National Library of Canada
Bibliothèque nationale du Canada

Canadian Theses Service
Service des thèses canadiennes

Ottawa, Canada
K1A 0N4

NOTICE

The quality of this microform is heavily dependent upon the quality of the original thesis submitted for microfilming. Every effort has been made to ensure the highest quality of reproduction possible.

If pages are missing, contact the university which granted the degree.

Some pages may have indistinct print especially if the original pages were typed with a poor typewriter ribbon or if the university sent us an inferior photocopy.

Reproduction in full or in part of this microform is governed by the Canadian Copyright Act, R.S.C. 1970, c. C-30, and subsequent amendments.

AVIS

La qualité de cette microforme dépend grandement de la qualité de la thèse soumise au microfilmage. Nous avons tout fait pour assurer une qualité supérieure de reproduction.

S'il manque des pages, veuillez communiquer avec l'université qui a conféré le grade.

La qualité d'impression de certaines pages peut laisser à désirer, surtout si les pages originales ont été dactylographiées à l'aide d'un ruban usé ou si l'université nous a fait parvenir une photocopie de qualité inférieure.

La reproduction, même partielle, de cette microforme est soumise à la Loi canadienne sur le droit d'auteur, SRC 1970, c. C-30, et ses amendements subséquents.

NL-339 (r. 88/04) c

Canada

UNIVERSITY OF ALBERTA

A METHOD FOR EVALUATING THE TRANSIENT CREEP OF POTASH

by

ANDRE PACHECO DE ASSIS

A THESIS

SUBMITTED TO THE FACULTY OF GRADUATE STUDIES AND RESEARCH

IN PARTIAL FULFILMENT OF THE REQUIREMENTS FOR THE DEGREE OF

DOCTOR OF PHILOSOPHY

DEPARTMENT OF CIVIL ENGINEERING

EDMONTON / ALBERTA

SPRING OF 1990

National Library of Canada
Bibliothèque nationale du Canada

Canadian Theses Service
Service des thèses canadiennes

Ottawa, Canada
K1A 0N4

NOTICE

The quality of this microform is heavily dependent upon the quality of the original thesis submitted for microfilming. Every effort has been made to ensure the highest quality of reproduction possible.

If pages are missing, contact the university which granted the degree.

Some pages may have indistinct print especially if the original pages were typed with a poor typewriter ribbon or if the university sent us an inferior photocopy.

Reproduction in full or in part of this microform is governed by the Canadian Copyright Act, R.S.C. 1970, c. C-30, and subsequent amendments.

AVIS

La qualité de cette microforme dépend grandement de la qualité de la thèse soumise au microfilmage. Nous avons tout fait pour assurer une qualité supérieure de reproduction.

S'il manque des pages, veuillez communiquer avec l'université qui a conféré le grade.

La qualité d'impression de certaines pages peut laisser à désirer, surtout si les pages originales ont été dactylographiées à l'aide d'un ruban usé ou si l'université nous a fait parvenir une photocopie de qualité inférieure.

La reproduction, même partielle, de cette microforme est soumise à la Loi canadienne sur le droit d'auteur, SRC 1970, c. C-30, et ses amendements subséquents.

ISBN 0-315-60321-6

NL-339 (r. 88/04) c

Canada

UNIVERSITY OF ALBERTA

RELEASE FORM

NAME OF AUTHOR: ANDRE PACHECO DE ASSIS

TITLE OF THESIS: A METHOD FOR EVALUATING THE TRANSIENT CREEP OF POTASH

DEGREE FOR WHICH THESIS WAS PRESENTED: DOCTOR OF PHILOSOPHY

YEAR THIS DEGREE GRANTED: SPRING OF 1990

Permission is hereby granted to THE UNIVERSITY OF ALBERTA LIBRARY to reproduce single copies of this thesis and to lend or sell such copies for private, scholarly or scientific research purposes only.

The author reserves other publication rights, and neither the thesis nor extensive extracts from it may be printed or otherwise reproduced without the author's written permission.

(SIGNED) .....

PERMANENT ADDRESS:

HIGS 705 - Bloco D - Casa 74

CEP 70350 - Brasilia / DF

Brazil - Tel.: (061) 2438980

DATED: January 12th, 1990.

UNIVERSITY OF ALBERTA

FACULTY OF GRADUATE STUDIES AND RESEARCH

The undersigned certify that they have read, and recommend to the Faculty of Graduate Studies and Research, for acceptance, a thesis entitled *A Method for Evaluating the Transient Creep of Potash* submitted by *Andre Pacheco de Assis* in partial fulfilment of the requirements for the degree of *Doctor of Philosophy*.

Dr. D.M. Cruden .....

Supervisor

Dr. K. Barron .....

Dr. R. Gerard .....

Dr. P.K. Kaiser .....

Dr. J.D. Scott .....

Dr. J.J.K. Daemen .....

External Examiner

Date: January 4th, 1990.

UNIVERSITY OF ALBERTA

FACULTY OF GRADUATE STUDIES AND RESEARCH

The undersigned certify that they have read, and recommend to the Faculty of Graduate Studies and Research, for acceptance, a thesis entitled *A Method for Evaluating the Transient Creep of Potash* submitted by *Andre Pacheco de Assis* in partial fulfilment of the requirements for the degree of *Doctor of Philosophy*.

Dr. D.M. Cruden .....

Supervisor

Dr. K. Barron .....

Dr. R. Gerard .....

Dr. P.K. Kaiser .....

Dr. J.D. Scott .....

Dr. J.J.K. Daemen .....

External Examiner

Date: January 4th, 1990.

ABSTRACT

Underground structures in salt deposits exhibit time-dependent closures. This research aimed at obtaining creep model parameters from laboratory tests and at the evaluation of their predictive capability. Model predictions and hollow cylinder test results are compared. Hollow cylinder experiments were selected because they simulate circular openings in homogeneous stress fields representative of underground structures in salt formations.

Potash was chosen as a testing material to study the material behaviour. Laboratory facilities were developed to apply and control accurately and independently various testing parameters such as stress, deformation and temperature. This laboratory testing system executes long-term tests following triaxial or hollow cylinder stress paths. Specimen preparation and testing procedures were established to minimize sample disturbance and to provide reproducible test results.

The creep models adopted to describe the behaviour of salt rocks were first reviewed. Analytical solutions for the thick-walled cylinder were then derived for plane strain and axisymmetric loading conditions, and several creep models to include the geometric component. These solutions were based on viscoelasticity or viscoplasticity. Four solutions, including the power, structural, Kelvin and generalized Kelvin (fluid) models, were chosen to predict the transient creep response of hollow cylinder bore convergences.

A laboratory testing program was executed to provide the creep model parameters following two triaxial stress paths (conventional and J1-constant). Creep tests at stages previously loaded by J1-constant paths exhibited considerably higher deformation. Model parameters were obtained by non-linear regression analyses. An evaluation using the triaxial data showed that the models predict the actual data well for times within test duration limits. Extrapolation to times beyond the test duration leads to increasingly large errors, particularly for the rheological models.

The model predictions were also compared with the hollow cylinder test results. The structural law yielded reasonable predictions in terms of magnitude and trend of the strain rate data. The generalized Kelvin model exhibited the best predictions, but extrapolation to times beyond the test duration must be restricted. The power law predicted the magnitude and form of the creep curve reasonably well. It has considerable potential to predict field observations of transient creep from laboratory transient creep tests.

ACKNOWLEDGEMENT

This thesis is the product of the support I have received for the last five years. Now with a great relief that it is finished, I would like to express my gratitude.

The Conselho Nacional de Desenvolvimento Cientifico e Tecnologico, CNPq (National Research Council of Brazil), provided my financial support, which is most appreciated. I cannot forget the Brazilian people whose tax and sacrifice provide funding to this research council. To them I am grateful. The testing equipment developed for this research was built with funds from a strategic research grant on borehole stability (P.K. Kaiser and J.D. Scott) by the National Sciences and Engineering Research Council of Canada (NSERC). Furthermore, related research expenses were covered by the NSERC operating grant of Dr. P.K. Kaiser.

My supervisors deserve special thanks for their continuous guidance, dedication and patience. Dr. Peter Kaiser introduced me to this fascinating topic. He never measured any efforts to give me the ideal conditions of work. Dr. Dave Cruden kindly accepted to continue this supervision when Dr. Kaiser left the University of Alberta. Their friendship and enthusiasm were the support I needed when difficult moments came out. To both of them, I express my profound gratitude.

Besides my supervisors, I also received technical input from many other people. Sean Maloney taught me the secrets of a laboratory testing equipment and assisted in the design

and implementation. Without his help, it is difficult to imagine the equipment we built. The entire testing system has now been moved to the Geomechanics Research Centre at Laurentian University where Dr. P.K. Kaiser and Mr. Sean Maloney are continuing their rock mechanics research. Sean also contributed to the reviewing and editing of this thesis. Roy Gitzel and Dale Lathe (Civil Electronics Division) helped develop the hardware and software of the testing control system. The machinists, Gary Morrison, Ken Ellis and Andy Gawlak, did a great job and I remember the numerous times I came with problems and they found the solutions. The technicians, Gerry Cyre and Steve Gamble, were always enthusiastic about this project. Especially Steve, spent more than two years in this 'heavy' job, and I am sure he was the happiest person when I finished my laboratory testing program. Ronaldo Ferreira provided support for the data reduction and Tanya Schulz for the typing. To all I express my sincere thanks.

I am also indebted to Dr. Maurice Dusseault and James Baleshta (University of Waterloo) for their advice and for sharing their experience with their laboratory testing system. Many features of the system described in this thesis originated from their early work on salt testing. Also, to Dr. Parviz Mottahed, Terry Danyluk and Tommy Tang (PCS) for offering the potash samples needed for this research and for the assistance during sampling.

More than technical support is needed to complete a thesis successfully. Friendship and moral support are also essential. Dr. Gentil Lucena (CNPq) trusted in my potential in a very delicate and decisive moment to initiate this journey. To my Brazilian friends, my deepest gratitude for their friendship and so many happy memories. Special thanks to Paulo and Lucila for their unmeasurable dedication during my settlement in Canada; to Julio Alencar for his company during those first and most difficult months; to Angela Kupper for her enormous patience being my office mate for so long time and many coffees; to Antonio and Ana Rita for sharing with me countless kilometres during our unforgettable vacations; and to Sergio, Marisa, Carlos and Carla for providing me with a home and not only with just a place to stay during the last months.

I wish to express my respect and the best of my feelings to my parents, Antonio and Desiree. Their love, care, incentive and support have been an essential source of strength at all stages of my life. Also, I am deeply thankful to my parents in-law, Joao and Thais, for their background support during the past years.

The development of this thesis would not have been possible without the continuous love and support of my family. Especially to my wife Sandra, for her love, affection and dedication, I express my deepest appreciation and profound thanks. Our sons, Bernardo and Daniel, have contributed to the happiness, joy and mean of our lives. To

my beloved family I am grateful. Also, I am hopeful that now we will spend more time together.

Finally, I thank God for giving me this opportunity and moreover, I pray for the strength needed to honour such a responsibility.

Table of Contents

Chapter Page

1. INTRODUCTION 1

1.1 Underground Structures in Salt Rocks 1

1.2 Variables Controlling the Deformation of Underground Structures in Salt Rocks 6

1.3 Definition of the Problem 8

1.4 Scope of Thesis 11

2. TIME-DEPENDENT DEFORMATION MECHANISMS AND CONSTITUTIVE MODELS 18

2.1 Introduction 18

2.2 Phenomenological Creep Response 20

2.3 Time-Dependent Models 23

2.3.1 Empirical Creep Laws 24

2.3.1.1 Power Law 25

2.3.1.2 Logarithmic Law 26

2.3.1.3 Exponential-Temperature Law 27

2.3.1.4 Exponential-Time Law 28

2.3.2 Microphysical Creep Laws 31

2.3.2.1 Mechanism 1: Defectless Flow 33

2.3.2.2 Mechanism 2: Dislocation Glide ...33

2.3.2.3 Mechanism 3: Dislocation Climb ...34

2.3.2.4 Mechanism 4: Diffusional Creep ...35

2.3.2.5 Mechanism 5: Undefined Mechanism .36

2.3.2.6 Physical Models for Transient Creep Strain 37

2.3.3 Rheological Models 39

2.3.3.1 Maxwell Model 40

2.3.3.2 Kelvin Model 41

2.3.3.3 Generalized Kelvin (3-parameter solid) Model 42

2.3.3.4 Generalized Kelvin (3-parameter fluid) Model 43

2.3.3.5 Burgers Model 44

2.3.4 Constitutive Modelling of Salt Rocks 46

2.4 In-Situ Observations 49

2.5 Conclusions 51

3. ANALYTICAL SOLUTIONS FOR THE THICK-WALLED CYLINDER ..59

3.1 Introduction 59

3.2 Elastic Solution for the Thick-Walled Cylinder ..60

3.2.1 Axisymmetric Loading State 62

3.2.2 Plane Strain State 63

3.2.3 Loading Conditions 64

3.2.3.1 Hydrostatic Loading 65

3.2.3.2 Axisymmetric Loading 66

3.2.3.3 Plane Strain 67

3.2.4 Elastic Equations for Hollow Cylinder Calibration Tests 69

3.3 Viscoelastic Solutions for the Thick-Walled Cylinder 69

3.3.1 Maxwell Model 79

3.3.2 Kelvin Model 80

3.3.3 Generalized Kelvin (solid) Model 81

3.3.4 Generalized Kelvin (fluid) Model 82

3.3.5 Burgers Model 83

3.4 Elastic-Viscoplastic Solutions for the Thick-Walled Cylinder 85

3.4.1 Plane Strain with Power Law 91

3.4.2 Plane Strain with Structural Law 91

3.4.3 Axisymmetric Loading with Power Law 91

3.4.4 Axisymmetric Loading with Structural Law .91

3.5 Summary and Conclusions 92

4. LABORATORY TESTING FACILITIES 98

4.1 Introduction 98

4.2 Experimental Techniques for Time-Dependent Properties 102

4.3 The High Pressure and Temperature System 104

4.3.1 Testing Cells and Axial Loading Systems (Appendix A) 105

4.3.2 Pressure System (Appendix B) 106

4.3.3 Temperature System (Appendix B) 108

4.3.4 Control and Data Acquisition System (Appendix C) 109

4.3.5 Monitoring (Appendix D) 112

4.3.6 Calibration Tests (Appendix D) 113

4.4 The HPTS Performance and Suggestions for Further Improvements 113

4.4.1 Testing Cells and Axial Loading Systems .113

4.4.2 Pressure System 116

4.4.3 Temperature System 116

4.4.4 Control and Data Acquisition System 117

4.4.5 Monitoring 120

4.5 Summary and Conclusions 120

5. LABORATORY TESTING PROGRAM 128

5.1 Introduction 128

5.2 Sampling 129

5.2.1 Sampling Location 131

5.2.2 Sample Transportation 132

5.2.3 Core Drilling Technique 132

5.2.4 Specimen Preparation 135

5.2.4.1 Preparation of Cylindrical Specimens 136

5.2.4.2 Preparation of Hollow Cylinder Specimens 138

5.2.5 Specimen Characterization and Storage ...140

5.3 Ultrasonic Velocity Tests 141

5.4 Triaxial Testing Program 144

5.4.1 Conventional Triaxial Compression (CTC) Tests 150

5.4.1.1 CTC Test 1 (Table and Plate E.1, Figs. E.1 and E.2) 150

5.4.1.2 CTC Test 2 (Table and Plate E.2, Figs. E.3 and E.4) 151

5.4.1.3 CTC Test 3 (Table and Plate E.3, Figs. E.5 and E.6) 152

5.4.1.4 CTC Test 4 (Table and Plate E.4, Figs. E.7 and E.8) 153

5.4.2 J1-Constant Triaxial Compression (JTC) Tests 154

5.4.2.1 JTC Test 1 (Table and Plate E.5, Figs. E.9 and E.10) 155

5.4.2.2 JTC Test 2 (Table and Plate E.6, Figs. E.11 and E.12) 155

5.4.2.3 JTC Test 3 (Table and Plate E.7, Figs. E.13 and E.14) 156

5.5 Hollow Cylinder Testing Program 158

5.5.1 HCAL Tests 160

5.5.1.1 HCAL Test 1 160

5.5.1.2 HCAL Test 2 160

5.5.1.3 HCAL Test 3 161

5.5.1.4 HCAL Test 4 161

5.5.2 HCPS Tests 162

5.5.2.1 HCPS Test 1 162

5.5.2.2 HCPS Test 2 163

5.6 Summary and Conclusions 163

6. INTERPRETATION OF THE LABORATORY TEST RESULTS AND EVALUATION OF THE CONSTITUTIVE CREEP MODELS 182

6.1 Introduction 182

6.2 Interpretation of the Hydrostatic Loading Results 185

6.2.1 Hydrostatic Loading 187

6.2.2 Hydrostatic Unload/Reload Cycles 188

6.2.3 Hydrostatic Creep Stage 189

6.3 Interpretation of the Triaxial Test Results 192

6.3.1 Triaxial Loading 193

6.3.2 Triaxial Creep Stage 195

6.4 Creep Model Parameters 199

6.5 Interpretation of the Hollow Cylinder Test Results 205

6.5.1 Deviatoric Pressure Loading 206

6.5.2 Hollow Cylinder Creep Stage 208

6.6 Evaluation of Creep Models 210

6.6.1 Model Test Results 211

6.6.2 Analytical Solution Predictions 213

6.6.2.1 Generalized Kelvin (Fluid) Model 213

6.6.2.2 Power Law 216

6.6.2.3 Structural Law 218

6.6.3 Comparison Between Creep Model Predictions and Hollow Cylinder Bore Convergence 220

6.7 Summary and Conclusions 226

7. SUMMARY, CONCLUSIONS AND SUGGESTIONS FOR FURTHER RESEARCH 270

7.1 Introduction 270

7.2 Summary 271

7.3 Conclusions 277

7.4 Suggestions for Further Research 282

REFERENCES 287

A. TESTING CELLS AND AXIAL LOADING SYSTEMS 305

A.1 Introduction 305

A.2 Design of the Testing Cells and Axial Loading Systems 306

A.3 Description and Specification of the Testing Cells and Axial Loading Systems 307

A.3.1 Pedestal, PD (Fig. A.3) 307

A.3.2 Bottom Cap, BC (Figs. A.4 and A.5) 308

A.3.3 Bottom Ring, BR (Fig. A.6) 308

A.3.4 Specimen Support, SS (Figs. A.7 and A.8) 308

A.3.5 Top Ring, TR (Fig. A.9) 309

A.3.6 Cell Chamber, CC (Fig. A.10) 309

A.3.7 Top Cap, TC (Figs. A.11 and A.12) 309

A.3.8 Diameter Reducer, DR (Fig. A.13) 309

A.3.9 Axial Ram, RM (Figs. A.14, A.15 and A.16) 309

A.3.10 Bolts, BT 310

A.3.11 Axial Loading Frame for Cell No. 1 310

A.3.12 Piston Chamber, PC (Fig. A.17) 310

A.3.13 Axial Piston, PP (Figs. A.18 and A.19) ..310

A.3.14 Piston Cap, CP (Fig. A.20) 311

A.3.15 Membranes 311

A.3.16 Seals 311

A.3.17 Insulator Caps, TS 312

A.3.18 Lower Platen, LP 312

A.4 Assembly and Disassembly Procedures 312

A.4.1 Assembly Procedure 312

A.4.2 Charging Procedure 315

A.4.3 Purging Procedure 315

A.4.4 Disassembly Procedure 316

A.5 Structural Performance of the Testing Cells 317

B. PRESSURE AND TEMPERATURE SYSTEMS 341

B.1 Introduction 341

B.2 Pressure System 341

B.2.1 Low Pressure Side 341

B.2.2 Accumulator/Intensifier/Volume Change Device 342

B.2.3 High Pressure Side 344

B.3 Temperature System 345

B.3.1 Cell Temperature 345

B.3.2 Bore Temperature 345

C. CONTROL AND DATA ACQUISITION SYSTEM 352

C.1 Introduction 352

C.2 Hardware 352

C.3 Software 354

C.3.1 Program HPTSCAL (Fig. C.3) 354

C.3.1.1 Running Program HPTSCAL 354

C.3.1.2 Listing of Program HPTSCAL 355

C.3.2 Program HPTSCON (Fig. C.4) 357

C.3.2.1 Running Program HPTSCON 357

C.3.2.2 Listing of Program HPTSCON 358

C.3.3 Program HPTS 361

C.3.3.1 Running Program HPTS 362

C.3.3.2 Entering Test Parameter Setup from Disk A (Fig. C.13) 363

C.3.3.3 Entering Data from the Keyboard (Fig. C.13) 363

C.3.3.4 Starting Routines 366

C.3.3.5 Monitor Screen Control 366

C.3.3.6 HPTS Data Output 368

C.3.3.7 Listing of Program HPTS 368

D. INSTRUMENTATION AND SYSTEM CALIBRATION 408

D.1 Introduction 408

D.2 Transducer Calibration 408

D.2.1 Pressure Transducers 409

D.2.2 Linear Variable Displacement Transducers 409

D.2.3 Volume Change Device 410

D.2.4 Bore Convergence Device 410

D.2.5 Thermocouples and RTDs 411

D.3 System Calibration 411

D.3.1 Hydrostatic Loading (HL) Tests 412

D.3.2 Conventional Triaxial Compression (CTC) Tests 413

D.3.3 J1-Constant Triaxial Compression (JTC) Tests 413

D.3.4 Hollow Cylinder (HC) Tests 414

D.4 Conclusion 414

E. TRIAXIAL TESTING PROGRAM DATA 431

List of Tables

Table | Page

1.1 Underground structures in salt formations 16

3.1 Deviatoric time differential and Laplace transformed operators for five linear viscoelastic models 95

4.1 Correction equations for triaxial tests 123

4.2 Correction equations for hollow cylinder tests 124

5.1 Physical measurements of cylindrical specimens 166

5.2 Physical measurements of hollow cylinder specimens 167

5.3 Ultrasonic velocity test results for cylindrical specimens (* not considered in the average) 168

5.4 Ultrasonic velocity test results for hollow cylinder specimens (* data sheet lost) 169

6.1 Comparison of cylindrical specimen deformations under hydrostatic loading and ultrasonic wave test results 232

6.2 Comparison of hollow cylinder specimen deformations under hydrostatic loading and ultrasonic wave test results 233

6.3 Power law parameters obtained from non-linear regression analyses (BMDP) 234

6.4 Structural law parameters obtained from non-linear regression analyses (BMDP) 235

6.5 Kelvin model parameters obtained from non-linear regression analyses (BMDP) 236

6.6 Generalized Kelvin (fluid) model parameters obtained from non-linear regression analyses (BMDP) 237

6.7 Comparison of creep model parameters obtained from non-linear analyses (BMDP), using half (H) and full (F) test duration 238

Table Page

6.8 Creep model evaluation program (number in the box indicates the equation number needed to calculate the desired variable) 239

A.1 Materials and properties of the testing cell and axial loading system components 319

C.1 Electronic instrument parameters 391

C.2 Files and routines contained in the disk drives 392

D.1 Transducer conversion factors 415

D.2 Correction factors for axial pressure transducers 416

D.3 Deformation equations for aluminium cylindrical specimens 417

D.4 Best-fit equations for aluminium cylindrical specimens 418

D.5 Deformation equations for aluminium hollow cylinder specimens 419

D.6 Best-fit equations for aluminium hollow cylinder specimens 420

E.1 CTC Test 1 432

E.2 CTC Test 2 433

E.3 CTC Test 3 434

E.4 CTC Test 4 435

E.5 JTC Test 1 436

E.6 JTC Test 2 437

E.7 JTC Test 3 438

List of Figures

Figure Page

1.1 Scope of this study (topics inside dashed boxes are not covered by this research) 17

2.1 Idealized phenomenological creep response 56

2.2 Deformation-mechanism map for pure halite; d= 3 mm, T_m= 1074°K and G= 11 GPa (modified after Munson and Dawson, 1984) 57

2.3 Linear viscoelastic rheological models 58

3.1 Definition of the terms used in the elastic equations for thick-walled cylinders (pressures and displacements are shown in positive directions) 96

3.2 Volume change expressions for thick-walled cylinders 97

5.1 Physical measurements of specimens (example for Specimen TR01) 170

5.2 Densities and ultrasonic wave velocities of cylindrical specimens 171

5.3 Densities and ultrasonic wave velocities of hollow cylinder specimens 172

6.1 Triaxial testing program - Hydrostatic loading - Stress vs strain curves 240

6.2 Hollow cylinder testing program - Hydrostatic loading - Stress vs strain curves 241

6.3 Triaxial testing program - Hydrostatic loading - Strain vs time curves 242

6.4 Hollow cylinder testing program - Hydrostatic loading - Strain vs time curves 243

6.5 Triaxial testing program - Hydrostatic loading - Strain rate vs time (log) curves for all specimens 244

6.6 Triaxial testing program - Hydrostatic loading - Strain rate (log) vs time (log) curves for all specimens 245

6.7 CTC Tests 1 and 2 - Stress vs strain curves 246

Figure Page

6.8 CTC Tests 3 and 4 - Stress vs strain curves (1st triaxial loading stage) 247

6.9 JTC Tests - Stress vs strain curves (1st triaxial loading stage) 248

6.10 CTC Tests - Strain vs time curves (σ_1/σ_3 MPa) 249

6.11 JTC Tests - Strain vs time curves (σ_1/σ_3 MPa) 250

6.12 CTC Test 1 (1st creep stage) - Comparison between creep model predictions and actual creep data 251

6.13 CTC Test 3 (1st creep stage) - Comparison between creep model predictions and actual creep data 252

6.14 CTC Test 3 (2nd creep stage) - Comparison between creep model predictions and actual creep data 253

6.15 CTC Test 4 (1st creep stage) - Comparison between creep model predictions and actual creep data 254

6.16 CTC Test 4 (2nd creep stage) - Comparison between creep model predictions and actual creep data 255

6.17 JTC Test 1 (1st creep stage) - Comparison between creep model predictions and actual creep data 256

6.18 JTC Test 2 (1st creep stage) - Comparison between creep model predictions and actual creep data 257

6.19 JTC Test 2 (2nd creep stage) - Comparison between creep model predictions and actual creep data 258

6.20 JTC Test 3 (1st creep stage) - Comparison between creep model predictions and actual creep data 259

6.21 CTC Test 1 (1st creep stage) - Comparison between creep model predictions and actual creep data, using half (H) test duration 260

Figure Page

6.22 CTC Test 3 (1st creep stage) - Comparison between creep model predictions and actual creep data, using half (H) test duration 261

6.23 CTC Test 1 (1st creep stage) - Comparison between creep model and extrapolated model predictions 262

6.24 CTC Test 3 (1st creep stage) - Comparison between creep model and extrapolated model predictions 263

6.25 HC Tests - Deviatoric pressure vs bore convergence curves (1st deviatoric loading stage) 264

6.26 HC Tests - Bore convergence vs time curves 265

6.27 Suggested triaxial creep testing program to generate model parameters needed to predict hollow cylinder results 266

6.28 HCAL4CP1 and HCPS2CP1 creep stages - Evaluation of the generalized Kelvin model 267

6.29 HCAL4CP1 creep stage - Evaluation of the power (PW) and structural (ST) laws 268

6.30 HCPS2CP1 creep stage - Evaluation of the power (PW) and structural (ST) laws 269

A.1 Cell No. 1 - Triaxial test setup 320

A.2 Cell No. 2 - Hollow cylinder test setup 321

A.3 Pedestal, PD 322

A.4 Bottom cap, BC - Top view 323

A.5 Bottom cap, BC - Sections 324

A.6 Bottom ring, BR (* for 100 mm diameter specimen; 171.0 for 140 mm diameter specimen) 325

A.7 Specimen support, SS - Cylindrical specimens 326

A.8 Specimen support, SS - Hollow cylinder specimens 327

Figure Page

A.9 Top ring, TR (* for 100 mm diameter specimen; 171.0 for 140 mm diameter specimen; **167.0 for 140 mm diameter specimen) 328

A.10 Cell chamber, CC 329

A.11 Cell No. 1 - Top cap, TC 330

A.12 Cell No. 2 - Top cap, TC 331

A.13 Diameter reducer, DR - From 140 to 100 mm 332

A.14 Cell No. 1 - Axial ram, RM - Triaxial test setup 333

A.15 Cell No. 1 - Axial ram, RM - Hollow cylinder test setup 334

A.16 Cell No. 2 - Axial ram, RM - Hollow cylinder test setup 335

A.17 Piston chamber, PC 336

A.18 Axial piston, PP 337

A.19 Seal cap, CS 338

A.20 Piston cap, CP 339

A.21 Cell No. 1 - Structural performance tests - Strain gauge measurements (microstrain) 340

B.1 Pressure system for two testing cells (symbols are defined on Figs. B.2 to B.4) 347

B.2 Low pressure side 348

B.3 AIVC device (modified after Maloney, 1986) 349

B.4 High pressure side 350

B.5 Performance curve - AIVC No. 2 (modified after Maloney, 1986) 351

C.1 Pressure and control system (modified after Maloney, 1986) 393

C.2 Hardware layout 394

C.3 Flow chart for Program HPTSCAL 395

Figure Page

C.4 Flow chart for Program HPTSCON 396

C.5 Flow chart for Program HPTS 397

C.6 Program HPTS - Flow chart for the main routines 398

C.7 Program HPTS - Flow chart for Routine 4000 399

C.8 Program HPTS - Flow chart for Routine 4500 400

C.9 Program HPTS - Flow chart for Routine 6000 401

C.10 Program HPTS - Flow chart for Routine 7000 402

C.11 Program HPTS - Flow chart for Routine 8000 - Part 1 403

C.12 Program HPTS - Flow chart for Routine 8000 - Part 2 404

C.13 Program HPTS - Flow chart for Routine 30000 405

C.14 Program HPTS - Flow chart for Routine 31000/32000 406

C.15 Example of data input methodology 407

D.1 Bore convergence device (units in inches) 421

D.2 System 1 - HL calibration tests for cylindrical specimens 422

D.3 System 2 - HL calibration tests for hollow cylinder specimens - A 423

D.4 System 2 - HL calibration tests for hollow cylinder specimens - B 424

D.5 System 1 - CTC calibration tests 425

D.6 System 1 - JTC calibration tests 426

D.7 System 2 - HC calibration tests under plane strain - A 427

D.8 System 2 - HC calibration tests under plane strain - B 428

Figure Page

D.9 System 2 - HC calibration tests under axisymmetric loading - A 429

D.10 System 2 - HC calibration tests under axisymmetric loading - B 430

E.1 CTC Test 1 (899 points) - Measured and prescribed stress paths 439

E.2 CTC Test 1 (899 points) - Axial displacement and volume change responses 440

E.3 CTC Test 2 (483 points) - Measured and prescribed stress paths 441

E.4 CTC Test 2 (483 points) - Axial displacement and volume change responses 442

E.5 CTC Test 3 (762 points) - Measured and prescribed stress paths 443

E.6 CTC Test 3 (762 points) - Axial displacement and volume change responses 444

E.7 CTC Test 4 (1058 points) - Measured and prescribed stress paths 445

E.8 CTC Test 4 (1058 points) - Axial displacement and volume change responses 446

E.9 JTC Test 1 (224 points) - Measured and prescribed stress paths 447

E.10 JTC Test 1 (224 points) - Axial displacement and volume change responses 448

E.11 JTC Test 2 (276 points) - Measured and prescribed stress paths 449

E.12 JTC Test 2 (276 points) - Axial displacement and volume change responses 450

E.13 JTC Test 3 (349 points) - Measured and prescribed stress paths 451

E.14 JTC Test 3 (349 points) - Axial displacement and volume change responses 452

List of Plates

Plate Page

4.1 HPTS Testing Cells; (A) Cell No. 1 and reaction frame; (B) Cell No. 2 (self-framed cell) 125

4.2 HPTS Pressure System; (A) General view of the intensifiers; (B) AIVC device 126

4.3 HPTS Control, Data Acquisition and Monitoring; (A) Control panel; (B) Bore convergence device 127

5.1 Laboratory Core Drilling Scheme; (A) General view; (B) Core barrel positioned over block sample 173

5.2 Cylindrical Specimen Preparation; (A) End cutting by diamond cut-off saw; (B) Lathe and large-scale vacuum cleaner 174

5.3 Cylindrical Specimen Preparation; (A) Specimen inside the line centered mandrel; (B) End preparation using lathe 175

5.4 Cylindrical Specimen Preparation; (A) Finishing and polishing using a high speed grinder; (B) End finishing using a grinding table 176

5.5 Hollow Cylinder Specimen Preparation; (A) Guide for drilling central hole; (B) Core and mandrel 177

5.6 Hollow Cylinder Specimen Preparation; (A) Side preparation using lathe; (B) End preparation using lathe 178

5.7 Specimen Characterization Using P/S Wave Tests; (A) Cylindrical specimens; (B) Hollow cylinder specimens 179

5.8 HCAL Test 2 - Specimen HC05; (A) Before testing; (B) After testing 180

5.9 HCAL Test 4 - Specimen HC01; (A) Before testing; (B) After testing 181

E.1 CTC Test 1 - Specimen TR02; (A) Before testing; (B) After testing 453

E.2 CTC Test 2 - Specimen TR03; (A) Before testing; (B) After testing 454

Plate Page

E.3 CTC Test 3 - Specimen TR04; (A) Before testing; (B) After testing 455

E.4 CTC Test 4 - Specimen TR06; (A) Before testing; (B) After testing 456

E.5 JTC Test 1 - Specimen TR05; (A) Before testing; (B) After testing 457

E.6 JTC Test 2 - Specimen TR07; (A) Before testing; (B) After testing 458

E.7 JTC Test 3 - Specimen TR08; (A) Before testing; (B) After testing 459

LIST OF SYMBOLS, NOMENCLATURE AND ABBREVIATIONS

a ... average of various diffusion paths in diffusional creep laws

a ... inner radius of thick-walled cylinders

a ... time exponent in transient creep laws

a_0 ... original inner radius for thick-walled cylinders

A ... empirical constant in creep laws

AISI ... American Iron and Steel Institute

AIVC ... accumulator/intensifier/volume change

AL ... axisymmetric loading

AP ... after specimen preparation

ASTM ... American Society for Testing and Materials

A_t ... total cross-sectional area of bolts

AT ... after testing

AVG ... average

A/D ... analog/digital

b ... outer radius of thick-walled cylinders

b ... temperature exponent in transient creep laws

b_1 ... strain rate at unit time in structural creep laws

b_2 ... strain-hardening parameter in structural creep laws

B ... empirical constant in creep laws

B ... temperature-dependent diffusivity term in solution-precipitation creep laws

BC ... bore convergence

BC ... bottom cap

BP ... before specimen preparation

BR ... bottom ring

BT ... before testing

BT ... bolts

c ... stress exponent in transient creep laws

cm ... centimetre

C ... Celsius

C ... empirical constant in creep laws

C ... grain boundary structure parameter in solution-precipitation creep laws

CAL ... calibration

CANMET ... Canada Centre for Mineral and Energy Technology

CC ... cell chamber

CJC ... cold junction compensation

CL ... supporting column

CP ... piston cap

CS ... seal cap

CTC ... conventional triaxial compression

d ... diameter, grain diameter or mean grain diameter

d ... stress exponent in steady-state creep laws

d_b ... bore diameter of hollow cylinder specimens

d_i ... inside diameter

d_{ij} ... deviatoric strain tensor

d_o ... outside diameter

D ... empirical constant in creep laws

D ... specimen diameter

DA ... axial displacement

Db ... grain boundary diffusion coefficient in diffusional creep laws

DOS ... directory operation system for IBM microcomputers

DR ... diameter reducer

e ... temperature exponent in steady-state creep laws

e_a ... asymptotic transient creep strain in exponential-time creep laws

e.g. ... exempli gratia (for example)

et al. ... et alli (and others)

etc. ... et cetera (and so on)

E ... Young's modulus or spring constant

E_u ... ultrasonic elastic modulus

EXP(x), exp(x) ... exponential function of 'x'

f(x) ... function of 'x'

g ... gram

G ... shear modulus

GK ... generalized Kelvin creep model

GPa ... gigapascal

h ... hour

H ... height

HC ... hollow cylinder

HCAL ... hollow cylinder/axisymmetric loading

HCPS ... hollow cylinder/plane strain

HL ... hydrostatic loading

HPTS ... high pressure and temperature system

HRC ... Rockwell C hardness

i.e. ... id est (that is to say)

ID ... internal diameter; strain gauge average (bore convergence)

IDA ... internal diameter; strain gauge A

IDB ... internal diameter; strain gauge B

ISRM ... International Society for Rock Mechanics

I/O ... input/output

J1 ... first deviatoric stress invariant

J2 ... second deviatoric stress invariant

JTC ... J1-constant triaxial compression

k ... inside to outside pressure ratio

kBytes ... kilobytes

kg ... kilogram

kN ... kilonewton

kPa ... kilopascal

K ... Kelvin

K ... Boltzmann's constant

K ... bulk modulus

K ... empirical constant in creep laws

KL ... Kelvin creep model

K_o ... horizontal to vertical effective stress ratio

L ... length

L_0 ... original specimen length

LED ... liquid electronic display

LNG ... liquefied natural gas

LP ... lower platen

LPG ... liquefied petroleum gas

LVDT ... linear variable displacement transducer

m ... metre

min ... minute

ml ... millilitre

mm ... millimetre

ms ... millisecond

mV ... millivolt

M ... bending moment

M1 ... metering valve connected to solenoid valve S1

M2 ... metering valve connected to solenoid valve S2

MB ... bore membrane

MBytes ... megabytes

MC ... cell membrane

MN ... meganewton

MPa ... megapascal

n ... stress exponent in creep laws

N ... newton

NWSP ... National Waste Terminal Storage Program

ODA ... specimen diameter deformation

P ... compression wave (ultrasonic tests)

P, p ... pressure, hydrostatic pressure, geostatic pressure or mean pressure

PA, p_a ... axial pressure

PC ... piston chamber

PCS ... Potash Corporations of Saskatchewan

PD ... pedestal

PE, p_e ... external (cell) pressure

PI, p_i ... internal (bore) pressure

P_i ... Laplace transform operator for the stress tensor

$\hat{P}_i$ ... time differential operator for the stress tensor

PO, p_o ... outside pressure

PP ... axial piston

PS ... plane strain

PVC ... polyvinyl chloride

PW ... power creep law

Q ... activation energy

Q_i ... Laplace transform operator for the strain tensor

$\hat{Q}_i$ ... time differential operator for the strain tensor

r ... radius

R ... universal gas constant

RAM ... random access memory

RM ... axial ram

RTD ... resistance temperature device

R-P ... room and pillar

s ... second

s ... Laplace transform variable

S ... shear wave (ultrasonic tests)

S1 ... solenoid valve to increase pressure

S2 ... solenoid valve to decrease pressure

SB ... bore seal

SC ... chamber seal

SG ... after contact with water absorbent material

S_{ij} ... deviatoric stress tensor

SM ... membrane seal

SP ... piston seal

S_r ... deviatoric radial stress

SS ... specimen support

SS ... stainless steel

ST ... structural creep law

t ... thickness

t ... time

T ... temperature

TC ... top cap

TE ... external (cell) temperature

TI ... internal (bore) temperature

T_m ... melting temperature

TR ... top ring

TS ... insulator cap

u ... displacement in the radial direction

v ... displacement in the tangential direction

vs ... versus

V ... volts

V ... volume

V_0 ... original specimen volume

V1 ... ball valve to bypass solenoid valve S1

V2 ... ball valve to bypass solenoid valve S2

V3 ... ball valve to isolate the low pressure side

VB_0 ... original hollow cylinder bore volume

VC ... volume change

VCA ... axial volume change

VCE ... external (cell) volume change

VCI ... internal (bore) volume change

V_p ... ultrasonic compression wave velocity

V_s ... ultrasonic shear wave velocity

w ... average width of grain boundary in diffusional creep laws

w ... displacement in the axial (longitudinal) direction

W ... watts

yr ... year

z ... longitudinal dimension (axial direction)

° ... degree

$\dot{}$ ... derivative with respect to time

β ... relaxation frequency in exponential-time creep laws

γ ... unit weight

Δ ... change

ϵ ... strain

ϵ_a ... accelerating creep strain

ϵ_e ... elastic strain

ϵ_e^c ... effective or equivalent creep strain

ϵ_{ii} ... hydrostatic strain tensor

ϵ_{ij} ... total strain tensor

ϵ^{c}_{ij} ... plastic creep strain tensor

ϵ^{e}_{ij} ... elastic strain tensor

ϵ_{o} ... instantaneous strain

ϵ_{p} ... plastic strain

ϵ_{r} ... total radial strain

ϵ^{c}_{r} ... plastic creep radial strain

ϵ^{e}_{r} ... elastic radial strain

ϵ_{ss} ... steady-state creep strain

ϵ_{t} ... transient creep strain

ϵ_{v} ... volumetric strain

ϵ_{z} ... axial strain

η ... viscosity

λ ... empirical constant in temperature-exponential creep laws

ν ... Poisson's ratio

ν_{u} ... ultrasonic Poisson's ratio

π ... 3.141592

ρ ... density

σ ... stress

σ_{11}, σ_{22}, σ_{33} ... principal stresses

σ_c ... uniaxial compressive strength

σ_e ... effective or equivalent stress

σ_{ii} ... hydrostatic stress tensor

σ_o ... natural in-situ stress or constant stress

σ_r ... radial stress

σ_y ... yield limit stress

σ_z ... axial stress

σ_θ ... tangential stress

τ ... shear stress

ω ... molecular volume in diffusional creep laws

1. INTRODUCTION

1.1 Underground Structures in Salt Rocks

Salt rocks belong to a group of sedimentary rocks, called evaporites, deposited by the evaporation of saline water. They are usually named after the dominant salt mineral. The most common of these evaporites are gypsum and anhydrite, followed by halite, often called salt rock and then, potash in which sylvite, carnallite, langbeinite and kainite are occurred. There are also associations of minerals which have formed together (parageneses). For example, halite parageneses are very common. The association of halite and sylvite is called sylvinite and the combination with carnallite is known as carnallinite. The origin, composition and sedimentology of salt formations are described in detail by Borchert and Muir (1964), Braitsch (1971), Sonnenfeld (1984) and Warren (1989).

Salt rocks, especially halite and potash salts, present some basic characteristics which are consequences of their genesis. First, they are readily dissolved in water. Second, they deform permanently over a wide range of stress and temperature. This deformability may prevent gaps and joints from opening up which implies a third basic characteristic, that is a practical impermeability. The last characteristic is their abundant presence in many sedimentary formations.

The economic value and importance of salt rocks have been recognized since the beginning of mankind. Common salt,

either mined or quarried, is amongst man's first commodities. On the other hand, potash salts had no large scale practical use until the nineteenth century. Potash salts are mainly used for fertilizers, but also for many chemical industry products.

Besides the mining exploitation of salt deposits, salt formations are often identified as possible boundary rocks for gas and oil reservoirs. Traditionally, it is believed that crude oil is generated in source rocks (e.g., shales and limestones), percolates into reservoir rocks and accumulates there if a suitable trap exists. Bedded and domal salts are well known hydrocarbon traps (Halbouty, 1979). About 70% of the world's oil fields in carbonate rocks have a relationship to salt formations. This association is more than fortuitous since salt deposits constitute less than 2% of the world's platform sediments (Warren, 1989). Sonnenfeld (1985) and Schreiber (1988) have suggested that salt rocks may also be a hydrocarbon source rock. About 50% of the world's oil may have originated as explained by this new thinking (Evans and Kirkland, 1988).

The basic characteristics of salt rocks have made these rocks the host for an increasing number of underground structures, used as storage for crude oil, compressed air or gas (e.g., LPG, LNG) and fluid or solid waste. Lately, old salt mines or salt caverns are being recommended as repositories for radioactive waste. Table 1.1 shows some underground structures in salt rocks, their utilization and

data on their development and operation.

Conventional salt mining creates an opening without internal pressure. The inside temperature is usually controlled to promote a comfortable work environment and ranges from 25 to 30°C. Depending on the layout and transport routes, some rooms are only active for a few months and others may stay in service for many years. Instability modes in salt mines are mostly related to excessive creep deformation, pillar collapse and groundwater inflow. Rooms completely closed by excessive creep and mines lost due to flooding are common problems in the salt mining industry.

The typical loading history of a nuclear repository would start with zero internal pressure for the initial operation period (≈50 yr) and, after backfilling, the pressure would increase gradually up to the geostatic pressure ($p = \gamma H$). Similarly the temperature would start at room temperature and could reach values up to 250°C (Wieczorek et al., 1988), depending on the kind of nuclear waste stored (e.g., sludge from reactor fuel). Major problems are associated with excessive salt deformation which, besides the instability modes described for salt mines, could overload waste containers, borehole casings and shaft liners or may affect the opening, backfill and shaft seals (Fuenkajorn and Daemen, 1988a and b). Other problems are related to high temperature, that besides the recognized direct and strong influence on creep rates and other

mechanical properties of salt rocks, also causes cleavage of certain mineral salts (e.g., carnallite), migration of brine, mineral transformations due to thermo-metamorphism and thermally induced stresses and strains (Albrecht et al., 1980).

Some salt mines and most fluid storage caverns are excavated by solution mining. The magnitude of pressure acting inside the storage caverns depends on the type of stored fluid, but it always has a cyclic pattern due to the storage operation. Passaris (1979), Thoms et al. (1980), Thoms and Gehle (1982) and Horseman and Passaris (1984) presented a typical internal pressure history of a gas storage cavity. Initially, the pressure is the overburden pressure which is dropped to the brine head during excavation and then to zero when brine is pumped out at the end of excavation. Then, the cyclic pattern starts with the internal pressure ranging from minimum to maximum values depending on the fluid demand. The temperature in gas caverns is extremely dependent on internal pressure and the type of gas stored. It can reach -50°C or less for certain gases (Rocha, 1980). The cyclic pattern of internal pressure also exists for liquid storage, but the pressure value approximates the hydrostatic pressure in the liquid. Temperature can be taken as ambient, although certain liquids are stored at very low temperatures (-50°C). The lifetime of storage caverns is expected to be in the order of decades (≈50 yr).

Excessive deformation due to creep is, once more, the most common source of problems in storage caverns. Creep can drastically reduce the cavern volume in just a few years and the volume loss may be as great as 20% in the first year (Hardy, 1982; Coates et al., 1983). The low frequency cyclic fluctuations of the internal pressure reduce temporarily the effective confining pressure and may also cause a gradual weakening of the rock media by as much as 50% (Thoms et al., 1980; Passaris, 1982). Potts et al. (1980) and Rocha (1980) stated that low temperature caused by rapid withdrawal of gas may produce tensile stresses, microfracturing and local failures in the cavity walls. For oil storage, the interaction between liquid and cavity wall makes the walls wet by liquid penetration, reducing the effective stress at boundaries and leading to accelerating closure or even ultimate failure. Furthermore, chemical reactions may lead to rock deterioration and generate an unstable opening shape.

As salt deposits are common oil traps and also hydrocarbon source rocks, boreholes for hydrocarbon extraction are often drilled through salt. Problems encountered in drilling through salt deposits include borehole collapse with loss of equipment by creep closure. During borehole drilling, the internal pressure can be assumed as the circulation fluid head, the temperature is ambient and the period of time for this operation is in the order of months. Another critical phase for borehole

stability is the stage of secondary recovery. When a well is presenting low productivity due to high liquid viscosity or product scarcity, steam, at up to 65°C, is injected through the well to facilitate oil drainage. The bore pressure is essentially unchanged from borehole drilling, but the high temperature during secondary recovery accelerates creep deformation. The stand-up time can range from months to a few years.

1.2 Variables Controlling the Deformation of Underground Structures in Salt Rocks

From the previous descriptions of underground structures in salt formations, some common problems can be recognized. Most of them are related to the same basic characteristics which made salt deposits favourable for those structures. Solubility favours solution mining but causes major concerns in conventional salt mines, radioactive waste repositories and borehole drilling. Time-dependent deformation ensures a practical impermeability and fracture-free body to salt rocks. This favours salt mines, storage caverns and nuclear disposal in one aspect, but when the creep deformation is excessive, it causes serious problems for many types of underground structures. Temperature directly affects the creep rate. Interaction between stored matter and rock may induce chemical reactions, cause effective stress reduction at the cavity boundaries, affect creep deformation and ultimate

failure parameters, and deteriorate the rock mass.

The great variety of problems encountered in underground structures in salt rocks can be identified according to the type of structure, interaction of stored matter and rock, cavern operation and type of salt deposit. Some problems such as leakage, slabbing and excessive fracturing, can be considered as consequences of the previous problems (in particular, excessive creep deformation). Several variables dominating each specific problem can be identified and may be of primary or secondary importance.

The major and most common problem in all structures in salt formations is the time-dependent deformation. The variables that affect the creep rates, are related to:

1. The type of salt formation: its stress history, mineral composition, crystal size, natural moisture content and inhomogeneity.
2. The development and operation of the cavity: the stress path, confining stress level, deviatoric stress and temperature.
3. The interaction between stored matter and rock mass: chemical reactions, solution processes, effective stress and mechanical property changes.
4. The testing procedures employed to determine the creep properties in laboratory and in situ: quality (disturbance) of specimens, specimen sizes (scale effects) and quality of test control, both applied and

measured testing parameters such as load, stress, deformation, temperature, stress or deformation rates, etc.

1.3 Definition of the Problem

The investigation of the effects of the above variables upon the time-dependent behaviour of salt rocks and consequently, upon the closure of underground openings constitutes the core problem of this research. The primary objective of this study of creep properties is to assess the value of laboratory tests to predict or evaluate the field performance of a natural formation. Rheological studies must attempt to simulate the actual mechanical behaviour of matter as close as possible. The intent of such studies is to determine constitutive laws which describe the deformation behaviour, as far as the material dependence on time, stress and temperature are concerned, and to relate it to the conditions encountered in the field (Langer, 1979; 1984). The problem can be itemized as follows:

1. Study of creep models used for describing the time-dependent behaviour of salt rocks. Microphysical aspects should be considered to establish the most appropriate models.
2. Laboratory studies to determine the parameters needed for the creep models.
3. Theoretical investigations to implement creep models into analytical or numerical formulations and to predict

in-situ measurements.

4. In-situ measurements to confirm the theoretical predictions obtained from creep models with parameters based on laboratory results.

The approach adopted in this research attempts to assess the validity of using creep models with parameters obtained from laboratory triaxial tests to predict in-situ measurements. The step from laboratory to field, however, is too large and this investigation addresses only an intermediate step from laboratory tests of one stress path and geometry to another test of different stress path and geometry. In this research, the underground opening is replaced by a hollow cylinder. Hollow cylinder tests are model simulation of circular openings in homogeneous stress fields. Therefore, they resemble underground cavities in salt deposits. The study presented in the following contains:

1. A review of creep models usually adopted to describe creep deformation of salt rocks.
2. The development of a triaxial and hollow cylinder testing system.
3. A laboratory triaxial testing program to study various effects on the time-dependent behaviour of salt rocks and to determine creep model parameters for a potash.
4. Formulation of analytical solutions for the thick-walled cylinder based on several creep models.
5. Model tests on hollow cylinder specimens to confirm the

theoretical predictions.

The primary focus is on the assessment of how to perform the transition from laboratory triaxial stress paths to hollow cylinder tests. If this procedure can be established, hollow cylinder tests may play an important role in evaluating the predictive capability of creep models. The extrapolation to actual in-situ performance should then be a matter of scale effects.

More specifically, this study analyses only a few of the variables previously mentioned and is limited to one salt deposit. The salt rock studied is potash (sylvinite; 55% halite, 40% sylvite and 5% clay) from two mines of the Potash Corporations of Saskatchewan (PCS). All effort is concentrated on the variables related to the development and operation of cavities in salt formations (e.g., stress path, confining stress level, differential stress and temperature). Although temperature is controlled, all tests were executed under isothermal conditions (25°C) and the effects of temperature changes and gradients are relegated to future studies. Only the short-term response (transient creep) is evaluated. Factors related to the testing procedures are also examined.

Stress level, applied differential stress and temperature effects have been investigated by many researchers, but no conclusive and unique model has been satisfactorily defined. Even taking into account the natural variability of the material and that certain deformation

mechanisms can be dominant for specific conditions of stress and temperature, the results of these analyses have shown many discrepancies. Effects of testing procedures may be one of the responsible factors for the failure to arrive at unique results. It is necessary to define a standard testing procedure to minimize specimen disturbances and laboratory interferences on data. Furthermore, effects of the stress paths are recognized to be one of the sources of the discrepancies in the test results and clearly need to be addressed for model predictions. These are two fundamental aspects which have to be investigated for a better understanding of the mechanical behaviour of salt rocks.

1.4 Scope of Thesis

Chapter 1 gives a general view of the problems associated with underground structures placed in evaporite deposits. The main variables that affect the performance of these structures in salt rocks have been discussed and special attention has been drawn to confining stress level, differential stress, temperature and loading sequence during development and operation of cavities in salt deposits. The problem related to the time-dependent behaviour of salt rocks and consequent closure of openings has been defined. The approach adopted in this research to deal with it has been outlined.

Chapter 2 presents a review of the models normally adopted to describe creep deformation of salt rocks as a

function of stress, temperature and time. The creep models are divided into three groups. First, the empirical laws which are, basically, curve fitting equations of either laboratory or in-situ data. The second group comprises the rheological models, with spring, dashpot and friction elements assembled in series or in parallel. The third group, physical models, uses equations derived from the microphysical mechanisms of deformation. The resulting constitutive model is assembled by the substitution of each strain component by the appropriate deformation law (elastic, plastic, creep). This chapter also reviews some case-histories, describing the type of creep response measured in the field.

Chapter 3 presents several closed-form solutions based on elasticity, viscoelasticity (rheological models) and viscoplasticity (empirical and physical laws) for a thick-walled cylinder. This is the geometric shape that best resembles cavities in salt deposits. These solutions are later used for the interpretation of test data and for the comparison with hollow cylinder test results.

Chapter 4 reviews the current practice of creep testing. A detailed description of the laboratory facilities developed during this research for testing solid and hollow cylindrical specimens is presented. This apparatus is able to follow any axisymmetric stress path, control independently pressure and temperature, and perform data acquisition. The performance of the apparatus is discussed

and suggestions for further improvements are provided.

Chapter 5 describes the experimental work, from specimen preparation to test results. The specimen preparation procedure is outlined in detail because of the difficulties normally encountered in obtaining good quality specimens of natural potash. The testing program followed two triaxial stress paths, conventional triaxial compression and J1-constant triaxial compression, to obtain the creep properties of the potash. Also, a set of model tests, using hollow cylinder specimens, were executed to determine the creep response of a circular opening in the same potash.

Chapter 6 presents the interpretation of the laboratory triaxial test results and a discussion of the effects of the confining stress level, deviatoric stress and stress path. Creep model parameters are obtained from the triaxial creep tests using non-linear regression analyses. An evaluation of several creep models is performed in terms of how well these models can predict the time-dependent behaviour under different stress paths and for different geometries. For the later purpose, the model parameters are combined with analytical solutions to predict the hollow cylinder test results. The comparison between creep model predictions and model test results assesses the validity of obtaining parameters from triaxial tests to predict more realistic test results.

In Chapter 7, a summary and the major conclusions are presented. These include an evaluation of the equipment

performance, testing program and procedures, and how well creep parameters obtained from triaxial creep tests predict the results of hollow cylinder tests. Suggestions for further research, based on the successes and problems encountered in this work, are presented.

Appendices A to D describe in detail the apparatus developed for this research to test time-dependent deformation of rocks. Appendix A presents the design and specifications of the two testing cells. Assembly and disassembly procedures are also provided. Appendix B outlines the pressure and temperature systems, including the operation procedures. Appendix C describes the control and data acquisition system. The hardware is briefly explained and the software is presented in the form of a user's manual. Appendix D reviews the instrumentation used and explains how the laboratory equipment was calibrated. The correction curves are shown. Appendix E presents the plates and data of the triaxial testing program.

Figure 1.1 shows how this study fits in a generic work frame to investigate the mechanical behaviour of salt rocks and associated underground structures. It defines the problem and presents the three major areas of study: theoretical, laboratory and in-situ observations. The theoretical studies aim at the obtaining of constitutive models and their implementation into analytical or numerical formulations. The laboratory studies provide parameters for the constitutive models or the results of simulation tests.

Finally, the theoretical predictions are compared to the simulation test results or to in-situ measurements. From the results of this comparison, the predictive capability of creep models can be assessed.

Table 1.1 Underground structures in salt formations

Underground Structure			Structure Operation			
Development Method	Activity	Phase	Internal Media	Internal Pressure	Internal Temperature (°C)	Lifetime (yr)
Dry Mining	Waste Disposal	Open Cavern	Air	Zero	Transient (up to 250)	Decades (e.g., 50)
		Back-Filled Cavern	Mined Salt	Pressure of the Fill	Constant (e.g., 250)	Thousands (e.g., 10000)
	Salt Mining	Active Room	Air	Zero	Controlled Room Temperature (e.g., 27)	Less than 1 yr
Solution Mining		Access Route				Few (e.g., 10)
	Fluid Storage	Gas Storage	Compressed Air or Gas	Cyclic Compressed Pressure	Cyclic (down to -50)	Decades (e.g., 50)
		Liquid Storage	Crude Oil	Cyclic Hydrostatic Pressure	Room Temperature	
Borehole Drilling And Operation	Hydrocarbon Exploitation	Drilling	Mud	Hydrostatic Pressure	Room Temperature	Less than 1 yr
		Secondary Recovery	Oil		Up to 65	Few

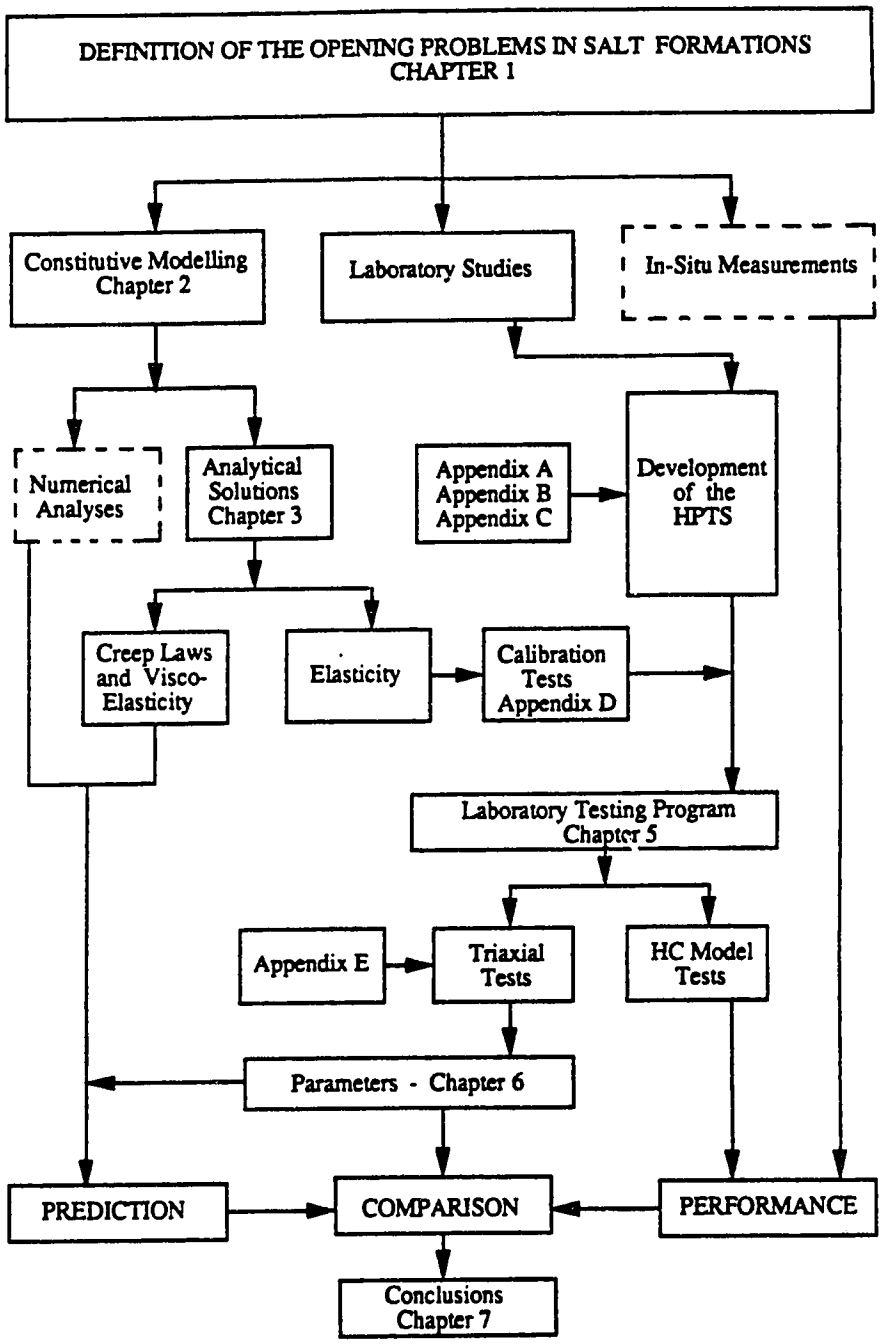

Figure 1.1 Scope of this study (topics inside dashed boxes are not covered by this research)

2. TIME-DEPENDENT DEFORMATION MECHANISMS AND CONSTITUTIVE MODELS

2.1 Introduction

The main objective of rheological studies is to determine the constitutive law which mathematically describes the behaviour of a material with time-dependent properties. This is desirable because the application of a mathematical model allows for a quantitative solution of complex events. Desai and Siriwardane (1984) suggested that the power of a constitutive law depends upon the extent to which the physical phenomenon has been understood and simulated. The behavioural response of a body is a function of the external excitation (e.g., pressure, temperature), internal constitution of the medium and body geometry. The geometric effect is usually isolated since it does not constitute a material property, however some properties may be size dependent. Therefore, the internal constitution of the material is of utmost importance.

The study of constitutive models can follow physical or phenomenological approaches (Nicolas and Poirier, 1976). The physical approach is founded on the microscopic level of deformation. Physical properties of rock-forming minerals, textures and preferred mineral orientations are used for establishing constitutive relations based on physical elementary units (e.g., single crystalline grains). The phenomenological approach assumes that the geometric

features of a deformed body reflect the geometric order of the differential displacements, rotations and strains, which occurred on the microscopic level, based on continuum mechanics. The material properties are global averages of local properties. This approach requires a model to explain the mechanism and kinematic path leading from initial to final geometric states.

In engineering applications, the response behaviour can be studied at the macroscopic level by continuum mechanics, without considering atomic and molecular structure. However, physical models have been gaining respect, if not to describe completely the behaviour of a body, at least to help better define phenomenological models which are closer to actual physical phenomena. The great difficulty in using physical models, based on theories of molecular behaviour at the microscopic level, arises from the nature of geotechnical materials. These are very complex combinations of mineral structures with defects, boundaries and impurities, which may dominate their behavioural response. Therefore, it seems to be almost impossible to establish physical models, even very complex ones, that are able to bridge the gap between the behaviour at microscopic and macroscopic levels.

On the other hand, phenomenological models are easier to obtain and can have some physical significance. Unfortunately, they are extremely dependent on the variables and parameters used for establishing them. Some of these

constitutive laws are only valid for a single class of materials, or even for a particular material under specific conditions of external excitation. These relationships are preferably called response functions rather than constitutive laws, as their validity is limited (Fluor Technology, 1987). A disadvantage is that researchers feel free to establish their own functions, giving a confusing number of relations for a similar response. Finally, it is important to note that the only rational way to determine the parameters for constitutive laws is to carry out appropriate laboratory or field tests.

This chapter presents a review of the creep laws, physical and phenomenological, usually used for describing the time-dependent behaviour of salt rocks. It also covers how a constitutive model is assembled by the association of several deformation laws describing the strain components (elastic, plastic and creep). Finally, some case-histories are briefly discussed to illustrate the type of creep measurements obtained in situ.

2.2 Phenomenological Creep Response

Time-dependent deformation is recognized as one of the most important properties of many rocks. It is significantly non-linear and consequently cannot be satisfactorily represented by linear constitutive laws. The complexity of non-linear theories of continuum mechanics has led researchers (Lama and Vutukuri, 1978b; Jaeger and Cook,

1979; Farmer, 1983) to suggest an idealized phenomenological creep response at constant state of external excitation.

The typical creep curve, shown by Fig. 2.1 for a constant stress state, may have up to four sections. Section AB represents the instantaneous strain, assumed to be elastic, due to the applied state of stress. Section BC presents a concave-downwards strain-time curve (strain rate decreasing with time) describing primary or transient creep. According to the above idealized phenomenological model, if the state of stress is released during the transient phase, all deformation would be recoverable (curve JKL), first the instantaneous strain (JK) and then the rest would tend asymptotically to zero (KL). Section CD represents secondary or steady-state creep characterized by a constant strain rate. The idealized phenomenological model suggests that if the differential stress is suddenly reduced to zero after the secondary phase has started, some deformation would be recoverable but part of the total deformation (permanent strain) would remain (curve RST). Many authors (e.g. Kaiser and Morgenstern, 1981) suggest that secondary creep may only exist under very special, rare conditions. Occasionally, tertiary or accelerating creep occurs leading rapidly to failure. It is represented in section DE by a concave-upwards curve with strain rate increasing with time.

Figure 2.1 also illustrates the dependence between creep rate and applied differential stress. The higher the applied differential stress, the larger the creep

deformation, for the same confining stress level.

Several criticisms can be directed at this idealized phenomenological model. It is still unclear how fast the load should be applied to isolate the instantaneous from the transient deformation. Also, some part of the instantaneous deformation could be permanent (plasticity). Furthermore, the unloading path described above, with all deformation recoverable for the transient phase and some recoverable deformation for the steady-state phase, has not been verified for many rock types.

Costa (1984) explained that creep and plasticity (irrecoverable strains) cannot be considered independent phenomena. They deal with permanent deformation of a body that occurs with time, but with different rates. However, for the sake of simplicity, they are mathematically separated; plasticity responsible for instantaneous permanent deformation and creep for that occurring with time. This idea of composing the total deformation by successive strain components can be convenient. Handin et al. (1986) presented an equation that would describe the total strain, ϵ, achieved over time, t, under constant deviatoric stress, σ:

$$\epsilon = \epsilon_e + \epsilon_p + \epsilon_t + \epsilon_{ss} + \epsilon_a \qquad [2.1]$$

where

ϵ ... total strain

ϵ_e ... perfectly elastic (instantaneous) strain

ϵ_p ... perfectly plastic (instantaneous) strain

ϵ_t ... transient creep strain

ϵ_{ss} ... steady state creep strain

ϵ_a ... accelerating creep strain.

The [illegible] o terms, representing instantaneous elastic and plas[illegible] [illegible]mations, are often ignored because they may be neg[illegible] . The elastic strain for salt rocks can be accurately described by the generalized Hooke's law. Plastic strain, if not totally ignored, is assumed to be incorporated in the time-dependent deformations. However, especially for underground structures subjected to continuous cycles of loading and unloading, plastic deformation may play a dominant role in the resulting deformation. Accelerating creep strain is the least known term of Eqn. 2.1. Although it is observed in laboratory tests, it is still barely understood and seldom appears in constitutive models. Transient and steady-state creep components are the most important, capable of yielding large deformations. They are described in the next section.

2.3 Time-Dependent Models

Many different models to describe the creep behaviour of rocks are reported in the literature. Most of these models were initially derived from studies of metals and then adapted to rock mechanics. They can be divided into three groups which are empirical, rheological and physical

models. They usually describe only portions of the typical creep curve shown in Fig. 2.1. Some models are only for transient creep, others are for steady-state creep alone and some combine both types of creep deformation. For the sake of simplicity, creep equations are presented in the form applicable to unconfined, uniaxial loading so that a clear understanding of each term of the equation can be achieved.

2.3.1 Empirical Creep Laws

Empirical models are mathematical equations obtained from curve fitting of laboratory or in-situ data. Cruden (1971a), Lama and Vutukuri (1978b) and Gangi (1981) presented a review of several empirical creep laws. A common assumption is that deformation depends only upon the values of applied stress and temperature at a particular time. Therefore, it is independent of the stress and temperature paths that were followed to reach that given state. As with any other curve fitting model, these response functions are dependent on the current external excitation state, material and testing conditions. The number of empirical models in the literature can be as many as the number of combinations among stress paths, external excitation states, testing conditions and materials. For instance, 24 different equations are suggested by Farmer (1983) for fitting a typical set of creep test data. Regardless of the large number of equations, the empirical creep laws can be divided into four major groups, according to the mathematical

function governing the equations. They are power, logarithmic, exponential-temperature and exponential-time laws.

2.3.1.1 Power Law

The power law can be expressed as:

$$\epsilon_t = K\ \sigma^c\ T^b\ t^a \qquad [2.2]$$

where

ϵ_t ... transient creep strain

σ ... deviatoric stress

T ... absolute temperature

t ... time

K, a, b, c ... empirical constants.

If the external excitation (stress and temperature) state is kept constant, Eqn. 2.2 can be reduced to:

$$\epsilon_t = A\ t^a \qquad [2.3]$$

where

$A = K\ \sigma^c\ T^b$

This law tends to an infinite transient strain rate at zero time because the time exponent 'a' is usually less than one. In the literature, there are many modifications that attempt to avoid this limitation (Costa, 1984).

The power law only describes the transient portion of the creep deformation curve, so that modified power laws are

often suggested to incorporate the steady-state creep portion. The expression then becomes:

$$\epsilon = \epsilon_t + \dot{\epsilon}_{ss}\, t \qquad [2.4]$$

where

ϵ_t ... given by Eqn. 2.2 or 2.3

$\dot{\epsilon}_{ss}$ ... steady-state creep rate.

The steady-state creep rate, $\dot{\epsilon}_{ss}$, can be described by a physical law (Section 2.3.3) or by an empirical equation. Fuenkajorn and Daemen (1988a) suggested:

$$\dot{\epsilon}_{ss} = B\, \sigma^d\, T^e \qquad [2.5]$$

For isothermal conditions, it reduces to:

$$\dot{\epsilon}_{ss} = D\, \sigma^d \qquad [2.6]$$

where

$D = B\, T^e$

B, d, e ... empirical constants.

2.3.1.2 Logarithmic Law

The logarithmic law has a form similar to the power law, but the time variable is governed by a logarithmic function. The general expression is:

$$\epsilon_t = K\ \sigma^c\ T^b\ \ln(t) \qquad [2.7]$$

The reduced form, for constant stress and temperature, is:

$$\epsilon_t = A\ \ln(t) \qquad [2.8]$$

This expression is a special case of the power law (Eqn. 2.3), where the time exponent is equal to -1 in the power law version for the creep rate equation.

The logarithmic law also presents an infinite transient strain rate at zero time. Modifications to overcome this inconvenience are also presented in the literature (Farmer, 1983; Costa, 1984).

Again, the logarithmic law only describes the transient creep strain. The same principle of introducing a second term to the equation to include the steady-state creep deformation ($\dot{\epsilon}_{ss}$) is often applied.

2.3.1.3 Exponential-Temperature Law

The exponential-temperature law describes the transient strain as an exponential function of the temperature. The remaining part of the equation is similar to the other empirical models as shown:

$$\epsilon_t = K\ \sigma^c\ t^a\ \exp(-\lambda/T) \qquad [2.9]$$

where λ is a further empirical constant.

For a constant state of stress and temperature, this expression reduces to an equation similar to the power law:

$$\epsilon_t = A\ t^a \qquad [2.10]$$

This transient creep law can also be extended to incorporate the steady-state creep deformation, as before.

2.3.1.4 Exponential-Time Law

The last group of empirical creep models is based on first order kinetics whereby the rate of change of the strain rate is proportional to its excess over the steady-state strain rate:

$$\frac{d\dot{\epsilon}}{dt} = -\beta\ (\dot{\epsilon} - \dot{\epsilon}_{ss}) \qquad [2.11]$$

where

$\dot{\epsilon}$ ... current creep rate

$\dot{\epsilon}_{ss}$ ... steady-state creep rate

β ... relaxation frequency.

Integrating Eqn. 2.11 twice with respect to time yields the expression for the creep strain:

$$\epsilon = e_a\ [1 - \exp(-\beta t)] + \dot{\epsilon}_{ss}\ t \qquad [2.12]$$

where

ϵ ... creep strain

e_a ... asymptotic transient creep strain (at $t = \infty$).

This law has been used with increasing frequency (Wagner et al., 1982; Senseny et al., 1983; Tammemagi et al., 1983; Senseny, 1985; Wagner and Senseny, 1986; Senseny, 1988) since the beginning of the 80s, when it was identified as the baseline creep law in the U.S. National Waste Terminal Storage Program (NWSP). The form of the exponential-time law given by equation Eqn. 2.12 relates the creep strain, composed of both transient and steady-state components, at constant stress and temperature to time. The first order kinetics is a valid formulation if the steady-state flow mechanism, $\dot{\epsilon}_{ss}$, is dominant (Gangi, 1981).

At first glance, the empirical models seem to have been derived in order to describe the transient creep strain only. Modified versions were then introduced to include the steady-state creep phase. The added term presents a constant steady-state creep strain rate which can be defined by other empirical equations, but more commonly by physical models (Section 2.3.2). One major problem is that the methods to determine the steady-state creep rate and the time at which it is established remain inconclusive (Fuenkajorn and Daemen, 1988a).

The most popular of the empirical models is the power law (Cruden, 1971a and 1974; Fairhurst et al., 1979; Dusseault and Mraz, 1983; Costa, 1984; Horseman and Passaris, 1984; Costa and Fairhurst, 1985; Handin et al.,

1986; Fuenkajorn and Daemen, 1988a and b), possibly because of its simplicity and good fit to the early creep stage results, especially for creep under constant stress and temperature. The logarithmic law has attracted very few followers lately. It is often argued that the logarithmic creep law provides a good fit for creep deformation at low temperature and for short time periods, but for other conditions it does not provide a satisfactory description of the observed behaviour (Herrmann et al., 1984). The explicit form of the exponential-temperature law can be very useful in analysing problems with changes in temperature during creep deformation. However, for isothermal conditions, it reduces to a power law form. Finally, the exponential-time law has increased in usage because it was chosen as a baseline creep law at the U.S. NWSP (Wawersik et al., 1982; Mellegard et al., 1983; Lux and Heusermann, 1983; Senseny et al., 1983; Herrmann et al., 1984; Senseny, 1985). It may yield a good fit if the mechanism that governs the steady-state creep is dominant.

Several salt researchers (Wagner et al., 1982; Herrmann et al., 1984; Fuenkajorn and Daemen, 1988a) have reviewed different empirical creep laws, applied them to the same data base and evaluated their performance. The results are inconclusive, but all authors agree that the models fit the laboratory data well. However, a wide scatter is encountered when they are used for long-term extrapolation purposes. This raises an important question on whether the quality of

fit criteria used are sufficient to assess the adequacy of the various models. Long-term extrapolations seem to be of extremely limited value and can only be solved by extremely long-term testing. Therefore, it appears to be very difficult to establish the steady-state creep strain rate from tests shorter than a few months, in the stress levels commonly encountered in engineering applications. However, some researchers advocate that steady-state creep can be achieved in a few hours or days (Dusseault and Mraz, 1983). The fact is that models describing only transient creep and models also including steady-state creep can fit laboratory data of tests run for short periods. However, Herrmann et al. (1984) advised that no conclusion should be drawn based on tests shorter than two years. The issue of whether a steady-state creep stage actually exists seems to be largely a question on accuracy or sufficient quality of fit.

2.3.2 Microphysical Creep Laws

Microphysical creep laws were derived from metallurgy and are based on deformation processes which take place in crystals (or at their boundaries). A crystal is defined as a three-dimensional periodic array of atoms in a stable position of equilibrium where the potential energy of the lattice is at a minimum. The elastic behaviour of crystals is due to interatomic forces which tend to maintain each atom in its equilibrium lattice position. Permanent deformations arise from lattice defects and consequent

changes of the lattice arrangement. Crystal defects are identified as sites where the periodicity of the lattice is disturbed. They can be point, line and planar defects. Point defects can be a nodal vacancy in the lattice, or an atom that occupies an interstitial position (self-interstitial), or impurities when alien atoms either substitute lattice atoms or occupy interstitial positions in the lattice. Line defects, also called dislocations, are characterized by a break in the periodicity of every point in a line. Finally, planar defects are two-dimensional breaks in lattice periodicity such as grain boundaries and interfaces between different minerals. Nicolas and Poirier (1976), Poirier (1985) and Ranalli (1987) present reviews of elements of crystallography, lattice defects and deformation mechanisms.

Deformation mechanisms are governed by the type of lattice defect and the state of stress and temperature. They are better represented by deformation-mechanism maps which specify the ranges of stress and temperature for each dominant mechanism. These maps are derived from lattice, atomic, physical and thermal properties of the mineral (crystal) under study. The procedure to determine a deformation-mechanism map is described in detail by Frost and Ashby (1982). Figure 2.2 shows an example of a deformation-mechanism map for pure halite where the normalized stress (deviatoric stress, σ, divided by the elastic shear modulus, G) is plotted against the homologous temperature (temperature, T, divided by the melting

temperature, T_m, of the mineral). The probable conditions of stress (0 to 70 MPa) and temperature (-50 to 250°C) for underground structures in salt deposits are also shown in the map. Deformation-mechanism maps, applications and respective equations for each mechanism are discussed by several salt researchers (Langer, 1979 and 1984; Pfeifle and Senseny, 1982; Munson and Dawson, 1984; Hambley et al., 1988; Blum and Fleischmann, 1988). Each mechanism and the respective constitutive equation, which only describes the steady-state creep strain, are discussed briefly.

2.3.2.1 Mechanism 1: Defectless Flow

At very high stresses, a crystal deforms by general flow even if it is initially free of defects. This mechanism is characterized by the ideal mineral shear strength derived from atomic binding properties. Defectless flow has very little engineering importance as the high stresses are seldom reached in practical applications (Munson and Dawson, 1984).

2.3.2.2 Mechanism 2: Dislocation Glide

Dislocation glide is also controlled by a flow process at high stresses. Deformation is the result of glide dislocations in sliding one ionic plane over another (on slip planes). These are usually impeded by lattice, grain boundaries, impurities and other intersecting dislocations. There are several equations for this slip deformation that differ in the function governing stress (exponential,

hyperbolic sine, etc). Only one typical expression is reported here:

$$\dot{\epsilon}_{ss} = C \exp(-Q/RT)\ f(B\sigma) \qquad [2.13]$$

where

$\dot{\epsilon}_{ss}$ ... steady-state creep strain rate

Q ... activation energy

R ... universal gas constant

T ... absolute temperature

σ ... differential stress

f ... function of

B, C ... constants.

2.3.2.3 Mechanism 3: Dislocation Climb

Dislocation climb is the most common mechanism investigated by salt researchers. It is controlled by a thermally activated equilibrium process and occurs at moderate to high temperature when blocked dislocations move out of their glide planes. The expression for dislocation climb depends on the type of climb, but a commonly encountered form is:

$$\dot{\epsilon}_{ss} = A \exp(-Q/RT)\ \sigma^n \qquad [2.14]$$

where

A, n ... constants.

2.3.2.4 Mechanism 4: Diffusional Creep

Diffusional creep is also a thermally activated mechanism where the grain shape changes by transport of material. Two types of diffusion are possible. Nabarro-Herring creep occurs when the transport in single crystals to crystal boundaries is by volume diffusion (it vanishes for grain diameters of pure halite less than 0.33 mm). Coble creep describes mass diffusion along polycrystal grain boundaries. Only the equation for Coble creep is presented since conditions for its generation are closer to those for underground structures:

$$\dot{\epsilon}_{ss} = \frac{a\ \sigma\ Db\ w\ \omega}{d^3\ K\ T} \qquad [2.15]$$

where

a ... average of various diffusion paths

K ... Boltzmann's constant

Db ... grain boundary diffusion coefficient

w ... average width of grain boundary

ω ... molecular volume

d ... mean grain size.

It is of interest to notice that Coble creep is extremely dependent on grain size, indicating difficulties in applying this creep law to geotechnical materials. More information on the diffusion creep equation parameters can be obtained from Poirier (1985) and Ranalli (1987).

2.3.2.5 Mechanism 5: Undefined Mechanism

The least known mechanism defining the steady-state creep strain rate happens to be the most relevant to the design of underground structures in salt deposits. In order to describe this mechanism, it is a common practice by salt researchers to assume empirical equations, either borrowed from one of the surrounding mechanisms (Skrotzki and Haasen, 1988a) or obtained by combining other thermally activated mechanisms (Pfeifle and Senseny, 1982). Lately, new mechanisms have been suggested for low stress and temperature conditions. Urai et al. (1986) and Spiers et al. (1988) suggested a solution-precipitation creep mechanism which is controlled by the liquid phase (brine films) present between grain boundaries. In a polycrystal, small amounts of moisture are sufficient to allow solution creep. Therefore, changes in moisture during sampling and testing may mislead laboratory results, if this mechanism is as dominant as suggested by them. The very small creep rates defined by this mechanism can be described by:

$$\dot{\epsilon}_{ss} = \frac{A\ B\ C\ \sigma}{K\ T\ d^3} \qquad [2.16]$$

where

A ... constant

B ... temperature-dependent diffusivity term

C ... grain-boundary structure parameter.

Although there are numerous limitations for applying these microphysical mechanisms to real polycrystalline rocks (different minerals, impurities, etc.), many models use these structural equations as the basis of constitutive laws for the steady-state creep rate. Many of the parameters present in the equations have little significance for real rocks because they are obtained from the properties of pure crystals. However, at least the form of the equations is representative of a certain microphysical mechanism of deformation. It is quite common practice to convert the physical constants in the equations from their physical meaning into curve-fitting parameters.

2.3.2.6 Physical Models for Transient Creep Strain

Physical models seldom define an equation for transient creep strain. Munson and Dawson (1982) suggested an explanation for transient deformation based on the competition between work hardening and recovery, where the steady-state creep strain occupies the equilibrium position. The exponential-time creep law establishes a dominant mechanism of steady-state creep strain and introduces the transient creep strain as a transition from zero to ϵ_{ss}, defined by the first order kinetics formulation. Fuenkajorn and Daemen (1988a) presented an extension of the dislocation climb equation to describe the transient creep strain:

$$\epsilon_t = K\ \sigma^c\ t^a\ \exp(-Q/RT) \qquad [2.17]$$

where

ϵ_t ... transient creep strain

t ... time

K, a, c ... constant.

Another alternative for evaluating the transient creep strain based on physical mechanisms is provided by the structural theory of brittle creep (Cruden, 1970, 1971a to c and 1983; Lama and Vutukuri, 1978b; Sano, 1978). This theory is founded on the concept of the stress-aided corrosion of the tips of microcracks within the material. The principal contribution to the transient creep at low pressure and temperature would come from straining near the tips of propagating cracks. Once these cracks have propagated, they are stable (crack hardened). The temperature dependence results from corrosion, and consequent crack growth, as a rate process with an activation energy. It is not intended to present here the assumptions involved and the whole derivation of the structural theory of brittle creep, which are described in detail by Cruden (1970 and 1971b), Lama and Vutukuri (1978b) and Sano (1978). The particular equation for isothermal conditions and constant stress can be written as:

$$\dot{\epsilon}_t = b_1 \, t^{b2} \qquad [2.18]$$

where

$\dot{\epsilon}_t$ ... transient creep strain rate

b_1 ... strain rate at unit time

b_2 ... strain-hardening parameter

t ... time.

Further research has extended this theory to multi-increment loading (Cruden, 1971b and 1983; Sano, 1978) and to constant strain rate compression tests (Sano, 1978). These features allow the prediction of the creep response at a given stress level based upon the response of the previous stress state and also to take into account the time spent to load the specimen to a certain stress level.

2.3.3 Rheological Models

Rheological models can also be used for simulating the time-dependent response of materials. They represent the solutions to certain differential equations, under given testing conditions, without offering any hint as to the deformation mechanism. These models are composed by the association, in series or in parallel, of elastic (spring), viscous (dashpot) and plastic (frictional contact) elements. Two principles govern the association of elements. In series, the total strain of the association is equal to the summation of the individual element strains. In parallel, the total stress applied to the association is equal to the summation of the individual element stresses. Figure 2.3 shows examples of some rheological models. By varying the number and configuration of the basic elements, models of increasing complexity may be achieved, with the element

parameters (E, ν, σ_y) chosen in such a way as to produce the best-fit to creep test data (Farmer, 1983).

Depending on the number and configuration of elements, rheological models can be classified as linear viscoelastic, non-linear viscoelastic, elastic viscoplastic, viscoelastic plastic and viscoelastic, viscoplastic models. Jaeger and Cook (1979), Farmer (1983), Costa (1984) and Fuenkajorn and Daemen (1988a) presented a review of several of these models. Flügge (1967), Findley et al. (1976) and Asszonyi and Richter (1979) discussed in detail the mathematical formulations and applications of linear and non-linear viscoelastic models. Because this matter is well documented elsewhere, only some linear viscoelastic models (Figure 2.3) are reviewed in this thesis.

Linear viscoelastic models present a linear relationship between strain rate and applied stress, and the law of superposition is applicable. Figure 2.3 shows the element configurations and creep responses for five linear, viscoelastic models. Their constitutive equations are given below.

2.3.3.1 Maxwell Model

For two elements associated in series, the total strain is:

$$\epsilon = \epsilon_1 + \epsilon_2 \ldots \dot{\epsilon} = \dot{\epsilon}_1 + \dot{\epsilon}_2$$

where

$$\epsilon_1 = \sigma/E \ldots \dot{\epsilon}_1 = \dot{\sigma}/E$$

$$\dot{\epsilon}_2 = \sigma/\eta$$

Then, the differential form of the Maxwell model can be written as:

$$E\,\sigma + \eta\,\dot{\sigma} = E\,\eta\,\dot{\epsilon} \qquad [2.19]$$

Imposing a constant stress $\sigma = \sigma_0$ gives:

$$\sigma_0 = \eta\,\dot{\epsilon}$$

Integrating and applying the boundary conditions (ϵ = [illegible] for t = 0) lead to:

$$\epsilon = \epsilon_0 + \frac{\sigma_0}{\eta}\,t \qquad [2.20]$$

where

ϵ ... creep strain

ϵ_0 ... instantaneous strain equal to σ_0/E

σ_0 ... applied constant stress

E ... spring constant

η ... viscosity

t ... time.

The Maxwell model describes only the steady-state creep and instantaneous strains.

2.3.3.2 Kelvin Model

The total stress for two elements associated in parallel is:

$$\sigma = \sigma_1 + \sigma_2$$

where

$$\sigma_1 = E\,\epsilon$$

$$\sigma_2 = \eta \dot{\epsilon}$$

Then, the differential form of the Kelvin model can be written as:

$$\sigma = E \epsilon + \eta \dot{\epsilon} \qquad [2.21]$$

Imposing a constant stress $\sigma = \sigma_0$ gives:

$$\sigma_0 = E \epsilon + \eta \dot{\epsilon}$$

Integrating and applying the boundary conditions given before lead to:

$$\epsilon = \frac{\sigma_0}{E} [1 - \exp(-a\ t)] \qquad [2.22]$$

where

$$a = E/\eta$$

The Kelvin model describes the transient creep strain for materials with a creep rate equal to zero at infinite time.

2.3.3.3 Generalized Kelvin (3-parameter solid) Model

A spring element is added in series to a Kelvin unit to describe the initial or instantaneous deformation. Applying the stress and strain equations to the elements in series and in parallel yields:

$$\epsilon = \epsilon_1 + \epsilon_2$$

$$\sigma = E_1 \epsilon_1$$

$$\sigma = E_2 \epsilon_2 + \eta_2 \dot{\epsilon}_2$$

Eliminating ϵ_1 and ϵ_2 from the above equations leads to the differential form of the generalized Kelvin (solid) model:

$$(E_1 + E_2)\ \sigma + \eta_2\ \dot{\sigma} = (E_1\ E_2)\ \epsilon + (E_1\ \eta_2)\ \dot{\epsilon} \qquad [2.23]$$

Imposing a constant stress $\sigma = \sigma_0$ gives:

$$(E_1 + E_2)\ \sigma_0 = E_1\ (E_2\epsilon + \eta_2\dot{\epsilon})$$

Integrating and applying boundary conditions ($\epsilon = \sigma_0/E_1$ for $t = 0$) lead to:

$$\epsilon = \epsilon_0 + \frac{\sigma_0}{E_2}\ [1 - \exp(-a_2\ t)] \qquad [2.24]$$

where

$$\epsilon_0 = \sigma_0/E_1$$

$$a_2 = E_2/\eta_2$$

This model can describe the instantaneous deformation and the transient strain, but not the steady-state creep strain.

2.3.3.4 Generalized Kelvin (3-parameter fluid) Model

This model is also an extension of the Kelvin model where a dashpot element is added in series to describe the steady-state creep deformation. The stress and strain equations for the elements in series and in parallel are:

$$\epsilon = \epsilon_1 + \epsilon_2$$

$$\sigma = \eta_1\ \dot{\epsilon}_1$$

$$\sigma = E_2\ \epsilon_2 + \eta_2\ \dot{\epsilon}_2$$

Eliminating ϵ_1 and ϵ_2 from the above equations leads to the differential form of the generalized Kelvin (fluid) model:

$$E_2\ \sigma + (\eta_1 + \eta_2)\ \dot{\sigma} = E_2\ \eta_1\ \dot{\epsilon} + \eta_1\ \eta_2\ \ddot{\epsilon} \qquad [2.25]$$

Imposing a constant stress state $\sigma = \sigma_0$ gives:

$$E_2\ \sigma_0 = E_2\ \eta_1\ \dot{\epsilon} + \eta_1\ \eta_2\ \ddot{\epsilon}$$

Integrating and applying boundary conditions lead to:

$$\epsilon = \frac{\sigma_0}{E_2}\ [1 - \exp(-a_2\ t)] + (\frac{\sigma_0}{\eta_1})\ t \qquad [2.26]$$

where

$$a_2 = E_2/\eta_2$$

This model describes the transient and steady-state creep strains, but it cannot fit instantaneous deformation data.

2.3.3.5 Burgers Model

Burgers model is a combination of both generalized Kelvin models (solid and fluid) where spring and viscous elements are added in series to a Kelvin unit to include the instantaneous and steady-state creep responses. The stress and strain equations for elements in series and in parallel are:

$$\epsilon = \epsilon_1 + \epsilon_2$$

$$\dot{\epsilon}_1 = \dot{\sigma}/E_1 + \sigma/\eta_1$$

$$\sigma = \eta_2\dot{\epsilon}_2 + E_2\epsilon_2$$

Eliminating ϵ_1 and ϵ_2 from the above equations leads to the differential form of the Burgers model:

$$E_1\ E_2\ \sigma + (E_1\ \eta_1 + E_1\ \eta_2 + E_2\ \eta_1)\ \dot{\sigma} + \eta_1\ \eta_2\ \ddot{\sigma} = \ldots$$

$$\ldots = E_1\ E_2\ \eta_1\ \dot{\epsilon} + E_1\ \eta_1\ \eta_2\ \ddot{\epsilon} \qquad [2.27]$$

Imposing a constant stress $\sigma = \sigma_0$ gives:

$$E_2\ \sigma_0 = E_2\ \eta_1\ \dot{\epsilon} + \eta_1\ \eta_2\ \ddot{\epsilon}$$

Integrating and applying the boundary conditions lead to:

$$\epsilon = \epsilon_0 + \frac{\sigma_0}{E_2}\ [1 - \exp(-a_2\ t)] + \frac{\sigma_0}{\eta_1}\ t \qquad [2.28]$$

where

ϵ_0 ... instantaneous strain equal to σ_0/E_1

$a_2 = E_2/\eta_2$

The Burgers model is able to reproduce all creep strain components up to the steady-state portion, with the exception of accelerating creep. Cracking elements as introduced by Kovari (1977) and Kaiser and Morgenstern (1981) would be needed to describe accelerating creep by rheological models.

There are an infinite number of possible models which could be used for fitting strain-time curves at different stress and temperature levels. The model that best-fits the data curve may offer some suggestions on the mechanical behaviour of the material. Temperature effects are implicit in the element parameters fitted for each stress and temperature condition. Regardless of the element build-up technique employed to simulate a certain mechanical deformation response, rheological models can be considered a curve-fitting technique and are therefore an empirical method. Salt researchers are attracted to this approach

since the models are easy to establish, understand, modify and validate without knowing the actual deformation mechanism (Fuenkajorn and Daemen, 1988a). Furthermore, closed-form solutions can be derived for many practical problems.

2.3.4 Constitutive Modelling of Salt Rocks

Keeping in mind Eqn. 2.1 for the strain response of a body creeping under a constant state of stress and temperature, the constitutive modelling of the material should be built up based upon the deformation laws for each term of the general equation. The deformation equations, reviewed previously, for the uniaxial stress state have to be extended for a generalized state of stress which would be representative of the conditions under analysis. Fossum et al. (1988) suggested how to cast one-dimensional laboratory equations into three-dimensional form and also presented some examples illustrating the differences in the final forms due to the chosen assumptions.

Elastic instantaneous deformation is always described by the classical theory of elasticity and can be easily extended to the generalized form of Hooke's law. Plastic instantaneous deformation is usually neglected. However, it can be described by the theory of plasticity which requires a number of assumptions such as the yield criterion, flow rule, isotropy, hardening response, etc. Desai and Varadarajan (1987) and Varadarajan and Desai (1987)

presented a constitutive model based upon the plasticity theory for the short-term behaviour of salt rocks. This model includes features such as state of stress, hardening, stress path, cohesive and tensile strengths, volume change and variations in the yield behaviour with the mean pressure. The parameters are obtained from conventional and true triaxial laboratory tests under different initial stress levels and stress paths.

Time-dependent deformation equations also need to be extended to a generalized state of stress and again, several assumptions are needed. Common assumptions are material incompressibility, isotropy, strain rate dependence on the deviatoric stress tensor only (independent of the hydrostatic state of stress) and coincidence of the deviatoric stress and creep strain rate tensors (Costa, 1984). Usually, constitutive models for salt rocks do not include a deformation law for accelerating creep.

Transient creep strain is often described by empirical laws and the power law is the most popular form. Another common choice is to define the transient creep strain as a first-order kinetics approximation about the steady-state creep rate (exponential-time law), although it is still totally empirical. Cruden (1971a) suggested the use of equations based only on physical mechanisms such as the structural theory of brittle creep. Other researchers believe that transient behaviour is only a very short-time response due to sampling damage, internal stress

redistribution in a non-linear polycrystal and strain hardening due to defect annealing (Dusseault and Mraz, 1983; Hambley et al., 1988), or just a response of imperfect laboratory conditions, where hardening may be induced due to friction between the specimen and platens (Baar, 1977). For these cases, the transient behaviour would be explained as a response to either a non-uniform stress state, caused by modification in the stress field (e.g., excavation) and being equilibrated due to stress redistribution, which may take from two months to one year, or a combined effect of multi-mechanisms of steady-state deformation.

Modelling of the steady-state creep strain may be another complex procedure. The most popular steady-state law is that which governs dislocations. Some salt investigators believe in several independent mechanisms occurring individually, as suggested by deformation mechanism maps. Each pair of temperature and stress values would define a regime of deformation and consequently, a specific steady-state strain rate equation. Other researchers would rather use multiple independent mechanisms of deformation, which contribute simultaneously to the final steady-state creep strain rate (e.g., Parrish and Gangi, 1981). Dawson and Munson (1983) and Munson and Dawson (1984) used the dislocation equation as a baseline and a similar equation with different coefficients to describe the steady-state creep strain rate in the undefined mechanism region. Dusseault and Mraz (1983) and Dusseault et al. (1987) also

presented examples of multiple mechanism laws for the steady-state creep strain. The material behaviour is controlled by diffusion (very slow rates due to ionic transfer in intercrystalline moisture films) for stresses below the Prandtl Yield Limit and above this shear stress activation level it follows a dislocation law. Wagner and Senseny (1986) also illustrated the use of multiple mechanism equations, evaluating the predictive capability of seven constitutive models.

2.4 In-Situ Observations

Most of the work done in situ refers to measurements of shaft and borehole convergences, and room and pillar deformations. Even those researchers, who heavily advocate steady-state creep, pointed out that a period of transience, ranging from a few months to a year, is necessary to reach a secondary creep strain rate (Baar, 1971 and 1977).

Lama and Vutukuri (1978b) summarized five previous works on in-situ creep of salt rocks and presented the deformation equations for opening closure and pillar deformation. All equations have a transient form, being either a power or a logarithmic law. Cook (1983) monitored the long-term closure (6 years) of a shaft excavated through evaporite deposits and found that the power law fitted the data best. Coates et al. (1983) also preferred the power law to fit data from three case-histories of salt caverns. Costa (1984) implemented a power law obtained from laboratory

results in a finite element code to predict the creep deformation of a potash mine in Brazil and then compared the results to in-situ measurements with good agreement (Costa and Fairhurst, 1985). Fernandez and Hendron (1984) performed in-situ borehole tests in a deep salt formation for eleven months and concluded that steady-state creep did not develop around the well. A power law fitted the in-situ data although the time exponent was not constant for all stress levels, suggesting a change of the primitive structure and consequent deformation mechanism, leading to different creep rates. Cominco (1985) instrumented several sections of a deep potash mine in Saskatchewan for one year. All measurements related to room closure showed decreasing creep rates with time. The above works indicate that in-situ opening closure data present a transient response at least during the first years.

There are other sites where researchers tried to adjust in-situ data to a pre-chosen steady-state creep equation, neglecting the transient trend of the data (Hunsche et al., 1983; Ladanyi and Gill, 1983a and b; Herget and Mackintosh, 1987). Dawson and Munson (1983) used their multiple mechanism steady-state creep model, based upon laboratory parameters, to numerically predict the deformations around a room in a deep potash mine. Calculated and field results compared favourably for the considered time (8 years), but the in-situ creep rates tended to diminish with time while the predicted curves increase with time. Any extrapolation,

based on the predicted curves, to times beyond that considered, would differ completely (overpredict) when compared to the field data. The same findings were obtained by DeVries (1988), who numerically simulated in-situ corejack test results using three different constitutive models based on steady-state creep. Preece (1987) presented numerical calculations of borehole closure using a finite element program with a secondary creep model to predict measured values of wellhead pressure, volume and convergence. The calculations underpredicted the volume and convergence by factors of between 2.5 and 4.

Finally, Mogharrebi and Thoms (1980) and Thoms and Gehle (1983) investigated the in-situ behaviour of salt from the closure of two deep boreholes. One of the boreholes indicated the traditional behaviour of salt with rapid rates of radial displacements following loading and then gradual decreasing rates. By contrast, the second borehole presented erratic data, possibly indicating that large scale in-situ effects (e.g., geological features) may dominate the closure behaviour. This seems to indicate that other factors such as geologic features, may quite often dominate the in-situ response of an underground structure in evaporites.

2.5 Conclusions

A large number of creep models describe at least transient and secondary creep, although most of the in-situ measurements indicate only a transient trend. This fact does

not exclude that the material is not behaving under a steady-state creep law. Geometric transient response of an opening must not be confused with material transient response.

Material transient response occurs when a body is subjected to a constant state of external excitation (e.g., temperature, stress) and presents time-dependent strain rates, which are very high just after loading and then gradually decrease possibly to a steady-state creep strain rate. This is a material property and should be applicable throughout the body.

The geometric transient response of an opening is a response of the structure and is highly dependent on the geometry. The geometry of the problem may induce non-uniform stress distribution in the body (stress gradients). Taking the radial axis of a circular opening as an example, each point along it is subjected to a different state of stress due to the stress distribution around the opening. Each point along the radius presents a different creep response depending on the acting stress level and creep law. Compatibility must be maintained and the summation of all creep strain contributions constitutes the convergence response for that particular radial axis. In addition, geometric changes of the opening cannot be neglected for large deformations. Due to the differences in the stress state acting at each point, and possibly geometric change of the opening, the final convergence is a transient curve

which is identified as a geometric transient response even if each point within the material behaves according to a steady-state creep deformation law.

Material transient creep is a point that deserves more attention from salt researchers. This became evident in the workshop on constitutive laws for salt rocks, held during the 6th ISRM in Montreal (1987) when several salt research groups from different countries, had the opportunity to discuss how salt behaviour is modelled. Transient creep was recognized by all to be important, but it was poorly represented. The reasons range from the fact that transient creep is influenced by many factors and is therefore difficult to model (Wallner, 1987), to the fact that a transient law is very expensive to adopt in numerical analyses (Munson, 1987). These factors and others such as sampling disturbance (Dusseault and Mraz, 1983) and laboratory platen friction (Baar, 1977) which may induce transient response, are valid, but the failure in extrapolating creep models to long-term predictions has indicated the need for further work on transient creep laws. Transient creep may represent only a small percentage of the total creep strain but it plays an important role in defining the shape of the creep curve, which is essential for reasonable data extrapolations.

In addition, it is clear that in-situ creep rates tend to decrease with time while the calculated curves based on steady-state creep laws, although matching the results for

the calibration time, show the opposite. It also seems that laboratory tests of a few weeks duration cannot be used for predicting steady-state creep, especially in the ranges of stress and temperature that are of interest to engineering applications. Laboratory tests with minimum friction and load control problems, should last several months to a year to be conclusive in this matter (Fuenkajorn and Daemen, 1988a).

A last point of interest is the number of creep laws and combined constitutive models for salt behaviour in the literature. An infinite number of curve fitting equations and combinations are still possible. Since the beginning of this decade, there is a tendency towards evaluating existing laws and models, instead of proposing new ones. Restrictions such as a basis in physical theories, have been helpful in the selection criterion of models to be adopted.

In conclusion, the development of laboratory facilities that include specimen preparation and testing methodologies converging to standard procedures in order to minimize sources of errors and erratic responses, is very desirable. This laboratory program would produce data from specimens, carefully prepared in the same manner and tested under rigorous conditions of environmental and pressure control. Data from different stress levels, deviatoric stresses and stress path tests would be used for obtaining parameters for several creep laws. These creep laws would be implemented into analytical and numerical formulations to predict the

results of model tests of circular openings with appropriate geometry and stress field conditions. It seems that by exploring this methodology and its possible variations, a better understanding of creep laws and geometric effects on the time-dependent response of openings can be achieved and the constitutive model predictive capability evaluated.

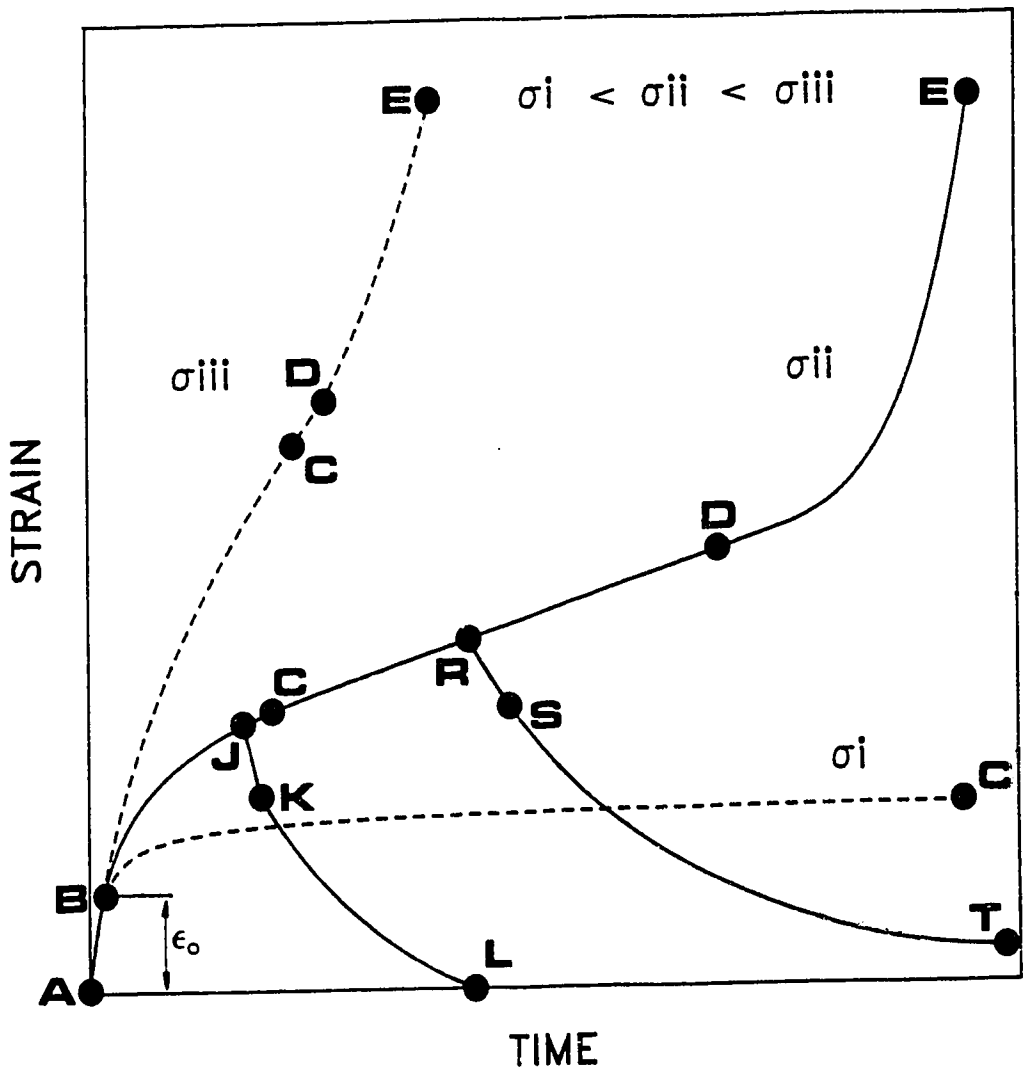

Figure 2.1 Idealized phenomenological creep response

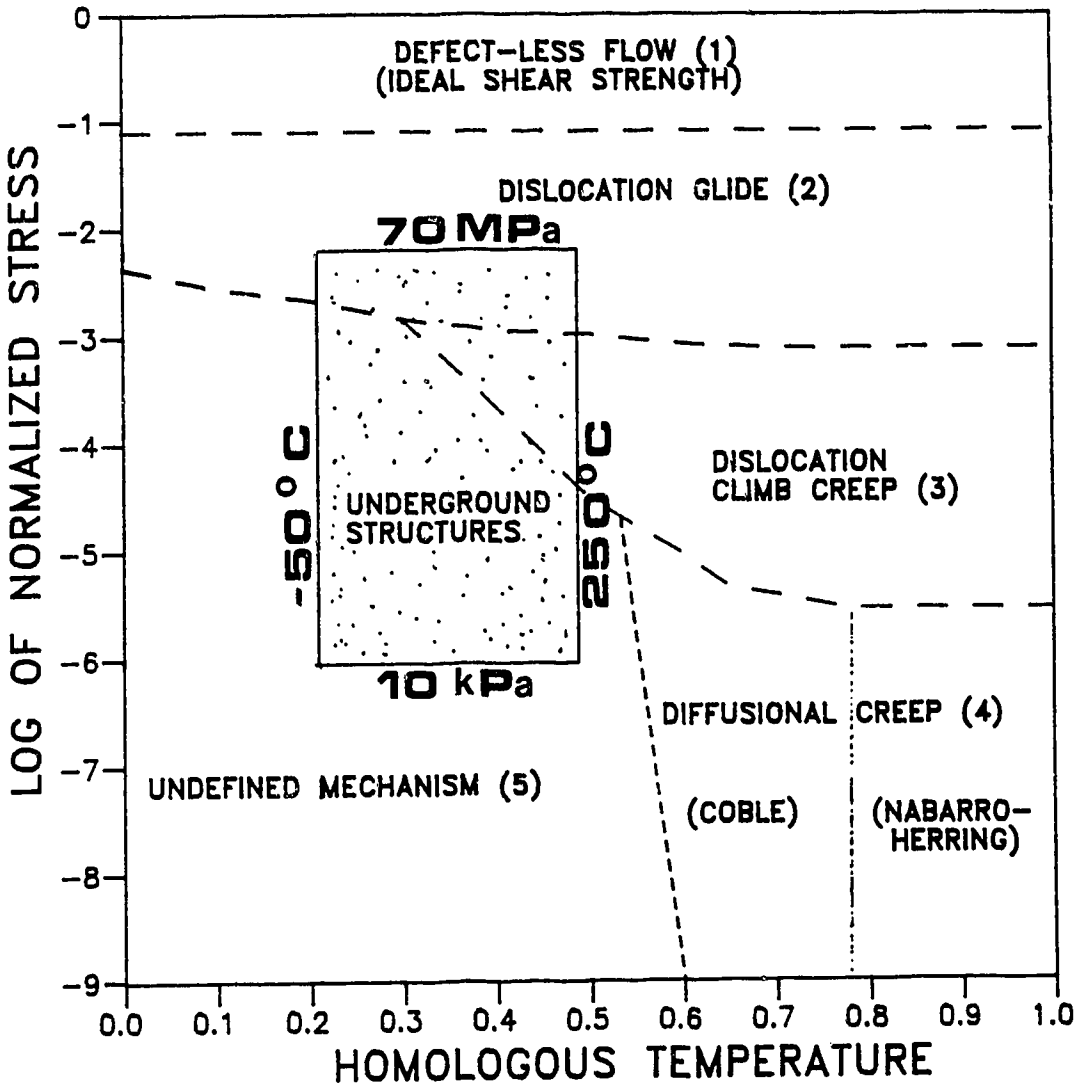

Figure 2.2 Deformation-mechanism map for pure halite; d= 3 mm, T_m= 1074°K and G= 11 GPa (modified after Munson and Dawson, 1984)

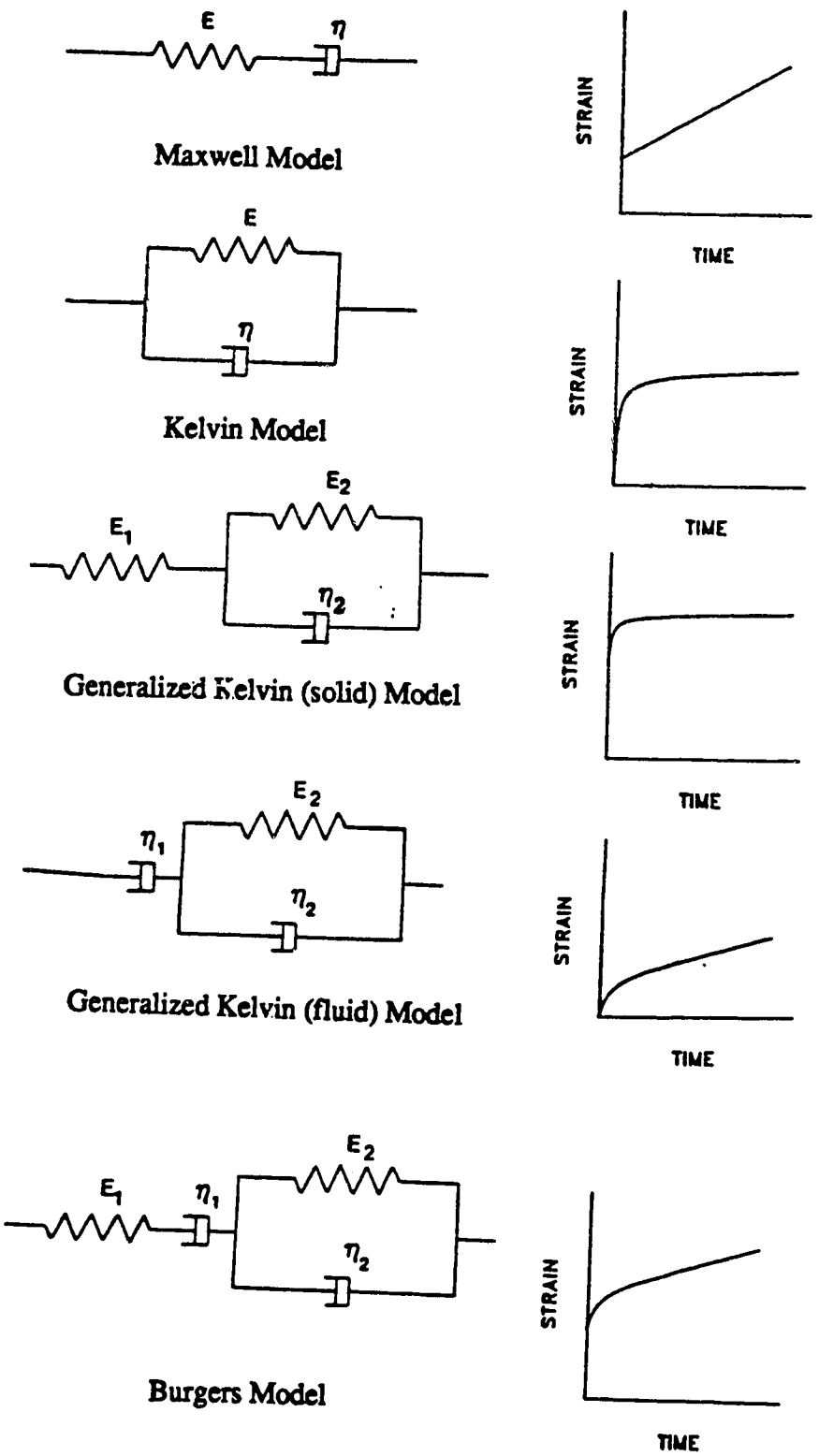

Figure 2.3 Linear viscoelastic rheological models

3. ANALYTICAL SOLUTIONS FOR THE THICK-WALLED CYLINDER

3.1 Introduction

The thick-walled cylinder has a shape which resembles in-situ circular openings. The explanation of how hollow cylinder specimens can be tested to simulate circular openings in homogeneous stress fields is presented in Chapter 4, as well as the advantages and drawbacks of using such specimens. Although some underground structures in salt deposits have cross-sections other than circular, this geometric shape approximates most of the cases and even if not, it may be used for preliminary studies. This chapter aims to present closed-form solutions for the thick-walled cylinder assuming different material constitutive models and loading conditions.

Constitutive model parameters are obtained from laboratory testing data (Chapter 6). These parameters are input into analytical solutions (one for each respective constitutive law and loading condition), which are used for predicting the hollow cylinder test results and therefore, for evaluating the predictive capability of the constitutive model. Several material behaviour models (Chapter 2) can be taken, but closed-form analytical solutions are only convenient for few simple models. Numerical analyses are recommended for the evaluation of more complicated constitutive models and for the assessment of geometry change effects (large deformations) with related stress

redistribution. These analyses are relegated to further research. Only elastic, linear viscoelastic and elastic-viscoplastic analytical solutions are reviewed in the following sections.

3.2 Elastic Solution for the Thick-Walled Cylinder

The elastic solution for the thick-walled cylinder does not predict the time-dependent response of circular openings in homogeneous stress fields. This solution is still briefly reviewed because it helps the interpretation of calibration tests using an aluminum hollow cylinder specimen and it also constitutes the baseline of many linear viscoelastic analytical solutions. The complete derivation of the elastic equations for a thick-walled cylinder can be found in classical text-books on the theory of elasticity (Fang, 1965; Chou and Pagano, 1967; Timoshenko and Goodier, 1970). Obert and Duvall (1967) also presented these equations, including applications to rock mechanics problems such as the elastic convergence of circular openings.

The elastic solution for the stress distribution on an axisymmetric problem such as a thick-walled cylinder, is obtained in terms of equilibrium and compatibility equations, Hooke's law and the Airy's stress function. Airy's functions are stress systems that satisfy the equilibrium and compatibility equations and reduce elastostatic problems in plane stress and plane strain states to boundary condition problems of a biharmonic

equation. Applying the boundary conditions shown on Fig. 3.1, the stress distribution equations for a thick-walled cylinder acted on by internal and external pressures are:

$$\sigma_r = \frac{A}{r^2} + B \qquad [3.1]$$

$$\sigma_\theta = -\frac{A}{r^2} + B \qquad [3.2]$$

$$\tau_{r\theta} = 0 \qquad [3.3]$$

where

$$A = \frac{-a^2\ b^2\ (p_e - p_i)}{b^2 - a^2} \qquad [3.4]$$

$$B = \frac{p_e\ b^2 - p_i\ a^2}{b^2 - a^2} \qquad [3.5]$$

σ_r ... radial stress

σ_θ ... tangential stress

$\tau_{r\theta}$ ... shear stress in the r-θ plane

a ... inner radius

b ... outer radius

r ... radius ($a < r < b$)

p_e ... external pressure

p_i ... internal pressure.

The strain state in a long thick-walled cylindrical body acted on by external and internal uniform pressures, and also by a uniform axial load can be approximated by a

plane strain state (Fang, 1965). The strain in the axial direction is assumed to be zero or constant. A constant axial strain may be imposed to a plane strain state without any change in the stresses on the r-θ plane (perpendicular to the axial direction). An extension of the plane strain definition can be formulated by requiring that the axial strain be a constant, the displacements 'u' and 'v' be functions of 'r' and 'θ' only and the displacement 'w' be a linear function of the axial direction 'z' only (Fang, 1965). To avoid confusion between these two plane strain states, it is simply called 'plane strain', PS, when the axial strain is zero and 'axisymmetric loading', AL, when the axial strain is constant, but non-zero. Both states are very useful for analysing the behaviour of circular openings in homogeneous stress fields.

3.2.1 Axisymmetric Loading State

For the axisymmetric loading state with uniform and constant longitudinal load, a constant axial strain is imposed to the thick-walled cylinder. It is defined by Hooke's law. Substitution of the stress distribution equations (Eqns. 3.1 to 3.3) into the strain-stress relations (Hooke's law) leads to strain equations which are functions of the internal and external pressures, elastic constants and geometric parameters. The strain equations combined with the strain-displacement relations leads to the conclusion that the displacement 'v' (θ direction) can only

be a rigid body displacement, then assumed as zero. The final displacement expressions for the axisymmetric loading state resume to:

$$w = \frac{1}{E} (\sigma_z - 2\nu B) z \qquad [3.6]$$

$$u = \frac{1+\nu}{E} [B(1-2\nu)r - \frac{A}{r}] - \frac{\nu}{E} (\sigma_z - 2\nu B)r \qquad [3.7]$$

where

u ... displacement in the radial direction

w ... displacement in the axial direction

ν ... Poisson's ratio

E ... Young's modulus

σ_z ... axial stress

z ... longitudinal dimension (axial direction)

A and B ... given by Eqns. 3.4 and 3.5.

The radial displacement at the hollow cylinder walls (r=a and r=b) is given by the expressions:

$$u_a = \frac{1+\nu}{E} [B(1-2\nu)a - \frac{A}{a}] - \frac{\nu a}{E} (\sigma_z - 2\nu B) \qquad [3.8]$$

$$u_b = \frac{1+\nu}{E} [B(1-2\nu)b - \frac{A}{b}] - \frac{\nu b}{E} (\sigma_z - 2\nu B) \qquad [3.9]$$

3.2.2 Plane Strain State

When a plane strain state with an axial strain equal to zero exists, the axial stress is given by:

$$\sigma_z = 2\nu B \qquad [3.10]$$

Following the same path of equation substitutions as for the axisymmetric loading state, the displacement equations are found. They only differ in the last term that reflects the contribution of the constant axial strain. The radial displacement expression for the plane strain state is:

$$u = \frac{1+\nu}{E} [B(1-2\nu)r - \frac{A}{r}] \qquad [3.11]$$

The radial displacement at the hollow cylinder walls is given by the expressions:

$$u_a = \frac{1+\nu}{E} [B(1-2\nu)a - \frac{A}{a}] \qquad [3.12]$$

$$u_b = \frac{1+\nu}{E} [B(1-2\nu)b - \frac{A}{b}] \qquad [3.13]$$

3.2.3 Loading Conditions

Several pressure paths can be followed under one of the two previous plane strain states. Three particular loading conditions are of special interest for the hollow cylinder laboratory testing program (Chapter 5). First, hollow cylinder specimens are hydrostatically loaded ($p_a = p_e = p_i = p$) up to a certain stress level, equivalent to the in-situ homogeneous stress field. Second, the internal pressure can be manipulated, keeping both the external and axial

pressures constant (axisymmetric loading). Third, the internal pressure can also be changed, maintaining the external pressure constant and adjusting the axial stress in such a manner as to keep the axial strain equal to zero (plane strain).

3.2.3.1 Hydrostatic Loading

Hydrostatic loading is a special case of the axisymmetric loading state where the three pressures, axial, external and internal, are kept at the same value ($p_a = p_e = p_i = p$) and changed simultaneously. Equations 3.4 and 3.5 are reduced to:

$$A = 0$$

$$B = p$$

where 'p' is called hydrostatic pressure.

Substitution of the A and B values into the displacement equations (Eqns. 3.6, 3.8 and 3.9) for the axisymmetric loading state provides:

$$w = C\ p\ z \qquad [3.14]$$

$$u_a = C\ p\ a \qquad [3.15]$$

$$u_b = C\ p\ b \qquad [3.16]$$

where

$$C = \frac{1-2\nu}{E} \qquad [3.17]$$

3.2.3.2 Axisymmetric Loading

After consolidation of the hollow cylinder specimen at a certain hydrostatic pressure, the internal pressure may be changed, keeping the axial and external pressures constant. The deformation occurred in the specimen due to this loading phase only, can be evaluated in terms of pressure changes (Δp), as defined below:

$$p_a = p_e = \text{constant} = p_o$$

$$\Delta p_o = 0$$

$$\Delta p_i = p_i - p_o$$

where 'p_o' is called outside pressure.

Substituting these above relations into Eqns. 3.4 and 3.5 gives:

$$\Delta A = \frac{\Delta p_i \; a^2 \; b^2}{b^2 - a^2} \qquad [3.18]$$

$$\Delta B = \frac{-\Delta p_i \; a^2}{b^2 - a^2} \qquad [3.19]$$

Substitution of Eqns. 3.18 and 3.19 into Eqns. 3.6, 3.8 and 3.9 leads to the displacement change equations:

$$\Delta w = R\ \Delta p_i \qquad [3.20]$$

$$\Delta u_a = -S\ \Delta p_i \qquad [3.21]$$

$$\Delta u_b = -T\ \Delta p_i \qquad [3.22]$$

where R, S and T are constant for the same material and geometry. They are defined by the following expressions:

$$R = \frac{\nu z}{E}\left(\frac{2a^2}{b^2-a^2}\right) \qquad [3.23]$$

$$S = \frac{a}{E}\left(\frac{a^2+b^2}{b^2-a^2} + \nu\right) \qquad [3.24]$$

$$T = \frac{1}{E}\left(\frac{2a^2b}{b^2-a^2}\right) \qquad [3.25]$$

3.2.3.3 Plane Strain

After consolidation of the hollow cylinder specimen at a certain hydrostatic pressure, the internal pressure may be changed, keeping the external pressure constant and adjusting the axial stress as to maintain the axial strain equal to zero. Again, the specimen deformation is evaluated in terms of pressure changes in relation to the previous hydrostatic pressure state, as defined by the following expressions:

$$p_e = \text{constant}$$

$$\Delta p_e = 0$$

$$\Delta p_i = p_i - p_e$$

Substituting the above relations into Eqns. 3.4 and 3.5 leads to the same expressions as defined by Eqns. 3.18 and 3.19. The only difference lies in the definition of Δp_i for each loading condition. Substitution of Eqn. 3.18 into Eqn. 3.10 leads to the axial stress change needed to keep the plane strain state:

$$\Delta\sigma_z = -O\ \Delta p_i \qquad [3.26]$$

where

$$O = \frac{2\nu a^2}{b^2-a^2} \qquad [3.27]$$

Substitution of Eqns. 3.18 and 3.19 into Eqns. 3.12 and 3.13 leads to the radial displacement change equations at the hollow cylinder walls:

$$\Delta u_a = -\ M\ \Delta p_i \qquad [3.28]$$

$$\Delta u_b = -\ N\ \Delta p_i \qquad [3.29]$$

where

$$M = \left(\frac{1+\nu}{E}\right)\ \left(\frac{a}{b^2-a^2}\right)\ [a^2(1-2\nu)+b^2] \qquad [3.30]$$

$$N = \left(\frac{1-\nu^2}{E}\right)\ \left(\frac{2a^2b}{b^2-a^2}\right) \qquad [3.31]$$

3.2.4 Elastic Equations for Hollow Cylinder Calibration Tests

Four transducers, an axial displacement (DA) LVDT, external and internal volume change (VCE and VCI) devices and a bore convergence (BC) device, measure the deformation of hollow cylinder specimens. The elastic equations provide the means to evaluate these measurements during the calibration tests using an aluminum hollow cylinder specimen. The appropriate elastic equation for each variable depends on the loading condition. The axial displacement of the aluminum specimen is given by either Eqn. 3.14 or 3.20. For the plane strain state, when the axial displacement is zero, the axial stress can be evaluated using Eqn. 3.26. The bore convergence is calculated by one of the Eqns. 3.15, 3.21 or 3.28. The bore and cell volume changes are calculated based on the radial displacements at the hollow cylinder walls, following the sketch and expressions shown in Fig. 3.2. The final expressions for the deformations of the aluminum hollow cylinder specimen are presented in Table D.5.

3.3 Viscoelastic Solutions for the Thick-Walled Cylinder

The analysis of stress and deformation requires the equilibrium, kinematic and constitutive equations, besides boundary conditions. The constitutive equations define the major difference in the behaviour of a body. The elastic solution is a limiting case of the behaviour of a

viscoelastic body. Assuming the material is isotropic and homogeneous, it is possible to establish an elastic-viscoelastic analogy (correspondence principle) and find the time-dependent solution of the viscoelastic problem based on the elastic solution, using Laplace transformation. Flügge (1967) and Findley et al. (1976) presented this formulation in detail. Only the basic and major steps are reviewed here.

The general differential equation of any linear viscoelastic model for a simple state of stress has the form:

$$p_0\sigma + p_1\dot{\sigma} + p_2\ddot{\sigma} + \ldots = q_0\epsilon + q_1\dot{\epsilon} + q_2\ddot{\epsilon}\ldots \qquad [3.32]$$

or

$$\sum_0^m p_k \frac{d^k\sigma}{dt^k} = \sum_0^n q_k \frac{d^k\epsilon}{dt^k} \qquad [3.33]$$

where p_k, q_k are material constants.

The parameter 'p_0' is usually set to one without any loss of generality of these equations. Each viscoelastic model has a certain number of non-zero coefficients 'p_k' and 'q_k'. Equation 3.33 can also be written in the form of linear differential operators with respect to time:

$$\hat{P}\,\sigma = \hat{Q}\,\epsilon \qquad [3.34]$$

where

$$\hat{P} = \sum_{0}^{m} p_k \frac{d^k}{dt^k}$$

$$\hat{Q} = \sum_{0}^{n} q_k \frac{d^k}{dt^k}.$$

In viscoelastic bodies, all stresses, strains and displacements may be time dependent. Then, the general differential equation for viscoelastic models can be rewritten in terms of Laplace transform operators, where the variables and time differential operators are substituted by polynomials of the transform variable 's':

$$\begin{aligned} P(s)\ \sigma(s) &= (p_0 + p_1 s + p_2 s^2 + \ldots)\ \sigma(s) \\ &= (q_0 + q_1 s + q_2 s^2 + \ldots)\ \epsilon(s) \\ &= Q(s)\ \epsilon(s) \end{aligned} \qquad [3.35]$$

where

P ... Laplace transform operator for the stress tensor

Q ... Laplace transform operator for the strain tensor.

The correspondence principle states that if a fictitious elastic problem where all variables are functions of the transform parameter 's' can be solved to find the stress and strain distributions, then a subsequent inverse Laplace transformation gives the stress and strain distributions as a function of time for the viscoelastic problem (Findley et al., 1976). Although the correspondence principle is quite general, it cannot be used in problems where the interface of stress and displacement boundaries

(boundary value problems) is not constant and also in thermo-viscoelastic problems when the temperature is transient. Tables with the time differential and Laplace transform operators for several viscoelastic models are presented by Flügge (1967), Findley et al., (1976) and Fuenkajorn and Daemen (1988a). Table 3.1 shows them for the five linear viscoelastic models used in the analytical solutions presented in this chapter.

Equation 3.35 can be extended to a multiaxial stress state by comparison with the generalized elastic solution (Hooke's law). The total elastic deformation of a body can be decomposed into two components due to the hydrostatic and deviatoric stress tensors. The equations are:

$$S_{ij} = 2G\ d_{ij} \qquad [3.36]$$

$$\sigma_{ii} = 3K\ \epsilon_{ii} \qquad [3.37]$$

where

S_{ij} ... deviatoric stress tensor

d_{ij} ... deviatoric strain tensor

σ_{ii} ... hydrostatic stress tensor

ϵ_{ii} ... hydrostatic strain tensor

G ... shear modulus

K ... bulk modulus.

Applying Eqn. 3.35 to Eqns. 3.36 and 3.37, they become:

$$P_1\ S_{ij}(s) = Q_1\ d_{ij}(s) \qquad [3.38]$$

$$P_2\ \sigma_{ii}(s) = Q_2\ \epsilon_{ii}(s) \qquad [3.39]$$

where

P_1, Q_1 ... Laplace transform operators for the deviatoric component

P_2, Q_2 ... Laplace transform operators for the hydrostatic component.

The elastic-viscoelastic analogy (correspondence principle) between Eqns. 3.36 and 3.38, and between Eqns. 3.37 and 3.39 gives:

$$2G(s) = \frac{Q_1}{P_1} \qquad [3.40]$$

$$3K(s) = \frac{Q_2}{P_2} \qquad [3.41]$$

As elastic problems are commonly written in terms of Young's modulus and Poisson's ratio, it is of interest to use the relationships among E, ν, K and G (Desai and Siriwardane, 1984) and derive E and ν expressions in function of P_i and Q_i, based on Eqns. 3.40 and 3.41. The resulting equations for the viscoelastic Young's modulus and Poisson's ratio are:

$$E(s) = \frac{3Q_1Q_2}{P_2Q_1 + 2P_1Q_2} \qquad [3.42]$$

$$\nu(s) = \frac{P_1Q_2 - P_2Q_1}{P_2Q_1 + 2P_1Q_2} \qquad [3.43]$$

The elastic-viscoelastic correspondence principle is now applied to the thick-walled cylinder problem. The stress distribution (r-θ plane) in an elastic thick-walled cylinder (Eqns. 3.1 and 3.2) is independent of the elastic constants. Therefore, the stress distribution in a linear viscoelastic thick-walled cylinder of the same geometry is equal to the elastic stress distribution. The elastic deformation equations depend on the elastic constants, then the viscoelastic deformation equations are functions of the viscoelastic Young's modulus and Poisson's ratio. The radial displacement equations for axisymmetric loading and plane strain states (Eqns. 3.7 and 3.11, respectively) can be rearranged to the following more convenient expressions:

<u>Axisymmetric Loading</u>

$$p_e = p_a = p$$

$$p_i = kp$$

$$u = \left(\frac{1+\nu}{E}\right)\left(\frac{p}{b^2-a^2}\right)\left[(b^2-ka^2)(1-2\nu)r + (1-k)\frac{a^2b^2}{r}\right] - \ldots$$

$$\ldots - \frac{p\nu r}{E}\left[1 - 2\nu\left(\frac{b^2-ka^2}{b^2-a^2}\right)\right] \qquad [3.44]$$

where

k ... ratio between the inside (p_i) and outside pressures.

Plane Strain[1]

$p_e = p$

$p_i = kp$

$$u = \left(\frac{1+\nu}{E}\right) \left(\frac{p}{b^2-a^2}\right) \left[(b^2-ka^2)(1-2\nu)r + (1-k)\frac{a^2b^2}{r}\right] \qquad [3.45]$$

Substituting the elastic constants and variables (pressures and displacements) by parameters in terms of the Laplace transform variable 's', leads to:

$$u(s)_{AL} = \left[\frac{1+\nu(s)}{E(s)}\right] \left[\frac{p(s)}{b^2-a^2}\right] \left[(b^2-ka^2)\{1-2\nu(s)\}r + \ldots\right.$$

$$\left.\ldots + (1-k)\frac{a^2b^2}{r}\right] - \frac{p(s)\nu(s)r}{E(s)} \left[1 - 2\nu(s)\left(\frac{b^2-ka^2}{b^2-a^2}\right)\right] \qquad [3.46]$$

and

$$u(s)_{PS} = \left[\frac{1+\nu(s)}{E(s)}\right] \left[\frac{p(s)}{b^2-a^2}\right] \left[(b^2-ka^2)\{1-2\nu(s)\}r + \ldots\right.$$

$$\left.\ldots + (1-k)\frac{a^2b^2}{r}\right] \qquad [3.47]$$

Substituting Eqns. 3.42 and 3.43 into Eqns. 3.46 and 3.47 leads to the general radial displacement equations of a thick-walled cylinder under axisymmetric loading and plane

---

[1] Fuenkajorn and Daemen (1988a) analysed a plane strain problem, but they presented the radial displacement equation (Eqn. 3.17, p. 220) for a thick-walled cylinder under plane stress.

strain states, respectively:

$$u(s)_{AL} = [\frac{p(s)}{b^2-a^2}] \frac{P_1}{Q_1} [(b^2-ka^2) (\frac{3P_2Q_1}{2P_1Q_2+P_2Q_1})r + \ldots$$

$$\ldots + (1-k)\frac{a^2b^2}{r}] - (\frac{P_1Q_2-P_2Q_1}{3Q_1Q_2})p(s)r [1 - \ldots$$

$$\ldots - 2(\frac{P_1Q_2 - P_2Q_1}{P_2Q_1 + 2P_1Q_2})(\frac{b^2-ka^2}{b^2-a^2})] \qquad [3.48]$$

$$u(s)_{PS} = [\frac{p(s)}{b^2-a^2}] \frac{P_1}{Q_1} [(b^2-ka^2) (\frac{3P_2Q_1}{2P_1Q_2+P_2Q_1})r + \ldots$$

$$\ldots + (1-k) (\frac{a^2b^2}{r})] \qquad [3.49]$$

These general equations can be written for particular cases. Common assumptions are:

1. The pressure 'p' is applied instantaneously (time independent), then the function p(s) can be replaced by a loading step function:

$$p(s) = p/s \qquad [3.50]$$

2. The material is time independent under hydrostatic stress, which means that no creep occurs in a hydrostatic stress field. In this case, the hydrostatic Laplace transform operators (Eqns. 3.39 and 3.41) become:

$$P_2 = 1 \qquad [3.51]$$

$$Q_2 = 3K \qquad [3.52]$$

Consequently, the viscoelastic Young's modulus (Eqn. 3.42) and Poisson's ratio (Eqn. 3.43) reduce to:

$$E(s) = \frac{9KQ_1}{Q_1 + 6KP_1} \qquad [3.53]$$

$$\nu(s) = \frac{3KP_1 - Q_1}{Q_1 + 6KP_1} \qquad [3.54]$$

3. The deviatoric behaviour of the material is defined by one of the linear viscoelastic models (Eqns. 2.19, 2.21, 2.23, 2.25 or 2.27). The respective deviatoric Laplace transform operators, P_1 and Q_1, are shown in Table 3.1.

Substituting Eqns. 3.50, 3.53 and 3.54 into Eqns. 3.48 and 3.49 gives:

<u>Axisymmetric Loading</u>

$$u(s) = D\left[F\left\{\frac{3P_1}{s(6KP_1+Q_1)}\right\} + H\left(\frac{P_1}{sQ_1}\right)\right] - \ldots$$

$$\ldots - J\left[\frac{3KP_1-Q_1}{s(9KQ_1)} - L\left\{\frac{(3KP_1-Q_1)^2}{s(9KQ_1)(6KP_1+Q_1)}\right\}\right] \qquad [3.55]$$

<u>Plane Strain</u>

$$u(s) = D\left[F\left\{\frac{3P_1}{s(6KP_1+Q_1)}\right\} + H\left(\frac{P_1}{sQ_1}\right)\right] \qquad [3.56]$$

where D, F, H, J and L are constants for a given geometry and stress state. Their expressions are:

$$D = p / (b^2 - a^2) \quad [3.57]$$

$$F = r (b^2 - k a^2) \quad [3.58]$$

$$H = [(1 - k) a^2 b^2] / r \quad [3.59]$$

$$J = p r \quad [3.60]$$

$$L = [2 (b^2 - k a^2)] / (b^2 - a^2) \quad [3.61]$$

To obtain the radial displacement equation in function of time for a certain viscoelastic model, one has to:

1. Substitute the respective deviatoric Laplace transform operators, P_1 and Q_1 (Table 3.1), which define the viscoelastic model, into Eqn. 3.55 or 3.56, according to the desirable loading condition.
2. Rearrange the expression into a series (summation) of functions of the transform variable 's'. Each individual function of 's' has to have an inverse Laplace transform, which can be found in books that publish a list of Laplace transform pairs (e.g., Spiegel, 1965; Roberts and Kaufman, 1966; Abramowitz and Stegun, 1972).
3. Exchange the functions of the transform variable 's' by their respective inverse Laplace transforms, which are functions of the time 't'.
4. The final radial displacement expression is a function of time, viscoelastic constants, applied pressure field and geometry.

This whole process is lengthy and tedious. Therefore, only the final forms of the radial displacement equations (function of time) are presented for both axisymmetric loading and plane strain. One might have already noticed that the axisymmetric solution is an extension of the plane strain solution, where the effects of the constant axial strain are added. To avoid repeating of terms, the axisymmetric solutions, $u(t)_{AL}$, are written in function of the plane strain solutions, $u(t)_{PS}$.

3.3.1 Maxwell Model

Plane Strain

$$u(t)_{PS} = D\left[\frac{F}{2K}\left\{1 - \frac{E}{6k+E}\,EXP(-a\,t)\right\} + H\left(\frac{1}{E} + \frac{t}{\eta}\right)\right] \qquad [3.62]$$

where

$$a = \frac{6KE}{(6K+E)\eta}$$

u(t) ... radial displacement in function of time

t ... time

K ... bulk modulus

E, η ... viscoelastic constants

D, F, H ... constants given by Eqns. 3.57 to 3.59, respectively.

Axisymmetric Loading

$$u(t)_{AL} = u(t)_{PS} - J\,[\frac{3K-E}{9KE} + \frac{t}{3\eta} - L\,\{\frac{t}{6\eta} + \ldots$$

$$\ldots + \frac{6K-5E}{36KE}\,(1 - EXP(-a\ t)) + \frac{(3K-E)^2}{9KE\eta(6K+E)}\,EXP(-a\ t)\}] \quad [3.63]$$

where

J, L ... constants given by Eqns. 3.60 and 3.61, respectively.

3.3.2 Kelvin Model

Plane Strain

$$u(t)_{PS} = D\,[\frac{3F}{6K+E}\,\{1 - EXP(-a\ t)\} + \ldots$$

$$\ldots + \frac{H}{E}\,\{1 - EXP(-\beta\ t)\}] \quad [3.64]$$

where

$$a = \frac{6K+E}{\eta}$$

$$\beta = \frac{E}{\eta}$$

Axisymmetric Loading

$$u(t)_{AL} = u(t)_{PS} - J\,[\frac{3K-E}{9KE} - \frac{1}{3E}\,EXP(-\beta\ t) - \ldots$$

$$\ldots - \frac{L}{9K}\,\{\frac{(3K-E)^2}{E(6K+E)} - W_1\,EXP(-\beta\ t) + W_2\,EXP(-a\ t)\}] \quad [3.65]$$

where

$$W_1 = \frac{12KE\eta(3K-E) + (3K-E)^2 + E^2}{6KE}$$

$$W_2 = \frac{-12K\eta(3K-E)(6K+E) + (3K-E)^2 + (6K+E)^2}{6K(6K+E)}$$

3.3.3 Generalized Kelvin (solid) Model

Plane Strain

$$u(t)_{PS} = D\left[\frac{3F}{6K(E_1+E_2)+E_1E_2}\left\{E_1 + E_2 - \frac{E_1^2}{6K+E_1}\,\mathrm{EXP}(-\alpha\ t)\right\} + \ldots\right.$$

$$\left.\ldots + \frac{H}{E_1E_2}\left\{E_1 + E_2 - E_1\ \mathrm{EXP}(-\beta\ t)\right\}\right] \qquad [3.66]$$

where

$$\alpha = \frac{6K(E_1+E_2) + E_1E_2}{(6K+E_1)\eta_2}$$

$$\beta = \frac{E_2}{\eta_2}$$

Axisymmetric Loading

$$u(t)_{AL} = u(t)_{PS} - J\left[\frac{3K(E_1+E_2) - E_1E_2}{9KE_1E_2} - \ldots\right.$$

$$\ldots - \frac{1}{3E_2}\,\mathrm{EXP}(-\beta\ t) - \frac{L}{9K}\left\{\frac{[3K(E_1+E_2) - E_1E_2]^2}{E_1E_2[6K(E_1+E_2) + E_1E_2]} + \ldots\right.$$

$$\left.\ldots + W_1\ \mathrm{EXP}(-\beta\ t) + W_2\ \mathrm{EXP}(-\alpha\ t)\right\}\Big] \qquad [3.67]$$

where

$$W_1 = 2[3K(E_1+E_2) - E_1E_2](3K-E_1)\eta_2 - \ldots$$

$$\ldots - \frac{[3K(E_1+E_2)-E_1E_2]^2 + (3K-E_1)^2 E_2^2}{6K E_1^2 E_2}$$

$$W_2 = 2[3K(E_1+E_2) - E_1E_2](3K-E_1)\eta_2 + \ldots$$

$$\ldots + \frac{[3K(E_1+E_2)-E_1E_2]^2(6K+E_1)^2 + (3K-E_1)^2[6K(E_1+E_2)+E_1E_2]^2}{6K E_1^4 E_2}$$

3.3.4 Generalized Kelvin (fluid) Model

Plane Strain

$$u(t)_{PS} = D\ [\frac{3F}{(\gamma-a)\eta_1\eta_2}\ \{-\frac{E_2}{a\ \gamma}\ (a\ (1 - EXP(-\gamma\ t)) - \ldots$$

$$\ldots - \gamma\ (1 - EXP(-a\ t))) + (\eta_1+\eta_2)(EXP(-a\ t) - \ldots$$

$$\ldots - EXP(-\gamma\ t))\} + \frac{H}{\eta_1 E_2}\ \{E_2\ t + \eta_1\ (1 - EXP(-\beta\ t)\}] \qquad [3.68]$$

where

a, γ ... are roots of:

$$6KE_2 + [6K(\eta_1+\eta_2) + E_2\eta_1]s + \eta_1\eta_2 s^2 = 0$$

$$\beta = \frac{E_2}{\eta_2}$$

Axisymmetric Loading

$$u(t)_{AL} = u(t)_{PS} - \ldots$$

$$\ldots - J\,[\frac{t}{3\eta_1} + \frac{3K-E_2}{9KE_2}\,\{1 - EXP(-\beta\ t)\} - \frac{1}{9K}\,EXP(-\beta\ t) - \ldots$$

$$\ldots - \frac{L}{9K}\,\{\frac{\alpha\beta\gamma W_3 - (\alpha\beta+\beta\gamma+\gamma\alpha)W_4}{\alpha^2\ \beta^2\ \gamma^2} + \frac{W_4\ t}{\alpha\ \beta\ \gamma} - \ldots$$

$$\ldots - \frac{-\ \alpha^4 + W_1\alpha^3 - W_2\alpha^2 + W_3\alpha - W_4}{\alpha^2\ (\beta-\alpha)\ (\gamma-\alpha)}\ EXP(-\alpha\ t) - \ldots$$

$$\ldots - \frac{-\ \beta^4 + W_1\beta^3 - W_2\beta^2 + W_3\beta - W_4}{\beta^2\ (\alpha-\beta)\ (\gamma-\beta)}\ EXP(-\beta\ t) - \ldots$$

$$\ldots - \frac{-\ \gamma^4 + W_1\gamma^3 - W_2\gamma^2 + W_3\gamma - W_4}{\gamma^2\ (\alpha-\gamma)\ (\beta-\gamma)}\ EXP(-\gamma\ t)\}] \qquad [3.69]$$

where

$$W_1 = \frac{2E_2\eta_1 - 6K(\eta_1+\eta_2)}{\eta_1\eta_2}$$

$$W_2 = [\frac{6K(\eta_1+\eta_2) - E_2\eta_1}{\eta_1\eta_2}]^2 - \frac{6KE_2}{\eta_1\eta_2}$$

$$W_3 = \frac{6KE_2\ [3K(\eta_1+\eta_2) - E_2\eta_1]}{(\eta_1\eta_2)^2}$$

$$W_4 = (\frac{3KE_2}{\eta_1\eta_2})^2$$

3.3.5 Burgers Model

<u>Plane Strain</u>

$$u(t)_{PS} = D\,[\frac{3F}{(\alpha-\gamma)(6K+E_1)\eta_1\eta_2}\,\{\frac{E_1E_2}{\alpha\gamma}\,(\alpha\ (1 - EXP(-\gamma\ t)) - \ldots$$

$$\ldots - \gamma\ (1 - \mathrm{EXP}(-\alpha\ t))) - (E_1\eta_1 + E_1\eta_2 + E_2\eta_1)\ \ldots$$

$$\ldots\ (\mathrm{EXP}(-\alpha\ t) - \mathrm{EXP}(-\gamma\ t))\} + \frac{H}{\eta_1 E_1 E_2}\ \{E_1E_2t + \ldots$$

$$\ldots + \eta_1(E_1+E_2)(1 - \mathrm{EXP}(-\beta\ t)) + \eta_1E_2\ \mathrm{EXP}(-\beta\ t)\}] \qquad [3.70]$$

where

α, γ ... are roots of:

$$6KE_1E_2 + [6K(E_1\eta_1+E_1\eta_2+E_2\eta_1) + E_1E_2\eta_1]s + (6K+E_1)\eta_1\eta_2 s^2 = 0$$

$$\beta = \frac{E_2}{\eta_2}$$

<u>Axisymmetric Loading</u>

$$u(t)_{AL} = u(t)_{PS} - J\ [\frac{t}{3\eta_1} + \frac{3K\eta_1(E_1+E_2) - E_1\eta_1}{9KE_1E_2\eta_1}\ \ldots$$

$$\ldots\ \{1 - \mathrm{EXP}(-\beta\ t)\} + \frac{3K-E_1}{9KE_1}\ \mathrm{EXP}(-\beta\ t) - \ldots$$

$$\ldots - \frac{L\ (3K-E_1)^2}{9KE_1(6K+E_1)}\ \{\frac{\alpha\beta\gamma W_3 - (\alpha\beta+\beta\gamma+\gamma\alpha)\ W_4}{\alpha^2\ \beta^2\ \gamma^2} + \frac{W_4\ t}{\alpha\ \beta\ \gamma} - \ldots$$

$$\ldots - \frac{-\ \alpha^4 + W_1\alpha^3 - W_2\alpha^2 + W_3\alpha - W_4}{\alpha^2\ (\beta-\alpha)\ (\gamma-\alpha)}\ \mathrm{EXP}(-\alpha\ t) - \ldots$$

$$\ldots - \frac{-\ \beta^4 + W_1\beta^3 - W_2\beta^2 + W_3\beta - W_4}{\beta^2\ (\alpha-\beta)\ (\gamma-\beta)}\ \mathrm{EXP}(-\beta\ t) - \ldots$$

$$\ldots - \frac{-\ \gamma^4 + W_1\gamma^3 - W_2\gamma^2 + W_3\gamma - W_4}{\gamma^2\ (\alpha-\gamma)\ (\beta-\gamma)}\ \mathrm{EXP}(-\gamma\ t)\}] \qquad [3.71]$$

where

$$W_1 = \frac{6K(E_1\eta_1+E_1\eta_2+E_2\eta_1) - 2E_1E_2\eta_1}{(3K-E_1)\eta_1\eta_2}$$

$$W_2 = [\frac{3K(E_1\eta_1+E_1\eta_2+E_2\eta_1) - E_1E_2\eta_1}{(3K-E_1)\eta_1\eta_2}]^2 + \frac{6KE_1E_2}{(3K-E_1)\eta_1\eta_2}$$

$$W_3 = \frac{6KE_1E_2\ [3K(E_1\eta_1+E_1\eta_2+E_2\eta_1) - E_1E_2\eta_1]}{[(3K-E_1)\eta_1\eta_2]^2}$$

$$W_4 = [\frac{3KE_1E_2}{(3K-E_1)\eta_1\eta_2}]^2$$

3.4 Elastic-Viscoplastic Solutions for the Thick-Walled Cylinder

Elastic-viscoplastic solutions for the thick-walled cylinder are based on the total strain equation (Eqn. 2.1), where the irrecoverable strain components are defined by the theory of plasticity. Examples of this type of analytical solution are given by Hardy et al. (1983), Van Eekelen (1983), Cristescu (1985) and Fuenkajorn and Daemen (1988a). The basic approach includes some simplifications to Eqn. 2.1, which is reduced to:

$$\epsilon_{ij} = \epsilon^e_{ij} + \epsilon^c_{ij} \qquad [3.72]$$

where

ϵ_{ij} ... total strain tensor

ϵ^e_{ij} ... linear elastic (recoverable) strain tensor

ϵ^c_{ij} ... plastic creep (irrecoverable) strain tensor.

The elastic strain tensor is well defined by the generalized

Hooke's law. The plastic strain tensor is described by a creep law (Chapter 2) and can be obtained from the theory of plasticity. Assumptions related to material properties, flow potential, flow rule and so on, have to be made.

Equation 3.72 has to be extended to a multiaxial stress state. The common form to do that is founded on the theory of total deformation (introduced by Odqvist in 1966), which is generalized to include any creep law (transient and steady-state portions). Costa (1984) reviewed in detail this whole formulation. The resulting equation depends on several assumptions associated with the theory of plasticity such as isotropy, incompressibility during creep, coaxiality of the stress and strain tensors, and infinitesimal strains. The difference among solutions published in the literature usually lies in the chosen creep law. For instance, Hardy et al. (1983) selected a dislocation law (Eqn. 2.4) to define the plastic creep strain while Fuenkajorn and Daemen (1988a) preferred the power law (Eqn. 2.2). The final expression of the creep strain rate for a multiaxial stress state, taking into account the above assumptions is:

$$\dot{\epsilon}^c_{ij} = \frac{3}{2} \frac{\dot{\epsilon}^c_e}{\sigma_e} S_{ij} \qquad [3.73]$$

where

$\dot{\epsilon}^c_{ij}$ ... creep strain rate tensor

$\dot{\epsilon}^c_e$ ... effective or equivalent creep strain rate

σ_e ... effective or equivalent stress

S_{ij} ... deviatoric stress tensor.

The effective or equivalent stress can be defined by the Von Mises yield criterion, assuming associated flow rule. In this case, the equivalent stress is only dependent on the second stress invariant (J2) and is expressed as:

$$\sigma_e = (J2)^{1/2} \qquad [3.74]$$

where

$$J2 = \frac{1}{6}\left[(\sigma_{11}-\sigma_{22})^2 + (\sigma_{22}-\sigma_{33})^2 + (\sigma_{33}-\sigma_{11})^2\right] \qquad [3.75]$$

The effective or equivalent creep strain rate is defined by a creep law, as for example the power law for isothermal conditions:

$$\epsilon_e^c = K\ \sigma_e^c\ t^a \ \ldots\ \dot{\epsilon}_e^c = K\ \sigma_e^c\ a\ t^{a-1} \qquad [3.76]$$

or the structural creep law:

$$\dot{\epsilon}_e^c = b_1\ t^{b2} \ \ldots\ \epsilon_e^c = \frac{b_1}{b_2+1}\ t^{b2+1} \qquad [3.77]$$

where

t ... time

a, b_1, b_2, c, K ... material constants.

Any other creep law could be chosen, but as transient creep is of particular interest in this research, the two above

laws were selected.

Applying the above concepts to the thick-walled cylinder problem, it is possible to derive the radial displacement expression, as a function of time, either for plane strain or axisymmetric loading conditions. The radial strain can be divided into two components, as shown in Eqn. 3.72:

$$\epsilon_r = \epsilon_r^e + \epsilon_r^c \qquad [3.78]$$

where

ϵ_r ... total radial strain

ϵ_r^e ... linear elastic (recoverable) radial strain

ϵ_r^c ... plastic creep (irrecoverable) radial strain.

The elastic radial strain can be calculated for each loading condition, using the generalized Hooke's law. It depends on the thick-walled cylinder geometry, axial, internal and external pressures, and elastic constants. The expressions for plane strain and axisymmetric loading conditions are respectively:

$$\epsilon_r^e = \frac{1+\nu}{E} \left[B(1-2\nu) + \frac{A}{r^2}\right] \qquad [3.79]$$

$$\epsilon_r^e = \frac{1+\nu}{E} \left[B(1-2\nu) + \frac{A}{r^2}\right] - \frac{\nu}{E} (\sigma_z - 2\nu B) \qquad [3.80]$$

where

E ... Young's modulus

ν ... Poisson's ratio

σ_z ... axial stress (assumed = p_a)

r ... radius

A, B ... given by Eqns. 3.4 and 3.5, respectively.

The radial creep strain rate, as defined by Eqn. 3.73, can be expressed as:

$$\dot{\epsilon}_r^c = \frac{3}{2} \frac{\dot{\epsilon}_e^c}{\sigma_e} S_r \qquad [3.81]$$

where

S_r ... deviatoric radial stress.

The power law (Eqn. 3.76) or the structural law (Eqn. 3.77) can be extended to describe the effective creep strain rate. The final expressions for the radial creep strain and strain rate become:

<u>Power Law</u>

$$\dot{\epsilon}_r^c = \frac{3}{2} K \sigma_e^{(c-1)} a \; t^{(a-1)} S_r \qquad [3.82]$$

Integrating once with respect to time leads to:

$$\epsilon_r^c = \frac{3}{2} K \sigma_e^{(c-1)} t^a S_r \qquad [3.83]$$

<u>Structural Loading</u>

$$\dot{\epsilon}_r^c = \frac{3}{2} \frac{b_1}{\sigma_e} t^{b2} S_r \qquad [3.84]$$

Integrating once with respect to time leads to:

$$\epsilon_r^c = \frac{3}{2}\frac{b_1}{\sigma_e}\frac{t^{(b2+1)}}{b_2+1} S_r \qquad [3.85]$$

Combining the elastic radial strain expressions for different loading conditions (Eqns. 3.79 and 3.80) with the creep strain equations (Eqns. 3.83 and 3.85) for different models and substituting into Eqn. 3.78 give four possible expressions for the total radial strain, as a function of time. The radial strain expressions are presented for each loading condition and creep law. These expressions are also a function of the equivalent and deviatoric radial stresses, which in cylindrical coordinates are given by:

$$\sigma_e = [\frac{1}{6}\{(\sigma_r-\sigma_\theta)^2 + (\sigma_\theta-\sigma_z)^2 + (\sigma_z-\sigma_r)^2\}]^{1/2} \qquad [3.86]$$

$$S_r = \sigma_r - \frac{\sigma_r+\sigma_\theta+\sigma_z}{3} \qquad [3.87]$$

where

σ_r, σ_θ ... given by Eqns. 3.1 and 3.2, respectively

σ_z ... axial stress.

The axial stress is assumed to be equal to the axial pressure (p_a) for axisymmetric loading condition or is given by Eqn. 3.10 for plane strain.

3.4.1 Plane Strain with Power Law

$$\epsilon_r(t) = \frac{1+\nu}{E} \left[B\ (1-2\nu) + \frac{A}{r^2}\right] + \frac{3}{2} K\ \sigma_e^{(c-1)} t^a\ S_r \qquad [3.88]$$

3.4.2 Plane Strain with Structural Law

$$\epsilon_r(t) = \frac{1+\nu}{E} \left[B\ (1-2\nu) + \frac{A}{r^2}\right] + \frac{3}{2} \frac{b_1}{\sigma_e} \frac{t^{(b2+1)}}{b_2+1}\ S_r \qquad [3.89]$$

3.4.3 Axisymmetric Loading with Power Law

$$\epsilon_r(t) = \frac{1+\nu}{E} \left[B\ (1-2\nu) + \frac{A}{r^2}\right] - \frac{\nu}{E} (\sigma_z - 2\nu B) + \ldots$$

$$\ldots + \frac{3}{2} K\ \sigma_e^{(c-1)} t^a\ S_r \qquad [3.90]$$

3.4.4 Axisymmetric Loading with Structural Law

$$\epsilon_r(t) = \frac{1+\nu}{E} \left[B\ (1-2\nu) + \frac{A}{r^2}\right] - \frac{\nu}{E} (\sigma_z - 2\nu B) + \ldots$$

$$\ldots + \frac{3}{2} \frac{b_1}{\sigma_e} \frac{t^{(b2+1)}}{b_2+1}\ S_r \qquad [3.91]$$

The radial strain equations (Eqns. 3.88 to 3.91) could be integrated once with respect to radius, to give radial displacement expressions, assuming small strains ($\epsilon_r=\partial u/\partial r$). The elastic radial displacement components were already defined by Eqns. 3.7 and 3.11 for axisymmetric loading and plane strain, respectively. Unfortunately, the problem relies on the integrals of the creep radial strain expressions (Eqns. 3.83 and 3.85). The solution is a series of integrals that can only be solved numerically.

3.5 Summary and Conclusions

The elastic solution for the thick-walled cylinder was reviewed in order to help interpret the cell structural performance and calibration tests (Appendices A and D, respectively). The elastic solution also serves as the basis for linear viscoelastic solutions, where the correspondence principle is applied to obtain time-dependent radial displacement equations. Other solutions based on more complex rheological models are available in the literature (e.g., Ottosen, 1986), but the final forms of the equations are very complicated and numerical solution techniques are required. Also, elastic-viscoplastic analytical solutions were derived based on the theory of plasticity, where the plastic strain component was described by a creep law (Chapter 2).

Analytical solutions are limited by several assumptions related to material properties, loading conditions, flow

potential, infinitesimal strains, etc. Even so, analytical solutions can be very helpful for preliminary understanding of the constitutive model parameters, how they affect the final bore convergence and for checking numerical solutions before simulating more complex geometry, stress path, pressure field and material inhomogeneity. The analytical solutions derived in this chapter are used for predicting the hollow cylinder test results (Chapter 6) and for evaluating the predictive capability of these creep models.

Numerical analyses should follow as the next logical step, but it is left for future investigation. Numerical analyses allow the use of more complex creep models, geometries, pressure fields and loading conditions. Appropriate numerical formulation permits the analysis of geometric non-linearity effects (i.e., change of geometry and consequent stress redistribution), besides the material non-linearity effects. This tool is essential to assess the predictive capability of creep models, because in-situ measurements of opening closure are the resulting response of material and geometric non-linearities.

Once more, the success of analytical solutions and numerical analyses, involving comparison between predicted and measured deformation and extrapolations for further deformation, relies on the quality of the laboratory data used for generating the creep model parameters. The next two chapters (Chapters 4 and 5) describe the laboratory facilities, specimen preparation and testing procedures

developed during this research as an attempt to obtain reliable data.

Table 3.1 Deviatoric time differential and Laplace transformed operators for five linear viscoelastic models

Viscoelastic Model	Deviatoric Time Differential Operators	Deviatoric Laplace Transformed Operators
Maxwell	$\hat{P}_1 = E + \eta\frac{\partial}{\partial t}$ $\hat{Q}_1 = E\,\eta\frac{\partial}{\partial t}$	$P_1 = E + \eta s$ $Q_1 = E\,\eta\, s$
Kelvin	$\hat{P}_1 = 1$ $\hat{Q}_1 = E + \eta\frac{\partial}{\partial t}$	$P_1 = 1$ $Q_1 = E + \eta s$
Generalized Kelvin (solid)	$\hat{P}_1 = E_1 + E_2 + \eta_2\frac{\partial}{\partial t}$ $\hat{Q}_1 = E_1E_2 + E_1\eta_2\frac{\partial}{\partial t}$	$P_1 = E_1 + E_2 + \eta_2\, s$ $Q_1 = E_1E_2 + E_1\eta_2 s$
Generalized Kelvin (fluid)	$\hat{P}_1 = E_2 + (\eta_1+\eta_2)\frac{\partial}{\partial t}$ $\hat{Q}_1 = E_2\eta_1\frac{\partial}{\partial t} + \eta_1\,\eta_2\frac{\partial^2}{\partial t^2}$	$P_1 = E_2 + (\eta_1+\eta_2)s$ $Q_1 = E_2\eta_1 s + \eta_1\,\eta_2 s^2$
Burgers	$\hat{P}_1 = E_1E_2 + (E_2\eta_1 + E_1\eta_1 + E_1\eta_2)\frac{\partial}{\partial t} + \eta_1\,\eta_2\frac{\partial^2}{\partial t^2}$ $\hat{Q}_1 = E_1E_2\eta_1\frac{\partial}{\partial t} + E_1\eta_1\,\eta_2\frac{\partial^2}{\partial t^2}$	$P_1 = E_1E_2 + (E_2\eta_1 + E_1\eta_1 + E_1\eta_2)\, s + \eta_1\,\eta_2 s^2$ $Q_1 = E_1E_2\eta_1 s + E_1\eta_1\,\eta_2 s^2$

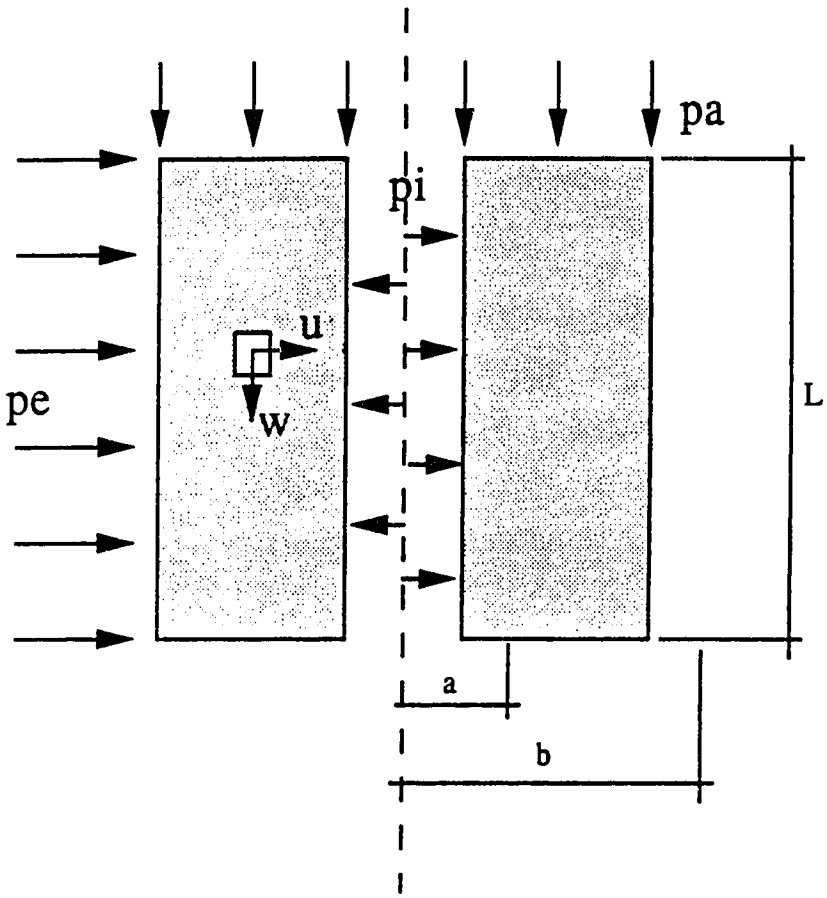

Figure 3.1 Definition of the terms used in the elastic equations for thick-walled cylinders (pressures and displacements are shown in positive directions)

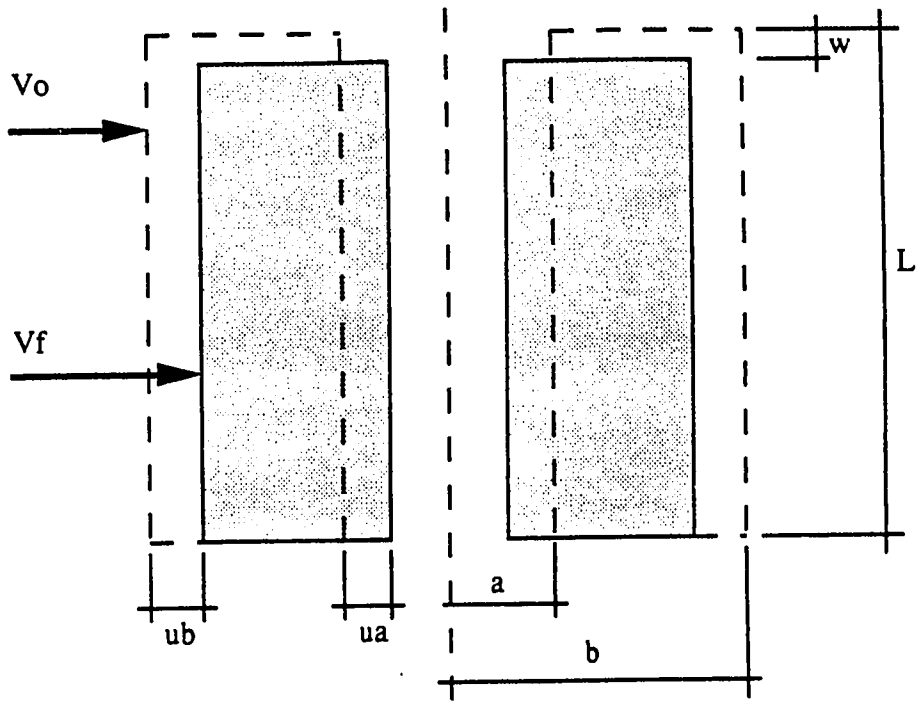

$$\triangle VCI = (VCI)f - (VCI)o$$

where

$$(VCI)f = \pi\,(a - ua)^2 (L - w)$$

$$(VCI)o = \pi\, a^2 L$$

$$\triangle VCI = \pi\,[(ua^2 - 2a\,ua)\,L - (a - ua)^2 w]$$

$$\triangle VCE = (VCE)f - (VCI)o$$

where

$$(VCE)f = \pi (b - ub)^2 (L - w)$$

$$(VCE)o = \pi\, b^2 L$$

$$\triangle VCE = \pi\,[(ub^2 - 2b\,ub)\,L - (b - ub)^2 w]$$

Figure 3.2 Volume change expressions for thick-walled cylinders

4. LABORATORY TESTING FACILITIES

4.1 Introduction

The increasing demand for salt rocks as a mining product and as a medium for either fluid or radioactive waste storage, and the borehole closure problems encountered in these rocks, have placed pressure on the quality of laboratory experiments. One of the contributing factors to the quality of laboratory experiments is the apparatus used for producing them. Hardy et al. (1984) and Dusseault et al. (1985) reviewed the type of data needed to evaluate the behaviour of openings in salt rocks. Ideally, laboratory facilities should provide the means to evaluate strength and deformation properties under variable pressure and temperature conditions. Based on these required critical properties, the equipment and testing procedures have to be developed. Tullis and Tullis (1986) presented a complete review of experimental rock testing techniques. Details on factors affecting testing response, pressure, loading and temperature systems, sealing and monitoring are provided. In similar work, Handin et al. (1986) discussed techniques of experimental deformation applied to salt rock.

Besides triaxial testing facilities, it would be beneficial to incorporate the capability of testing other specimen geometries and stress paths. More recently, hollow cylinder tests have been identified as most promising for studying the behaviour of circular openings in homogeneous

stress fields because they are simulations of in-situ geometries and stress fields (Daemen, 1981; Dusseault et al., 1985). Hambley et al. (1988) suggested the hollow cylinder apparatus with independent axial, internal and external pressure control, as a future means of simulating in-situ conditions more closely. Jaeger and Cook (1979) called it the most ready available method of studying the strength and deformation of rock under a wide variety of unequal principal stresses.

The use of hollow cylinder specimens of geotechnical materials is not new. Hoskins (1969) reported on hollow cylinder tests in rock conducted in 1912 by Adams. Hight et al. (1983) reviewed the hollow cylinder technique in soils since 1957. Most of these works were undertaken to investigate the shape of yield surfaces, the effects of principal stress rotation and failure modes (Sterne, 1981; Hight et al., 1983; Sayao and Vaid, 1988). These researchers usually preferred thin-walled hollow cylinder specimens with a ratio of internal to external diameter of 0.5 to 0.8, because they offer reduced end effects and the stress across the walls can be approximated by a constant stress without introducing major errors.

Lately, when hollow cylinder tests have been used more often as model experiments simulating in-situ geometries and stress fields, thick-walled hollow cylinder specimens, with a diametric ratio of 0.25 to 0.5, have been preferred (Dusseault, 1981; Sterne, 1981; Wawersik and Morgan, 1987;

Branco, 1988; Fuenkajorn and Daemen, 1988a). Actually, a maximum ratio of 0.25 is advisable in order to avoid boundary effects. When this ratio is used, the elastic solution for the stress distribution in thick-walled hollow cylinders, under zero internal pressure, gives a deviatoric stress at the outer radius of only 6.7% of the maximum value at the inner radius. This means that a homogeneous stress field is almost reestablished at the outer boundary (no boundary stress effect), although there is still some displacement boundary effect ('u' not equal to zero or not equal to that of external media).

Hight et al. (1983) reviewed the general principles of hollow cylinder tests. Internal and external pressures act through flexible membranes so that there are no shear stresses on the vertical boundaries. Neglecting end effects, there are also no shear stresses on the circumferential surfaces throughout the wall. Consequently, the radial and tangential stresses are always principal stresses. The third principal stress is the axial stress. The hollow cylinder apparatus presents the advantages of independent control of the three principal stresses and of simplified evaluation of strains by measuring volume changes occurring within the cell and bore. Besides, it offers the opportunity of extending the stress path approach to include simulations of in-situ geometries, stress fields, axial loading conditions (axisymmetric or plane strain) and also independent control of the thermal regime by regulating bore and cell

temperatures.

This is done by hydrostatically loading the specimen to the equivalent in-situ stress and temperature fields. Then, maintaining the external pressure and temperature constant, the internal pressure and temperature can be changed according to the class of geotechnical problem to be modelled (Table 1.1). The axial stress is controlled according to the desired axial loading condition, whether axisymmetric loading or plane strain. In the former condition, which is more appropriate for shafts and boreholes, the axial stress is maintained constant. In the latter, more appropriate for mining, caverns and tunnelling, the axial stress is controlled in such a way as to maintain zero axial strain.

The major drawback in the use of hollow cylinder specimens, besides their more complicated specimen preparation and assembly procedures, is the non-uniformity of the stress distribution across the thick wall, due to the curvature of the specimen surfaces and restraint at end loading platens. The latter cause of stress non-uniformity can be minimized, but the former requires assumptions about the constitutive behaviour of the material in order to do a stress-strain analysis.

4.2 Experimental Techniques for Time-Dependent Properties

Time-dependent properties were considered the priority in the development of a new apparatus. Findley et al. (1976) reviewed the general principles and precautions which should be considered in setting up an experimental apparatus for creep tests. First, creep tests are constant stress and not constant load experiments. This problem mainly concerns the axial loading system. Constant load tests are usually satisfactory for small changes of the cross-section, but not for materials that undergo large deformations such as salt rocks. In this case, the axial load has to be corrected to account for the changes of the cross-section and thereby produce constant stress. For triaxial tests, the assumption of no volume change in the specimen during creep tests is commonly used (Wawersik and Preece, 1984). Now, with computer control of testing apparatuses, better maintenance of the constant axial stress is possible by measuring the specimen volume change and axial displacement, calculating the current cross-section and then, correcting the axial load.

Creep tests are also conducted under the assumption that the load is applied instantaneously and then remains constant. This is, of course, not possible and, in practice, the load is applied in a short time compared to the creep test duration. There are creep models (e.g., Sano, 1978) that consider the time taken for loading the specimen. As different rates of loading also affect the resulting creep,

the loading rate should also be controlled.

Other important aspects of creep apparatuses commented on by Findley et al. (1976), are the loading system, temperature and monitoring. Cook (1981) and Hardy et al. (1984) presented a review of several types of loading systems used in creep tests, outlining the advantages and drawbacks of each one. Friction is usually a problem in any loading system and should be kept to a minimum. For this reason, the load measuring device should be placed between the specimen and loading system. Rolling diaphragm pistons usually yield good results, especially when they are servo-controlled to provide a controllable and repeatable loading pattern. Temperature has also to be controlled during creep tests, not only because it affects creep rates, but because temperature fluctuations can cause fluctuations in pressure and transducer outputs. A uniform temperature can be applied to a specimen using a fluid heat-transfer medium, regulated by a closed-loop automatic controller. A controlled environment room is also advisable. Finally, monitoring has to be continuous and reliable for long periods. Zero drifts of electronic instruments are usually a problem for tests of long durations. Local point deformation instruments, although desirable as a second source of information, are not recommended as key instruments. It is preferable to use devices measuring average responses.

In addition to all of the above requirements, an ideal laboratory apparatus for obtaining creep properties should

be able to operate under conditions closer to those experienced in situ. Maybe the most dramatic improvements in laboratory testing during the last decade resulted from the incorporation of modern electronics in the control and data acquisition systems. Moore (1980a to f, 1981a and b) explained how physical parameters such as temperature, pressure and displacement, which are measured by analog devices, can be converted to digital outputs and then, be regulated with a microprocessor, in the 'closed-loop' controller. Since then, several triaxial testing facilities have been developed (Wawersik and Preece, 1984; Hardikar et al., 1987; Baleshta and Dusseault, 1988 ; Reeves, 1988) and a substantial evolution in terms of features, accuracy, capability, versatility, sophistication, operation, programming and data reduction, has taken place.

4.3 The High Pressure and Temperature System

Based on the characteristics required for an ideal testing apparatus to investigate time-dependent properties, a high pressure and temperature system, called HPTS, was developed at the University of Alberta during this research. The HPTS was based heavily on a triaxial testing system developed at the University of Waterloo (Baleshta and Dusseault, 1988). Hollow cylinder testing capabilities and temperature control systems were incorporated in this project. The concepts, design and specifications involved in the development of the HPTS are provided in Appendices A to

D. Laboratory facilities for this research were composed of an environmentally controlled room, with the temperature set to 25 +/- 0.5°C and relative humidity to 50 +/- 5%, facilities for specimen preparation (Chapter 5) and apparatus assembly (Appendix A), and the HPTS itself.

The HPTS consists of two testing cells, loading, pressure, temperature, data acquisition and control systems, and monitoring. Although all these components are interrelated, for the sake of simplicity, they are described separately. The development and construction of this system constitutes a major component of this thesis. From design to calibration and system verification more than two and a half years lapsed. Maloney (Maloney, 1986) has contributed in designing the pressure system and R. Gitzel (from Civil Electronics Division) in assembling the hardware of the control and data acquisition system and, in writing the preliminary version of the software.

4.3.1 Testing Cells and Axial Loading Systems (Appendix A)

The HPTS has two cells (Figs. A.1 and A.2) designed to test both solid and hollow cylindrical specimens. Cell dimensions were decided according to desired specimen sizes and geometric constraints. The internal diameter (bore) of hollow cylinder specimens was set to 32 mm, based on the minimum room needed to accommodate a membrane, seals, fluid circulation tubes and instrumentation. Ideal specimen diameters and heights are discussed in Chapter 5. Currently,

both testing cells accommodate specimen diameters up to 140 mm and heights up to 200 mm. Confining (cell or external) and bore (internal) pressures of up to 70 MPa can be applied.

The cells are identical except for the axial loading systems. Cell No. 1 needs a reaction frame which has an axial loading capacity of 1 MN (Plate 4.1a). Cell No. 2 is a self-contained cell with a second chamber which provides the axial loading system (Plate 4.1b). Its axial loading capacity varies from 1 MN, using the modified pressure intensifier, to 3 MN, using the standard intensifier (Appendix B). The axial loading is transmitted to the specimen through the axial ram and specimen support, which both have highly polished spherical seats. These seats combined with the lubricant applied between the specimen and contact parts help minimize friction and end effects.

4.3.2 Pressure System (Appendix B)

The HPTS delivers pressure to both testing cells, each having three independent (axial, bore or internal and cell or external) pressure controls (Fig. B.1). Each pressure circuit is composed of microprocessor activated low pressure components, a pressure intensifier (AIVC) device and high pressure parts. A common source of low pressure, bottled nitrogen, delivers regulated pressure at 2 MPa to the low pressure side (Fig. B.2), where it is controlled by a set of (ball, metering and normally-closed solenoid) valves. The

ball valves are for manual pressure control. Each pair of metering and solenoid valves regulate the amount of nitrogen delivered by each pulse of the solenoid valves when they are energized by the control system (Appendix C). Continuous energizing allows the pressure in the intensifier chamber to increase gradually from zero to a desired value.

The low pressure is boosted by the accumulator, intensifier and volume change (AIVC) device (Plate 4.2 and Fig. B.3). It acts as an accumulator by storing a quantity of compressed nitrogen which buffers the pressurized volume, during valve operation, leakage and temperature fluctuations. It also acts as a pressure intensifier due to the difference in the piston cross-sections (standard and modified intensifier ratios are 1:35 and 1:12, respectively). The gas/oil interface is a Bellofram rolling diaphragm seal which minimizes friction. The typical friction to initiate movement in the intensifiers is in the order of 100 kPa, but one of them presented values up to 350 kPa. Finally, this device also acts as volume change indicator by monitoring the displacement of the low pressure piston using the volume change device (Appendix D). The maximum stroke is limited by the diaphragm seal, being 190 mm for the selected seal. This gives high pressure supply volumes of 65 and 180 ml for the standard and modified intensifiers, respectively.

High pressure volumes, ordinary hydraulic oil for axial and silicone oil for bore and cell axes, are delivered to

the high pressure side (Fig. B.4). A set of high pressure valves are used for manual operation, control and maintenance. High pressure lines are connected to cells by quick-connectors which are convenient, easy to operate and avoid loss of fluid. Pressure gauges and transducers measure the pressure just before delivery to the testing cells.

4.3.3 Temperature System (Appendix B)

The HPTS facilities can control temperature in two ways. First, the apparatus is housed in a controlled environment room, with the ambient temperature set to 25 +/- 0.5°C. Second, the HPTS can independently control oil temperatures in the bore and cell axes. The cell temperature is closed-loop controlled by a system of heaters, resistance temperature devices (RTDs) and a microcomputer. Two heating mats, wrapped around the cell chamber, are connected to the heater controller which is computer directed. RTDs measure the temperature of the confining fluid and depending on the value, a computer signal is sent back to the heating elements (on/off). The cell temperature is controlled from ambient to temperatures up to 80 +/- 0.1°C.

On the other hand, the bore temperature is regulated by a thermostatic bath and fluid circulation through the bore coils. It is monitored by thermocouples. Presently, the HPTS does not control the bore temperature by a closed-loop process, but it can easily be done. Although the temperature control system is already implemented, it has not yet been

fully tested. Temperature dependent aspects of this study were relegated to future studies.

4.3.4 Control and Data Acquisition System (Appendix C)

For precise load and temperature application over the long duration of creep tests, a closed-loop control process was highly desirable to regulate the testing parameters (pressure, displacement, volume change and temperature). A basic control and data acquisition system is composed of two strongly interdependent parts, hardware and software. It comprises six stages: signal acquisition, signal conditioning, analog-to-digital conversion, signal transmission, signal processing and data storage (Reeves, 1988).

Hardware employed by the HPTS consists of an IBM-XT compatible computer with multifunction and graphic cards, clock, one hard and two floppy disks, monochrome display and printer, and a data acquisition and control interface board with extension boards.

Signal acquisition is done by a wide variety of instruments (pressure transducers, LVDTs, strain gauges, RTDs and thermocouples) with different analog signal output ranges. Instruments, depending on the analog output range, were divided into two groups. The first group, LVDTs, was connected to an EXP-16 board, set to a gain of one. The second group, composed of all other instruments was connected to a second EXP-16 board, set to a gain of 100.

EXP-16 boards are expansion, multiplexer and instrumentation amplifier boards which also do signal filtering and conditioning. Each EXP-16 board is connected to one of the eight single analog input channels of the DASH-8 board which is an eight channel, twelve bit, high speed analog to digital (A/D) converter and timer/counter board. A/D conversion time is typically 25 microseconds which is far less than the speed of the QUICKBASIC (software language) compiler.

Digital data are used by the HPTS software and stored in the random access memory (RAM). Testing parameters, in digital form, are processed and compared to the reference values prescribed by the software. Depending on the results of the comparison, the computer transmits a digital signal to energize the appropriate, normally-closed solenoid valves and heaters.

Signal transmission to solenoid valves and heaters is done by the PIO12 card which is a 24 bit, parallel, digital input/output (I/O) interface.

Finally, data are stored on hard disk when certain control conditions are fulfilled. Presently, load, time interval (1 to 120 min) and manual intervention are used as control triggers for data storage.

The HPTS software is written in QUICKBASIC and compiled to an executable version. It is composed of three computer programs. Program HPTSCAL manages the instrument calibrations and helps position the instrument output range

before starting a test. Program HPTSCON sets the file with the conversion factors (analog output to physical measurements) for all instruments. And Program HPTS does the testing control and data acquisition.

Program HPTS starts by resetting and dimensioning variables, setting up trapping error and function-key routines, loading parameters for accessory boards and reading the conversion factors for the instruments. Then, testing parameter data are entered. A user manual with programming tips and flow charts is presented in Appendix C.

Finally, the HPTS software runs the testing control and data acquisition routines. Signal sampling (A/D channels) is done by a low speed data logging routine. Channels are read a chosen number of times to be as reliable as possible. The average of readings is saved for further comparison, displaying and storing. The control routines use the sampling data to decide on the settings of digital switches which energize solenoid valves and heaters. Currently, the HPTS can use several control limits such as pressure, volume change, displacement and temperature, but gradient control (e.g., stress and strain rates) has not been implemented yet. Testing parameters, reference and current values, are on-line displayed after each software cycle (2 s). A menu of options is also shown on the display screen, allowing several intervening and reprogramming options. Data are stored on hard disk after a certain control condition is fulfilled. Load is the control condition during loading

stages and time interval (ranging from 1 to 120 min) during creep stages. Data are written in a simple compact form readily accepted by most spreadsheet programs. Post-processing activities and graphics are accomplished using spreadsheet and graphic software.

Plate 4.3a shows a general view of the control panel and data acquisition system.

4.3.5 Monitoring (Appendix D)

The HPTS monitors up to 32 transducers, sixteen for each testing cell. The instrument configuration for each system comprises three volume change devices (axial, bore and cell), one axial displacement LVDT, four spare LVDTs, three pressure transducers (axial, bore and cell), one bore convergence device with two strain gauge pairs (Plate 4.3b), one specimen diameter deformation device, one thermocouple (bore) and one resistance temperature device (cell). Signal acquisition is done by these transducers transforming a continuously varying physical quantity (pressure, displacement, temperature) into a directly proportional, continuously varying analog output. All transducers were calibrated to obtain the conversion factors which give the relation between physical quantity and analog or digital output. No performance tests for evaluating the instrument zero drifts were executed since this laboratory program focused on short-term creep tests only.

4.3.6 Calibration Tests (Appendix D)

A series of calibration tests were performed using both solid and hollow cylindrical aluminum specimens with the ideal dimensions of actual specimens. Aluminum specimen deformations for several loading conditions were calculated using the theory of elasticity. The difference between the deformations measured by the system transducers and those calculated by the theory of elasticity, gives the correction or calibration curve for a specific transducer under the corresponding loading condition and specimen size. The calibration curves were written as polynomial equations to facilitate the correction of raw data. Tables 4.1 and 4.2 show the final equations of the correction curves used in this laboratory testing program.

The calibration tests can be used as a first analysis of the system performance. Most ot the data has a quite consistent trend for all tests. Pressure and other testing parameter control can be considered satisfactory. The system only failed to record accurately very small volume changes. More performance data are discussed in Chapter 5.

4.4 The HPTS Performance and Suggestions for Further Improvements

4.4.1 Testing Cells and Axial Loading Systems

The structural performance of the testing cells, in terms of design criteria, was evaluated by comparing the

measurements of ten strain gauges, installed on several cell components, to the equivalent predicted deformations, obtained by closed-form solutions (Appendix A). The cylindrical chambers behaved exactly according to the prediction, but bolts and end caps measured deformations less than half of the predicted values. Leakage through fittings was not a problem, but occurred between seals and membranes, when specimens underwent large diametric expansion (Chapter 5). Also the electrical wire connector in Cell No. 2 leaked, but this was due to poor installation and not to design.

Assembly and disassembly were relatively slow processes, requiring two people and a crane for four hours. However, considering that the HPTS is employed for long-term tests, the time involved in the assembly and disassembly procedures is not excessive. Several modifications could speed up these procedures. The number of bolts can be reduced using bolts with greater cross-sectional area, but a minimum of eight should be obeyed to ensure uniform load distribution. Also, the specimen support (Figs. A.7 and A.8) does not have to be screwed to the bottom end cap. A few pins could be used for keeping it aligned and for avoiding rotation. Cell No. 2 could be designed 'upside down' with the piston chamber being on the bottom. This would save time during assembly and disassembly of the axial loading system after each test. This design alternative would require several changes in the testing cell components (rings) and

assembly procedure in order to ensure correct sealing.

In summary, the suggestions for improvements of the testing cells and axial loading systems are:

1. A higher cylindrical chamber to accommodate specimen heights up to 250 mm, permitting tests of cylindrical specimens with a length to diameter (L/D) ratio up to 2.5, if D = 100 mm.
2. Longer contact between the top membrane seal (SM) and the external membrane (MC), to accommodate larger diametric expansion of specimens, thereby avoiding leakage.
3. Specimen support (SS) with pins for maintaining alignment and avoiding rotation, instead of screws, to ease assembly and disassembly procedures. Also, incorporation of a spherical seat in the specimen supports to improve axial loading conditions.
4. Specimen support (SS) and axial ram (RM) diameters larger than the specimen diameter would avoid punching of specimens under large diametric deformation by the end platens. However, this may result in difficult membrane sealing.
5. A reduction in the number of bolts, by increasing the cross-sectional area of individual bolts, would ease assembly and disassembly procedures.
6. Redesign Cell No. 2, with the piston and cell chambers in the reverse position, to ease assembly and disassembly procedures and with the axial piston (PP)

moving upwards to avoid gravity effects.

4.4.2 Pressure System

In general, the pressure system has worked satisfactorily. No leakage has been observed. The major limitation is the limited stroke of the intensifier piston. Overcoming this problem would involve a set of electrical high pressure pumps and high pressure solenoid valves, which would certainly not be cost effective. Another weak point of the pressure system resides in the Bellofram rolling diaphragm. Any mistake or carelessness during the intensifier assembly may destroy the diaphragm or damage it, reducing its lifetime. As in any pressure system, friction is a problem, but it can be minimized by using low friction seals and by machining very smooth contacts between metal parts. Each of the six intensifiers presented a different degree of friction (50 to 350 kPa to initiate movements).

In summary, the only practical suggestion for improvements of the pressure system is:

1. Run a set of performance tests for each intensifier, in order to make adjustments and minimize friction.

4.4.3 Temperature System

Although this system is already implemented (Appendix B), it has not yet been tested. Therefore, performance has not been evaluated. However, at least two improvements could be implemented to increase its flexibility and efficiency:

1. Increase the range of temperature control to allow simulations of compressed air storage (-50°C) and nuclear waste repositories (250°C).
2. Regulate the bore temperature system by a closed-loop controller (microcomputer).

4.4.4 Control and Data Acquisition System

This is where more improvements can be made, not because the performance was unsatisfactory, but because this system manages all others and controls the data acquisition and test sequence. It is the core of the HPTS. The control system has performed very well, especially during creep stages. During load stages, for each load step, the system first loads the axial axis, then the internal and external pressure axes. Currently, the load step is considered complete and data are recorded when the last (external pressure) axis is at the prescribed level, without rechecking the other pressure axes. It has been noticed that loading of one axis may affect the pressure in another axis. This is particularly true for hydrostatic loading of hollow cylinder specimens, where manual corrections were needed to keep all pressures at their prescribed values. A better loading control can be easily implemented, via software, making the microcomputer recheck the load step routine until all pressure values are equal to the prescribed ones prior to data recording and step advancement.

Another important improvement to the control system lies in the controlled loading rate. At the beginning of a test, the system is under low pressure. Consequently, each pulse of the solenoid valve releases a larger equivalent pressure to the system than when it is under high pressure, therefore following a non-uniform rate of loading. Two options can provide a controlled loading rate in the HPTS. First, divide the pressure range into intervals, in which the open time of the solenoid valve would differ in such a way as to deliver the same equivalent pressure to the system. For instance, the solenoid time would be 100 ms for pressures between 0 and 5 MPa, 200 ms for pressures between 5 and 10 MPa and so on. The appropriate opening time for each pressure interval to yield an average constant loading rate would be obtained from a set of performance tests, covering all pressure ranges. The second option would consist of having a set of solenoid valves, each one set with a different opening time. This set of valves would be shared by all pressure axes. The microcomputer would calculate the current loading rate, compare it to the prescribed rate and then decide which valve should be energized to produce the average constant loading rate.

The data acquisition system has presented no problems and major improvements are not needed for the time being.

Finally, the software itself can always be improved. It is well documented (Appendix C) and the basic features to operate the HPTS are available. Nevertheless, more

information on the display screen during test execution would be very helpful and would facilitate testing decisions. Multiple screens should be implemented. For instance, the standard screen would show the main menu of options and current situation of the test. A second screen, when called, would show the values being monitored by all transducers at that moment. Finally, a third screen would plot the measurements for specified transducers, from the beginning of the test to the current situation.

In summary, the suggestions for improvements of the control and data acquisition system are:

1. Implementation of facilities for controlled strain rate tests.
2. Modification of the software to produce controlled average loading (stress) rates.
3. Modification of the software to perform more accurate loading stages, particularly hydrostatic loading.
4. Modification of the software to obtain more information on the display screen, during test execution, in order to follow more closely the experiment and to facilitate any decision which may be needed.
5. Use of faster computers to provide better test control, especially during loading stages and when high strain rates occur.

4.4.5 Monitoring

Commercial instruments such as pressure transducers and LVDTs, performed according to their specifications. In-house fabricated instruments, the volume change device, the bore convergence device and the specimen diameter deformation device, did not al[illegible]form as desired (Appendix D). The specimen diameter [illegible] device displayed non-linearity during the calib[illegible]cs and subsequently, was not used in this laboratory testing program. Major modifications would have to be made in order for it to perform satisfactorily. Volume change devices have worked very well. For small volume changes however, a step function was noticed in the measurements due to friction in the intensifier pistons. The bore convergence device has also performed very well. Its only drawback is that it cannot measure diametric extension, therefore being only appropriate for bore closure tests.

4.5 Summary and Conclusions

A review of experimental techniques of rock deformation and, in particular, those dedicated to time-dependent properties is presented. The hollow cylinder apparatus is suggested to be the most ready simulator of circular openings in homogeneous stress fields. Therefore, it is ideal for modelling underground structures in salt rocks.

The laboratory facilities developed in this research, incorporate all requirements for modern triaxial testing,

time-dependent studies and hollow cylinder tests. The HPTS presents improvements over other systems such as independent computer control of axial (to 210 MPa), internal (to 70 MPa) and external (to 70 MPa) pressures, bore and cell temperatures (ambient to 80°C), data acquisition and monitoring. Also, the axial loading and pressure systems were carefully designed to minimize frictions and end effects. Using this laboratory system, it is possible to execute tests following any triaxial stress and hollow cylinder paths. The computer control of the testing parameters ensures corrections at any time in order to keep the testing conditions within a narrow range of variations. All these aspects are essential to produce the reliable data so needed to investigate time-dependent properties of rocks.

Although the HPTS performance was very satisfactory, there is room for improvement. The major limitation relies on the rate control of stress, deformation and temperature not yet implemented. Other modifications are suggested for each component of the system. Basically, they are related to increased flexibility and efficiency. Reeves (1988) suggested that good software can compensate for hardware deficiencies, but excellent hardware can be crippled by inadequate software. For the HPTS, the available hardware is not fully exploited by the current software. Therefore, many improvements can be achieved by simply refining the software. On-line configuration changes and real-time graphics would be very desirable to follow closely the

specimen response during testing.

Table 4.1 Correction equations for triaxial tests

HL	DA (mm)	= 0.00843.P
	VC (ml)	= -0.09370.$(P)^2$ + 15.2473.P
CTC	△DA (mm)	= 0.00285.(PA-PE)
	△VC (ml)	= 0
JTC	△DA (mm)	= 0.00135.(PA-PE)
	△VC (ml)	= -0.00580.$(PA-PE)^2$ - 2.82927.(PA-PE)

P ... mean pressure (MPa) = (PA+2PE)/3

PA ... axial stress (MPa)

PE ... confining pressure (MPa)

Table 4.2 Correction equations for hollow cylinder tests

HCHL	DA (mm)	= 0.02358.P
	VCE (ml)	= 0.00199.$(P)^3$ - 0.16069.$(P)^2$ + 12.1601.P
	VCI (ml)	= 0.00032.$(P)^3$ - 0.01873.$(P)^2$ + 0.64077.P
	ID (mm)	= 0.00354.P
HCAL	△DA (mm)	= 0
	△VCE (ml)	= 0
	△VCI (ml)	= 0.28750.(PI-PO)
	△ID (mm)	= -0.00400.(PI-PO)
HCPS	△DA (mm)	= 0
	△VCE (ml)	= 0
	△VCI (ml)	= 0.32085.(PI-PE)
	△ID (mm)	= -0.00396.(PI-PE)

P ... mean pressure (MPa) = (PA+PE+PI)/3
PO ... outside pressure (MPa) = (PA+PE)/2
PA ... axial stress
PE ... external pressure
PI ... internal pressure

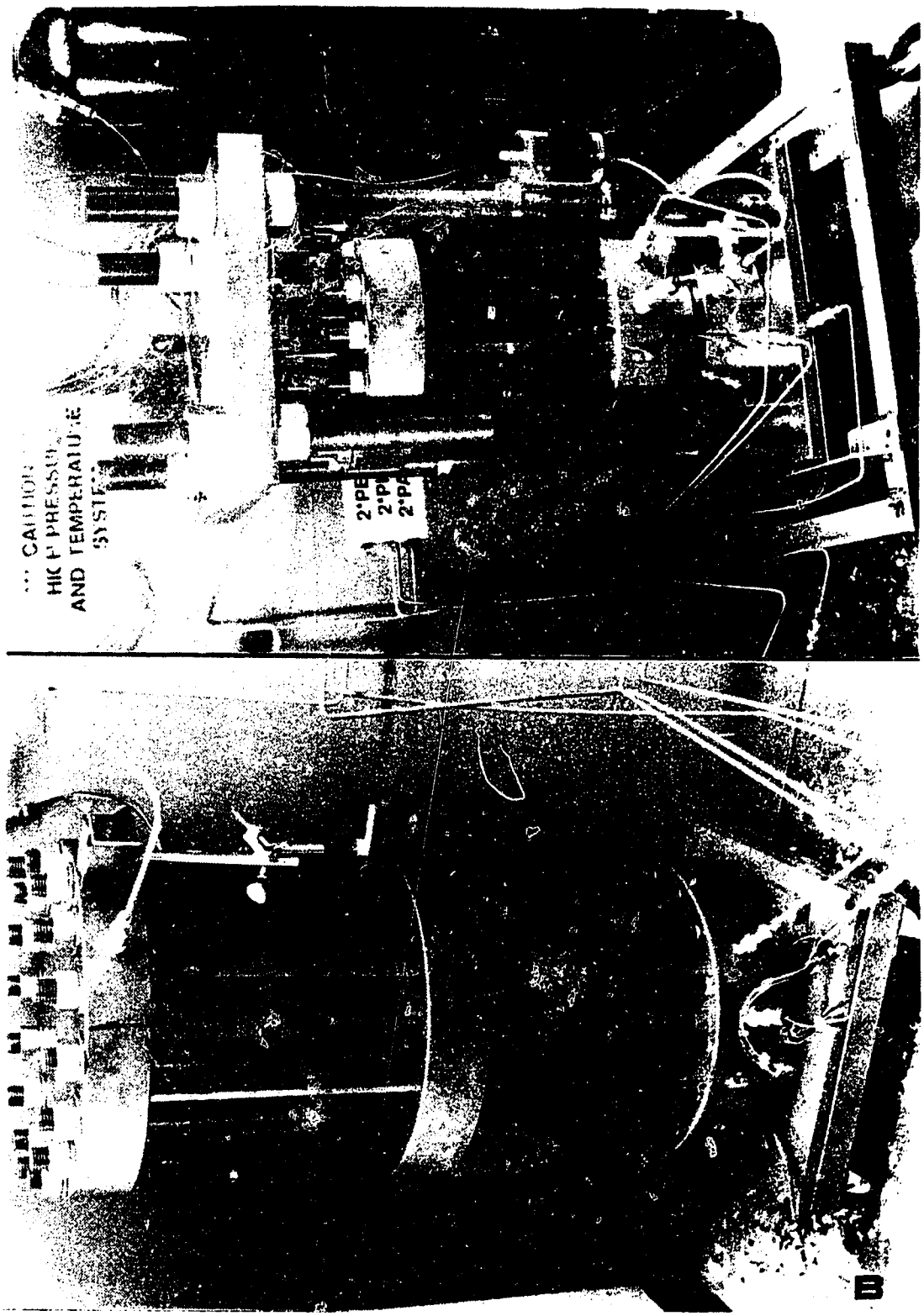

Plate 4.1 HPTS Testing Cells; (A) Cell No. 1 and reaction frame; (B) Cell No. 2 (self-framed cell)

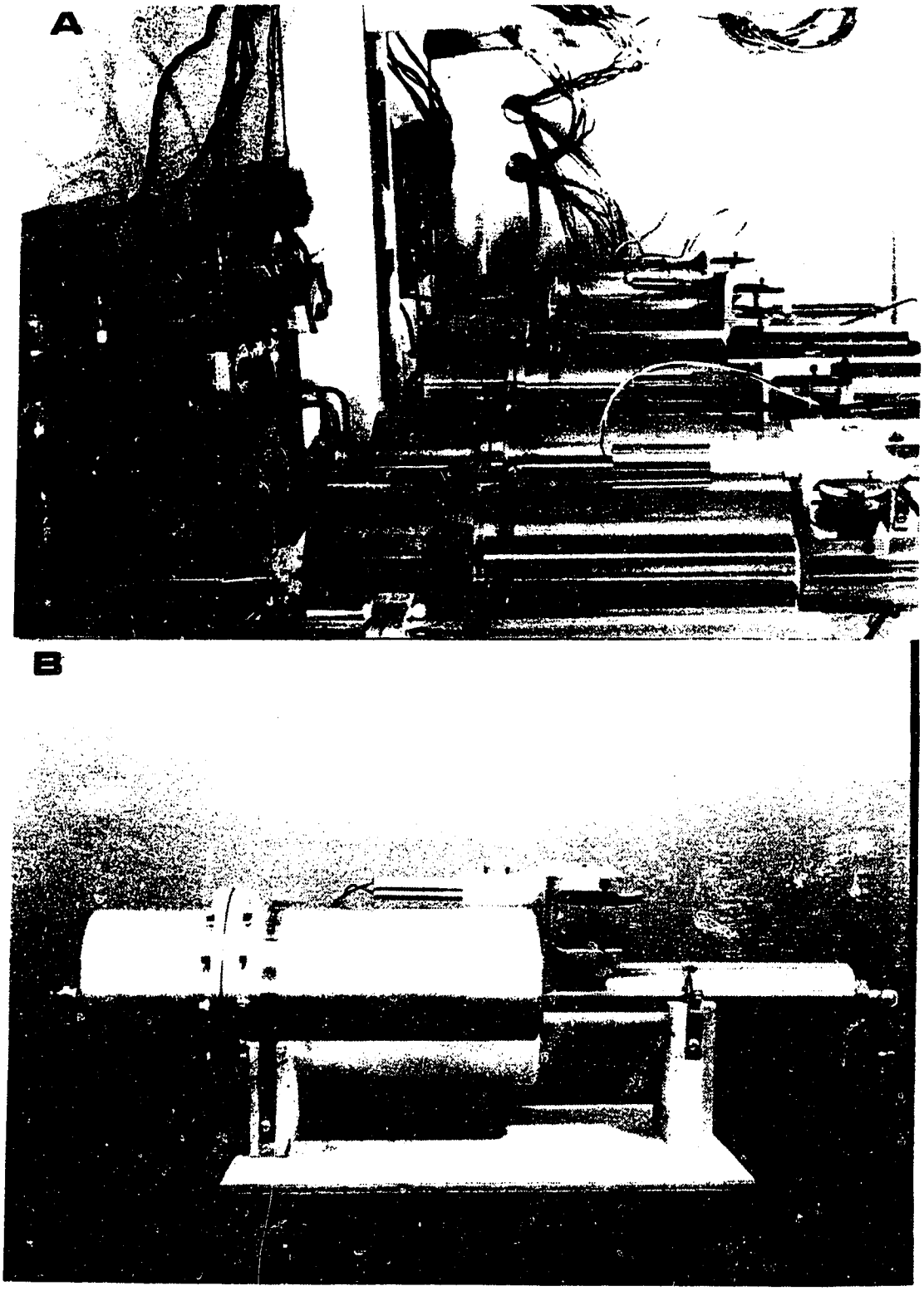

Plate 4.2 HPTS Pressure System; (A) General view of the intensifiers; (B) AIVC device

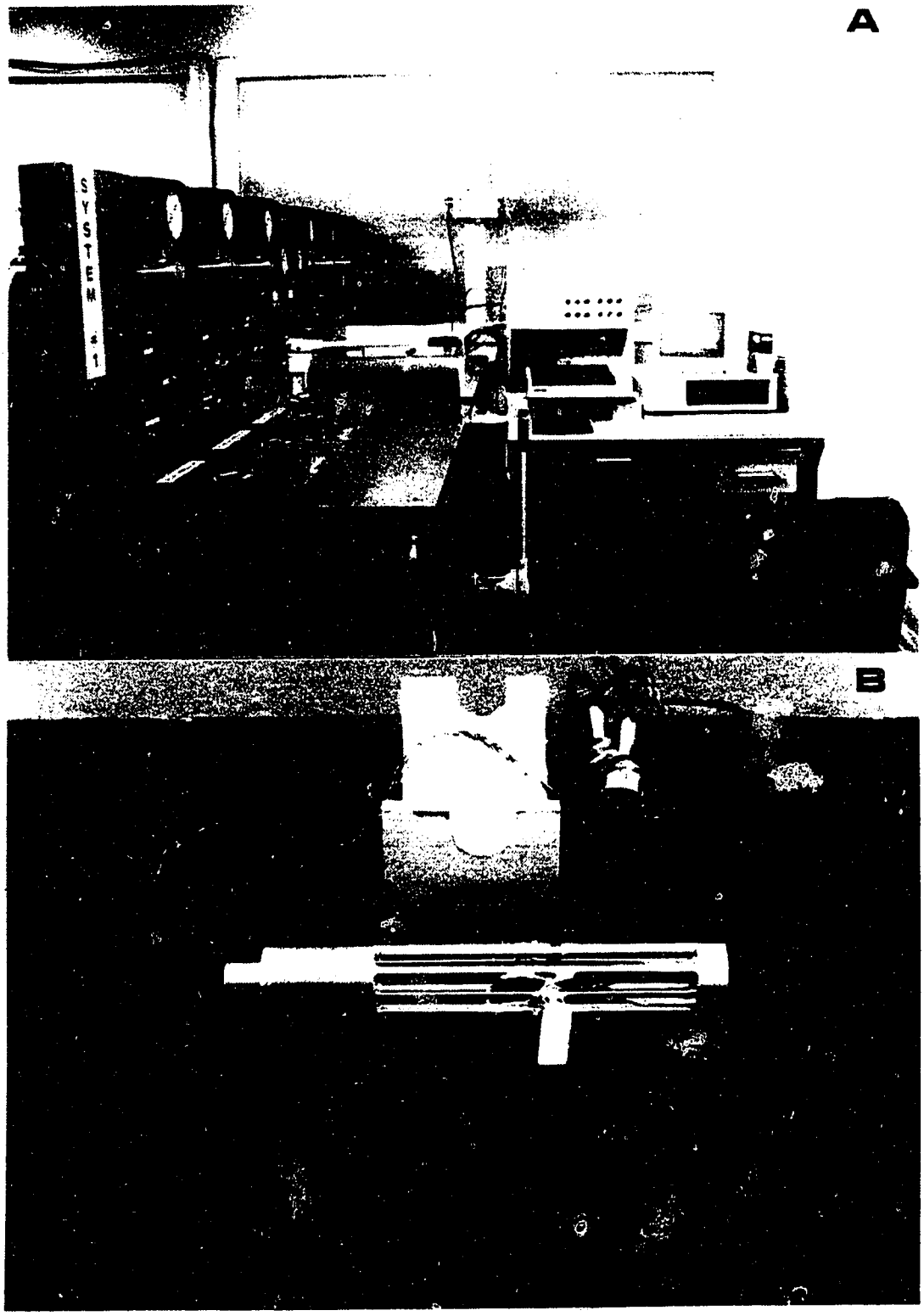

Plate 4.3 HPTS Control, Data Acquisition and Monitoring; (A) Control panel; (B) Bore convergence device

5. LABORATORY TESTING PROGRAM

5.1 Introduction

As mentioned in the previous chapters, a laboratory testing program constitutes an essential part of the study of material properties and structure performance. Computer analyses have also increasingly demanded reliable laboratory data as input for sophisticated constitutive laws. High quality laboratory data are a result of a complex process which starts with sampling, goes through a well-designed laboratory testing program and ends at the reduction of data which are corrected for system compliance. Data should be presented in standard plots, as raw as possible, avoiding any kind of assumptions, curve fitting and interpretation in order to be a faithful and reliable source of information for further analyses.

Statistically speaking, laboratory data must also be representative of the material tested and of the response to the tests carried out. The minimum number of specimens for each material sample and type of test are suggested by several researchers (Vutukuri et al., 1974; Gyenge and Ladanyi, 1977). Although this laboratory testing program is an attempt to produce reliable data, these data cannot be considered statistically representative, due to the small number of available samples. Only one specimen was tested for each stress state in a particular stress path.

This chapter describes in detail the sampling and testing procedures. These procedures were established to minimize the differences among specimens and therefore produce more uniform test results. Tests are reviewed, reporting problems and difficulties encountered during execution, and their respective solutions.

5.2 Sampling

Sampling is understood as the entire process from the selection of sampling locations until the delivery of a specimen for testing. It is composed of several procedures including selection of sampling locations, acquisition, transportation, preparation, storage and characterization. These procedures are influenced by geological conditions, by the purpose of the investigation and by other conditions such as accessibility of the test site or availability of appropriate samples (Gyenge and Ladanyi, 1977). A specimen for determining strength and deformation properties should fulfill the following requirements:

1. Be representative of the entire rock mass.
2. Be free of cracks and other weaknesses in the case of intact material.
3. Have ends parallel to each other and perpendicular to the longitudinal axis.
4. Have sides straight, smooth and free of abrupt irregularities.

ISRM (1983) and ASTM D4543-85 (1988) present limits and

tolerances for the above requirements. There is agreement that the most common specimen shape is a right circular cylinder. Specimen diameter and length to diameter ratio (L/D) are discussed later.

Reeves and Unrau (1988) reported on the complexity of natural potash. It is difficult to obtain and prepare specimens which satisfy desirable specifications. Many researchers prefer artificial to natural specimens where crystal size, impurities, inclusions, secondary minerals and bedding planes can be controlled (Le Comte, 1965; Friedman et al., 1984; Gangi et al., 1984; Guessous et al., 1987 and 1988; Bakhtar et al., 1988). Natural potash was chosen to avoid structural simplifications which could eliminate behavioural aspects (Fuenkajorn and Daemen, 1988a), although some studies suggest no major differences between pure and real salts (Friedman et al., 1984; Gangi et al., 1984).

In the case of sampling natural potash, all reasonable efforts should be made to prepare specimens in accordance with the standard tolerances. Wawersik and Preece (1984), Dusseault et al. (1985), Senseny (1985), Reeves and Unrau (1988) and especially Fuenkajorn and Daemen (1988a) present guides and procedures for sampling natural salt. The procedures used in this sampling program are briefly described, with more emphasis on the stages that differed from standard practices. The results of the specimen preparation procedure were very satisfactory, producing specimens of high quality and within standard tolerances.

5.2.1 Sampling Location

Due to the complexity of rock as an engineering material, where the mechanical properties can greatly vary as a function of lithology, stress history, weathering and other natural geologic processes, samples should be collected from all portions of the deposit in order to truly represent the entire rock mass (ASTM D4543-85, 1988). Two different sites in Saskatchewan were selected for sampling. They were the Allan and Cory Divisions of the Potash Corporations of Saskatchewan (PCS), located near the city of Saskatoon. These potash mines are at depths of 1012 m (Cory) and 1036 m (Allan) and exploit bedded, horizontal ($\approx 0.2^{\circ}$) Devonian deposits (Patience Lake), 3.3 m thick, of the Prairie Evaporite Formation (Monenco, 1984). The average mineral contents are 55% halite (NaCl - milky white), 40% sylvite (KCl - colorless to pink) and 5% impurities (clay, carnallite and anhydrite).

Samples were collected from several locations at each site, in the form of large blocks from the excavation face, on two different occasions (September, 1986 and May, 1987). It is known that these kind of blocks are subjected to microcracks due to stress relief but they were the most readily available source of samples. A geologist from PCS helped select blocks. They were chosen based on the absence of fissures and open cracks, and minimal structural differences such as crystal size, deposition layers and mineral composition. Later, cores from the Allan Division

(PCS) were also obtained but no details of the drilling technique applied and sampling locations were available. Analysing them, they seem to have been drilled horizontally from the mine wall, parallel to the bedding planes.

5.2.2 Sample Transportation

Blocks and cores from both trips were transported by truck. They were protected from the effects of weathering by plastic covers. The samples were placed on foam in a wood box to prevent excessive jarring which could induce fresh cracks or extension of any pre-existing ones.

5.2.3 Core Drilling Technique

There are two ways of obtaining cores for laboratory testing. The first is by in-situ core drilling and the second by laboratory core drilling from block samples. The in-situ core drilling has the advantage of obtaining samples from inaccessible regions, at specified locations, directions and depths, far away from the excavation face and zones of disturbance. Dusseault et al. (1985) suggested that samples should be obtained at least 2 m beyond a free face to avoid opening disturbance. The second technique, laboratory core drilling, although more prone to disturbance, is more practical and sometimes the only feasible source of samples. In this sampling program, both coring techniques were used, although there are no details of the in-situ coring technique used by the PCS workers. Six

cores of 146 mm diameter were received from the Allan Division (PCS), in satisfactory condition, with only some surface waviness. This was also noted in cores obtained from the laboratory coring program.

The laboratory coring program on the block samples from the Cory Division (PCS) consumed a great deal of time, effort and material, and is therefore described in some detail. Much information was gained from the literature (Gyenge and Ladanyi, 1977; Wawersik and Preece, 1984; Dusseault et al., 1985) but the final procedure was a combination of these previous experiences and trial and error. Most of the problems were directly related to the structure of the material. Potash is a soft material with a polycrystalline structure, extremely brittle when unconfined and subjected to high temperatures, and soluble in water. The dust generated from dry coring is extremely corrosive to other metals. The final drilling procedure had to avoid:

1. Heat generation and vibration from drilling equipment and core barrel.
2. Use of water in circulation fluid, with the exception of brine.
3. Dust contamination.

Several measures were taken to meet these requirements. Only the final and successful procedure is described:

1. The blocks, encased in plastic bags, were positioned and cast in concrete to eliminate vibration during coring.
2. The portable coring unit (light weight, with electric

motor) was jacked against a steel beam system to minimize vibration (Plate 5.1a).

3. The selected core barrel (ID = 101.6 mm), a single tube with segmented diamond bit ('tooth' type) to facilitate fluid circulation and having sufficient internal clearance to avoid transfer of heat generated during drilling, was positioned over the block (Plate 5.1b).
4. Dry coring using compressed air (at 350 kPa) was used due to the hydroscopic nature of the material. Compressed air also helps cool the samples due to its low temperature.
5. A large vacuum cleaner was used for overcoming the dust problem.
6. Coring was conducted at low rotation speed of the core barrel. Slow and with small pressure at the beginning until the hole is well defined. Then, to continue the drilling process, small pressure (approximately equivalent to the self-weight of the barrel) and large inflow of compressed air to cool the sample and reflush the drill hole.
7. After drilling for 10 to 15 min, the coring unit was turned off and an equal period was allowed for cooling of the sample with the air circulation still on.

With this procedure, the laboratory core drilling program was completed, without any major problems, other than some waviness on the sample surface. All cores were drilled perpendicular to the bedding planes. The average drilling

rate was 20 cm/h. It is worth noting that this drilling program was conducted outside during the winter, when the benefits of the natural cold temperatures could be used. This also helped control any corrosive dust contamination.

5.2.4 Specimen Preparation

The aim of the specimen preparation technique is to transform a roughly cylindrical shaped core into an acceptable test specimen. Laboratory tests need specimens of a certain specified size, shape and number (Gyenge and Ladanyi, 1977).

This laboratory testing program required two kinds of specimens, solid and hollow cylindrical specimens. The specimen size is governed by crystal size, testing equipment specifications and availability of cores. The diameter of specimens from polycrystalline rocks such as potash, should be at least ten times the average crystal size, in order to avoid excessive influence of a particular crystal on the mechanical behavioural response. The crystal sizes of samples from the Cory Division (PCS) range from 1 to 20 mm, but the majority of crystals lies between 4 to 7 mm. The samples from the Allan Division (PCS) present the same average crystal sizes, but a narrower range of extremes (1 to 10 mm). Testing equipment specifications limit the specimen diameter to 140 mm and the length to 200 mm. Although the length to diameter (L/D) ratio should be between two and three, availability of cores with length in

that order was a problem. An attempt was made to keep the specimens within these limits, except for hollow cylinder specimens where the thick wall (54 mm) should be ten average grain sizes (≈50 to 100 mm).

After the laboratory coring program, the samples were found to be very fragile and special care was deemed necessary during specimen preparation. The main problems were related to dislodgement of crystals during end cutting and surface lathing. After several unsuccessful attempts, the procedure described in the following section was established.

5.2.4.1 Preparation of Cylindrical Specimens

Cylindrical specimens for triaxial tests were prepared from block samples obtained from the Cory Division (PCS). The specimen diameter was set at 100 mm and the length at 200 mm, whenever possible. Due to the waviness in the circumferential surface of the samples, some finished specimen diameters were a few millimeters below 100 mm. For future laboratory coring, it is suggested that a core barrel with inside diameter of at least 5 mm greater than the desired specimen diameter be used. The procedure for preparation of the cylindrical specimens is as follows:

1. Core ends were cut by a diamond cut-off saw in order to produce close to parallel ends. A metal ring applying some confinement to the edge crystals was place near (approximately 2 mm) the surface to be cut (Plate 5.2a) to avoid crystal dislodgement.

2. A thin uniform layer of epoxy was spread near the core edges and on small cavities along the sides.
3. For side preparation, cores were centered in a lathe (Plate 5.2b). The lathe was set to a cartridge feed of 5 threads/mm and to a cutting depth between 0.025 and 0.05 mm, depending on the desired degree of smoothness. No cooling was applied. Side preparation took about four hours per specimen but the results were worthwhile.
4. For end preparation, cores were placed inside a modified line centered mandrel which held the cores firmly (Plate 5.3a). A thin, uniform layer of epoxy was again applied on the end surfaces. The mandrel was centered in the chuck of the lathe using a dial gauge and firmly secured. A diamond bit cut the ends, resulting in flat, smooth parallel surfaces perpendicular to the longitudinal axis (Plate 5.3b).
5. Finishing the specimen sides and ends was done by filling hollows with epoxy and smoothing ridges with a high speed grinder, Dremel Model 395 (Plate 5.4a). Occasionally, a grinding table with 600 grit was used when a smoother end was required (Plate 5.4b). The epoxy applied during specimen preparation was removed during lathing, with the exception of small quantities used for filling hollows on the sides and ends.

5.2.4.2 Preparation of Hollow Cylinder Specimens

Hollow cylinder (HC) specimens are considered to be of specialized nature and very little is available in terms of standardized procedures for their preparation. Vutukuri et al. (1974) gives some preparation hints. The same tolerances as for the solid cylindrical specimens were followed, in addition to having the internal bore concentric with the outer circumferential surface of the specimen. The HC specimens were prepared from cores (D= 146 mm) obtained from the Allan Division (PCS). The inside diameter was set to 32 mm (testing equipment specifications) and the outside to 140 mm. The resulting wall thickness of 54 mm keeps the minimum specimen dimension to average crystal size ratio in the order of ten. Also, for the circular opening simulation tests (HC tests), it is recommended that the outer to inner diameter ratio be greater than four to avoid boundary stress effects. The specimen length is not a major limitation for circular opening simulation tests, but it should be larger than one diameter to minimize end effects (less than 200 mm due to equipment limitations).

Few hollow cylinder tests simulating openings in salt or potash have been published in the literature. Wawersik and Morgan (1987) tested hollow cylinder specimens of salt rock (halite) with 165 mm length, 127 mm outside and 38 mm inside diameters. Fuenkajorn and Daemen (1988a and b) carried out a borehole closure testing program on salt (halite) specimens with a length of 300 mm, outside diameter

of 150 mm and inside diameter of 25.4 mm.

Basically, the same specimen preparation procedure as for cylindrical specimens was adopted. The procedure for hollow cylinder specimen preparation is now described, stressing the points which differ from the cylindrical specimen preparation procedure:

1. Core ends were cut using a diamond cut-off saw.
2. Cores were firmly held by a chuck. A guide for drilling the central hole was positioned on the top end of the core (Plate 5.5a). This central hole guide is important to ensure that the diamond core barrel does not deviate from the desired longitudinal axis.
3. The chuck was positioned in a drill press. The internal bore was drilled by a diamond core barrel with outside diameter of 32 mm. Air was used as coolant and the drilling rate was about 5 cm/min. This procedure, although requiring special care in centering the core barrel guide and in positioning the chuck with the core in the drill press, did not present any problems. The results in terms of inner hole alignment and quality were satisfactory.
4. For side preparation, a solid shaft (mandrel) was placed through the inner hole and held firmly by the chuck of the lathe (Plate 5.5b). Ring nuts were used for tightening the core to the mandrel to avoid any relative rotation. A diamond bit cut the outside diameter and smoothed the circumferential surface. This procedure

produced concentric inside and outside diameters (Plate 5.6a).

5. For end preparation, the procedure was the same as for the cylindrical specimens, using epoxy, a line-centered mandrel, lathe and diamond bit (Plate 5.6b).

This procedure for hollow cylinder specimen preparation was very successful. Not only did it produce right circular cylinders but it also ensured that the inner hole was concentric with the outside circumferential surface. The differences in the bore alignment were less than 0.1 mm.

5.2.5 Specimen Characterization and Storage

After preparation, all specimens were measured (electronic caliper, +/-0.01 mm), weighed (electronic scale, +/-0.1 g), labelled and photographed. Then, the specimens were encased in a plastic bag, placed inside an air-tight wood box and surround with water absorbent material (silica-gel), in order to keep the moisture content as low as possible. This wood chamber containing the specimens was kept in an environmentally controlled room, with the temperature set at 25 +/- 0.5°C and relative humidity to 50 +/- 5%.

Five length and five diameter measurements were recorded for each specimen. The length values were taken equally distributed around the specimen while the diameter values were the average of two measurements taken 90° apart at 0.0L, 0.25L, 0.5L, 0.75L and 1.0L, where L is the

specimen length (Fig. 5.1). Tables 5.1 and 5.2 show the average physical measurements of solid and hollow cylindrical specimens before preparation (BP), before testing (BT) and after testing (AT). From these tables, one can detect the effectiveness of the specimen preparation technique and the final dimensions of specimens after testing.

The cylindrical specimens, obtained from the Cory Division (PCS) with grain sizes between 1 and 20 mm (average 4 to 7 mm), exhibited densities around 1990 kg/m³ (Table 5.3) while the hollow cylinder specimens, taken from the Allan Division (PCS) with grain sizes between 1 to 10 mm (average 4 to 7 mm), possessed a more compact structure with densities in the order of 2140 kg/m³ (Table 5.4).

5.3 Ultrasonic Velocity Tests

Ultrasonic velocity tests, measuring the compression wave and the shear wave velocities, V_p and V_s, were conducted on all specimens at several stages of the testing program. Standard procedures suggested in the literature (Gyenge and Herget, 1977; ISRM, 1978; ASTM D2845-83, 1988) were closely followed. The equipment (Gould advance OS-3300B oscilloscope, Terrametrics sonic pulse generator and transducers) was calibrated to obtain the zero time correction. Cylindrical specimens were tested along their central longitudinal axis and the hollow cylinder specimens on the thick wall at 90° intervals. The P- and S-wave

velocities for cylindrical and hollow cylinder specimens are summarized in Tables 5.3 and 5.4, respectively. For each pair of P- and S-wave velocities, the equivalent ultrasonic elastic constants, E_u and ν_u, were evaluated as also shown in Tables 5.3 and 5.4. The last column of the these tables presents the average and the standard deviation of the specimen results. These results are affected by moisture content, specimen preparation and loading history of specimens.

Cylindrical specimens (Plate 5.7a) were tested four times: just after specimen preparation (AP), after two weeks of contact with the water absorbent material (SG), just before testing (BT) and after testing (AT). In the second phase (SG), a consistent increase of the ultrasonic velocities compared to the velocities in the first phase (AP) was noticed. The chance of this occurring due to randon change is ≈0.004. From the results of this phase, Specimen TR01 was discarded for testing (V_p= 1849 m/s against an average of 3395 +/- 322 m/s). The third phase (BT) results did not show significant changes relative to the second phase (SG) results. The results of the fourth phase (AT) are discussed in Section 5.4 (individual description of the triaxial tests), because the stress path and state of specimens after testing clearly affect the densities and wave velocities. Figure 5.2 presents the evolution of the densities and ultrasonic velocities for cylindrical specimens during the testing program.

The hollow cylinder specimens (Plate 5.7b) were tested three times: before specimen preparation (BP), before testing (BT) and after testing (AT). The cores from Allan Division (PCS) were kept in water absorbent material until specimen preparation, when they were ultrasonic tested just before specimen preparation (BP) started. They were tested again before testing (BT). A comparison of the results of the first two phases (BP and BT) shows the effect of specimen preparation. The results of the second (BT) phase are consistently lower. Although no ultrasonic tests were run immediately following preparation, the specimens were measured and weighed. Some differences in the specimen weights were recorded between the after specimen preparation (AP) and before testing (BT) phases. These were not noticed in the cylindrical specimens. Figure 5.3 shows the average of the four ultrasonic tests, taken 90° apart, for each hollow cylinder specimen at the three phases of the testing program.

The ultrasonic velocities were consistently higher and presented less scatter in the hollow cylinder specimens than in the cylindrical specimens. This can be explained by the more compact structure of the potash from the Allan Division (PCS) since this material has higher density and smaller grain sizes (Lama and Vutukuri, 1978a). Also hollow cylinder specimens were obtained from cores, taken inside the mine wall, while the cylindrical specimens were prepared from block samples taken from the excavation face, therefore with

more damage.

The ultrasonic velocity tests provided estimates of the elastic constants (Jaeger, 1962; ASTM D2845-83, 1988)[2]. The ultrasonic elastic constants are known to be different from those obtained by static tests (Lama and Vutukuri, 1978a; Van Heerden, 1987; Eissa and Kazi, 1988), especially in specimens without any reconditioning. Tables 5.3 and 5.4 show the values of the ultrasonic elastic constants, E_u and ν_u, at all testing phases. Just before testing, the average ultrasonic Young's moduli for solid and hollow cylindrical specimens, ranged from 13 to 20 GPa (average 16.1 +/- 2.8 GPa) and from 22 to 24 GPa (average 22.8 +/- 1.7 GPa), respectively and the average Poisson's ratios were 0.31 +/- 0.05 and 0.29 +/- 0.04, respectively.

5.4 Triaxial Testing Program

In the last decade, there have been several efforts to determine the mechanical properties of salt rocks. Hardy et al. (1984) and Dusseault et al. (1985) discussed the type of laboratory data needed to study the behaviour of openings in salt rocks. Hardy (1988) pointed out that of all laboratory work, 46% provided creep data for the evaluation of the time-dependent response, 23% strength data for the assessment of failure criteria, and 31% produced elastic constants for the description of the elastic or instantaneous response. Several researchers have not only

---

[2] Expressions for calculating ultrasonic elastic constants presented by Gyenge and Herget (1977) are not correct.

carried out laboratory testing programs, but have also established effective triaxial testing procedures (Wawersik and Preece, 1984; Dusseault et al., 1985; Reeves and Unrau, 1988; Fuenkajorn and Daemen, 1988a).

Several factors are known to affect the mechanical response of salt rocks (Lama and Vutukuri, 1978b). Some of these factors such as texture (Skrotzki and Haasen, 1988b), mineral composition, water content (Urai et al., 1986; Spiers et al., 1988), origin (Hansen et al., 1984), impurities (Heard and Ryerson, 1986; Hansen et al., 1988), stress history (Lindner and Brady, 1984) and crystal size, are related to the material itself and its development history. Other factors such as applied deviatoric stress, strain rate, stress rate, stress level, stress path, temperature, specimen size and sampling, are related to the testing procedure. Most researchers have concentrated on the effects of temperature, confining stress level and deviatoric stress, using uniaxial and conventional triaxial compression tests. Few have studied the other factors. Senseny (1984) discussed the effects of specimen size and stress path. Farmer and Gilbert (1984) conducted tests at different strain rates. Guessnoss et al. (1987 and 1988) simulated the effect of damage due to sampling. All these aspects have caused salt-rock researchers to seek more appropriate and effective testing procedures, almost always different from those standardized by societies such as ISRM and ASTM.

This triaxial testing program has no intention of evaluating all testing parameters that could affect the mechanical response of salt rocks, more specifically potash. Only stress path, stress level, deviatoric stress and temperature are focused. The high pressure and temperature system (HPTS) was designed to control stress, following any axisymmetric stress path and including creep stages for long periods. Features such as controlled stress and strain rates, are not available yet. Control of temperature is also implemented in the HPTS, but all tests were run at constant room temperature (25 +/- 0.5°C). Basically, the triaxial testing program covered the time-dependent response of cylindrical specimens under different loading conditions and subjected to two stress paths, conventional triaxial compression (CTC) and J1-constant triaxial compression (JTC). The latter path was chosen to more closely follow the state of stress and stress path near a circular opening. Quick unload/reload cycles were also executed during the tests for the evaluation of elastic constants.

The triaxial testing procedure is summarized below:

1. The testing cell is assembled in the triaxial setup according to the specimen size (Appendix A). A thin coat of dry lubricant is applied to the specimen ends and loading platens to reduce friction effects. Dry lubricant is also applied to the membranes to facilitate their recovery after testing without damaging either the specimen or membrane.

2. The specimen is hydrostatically loaded to a stress level representative of the natural in-situ stresses. Confining and axial pressures are increased such that the axial stress on the specimen always exceeds the confining pressure but by no more than 1/10 of the uniaxial compressive strength, σ_c (ISRM, 1983). Senseny (1985) suggested a load increment of 5% of the desired confining pressure. Loading steps of 1 MPa were applied in this testing program since the desired stress level was 20 MPa and the uniaxial compressive strength for salt rocks ranges from 10 to 40 MPa (Lama and Vutukuri, 1978a) with a typical average of 23 MPa (Kelsall and Nelson, 1983). Pressures are kept constant at this natural in-situ stress level for 72 hours to reverse post-sampling stress relief effects (crack closure, etc.). Wawersik and Preece (1984) and Senseny (1985) suggested eight to twelve hours (overnight), but Reeves and Unrau (1988) recommended that the in-situ stress state should be maintained until changes in the strain readings (axial and radial) fall below ten microstrains per day. The latter criterion seems to be more appropriate but a minimum period of 72 hours should also be obeyed according to our experience (Chapter 6).
3. The specimen is loaded, as quickly as possible, to the first stage of deviatoric stress, according to the prescribed stress path. This deviatoric stress state is then maintained for a certain period of time as a creep

stage. Some tests employ multiple loading stages in order to obtain more information per specimen, due to the limited number of available specimens and the very extensive amount of time taken for specimen preparation and cell assembly (Reeves and Unrau, 1988).

Cross-sectional area correction was not made during testing. Therefore, they were constant axial load tests and not as they are supposed to be, constant axial stress tests. This, although seemingly contradictory to earlier test requirements, can be justified. In order to carry out a test with cross-sectional area correction, two requirements must be fulfilled: both the instruments monitoring the area change and their calibration curves must be reliable. Furthermore, the correction curve and area change have to be input to the microprocessor, so that it can evaluate the current cross-sectional area and make adjustments to the axial loading, in such a way as to produce a constant axial stress. If errors in these requirements occurred, the laboratory system would produce a completely erratic stress path and the whole test could be lost. In regard to monitoring, high quality instruments and data acquisition (hardware and software) are necessary to obtain reliable measurements (avoiding electronic noise and extreme signal peaks). Calibration curves have to be repeatable and applicable to all ranges of pressure and deformation. Such confidence in a system is only achieved after much experience and many tests.

The HPTS has just been developed and used for the first time during this research. Although the calibration tests were carefully programmed and executed, it was decided to evaluate the system further, before implementing a software routine for cross-sectional area correction. Some researchers (e.g., Wawersik, 1985) prefer an intermediate solution, only relying on axial displacement measurements and assuming no volume change during creep, to perform the area correction. This assumption may lead to the same type of errors as assuming no area correction. In conclusion, while the ideal is to execute constant axial stress creep tests, these can only be achieved after experience and confidence are gained with the laboratory system, thereby avoiding loss of specimens, data and time.

For triaxial tests, the axial (PA) and confining (PE) pressure transducers, axial displacement (DA) LVDT and cell volume change (VCE) device were monitored (Appendix C). The HPTS was programmed to follow a given stress path. Some reprogramming was necessary in view of the observed specimen responses. These changes, whenever they occurred, are indicated in the individual test description. The actual stress path and data for each test are presented in Appendix E as well as the plates taken before and after testing the specimens. Physical measurements of the cylindrical specimens before and after testing are shown in Table 5.1. Finally, it is important to mention that only the first stages of all tests were programmed to obtain the data

needed for this research (Chapter 6). The other stages were for testing the HPTS performance under limit conditions of applied stress and deformation, since it was the first time this system tested geotechnical materials.

5.4.1 Conventional Triaxial Compression (CTC) Tests

Conventional triaxial compression (CTC) tests are those in which the confining pressure (PE) is kept constant and the axial stress (PA) increases. Creep stages were added at certain deviatoric stress (PA-PE) levels. Four CTC tests were conducted. They are described in chronological order.

5.4.1.1 CTC Test 1 (Table and Plate E.1, Figs. E.1 and E.2)

This test was designed to measure the ultimate strength. No creep stages under triaxial loading were initially programmed. Specimen TR02 was hydrostatically loaded to 20 MPa. An unload/reload cycle to 10 MPa was performed before the specimen underwent a creep stage for three days. Another unload/reload cycle was executed and then, the specimen was hydrostatically unloaded to 5 MPa. Keeping the confining pressure constant at 5 MPa, the specimen followed a conventional triaxial compression path. The system reached its axial loading capacity (120 MPa for a cylindrical specimen of 100 mm diameter) and the specimen did not fail. At this time, a creep stage (PA = 120 MPa and PE = 5 MPa) was included. The test ended due to a sudden drop of the axial pressure and an increase of the axial

displacement. This may have resulted from the crushing of the insulator caps since no cracks or other signs of failure were found on the specimen surface. Measurements after testing showed an increase of the density and compression wave velocity, which indicate a more compact structure after testing. One problem noticed was that the external volume change device (VCD) stopped recording during the hydrostatic creep stage. The problem was identified as a malfunction of the LVDT, which was subsequently replaced.

5.4.1.2 CTC Test 2 (Table and Plate E.2, Figs. E.3 and E.4)

This test was also designed to measure the ultimate strength. No creep stages under triaxial loading were initially programmed. The system hydrostatically loaded Specimen TR03 to 20 MPa. An unload/reload cycle to 10 MPa was carried out and followed by a creep stage for three days. Another unload/reload cycle to 15 MPa was performed before starting the conventional triaxial compression path with the confining pressure constant at 20 MPa. The test ended due to leakage between the top cap and the axial ram. Investigation showed that when specimens undergo large axial displacement and consequently large radial strain, the external membrane gets shorter, thereby losing the contact point with the top seal and causing the leak. Unfortunately, this problem cannot be overcome without major changes in the equipment design (Chapter 4). This leak caused some wetting of the specimen by silicon oil, which was later confirmed by

higher specimen weights after testing. This may also have affected the results of the last series of ultrasonic velocity tests (Section 5.3) which showed a decrease in the compression wave velocity. Examining the shape of the specimen after testing, two aspects were noticed. First, it was suspected that the insulator caps (sulfaset) were not working properly. An outer ring of the bottom sulphur cap was completely destroyed and the remaining part, with a diameter smaller than the specimen, was very stiff. Therefore, it induced a punch failure mode in the specimen. Second, some vertical cracks were present at the circumferential surface of the specimen. It is believed that these cracks were caused by the sudden depressurization of the chamber due to the leak (PE = 0), causing the specimen to be subjected momentarily to an unconfined state under a very high axial stress. These cracks were responsible for a looser structure, yielding lower values of density and ultrasonic wave velocities.

5.4.1.3 CTC Test 3 (Table and Plate E.3, Figs. E.5 and E.6)

Specimen TR04 was hydrostatically loaded to 20 MPa and an unload/reload cycle to 15 MPa performed. A three-day long creep stage under hydrostatic loading followed. Another unload/reload cycle to 15 MPa was executed and then, a conventional triaxial compression path with the confining pressure at 20 MPa was followed. Three creep stages were programmed with axial stresses of 30, 40 and 50 MPa,

respectively. The test was also terminated during the third creep stage, due to a leak between the top cap and axial ram. The deformation occurred very quickly, leading to problems in the pressure control system. Pressure intensifiers are limited by the travel (stroke) distance of the piston. Recharging of the intensifiers is a manual operation as explained in Appendix B. When full extension is reached during the night, the system is unable to maintain a constant pressure and a pressure drop occurs as the specimen deforms. This problem always took place overnight during the last creep stage. The two problems described in the previous tests were also evident in this test. The malfunctioning of the insulator caps was confirmed and this led to the design of a highly polished, lower platen (stainless steel SS-316), with a spherical seat. This new platen was used in all remaining tests. Again, the specimen exhibited some cracks and a decrease in the density and compression wave velocity values, indicating a looser structure due to fracturing.

5.4.1.4 CTC Test 4 (Table and Plate E.4, Figs. E.7 and E.8)

The system hydrostatically loaded Specimen TR06 to 20 MPa and performed an unload/reload cycle to 15 MPa. The specimen was kept under creep for three days, when another unload/reload cycle to 15 MPa was carried out. Then, the specimen was hydrostatically loaded to 35 MPa, where the conventional triaxial compression path started. Three creep stages were initially programmed with axial stresses of 60,

85 and 110 MPa, respectively. Before starting the third creep stage, the test was reprogrammed, because very small deformations had been measured to this point. The confining pressure was dropped to 20 MPa and two new creep stages, with axial stresses at 45 and 70 MPa, were added. Two additional creep stages were included with the confining pressure dropped to 5 MPa and the axial stresses increased to 55 and 105 MPa, respectively. The test ended before starting the last creep stage (PA= 105 MPa) due to a leak between the top cap and the axial ram. The specimen shape after testing was almost cylindrical, slightly barreled, with ends perfectly parallel to each other and normal to the longitudinal axis. This shows the effectiveness of the new lower platen with spherical seat. With no cracks and a more compact structure after testing, the ultrasonic tests recorded higher values for the wave velocities.

5.4.2 J1-Constant Triaxial Compression (JTC) Tests

The specimens are first loaded hydrostatically to a certain stress level, defined by the first stress invariant ($J1 = PA + 2PE$). Then, they are loaded such that the axial stress (PA) is increased and the confining pressure (PE) is decreased ($\Delta PA = -\Delta PE/2$), keeping the same original value of the first stress invariant (J1). Creep stages were added at certain deviatoric stress (PA-PE) levels. Three JTC tests were conducted and are described below.

5.4.2.1 JTC Test 1 (Table and Plate E.5, Figs. E.9 and E.10)

Specimen TR05 was hydrostatically loaded to 15 MPa and maintained under creep for three days. An unload/reload cycle to 10 MPa was performed and then, the J1-constant triaxial compression path started. Three creep stages were initially programmed. For each creep stage, the axial stress was increased by 10 MPa and the confining pressure reduced by 5 MPa. Just before beginning the second creep stage, the test ended due to a leak between the top cap and the axial ram. Again, the specimen shape after testing was only slightly barreled and it did not exhibit any cracks. Higher values of density and ultrasonic velocities were recorded after testing.

5.4.2.2 JTC Test 2 (Table and Plate E.6, Figs. E.11 and E.12)

Specimen TR07 was hydrostatically loaded to 25 MPa and an unload/reload cycle to 15 MPa performed. The specimen underwent a hydrostatic creep stage for three days, when the J1-constant triaxial compression path began. Three creep stages were initially programmed. For each creep stage, the axial stress was increased by 10 MPa and the confining pressure reduced by 5 MPa. The test terminated during the second creep stage due to a leak between the top cap and the axial ram. Although the specimen shape, after testing, remained cylindrical with some barrelling and the ends in perfect condition, the specimen exhibited some fracturing

near the surface due, probably, to the loss of confining pressure at high axial stress (45 MPa). Ultrasonic velocity tests gave results in agreement with those from other specimens (higher values after testing), leading to the conclusion that the inside core of the specimen was intact and fracturing occurred only at the surface. The density decreased due to surficial cracking.

5.4.2.3 JTC Test 3 (Table and Plate E.7, Figs. E.13 and E.14)

The system hydrostatically loaded Specimen TR08 to 35 MPa, performed an unload/reload cycle to 25 MPa and executed a creep stage for three days. Then, the J1-constant triaxial compression path started. Three creep stages were initially programmed. For each creep stage, the axial stress was increased by 20 MPa and the confining pressure reduced by 10 MPa. The test ended in the first creep stage due to a leak between the top cap and the axial ram. Great difficulty was encountered in controlling the pressure during the creep stage due to the fast rate of deformation. The problem of limited intensifier piston stroke described previously, was also encountered. Once more higher values of density and ultrasonic velocities were measured after testing.

It is important to note that all tests ended due to the leak between the top cap and the axial ram have subjected the specimens to axial deformations of at least 10%. Therefore, before leakage and test termination, reliable

data were obtained for all those specimens (Chapter 6).

Comparison of the density and ultrasonic wave velocity values, before and after testing, shows some interesting results, although no conclusions can be drawn on the effects of different stress paths (CTC and JTC tests). Neglecting the specimens (TR03 and TR04) that exhibited cracks and fractures, all presented higher values of density and compression wave velocities and consequently greater ultrasonic elastic constants, after testing, even those undergoing 10 to 15% of creep deformation. This suggests the development of a more compact structure. Fairhurst et al. (1979) found a similar result when they compared the unconfined strengths of specimens subjected to creep (but not failed) with those of specimens of the same composition and grain size. The strength after creep was considerable greater than that of a virgin specimen. On the other hand, if fracturing is induced by excessive creep deformation or for any other reason, the rock structure deteriorates very rapidly and fails, as shown by the other specimen results. These results indicate that salt specimens do not lose their load-supporting capability with creep deformation, provided they are not subject to loads sufficient to produce tertiary creep (Fairhurst et al., 1979).

5.5 Hollow Cylinder Testing Program

Although hollow cylinder tests in laboratory programs of geotechnical materials have been conducted regularly since 1957, very few tests have been done as circular opening simulation tests, especially in salt rock. Lately, salt rock researchers (Wawersik and Morgan, 1987; Fuenkajorn and Daemen, 1988a and b; Hambley et al., 1988) have indicated that the use of hollow cylinder cells with independent axial, internal and external pressure control would provide an important means of addressing the behaviour of circular openings in salt rocks subjected to uniform stress fields. There is no testing procedure established yet for this kind of experimentation. A testing procedure similar to that specified for triaxial testing was therefore adopted:

1. The specimen was assembled in the cell following the procedure for hollow cylinder specimen set-up (Appendix A).
2. The specimen was hydrostatically loaded to the equivalent in-situ stress field and maintained at this level for 72 hours.
3. A deviatoric pressure (PI-PE) was applied to the specimen by changing the internal pressure (PI) and keeping the external pressure (PE) constant. The internal pressure could be increased or decreased depending on the effect to be modelled.
4. The axial stress (PA) was either kept constant for

axisymmetric loading (HCAL) tests or changed in such a manner as to maintain zero axial displacement for plane strain (HCPS) tests.

5. A creep test for a given period of time and loading condition was conducted. Occasionally, multi-stage tests were performed to get more information from a single specimen, even though the complications due to stress history dependence of salt rock were recognized.

The hollow cylinder tests were divided into two groups according to the axial loading condition:

i) HCAL - hollow cylinder axisymmetric loading tests with constant axial stress.

ii) HCPS - hollow cylinder plane strain tests with axial stress changes in order to maintain zero axial displacement.

Table 5.2 presents the physical measurements of the hollow cylinder specimens before and after testing. Hollow cylinder experiments are described below drawing particular attention to the stress paths followed and to the problems that occurred during their execution. Results are presented in Chapter 6. Again, the first stages of the hollow cylinder tests were designed to provide the data needed for comparison with the creep model predictions. Then, other stages followed to evaluate the system performance under limit conditions of applied deviatoric pressure.

5.5.1 HCAL Tests

Four hollow cylinder tests under constant axial stress (axisymmetric loading) were carried out.

5.5.1.1 HCAL Test 1

Specimen HC04 was hydrostatically loaded to 15 MPa. This mean pressure was kept constant for three days, when an unload/reload cycle to 10 MPa was performed. Then, the specimen was subjected to three creep stages of three days each, with internal pressures at 10, 5 and 1.5 MPa. The internal pressure was then increased to 15 MPa and maintained for one day (hydrostatic pressure). The specimen was subjected to three more creep stages of three days each, but with internal pressures of 20, 25 and 30 MPa. During the last creep stage (PI= 30 MPa), the system encountered difficulties in maintaining a constant internal pressure and leakage was detected in the internal volume. This problem was the first indication that leakage could be a problem in HC tests, when the internal pressure is much higher than the outside pressure (axial and external).

5.5.1.2 HCAL Test 2

Specimen HC05 was hydrostatically loaded to 35 MPa. A quick unload/reload cycle to 25 MPa was performed and then, the specimen was subjected to a hydrostatic creep stage for three days. As described for HCAL Test 1, three creep stages with internal pressure reduction (25, 15 and 5 MPa) and three other stages with internal pressure increases (45, 55

and 65 MPa) were programmed. Unfortunately, this test encountered problems in the pressure control from the beginning. Some internal leaking in the bore volume was noticed during the hydrostatic creep stage. During the first creep stage (PI= 25 MPa), the experiment was terminated due to excessive leakage. The cause of the leakage was difficult to determine, since all pressures dropped rapidly. The cell was disassembled for a complete review of all fittings and parts. The specimen was recovered and exhibited radial cracks (Plate 5.8), indicating that, at least momentarily, the internal pressure was higher than the external pressure.

5.5.1.3 HCAL Test 3

The third test of this series was performed on Specimen HC02. It was designed to be similar to HCAL Test 2, but at a lower stress level. The specimen was loaded to 25 MPa and an unload/reload cycle to 15 MPa executed. During the hydrostatic creep stage (after 2000 min), the external pressure started dropping due to leakage through the external electrical connector. The test was ended and the connector replaced by a plug. A series of performance tests were subsequently undertaken to ensure the adequacy of the remedial measures.

5.5.1.4 HCAL Test 4

Since the deformations measured in hollow cylinder tests up to this point were very small, the last HC axisymmetric loading test was designed to incorporate only

two, albeit longer, creep stages. Specimen HC01 was hydrostatically loaded to 20 MPa and allowed to creep for three days. Then, the internal pressure was dropped to 1 MPa where it was maintained for four weeks. The internal pressure was then increased to 39 MPa and maintained for a few days. The system encountered difficulties in maintaining the internal pressure constant at this level and the test was ended.

5.5.2 HCPS Tests

Two hollow cylinder tests under plane strain in the axial direction (DA= 0) were executed.

5.5.2.1 HCPS Test 1

Specimen HC03 was loaded to 35 MPa and kept under hydrostatic creep for three days. Two creep stages of seven days each, with internal pressures at 18 and 1 MPa followed. Then, the internal pressure was increased to the hydrostatic stress level (35 MPa) and maintained for one day. The third creep stage with an internal pressure of 35 MPa ran only for a few days, when difficulties in controlling the internal pressure were again encountered. Problems also developed in the internal pressure intensifier due to excessive piston friction (350 kPa) and in the bore convergence device (malfunction of the electronic connection). Unfortunately, all bore convergence data were lost. A complete inspection of the internal pressure intensifier was performed and the rolling diaphragm and seals replaced.

5.5.2.2 HCPS Test 2

Specimen HC06 was hydrostatically loaded to 20 MPa and allowed to creep for three days. Two creep stages of seven days each, with internal pressures of 11 and 2 MPa followed. The internal pressure was increased to 20 MPa and maintained for one day. Two more creep stages of seven days each, with internal pressures of 29 and 38 MPa were executed. During the last creep stage, the internal pressure could not be maintained within the specifications and the test was ended.

5.6 Summary and Conclusions

A laboratory program of triaxial and hollow cylinder tests in potash was executed. Specimens for the triaxial testing program were prepared from block samples obtained from the Cory Division (PCS) and specimens for the hollow cylinder testing program were prepared from cores obtained from the Allan Division (PCS). Laboratory core drilling techniques and specimen preparation procedures were successfully implemented. The geometric measurement tolerances reached were in the order of 0.1 mm. Ultrasonic velocity tests were carried out on all specimens. They show some effects of specimen preparation, moisture content and loading history. It was demonstrated that the specimens prepared from the Allan Division cores have higher densities and ultrasonic velocities than those from the Cory Division. This was due to the quality of the sampling procedure and mainly to the material itself. Potash from the Allan

Division presented smaller grains and a more compact structure.

The laboratory triaxial testing program concentrated on the time-dependent properties of the specimens, although some quick unload/reload cycles were executed to evaluate the elastic/instantaneous properties. Triaxial tests followed two different stress paths, conventional triaxial compression (CTC) and J1-constant triaxial compression (JTC), including creep stages at several confining and deviatoric stress levels. Insulator (sulfaset) caps were unable to accommodate large diametric deformations and were replaced by a lower platen with a spherical seat. The shape of specimens after testing remained almost cylindrical with satisfactory end conditions, even after undergoing axial deformations of 5 to 15%.

The hollow cylinder testing program ran satisfactorily except for the two tests that presented leakage through the electrical connector. In general, the deformations measured were small and the shapes of the specimens after testing were similar to those before testing (Plate 5.9). Longer duration tests will be needed for more conclusive data on the simulation of circular openings in salt rocks using hollow cylinder tests as model experiments.

The laboratory testing system (HPTS) proved to be efficient, although leakage problems developed after large deformations (≃15%) during triaxial testing. Also, pressure control difficulties were encountered when the internal

pressure was higher than the external pressure in hollow cylinder tests. Most of these problems occurred during the test stages designed to evaluate the HPTS performance under limit conditions (e.g., excessive deformation or high deviatoric stress). Before the problems have happened, the system had proven to provide reliable data, as shown in Chapter 6. Although the equipment and testing procedures could be improved, the HPTS was found to present the desired flexibility to accommodate different specimen sizes, test types and stress paths. It demonstrated considerable potential for determining time-dependent, strength and elastic properties, and for simulating in-situ conditions near underground openings.

Table 5.1 Physical measurements of cylindrical specimens

Specimen No.		TR01	TR02	TR03	TR04	TR05	TR06	TR07	TR08
L (mm)	BT	153.43 +/-0.09	171.20 +/-0.06	179.62 +/-0.06	180.25 +/-0.04	187.67 +/-0.05	192.81 +/-0.05	200.52 +/-0.03	205.13 +/-0.06
	AT	-x-	159.43 +/-0.68	163.25 +/-0.72	154.37 +/-0.35	161.61 +/-0.02	170.75 +/-0.44	179.80 +/-0.09	179.67 +/-0.15
D (mm)	BT	99.36 +/-0.07	97.82 +/-0.07	98.22 +/-0.04	99.84 +/-0.11	99.26 +/-0.10	98.44 +/-0.06	100.16 +/-0.06	100.23 +/-0.07
	AT	-x-	99.65 +/-0.26	106.07 +/-2.32	113.90 +/-2.73	106.11 +/-2.23	104.37 +/-2.67	109.36 +/-5.44	105.39 +/-2.25
L/D	BT	1.54	1.75	1.83	1.81	1.89	1.96	2.00	2.05
	AT	-x-	1.60	1.54	1.36	1.52	1.64	1.64	1.70
V (cm^3)	BT	1190	1283	1361	1411	1452	1467	1580	1619
	AT	-x-	1243	1447	1575	1429	1463	1689	1567

Table 5.2 Physical measurements of hollow cylinder specimens

Specimen No.		HC01	HC02	HC03	HC04	HC05	HC06
L (mm)	BP	165.34+/-0.34	158.58+/-0.62	209.28+/-0.76	209.60+/-1.14	194.16+/-0.71	179.08+/-0.49
	BT	162.15+/-0.09	155.90+/-0.05	181.09+/-0.02	204.98+/-0.09	191.14+/-0.09	175.83+/-0.03
	AT	162.65+/-0.25	155.18+/-0.13	181.88+/-0.07	205.00+/-0.08	186.93+/-0.10	175.52+/-0.19
D (mm)	BP	142.82+/-0.28	142.92+/-0.26	144.08+/-0.60	142.30+/-0.54	143.58+/-0.38	142.62+/-0.19
	BT	139.46+/-0.09	138.61+/-0.14	139.35+/-0.04	137.96+/-0.10	139.00+/-0.06	139.00+/-0.03
	AT	139.06+/-0.09	139.10+/-0.10	138.25+/-0.26	137.86+/-0.07	140.83+/-0.37	138.94+/-0.08
L/D	BP	1.16	1.11	1.45	1.47	1.35	1.26
	BT	1.16	1.12	1.30	1.49	1.38	1.26
	AT	1.17	1.12	1.32	1.49	1.33	1.26
d_b (mm)	BT	31.92+/-0.06	31.93+/-0.09	32.03+/-0.05	31.55+/-0.01	32.00+/-0.06	31.96+/-0.05
	AT	31.48+/-0.31	31.83+/-0.11	*	31.90+/-0.01	33.19+/-0.28	31.96+/-0.23
V (cm^3)	BP	2649	2544	3412	3333	3144	2861
	BT	2347	2228	2616	2904	2747	2527
	AT	2344	2235	2584	2896	2750	2520

* not measured

Table 5.3 Ultrasonic velocity test results for cylindrical specimens (* not considered in the average)

Spec.No.		TR01 *	TR02	TR03	TR04	TR05	TR06	TR07	TR08	AVG
ρ kg/m^3	AP	1974	2009	1995	2007	2013	2009	2058	1991	2012 +/-22
	SG	1974	2009	1995	2006	2012	2009	2058	1991	2011 +/-22
	BT	-	2008	1995	2006	2012	2009	2058	1991	2011 +/-22
	AT	-	2078	1877	1797	2045	2016	1925	2056	1971 +/-106
V_p m/s	AP	1582	1529	2871	3679	2932	3268	3399	3156	2976 +/-695
	SG	1849	2853	3151	3835	3412	3506	3646	3363	3395 +/-322
	BT	-	2853	2945	3679	3181	3214	3518	3108	3214 +/-295
	AT	-	3623	2120	1288	3673	3561	3826	3152	3035 +/-962
V_s m/s	AP	908	839	1648	1733	1360	1769	1892	1465	1529 +/-354
	SG	1030	1571	1590	1918	1721	1948	2025	1799	1796 +/-178
	BT	-	1600	1590	1897	1754	1854	1947	1668	1759 +/-145
	AT	-	1594	1020	377	1701	1943	1635	1695	1424 +/-540
E_u MPa	AP	4082	3634	13536	16368	10150	16257	18787	11650	12912 +/-5055
	SG	5338	12705	13402	19670	15859	19463	21557	16754	17059 +/-3334
	BT	-	13067	13049	19045	15866	17274	19954	14373	16090 +/-2782
	AT	-	14571	5260	742	16223	19635	14399	15357	12312 +/-6724
ν_u	AP	0.254	0.284	0.249	0.357	0.362	0.293	0.276	0.363	0.312 +/- 0.047
	SG	0.275	0.283	0.329	0.333	0.329	0.277	0.277	0.299	0.304 +/- 0.026
	BT	-	0.271	0.294	0.319	0.282	0.251	0.279	0.298	0.285 +/- 0.022
	AT	-	0.380	0.349	0.453	0.363	0.288	0.388	0.297	0.360 +/- 0.056

Table 5.4 Ultrasonic velocity test results for hollow cylinder specimens (* data sheet lost)

Spec. No.		HC01	HC02	HC03	HC04	HC05*	HC06	AVG
ρ kg/m^3	BP	2137	2132	2091	2117	2083	2138	2116 +/-24
	AP	2162	2172	2119	2133	2111	2171	2145 +/-28
	BT	2155	2174	2114	2131	2111	2165	2141 +/-27
	AT	2159	2167	2140	2137	2108	2171	2147 +/-24
V_p m/s	BP	4134	3604	3805	3553	3807	4165	3845 +/-257
	BT	4042 +/-263	3660 +/-245	3653 +/-256	3728 +/-79		3536 +/-91	3724 +/-252
	AT	3691 +/-72	3786 +/-76	3798 +/-227	4339 +/-46		3883 +/-133	3899 +/-260
V_s m/s	BP	2093	2059	2032	2015	2039	2082	2053 +/-30
	BT	1969 +/-97	1928 +/-101	2013 +/-55	2138 +/-77		2052 +/-63	2020 +/-103
	AT	2120 +/-69	2050 +/-59	2129 +/-58	2516 +/-32		2198 +/-105	2202 +/-178
E_u MPa	BP	24850	22744	22456	21720	22491	24716	23163 +/-1301
	BT	22421 +/-1967	22405 +/-2353	22062 +/-1542	24354 +/-942		22701 +/-1167	22788 +/-1704
	AT	24260 +/-887	23539 +/-1229	24609 +/-1332	34044 +/-817		26499 +/-2047	26590 +/-4128
ν_u	BP	0.328	0.258	0.301	0.263	0.299	0.333	0.297 +/- 0.031
	BT	0.340 +/- 0.033	0.315 +/- 0.016	0.286 +/- 0.021	0.252 +/- 0.042		0.245 +/- 0.026	0.288 +/- 0.045
	AT	0.251 +/- 0.037	0.293 +/- 0.008	0.268 +/- 0.035	0.242 +/- 0.009		0.262 +/- 0.034	0.263 +/- 0.031

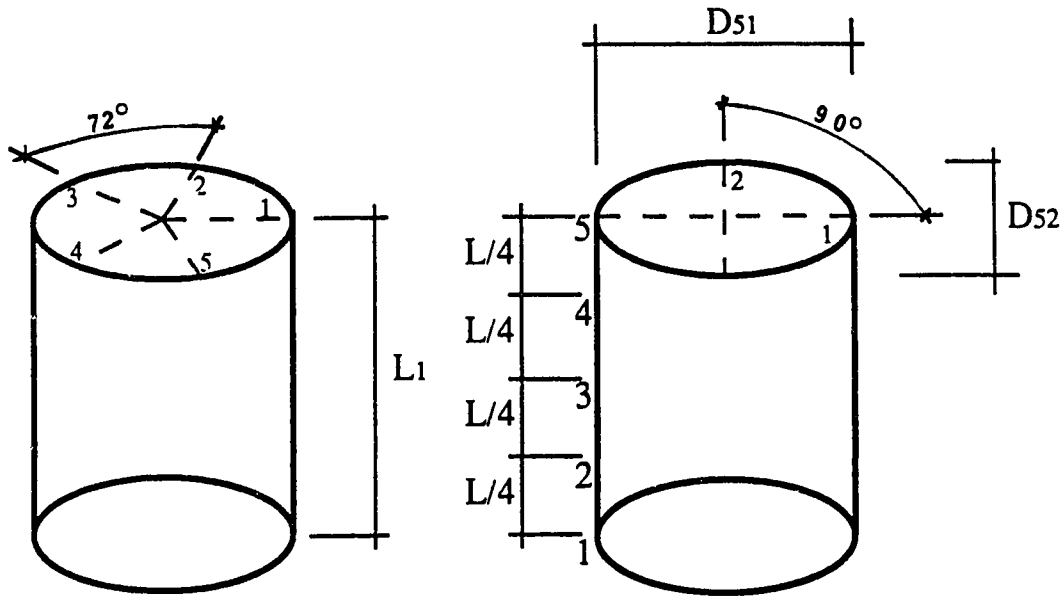

$$Di = (Di1 + Di2) / 2$$

$$L = \sum_{1}^{5} Li / \sum_{1}^{5} i \qquad D = \sum_{1}^{5} Di / \sum_{1}^{5} i$$

i	1	2	3	4	5	Average
L	153.48	153.51	153.40	153.28	153.48	153.43
D	99.46	99.39	99.36	99.30	99.30	99.36

Figure 5.1 Physical measurements of specimens (example for Specimen TR01)

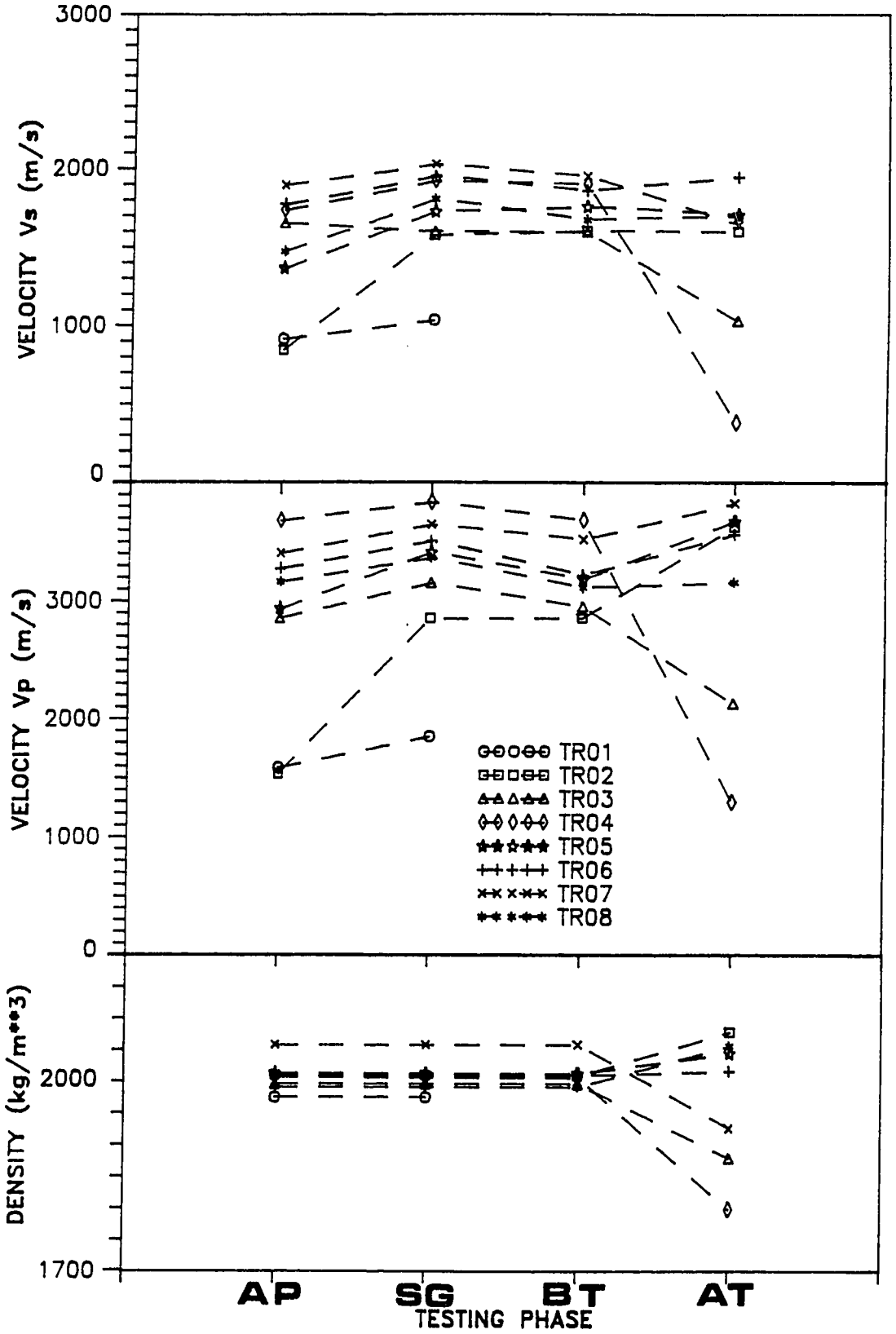

Figure 5.2 Densities and ultrasonic wave velocities of cylindrical specimens

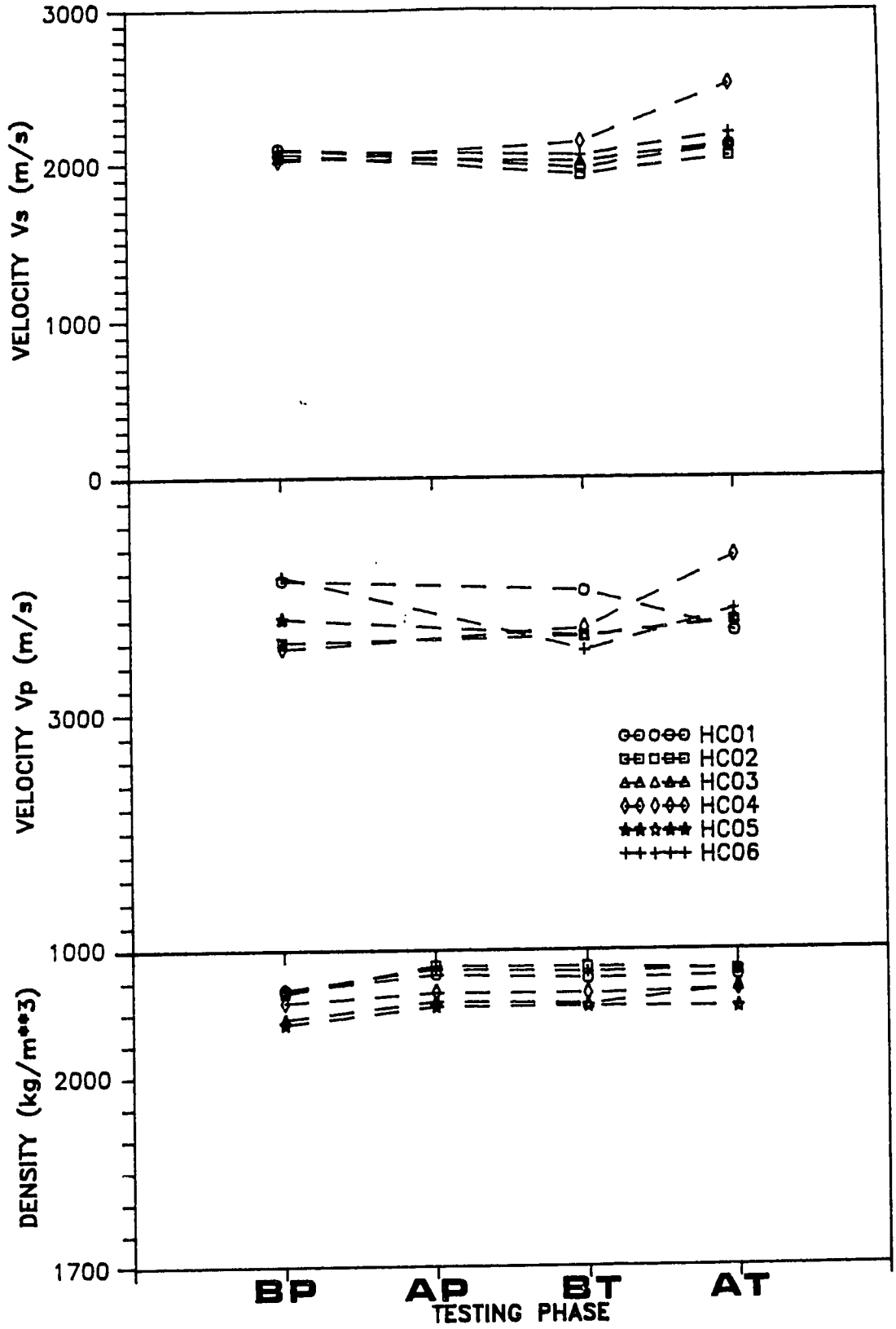

Figure 5.3 Densities and ultrasonic wave velocities of hollow cylinder specimens

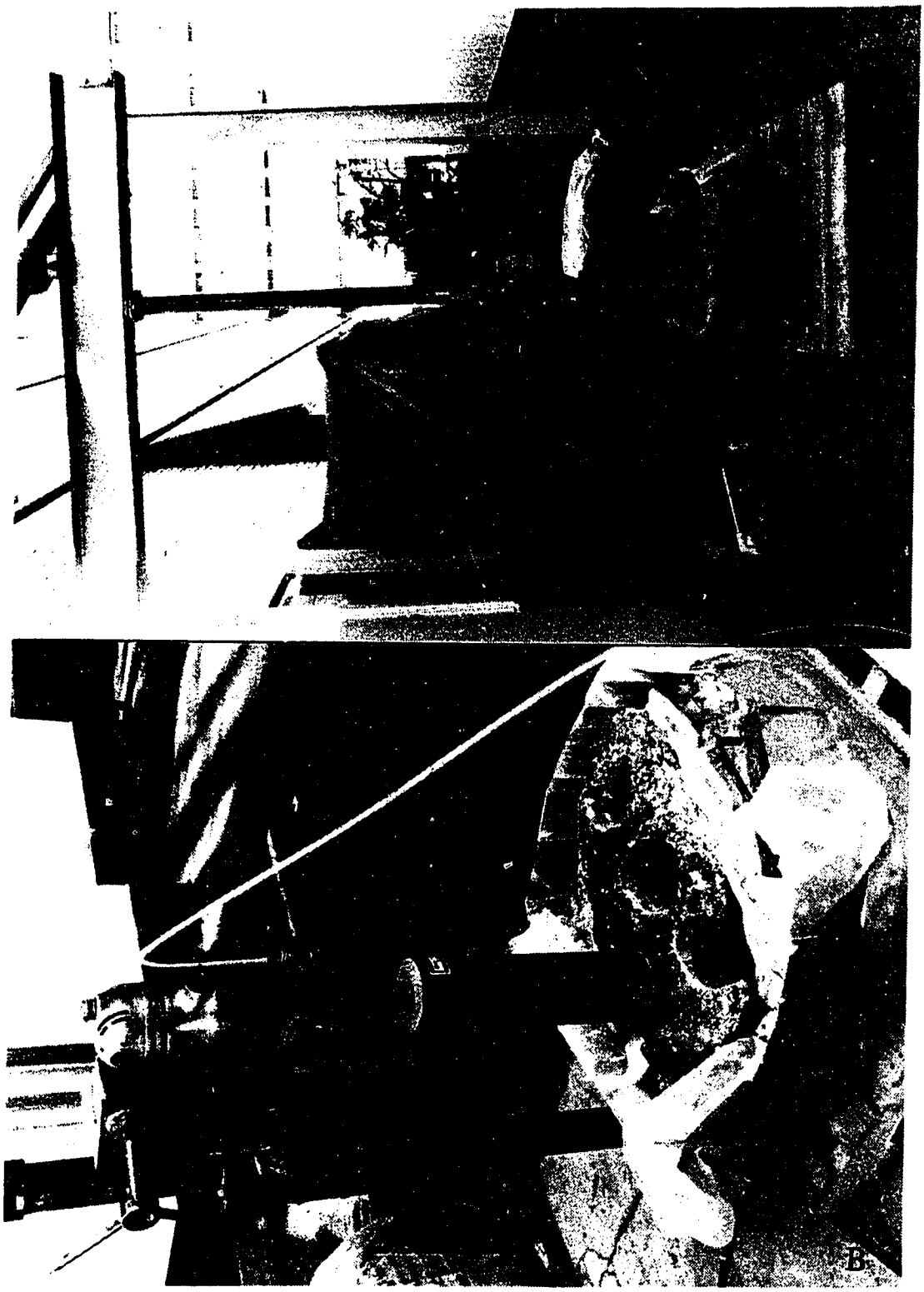

Plate 5.1 Laboratory Core Drilling Scheme; (A) General view; (B) Core barrel positioned over block sample

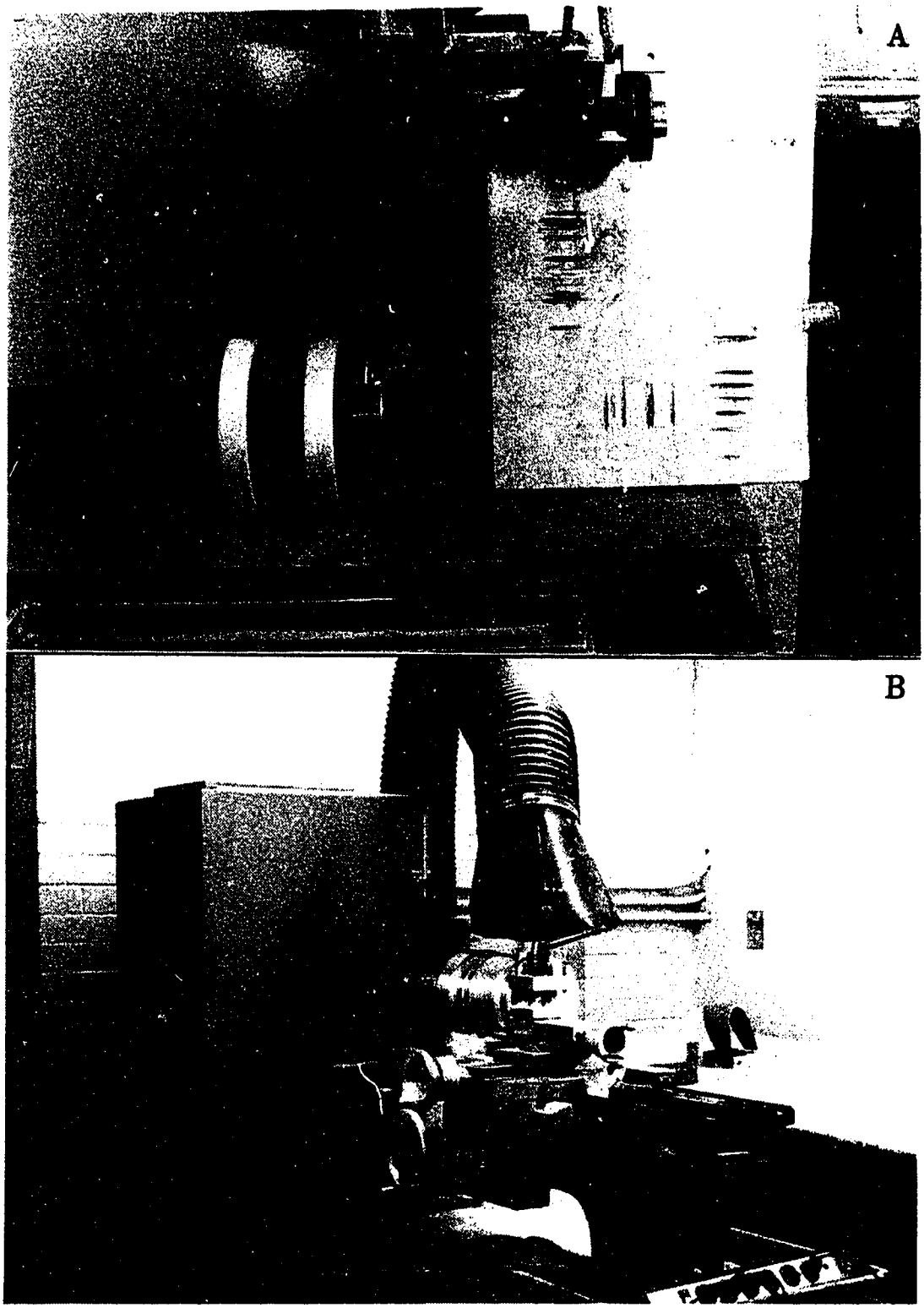

Plate 5.2 Cylindrical Specimen Preparation; (A) End cutting by diamond cut-off saw; (B) Lathe and large-scale vacuum cleaner

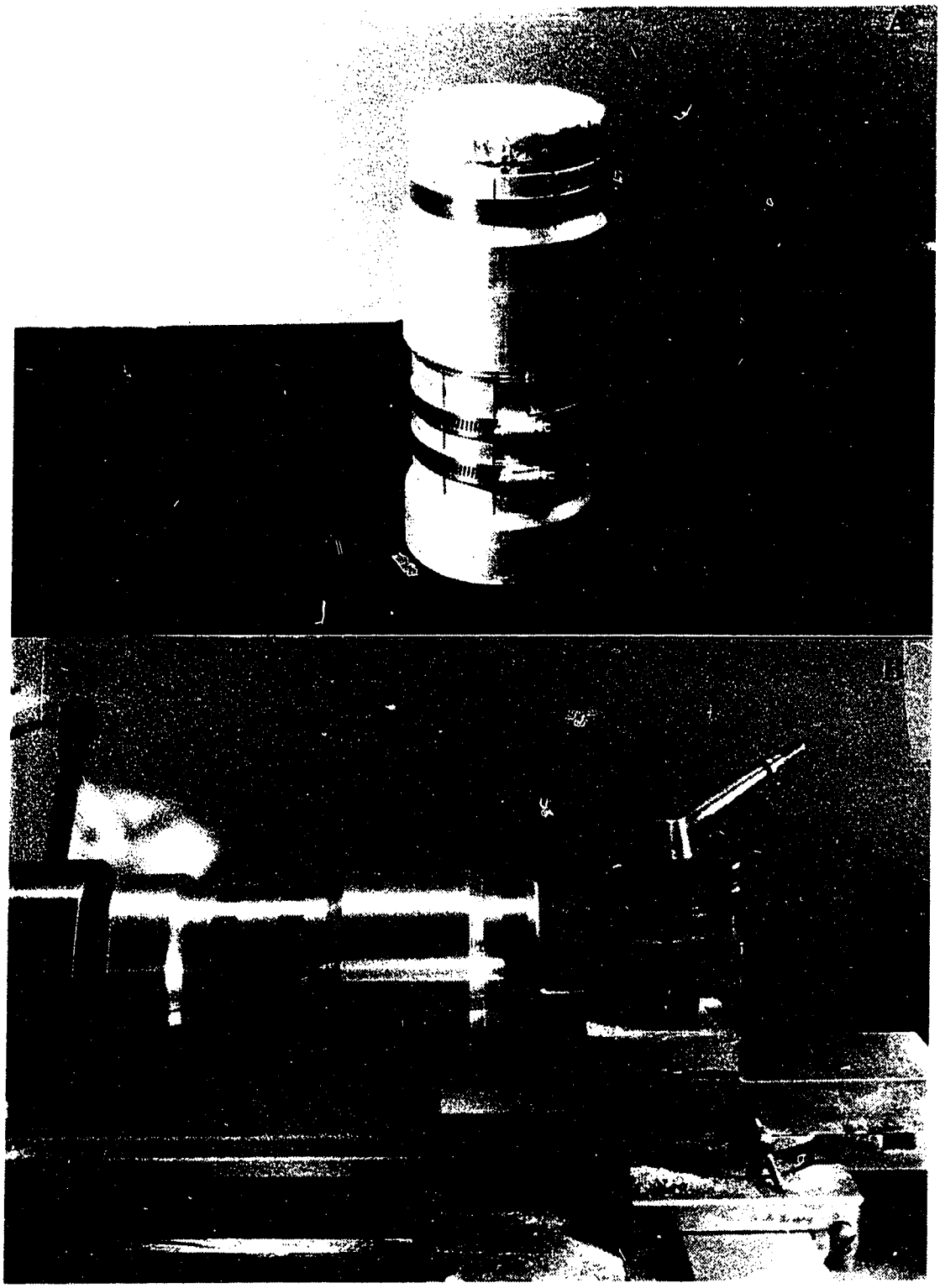

Plate 5.3 Cylindrical Specimen Preparation; (A) Specimen inside the line centered mandrel; (B) End preparation using lathe

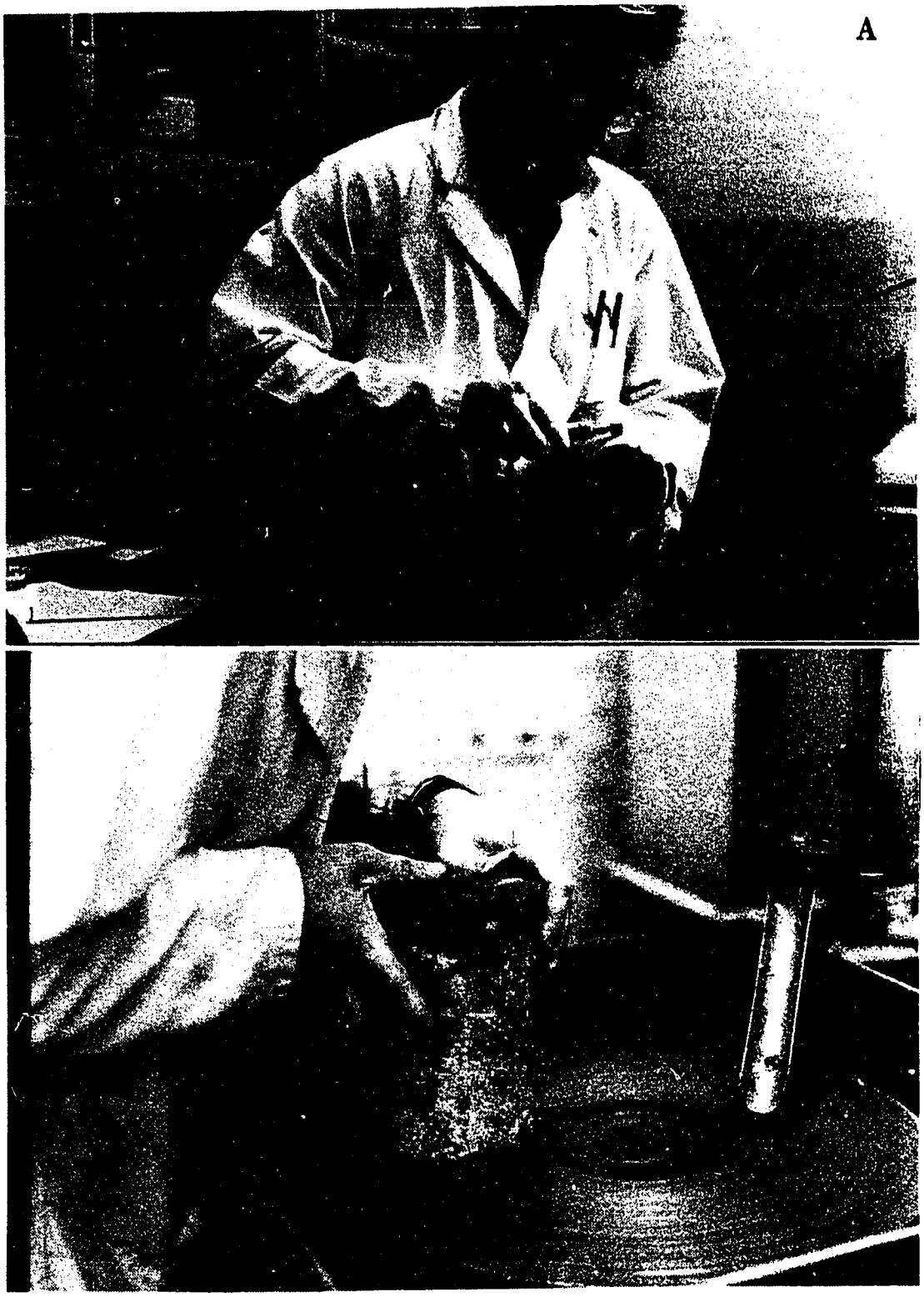

Plate 5.4 Cylindrical Specimen Preparation; (A) Finishing and polishing using a high speed grinder; (B) End finishing using a grinding table

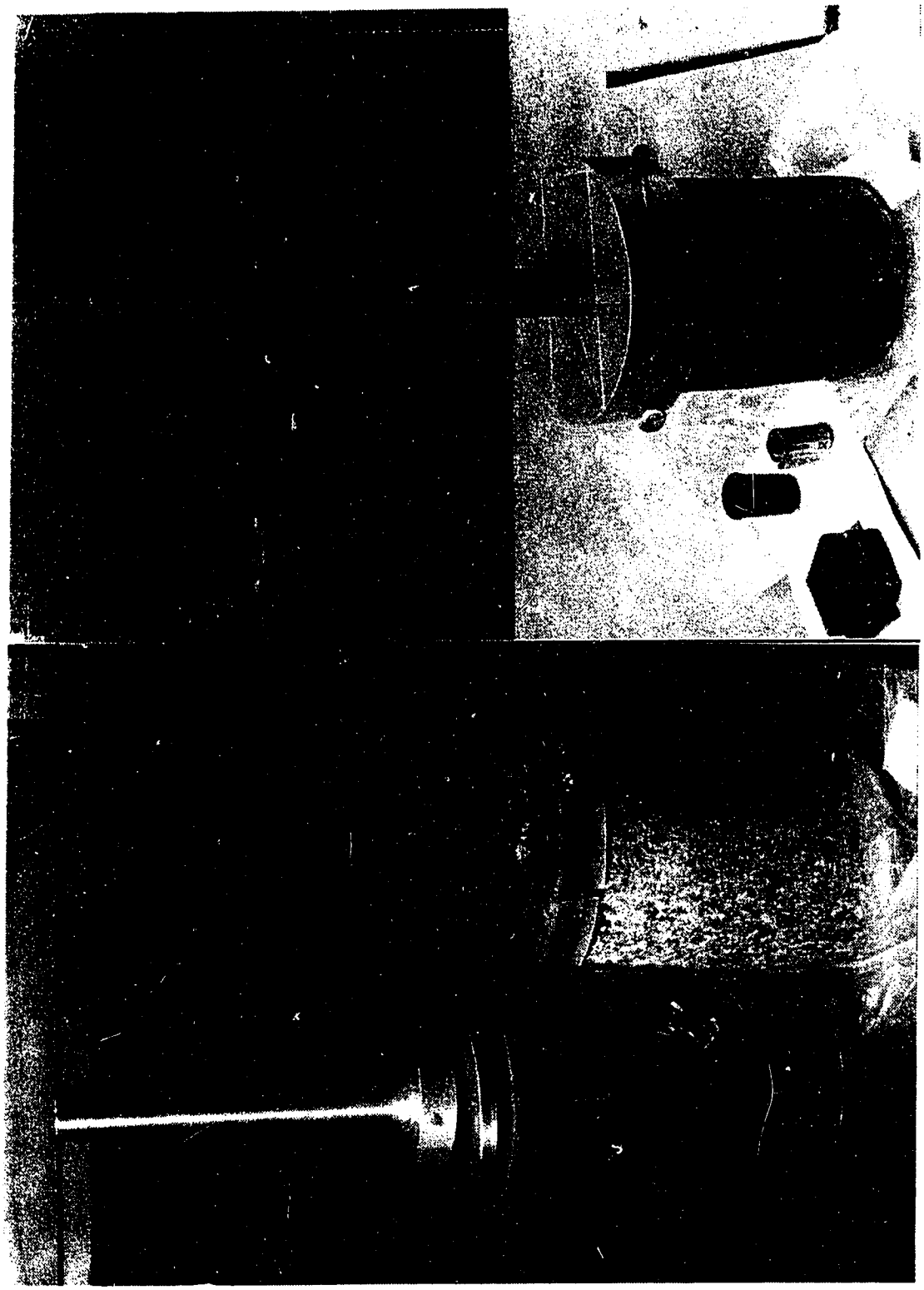

Plate 5.5 Hollow Cylinder Specimen Preparation; (A) Guide for drilling central hole; (B) Core and mandrel

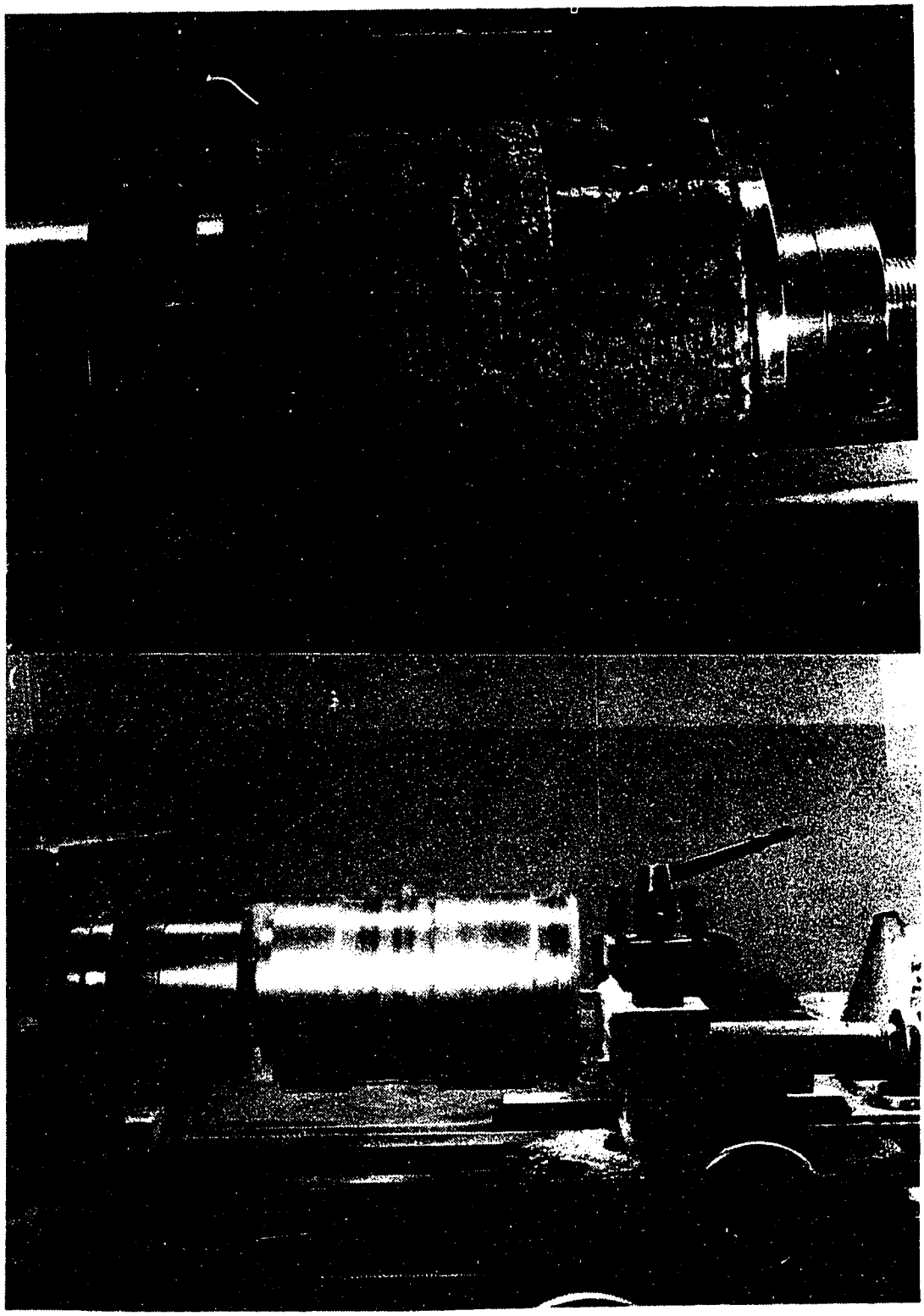

Plate 5.6 Hollow Cylinder Specimen Preparation; (A) Side preparation using lathe; (B) End preparation using lathe

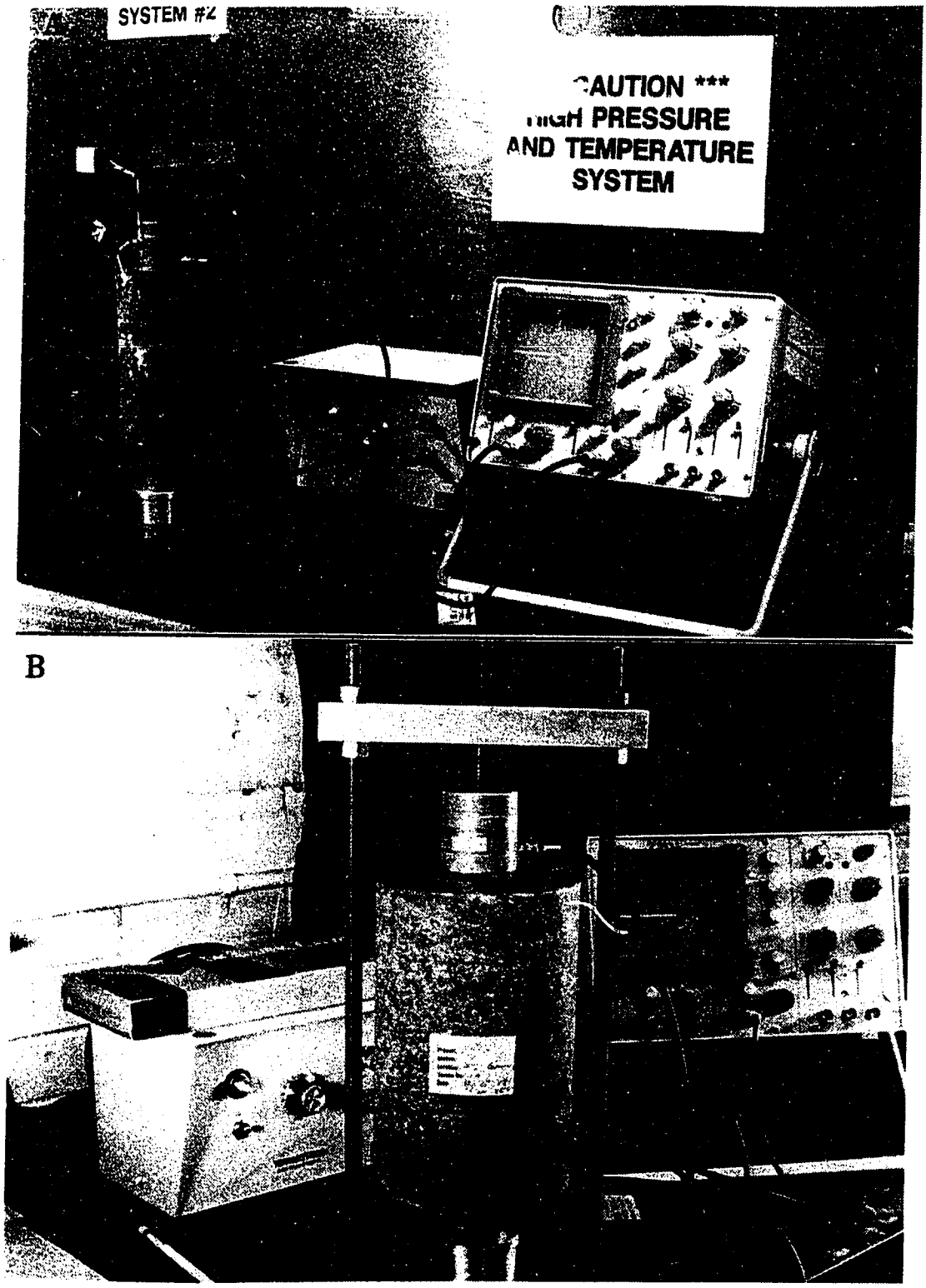

Plate 5.7 Specimen Characterization Using P/S Wave Tests; (A) Cylindrical specimens; (B) Hollow cylinder specimens

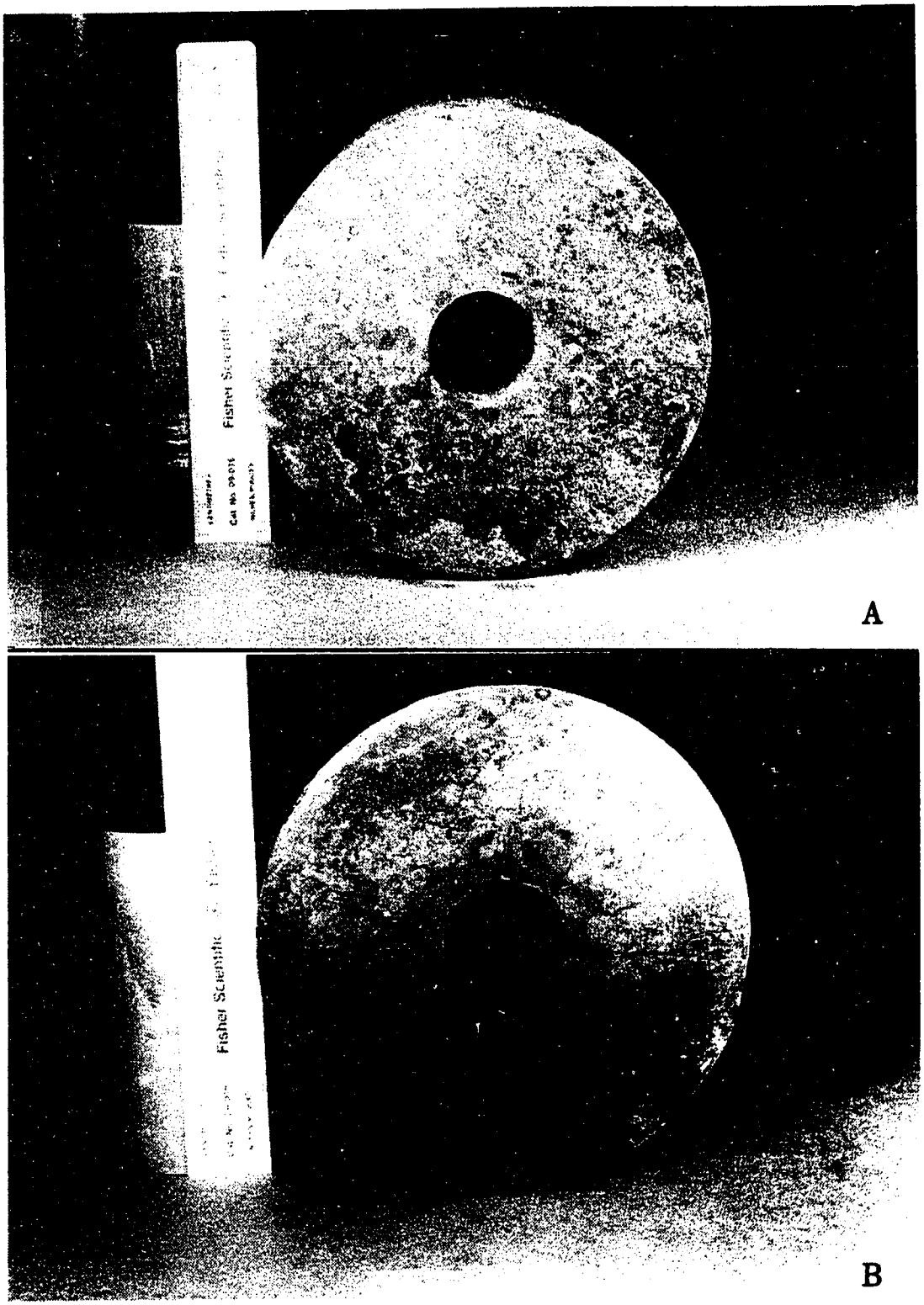

Plate 5.8 HCAL Test 2 - Specimen HC05; (A) Before testing; (B) After testing

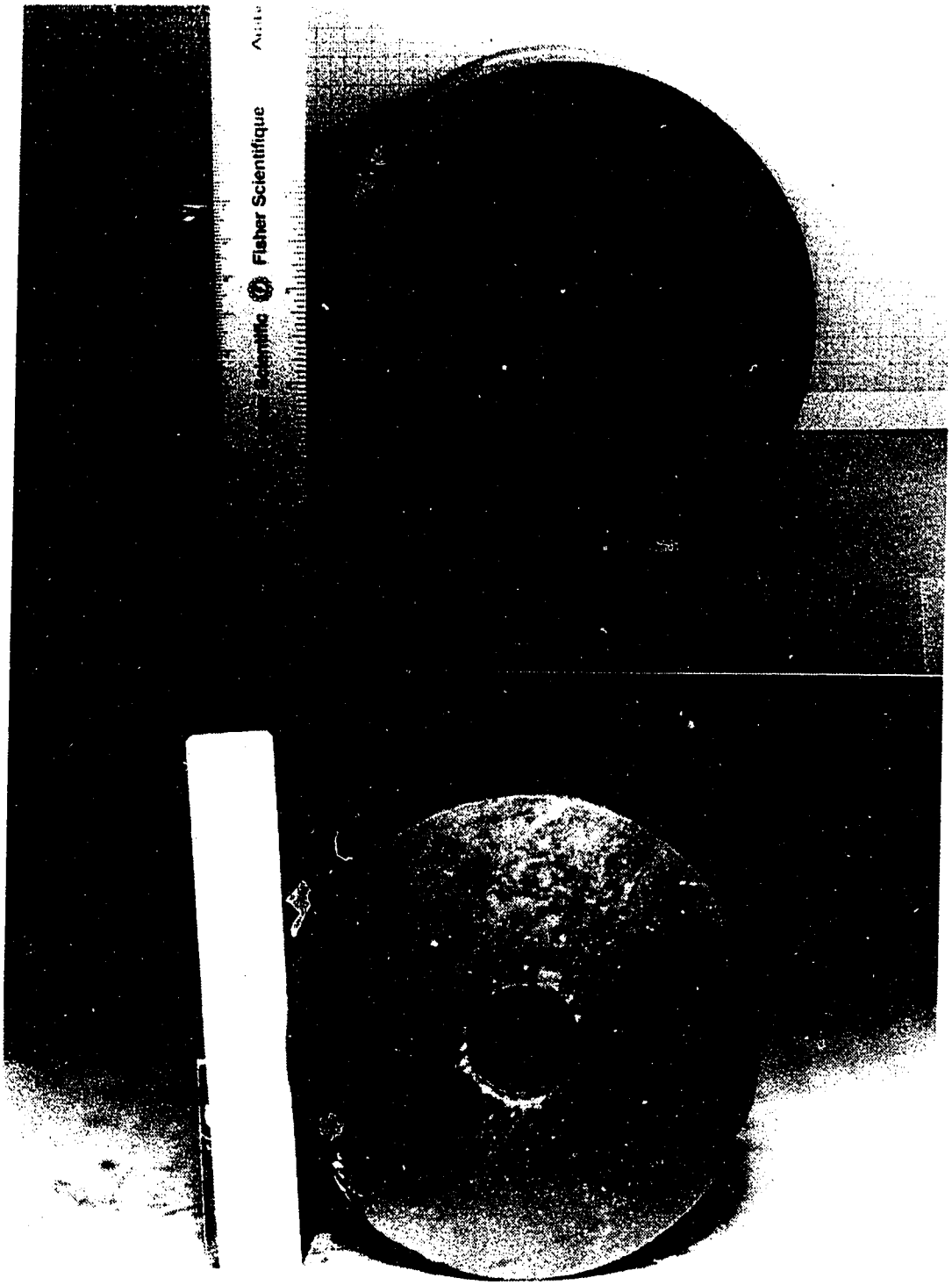

B

Plate 5.9 HCAL Test 4 - Specimen HC01; (A) Before testing; (B) After testing

6. INTERPRETATION OF THE LABORATORY TEST RESULTS AND EVALUATION OF THE CONSTITUTIVE CREEP MODELS

6.1 Introduction

This chapter links all preceding chapters, demonstrating how constitutive creep laws (Chapter 2) can be derived from triaxial tests, following different stress paths and evaluated by using hollow cylinder specimens as a model for openings in the same material. Triaxial testing data (Chapter 5) are interpreted and creep model parameters obtained. Model parameters are used as input to the analytical solutions for the thick-walled cylinder (Chapter 3) and the predictions for each constitutive law and triaxial path are compared with hollow cylinder test results.

Despite some limitations such as scale effects, sampling disturbance, stress history dependence and inhomogeneity, hollow cylinder tests are faithful representation of the homogeneous stress field, circular opening geometry and stress paths followed during the excavation and operation of an underground structure. They constitute a major contribution in understanding how well different constitutive laws with parameters obtained from triaxial tests are able to predict opening closures.

This chapter starts interpreting the hydrostatic loading data of all specimens (triaxial and hollow cylinder tests). Triaxial test data are divided into triaxial loading

and creep stage data, regardless of the stress path followed (CTC or JTC tests). Triaxial creep stage data are fitted according to specific creep models, in order to get the parameters for the respective analytical solutions, needed for predicting the hollow cylinder test results. Hollow cylinder data are also divided into two data sets for deviatoric pressure loading and creep stages. Finally, a comparison between creep model predictions based on triaxial data and hollow cylinder bore deformation is presented and discussed.

Before presenting these results, it is important to define how deformations are calculated based on transducer measurements. Because creep tests can lead to large deformations, strains are defined in terms of the current geometry state of the specimen, as described by the following expressions:

$$\epsilon_z = \frac{DA}{L_0 - DA} \qquad [6.1]$$

$$\epsilon_v = \frac{VC}{V_0 - VC} \qquad [6.2]$$

$$\dot{\epsilon}_{i+1} = \frac{\epsilon_{i+1} - \epsilon_i}{t_{i+1} - t_i} \qquad [6.3]$$

where

ϵ_i ... strain at time i

ϵ_{i+1} ... strain at time i+1

$\dot{\epsilon}_{i+1}$ ... strain rate at time i+1

ϵ_v ... volumetric strain (+...reduction)

ϵ_z ... axial strain (+...shortening)

L_0 ... original specimen length for that stage

V_0 ... original specimen volume for that stage

DA ... axial displacement for that stage

VC ... volume change for that stage

t ... time.

For the data reduction of triaxial creep tests, the axial pressure was converted into axial stress without any corrections for cross-sectional area change, although it is known that an error of 10 to 20% in the axial stress value can easily occur at the end of the test. Therefore, the axial stress values referred in the plots are related to the initial cross-section of the specimen. For hollow cylinder tests under axisymmetric loading, the axial pressure was also converted into axial stress without any corrections due to cross-sectional area changes, but for this type of experiment the error is negligible. For hollow cylinder tests under plain strain, the axial displacement measured by the LVDT 'DA' was assumed to be the axial displacement of the specimen, without any correction for system compliance. These corrections for cross-sectional area changes and system compliance could be easily implemented in the HPTS software, but this is left for a future stage, when more experience has been gained with the system.

6.2 Interpretation of the Hydrostatic Loading Results

A typical hydrostatic loading phase started with loading the specimen from zero to a certain stress level, usually representing the original in-situ stress state. Occasionally, a quick hydrostatic unload/reload cycle was performed to evaluate the elastic parameters before specimen reconditioning. Then, a three-day long hydrostatic creep stage was imposed to reverse sampling disturbance. Another quick hydrostatic unload/reload cycle was sometimes executed to determine the elastic constants after specimen reconditioning. Finally, the specimen was hydrostatically loaded to the stress level where the triaxial or hollow cylinder path should start.

The hydrostatic loading phase involves three data sets: hydrostatic loading itself, hydrostatic unload/reload cycles and hydrostatic creep stage. The objective is to load the specimen to its original in-situ stress field (or any other stress level) and to keep it under hydrostatic creep till post-sampling cracks and fissures are closed.

Although it is believed that it is impossible to reverse all sampling disturbance, specimen reconditioning is essential for creep testing on salt rocks to minimize differences among specimens before testing and consequently produce more uniform test results. Lack of reconditioning may cause erratic data at the first testing stages, leading to difficulties during the interpretation of the transient response and compromising the creep curve shape. Many

authors (e.g., Senseny, 1984) found different behaviours of natural salt specimens during the transient phase and then, similar behaviours for later stages of the tests. Erratic transient data are often obtained and have been disregarded completely or may have misled data interpretation and performance predictions. Lack of reconditioning may also explain the tremendous scatter in unconfined creep test data and why it is difficult to match predictions based on this type of data with in-situ measurements.

In summary, three steps were implemented (and are recommended) to minimize differences among specimens in a testing program:

1. Ultrasonic wave tests for preliminary assessment of specimens.
2. Hydrostatic loading of specimens and hydrostatic creep testing for specimen reconditioning.
3. Use testing equipment with ultrasonic wave heads adapted to the loading platens and run ultrasonic tests during the hydrostatic creep stage to help determine when the specimen is ready for testing (not done in this program).

Support for these steps are given in Sections 6.2.1 and 6.2.3.

Because specimens may contain cracks and fissures due to sampling, hydrostatic loading data are neither used for calculating the current specimen geometry nor for obtaining parameters and deformation predictions. These data are only

analysed to assess the validity of the specimen reconditioning procedure.

6.2.1 Hydrostatic Loading

The response of all cylindrical specimens to hydrostatic loading is analysed first (Fig. 6.1). The mean pressure versus axial strain relationships are quite linear for all specimens. It can be seen how specimens respond differently to the same type and magnitude of loading, which reflect their initial post-sampling states. For instance, the four specimens prepared for CTC tests were loaded to 20 MPa. Their axial strains range from zero to 1% and the volumetric strains from one to 8%. Comparing the deformations of all cylindrical specimens (mean pressure at 20 MPa is taken as baseline) with the results of the ultrasonic wave tests (Table 6.1; phase BT - before testing), one can see how well the ultrasonic wave test can indicate the specimen post-sampling condition. Specimens TR03 and TR02 (CTC Tests 2 and 1, respectively) presented the lowest ultrasonic velocities and the highest deformation levels. On the other hand, specimens TR04 and TR08 (CTC Test 3 and JTC Test 3) showed the highest ultrasonic properties and the lowest measured deformation. Linear regressions between the ultrasonic velocities and the axial deformations yielded a correlation coefficient of -0.74, and between the ultrasonic velocities and the volumetric deformations a coefficient of -0.91.

Hollow cylinder specimen results are shown in Fig. 6.2. Again, the specimens respond differently to the same type of loading and show dependence on the post-sampling conditions. Table 6.2 illustrates how the ultrasonic tests also give an indication of the specimen post-sampling conditions. Notice that the hollow cylinder deformations are within a narrower range than those from cylindrical specimens. This was expected since the ultrasonic properties of the hollow cylinder specimens were higher and less scattered. Also, the correlation coefficients from linear regressions are lower than those reported for cylindrical specimens.

The hydrostatic loading results of solid and hollow cylindrical specimens reinforce the use of ultrasonic wave tests for preliminary selection of salt rock specimens for testing.

6.2.2 Hydrostatic Unload/Reload Cycles

Unload/reload cycles were performed before and after hydrostatic creep stages. The objectives were to evaluate the elastic constants before and after specimen reconditioning and to assess the effectiveness of the adopted test procedure. All CTC tests and JTC Test 2 included unload/reload cycles before and after the creep stage. In JTC Test 1 as well as HCAL Tests 2 and 3, cycles were only carried out prior to the creep stage and in JTC Test 3 and HCAL Test 1 only after the creep stage. Although the unload/reload curves are very consistent (both curves

follow the same path), they usually lead to negative bulk moduli. This may reflect some inadequacies in the calibration curves, obtained from the monotonic hydrostatic loading, for correcting deformation measurements from rapid hydrostatic unload/reload cycles. A set of calibration tests to improve rapid cycle data would be required, but as this type of data is not of sufficiently high priority for this study, tests were not repeated.

6.2.3 Hydrostatic Creep Stage

The hydrostatic creep stage was intended to reverse post-sampling cracking and closure of fissures, bringing the specimens to a natural state before running the experiments. The axial and volumetric time-dependent responses to hydrostatic creep of the cylindrical specimens are shown on Fig. 6.3. The specimen deformations in response to similar hydrostatic stress levels appear to be affected by the specimen condition (Table 6.1). Specimen TR02 (CTC Test 1) presented the highest axial deformation and specimen TR04 (CTC Test 3) the lowest one. All other specimens presented an intermediate level of deformation, with the axial and volumetric strains ranging from 0.7 to 1.6 and from 5 to 15 millistrains, respectively. Again, these findings are quite consistent with the ultrasonic test results.

Hollow cylinder results are presented on Table 6.2 and Fig. 6.4. The results seem to be still dominated by the post-sampling of the specimens, but not so clear as for the

cylindrical specimens.

At the end of hydrostatic creep stages, specimens are assumed to be reconditioned and ready for triaxial or hollow cylinder testing. The specimen reconditioning criterion adopted for this study was a minimum creep period of 72 h. This criterion has been used successfully by other researchers (e.g., Dusseault et al., 1985) and was demonstrated to be satisfactory for most of the specimens which presented stable levels of deformation rate. Only specimen TR08 (JTC Test 3) indicated a continuing trend of increasing axial deformation (Fig. 6.3). All hollow cylinder specimens showed volumetric strain curves that had not yet stabilized at low rates (Fig. 6.4).

A more detailed investigation of the strain rate trend with time was undertaken using the hydrostatic creep results from cylindrical specimens. Figure 6.5 shows the strain rate versus time (log) curves for the cylindrical specimens. Strain rate values were calculated at one-hour time intervals. From this figure, the importance of the first few hours of creep for specimen reconditioning can be noticed. The strain rates start with very discrepant values but converge to an asymptotic value. The oscillating range also diminishes considerably after one day of hydrostatic creep stage. These two findings, in addition to the fact that the shapes of the strain versus time curves (Fig. 6.3) get more uniform after the third day of hydrostatic creep stage, lead to the minimum three-day creep stage as a time criterion for

specimen reconditioning.

The time criterion should also be combined with a maximum strain-rate criterion. Reeves (1988) suggested that specimens should be considered reconditioned when the strain rate (axial and radial) falls below a certain limit (e.g., 10 microstrain per day). Figure 6.6 presents the strain rate (log) versus time (log) curves for the cylindrical specimens, so that the trend of the strain-rate values can be evaluated. The best-fit equations for all cylindrical specimens under hydrostatic creep are also given. It is important to mention that the strain-rate values (Fig. 6.6) are calculated taking the two closest data points resulting in the positive strain-rate value required by the log scale. This procedure may not be accurate at individual points, but certainly it reflects the average trend of strain rates during creep stages. The maximum strain-rate criterion for specimen reconditioning should be based on these averages because the strain-rate values oscillate. This is particularly true when the deformation level is very small and the measured deformation approximates the transducer accuracy, reflecting also some electronic shifts of the analog signals.

Tables 6.1 and 6.2 also present the strain-rate averages for the last day of hydrostatic creep stages for both specimen shapes. These values are at least one order of magnitude greater than the maximum strain-rate (axial and radial) criterion of 10 microstrain per day suggested by

Reeves (1988). Using the best-fit equations (Fig. 6.6), this suggested strain rate would be achieved only after six months of hydrostatic creep. This is an extremely long time for specimen reconditioning. A strain rate of 100 microstrains per day was adopted as a strain-rate criterion. This value is recommended for further tests on the same material. The time needed for specimen reconditioning, according to the best-fit equations, would be on the order of one week, which is a reasonable time for creep tests expected to last months or even years.

Some specimens were subjected to another hydrostatic unload/reload cycle just after the hydrostatic creep stage. Then, specimens were hydrostatically loaded to the stress levels, selected as the initial points of the triaxial or hollow cylinder stress paths. Actually, only CTC Tests 1 and 4 had to perform this loading to position the specimens to 5 and 35 MPa, respectively. All other tests started the triaxial stress or hollow cylinder path at the same stress level where the hydrostatic creep stage was performed.

6.3 Interpretation of the Triaxial Test Results

Triaxial tests were carried out following the stress paths presented in Chapter 5 and Appendix E. A typical triaxial test started from a hydrostatic stress state, followed by triaxially loading the specimen to a certain deviatoric stress level and subjecting it to a creep stage. Triaxial creep stages were short-term ($\simeq$1 week) to

investigate transient creep.

6.3.1 Triaxial Loading

Triaxial loading is the stage which starts at the hydrostatic stress level and positions the specimen at a certain deviatoric stress level. It can follow any triaxial stress paths (e.g., CTC or JTC). Figures 6.7 and 6.8 show the stress versus strain curves for the conventional triaxial compression (CTC) stress path, while Fig. 6.9 shows them for the J1-constant triaxial compression (JTC) path.

The first two CTC tests (Fig. 6.7) were originally designed to obtain the stress-strain curves of specimens, confined at different stress levels. At first glance, the curves seem opposite, with the specimen confined at a higher stress (CTC2) showing larger deformations. CTC Test 1 presents some irregularities in the stress versus axial strain data, between deviatoric stresses of 35 and 45 MPa, and then it follows a linear relationship ($E \simeq 3.3$ GPa) till reaching the axial loading capacity of the equipment. These erratic data might be explained by the crushing of the insulator caps, although they did not present signs of extensive failure after testing. It is difficult to justify this linear behaviour up to such high axial stresses, considering the low confining stress of 5 MPa.

CTC Test 2 presents more reasonable stress-strain curves. The insulator caps were found to have an outer ring of crushed material after testing. This cannot be seen from

the curves. The reduction of cross-sectional area due to the crushed outer ring may have caused an increase of the actual axial stress within the specimen. Based on geometric measurements of the insulator caps and specimen ends after testing, the actual axial stress at the cap could have been up to 50% higher than the reported values (Fig. 6.7).

CTC Tests 3 and 4 were programmed to investigate the creep response under different confining and deviatoric stresses. Figure 6.8 shows the stress-strain curves of the first triaxial loading stage. The volumetric strain curves of both tests are quite similar. The deviatoric stress versus axial strain curves although different are within a reasonable range of variation. The axial strain data of CTC Test 3 are quite inconsistent and could not be explained. On the other hand, the axial strain data of CTC Test 4 follows a linear relationship with the applied deviatoric stress ($E \simeq$ 6.5 GPa).

The JTC tests (Fig. 6.9) present consistent stress-strain curves. The three tests seem to follow the same strain path, independently of the stress level (first stress invariant). In other words, the specimen deformations appear to depend only on the applied deviatoric stresses.

If somehow, the deformations can be compared among all triaxial tests, considering either the confining stress at the end of the triaxial loading stage or the applied deviatoric stress, the J1-constant triaxial compression paths generate deformations of about one order of magnitude

larger than those from the conventional triaxial compression tests.

6.3.2 Triaxial Creep Stage

Each creep stage is characterized by the confining and deviatoric stress increment levels, assuming that all tests are isothermal. The previous stress path used and the time needed to load the specimen up to the stress state that defines the creep stage can also play an important role in the creep response. Therefore, creep stages for each type of triaxial stress path are analysed separately, only investigating the effects of the stress state on creep deformation. Then, a global analysis of all triaxial creep stages is made, attempting to assess the influence of the previous triaxial stress path on creep deformation.

Figure 6.10 depicts the five triaxial creep stages which had a previous CTC path. CTC1CRP1 (CTC Test 1 and 1st creep stage) creep stage presents the highest rate of deformation, what can be explained by the low confining stress (5 MPa) combined with a very high axial stress (115 MPa). The specimen failed after 2400 min of creep testing. CTC Test 3 subjected the specimen to two creep stages with the confining stress set to 20 MPa and axial stresses of 30 and 40 MPa, respectively. As expected, the first creep stage (CTC3CRP1) presents a lower rate and level of deformation because the applied deviatoric stress is smaller. The second creep stage (CTC3CRP2) shows much higher levels of creep

strain, which can be simply justified by the higher deviatoric stress. CTC Test 4 also presents two creep stages, with the confining stress set to 35 MPa and axial stresses of 60 and 85 MPa, respectively. Regardless of the different deviatoric stresses, the creep responses are very similar for both creep stages. CTC4CRP1 creep stage presents lower volumetric creep strain but in contrast, higher axial creep strain. It seems that for higher confining stresses, the creep response is less dependent on the deviatoric stress state. This clearly demonstrates a dependence of the creep response upon the confining stress level.

One important aspect that must be considered is that the specimen condition is not the same during the second creep stage. It is difficult to determine how much the first creep stage affects the second stage results. Cruden (1971b and 1983) has studied this in detail for unconfined compressive creep. He concluded that the form of the creep curve after a load increment depends on a creep parameter of the rock and on the size of the load increment, and varies with time. For CTC Test 3, it seems that the specimen condition during the second creep stage was much more favourable to creep deformation, considering that a doubling of the deviatoric stress level caused an increase in deformation of about fifteen times. On the other hand, for CTC Test 4, both creep stages present similar responses even though the deviatoric stress was also doubled. The small differences may be attributed to specimen condition

differences.

Comparing the five CTC creep stages, one can get a general view of the effects of the confining and applied deviatoric stresses on the creep response. CTC1CRP1 creep stage shows that low confining and high deviatoric stresses are the most favourable condition for generating creep deformation. CTC Test 3 shows the effects of the deviatoric stress, keeping the confining stress constant. The higher the applied deviatoric stress, the higher the creep strain. This dependence changes in magnitude for different confining stress levels, as shown by comparing the creep stage results between CTC Tests 3 and 4. CTC4CRP1 and CTC3CRP2 creep stages demonstrate the influence of the confining stresses, keeping almost the same deviatoric stress (25 and 20 MPa, respectively). The lower the confining pressure, the higher the creep response. These findings, although supported by the literature on salt, can only be presented in qualitative manner because of the few specimens and test stages for each loading condition.

The triaxial creep stage results of specimens previously loaded by a JTC stress path, are depicted on Fig. 6.11. JTC1CRP1 creep stage presents a classical creep response with high strain rates at the beginning of the experiment and gradual rate decreases with time. JTC Test 2 subjected the specimen to two creep stages. JTC2CRP1 creep stage (σ_1= 35 and σ_3= 20 MPa) shows an almost constant creep rate. JTC2CRP2 creep stage (σ_1= 45 and σ_3= 15 MPa) presents

a more classical response, but the test ended after 1200 min. Finally, JTC3CRP1 creep stage presents very high creep rates. Although the creep response resembles a step function because the pressure system was unable to follow such high deformation rates, a trend can be identified (shown on Fig. 6.11 by a dashed line).

A comparison of the four JTC creep stages leads to some interesting findings. JTC1CRP1 and JTC2CRP1 creep stages have the same deviatoric stress (15 MPa) but JTC2CRP1 presents higher axial deformation, even though its confining stress is twice as high as the JTC1CRP1 confining pressure. This finding is opposite to that found for the CTC creep stages and in the literature. However, it is reinforced by the comparison between the results of JTC2CRP2 and JTC3CRP1 creep stages, where the creep stage under higher confining stress (JTC3CRP1) presents higher axial and volumetric strains. No JTC creep stages present the same confining stresses, but taking similar confining levels, it seems that the dependence between applied deviatoric stress and creep response follows the same trend as for the CTC creep stages.

Analysing all triaxial creep stages (CTC and JTC tests), it seems that creep stages previously loaded by a JTC path present considerably higher levels of deformation. Also, the dependence upon confining and deviatoric stresses appears not to follow the same rules for both triaxial stress paths. As a matter of fact, they show an inverse relationship of the dependence between confining stress and

creep response, keeping other parameters constant. These findings suggest how previous stress paths can affect creep stage responses. Specimens subjected to creep stages under the same state of confining and deviatoric stresses, but previously loaded by different stress paths, also behave differently. The difference seems not only to be qualitative but also in the dependence relationships among parameters that influence creep response. However, these remarks should not be extrapolated to situations other than those tested by this testing program. The number of specimens tested for each loading condition is too small for any quantitative analysis.

6.4 Creep Model Parameters

Creep stages have controlling parameters such as confining stress level, deviatoric stress, temperature, that characterize them. Of course, there are other parameters (e.g., previous stress path, specimen condition, deformation level) that have been shown to affect the creep response, but their effects are difficult to assess quantitatively. It is important that the selected creep models include all controlling parameters and portions of the creep response (Fig. 2.1) of interest for the study.

This research aims to investigate the transient response of potash for different confining stress levels and deviatoric stresses, after the specimens were loaded by CTC and JTC stress paths. All experiments were conducted under

isothermal condition (25 +/- 0.5°C). Hence, the temperature does not appear explicitly in any chosen creep model. Also, the elastic or instantaneous data from the previous triaxial loading stages are not included. Only time-dependent data are analysed.

From all creep models reviewed in Chapter 2, one empirical (power law, PW), one microphysical (structural law, ST) and two rheological (Kelvin, KL and generalized Kelvin fluid, GK) models are selected, basically because they are most appropriate to describe transient creep and can easily be implemented in analytical solutions (Chapter 3). Although these models do not explicitly include the confining stress level and previous stress path, their effects on parameters can be evaluated at least qualitatively. The one-dimensional equations (Eqns. 2.2, 2.18, 2.22 and 2.26) for the chosen creep models have to be extended to the triaxial stress state and applied to the boundary conditions of a cylindrical specimen. Also, the assumptions related to creep behaviour, made in Chapter 3 (material incompressibility, isotropy and creep deformation only dependent on a J2-type flow), must be invoked. These assumptions lead to:

1. The effective or equivalent stress ($\sqrt{J2}$) reduces to a function of the deviatoric stress ($\sigma_{11}-\sigma_{33}$) only.
2. The generalized strain is a function of the axial strain only.
3. The chosen creep model equations can be rewritten,

substituting the uniaxial strain and stress by the axial strain and triaxial deviatoric stress, respectively. Other adjustments are implicit in the model constants. A more general interpretation of creep stage data can be done by assuming the volume as a variable, provided axial and radial strains are measured (as performed in this study). This would require more complex flow criteria to generalize the one-dimensional creep laws to multiaxial stress state. It is left for future analysis.

Having chosen the creep models, parameters are determined by the curve-fitting technique. Although this technique is well known, some salt researchers have concerns related to inappropriate use of it and have developed more specific formulations for each type of fit and creep model (e.g., Parrish and Gangi, 1981; Mrugala, 1984). For non-linear least squares methods, Senseny (1985) suggested that data must be weighed to compensate for the different lengths of time intervals that contain a particular data point. This is exactly the HPTS case, where the data acquisition system takes data more often at the beginning of creep stages than later. If data were not weighed, the data points at the beginning of the creep stage would dominate the shape of the best-fit curve. Both types of analysis (weighed and not weighed data) were performed in this research. The findings confirmed that weighed data give a better visually adjusted curve, although both curves presented similar correlation coefficients. The non-linear

regression analyses were performed using the BMDP Statistical Software, which is well documented by Dixon et al. (1988). Only the results of the analyses using weighed data are presented.

Three models (the empirical and the two rheological) fit creep strain versus time data, while the microphysical model fits creep strain rate versus time data. Tables 6.3 to 6.6 show the model parameters obtained from non-linear regression analyses. Figures 6.12 to 6.20 depict how well each particular model can predict the actual creep stage data. The strain-rate values used for fitting the structural law were calculated following the same procedure suggested in Section 6.2.3 (two closest data points giving a positive strain rate average).

The comparison between creep model predictions and actual data indicate that all creep models are able to describe the trend of actual data well, except the Kelvin model which tends to underpredict the measured data for time periods greater than half of the test duration. This fact can be explained by the nature of the Kelvin model equation, which searches for an asymptotic axial strain (= $\Delta\sigma/E$). For the same reason (model nature), the generalized Kelvin (fluid) model tends to overpredicted slightly the measured data at the end of the test, because it imposes a constant rate of deformation after a certain time limit. The other two models only depend upon the effectiveness of the curve-fitting technique.

The curve-fitting technique can be affected by many factors. The selected model equation is maybe the most important. Simply, some models cannot fit well the measured data. From all models tested in this research, the Kelvin model is the most likely to belong to this category. Also, the number and distribution of data points are important, but these factors affect all models. Applying weights to data points to compensate for their distribution and correcting the correlation coefficients to compensate for the different number of data points of each creep stage are necessary.

A second type of creep model evaluation considers that model equations are also for extrapolating further data beyond the test duration used for obtaining their parameters. Figures 6.21 and 6.22 present the model predictions for CTC1CRP1 and CTC3CRP1 creep stages. These curves are based on parameters obtained using only the data of the first half of the creep stage duration. Table 6.7 shows the creep model parameters for both half and full creep stage duration. Although there are differences between corresponding parameters, in general they can be considered very close. However, a comparison between Figs. 6.12 and 6.21, and between Figs. 6.13 and 6.22 shows that differences between predicted and measured strains increase, especially for the two rheological models. This is explained exactly by the nature of the model equations, which impose strain rate conditions at certain time limits. The power and structural

laws present slight differences. The latter is the most insensitive to this kind of model evaluation. These examples illustrate the importance of the test duration used for generating model parameters and consequent quality of extrapolations. They also reinforce the recent trend of thinking among salt researchers, that suggests long-term creep tests, regardless of the type of creep model chosen to fit the data (Herrmann et al., 1984; Bakhtar et al., 1988; Fuenkajorn and Daemen, 1988a).

The last point to be addressed in this section, is the use of model equations obtained from curve-fitting one type of data to predict other types. For instance, a model derived from strain versus time data may be used for predicting strain rate versus time data and vice-versa. This is possible simply by mathematical manipulation of the model equations. Although some physical significance can be attributed to some model parameters, they are in fact curve-fitting parameters. The best-fit equation for one type of data may be inappropriate for predicting different kinds of data, even so there might be some mathematical correlation.

CTC1CRP1 and CTC3CRP1 creep stages are again taken as an example. Figures 6.23 and 6.24 show the actual creep data, the model predictions for the data they were derived from and the model extrapolations to the other type of data set (* denotes model extrapolations). Comparison between model predictions and extrapolations show that the power

(PW) and structural (ST) laws produce curves with the same shape, only dislocated in the graph space. This is because both models are very similar in nature (both are power laws) and the differences lie in the type of data from which each model is derived. Despite these similarities, any extrapolation of a model derived from one data type to predict another kind of data can produce misleading results, as illustrated by the examples. In one example, model extrapolation underpredicted data and in the other it overpredicted without showing any logical dependence. The rheological model (KL and GK) extrapolations underpredicted the strain rate at the beginning of the creep stages. At the end of tests, the rheological models followed the imposition of their equations, with the Kelvin model giving approximate zero strain-rates and the generalized Kelvin model establishing a constant value.

In conclusion, it seems to be advisable that each creep model should only be used for predicting the same type of data it is derived from, because model parameters are in fact curve-fitting parameters.

6.5 Interpretation of the Hollow Cylinder Test Results

Hollow cylinder tests were carried out following the pressure paths presented in Chapter 5. A typical hollow cylinder test started from a hydrostatic stress state. Then, the specimen was loaded to a certain deviatoric stress level, by changing the internal pressure and keeping either

plane strain or axisymmetric loading condition. A creep stage followed each deviatoric stress level. Creep stages were short-term in order to compare their results with model equations obtained from triaxial creep stages, whose durations are similar.

As hollow cylinder tests are assumed as simulation tests of circular openings in homogeneous stress fields, their data are only corrected using the system calibration curves. No other interpretation is made.

6.5.1 Deviatoric Pressure Loading

Deviatoric pressure loading is the stage which starts at the hydrostatic stress level and positions the specimen at a certain deviatoric stress level, where a creep stage will be executed. It is done by changing the internal pressure, following either an axisymmetric loading or plane strain path. To perform a stress-strain analysis of hollow cylinder tests, it is necessary to assume a material constitutive law. Otherwise, the stress and strain values cannot be calculated due to the curvilinear nature of the boundary conditions. One common assumption is that the load is applied instantaneously and the specimen response is linear elastic. In this case, the stresses and strains can be evaluated using the equations presented in Section 3.2.

As hollow cylinder tests in this research are taken as model tests, in principle no assumption is made. The internal pressure change is plotted against the bore

convergence only. As the cross-sectional geometries of all specimens are very close, these two parameters can be considered proportional to the deviatoric stress and radial strain, respectively. The bore convergence can be either measured directly by the bore convergence device (BC measured) or calculated from the internal volume change measurements (BC from VCI), according to the following expression:

$$BC = a_0 - \left[\frac{VB_0 - \Delta VCI}{\pi(L_0 - DA)}\right]^{1/2} \qquad [6.4]$$

where

a_0 ... original bore radius for that stage

L_0 ... original specimen length for that stage

VB_0 ... original hollow cylinder bore volume for that stage

ΔVCI ... internal (bore) volume change.

Figure 6.25 presents the internal pressure change versus bore convergence for the deviatoric pressure loading starting at the hydrostatic stress level (1st deviatoric pressure loading). The bore convergence calculated from bore volume change measurements (BC from VCI), describes quite well those values measured directly by the bore convergence device (BC measured). However, the BC values measured directly present the same strain path for all specimens, being only dependent on the applied deviatoric pressure. The relationship can be assumed linear up to a deviatoric

pressure of 10 MPa (E≈ 3.3 GPa) and then, it becomes non-linear. The reason for this non-linearity can be simply that higher deviatoric pressures take more time to be applied, allowing some time-dependent deformation to be added to the total deformation.

6.5.2 Hollow Cylinder Creep Stage

Creep stages follow each deviatoric pressure loading. Only creep stages under internal pressure decreases ($p_i<p_e$) are analysed. Figure 6.26 presents the bore convergence, measured directly (BC measured) and calculated from VCI measurements (BC from VCI), versus time curves for all creep stages. The bore convergence data calculated from VCI measurements are, on average, twice as large as the measured values. They are not so consistent as those for the deviatoric pressure loading. The reason for these differences can be that the calculated bore convergence is very sensitive to the value of the VCI measurements. A small leak in the hollow cylinder bore volume, what is very likely to occur in long creep stages, affects the calculated bore convergence very much. This may lead to the conclusion that besides the internal volume change measurements, which give the average response of the bore convergence, point-deformation measurements as those provided by the bore convergence device must also be taken.

HCAL Test 1 (PO= 15 MPa) presents three creep stages (HCAL1CP1, HCAL1CP2 and HCAL1CP3) with internal pressures at

10, 5 and 1.5 MPa, respectively. The results are opposite to those expected, since the creep stage under lower deviatoric pressure (HCAL1CP1) presents higher deformations. HCAL Tests 2 and 3 do not have any creep stage data due to leaking problems during their execution (Chapter 5). HCAL Test 4 (PO= 20 MPa) has only one creep stage (HCAL4CP1) with internal pressure at 1 MPa, but it is longer. The bore convergence data show some discrepant measurements (increasing rates) between 30000 and 45000 min, with no apparent reason. The previous trend of decreasing rates is resumed later.

HCPS Test 1 (PE= 35 MPa) has two creep stages (HCPS1CP1 and HCPS1CP2) with internal pressures at 18 and 1 MPa, respectively. The bore convergence responses, calculated from VCI measurements (BC from VCI), present unexpectedly higher deformation levels for the first creep stage. Unfortunately, the bore convergence data, measured directly (BC measured), were lost due to electronic connection malfunction. HCPS Test 2 (PE= 20 MPa) has also two creep stages (HCPS2CP1 and HCPS2CP2) with internal pressure at 11 and 2 MPa, respectively. The results show a direct relationship between the applied deviatoric pressure and bore convergence.

6.6 Evaluation of Creep Models

The assessment of the predictive capability of creep models can be made by comparing analytical solution predictions to hollow cylinder bore convergence results. Creep model parameters are usually obtained from triaxial data. The first model evaluation is done by comparing how well the creep law can fit the triaxial data used for generating its parameters (Section 6.4). Then, parameters are input into analytical solutions, which have their own limitations from the assumptions made to derive them. When analytical solution predictions are compared to hollow cylinder test results, not only is the creep law being evaluated, but the whole formulation (creep model plus analytical solution). It is quite difficult to divorce the creep model effects from those related to the assumptions taken for the analytical formulation. Hollow cylinder tests as simulation experiments may play an important role helping establish the distinction between these effects. Also, numerical analyses incorporating more complex models and fewer formulation assumptions, would be beneficial to undertake this task.

For this research, three models (power, PW, structural, ST and generalized Kelvin fluid, GK) are chosen to have their predictive capacity assessed. The Kelvin model is not evaluated because its predictions compared to the actual triaxial data was considered the poorest (Section 6.4). The structural model is also selected, even though its

parameters are obtained by fitting strain-rate data. As discussed in the section on creep model parameters, model extrapolation from one type of data to another one may cause prediction errors, but this is one of the objectives of the creep model evaluation.

6.6.1 Model Test Results

The only hollow cylinder test deformation used for comparison with the analytical solution predictions is the borehole convergence (BC). The hollow cylinder bore convergence can be either measured directly (BC measured) by the bore convergence device (Appendix D) or calculated from the internal volume change measurements (BC from VCI), using Eqn. 6.4. HCAL Tests 1 and 4 and HCPS Tests 1 and 2 produced bore convergence creep data under axisymmetric loading and plane strain, which can be compared to the analytical solution predictions. However, only the results of the HCAL4CP1 and HCPS2CP1 creep stages are selected as database for the model evaluation.

Ideally, model test results should be compared directly to analytical solutions, without applying any restrictions related to material behaviour or boundary conditions. Analytical solutions have already their own assumptions needed to derive them. Unfortunately, some analytical solutions are not available for the type of deformation measured in model tests. In this case, it is necessary to convert the model test results into the variables given by

readily available analytical solutions. The solutions presented for the power and structural laws only describe the radial strain and not the radial displacement (bore convergence). Therefore, the radial strain at the hollow cylinder inner wall has to be calculated from the bore convergence measurements. Assuming small strains ($\epsilon=\partial u_r/\partial r$), the radial strain can be defined by the radial displacements between two points. If one of the points presents a negligible displacement, as assumed for the hollow cylinder outer wall, the final expression for the radial strain at the inner wall is:

$$\epsilon_{r,a} = \frac{BC}{\Delta r} \qquad [6.5]$$

where

$\epsilon_{r,a}$ ... radial strain at the hollow cylinder inner wall

BC ... bore convergence (radial displacement at the hollow cylinder inner wall)

Δr ... distance between the two points (hollow cylinder wall thickness).

Radial strain rates at the hollow cylinder inner wall could also be calculated applying two radial strains at different instants to Eqn. 6.3. These results could be compared to the predictions of the structural law, which fits directly strain rate data.

6.6.2 Analytical Solution Predictions

Analytical solution predictions of bore convergence can be obtained by applying boundary conditions (radius 'r' equal to hollow cylinder inner radius 'a') to radial strain or displacement equations.

6.6.2.1 Generalized Kelvin (Fluid) Model

The radial displacement equation, in function of time, for the generalized Kelvin (fluid) model is given by Eqn. 3.68 or 3.69, whether plane strain or axisymmetric loading condition, respectively. Applying boundary conditions (r=a) into Eqns. 3.57 to 3.61 and substituting the resulting relations into Eqns. 3.68 and 3.69, the bore convergence equations for each loading condition become:

<u>Plane Strain</u>

$$u_a(t)_{PS} = \frac{p}{b^2-a^2}\left[\frac{3a(b^2-ka^2)}{(\gamma-\alpha)\eta_1\eta_2}\left\{-\frac{E_2}{\alpha\,\gamma}\left(\alpha\,(1-\mathrm{EXP}(-\gamma\,t)) - \ldots\right.\right.\right.$$

$$\ldots - \gamma\,(1-\mathrm{EXP}(-\alpha\,t))) + (\eta_1+\eta_2)(\mathrm{EXP}(-\alpha\,t) - \ldots$$

$$\ldots - \mathrm{EXP}(-\gamma\,t))\} + \frac{(1-k)ab^2}{\eta_1 E_2}\{E_2\,t + \ldots$$

$$\left.\ldots + \eta_1\,(1-\mathrm{EXP}(-\beta\,t)\}\right] \qquad [6.6]$$

<u>Axisymmetric Loading</u>

$$u_a(t)_{AL} = u_a(t)_{PS} - \ldots$$

$$\ldots - p\ a\ [\frac{t}{3\eta_1} + \frac{3K-E_2}{9KE_2}\ \{1 - EXP(-\beta\ t)\} - \frac{1}{9K}\ EXP(-\beta\ t) - \ldots$$

$$\ldots - \frac{2(b^2-ka^2)}{9K(b^2-a^2)}\ \{\frac{\alpha\beta\gamma W_3 - (\alpha\beta+\beta\gamma+\gamma\alpha)W_4}{\alpha^2\ \beta^2\ \gamma^2} + \frac{W_4\ t}{\alpha\ \beta\ \gamma} - \ldots$$

$$\ldots - \frac{-\alpha^4 + W_1\alpha^3 - W_2\alpha^2 + W_3\alpha - W_4}{\alpha^2\ (\beta-\alpha)\ (\gamma-\alpha)}\ EXP(-\alpha\ t) - \ldots$$

$$\ldots - \frac{-\beta^4 + W_1\beta^3 - W_2\beta^2 + W_3\beta - W_4}{\beta^2\ (\alpha-\beta)\ (\gamma-\beta)}\ EXP(-\beta\ t) - \ldots$$

$$\ldots - \frac{-\gamma^4 + W_1\gamma^3 - W_2\gamma^2 + W_3\gamma - W_4}{\gamma^2\ (\alpha-\gamma)\ (\beta-\gamma)}\ EXP(-\gamma\ t)\}] \qquad [6.7]$$

where

a ... hollow cylinder inner radius

b ... hollow cylinder outer radius

E_2, η_1, η_2 ... viscoelastic constants

k ... ratio between the inside (p_i) and outside pressures

K ... bulk modulus

p ... outside pressure (for plane strain $p=p_e$; for axisymmetric loading $p=p_a=p_e$)

t ... time

u_a ... radial displacement at the hollow cylinder inner wall

$$W_1 = \frac{2E_2\eta_1 - 6K(\eta_1+\eta_2)}{\eta_1\eta_2}$$

$$W_2 = [\frac{6K(\eta_1+\eta_2) - E_2\eta_1}{\eta_1\eta_2}]^2 - \frac{6KE_2}{\eta_1\eta_2}$$

$$W_3 = \frac{6KE_2\ [3K(\eta_1+\eta_2) - E_2\eta_1]}{(\eta_1\eta_2)^2}$$

$$W_4 = (\frac{3KE_2}{\eta_1\eta_2})^2$$

α, γ ... are roots of:

$$6KE_2 + [6K(\eta_1+\eta_2) + E_2\eta_1]s + \eta_1\eta_2 s^2 = 0$$

$$\beta = \frac{E_2}{\eta_2}$$

All the above parameters have already been specified, except the bulk modulus. This constant should have been determined from the hydrostatic unload/reload cycles just after specimen reconditioning, but the testing results were not reasonable (Section 6.2.2). Consequently, it was calculated using the ultrasonic elastic constants. Ultrasonic constants are known to be higher than those obtained from static tests, but the elastic constants are also expected to be higher after specimen reconditioning than before testing. An average bulk modulus value of 22 GPa was assumed for specimens HC01 (HCAL Test 4) and HC06 (HCPS Test 2). Ideally, a parametric analysis should be executed to investigate how sensitive are the bore convergence predictions upon the assumed value of the bulk modulus.

Equations 6.6 and 6.7 are evaluated using a computer

program, written in FORTRAN. The constant values of a, b, E_2, η_1, η_2 and K are input and the program calculates the other constants, W_1, W_2, W_3, W_4, α, β and γ. Then, it reads from the datafile (hollow cylinder test output), the values of the axial, internal and external pressures and time, for each data point. The outside pressure is either assumed as equal to the external pressure for plane strain or taken as the average between the axial and external pressures (both values should be equal) for axisymmetric loading condition.

6.6.2.2 Power Law

The radial strain equation, in a function of time, for the power law is given by Eqn. 3.88 or 3.90, whether plane strain or axisymmetric loading condition, respectively. Only the time-dependent deformation component of the equations is considered, since the instantaneous response to the deviatoric pressure loading is not included in the hollow cylinder creep stage data. Applying boundary conditions (r=a) to the creep component of the above equations, the expression of the radial creep strain at the hollow cylinder inner wall becomes:

$$\epsilon_{r,a}(t) = \frac{3}{2} K \sigma_{e,a}^{(c-1)} t^a S_{r,a} \qquad [6.8]$$

where

$\epsilon_{r,a}$ ... radial creep strain at the hollow cylinder inner wall

a, c, K ... power law parameters

$\sigma_{e,a}$ ... effective or equivalent stress at the hollow cylinder inner wall

$S_{r,a}$ ... deviatoric radial stress at the hollow cylinder inner wall

t ... time.

What varies in Eqn. 6.8 for each loading condition is the definition of the axial which is implicit in the expressions for the e e and deviatoric radial stresses. The axial stress is either taken as the axial pressure for axisymmetric loading or given by Eqn. 3.10 for plane strain. Applying boundary conditions to Eqns. 3.4 and 3.5 and substituting the resulting relations into Eqns. 3.86 and 3.87, the final expressions for the effective and deviatoric radial stresses at the hollow cylinder inner wall are:

Axisymmetric Loading

$$\sigma_{e,a} = [\{\frac{-p(1-k)b^2}{b^2 - a^2}\}^2 + \frac{p^2}{3}(\frac{b^2-ka^2}{b^2-a^2} - 1)^2]^{1/2} \qquad [6.9]$$

$$S_{r,a} = \frac{-p(1-k)b^2}{b^2 - a^2} + \frac{p}{3}(\frac{b^2-ka^2}{b^2-a^2} - 1) \qquad [6.10]$$

Plane Strain

$$\sigma_{e,a} = [\{\frac{-p(1-k)b^2}{b^2 - a^2}\}^2 + \frac{p^2}{3}(1-2\nu)^2(\frac{b^2-ka^2}{b^2-a^2})^2]^{1/2} \qquad [6.11]$$

$$S_{r,a} = \frac{-p(1-k)b^2}{b^2 - a^2} + \frac{p}{3}(1-2\nu)\frac{b^2-ka^2}{b^2-a^2} \qquad [6.12]$$

where

a ... hollow cylinder inner radius

b ... hollow cylinder outer radius

k ... ratio between the inside and outside pressures

p ... outside pressure

ν ... Poisson's ratio.

All above parameters have been already specified, except the Poisson's ratio. It was calculated using the ultrasonic elastic constants. An average Poisson's ratio value of 0.333 was assumed for specimens HC01 (HCAL Test 4) and HC06 (HCPS Test 2). As suggested for the bulk modulus, a parametric analysis should be executed to investigate how sensitive are the bore convergence predictions to the assumed value of this constant.

6.6.2.3 Structural Law

The radial strain equation, in function of time, for the structural law is given by Eqn. 3.89 or 3.91, whether plane strain or axisymmetric loading condition, respectively. Again, only the time-dependent deformation component of the equations is considered. Applying boundary conditions (r=a) to the creep component of the above equations, the expression of the creep radial strain at the hollow cylinder inner wall becomes:

$$\epsilon_{r,a}(t) = \frac{3}{2}\frac{b_1}{\sigma_{e,a}}\frac{t^{(b2+1)}}{b_2+1} S_{r,a} \qquad [6.13]$$

where

$\epsilon_{r,a}$ ... radial creep strain at the hollow cylinder inner wall

b_1, b_2 ... structural law parameters

$\sigma_{e,a}$ ... effective or equivalent stress at the hollow cylinder inner wall

$S_{r,a}$ ... deviatoric radial stress at the hollow cylinder inner wall

t ... time.

Equations 6.9 and 6.10, and Eqns. 6.11 and 6.12 give the effective and deviatoric radial stresses for axisymmetric loading and plane strain conditions, respectively.

The expressions of the radial strain at the hollow cylinder inner wall for power and structural laws, Eqns. 6.8 and 6.13 respectively, can be easily evaluated using a spread sheet software for microcomputers. First, the equivalent and deviatoric radial stresses are calculated based on the readings of the internal and external pressures. For axisymmetric loading, the axial pressure readings can also be taken into account or simply, assumed as equal to the external pressure readings. Then, time 't' is read for each data point and the whole expression is calculated.

Radial strain rates can also be analysed following the same path of substitution indicated above, but using the creep strain rate equations (Eqns. 3.82 and 3.84). For the

structural law, this evaluation would be of special interest since its parameters are obtained from curve-fitting strain rate data.

6.6.3 Comparison Between Creep Model Predictions and Hollow Cylinder Bore Convergence

Two hollow cylinder creep stages, HCAL4CP1 and HCPS2CP1, were chosen as the database for the evaluation of the creep models. HCAL4CP1 creep stage was loaded under axisymmetric loading conditions (PO= 20 MPa; PI= 1 MPa) and ran for almost 55000 min. On the other hand, HCPS2CP1 creep stage was loaded under plane strain (PE= 20 MPa; PI= 11 MPa) and ran for 8000 min. Bore convergence data, both measured directly (BC measured) and calculated from VCI measurements (BC from VCI), are plotted to give a range of possible variations.

Comparing hollow cylinder test results with model predictions obtained from triaxial tests, raises an important question related to which triaxial stress state should be taken to generate the model parameters. The reason for this difficulty lies on the nature of hollow cylinder tests. Assuming linear elastic material behaviour, as an example only, the state of stress along the hollow cylinder wall varies at each radius point, as defined by Eqns. 3.1 and 3.2. As demonstrated in this chapter, creep model parameters are highly dependent on the confining and deviatoric stresses, among other factors. Therefore, the

selection of triaxial stress states that would be representative of hollow cylinder tests, seems to be the major task in performing a reasonable comparison between hollow cylinder test results and predictions of creep models based on triaxial creep data.

Three alternatives can be suggested to associate triaxial to hollow cylinder stress states. The first approach assumes an average stress state, defined by elasticity, just before starting creep stages (Sterne, 1981). The average elastic radial and tangential stresses can be calculated by integrating Eqns. 3.1 and 3.2 along the radius and dividing by the hollow cylinder wall thickness. The final expressions are:

$$\sigma_{r,avg} = \frac{(p_e b + p_i a)(b-a)}{b^2 - a^2} \qquad [6.14]$$

$$\sigma_{\theta,avg} = \frac{(p_e b - p_i a)(b+a)}{b^2 - a^2} \qquad [6.15]$$

Model parameters should be obtained from triaxial creep tests run at this average stress state. The second approach would involve a series of triaxial creep tests executed at different stress states, which are representative of the distribution of stresses along the hollow cylinder wall. Elasticity is again assumed for this matter. Model parameters should be obtained from curve-fitting all data at once. This is perhaps the most common practice. Finally, the third approach would also involve a triaxial creep testing

program. Model parameters are obtained for each creep stage. Then, relationships between the parameters and stress states should be described by equations (e.g., best-fits). The constant parameters in the analytical solutions should be substituted by these parameter equations. A similar approach was followed by Santarelli et al. (1986) and Santarelli and Brown (1987) to study the effects of the dependence between elastic constants and stress states on analytical solutions for boreholes.

This research is limited to the two first approaches only. The average elastic stresses are $\sigma_{r,avg}$ = 16.5 MPa and $\sigma_{\theta,avg}$ = 25.6 MPa for HCAL4CP1 creep stage and $\sigma_{r,avg}$ = 18.3 MPa and $\sigma_{\theta,avg}$ = 22.7 MPa for HCPS2CP1 creep stage. These values show how the average state of stress (high confining and relatively small deviatoric stresses) in the hollow cylinder wall can vary from those used in the triaxial testing program. Some triaxial creep tests had confining stresses of the same order of magnitude, but the applied deviatoric stresses were usually higher. This can justify the discrepancy between deformation levels measured in triaxial and hollow cylinder creep tests. Considering that the stress state of no single triaxial creep stage can be associated to the average hollow cylinder stress state, the second approach, involving average parameters for all creep stages, would be more appropriate for the creep model evaluation performed in this research.

For further research, a testing program of triaxial creep stages that approximates more closely the hollow cylinder stress distribution, can be suggested (Fig. 6.27):

1. Assume that the stress distribution in the hollow cylinder, immediately after the deviatoric pressure loading, can be described by Eqns. 3.1 and 3.2 (elasticity).
2. Divide the hollow cylinder wall into three thirds and calculate the stress states at the hollow cylinder inner wall (r=a) and at the limit points between the first and second ($r=r_1$), and between the second and third ($r=r_2$) thirds. It is assumed there are no boundary stress effects at the hollow cylinder outer wall (r=b), therefore the pressure is reestablished at its original value and there is no deviatoric stress at that point.
3. A fourth stress state equal to the average hollow cylinder stress state can also be considered.
4. Consolidate specimens under hydrostatic creep (both confining and axial stresses are equal). The duration of the hydrostatic creep stage should consider a specimen reconditioning criterion.
5. Load specimens triaxially to one of the creep states. Preferably, follow a J1-type stress path because it simulates better an opening excavation. Keep specimens under triaxial creep for a certain period of time. Multi-creep stage tests, although not ideal, can be tolerated when the level of deformations is still low.

6. Obtain creep model parameters by curve-fitting the data of creep stages. The average parameter approach (approach 2) should evaluate all creep stage data at once. The parameter equation approach (approach 3) finds the relationships between parameters and the radius 'r' (it is a indication of the stress state). Parameter equations as a function of radius could be very convenient to substitute into analytical solutions for the thick-walled cylinder.

Finally, Table 6.8 presents the creep model evaluation program performed in this thesis. The number indicated in the box is the equation number used for calculating the desired variable. For instance, the radial strain predictions for the HCAL4CP1 creep stage, using power law parameters based on CTC creep stages, are calculated by Eqns. 6.8, 6.9 and 6.10 and compared to hollow cylinder results calculated by Eqn. 6.5. For each hollow cylinder creep stage (HCAL4CP1 and HCPS2CP1), predictions based on both CTC and JTC creep stages were calculated. They are indicated in Figs. 6.28 to 6.30 by an abbreviation of the creep model name and the stress path. As an example, PW-ctc means predictions of the power law based on parameters obtained from CTC creep stages. The actual deformation on the figures was calculated either from the bore convergence measurements (from BC) or from the bore volume change measurements (from VCI). Figure 6.28 shows the comparison between the generalized Kelvin model predictions of radial

displacements (BC prediction) and the hollow cylinder bore convergence results (BC measured and BC from VCI). Only the predictions based on parameters from CTC tests are shown, because the predictions using parameters from JTC tests are about one order of magnitude greater. Power (PW) and structural (ST) law predictions of radial strain (ϵ_r) and radial strain rate ($\dot{\epsilon}_r$) are compared to hollow cylinder results calculated from bore convergence data (Fig 6.29 for HCAL4CP1 and Fig. 6.30 for HCPS2CP1). Again, only the predictions for radial strain obtained from CTC test parameters are provided.

Regardless of the creep model, all predictions based on parameters from JTC tests were at least one order of magnitude greater than the measured deformation. This is a consequence of the results of the triaxial testing program, where creep tests following a JTC path showed much higher time-dependent response than those following a CTC path. Unfortunately, no conclusions can be drawn on the preferable triaxial stress path, since all triaxial tests were executed with stress states higher than those encountered along the hollow cylinder wall. These conclusions could only be drawn, if the triaxial creep tests were executed following the testing program previously recommended (Fig. 6.27).

Figure 6.28 depicts that the generalized Kelvin model predictions based on CTC test parameters fit the magnitudes of the bore convergence well for both hollow cylinder creep stages. Although the predicted and measured values are

within a narrow range, the forms of the time-dependent curves are different. While the bore convergence curve (especially the BC measured) tends to a reduced rate with increasing time, the model prediction curve assumes a constant rate, as expected.

Figures 6.29 and 6.30 present the comparison amongst the power and structural law predictions, radial strain and radial strain rate. The power law results, based on CTC test parameters (PW-ctc), overpredicted the radial strain by a factor of two. The predictions of the structural law (ST-ctc) were higher (about five times). Despite the differences in magnitude, the shapes of the predicted and measured curves are alike, because both creep laws describe a transient response. For the radial strain rate, the power and structural laws provided reasonable predictions, although the structural law trend is closer to the actual data. These findings seem to confirm that creep models derived from a certain type of data should only be used for predicting the same type of data.

6.7 Summary and Conclusions

This chapter presented the laboratory test results and showed how an evaluation program of creep models based on triaxial data can be performed using hollow cylinder experiments as model tests.

Specimens were first hydrostatically loaded and kept under hydrostatic creep to reverse post-sampling cracks and

fissures. Hydrostatic loading data were neither used for calculating current geometries nor for obtaining model parameters. They were only analysed to investigate the efficiency of the specimen reconditioning procedure, which was based on a minimum time period of three days under hydrostatic creep. The results showed that ultrasonic wave tests provide a reasonable indication of specimen post-sampling conditions. The specimen reconditioning criterion based on a minimum time period of three days was sufficient for most specimens, but it can be improved if combined with a maximum strain rate criterion (e.g., 100 microstrains per day). Finally, a specimen reconditioning procedure was suggested to minimize differences among specimens and therefore, produce more uniform test results. This procedure is based on the preliminary selection of specimens using ultrasonic tests and hydrostatic creep till a certain specimen reconditioning criterion is met. Ultrasonic tests during the hydrostatic creep stage could also reinforce this procedure.

Triaxial creep tests were carried out on specimens previously loaded by CTC and JTC stress paths. The results of CTC creep stages are in agreement with the salt literature. Creep deformation is directly proportional to the applied deviatoric stress and inversely proportional to the confining stress. JTC creep stage results showed directly proportional relationships between creep deformation and both confining and deviatoric stresses. The

creep deformation dependence on the confining stress for JTC creep stages is a reverse relationship to that obtained from CTC creep stages. The higher the confining stress, the higher the creep deformation from JTC creep stages, keeping the other variables constant. Furthermore, the magnitude of creep deformation from JTC creep stages is considerably higher than that from CTC creep stages. It seems that the simultaneous increase of the axial stress and reduction of the confining stress is possibly favourable to crack propagation, which according to the structural theory of brittle creep, can positively contribute to the transient creep response. These speculations have to be confirmed by a more extensive testing program, since they can play an important role on creep model parameters.

Four creep models, power and structural laws, Kelvin and generalized Kelvin (fluid) models, were chosen to fit the transient creep stage data. Creep model parameters were obtained from non-linear regression analyses using the BMDP statistical software. Curve-fitting procedures based on weighed data were recommended to compensate for the different lengths of time interval that contains a particular data point (i.e., non-uniform data distribution along the time scale). Also, a correction of the correlation coefficients should be done to take into account the different number of data points for each creep stage.

Three types of model evaluation were done using triaxial creep data. First, model predictions were compared

to the actual creep data used for generating the model parameters. All creep models respond well to this evaluation, except the Kelvin model that showed a trend to underpredict the measured strains of the second half of the creep stage duration. This may point to the importance of the models selected to describe actual data. Their equations should be flexible enough to describe the trend of actual data, without any constraints (e.g., $\epsilon = \Delta\sigma/E$ for $t \to \infty$). The second evaluation used only data of the first half of the creep stage duration for obtaining model parameters. The second half of the creep stage duration was for comparing the model predictions. The differences increased for all models, but especially for the rheological ones as a result of their equation impositions of specified strain rates. This may indicate how important the duration of creep stages used for generating model parameters is, because these models are commonly used for predicting data well beyond the time limits of creep experiments. The last evaluation involved the use of model equations obtained from curve-fitting one type of data (e.g., strain) to extrapolate results of another type of data (e.g., strain-rate). The results showed that even though there may exist a relationship between both types of data, this procedure is usually not valid, because model parameters are in fact, curve-fitting parameters, which are highly dependent on the data type that generates them. Also, the problem of predicting strain from strain-rate data and vice-versa

relies on the difficulty of estimating the initial strain which mathematically is represent by the constants of integration.

Hollow cylinder data were presented and discussed. The responses to the deviatoric pressure loading presented some non-linearity, which is quite a characteristic of this material. Bore convergence results of creep stages showed a reasonable dependence on the applied state of stress, although some discrepant results were found. Some simplified equations were presented to convert the bore convergence results into radial strain and radial strain rate, in order to compare with analytical predictions.

Finally, an evaluation of creep models was performed. The difficulties of associating triaxial states of stress with hollow cylinder tests were examined. A procedure based on a triaxial creep testing program was suggested. It assumes an elastic stress distribution on the hollow cylinder, just before the creep stage starts. Triaxial creep tests would be carried out at stress states that are representative of the stress distribution along the hollow cylinder wall. Model parameters would be obtained from these triaxial creep stages. For this research, model parameters for the evaluation program were obtained from curve-fitting all creep stages at once. It is known that the triaxial creep stages were executed at deviatoric levels higher than those commonly found in hollow cylinder tests, what may have caused an overestimation of the model parameters and

consequently their predictions. All predictions based on parameters obtained from JTC tests were about one order of magnitude greater than the actual deformation.

The generalized Kelvin model predicted quite well the bore convergence of both hollow cylinder creep stages. Unfortunately, the forms of the predicted and measured curves are not similar and any extrapolation to times beyond the test duration could cause increasing errors. The structural law seems to be the most appropriate to describe the radial strain rate, because it is derived from the same type of data, gives a reasonable match of magnitudes and follows the trend of the actual data. The power law describes quite well the radial strain response. It slightly overpredicted the measured deformation, but the forms of the predicted and measured curves were similar. The reason for the overprediction may be attributed to the higher stress states used in the triaxial tests than in the hollow cylinder tests. Following the triaxial stress states suggested in the testing program, previously recommended to compare triaxial to hollow cylinder stress states, those differences may diminish. In conclusion, the power law appears to be the most adequate creep model to describe the transient response of circular openings in potash.

Table 6.1 Comparison of cylindrical specimen deformations under hydrostatic loading and ultrasonic wave test results

Test	Specimen No.	V_p (m/s)	Hydrostatic Loading (p at 20 MPa)		Hydrostatic Creep Stage			
			ϵ_z(%)	ϵ_v(%)	ϵ_z(%)	ϵ_v(%)	$\dot{\epsilon}_{z*}$ (μstrain per day)	$\dot{\epsilon}_{v*}$ (μstrain per day)
CTC1	TR02	2853	1.03	7.63	0.49	0.58	267	207
CTC2	TR03	2945	0.20	7.67	0.07	1.47	-254	241
CTC3	TR04	3679	0.02	1.13	0.05	1.36	102	518
CTC4	TR06	3214	0.28	5.16	0.11	1.74	62	67
JTC1	TR05	3181	0.42**	4.94	0.14	1.31	115	-99
JTC2	TR07	3108	0.60	3.00	0.15	1.12	-46	120
JTC3	TR08	3518	0.17	1.12	0.16	0.40	269	540

* average strain rates during the last day (1440 min) of hydrostatic creep stage

** assumed

Table 6.2 Comparison of hollow cylinder specimen deformations under hydrostatic loading and ultrasonic wave test results

Test	Specimen No.	V_p (m/s)	Hydrostatic Loading (p at 20 MPa)		Hydrostatic Creep Stage			
			ϵ_z(%)	ϵ_v(%)	ϵ_z(%)	ϵ_v(%)	$\dot{\epsilon}_{z*}$ (μstrain per day)	$\dot{\epsilon}_{v*}$ (μstrain per day)
HCAL1	HC04	3728	0.07**	2.9**	0.015	0.95	46	2000
HCAL2	HC05	3807***	0.18	2.8	0.043	0.90	49	841
HCAL3	HC02	3660	0.41	4.6	0.045	1.25	60	5668
HCAL4	HC01	4042	0.21	2.4	0.055	1.57	58	2378
HCPS1	HC03	3653	0.16	2.9	0.090	1.00	110	1787
HCPS2	HC06	3536	0.26	3.7	0.025	1.10	0	2881

* average strain rates during the last day (1440 min) of hydrostatic creep stage

** assumed

*** no available data for BT phase; BP-phase value is assumed

Table 6.3 Power law parameters obtained from non-linear regression analyses (BMDP)

$$\epsilon = B\ \Delta\sigma^{c}\ t^{a}$$

Creep Stage	B x 10^{-6} ($MPa^{-c}.min^{-a}$)	c	a
CTC1CRP1	4 x 10^{-1}	1.466	0.429
CTC3CRP1	130	-0.942	0.521
CTC3CRP2	27	-0.234	0.859
CTC4CRP1	7 x 10^{-6} *	5.221	0.365
CTC4CRP2	1786 *	-0.702	0.373
All CTCs	14	0.783	0.355
JTC1CRP1	1973	-0.593	0.435
JTC2CRP1	308	-0.987	0.873
JTC2CRP2	4406	-0.468	0.511
JTC3CRP1	5	2.284	0.280
All JTCs	3	1.943	0.472
All Tests	96	0.113	0.571

* parameter may not affect the function value

Table 6.4 Structural law parameters obtained from non-linear regression analyses (BMDP)

$$\dot{\epsilon} = b_1 \; t^{b_2}$$

Creep Stage	b_1 (min^{-b2}/day)	b_2
CTC1CRP1	0.240	-0.643
CTC3CRP1	0.038	-0.618
CTC3CRP2	0.017	-0.159
CTC4CRP1	0.434	-0.899
CTC4CRP2	0.601	-0.970
All CTCs	0.376	-0.779
JTC1CRP1	0.610	-0.708
JTC2CRP1	0.034	-0.159
JTC2CRP2	1.833	-0.658
JTC3CRP1	14.639	-0.986
All JTCs	2.721	-0.735
All Tests	0.516	-0.731

Table 6.5 Kelvin model parameters obtained from non-linear regression analyses (BMDP)

$$\epsilon = \Delta\sigma/E\,[1-\exp(-E/\eta \cdot t)]$$

Creep Stage	E (GPa)	η x 10^3 (GPa.min)
CTC1CRP1	12.4	4.2
CTC3CRP1	7.9	8.9
CTC3CRP2	0.5	3.4
CTC4CRP1	9.2	7.3*
CTC4CRP2	21.5	8.7*
All CTCs	11.6	4.6
JTC1CRP1	1.7	0.7
JTC2CRP1	0.1	1.8
JTC2CRP2	1.0	0.3
JTC3CRP1	0.5	0.1
All JTCs	0.5	0.2
All Tests	-20.2	39.2

* parameter may not affect the function value

Table 6.6 Generalized Kelvin (fluid) model parameters obtained from non-linear regression analyses (BMDP)

$$\epsilon = \Delta\sigma/E_2\,[1-\exp(-E_2/\eta_2 \cdot t)] + \Delta\sigma/\eta_1 \cdot t$$

Creep Stage	$\eta_1 \times 10^3$ (GPa.min)	E_2 (GPa)	$\eta_2 \times 10^3$ (GPa.min)
CTC1CRP1	43.5	20.6	3.3
CTC3CRP1	62.3	15.3	7.9
CTC3CRP2	4.5	26.0	2.6*
CTC4CRP1	154.0	12.0	7.4
CTC4CRP2	394.4	24.7	16.7
All CTCs	64.1*	17.5	3.7
JTC1CRP1	4.3	3.4	0.5
JTC2CRP1	34.5*	0.1	1.9
JTC2CRP2	1.5	2.6	0.3
JTC3CRP1	1.6	0.6	0.1
All JTCs	3.4	0.9	0.1
All Tests	13.0	41.8	0.5

* parameter may not affect the function value

Table 6.7 Comparison of creep model parameters obtained from non-linear analyses (BMDP), using half (H) and full (F) test duration

Creep Law	Test Duration	$B/b_1/-/\eta_1$	$c/-/E/E_2$	$a/b_2/\eta/\eta_2$
CTC1CRP1				
PW	H	1.2	1.240	0.429
	F	0.4	1.467	0.430
ST	H	0.281	-	-0.679
	F	0.241	-	-0.644
KL	H	-	14.0	3.6
	F	-	12.4	4.2
GK	H	35.3	22.6	3.3
	F	43.5	20.6	3.3
CTC3CRP1				
PW	H	125	-0.936	0.526
	F	130	-0.942	0.521
ST	H	0.033	-	-0.585
	F	0.039	-	-0.619
KL	H	-	9.9	7.3
	F	-	7.9	8.8
GK	H	48.0	19.1	7.3
	F	62.3	15.3	7.9

Table 6.8 Creep model evaluation program (number in the box indicates the equation number needed to calculate the desired variable)

HC Creep Stage	Triaxial Creep Type	Variables	Generalized Kelvin		Power Law		Structural Law	
			Predictions	HC Results	Predictions	HC Results	Predictions	HC Results
HCAL4 CP1	CTC	u	6.7	BC or 6.4	-	BC or 6.4	-	BC or 6.4
		ϵ_r	-	-	6.8/6.9/6.10	6.5	6.13/6.9/6.10	6.5
		$\dot{\epsilon}_r$	-	-	3.82/6.9/6.10	6.5/6.3	3.84/6.9/6.10	6.5/6.3
	JTC	u	6.7	BC or 6.4	-	BC or 6.4	-	BC or 6.4
		ϵ_r	-	-	6.8/6.9/6.10	6.5	6.13/6.9/6.10	6.5
		$\dot{\epsilon}_r$	-	-	3.82/6.9/6.10	6.5/6.3	3.84/6.9/6.10	6.5/6.3
HCPS2 CP1	CTC	u	6.6	BC or 6.4	-	BC or 6.4	-	BC or 6.4
		ϵ_r	-	-	6.8/6.11/6.12	6.5	6.13/6.11/6.12	6.5
		$\dot{\epsilon}_r$	-	-	3.82/6.11/6.12	6.5/6.3	3.84/6.11/6.12	6.5/6.3
	JTC	u	6.6	6.4	-	BC or 6.4	-	BC or 6.4
		ϵ_r	-	-	6.8/6.11/6.12	6.5	6.13/6.11/6.12	6.5
		$\dot{\epsilon}_r$	-	-	3.82/6.11/6.12	6.5/6.3	3.84/6.11/6.12	6.5/6.3

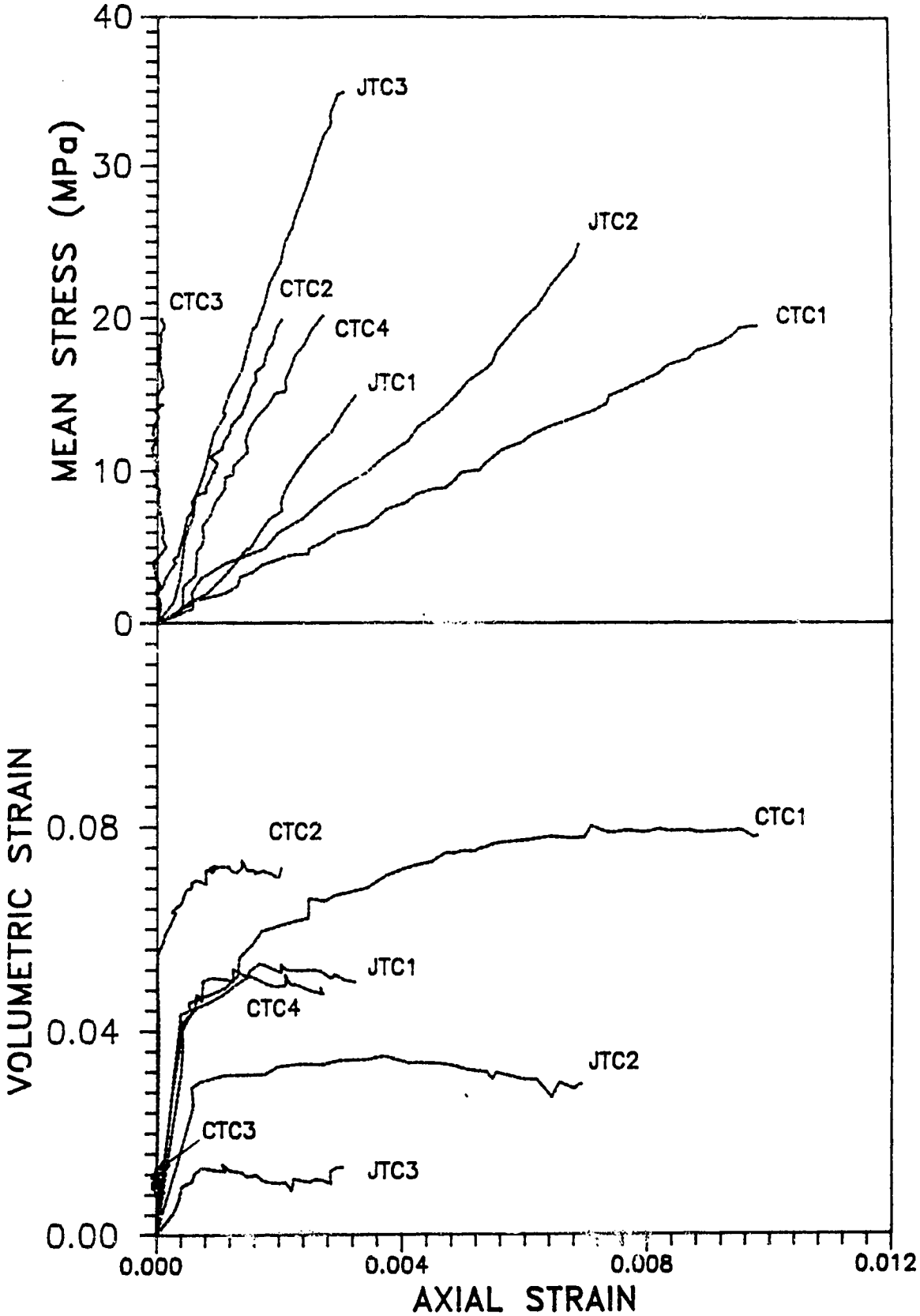

Figure 6.1 Triaxial testing program - Hydrostatic loading - Stress vs strain curves

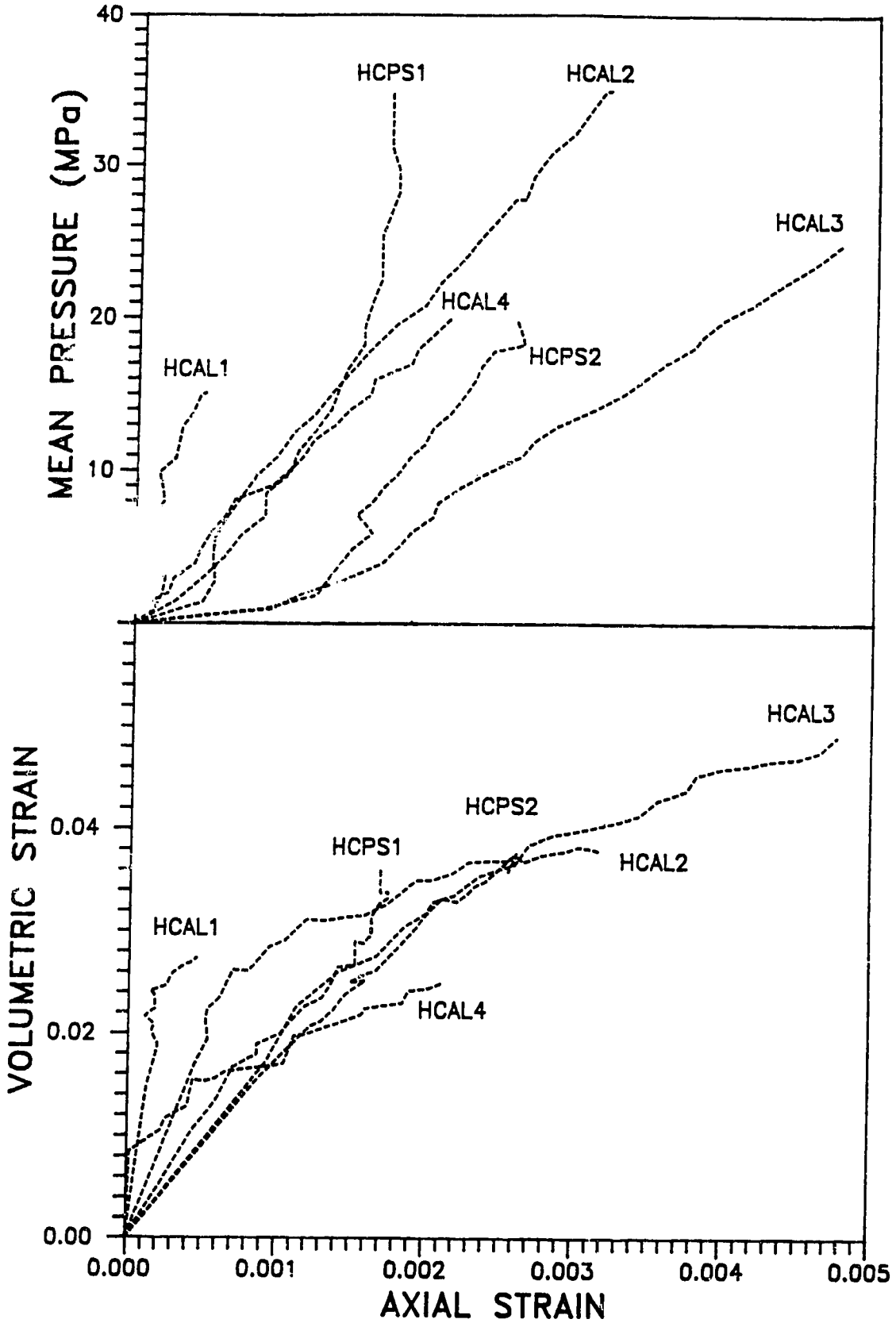

Figure 6.2 Hollow cylinder testing program - Hydrostatic loading - Stress vs strain curves

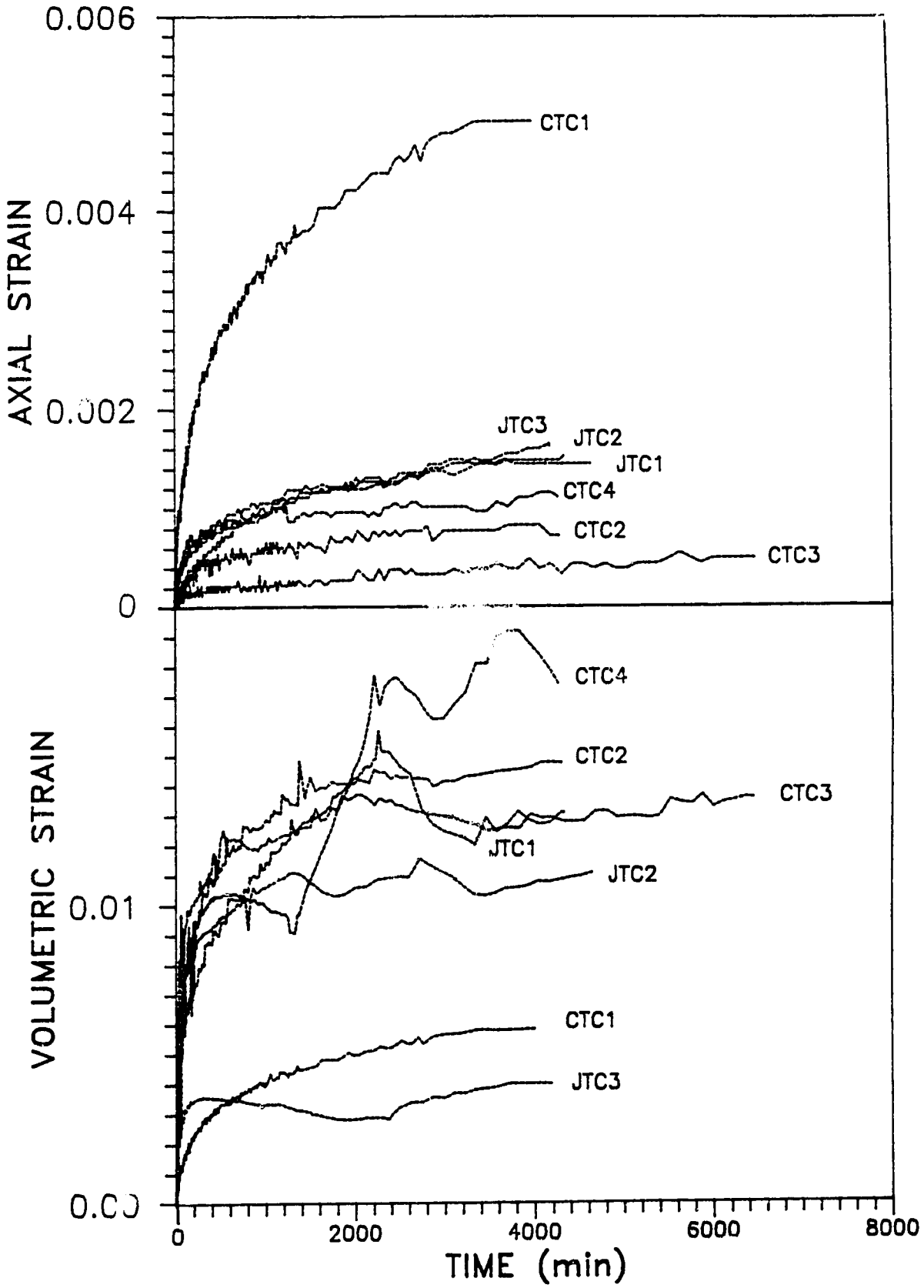

Figure 6.3 Triaxial testing program - Hydrostatic loading - Strain vs time curves

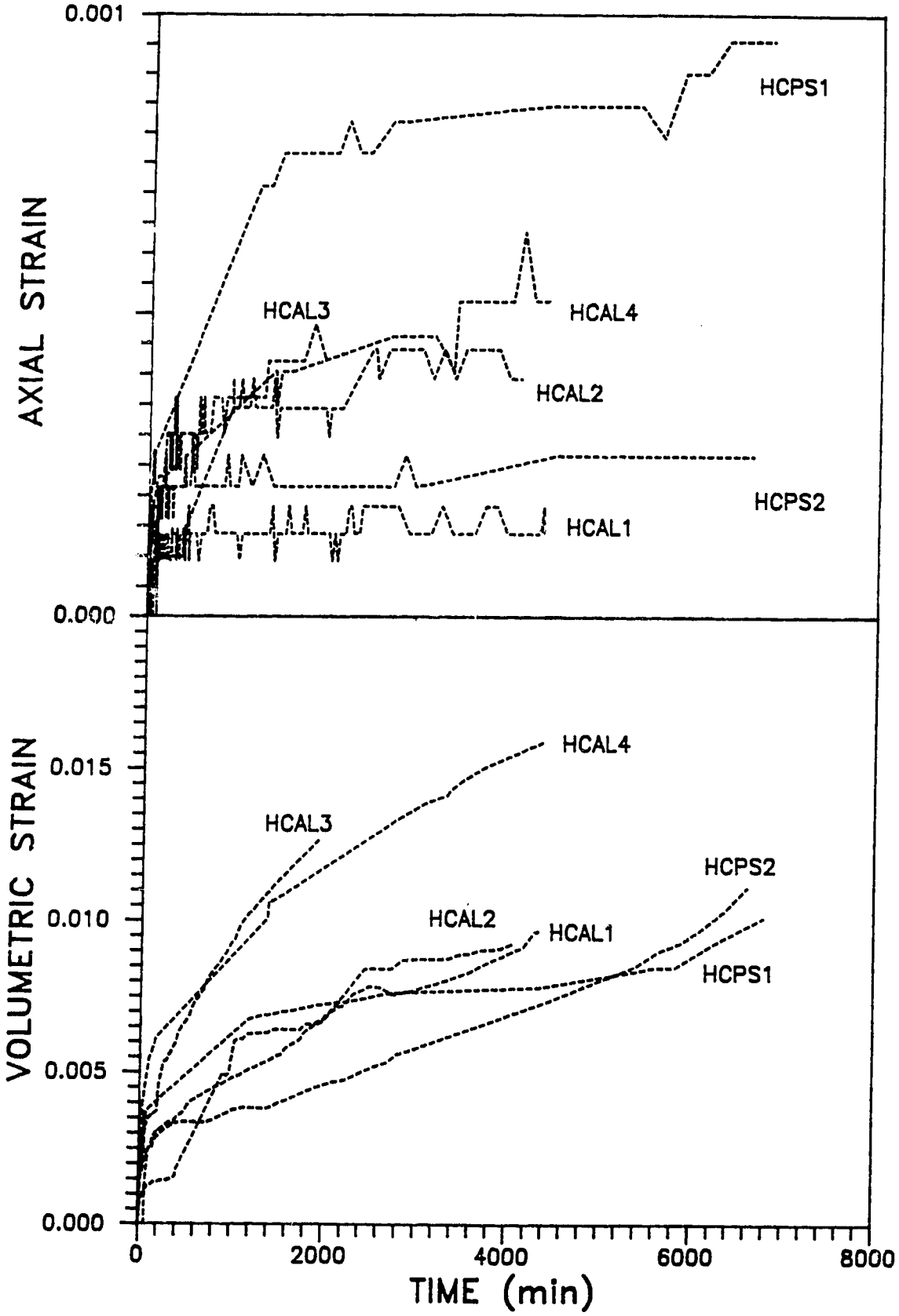

Figure 6.4 Hollow cylinder testing program - Hydrostatic loading - Strain vs time curves

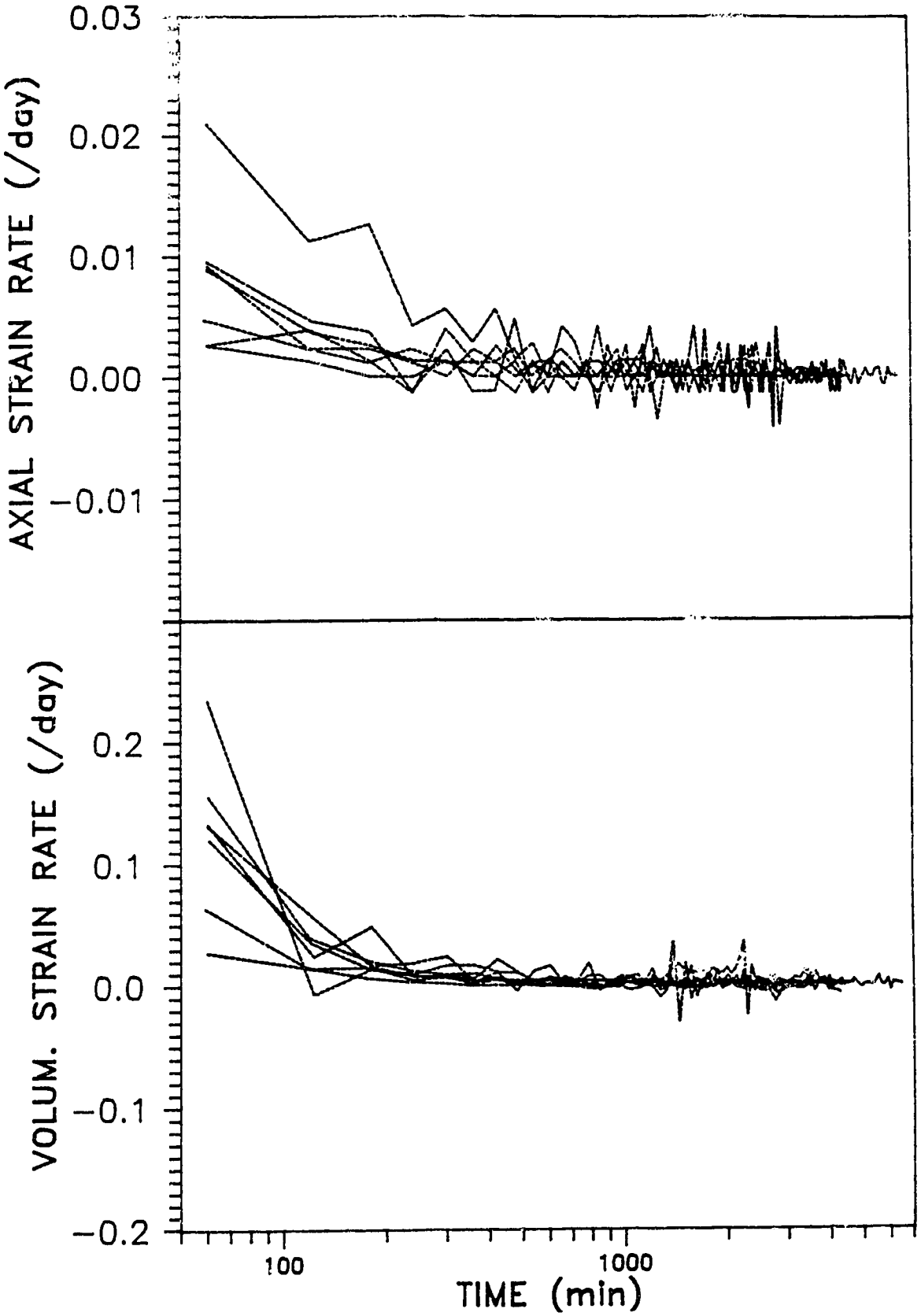

Figure 6.5 Triaxial testing program - Hydrostatic loading - Strain rate vs time (log) curves for all specimens

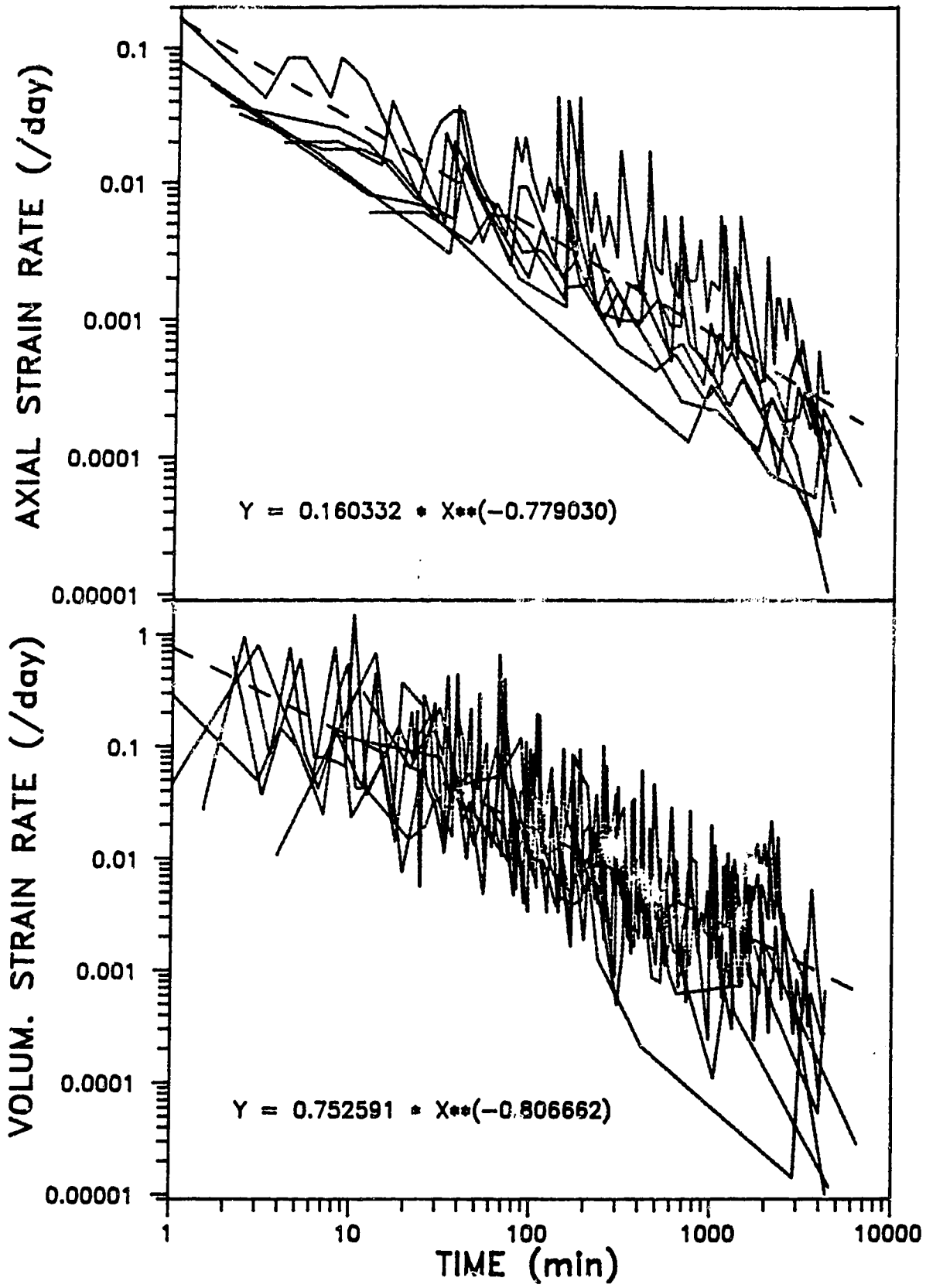

Figure 6.6 Triaxial testing program - Hydrostatic loading - Strain rate (log) vs time (log) curves for all specimens

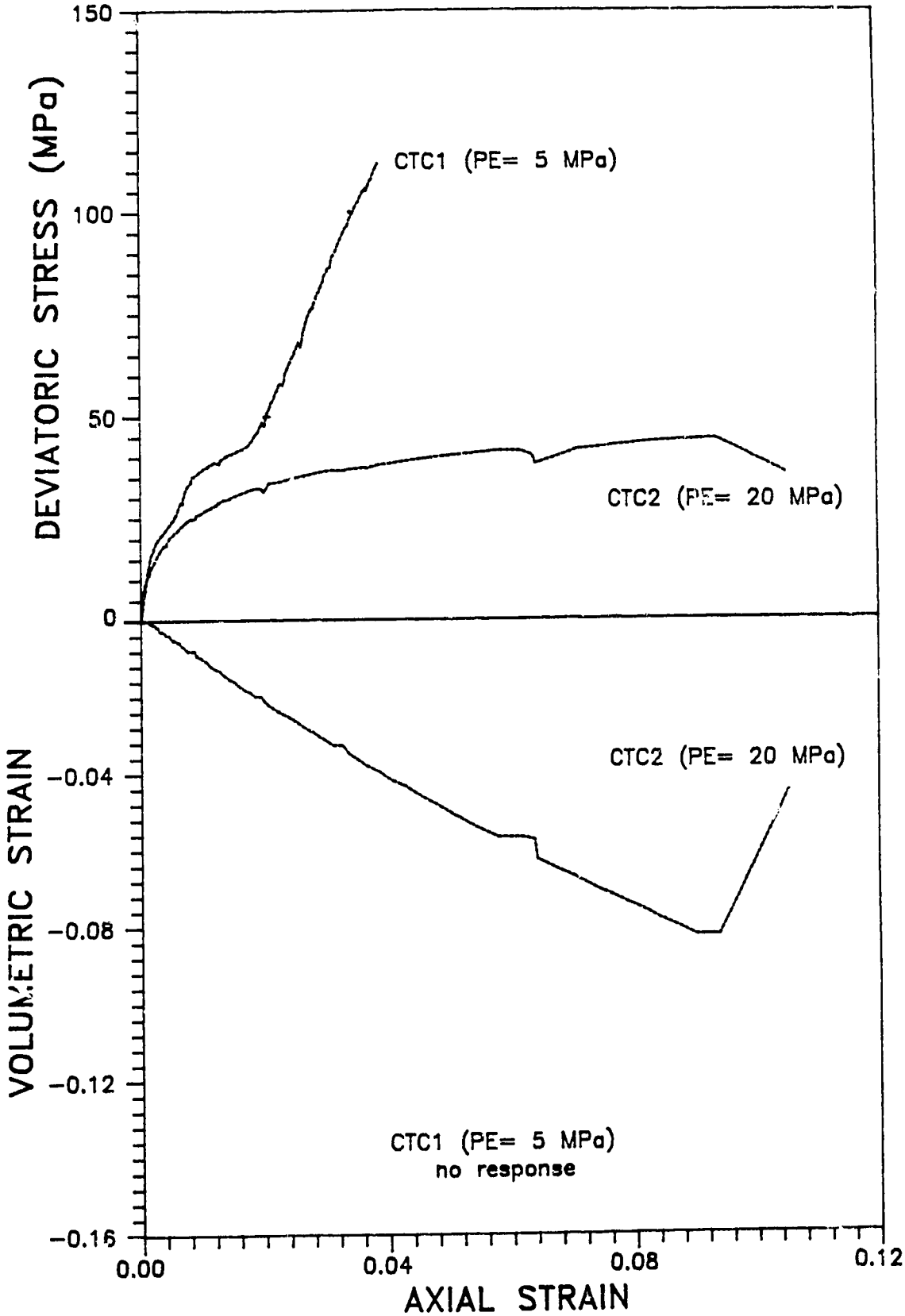

Figure 6.7 CTC Tests 1 and 2 - Stress vs strain curves

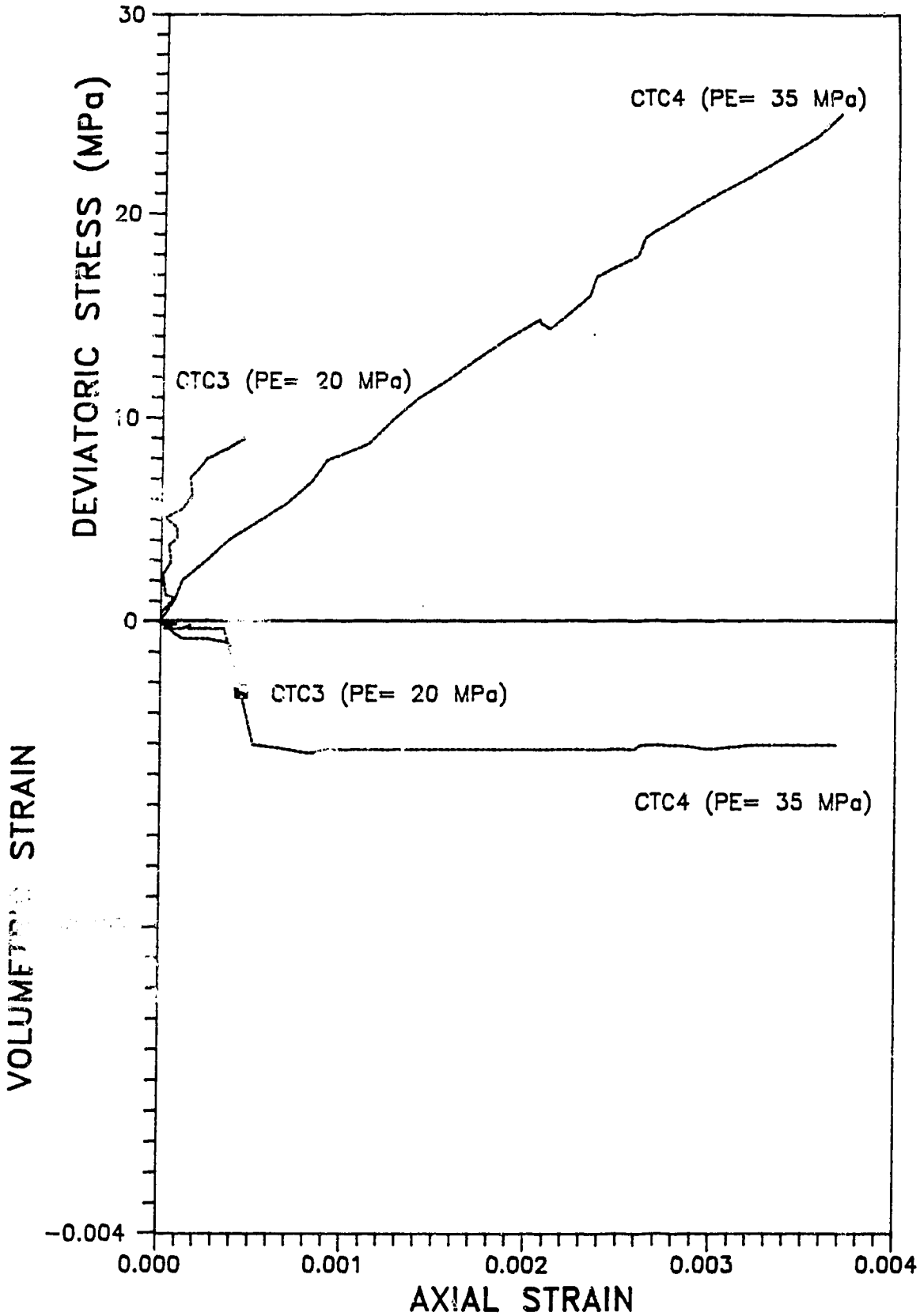

Figure 6.8 CTC Tests 3 and 4 - Stress vs strain curves (1st triaxial loading stage)

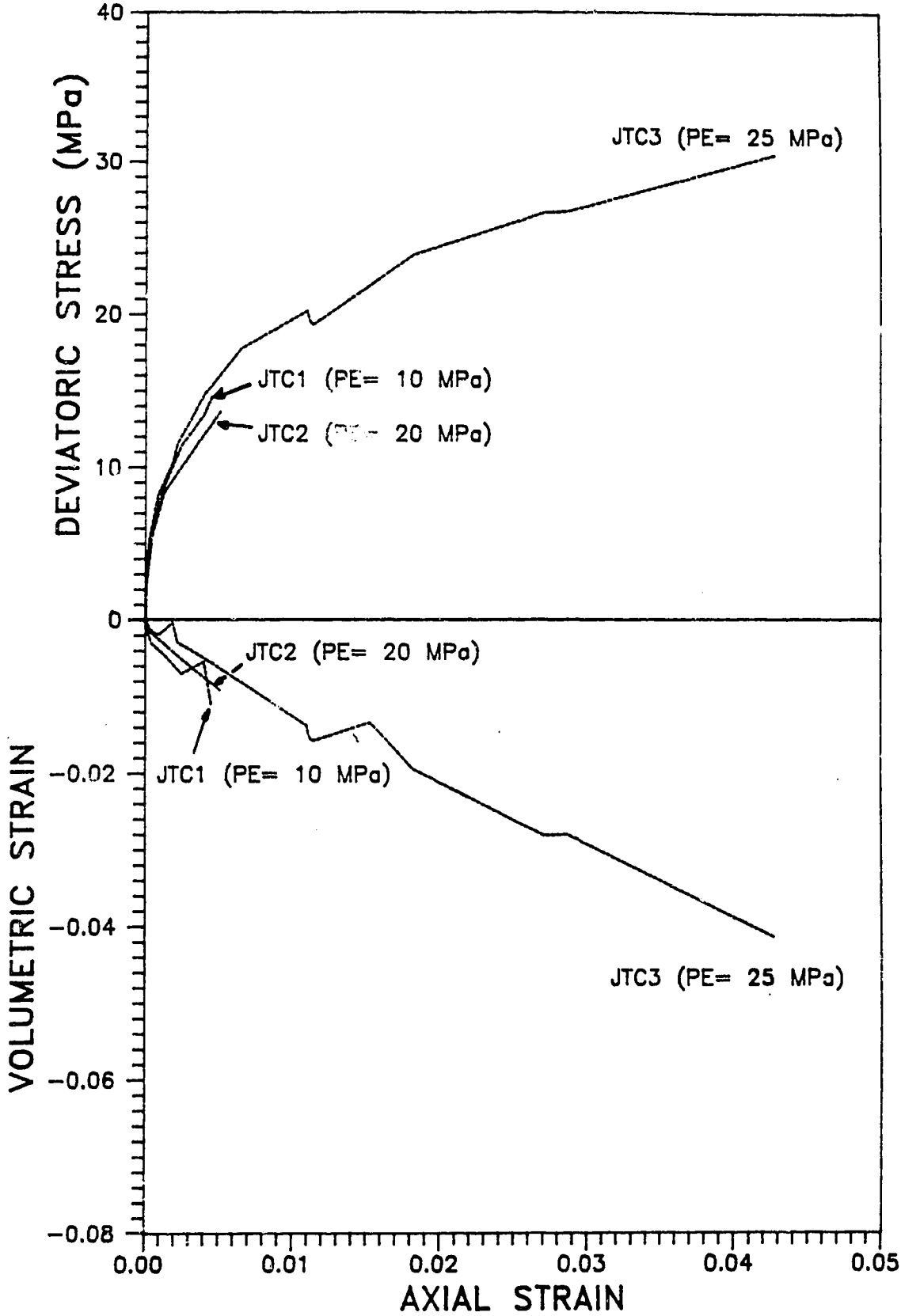

Figure 6.9 JTC Tests - Stress vs strain curves (1st triaxial loading stage)

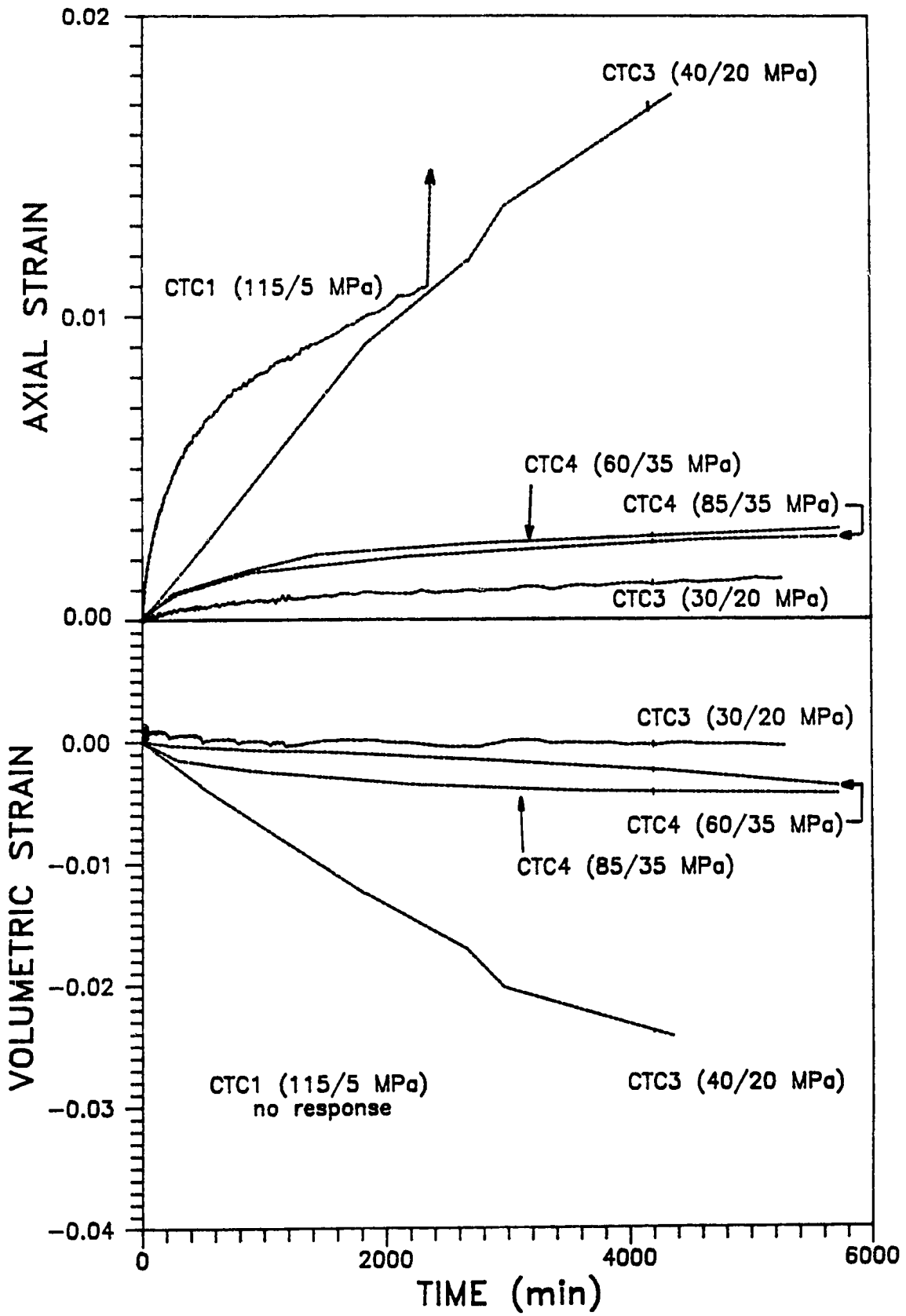

Figure 6.10 CTC Tests - Strain vs time curves (σ_1/σ_3 MPa)

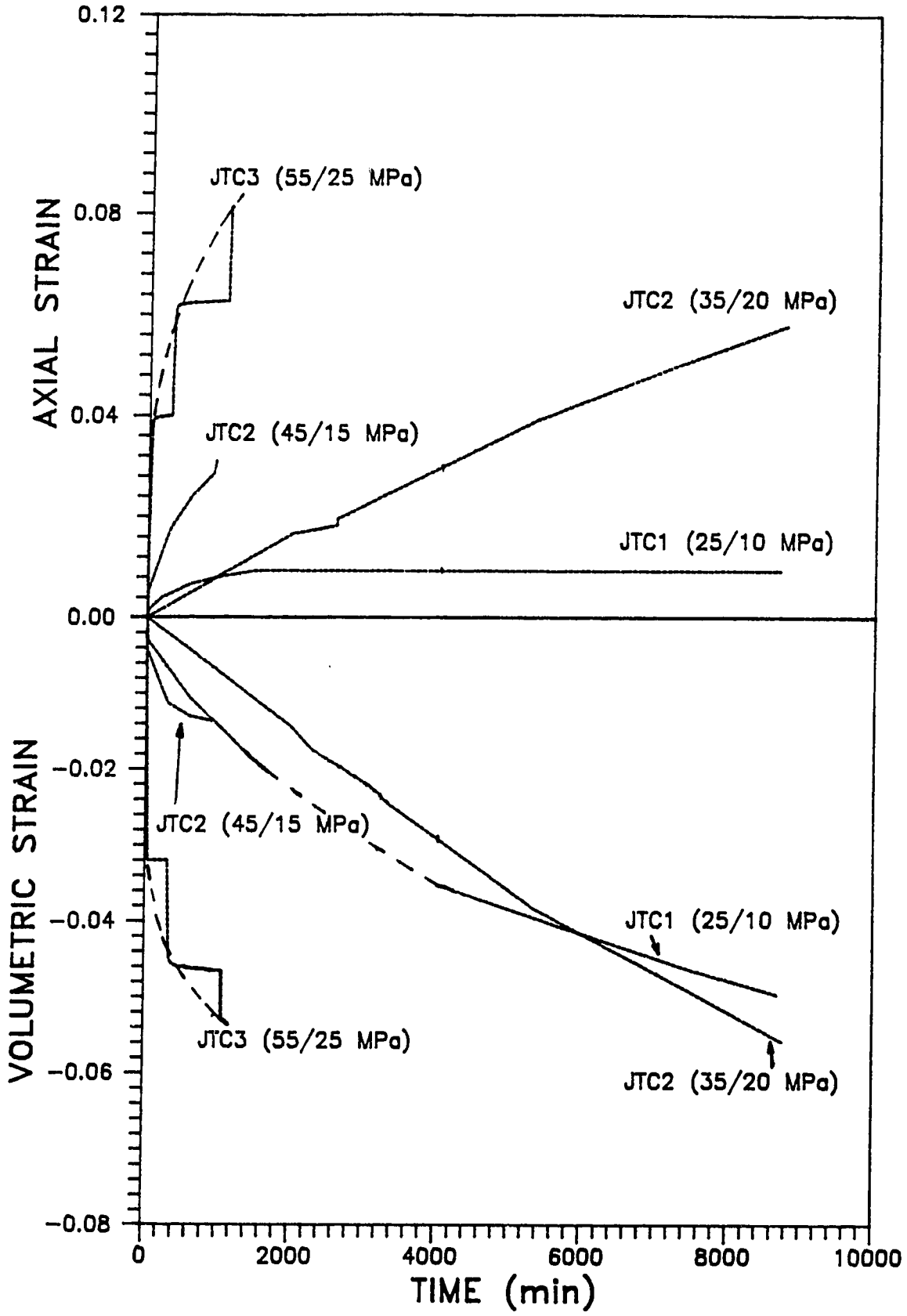

Figure 6.11 JTC Tests - Strain vs time curves (σ_1/σ_3 MPa)

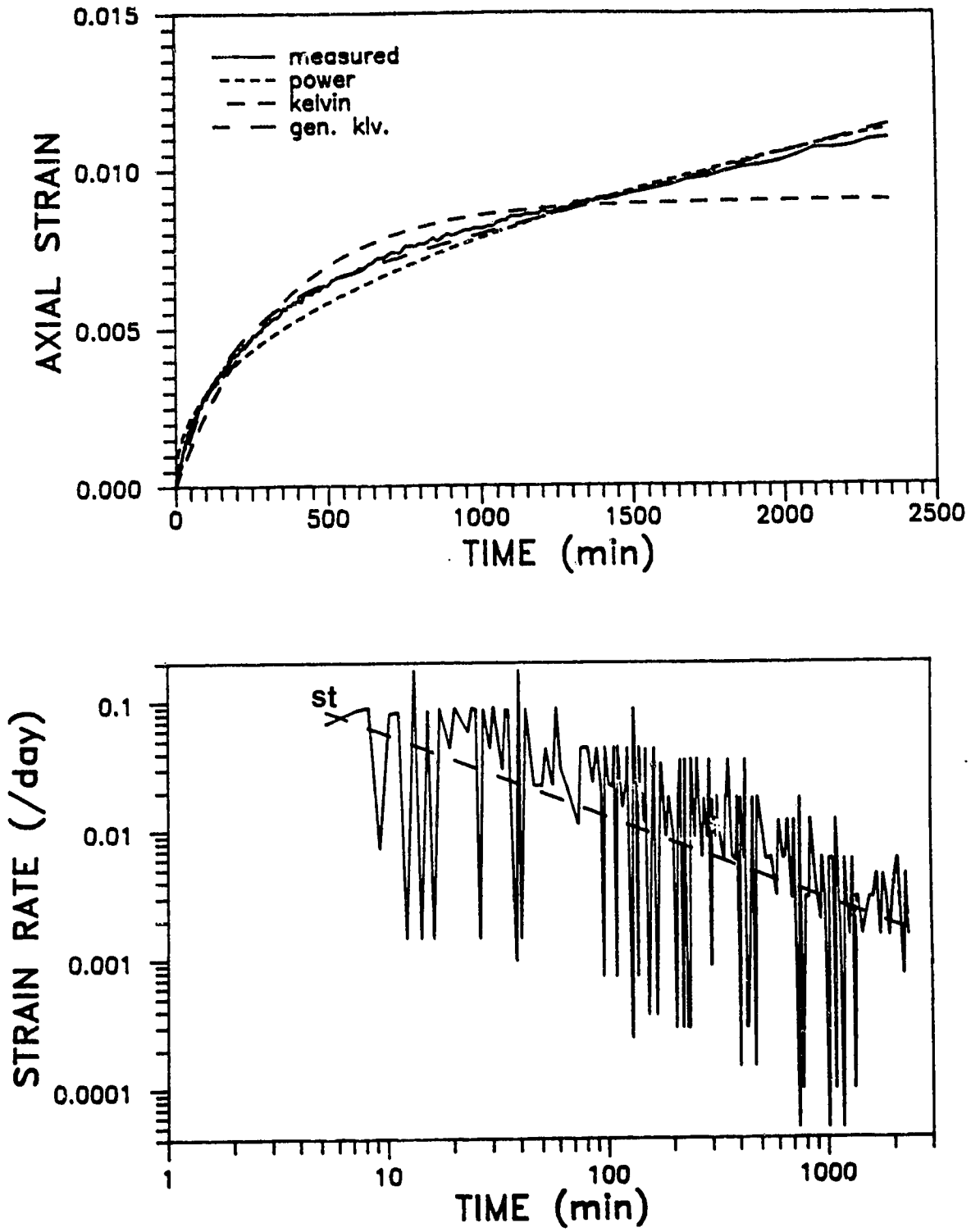

Figure 6.12 CTC Test 1 (1st creep stage) - Comparison between creep model predictions and actual creep data

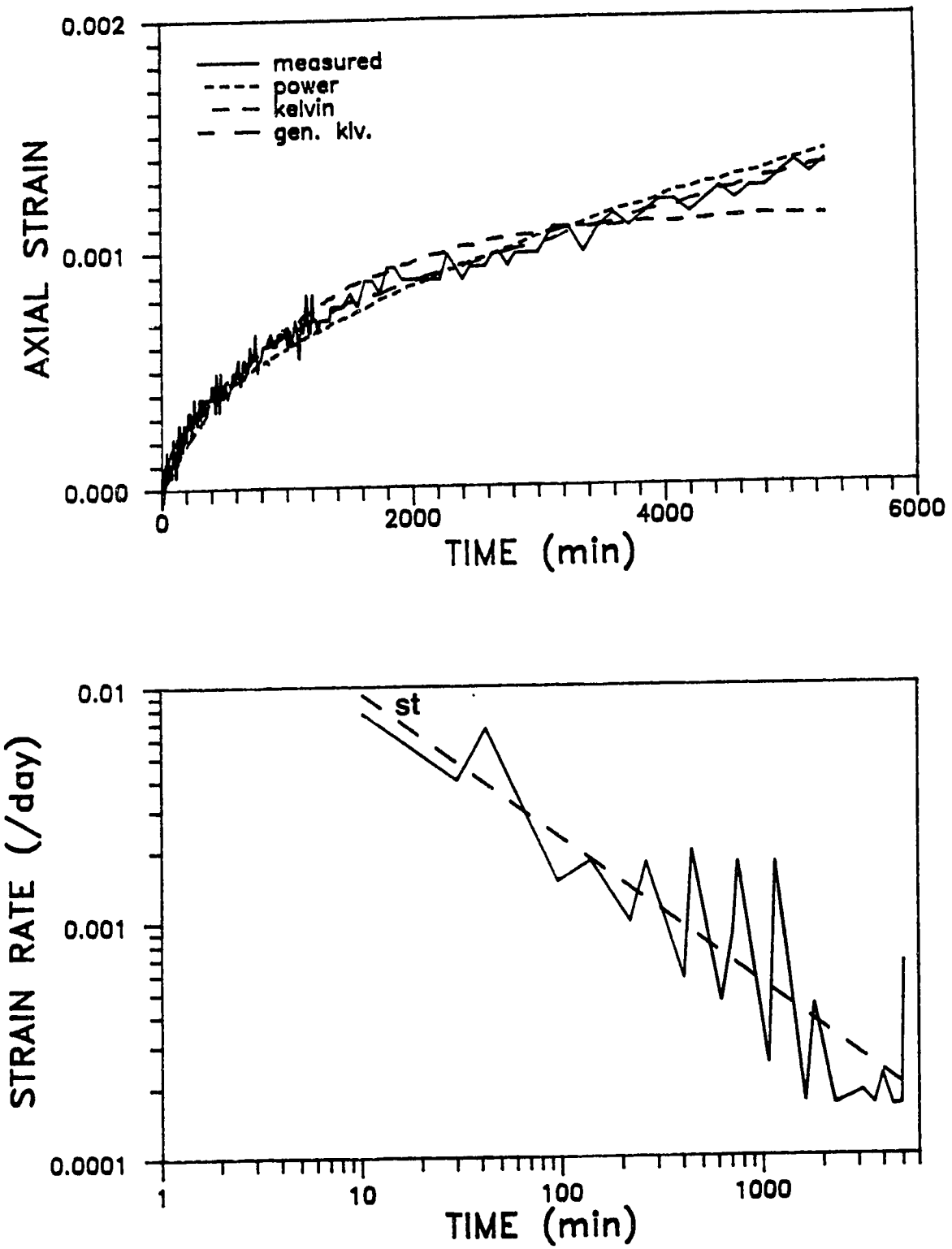

Figure 6.13 CTC Test 3 (1st creep stage) - Comparison between creep model predictions and actual creep data

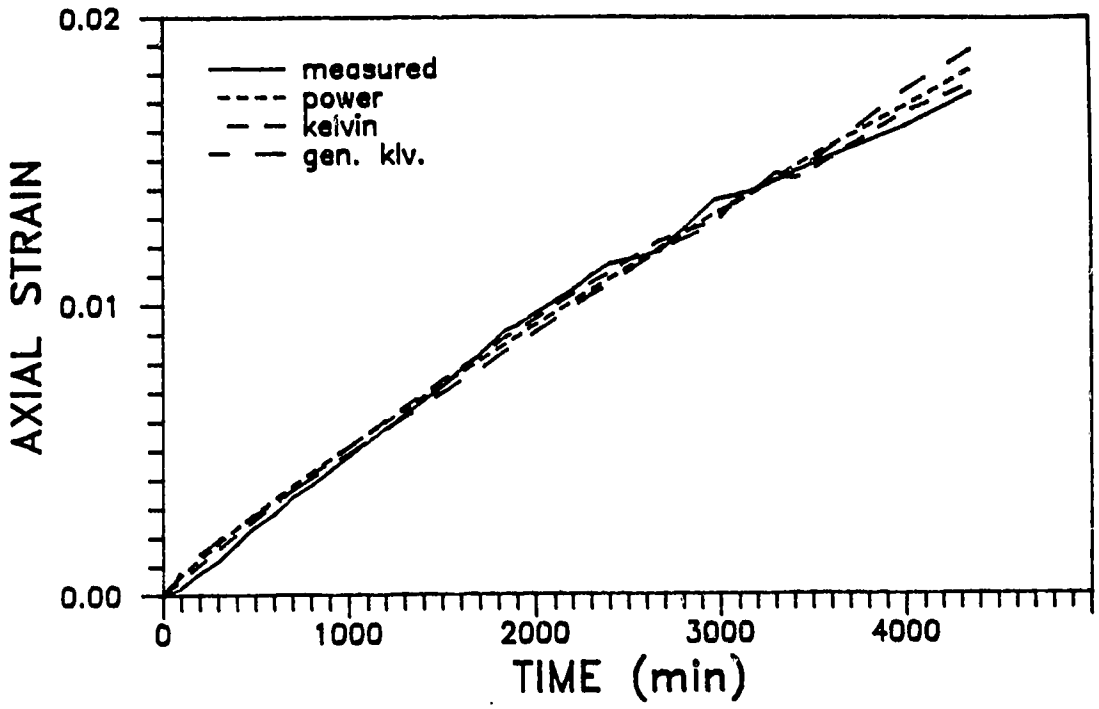

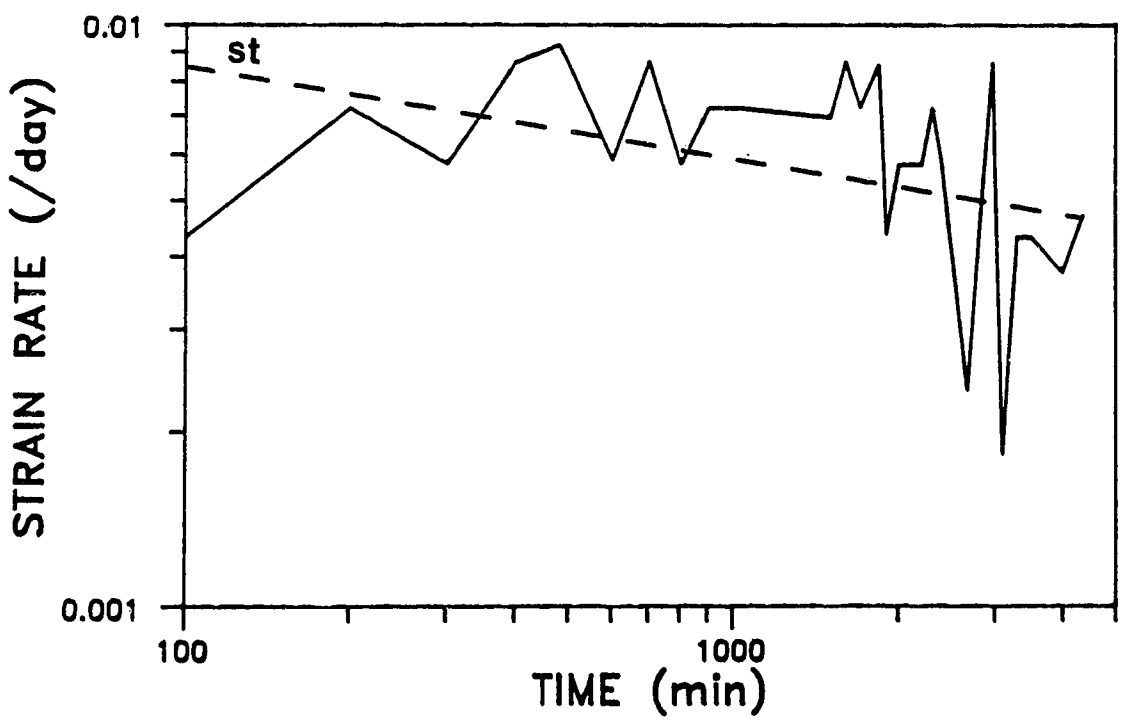

Figure 6.14 CTC Test 3 (2nd creep stage) - Comparison between creep model predictions and actual creep data

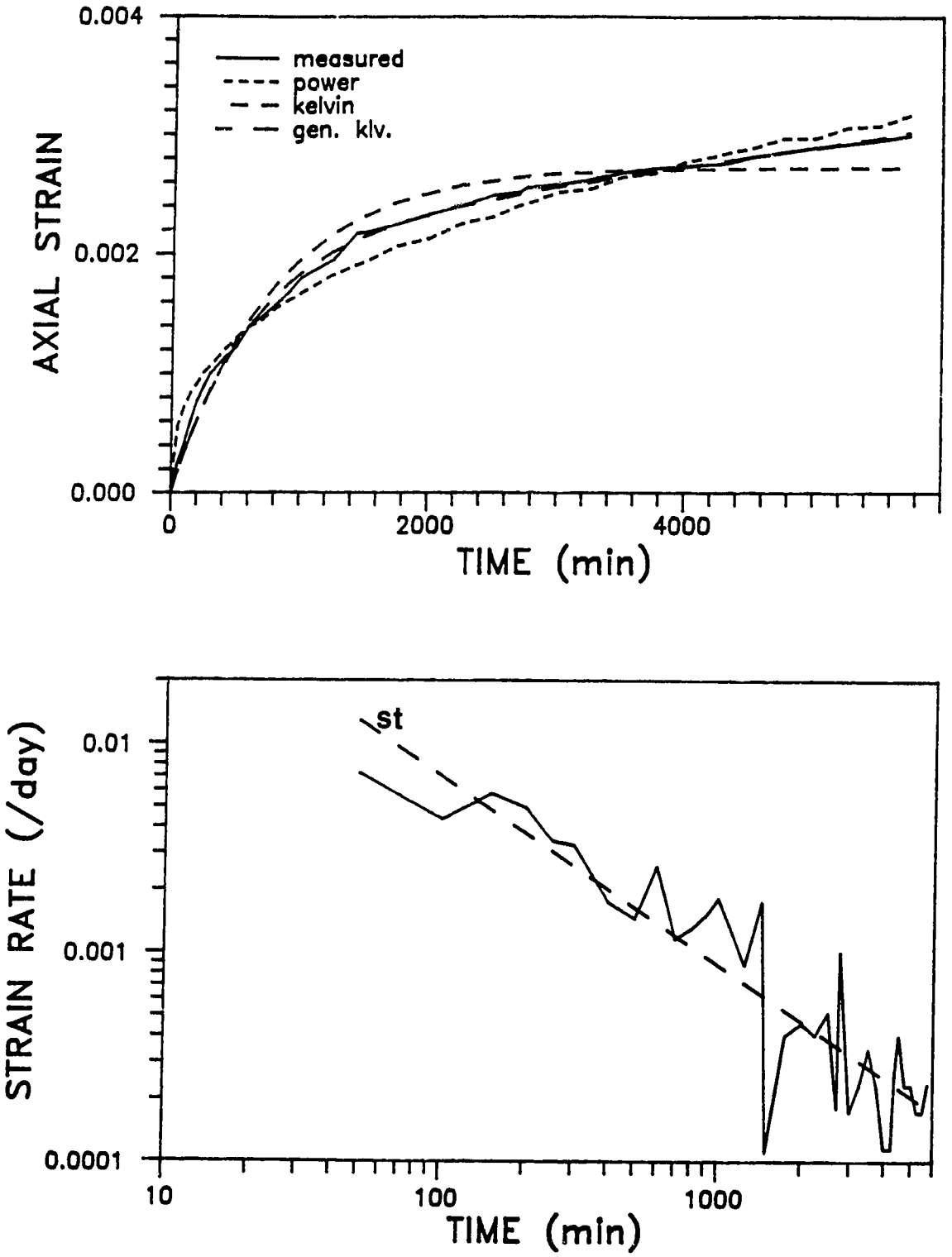

Figure 6.15 CTC Test 4 (1st creep stage) - Comparison between creep model predictions and actual creep data

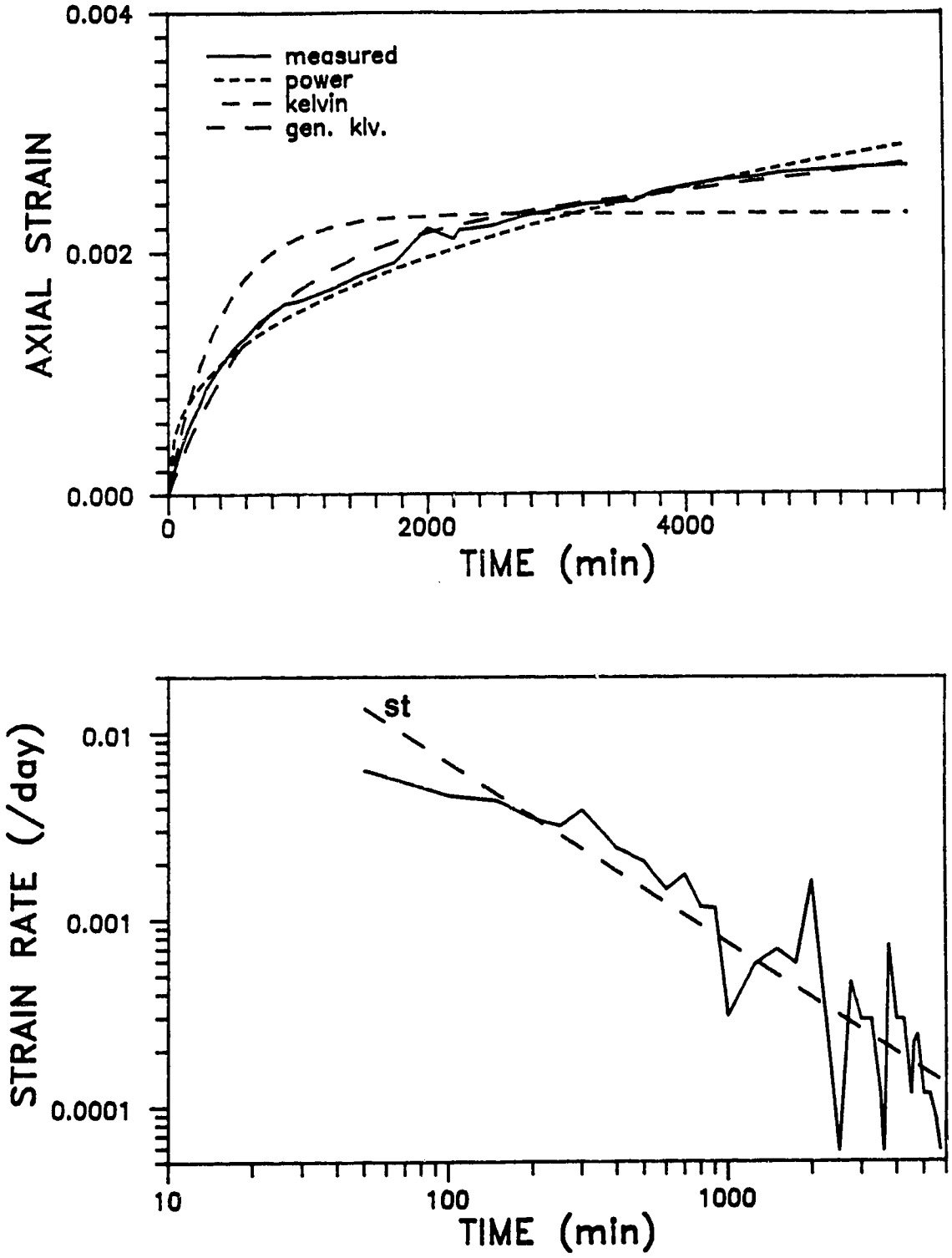

Figure 6.16 CTC Test 4 (2nd creep stage) - Comparison between creep model predictions and actual creep data

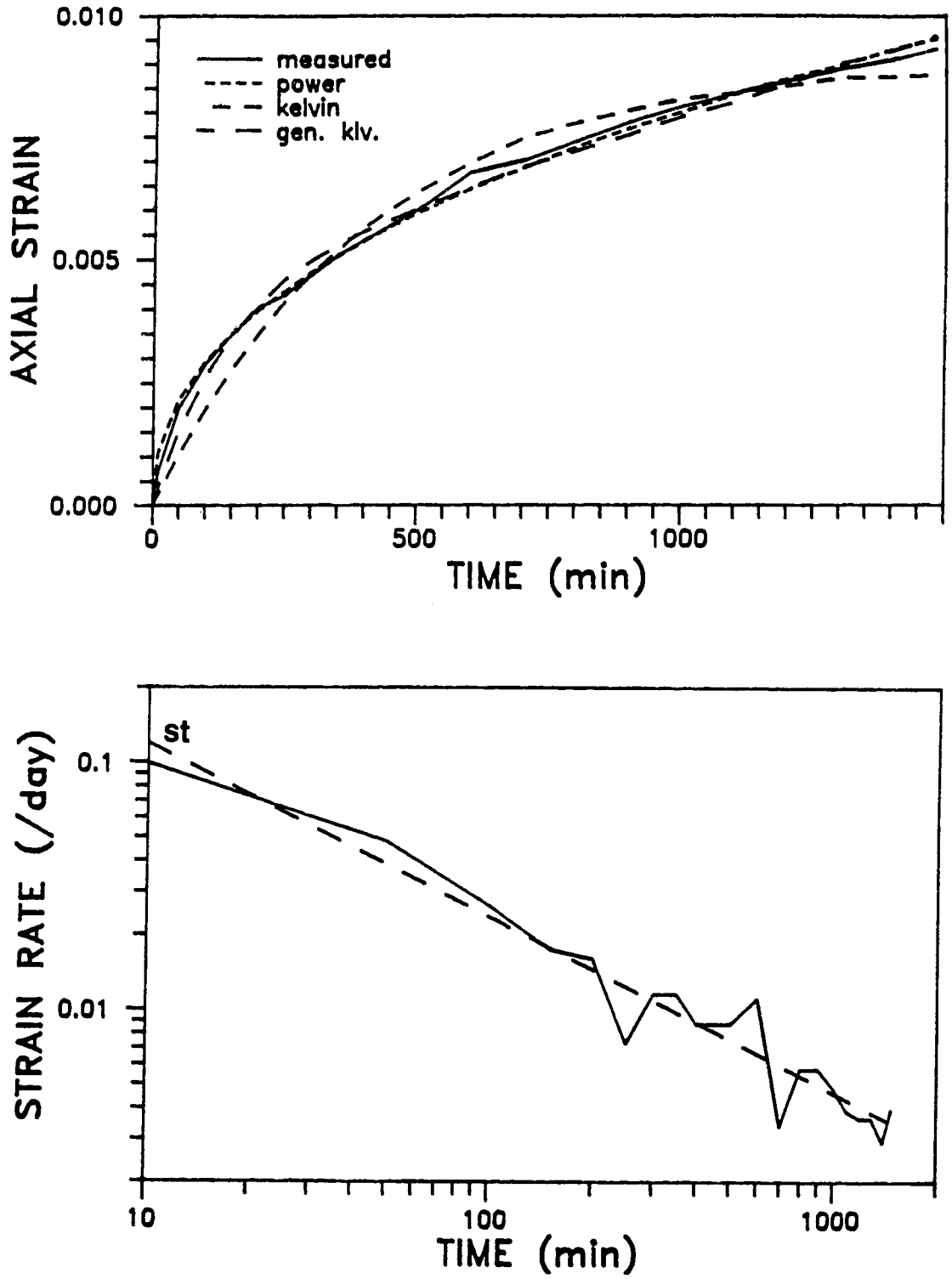

Figure 6.17 JTC Test 1 (1st creep stage) - Comparison between creep model predictions and actual creep data

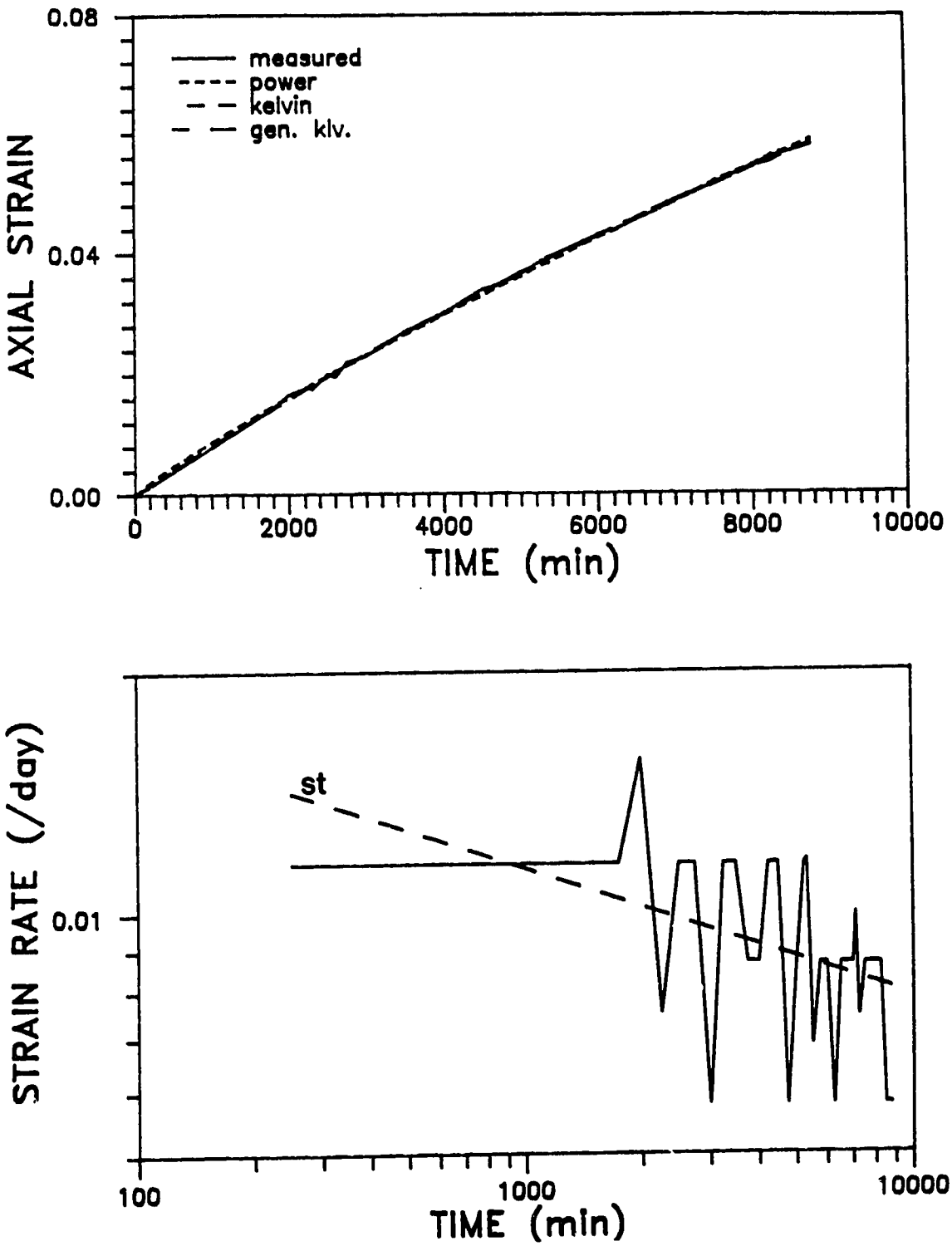

Figure 6.18 JTC Test 2 (1st creep stage) - Comparison between creep model predictions and actual creep data

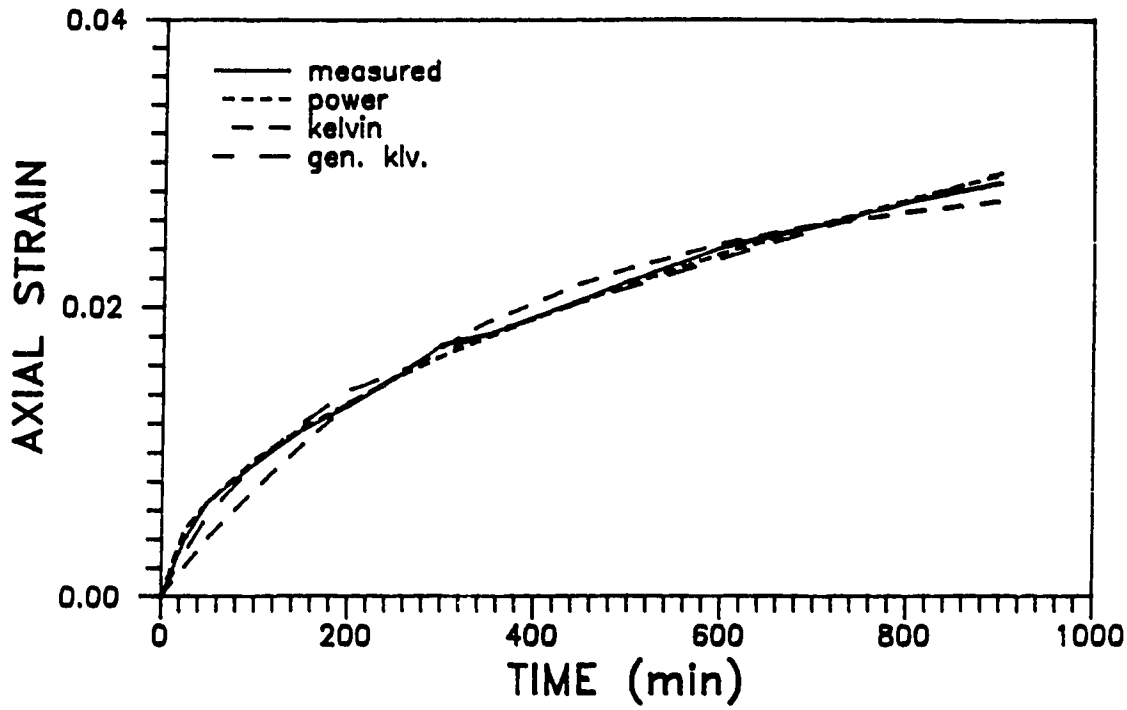

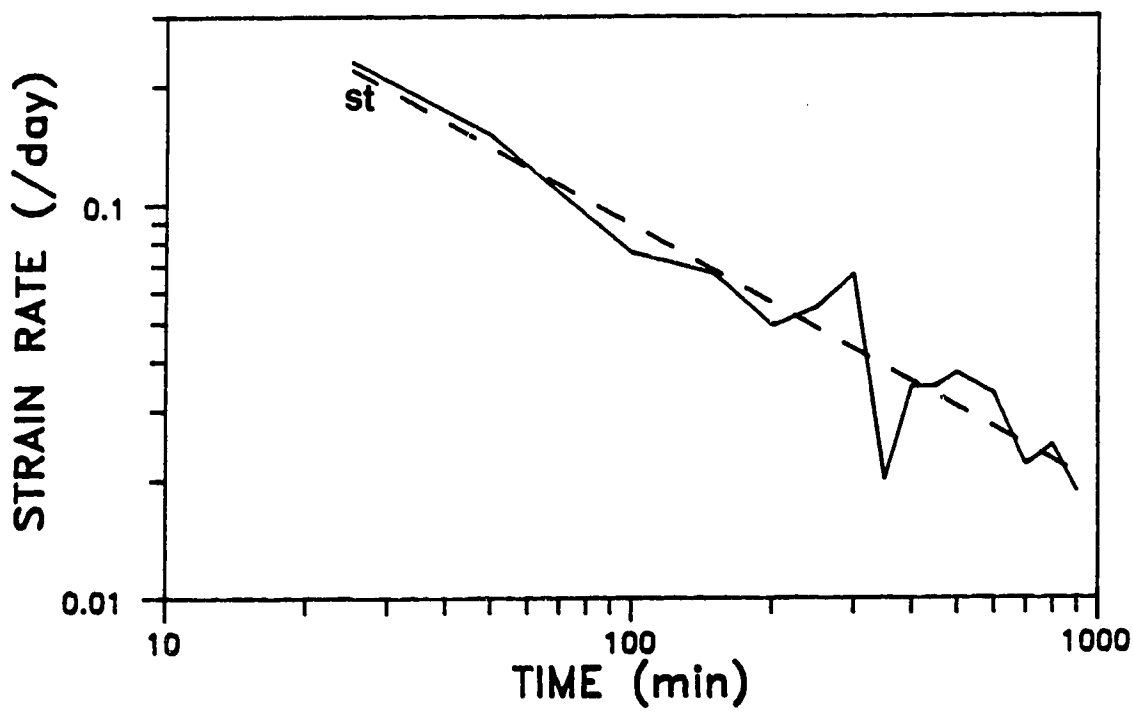

Figure 6.19 JTC Test 2 (2nd creep stage) - Comparison between creep model predictions and actual creep data

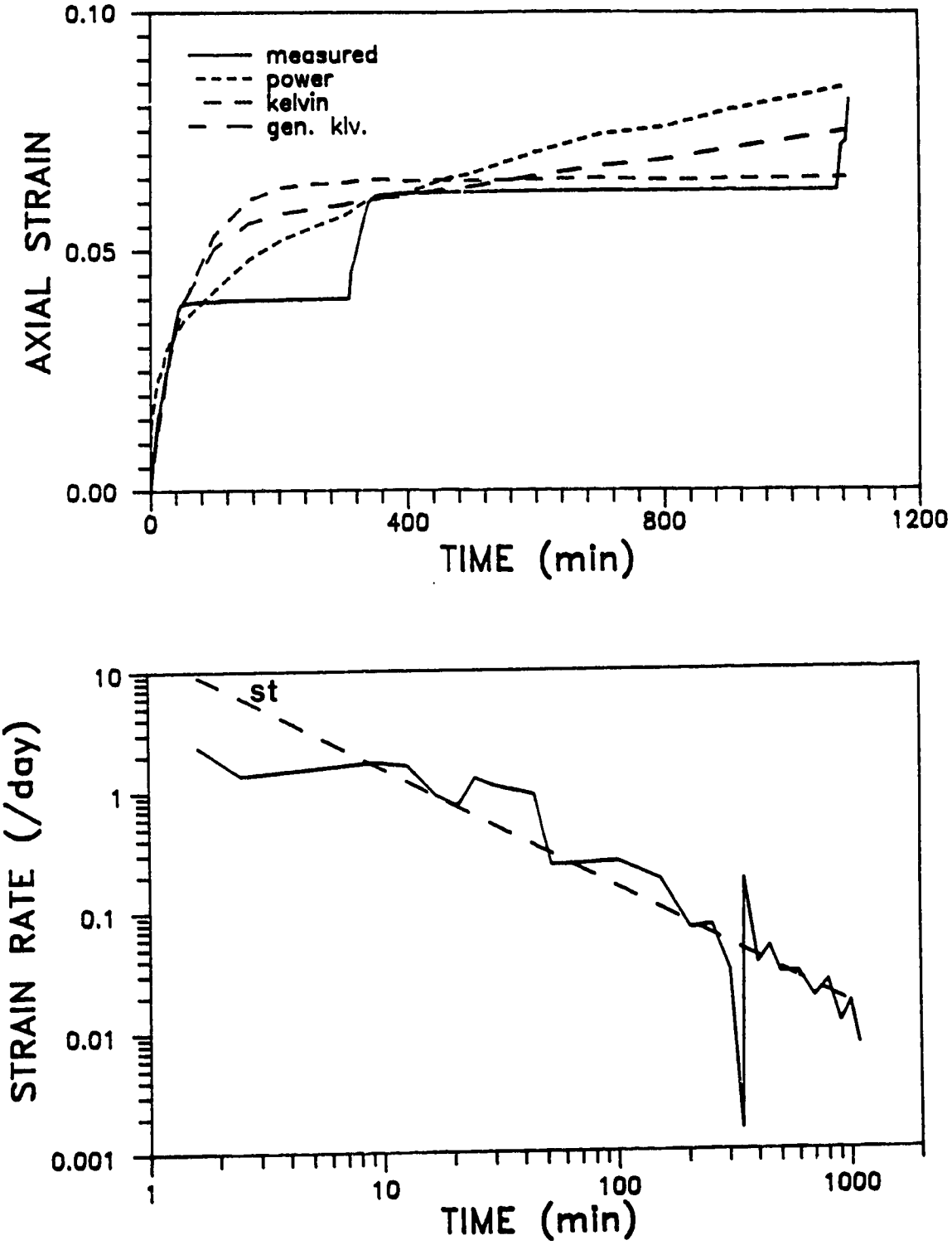

Figure 6.20 JTC Test 3 (1st creep stage) - Comparison between creep model predictions and actual creep data

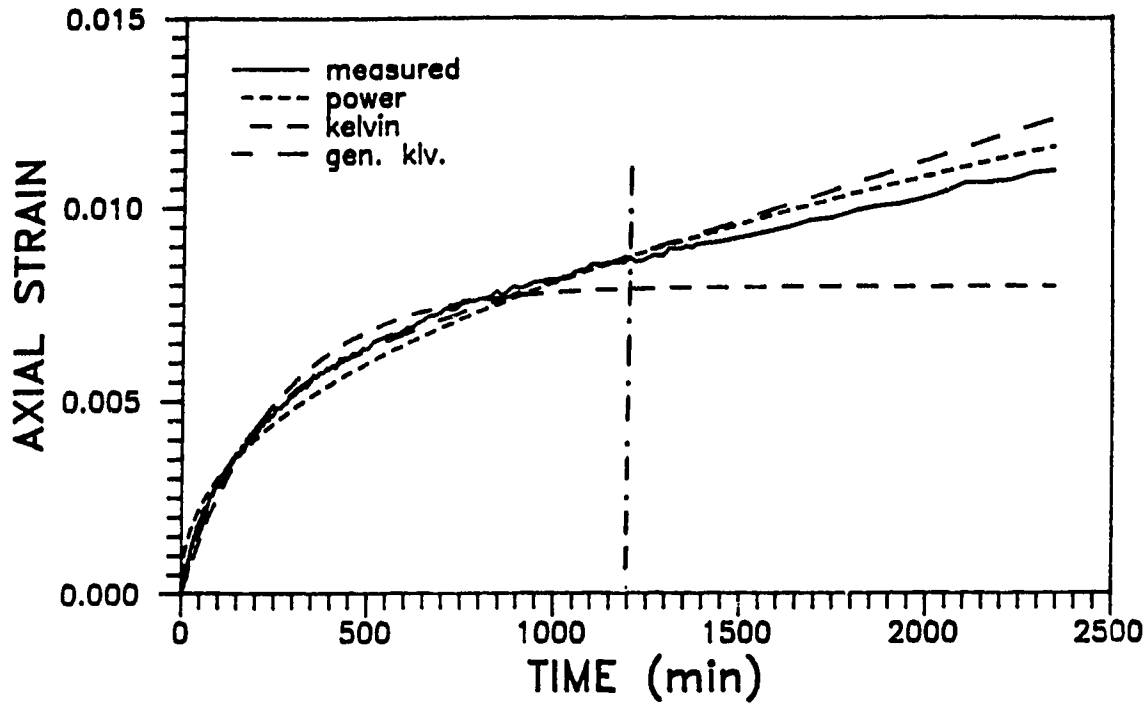

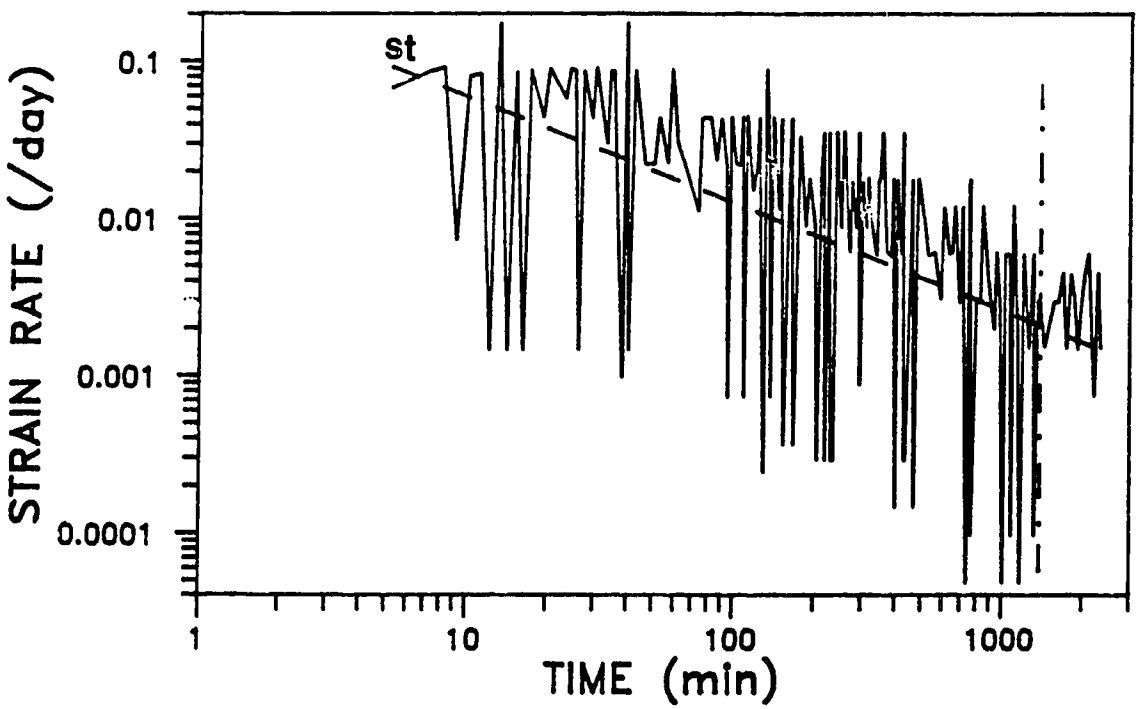

Figure 6.21 CTC Test 1 (1st creep stage) - Comparison between creep model predictions and actual creep data, using half (H) test duration

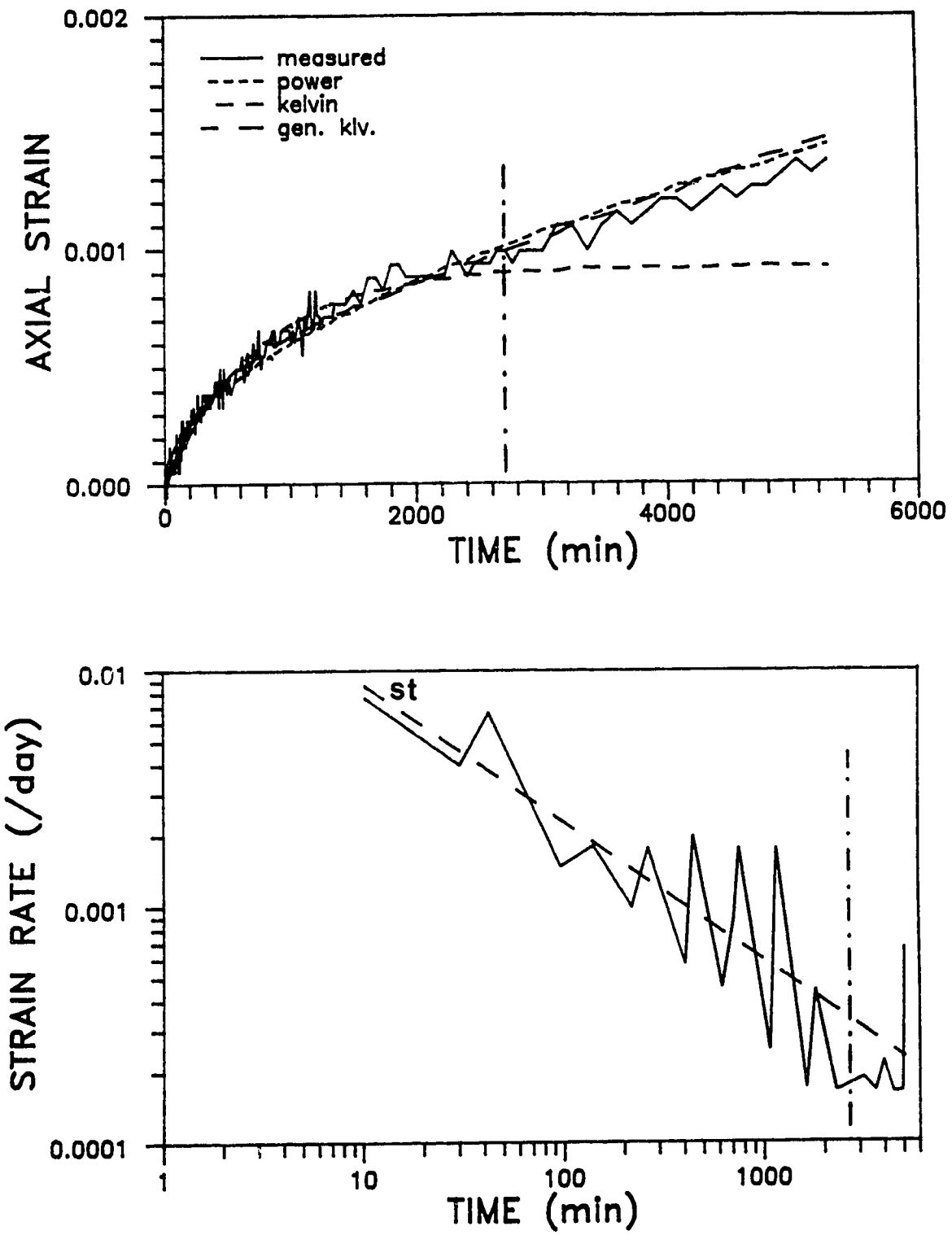

Figure 6.22 CTC Test 3 (1st creep stage) - Comparison between creep model predictions and actual creep data, using half (H) test duration

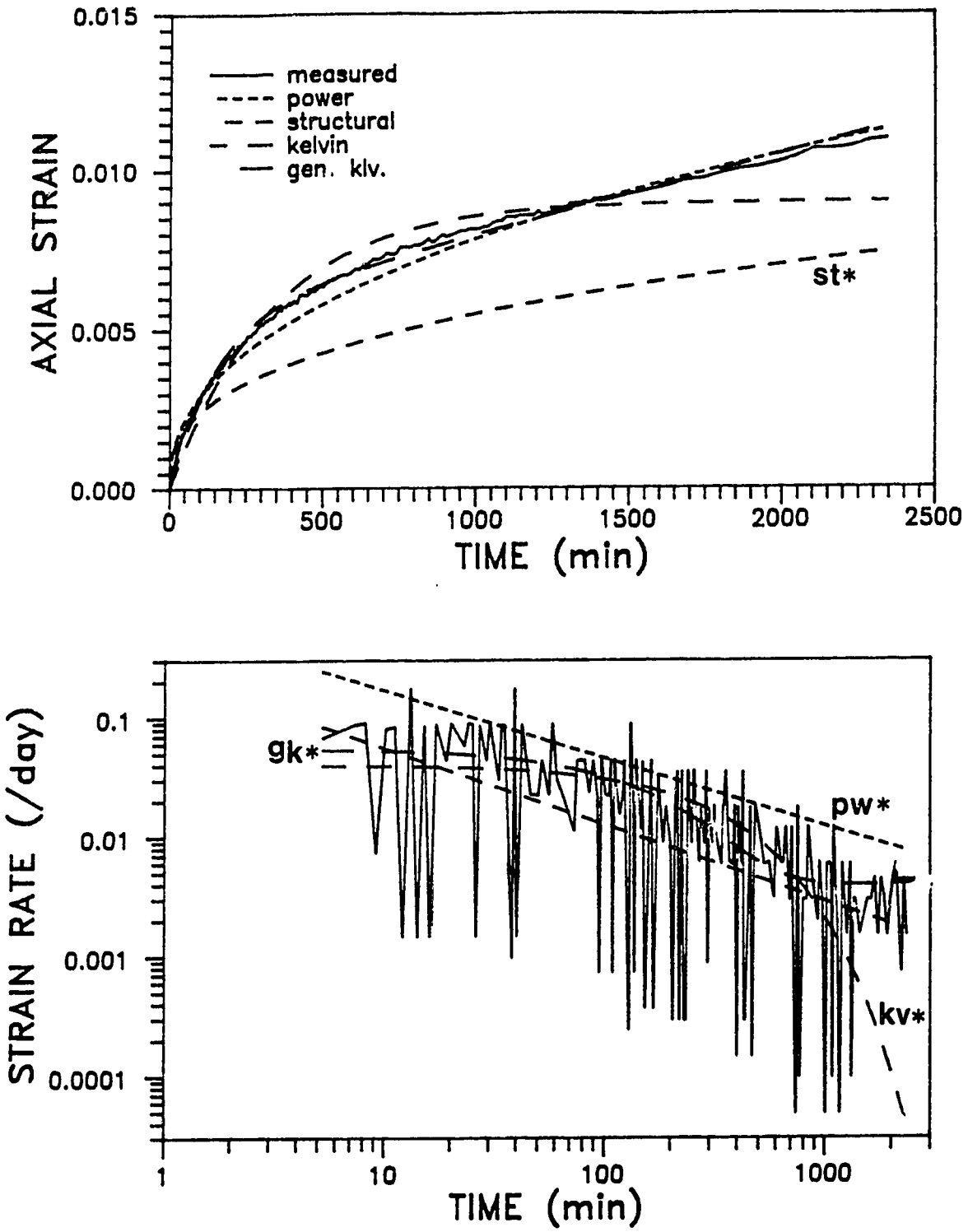

Figure 6.23 CTC Test 1 (1st creep stage) - Comparison between creep model and extrapolated model predictions

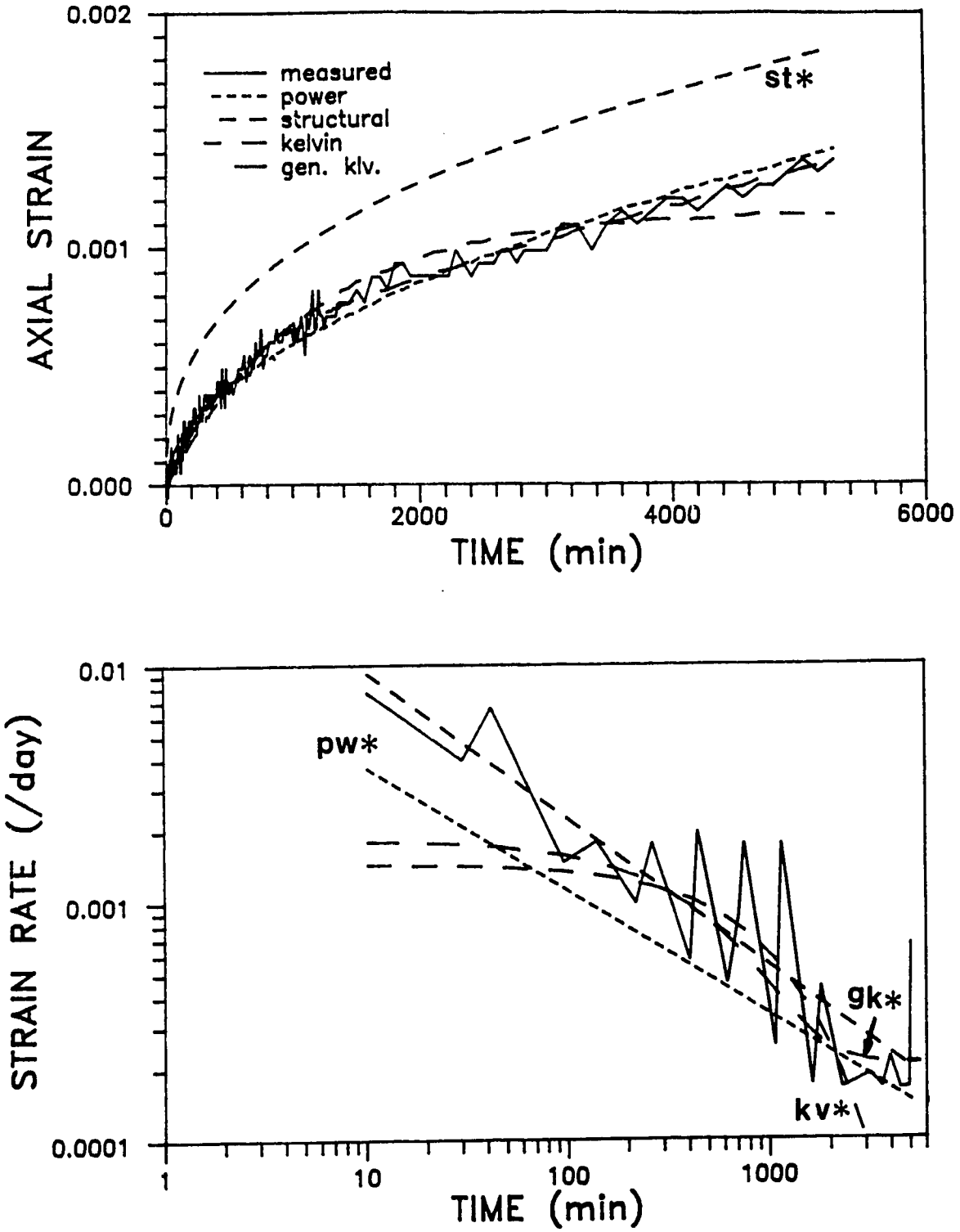

Figure 6.24 CTC Test 3 (1st creep stage) - Comparison between creep model and extrapolated model predictions

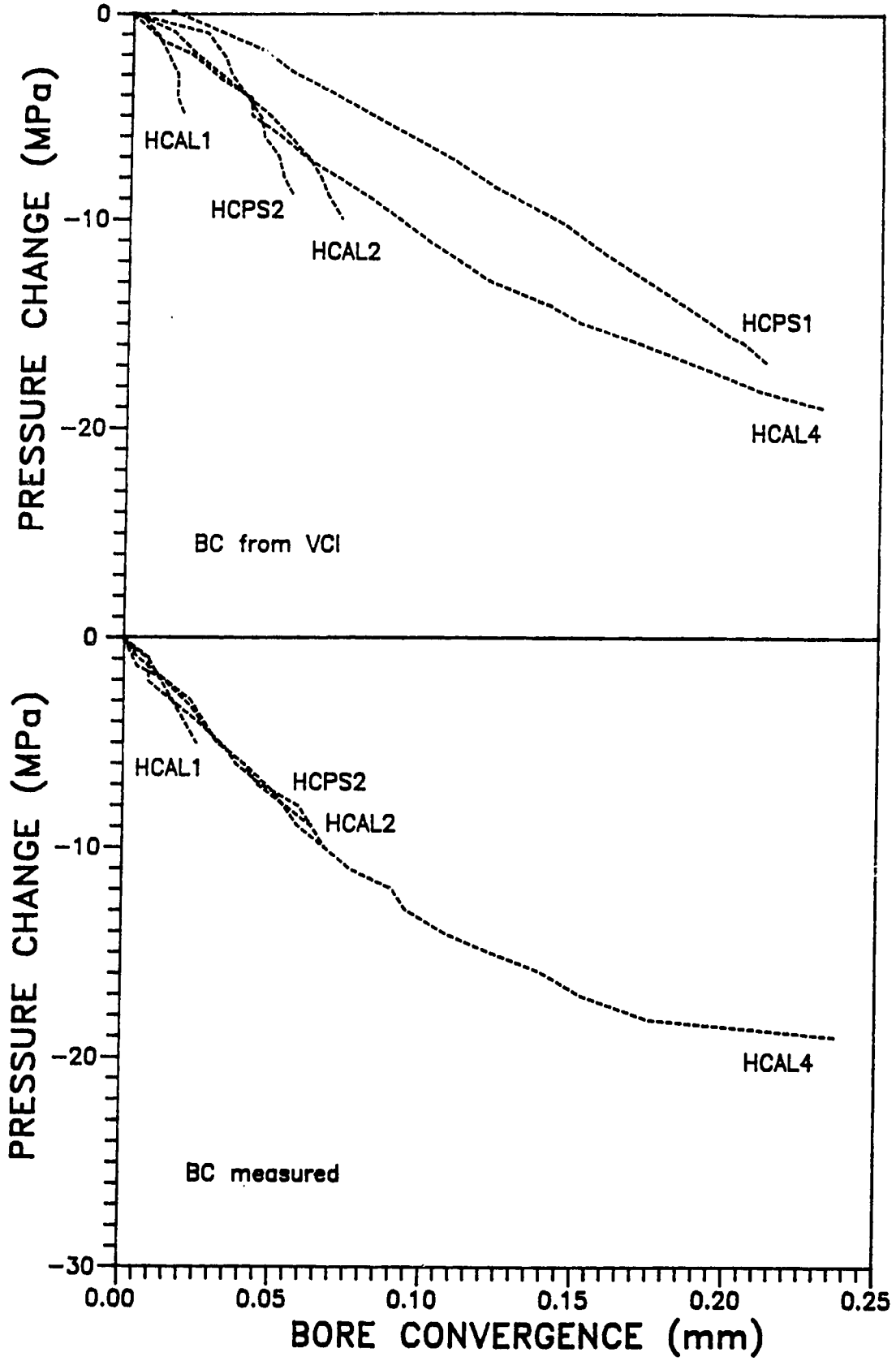

Figure 6.25 HC Tests - Deviatoric pressure vs bore convergence curves (1st deviatoric loading stage)

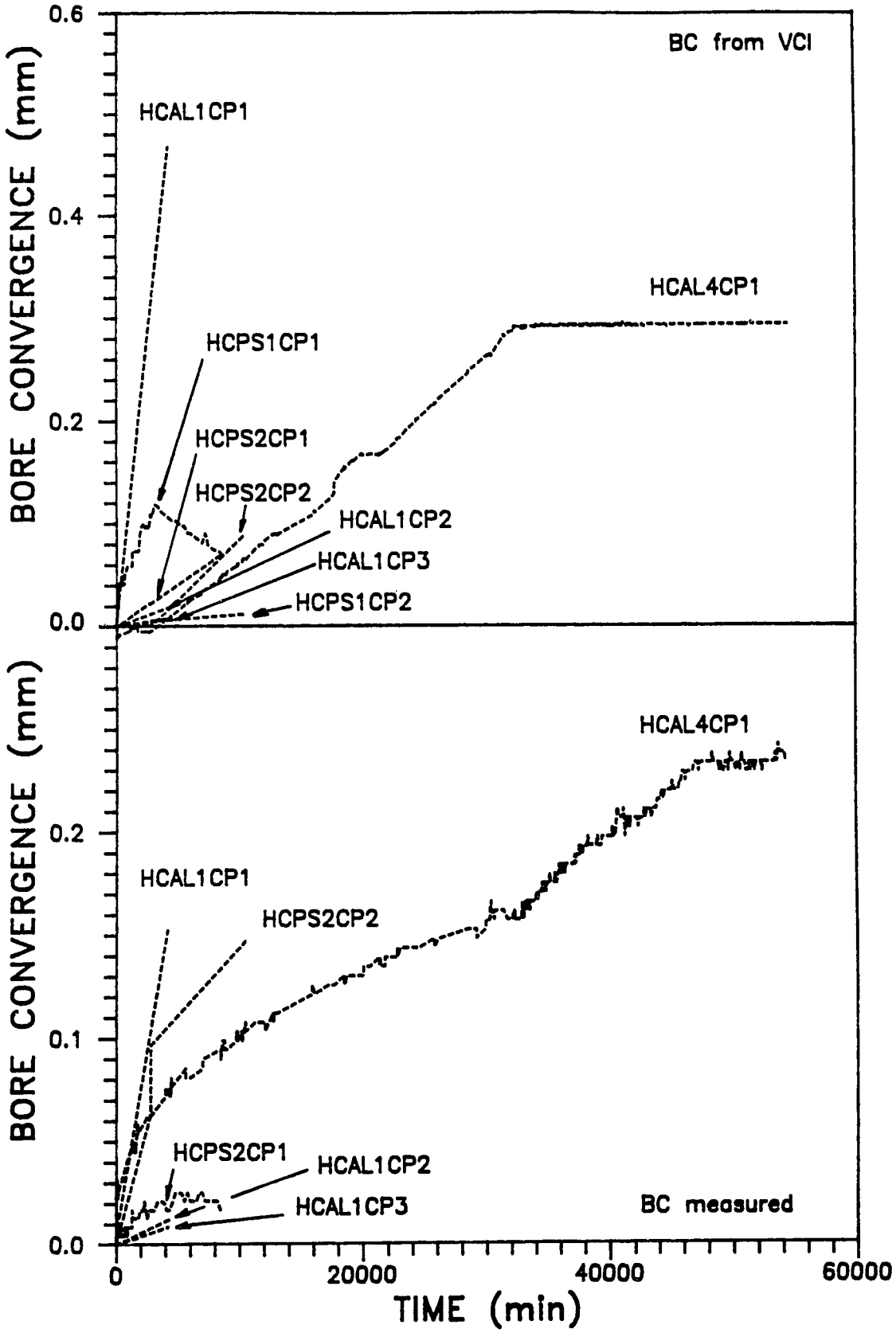

Figure 6.26 HC Tests - Bore convergence vs time curves

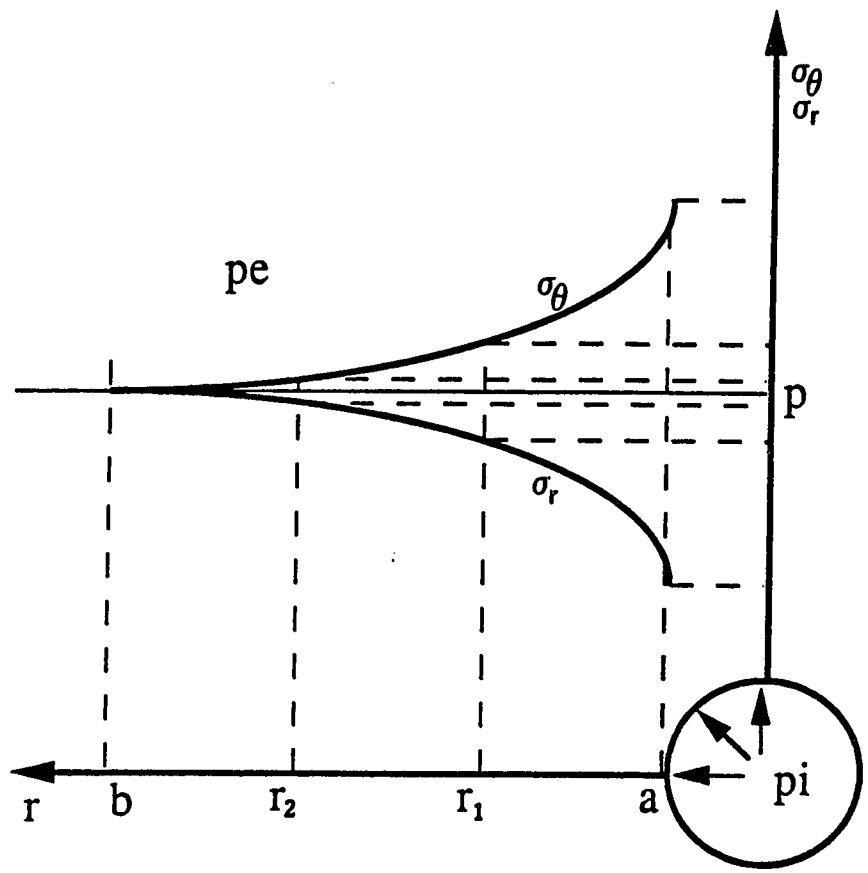

1. Consolidate specimens under hydrostatic creep
2. Load specimens triaxially following a J1-type stress path
3. Run creep tests at the stress states recommended above
4. Obtain model parameters from these creep stages

Figure 6.27 Suggested triaxial creep testing program to generate model parameters needed to predict hollow cylinder results

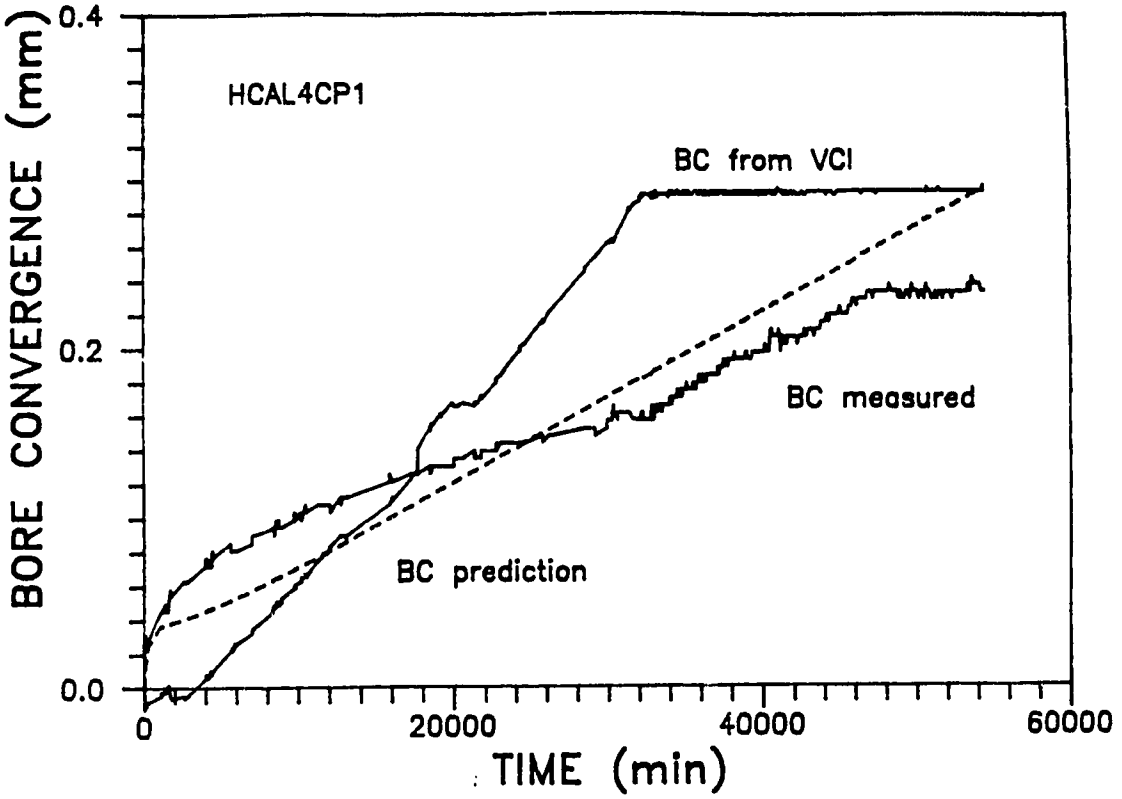

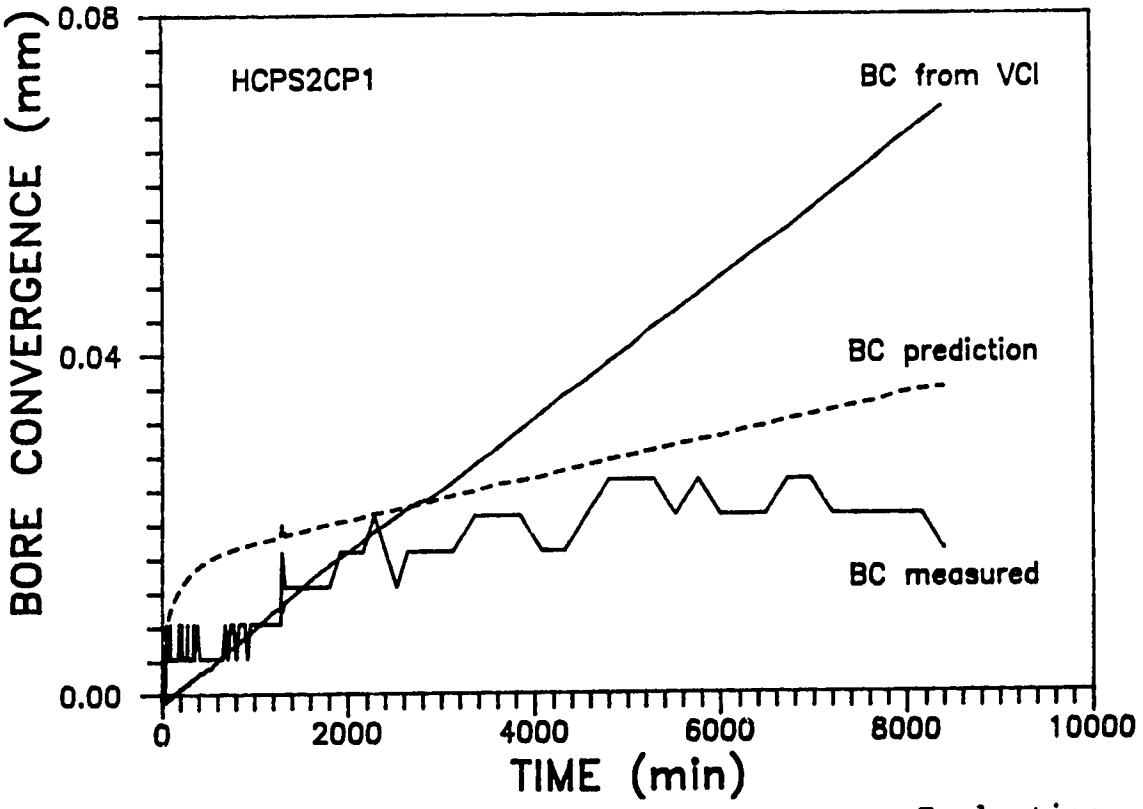

Figure 6.28 HCAL4CP1 and HCPS2CP1 creep stages - Evaluation of the generalized Kelvin model

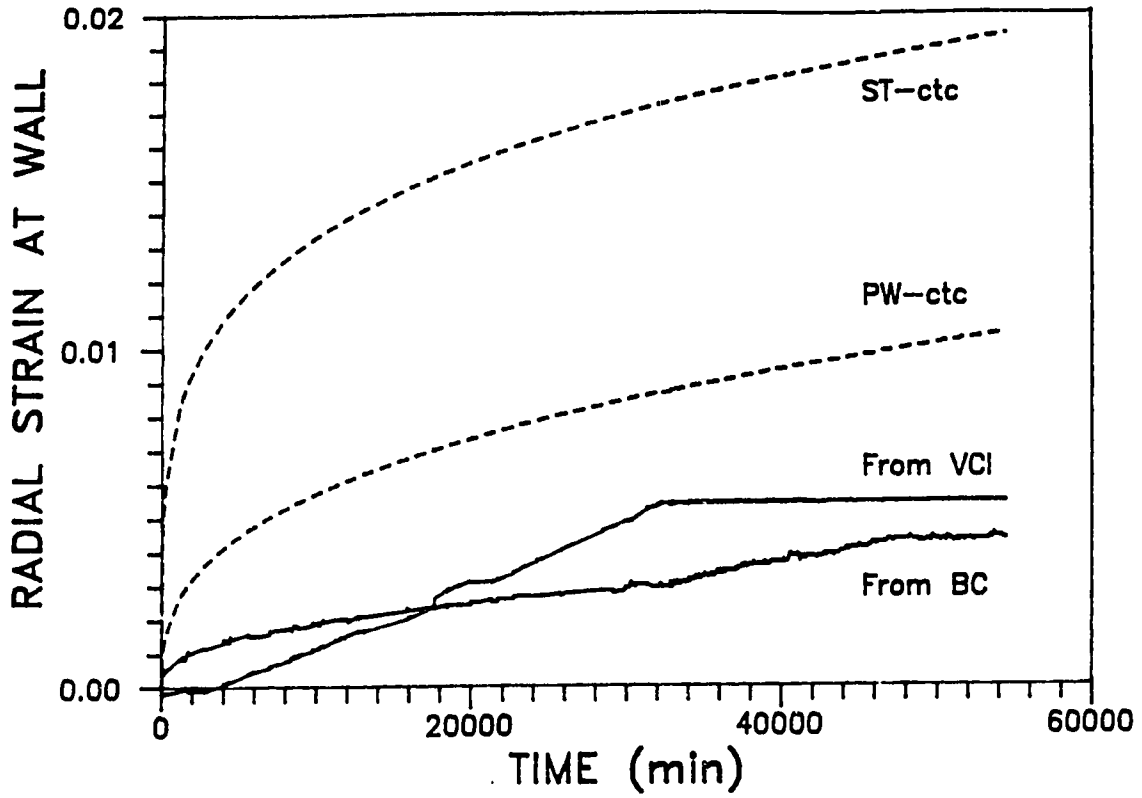

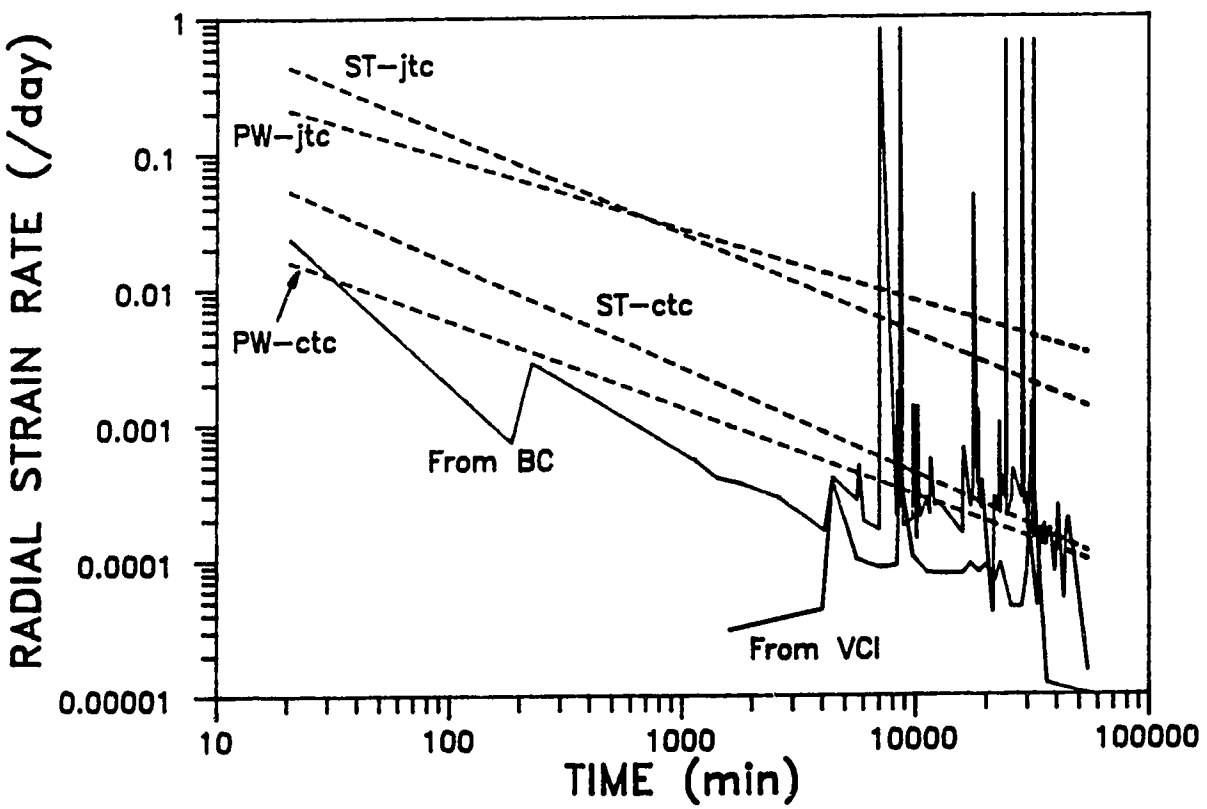

Figure 6.29 HCAL4CP1 creep stage - Evaluation of the power (PW) and structural (ST) laws

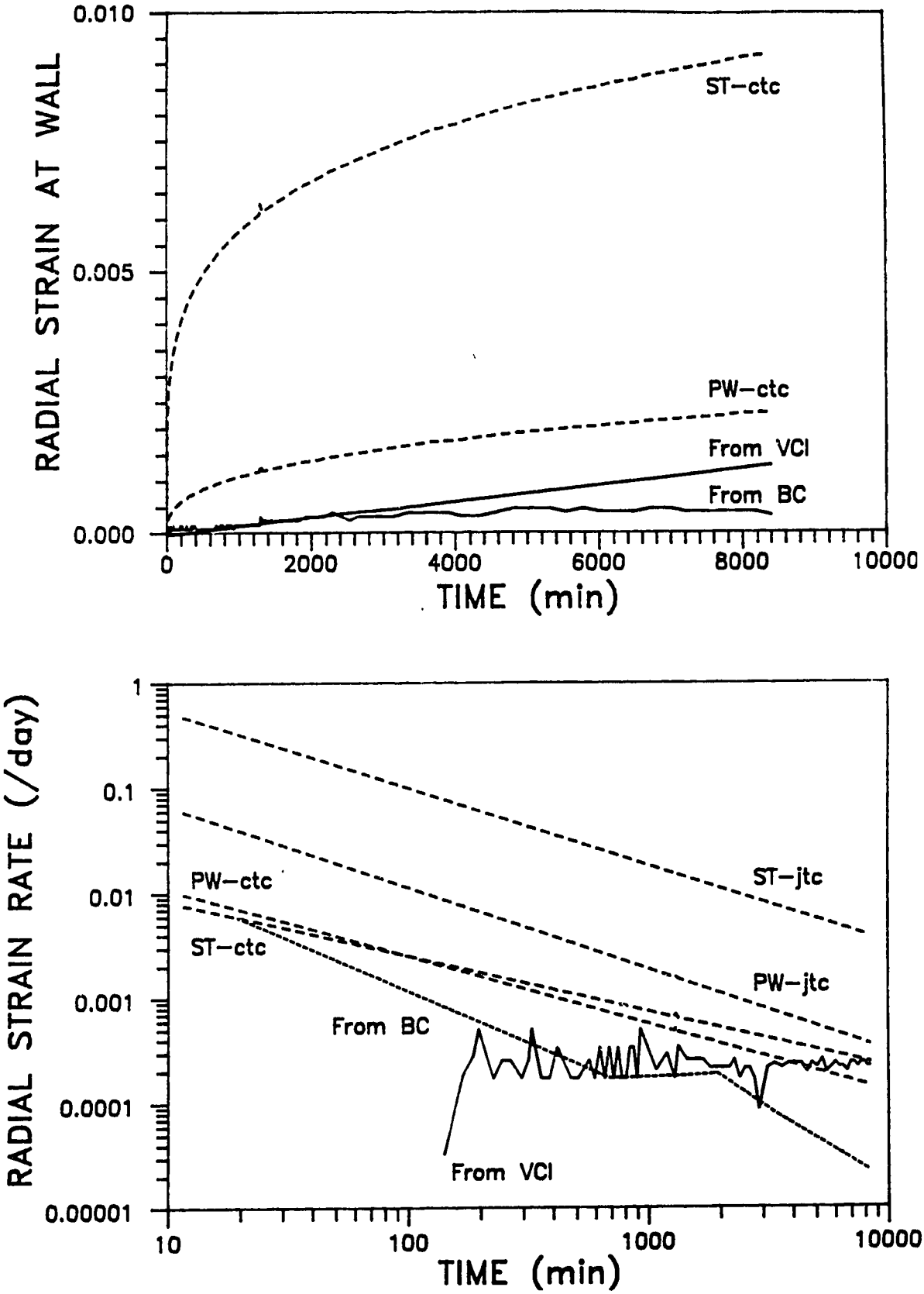

Figure 6.30 HCPS2CP1 creep stage - Evaluation of the power (PW) and structural (ST) laws

7. SUMMARY, CONCLUSIONS AND SUGGESTIONS FOR FURTHER RESEARCH

7.1 Introduction

Underground structures in salt formations such as mines, storage caverns, waste repositories and boreholes, usually exhibit problems related to the time-dependent behaviour of the material. Many variables may affect the creep properties of salt rocks. Some variables are associated with the type of salt deposit (e.g., grain size, natural moisture content, mineral composition, inhomogeneity and stress history). Others are due to the development and operation of the cavities (e.g., stress path, stress level, deviatoric stress and temperature). Some variables depend upon the interaction between stored matter and rock (e.g., chemical reactions and solution processes). Finally, there are other variables related to the testing procedures employed to determine the creep properties in laboratory or field. The resulting time-dependent deformation of the rock is influenced by the all above variables. Besides the material behaviour, the time-dependent response of the opening is also affected by its geometry. The geometry induces a stress distribution which dictates the state of stress for each point disturbed by the opening.

Potash from two mines of the Potash Corporations of Saskatchewan (PCS) was chosen as a testing material to study the creep properties (material behaviour). Only the variables related to the development and operation of

underground structures and to the testing procedure were selected to be more closely investigated by a laboratory testing program. Analytical solutions for the thick-walled cylinder were derived for several creep models to include the geometric component on the time-dependent response of openings. The major problem is translating the creep properties determined in the laboratory to models able to predict in-situ measurements.

7.2 Summary

The approach followed by this research included the laboratory study of creep properties of potash, the determination of parameters for several creep models and the use of these models combined with analytical solutions for predicting the results of hollow cylinder tests. Hollow cylinder experiments were chosen because they are a faithful simulation of circular openings in homogeneous stress fields such as underground structures in salt deposits. This approach required:

1. A review of creep laws usually adopted to describe the time-dependent behaviour of salt rocks.
2. Formulation of analytical solutions for the thick-walled cylinder, based on several creep models, to predict the deformation of circular openings.
3. A laboratory triaxial testing program to investigate the variables affecting the creep properties and to determine the creep model parameters.

4. A laboratory hollow cylinder testing program to simulate the in-situ response of circular openings in homogeneous stress fields.

Creep modelling of salt rock behaviour attempts to establish the constitutive laws that describe closely the material deformation as a function of the variables that affect it. The general deformation equation (Eqn. 2.1) separates the total deformation into instantaneous and time-dependent deformations. The instantaneous deformation which is composed of elastic and plastic components, commonly contributes to only a small percentage of the total deformation. Both components can be satisfactorily described by the generalized Hooke's law and theory of plasticity, respectively, although the selection of the appropriate parameters for these constitutive laws is not so obvious. The time-dependent deformation is described by creep models. These models are divided into empirical, physical and rheological groups. Empirical models are simply curve-fitting equations of laboratory or in-situ data. Physical models search for basic equations governing microphysical mechanisms of deformation, but the physical constants are often converted from their physical meaning to curve-fitting parameters. Rheological models are composed by the association of elastic, viscous and plastic elements, in such a manner as to resemble the response curve of mechanical bodies. Their element parameters are also obtained by the curve-fitting technique.

Due to the great number of creep models reported in the literature, this thesis focused on the evaluation of some existing models, instead of suggesting new ones. Only the models that included the variables associated with the development and operation of cavities in salt rocks were analysed. At least one model representative of each group was selected to evaluate the transient creep response of hollow cylinder tests. They were the power law (empirical), the structural law (physical), the Kelvin and generalized Kelvin (fluid) models (rheological).

Analytical solutions for the thick-walled cylinder were derived for different loading conditions (axisymmetric loading and plane strain in the axial direction) and creep models. The solutions for the rheological models assumed linear viscoelasticity. Solutions were presented for the Maxwell, Kelvin, generalized Kelvin solid and fluid, and Burgers models. The solutions for the empirical and physical laws were formulated adopting the theory of plasticity. Several assumptions were taken to describe the plastic strain component by a creep law (viscoplasticity). These analytical solutions, although limited to their own assumptions and by the combined creep model, are useful for the preliminary assessment of the predictive capability of creep models, when their predictions are compared with data from model tests or in-situ measurements.

The success of any comparison involving predictions based on laboratory tests, depends heavily on the quality of

the laboratory data. Laboratory facilities were developed in this research with two main objectives:

1. Standardize the specimen preparation and testing procedures in order to minimize the differences among specimens and the influences of testing parameters on the creep properties, and therefore obtain more uniform test results.
2. Provide the laboratory system with versatility to apply and control the same external excitation as in the field.

The laboratory system developed is able to follow any triaxial or hollow cylinder stress path. It controls independently two testing cells, each with three pressure axes and bore and cell temperatures, and does data acquisition. Any testing parameter such as stress, deformation or temperature, can be used as a control parameter during testing, but rate control has not been implemented yet. Besides triaxial creep tests to investigate the effects of several variables on the time-dependent behaviour of the material, this system can also execute model tests using hollow cylinder specimens to simulate the response of circular openings in homogeneous stress fields.

The specimen preparation procedure was described in detail due to the difficulties normally encountered to obtain high quality specimens from natural potash. Also, a specimen reconditioning procedure was implemented to reverse post-sampling cracks and fissures and therefore provide more

uniform test results. Based on the result analysis, an improved specimen reconditioning procedure was recommended for future tests in the same material. This suggested procedure comprises ultrasonic wave tests for preliminary assessment of specimens, hydrostatic creep stage till a specimen reconditioning criterion is met and ultrasonic tests during the hydrostatic creep stage to confirm the specimen condition.

The triaxial testing program concentrated on the stress path, stress level, deviatoric stress and temperature variables. The temperature was maintained at 25°C by an environmental-controlled room. Two triaxial stress paths were followed prior to the creep stages: conventional triaxial compression (CTC) and J1-constant triaxial compression (JTC). The stress path does not appear explicitly in the creep model equations, but its effects are implicit on the model parameters. Nine creep stages (five CTCs and four JTCs) at different stress states were analysed. The creep deformation dependence on confining stress levels for CTC creep stages and on applied deviatoric stresses for all creep stages are fully supported by the literature. The lower the confining stress, the higher the creep deformation and the higher the deviatoric stress, also the higher the creep deformation. However, for JTC creep stages, the dependence on the confining stress showed an reverse relationship. Finally, all JTC creep stages yielded higher deformation levels than the CTC creep stages.

Creep model parameters were obtained from the nine triaxial creep stages using non-linear regression analyses (BMDP statistical software). The models seemed to predict well the data which from they were derived, except the Kelvin model. Two more evaluations were performed with the selected creep models. One showed the importance of the creep test duration used for generating the creep parameters. The other indicated that models derived from a certain type of data (e.g., strain) should not be used for predicting other natures of data (e.g., strain rate), when both types of data are interrelated by the independent variable (e.g., time).

Hollow cylinder test results were presented. Two hollow cylinder creep stages, one following an axisymmetric loading and the other a plane strain state in the axial direction, were chosen as the database to be compared with the analytical solution predictions. Both creep stages exhibited transient responses of the bore convergence. The difficulties to compare triaxial to hollow cylinder stress states were analysed. A methodology to obtain model parameters from triaxial creep stages compatible with the stress states along the hollow cylinder wall was recommended for future studies (Fig. 6.27).

The creep model predictions were compared to the hollow cylinder results. All predictions based on parameters from JTC creep stages were considerably higher than the measured deformation. Predictions based on CTC creep stage parameters

were quite accurate in terms of magnitude. Some models also described the trend of actual data well. The approach taken seemed to have considerable potential to evaluate the predictive capability of creep models.

7.3 Conclusions

The conclusions of this research can be grouped into three major topics: the laboratory facilities, laboratory testing program and evaluation of creep models. The laboratory facilities were developed to study the time-dependent properties using a triaxial testing program and to obtain the creep response of hollow cylinder specimens. Besides the testing system, the laboratory facilities include the specimen preparation and testing procedures.

The major contribution of the laboratory testing system is the independent and accurate control of the external excitation (e.g., pressure, deformation and temperature). This allows the HPTS to follow any triaxial stress path needed to investigate the effects of several variables on creep properties. It also permits the execution of model tests which simulate circular openings in homogeneous stress fields. The results of these hollow cylinder tests may play an important role in the evaluation of the predictive capability of creep models. The HPTS proved to have the versatility to accommodate different specimen sizes and geometries, run any triaxial and hollow cylinder stress

paths and especially, to control precisely the testing parameters during creep stages.

The specimen preparation procedure established during this research produced high quality solid and hollow cylindrical specimens, in terms of geometric measurements and smoothness of the surfaces. It controls the aspects affecting specimen preparation from natural potash.

The testing procedure aimed to reduce the influence of testing parameters on the laboratory results. The specimen reconditioning program is of particular interest, since it attempted to minimize specimen differences and yield more uniform test results. The specimen reconditioning criterion, based on a minimum hydrostatic creep stage duration, proved to be satisfactory for most specimens. An analysis of the results led to a combined criterion based on a minimum hydrostatic creep stage duration of 72 h and a maximum creep rate of 100 microstrains per day. This criterion is recommended for future testing on the same material. Specimen reconditioning was shown to be essential for the study of transient creep properties.

The main achievement of the laboratory system developed and the specimen preparation and testing procedures established during this research is the obtaining of reliable data. The laboratory system ensures the control of testing parameters while the specimen preparation and testing procedures guarantee minimum differences among specimens.

The second group of conclusions is associated with the observations from the triaxial testing program results. These remarks should only be taken qualitatively due to the small number of specimens and tests for each loading condition. The results reinforce that the creep deformation is directly proportional to the applied deviatoric stress and inversely proportional to the confining stress. The exception is that the JTC creep stage results present a directly proportional relationship between creep deformation and confining stress. No reasonable explanation is found for this type of dependency. Also with no ready explanation, the triaxial tests following a JTC stress path exhibit considerably higher deformation than those following a CTC path. This is also noticed for the creep stages. As known, no stress path is followed during creep stages, since they are performed under a constant state of stress. However, the stress path followed to load the specimen to a particular creep stage affect the creep response. Those creep stages previously loaded by a JTC stress path present much higher deformation. The simultaneous increase of the axial stress and reduction of the confining pressure, which is a characteristic of JTC stress paths, is perhaps more favourable to crack propagation, which according to the structural theory of brittle creep, contributes positively to the transient creep response.

The last set of conclusions concerns the evaluation of creep models. From the curve-fitting procedure used for

obtaining the model parameters, it can be concluded that weighed data must be adopted to compensate for the different lengths of time interval that contains each data point, when the data distribution along the time scale is not uniform. Also, if correlation coefficients are used as a fit criterion, they have to be corrected to compensate for the different number of data points among tests.

Before comparing creep model predictions with the model test results, the creep models were evaluated using the same triaxial data from which their parameters were derived. All selected models seem to predict the actual data reasonably well, within the test duration limits. It is shown that the creep test duration is very important for the obtained parameters. Extrapolations to times beyond the test duration lead to increasing errors, particularly for models which equations have conditions such as constant or zero strain rate at a certain time. Also, models with parameters obtained from strain rate data yielded poor predictions of strain data and vice-versa. It indicates that if the dependent variables (e.g., strain and strain rate) are interrelated mathematically to the independent variable (e.g., time), models obtained by fitting one type of dependent variable data are not appropriate to predict the other type of dependent variable data. In conclusion, the transient creep response should be described by transient creep models with flexible equations (avoid conditions) and with parameters obtained from the same type of data to be

predicted and from creep tests with durations which are as long as possible.

The creep models were used for predicting two hollow cylinder creep stages. The predictions based on model parameters obtained from JTC creep stages are about one order of magnitude greater than the measured data. The creep models with parameters obtained from CTC creep stages predicted the measured deformation satisfactorily. The structural law exhibited the poorest prediction of radial strain as expected, since its parameters are fitted from strain rate data. On the other hand, it fitted the strain rate data quite well, in terms of magnitude and trend of the data. The rheological model presented the best fit in terms of magnitude, but it failed to resemble the form of the actual bore convergence curve. It seems obvious to yield increasing prediction errors for times beyond the creep experiment duration. The power law overpredicted slightly the measured deformation, but it resembled the measured creep curve quite well. The reason for this overprediction is possibly because the stress states of the CTC creep stages were higher than those encountered along the hollow cylinder wall. In conclusion, the structural law can be adopted successfully to describe the strain rates. The generalized Kelvin model should be used with restrictions, since it may lead to increasing errors beyond the duration of the creep test from which its parameters were derived. The power law appears to have more flexibility and potential

to describe the transient creep response of circular openings in homogeneous stress fields.

The main achievement of this creep model evaluation program is the establishment of a procedure to perform such an evaluation. A triaxial testing program to generate creep model parameters compatible with the hollow cylinder stress states was described and recommended. The analytical solutions proved to be useful for a preliminary evaluation. Finally, the approach, as a whole, seems to have considerable potential in evaluating the predictive capability of creep models. Calibrating the models with the hollow cylinder test results, the extrapolation to field conditions is then a matter of scale effects and opening geometry.

7.4 Suggestions for Further Research

The approach adopted in this research, involving the transition from laboratory studies to the in-situ performance of underground structures in salt rocks, can be optimized by future investigations in many ways. Suggestions for future research are now provided, especially those concerning with the improvement of the laboratory facilities, the laboratory testing program and the model evaluation procedure.

The improvement of the laboratory facilities for further studies must focus on its main objective which is the obtaining of reliable data. A list of improvements for

the laboratory testing system (HPTS) is provided in Chapter 4. Most of these recommendations are related to an increasing versatility and friendly usage of the system. However, some improvements affect directly the system performance in terms of the quality of the testing parameter control. These suggestions are:

1. Modification of the loading routine in the software to ensure a better stress control during the loading stages, in particular hydrostatic loadings.
2. Implementation of a software routine for correcting the cross-sectional area. This routine would permit the execution of constant axial stress creep stages, instead of constant axial load.
3. Implementation of a software routine for controlling the rate of testing parameters. This type of control (e.g., strain rate or stress rate) would eliminate more variables that may affect the creep properties.
4. Use of faster computers to provide immediate response when higher rates of deformation occur.

These recommendations for further research would contribute to a better control of the testing parameters which is extremely important to minimize their effects on the creep properties measured in laboratory.

The testing procedure established for this research can also be improved by increasing the quality of the specimens to yield more uniform testing results. It is suggested that ultrasonic wave tests are executed during the hydrostatic

creep stages to reinforce the adopted specimen reconditioning criterion. Also, unload/reload cycles before and after the hydrostatic creep stages would provide the means to evaluate the performance of the specimen reconditioning procedure. These suggestions for future studies would help standardize the specimen reconditioning procedure which is essential for the investigation of transient creep properties.

The laboratory triaxial testing program presented some interesting observations which certainly deserve more investigation. The creep stages, previously loaded by a JTC stress path, exhibited an unexpected relationship between the creep deformation and the confining stress. This matter has to be studied in detail by a testing program, including a larger number of specimens and tests for each loading condition. Also, the magnitude of the deformations measured from JTC tests was considerably higher than that from CTC tests. It is important to confirm this observation and study the physical mechanism responsible for this difference. The stress path effects on creep properties can play an important role in the predictions of in-situ measurements.

Also, some suggestions for further research are provided to improve the methodology for evaluating the predictive capability of creep models. First, it is necessary to improve the quality of the predictions. This can be done by either better creep model parameters or more accurate mathematical formulations. On the creep model

parameters, it is important to define the role of the triaxial stress path. In other words, which stress path yields parameters that better describe the time-dependent response of circular openings in homogeneous stress fields. To study this matter, it is suggested to execute a triaxial testing program, including CTC and JTC tests or even true triaxial tests, under the stress states recommended by the testing program described in Sec. 6.6 (Fig. 6.27). Also, the model parameters should be obtained from creep tests as long as possible, regardless of the type of the model selected to fit the data. To facilitate the implementation of creep parameters into analytical or numerical formulations, it is suggested that equations linking the creep model parameters to the independent variables (e.g., stress level, deviatoric stress and temperature) are obtained from the triaxial test results.

More accurate mathematical formulations can be achieved by the incorporation of fewer assumptions in the solutions. With the recent laboratory facilities, it is possible to measure the volume change during creep and adopt more complex constitutive models to describe the creep deformation. In this case, numerical analyses would be mandatory. They also allow the evaluation of the stress redistribution around the opening due to geometric changes. Especially for large deformations, this type of analysis is essential to evaluate the predictive capability of creep models. Finally, in-situ measurements should be included to

this evaluation procedure. They provide the scale effects and inhomogeneities that are so important for the performance of any structure built in geotechnical materials.

REFERENCES

Abramowitz, M., and Stegun, I.A. 1972. Handbook of mathematical functions. Dover Publications, New York, U.S.A., 1046 p.

Albrecht, H., Langer, M., and Wallner, M. 1980. Thermomechanical effects and stability problems due to nuclear waste disposal in salt rock. Proceedings, Subsurface Space: Rockstore '80, Pergamon Press, Toronto, vol. 2, pp. 801-809.

Asszonyi, C., and Richter, R. 1979. The continuum theory of rock mechanics. Trans Tech Publications, Clausthal, Germany, 332 p.

ASTM D2845-83 1988. Standard method for laboratory determination of pulse velocities and ultrasonic elastic constants of rock. Annual Book of ASTM Standards, Vol. 04.08, American Society for Testing and Materials, Philadelphia, U.S.A., pp. 317-321.

ASTM D4543-85 1988. Standard practice for preparing rock core specimens and determining dimensional and shape tolerances. Annual Book of ASTM Standards, Vol. 04.08, American Society for Testing and Materials, Philadelphia, U.S.A., pp. 727-730.

Baar, C.A. 1971. Creep measured in deep potash mines vs. theoretical predictions. Proceedings, 7th Canadian Rock Mechanics Symposium, Department of Energy, Mines and Resources, Ottawa, pp. 23-77.

Baar, C.A. 1977. Applied salt-rock mechanics 1: The in situ behavior of salt rocks. Elsevier, Amsterdam, Netherlands, 294 p.

Bakhtar, K., Hardy Jr., H.R., Richardson, A.M., and Mrugala, M.J. 1988. Experimental results and modeling of long-term creep behaviour of rock salt. Proceedings, 29th U.S. Symposium on Rock Mechanics, Balkema, Rotterdam, Netherlands, pp. 169-178.

Baleshta, J.R., and Dusseault, M.B. 1988. Triaxial testing of intact salt rocks: Pressure control, pressure systems, cell and frame design. ASTM STP 977, American

Society for Testing and Materials, Philadelphia, U.S.A., pp. 155-168.

Blum, W., and Fleischmann, C. 1988. On the deformation-mechanism map for rock salt. Proceedings, 2nd Conference on the Mechanical Behavior of Salt, Trans Tech Publications, Clausthal, Germany, pp. 7-22.

Borchert, H., and Muir, R.O. 1964. Salt deposits: The origin, metamorphism and deformation of evaporites. Van Nostrand, Toronto, 338 p.

Braitsch, O. 1971. Salt deposits: Their origin and composition, minerals, rocks and inorganic materials. Springer-Verlag, Berlin, Germany, 297 p.

Branco Jr., P. 1988. Isothermal behaviour of gassy soils. Ph.D. Thesis, Department of Civil Engineering, University of Alberta, Edmonton, 724 p.

Chou, P.C., and Pagano, N.J. 1967. Elasticity: Tensor, dyadic and engineering approaches. Van Nostrand, Toronto, 290 p.

Coates, G.K., Lee, C.A., McClain, W.C., and Senseny, P.E. 1983. Closure and collapse of man-made cavities in salt. Proceedings, 6th International Symposium on Salt, Salt Institute, Alexandria, U.S.A., vol. 2, pp. 139-157.

Cominco 1985. Collection and evaluation of field data around excavations in potash to evaluate excavation performance or concepts for new mining layouts. Prepared for CANMET, Project No. 310104, Cominco Ltd., 46 p.

Cook, N.G.W. 1981. Stiff testing machines, stick slip sliding and the stability of rock deformations. In Mechanical Behaviour of Crustal Rocks: The Handin Volume, Carter et al. (eds.), Geophysical Monograph 24, American Geophysical Union, pp. 93-102.

Cook, R.F. 1983. Long term closure of a shaft excavation through evaporite deposits. Proceedings, Potash Technology: Potash '83, Saskatoon, pp. 275-281.

Costa, A.M. 1984. An application of computational methods and rock mechanics principles to the design and analysis of underground mine excavations (in portuguese). Ph.D. Thesis, COPPE, Universidade Federal do Rio de Janeiro, Rio de Janeiro, Brazil, 3 volumes, 1488 p.

Costa, A.M., and Fairhurst, C. 1985. Comparison of numerical modeling with predictions from laboratory and field observations of deformation in a potash mine in Sergipe, Brazil. Proceedings, 26th U.S. Symposium on Rock Mechanics, Balkema, Rotterdam, Netherlands, pp. 239-249.

Cristescu, N. 1985. Viscoplastic creep of rocks around horizontal tunnels. International Journal of Rock Mechanics and Mining Science & Geomechanics Abstracts, 22: 453-459.

Cruden, D.M. 1970. A theory of brittle creep in rock under uniaxial compression. Journal of Geophysical Research, 75: 3431-3442.

Cruden, D.M. 1971a. A form of the creep law for rock under uniaxial compression. International Journal of Rock Mechanics and Mining Science, 8: 105-126.

Cruden, D.M. 1971b. Single increment creep experiments on rock under uniaxial compression. International Journal of Rock Mechanics and Mining Science, 8: 127-142.

Cruden, D.M. 1971c. The recovery of Pennant sandstone from uniaxial compressive load. Canadian Journal of Earth Sciences, 8: 518-522.

Cruden, D.M. 1974. The static fatigue of brittle rock under uniaxial compression. International Journal on Rock Mechanics and Mining Science & Geomechanics Abstracts, 11: 67-73.

Cruden, D.M. 1983. Creep in brittle rock after an increment of uniaxial load. Canadian Geotechnical Journal, 20: 836-839.

Daemen, J.J.K. 1981. Borehole studies of rock engineering problems in large scale laboratory equipment. Geophysical Research Letters, 8: 711-714.

DASH-8 Manual 1984. Metrabyte Corporation, Taunton, U.S.A., 91 p.

Dawson, P.R., and Munson, D.E. 1983. Numerical simulation of creep deformations around a room in a deep potash mine. International Journal on Rock Mechanics and Mining Sciences & Geomechanics Abstracts, 20: 33-42.

Desai, C.S., and Siriwardane, H.J. 1984. Constitutive laws for engineering materials with emphasis on geologic materials. Prentice-Hall, Englewood Cliffs, U.S.A., 468 p.

Desai, C.S., and Varadarajan, A. 1987. A constitutive model for quasi-static behavior of rock salt. Journal of Geophysical Research, 92: 11445-11456.

DeVries, K.L. 1988. Simulation of field tests in Avery Island dome salt. Proceedings, 29th U.S. Symposium on Rock Mechanics, Balkema, Rotterdam, Netherlands, pp. 413-420.

Dixon, W.J., Brown, M.B., Engelman, L., Hill, M.A., and Jennrich, R.I. 1988. BMDP statistical software manual. University of California Press, Berkeley, U.S.A., 2 volumes, 1234 p.

Dusseault, M.B. 1981. A versatile hollow cylinder triaxial device. Canadian Geotechnical Journal, 17: 1-7.

Dusseault, M.B., and Mraz, D.Z. 1983. Salt rock constitutive behavior. Proceedings, Potash Technology: Potash '83, Saskatoon, pp. 311-320.

Dusseault, M.B., Mraz, D.Z., Unrau, J.D., and Fordham, C. 1985. Test procedures of salt rock. Proceedings, 26th U.S. Symposium on Rock Mechanics, Balkema, Rotterdam, Netherlands, pp. 313-319.

Dusseault, M.B., Rothenburg, L., and Mraz, D.Z. 1987. The design of openings in saltrock using a multiple mechanism viscoelastic law. Proceedings, 28th U.S. Symposium on Rock Mechanics, Balkema, Rotterdam, Netherlands, pp. 633-642.

Eissa, E.A. and Kazi, A. 1988. Relation between static and dynamic Young's moduli of rocks. International Journal on Rock Mechanics and Mining Science & Geomechanics Abstracts, 25: 479-482.

Evans, R., and Kirkland, D.W. 1988. Evaporitic environments as a source of petroleum. In Evaporites and Hydrocarbons, B.C. Schreiber (ed.), Columbia University Press, New York, U.S.A., pp. 256-299.

EXP-16 Manual 1985. Metrabyte Corporation, Taunton, U.S.A., 21 p.

Fairhurst, C., St. John, C.M., Midea, N.F., De Eston, S.M., Fernandes, A.C., and Bongiovanni, L.A. 1979. Rock mechanics studies of proposed underground mining of potash in Sergipe, Brazil. Proceedings, 4th International Congress on Rock Mechanics, Balkema, Rotterdam, Netherlands, vol. 1, pp. 131-137.

Fang, Y.C. 1965. Foundations of solid mechanics. Prentice-Hall, Englewood Cliffs, U.S.A., 525 p.

Farmer, I.W. 1983. Engineering behaviour of rocks. Chapman and Hall, London, Great Britain, 208 p.

Farmer, I.W., and Gilbert, M.J. 1984. Time dependent strength reduction of rock salt. Proceedings, 1st Conference on the Mechanical Behavior of Salt, Trans Tech Publications, Clausthal, Germany, pp. 3-18.

Fernandez, G., and Hendron, A.J. 1984. Interpretation of a long-term in situ borehole test in a deep salt formation. Bulletin of the Association of Engineering Geologists, 21: 23-38.

Findley, W.N., Lai, J.S., and Onaran, K. 1976. Creep and relaxation of nonlinear viscoelastic materials with an introduction to linear viscoelasticity. North-Holland, Amsterdam, Netherlands, 367 p.

Flügge, W. 1967. Viscoelasticity. Blaisdell Publishing Co., Toronto, 127 p.

Fluor Technology 1987. Rock mechanics models evaluation report. Prepared for the U.S. Department of Energy, Report DOE/CH/46656-09, Fluor Technology Ltd., 151 p.

Fossum, A.F., Callahan, G.D., Van Sambeek, L.L., and Senseny, P.E. 1988. How should one-dimensional laboratory equations be cast into three-dimensional form? Proceedings, 29th U.S. Symposium on Rock Mechanics, Balkema, Rotterdam, Netherlands, pp. 35-41.

Friedman, M., Dula, W.F., Gangi, A.F., and Gazonas, G.A. 1984. Structural petrology of experimentally deformed synthetic rocksalt. Proceedings, 1st Conference on the Mechanical Behavior of Salt, Trans Tech Publications, Clausthal, Germany, pp. 19-36.

Frost, H. J., and Ashby, M.F. 1982. Deformation-mechanism maps: The plasticity and creep of metals and ceramics. Pergamon Press, Toronto, 166 p.

Fuenkajorn, K., and Daemen, J.J.K. 1988a. Borehole closure in salt. Prepared for the U.S. Nuclear Regulatory Commission, NUREG/CR-5243, Department of Mining and Geological Engineering, University of Arizona, Tucson, U.S.A., 450 p.

Fuenkajorn, K., and Daemen, J.J.K. 1988b. Borehole closure in salt. Proceedings, 29th U.S. Symposium on Rock Mechanics, Balkema, Rotterdam, Netherlands, pp. 191-198.

Gangi, A.F. 1981. A constitutive equation for one-dimensional transient and steady-state flow of solids. In Mechanical Behavior of Crustal Rocks: The Handin Volume, Carter et al. (eds.), Geophysical Monograph 24, American Geophysical Union, pp. 275-285.

Gangi, A.F., Parrish, D.K., and Handin, J. 1984. Transient and steady-state deformation of synthetic rocksalt. Proceedings, 1st Conference on the Mechanical Behavior of Salt, Trans Tech Publications, Clausthal, Germany, pp. 37-51.

Guessous, Z., Gill, D.E., and Ladanyi, B. 1987. Effect of simulated sampling disturbance on creep behaviour of rock salt. Rock Mechanics and Rock Engineering, 20: 261-275.

Guessous, Z., Ladanyi, B., and Gill, D.E. 1988. Effect of sampling disturbance on laboratory determined properties of rock salt. Proceedings, 2nd Conference on the Mechanical Behavior of Salt, Trans Tech Publications, Clausthal, Germany, pp. 137-158.

Gyenge, J., and Herget, G. 1977. Pit Slope Manual Supplement 3-2: Laboratory tests for design parameters. CANMET, Report 77-26, 74 p.

Gyenge, M., and Ladanyi, B. 1977. Pit Slope Manual Supplement 3-5: Sampling and specimen preparation. CANMET, Report 77-29, 30 p.

Halbouty, M.T. 1979. Salt domes: Gulf region, United States and Mexico. Gulf Publishing, 561 p.

Hambley, D.F., Dusseault, M.B., and Mraz, D.Z. 1988. Characterization of salt rock creep behaviour. Proceedings, 29th U.S. Symposium on Rock Mechanics, Balkema, Rotterdam, Netherlands, pp. 179-189.

Handbook of Steel Construction 1985. Canadian Institute of Steel Construction, 1018 p.

Handin, J., Russell, J.E., and Carter, N.L. 1986. Experimental deformation of rocksalt. In Mineral and Rock Deformation - Laboratory Studies: The Peterson Volume, Hobbs and Heard (eds.), Geophysical Monograph 36, American Geophysical Union, pp. 117-160.

Hansen, F.D., and Carter, N.L. 1984. Creep of Avery Island rocksalt. Proceedings, 1st Conference on the Mechanical Behavior of Salt, Trans Tech Publications, Clausthal, Germany, pp. 53-69.

Hansen, F.D., Mellegard, K.D., and Senseny, P.E. 1984. Elasticity of ten natural rock salts. Proceedings, 1st Conference on the Mechanical Behavior of Salt, Trans Tech Publications, Clausthal, Germany, pp. 71-83.

Hansen, F.D., Senseny, P.E., Pfeifle, T.W., and Vogt, T.J. 1988. Influence of impurities on the creep of salt from the Palo Duro Basin. Proceedings, 29th U.S. Symposium on Rock Mechanics, Balkema, Rotterdam, Netherlands, pp.

199-206.

Hardikar, M.A., Fahrenthold, E.P., and Gray, K.E. 1987. Microcomputer control of triaxial rock compaction and creep tests. Proceedings, 28th U.S. Symposium on Rock Mechanics, Balkema, Rotterdam, Netherlands, pp. 117-123.

Hardy Jr., H.R. 1982. Basic studies associated with the design of salt caverns for the storage of pressurized fluids. Proceedings, ISRM Symposium on Caverns and Pressure Shafts, Balkema, Rotterdam, Netherlands, vol. 2, pp. 903-921.

Hardy Jr., H.R., Chabannes, C.R., and Mrugala, M. 1983. Laboratory and theoretical studies relative to the design of salt caverns for the storage of natural gas. Proceedings, 6th International Symposium on Salt, Salt Institute, Alexandria, U.S.A., vol. 1, pp. 385-416.

Hardy Jr., H.R., Bakhtar, K., Mrugala, M., and Kimble Jr., E.J. 1984. Development of laboratory facilities for evaluating the creep behavior of salt. Proceedings, 1st Conference on the Mechanical Behavior of Salt, Trans Tech Publications, Clausthal, Germany, pp. 85-117.

Hardy Jr., H.R. 1988. Introductory remarks. Proceedings, 2nd Conference on the Mechanical Behavior of Salt, Trans Tech Publications, Clausthal, Germany, pp. 1-3.

Heard, H.C., and Ryerson, F.J. 1986. Effect of cation impurities on steady-state flow of salt. In Mineral and Rock Deformation - Laboratory Studies: The Peterson Volume, Hobbs and Heard (eds.), Geophysical Monograph 36, American Geophysical Union, pp. 99-115.

Herget, G., and Mackintosh, A.D. 1987. Mining induced stresses in Saskatchewan potash. Proceedings, 6th International Congress on Rock Mechanics, Balkema, Rotterdam, Netherlands, vol. 2, pp. 953-957.

Herrmann, W., Wawersik, W.R., and Montgomery, S.T. 1984. Review of creep modelling for rock salt. In Mechanics of Engineering Materials, Desai and Gallagher (eds.), John Wiley and Sons, Toronto, pp. 297-317.

Hight, D.W., Gens, A., and Symes, M.J. 1983. The development of a new hollow cylinder apparatus for investigating the effects of principal stress rotation in soils. Geotechnique, 33: 355-383.

Horseman, S., and Passaris, E.K.S. 1984. Creep tests for storage cavity closure prediction. Proceedings, 1st Conference on the Mechanical Behavior of Salt, Trans Tech Publications, Clausthal, Germany, pp. 119-157.

Hoskins, E.R. 1969. The failure of thick-walled hollow cylinders of isotropic rock. International Journal of Rock Mechanics and Mining Science & Geomechanics Abstracts, 6: 99-125.

Hunsche, U., Plischke, I., Nipp, H.K., and Albrecht, H. 1983. An in situ creep experiment using large rock salt pillar. Proceedings, 6th International Symposium on Salt, Salt Institute, Alexandria, U.S.A., vol. 1, pp. 437-454.

ISRM 1978. Suggested method for determining sound velocity. International Journal of Rock Mechanics and Mining Science & Geomechanics Abstracts, 15: 53-58.

ISRM 1983. Suggested method for determining the strength of rock materials in triaxial compression: revised edition. International Journal of Rock Mechanics and Mining Science & Geomechanics Abstracts, 20: 283-290.

Jaeger, J.C. 1962. Elasticity, fracture and flow with engineering and geological applications. Chapman and Hall, London, Great Britain, 268 p.

Jaeger, J.C., and Cook, N.G.W. 1979. Fundamentals of rock mechanics. Chapman and Hall, London, Great Britain, 593 p.

Kaiser, P.K., and Morgenstern, N.R. 1981. Phenomenological model for rock with time-dependent strength. International Journal of Rock Mechanics and Mining Science & Geomechanics Abstracts, 18: 153-165.

Kelsall, P.C., and Nelson, J.W. 1983. Geologic and engineering characteristics of Gulf region salt domes

applied to underground storage and mining. Proceedings, 6th International Symposium on Salt, Salt Institute, Alexandria, vol. 1, pp. 519-544.

Kovari, K. 1977. Micromechanics models of progressive failure in rock and rock-like materials. Proceedings, International Symposium on Geotechnics of Structurally Complex Formations, Capri, Italy, vol. 1, pp. 307-316.

Ladanyi, B., and Gill, D.E. 1983a. In situ determination of creep properties of rock salt. Proceedings, 5th International Congress on Rock Mechanics, Balkema, Rotterdam, Netherlands, vol. A, pp. 219-225.

Ladanyi, B., and Gill, D.E. 1983b. In situ measurements of creep properties of potash by a borehole dilatometer test. Proceedings, Potash Technology: Potash '83, Saskatoon, pp. 267-273.

Lama, R.D., and Vutukuri, V.S. 1978a. Handbook on mechanical properties of rocks, Vol. II. Trans Tech Publications, Clausthal, Germany, 481 p.

Lama, R.D., and Vutukuri, V.S. 1978b. Handbook on mechanical properties of rocks, Vol. III. Trans Tech Publications, Clausthal, Germany, 406 p.

Langer, M. 1979. Rheological behaviour of rock masses. Proceedings, 4th International Congress on Rock Mechanics, Balkema, Rotterdam, Netherlands, vol. 3, pp. 29-62.

Langer, M. 1984. The rheological behaviour of rock salt. Proceedings, 1st Conference on the Mechanical Behavior of Salt, Trans Tech Publications, Clausthal, Germany, pp. 201-240.

Le Comte, P., 1965. Creep in rock salt. Journal of Geology, 73: 469-484.

Lindner, E.N., and Brady, B.H.G. 1984. Memory aspects of salt creep. Proceedings, 1st Conference on the Mechanical Behavior of Salt, Trans Tech Publications, Clausthal, Germany, pp. 241-273.

Lux, K.H., and Heusermann, S. 1983. Creep tests on rock salt changing load as a basis for the verification of theoretical material laws. Proceedings, 6th International Symposium on Salt, Salt Institute, Alexandria, U.S.A., vol. 1, pp. 417-435.

Maloney, S. 1986. Design of pressure system. Report 86-5, NSERC Strategic Grant No. G1336, 45 p.

Mellegard, K.D., Pfeifle, T.W., and Senseny, P.E. 1983. Constitutive behavior of saline salt from the Cleveland mine. Proceedings, 6th International Symposium on Salt, Salt Institute, Alexandria, U.S.A., vol. 1, pp. 481-486.

Mogharrebi, M., and Thoms, R.L. 1980. In-situ behaviour of salt from closure of deep boreholes. Proceedings, 13th Canadian Rock Mechanics Symposium, Canadian Institute of Mining and Metallurgy, Montreal, pp. 198-203.

Monenco 1984. Alternatives to present potash mining practice in Canada. Prepared for CANMET, Project No. 310104, Montreal Engineering Company Ltd., 422 p.

Moore, C.A. 1980a. Modern electronics for geotechnical engineers: 1. Introduction to integrated circuits. Geotechnical Testing Journal, 3: 9-12.

Moore, C.A. 1980b. Modern electronics for geotechnical engineers: 2. Operational amplifiers. Geotechnical Testing Journal, 3: 13-17.

Moore, C.A. 1980c. Modern electronics for geotechnical engineers: 3. Voltage comparators. Geotechnical Testing Journal, 3: 66-68.

Moore, C.A. 1980d. Modern electronics for geotechnical engineers: 4. Wave form generators. Geotechnical Testing Journal, 3: 69-72.

Moore, C.A. 1980e. Modern electronics for geotechnical engineers: 5. Digital logic circuits. Geotechnical Testing Journal, 3: 124-126.

Moore, C.A. 1980f. Modern electronics for geotechnical

engineers: 6. Process control applications. Geotechnical Testing Journal, 3: 159-162.

Moore, C.A. 1981a. Modern electronics for geotechnical engineers: 7. Introduction to microprocessors. Geotechnical Testing Journal, 4: 26-30.

Moore, C.A. 1981b. Modern electronics for geotechnical engineers: 8. Microprocessor applications. Geotechnical Testing Journal, 4: 79-82.

Mrugala, M. 1984. Application of statistical methods to the determination of mechanical model parameters for salt. Proceedings, 1st Conference on the Mechanical Behavior of Salt, Trans Tech Publications, Clausthal, Germany, pp. 339-354.

Munson, D.E., and Dawson, P.R. 1982. A workhardening/recovery model of transient creep of salt during stress loading and unloading. Proceedings, 23rd U.S. Symposium on Rock Mechanics, Berkeley, U.S.A., Chapter 31, pp. 299-306.

Munson, D.E., and Dawson, P.R. 1984. Salt constitutive modeling using mechanism maps. Proceedings, 1st Conference on the Mechanical Behavior of Salt, Trans Tech Publications, Clausthal, Germany, pp. 717-737.

Munson, D.E. 1987. Personal communication. Workshop on Constitutive Laws for Salt Rocks, 6th International Congress on Rock Mechanics, ISRM, Montreal.

Nicolas, A., and Poirier, J.P. 1976. Crystalline plasticity and solid state flow in metamorphic rocks. John Wiley and Sons, Toronto, 444 p.

Obert, L., and Duvall, W.I. 1967. Rock mechanics and the design of structures in rock. John Wiley and Sons, Toronto, 650 p.

Ottosen, N.S. 1986. Viscoelastic-viscoplastic formulas for analysis of cavities in rock salt. International Journal of Rock Mechanics and Mining Science & Geomechanics Abstracts, 23: 201-212.

Parrish, D.K., and Gangi, A.F. 1981. A nonlinear least squares technique for determining multiple-mechanism, high-temperature creep flow laws. In Mechanical Behavior of Crustal Rocks: The Handin Volume, Carter et al. (eds.), Geophysical Monograph 24, American Geophysical Union, pp. 287-298.

Passaris, E.K.S. 1979. The rheological behaviour of rocksalt as determined in an in-situ pressurized test cavity. Proceedings, 4th International Congress on Rock Mechanics, Balkema, Rotterdam, Netherlands, vol. 1, pp. 257-264.

Passaris, E.K.S. 1982. Fatigue characteristics of rock salt with reference to underground storage caverns. Proceedings, ISRM Symposium on Caverns and Pressure Shafts, Balkema, Rotterdam, Netherlands, vol. 2, pp. 983-989.

Pfeifle, T.W., and Senseny, P.E. 1982. Steady-state creep of rock salt in geoengineering. Proceedings 23rd U.S. Symposium on Rock Mechanics, Berkeley, U.S.A., Chapter 32, pp. 307-314.

Poirier, J.P. 1985. Creep of crystals: High temperature deformation processes in metals, ceramics and minerals. Cambridge University Press, Cambridge, Great Britain, 260 p.

Polypak Seal Design Handbook, PPD 3800 1984. Parker Seal Group, Lexington, U.S.A., 68 p.

Popov, E.P. 1978. Mechanics of materials: SI version. Prentice-Hall, Englewood Cliffs, U.S.A., 590 p.

Potts, E.L.J., Thompson, T.W., Passaris, E.K.S., and Horseman, S.T. 1980. An investigation into underground gas storage in brine well cavities. Proceedings, 5th Symposium on Salt, Salt Institute, Alexandria, U.S.A., vol. 2, pp. 105-123.

Preece, D.S. 1987. Borehole creep closure measurements and numerical calculations at the Big Hill, Texas SPR storage site. Proceedings, 6th International Congress on Rock Mechanics, Balkema, Rotterdam, Netherlands, vol. 2, pp. 219-224.

Ranalli, G. 1987. Rheology of the Earth: Deformation and flow processes in geophysics and geodynamics. Allen and Unwin, London, Great Britain, 366 p.

Reeves, M.J. 1988. Microcomputer based data acquisition systems for triaxial testing of soft yielding rocks. ASTM STP 977, American Society for Testing and Materials, Philadelphia, U.S.A., pp. 107-118.

Reeves, M.J., and Unrau, J.D. 1988. Long-term testing of evaporites at the Saskatchewan Research Council's large-scale triaxial test facility. Proceedings, 90th Annual General Meeting, Canadian Institute of Mining and Metallurgy, Montreal, Paper No. 193, 18 p.

Roark, R.J., and Young, W.C. 1982. Formulas for stress and strain. McGraw-Hill, Toronto, 624 p.

Roberts, G.E., and Kaufman, H. 1966. Table of Laplace transforms. W.B. Saunders, 367 p.

Rocha, M. 1980. Storage in caverns: The problem of interaction between stored products and rock mass (in portuguese). Geotecnia, 28: 93-101.

Sano, O. 1978. Fundamental study on the mechanism of brittle fracture of rocks. Ph.D. Dissertation, Faculty of Engineering, Kyoto University, Japan, 268 p.

Santarelli, F.J., Brown, E.T., and Maury, V. 1986. Analysis of borehole stresses using pressure-dependent, linear elasticity. International Journal of Rock Mechanics and Mining Science & Geomechanics Abstracts, 23: 445-449.

Santarelli, F.J., and Brown, E.T. 1987. Performance of deep wellbores in rock with a confining pressure-dependent, elastic modulus. Proceedings, 6th International Congress on Rock Mechanics, Balkema, Rotterdam, Netherlands, vol. 2, pp. 1217-1222.

Sayao, A., and Vaid, Y.P. 1988. Stress path testing in hollow cylinder torsional device. Soil Mechanics Series No. 117, Department of Civil Engineering, University of British Columbia, Vancouver, 13 p.

Schreiber, B.C. 1988. Evaporites and Hydrocarbons. Columbia University Press, New York, U.S.A., 475 p.

Senseny, P.E., Pfeifle, T.W., and Mellegard, K.D. 1983. A constitutive law for salt derived from laboratory data. Proceedings, Potash Technology: Potash '83, Saskatoon, pp. 329-334.

Senseny, P.E. 1984. Specimen size and history effects on creep of salt. Proceedings, 1st Conference on the Mechanical Behavior of Salt, Trans Tech Publications, Clausthal, Germany, pp. 369-379.

Senseny, P.E. 1985. Determination of a constitutive law for salt at elevated temperature and pressure. ASTM STP 869, American Society for Testing and Materials, Philadelphia, U.S.A., pp. 55-71.

Senseny, P.E. 1988. Creep properties of four rock salts. Proceedings, 2nd Conference on the Mechanical Behavior of Salt, Trans Tech Publications, Clausthal, Germany, pp. 431-444.

Skrotzki, W., and Haasen, P. 1988a. The role of cross slip in the steady-state creep of salt. Proceedings, 2nd Conference on the Mechanical Behavior of Salt, Trans Tech Publications, Clausthal, Germany, pp. 69-81.

Skrotzki, W., and Haasen, P. 1988b. The influence of texture on the creep of salt. Proceedings, 2nd Conference on the Mechanical Behavior of Salt, Trans Tech Publications, Clausthal, Germany, pp. 83-88.

Sonnenfeld, P. 1984. Brines and evaporites. Academic Press, Toronto, 613 p.

Sonnenfeld, P. 1985. Evaporites as oil and gas source rocks. Journal of Petroleum Geology, 8: 253-271.

Spiegel, M.R. 1965. Laplace Transforms. McGraw-Hill, Toronto, 261 p.

Spiers, C.J., Urai, J.L., and Lister, G.S. 1988. The effect of brine (inherent or added) on rheology and deformation

mechanisms in salt rock. Proceedings, 2nd Conference on the Mechanical Behavior of Salt, Trans Tech Publications, Clausthal, Germany, pp. 89-102.

Sterne, K.B. 1981. Hollow cylinder testing of oil sands. M.Sc. Thesis, Department of Civil Engineering, University of Alberta, Edmonton, 228 p.

Tammemagi, H.Y., Fossum, A.F., and Senseny, P.E. 1983. Thermomechanical modeling and salt mining. Proceedings, 6th International Symposium on Salt, Salt Institute, Alexandria, U.S.A., vol. 1, pp. 373-383.

Thoms, R.L., Nathany, M., and Gehle, R.M. 1980. Low-frequency cyclic loading effects on rocksalt. Proceedings, Subsurface Space: Rockstore '80, Pergamon Press, Toronto, vol. 2, pp. 755-761.

Thoms, R.L., and Gehle, R.M. 1982. Experimental study of rocksalt for compressed air energy storage. Proceedings, ISRM Symposium on Caverns and Pressure Shafts, Balkema, Rotterdam, Netherlands, vol. 2, pp. 991-1002.

Thoms, R.L., and Gehle, R.M. 1983. Borehole tests to predict cavern performance. Proceedings, 6th International Symposium on Salt, Salt Institute, Alexandria, U.S.A., vol. 2, pp. 27-33.

Timoshenko, S.P., and Goodier, J.N. 1970. Theory of elasticity. McGraw-Hill, Toronto, 567 p.

Tullis, T.E., and Tullis, J. 1986. Experimental rock deformation techniques. In Mineral and Rock Deformation - Laboratory Studies: The Peterson Volume, Hobbs and Heard (eds.), Geophysical Monograph 36, American Geophysical Union, pp. 297-324.

Urai, J.L., Spiers, C.J., Zwart, H.J., and Lister, G.S. 1986. Weakening of rock salt by water during long-term creep. Nature, 324: 554-557.

Van Eekelen, H.A. 1983. Analytical solutions of some cavity creep problems in layered salt formation. Proceedings, 6th International Symposium on Salt, Salt Institute, Alexandria, U.S.A., vol. 1, pp. 487-500.

Van Eekelen, H.A., Hulsebos, T., and Urai, J.L. 1984. Creep of bischofite. Proceedings, 1st Conference on the Mechanical Behavior of Salt, Trans Tech Publications, Clausthal, Germany, pp. 389-405.

Van Heerden, W.L. 1987. General relations between static and dynamic moduli of rocks. International Journal of Rock Mechanics and Mining Science & Geomechanics Abstracts, 24: 381-385.

Varadarajan, A., and Desai, C.S. 1987. Multiaxial testing and constitutive modelling of rock salt. Proceedings, 2nd International Conference on Constitutive Laws for Engineering Materials, vol. 1, pp. 465-473.

Vutukuri, V.S., Lama, R.D., and Saluja, S.S. 1974. Handbook on mechanical properties of rocks, Vol. I. Trans Tech Publications, Clausthal, Germany, 281 p.

Wagner, R.A., Mellegard, K.D., and Senseny, P.E. 1982. Influence of creep law form on the predicted deformations in salt. Proceedings, 23rd U.S. Symposium on Rock Mechanics, Berkeley, U.S.A., Chapter 71, pp. 684-691.

Wagner, R.A., and Senseny, P.E. 1986. Evaluation of constitutive models for salt creep. Proceedings, 2nd International Symposium on Numerical Models in Geomechanics, M. Jackson and Son, Redruth, England, pp. 275-283.

Wallner, M. 1987. Personal communication. Workshop on Constitutive Laws for Salt Rocks, 6th International Congress on Rock Mechanics, ISRM, Montreal.

Warren, J.K. 1989. Evaporite sedimentology: Importance in hydrocarbon accumulation. Prentice-Hall, Englewood Cliffs, U.S.A., 285 p.

Wawersik, W.R., Herrmann, W., Montgomery, S.T., and Lauson, H.S. 1982. Excavation design in rock salt: Laboratory experiments, material modeling and validations. Proceedings, ISRM Symposium on Caverns and Pressure Shafts, Balkema, Rotterdam, Netherlands, vol. 3, pp. 1345-1356.

Wawersik, W.R., and Preece, D.S., 1984. Creep testing of salt: Procedures, problems and suggestions. Proceedings, 1st Conference on the Mechanical Behavior of Salt, Trans Tech Publications, Clausthal, Germany, pp. 421-429.

Wawersik, W.R. 1985. Determination of steady state creep rates and activation parameters for rock salt. ASTM STP 869, American Society for Testing and Materials, Philadelphia, U.S.A., pp. 72-92.

Wawersik, W.R., and Morgan, H.S. 1987. Evaluating design procedures for structures in rock salt. Proceedings, 28th U.S. Symposium on Rock Mechanics, Balkema, Rotterdam, Netherlands, pp. 107-115.

Wieczorek, K., Stanpendahl, G., and Rothfuchs, T. 1988. Deformational rock mass response during a nuclear waste repository simulation experiment at the ASSE salt mine. Workshop on Excavation Response in Deep Radioactive Waste Repositories: Implications in Engineering Design and Safety Performance, Atomic Energy of Canada, Winnipeg, 12 p.

TESTING CELLS AND AXIAL LOADING SYSTEMS

A.1 Introduction

This appendix presents the design criteria leading to the specifications for the construction of Cells No. 1 and No. 2 as part of the High Pressure and Temperature System (HPTS). These cells were designed to optimize desired capacities, flexibility of application, cost, ease of handling and safety.

Dimensions and capacity are a direct consequence of the needs of a laboratory testing program. The size of specimens was determined as described in Chapter 5 and the pressure and temperature ranges were set according to the studies to be carried out. With these cells, it is possible to follow any axisymmetric stress path. The cell (external) and bore (internal) pressures of up to 70 MPa can be applied independently. The axial load capacity for Cell No. 1 is 1 MN and for Cell No. 2 varies from 1 MN, using the modified pressure intensifier, to 3 MN, using the standard intensifier (Appendix B).

For versatility and flexibility of application, both cells were designed to use cylindrical specimens with a diameter of less than 140 mm. Currently, the HPTS accommodates two specimen diameters, 100 and 140 mm. The height of a specimen cannot exceed 200 mm. Hollow cylinder specimens can also be tested if the bore (internal) diameter is 32 mm. In summary, the HPTS can accommodate specimens of different sizes in either hollow cylinder or triaxial test modes.

Handling is another important design aspect. As the HPTS is intended for high pressure tests, almost all parts are made of steel and therefore too heavy to be handled by one person. Several tools were developed to make the assembly and disassembly procedures easier but two people and a small crane (5 kN) are needed for productive work. Both cells lie on carts with four roller wheels to facilitate transport in the laboratory.

Safety and cost are analyzed together in engineering. Due to the characteristics of the tests to be performed and the involved pressures, it was decided to be conservative in the design. A strength criterion simply based on the ratio of factorized loads to factorized material strength was used. Furthermore, the material elastic limit was used as a

design limit. Cost reduction was limited to making the best use of the specified materials. For instance, separating the cell chamber and end caps saved a considerable amount of material, labor and time compared to machining a solid piece of metal to make the cell.

A.2 Design of the Testing Cells and Axial Loading Systems

A strength criterion was used to design both cells. All external loads (forces and pressures) were increased by a load factor of 1.5 and the material strength was decreased by a resistance factor of 0.9, regardless of the metal. Some dimensions of the parts were determined based on geometric constraints such as specimen size, seal dimensions and internal space required for instrumentation and heating coils. The other dimensions were calculated using readily available engineering design equations (Popov, 1978 and Roark and Young, 1982). It is not intended to present all calculations, but some principles used for designing the main parts of the cells are reviewed below.

The bottom end cap was approximated as a flat, circular plate of constant thickness simply supported at the outer edge and the top end cap as an annular plate of constant thickness, with the outer edge simply supported and inner edge free. Both end caps are subjected to a uniform distributed pressure (70 MPa). Their thicknesses are given by:

$$t = (6M / \sigma)^{1/2} \qquad [A.1]$$

where

t ... thickness

σ ... material design stress reduced by the resistance factor

M ... maximum bending moment.

The bending moments are given by Roark and Young (1982), Table 24.2a for the top end cap and Table 24.10a for the bottom end cap. They are functions of the maximum internal pressure, geometric dimensions and elastic constants.

The cylindrical chambers were designed as a thick-walled cylinder under an uniform internal radial pressure (70 MPa). Its thickness is given by (Table 32.1a, Roark and Young, 1982):

$$t = a\,[\{(\sigma+p)/(\sigma-p)\}^{1/2} - 1] \qquad [A.2]$$

where

p ... maximum internal pressure increased by the load factor

a ... internal radius, defined by geometric constraints (0.1176 m).

Finally, the bolts were designed by following the recommendations of the Handbook of Steel Construction (1985), with an additional resistance factor of 0.75 for elements under tension. The total area of the bolts is given by:

$$A_t = (p\pi a^2) / \sigma \qquad [A.3]$$

The number of bolts depends on the area of the selected bolt. Bolts of 25.4 mm diameter were chosen.

Table A.1 presents the materials and properties used in designing the testing cell and axial loading system parts. When a material is not precisely specified, any one in that category can be used for manufacturing that part.

A.3 Description and Specification of the Testing Cells and Axial Loading Systems

Both testing cells are identical but the axial loading systems differ. Cell No. 1 needs a separate loading frame to apply axial stress to the specimen. Cell No. 2, a self-framed cell, has a second chamber which provides the load to the piston. Individual cell components are described below with emphasis on the differences between the cells. Figures A.1 and A.2 show Cell No. 1 in the triaxial setup and Cell No. 2 in the hollow cylinder setup, respectively.

A.3.1 Pedestal, PD (Fig. A.3)

The pedestal, PD, is a thick-walled cylinder fastened to the bottom cap, BC, by four steel socket head cap screws (d= 12.7 mm, 63 mm long). There are two slots in the wall to bring out the tubing and wiring for the bore temperature, pressure and instrumentation, in hollow cylinder tests.

A.3.2 Bottom Cap, BC (Figs. A.4 and A.5)

The bottom cap , BC, consists of a flat circular plate that is connected to the top cap, TC, by sixteen bolts, BT. The five holes in its center are used in hollow cylinder testing. Two holes (d= 6.4 mm) provide fluid circulation to control the temperature in the bore of hollow cylinder specimens. A circulation tube is welded to these holes when bore temperature control is necessary (Fig. A.2). Two holes (d= 3.2 mm) are used for filling the bore with silicone oil and for applying pressure. One of these holes has a tube to the top of the bore for deairing. The fifth hole (d= 4.8 mm) contains electrical connections for thermocouples and strain gauges. Two of the three holes marked 'x' are for filling the cell with silicone oil and for applying pressure. The other hole is for thermocouple and specimen diameter deformation device wiring. The remaining holes, eight holes (marked 'w'), eleven holes (marked 'z') and four holes (marked 'v'), are for securing accessory parts (specimen support, SS, bottom ring, BR, and pedestal, PD). The outer ring of sixteen holes are for the bolts, BT, which are connected to the top cap, TC. Finally, a circular depression (d_o= 32 mm, d_i= 19 mm and 7 mm deep) at the center of the plate is designed to contain the bore membrane, MB, and its lower lip seal (Fig. A.2).

A.3.3 Bottom Ring, BR (Fig. A.6)

The bottom ring, BR, gives support to the lip seals. It is fastened to the bottom cap, BC, by eleven steel socket head cap screws (d= 9.5 mm, 32 mm long). There are also three holes (d= 6.3 mm) with the same function as those marked 'x' for the bottom cap, BC. One of the pressurizing holes has been modified to accept a vertical tube from the top of the cell to bleed air. O-rings are used in all holes to prevent leakage between the bottom cap and ring. The other four holes (d= 3.2 mm and 13 mm deep) on the top of the ring are for holding the supporting columns, CL (d= 9.5 mm, 280 mm long). These columns provide support to the top ring, TR. The bottom ring must be changed with different specimen sizes.

A.3.4 Specimen Support, SS (Figs. A.7 and A.8)

The specimen support, SS, is fastened to the bottom cap, BC, by eight stainless steel socket head cap screws (d= 6.3 mm, 32 mm long). It should have the same diameter as the specimen.

A.3.5 Top Ring, TR (Fig. A.9)

The top ring, TR, has the same function as the bottom ring. However, there are two major differences. First, there are no holes for connections since they are made through the bottom cap, BC. Second, there is a 2 mm wide flange at its base to prevent the upper lip seals from falling into the cell during assembly. Only five holes are present in the top ring, TR, four holes for the supporting columns, CL, and one for the deairing tube. This part must also be changed with different specimen sizes.

A.3.6 Cell Chamber, CC (Fig. A.10)

The cell chamber, CC, consisting of a thick-walled cylinder, was machined smooth (0.0003 mm) on the internal wall, near the seal-contact regions to avoid high friction during assembly. To ease assembly, both ends were chamfered.

A.3.7 Top Cap, TC (Figs. A.11 and A.12)

The top cap, TC, is an annular circular plate. An axial ram fits into the centered hole for loading the specimens. With specimen diameters other than 140 mm, an adapter, DR (Fig. A.13), is needed to reduce the internal diameter. On top, there are twelve holes to fasten the diameter reducer, DR. The other sixteen holes are for the bolts, BT, which connect the bottom and top end caps. The top end caps differ slightly for each cell (Fig. A.11 for Cell No. 1 and Fig. A.12 for Cell No. 2).

A.3.8 Diameter Reducer, DR (Fig. A.13)

The diameter reducer, DR, is essentially a thick-walled cylinder which serves to reduce the internal diameter of the top cap, TC (140 mm) to that of the axial ram being used. There are twelve holes to fasten it to the top cap, TC, using high strength steel (grade 8) socket head cap screws (d= 12.7 mm, 32 mm long). Currently, the HPTS employs a reducer to accommodate the 100 mm diameter ram.

A.3.9 Axial Ram, RM (Figs. A.14, A.15 and A.16)

The axial ram, RM, has the same diameter as the specimens. It is divided into two or three pieces for the

triaxial or hollow cylinder set up, respectively. This was necessary to facilitate assembly and to ensure vertical loading with good contact. There is a central longitudinal hole through the exposed part of the ram to bleed air during assembly.

A.3.10 Bolts, BT

There are sixteen high strength steel bolts (d= 25.4 mm) for each cell. They only differ in length, 510 mm for Cell No. 1 and 860 mm for Cell No. 2. They are threaded (eight threads each 25.4 mm) for 75 mm at the ends. Nuts and washers are also made of high strength steel.

A.3.11 Axial Loading Frame for Cell No. 1

The axial loading frame for Cell No. 1 with a capacity of 1 MN was manufactured by Structural Behavior Engineering Laboratories. It has a squared bottom plate (470x470 mm, 60 mm thick) with a cylindrical piston of 229 mm diameter and 35 mm stroke, a squared top plate with the same dimensions and four bolts (d= 51 mm, 1.05 m long) connecting both plates.

Cell No. 2 is a self-framed cell and has an extra chamber, PC, cap, CP, and axial piston, PP (Fig. A.2).

A.3.12 Piston Chamber, PC (Fig. A.17)

The piston chamber, PC, has the same dimensions as the cell chamber, CC, but with the addition of a slot in the bottom end. This slot permits measurement of the displacement of the axial ram by an LVDT. The internal surface of the piston chamber, PC, was machined smooth (0.0003 mm) to reduce friction with the lip seals. The top end was chamfered to facilitate assembly.

A.3.13 Axial Piston, PP (Figs. A.18 and A.19)

The axial piston, PP, is a single acting ram which when externally pressurized transmits load to the axial ram, RM. A lip seal, SP, recessed in the top end of the piston reacts against the piston chamber, PC. A seal cap, CS (Fig. A.19), is fastened to the piston by four screws (d= 6.3 mm, 25 mm long). It keeps the seal in place during downward movement

of the piston. Two grooves are provided for wear rings (PARKER Molygard W2-9500-500, 3.2 mm thick, 12.7 mm wide), which help maintain the alignment and prevent metal-to-metal contact of moving parts. Finally, at the bottom end, a concentric, cylindrical guide was machined to match the axial ram, RM.

A.3.14 Piston Cap, CP (Fig. A.20)

The piston cap, CP, is a circular plate connected to the bottom cap, BC, by the sixteen bolts, BT. Pressurized fluid is supplied to the piston chamber, PC, through a central hole. A second hole is used to bleed air during filling.

Seals and membranes are important parts that should be compatible and custom fit to the specimen dimensions.

A.3.15 Membranes

All membranes are 3.2 mm thick, made of neoprene and have a Durometer Rating of 90. The external membrane, MC, has an inner diameter equal to the specimen diameter (e.g., 100 and 140 mm) and is 305 mm long. The bore membrane, MB, used for hollow cylinder tests, has an outer diameter equal to the bore diameter (32 mm) and is 273 mm long. These membranes are oil resistant, leak proof and reusable.

A.3.16 Seals

Seals are PARKER Polypak (molythane) lip seals. Three pairs are used in the cell itself. Cell No. 2 has an additional pair in the piston chamber, PC. The first pair (chamber seal, SC, #50008250-750B) are independent of the specimen size. They seal between the cell chamber, CC, and the top and bottom rings. The second pair (membrane seal, SM, #50005750-750B for 140 mm specimens and #50004250-750B for 100 mm specimens) seal between the external membrane, MC, and the rings. The third pair (bore seal, SB, #12500750-250B), used in hollow cylinder specimens, seal between the bore membrane, MB, and the circular slots in the bottom cap, BC, and in the axial ram, RM. The fourth pair (piston seal, SP, #50008250-750B) seal between the piston chamber, PC, and the axial piston, PP, and between the piston chamber, PC, and the piston cap, CP. For more details on design and specifications of the lip seals, see the Polypak Seal Design Handbook (1984).

A.3.17 Insulator Caps, TS

Insulator caps, TS, are used to insulate the specimen from the metal parts during temperature control tests. They are fabricated from sulfaset, a product with high strength and low friction properties. They have the same diameter as the specimen and their thickness is 12.5 mm. For hollow cylinder specimens, they must have a central hole with the same diameter as the bore (32 mm).

A.3.18 Lower Platen, LP

A lower platen, LP (d= 100 mm, 25 mm thick), with a highly polished spherical seat (radius of 143 mm), was designed to substitute the insulator caps which proved ineffective for high stress triaxial tests.

The structural parts, the bottom, top and piston end caps, the diameter reducer and both cell and piston chambers, are fabricated from high strength steel (AISI 4140). They were roughly machined, heat treated to a Rockwell C Hardness of 33 to provide sufficient strength and then machined to their final dimensions. The bolts were also made from high strength, heat treated steel (AISI 4340). The specimen supports, lower platen and axial rams that may contact corrosive materials (e.g., salt-rock specimens) are fabricated from stainless steel (316-SS). The pedestal, rings and columns are made from mild steel. And, the axial piston and seal cap are from aluminium (6061-T6). See Table A.1.

A.4 Assembly and Disassembly Procedures

The assembly and disassembly procedures depend on the specimen size and the type of test (i.e., whether one axis of pressure control for unconfined axial loading, two axes for triaxial loading or three axes for hollow cylinder tests). The procedures are described below with attention drawn to those steps which might differ in special cases. Four procedures are described: assembly, charging, purging and disassembly.

A.4.1 Assembly Procedure

Before starting assembly, all threads should be cleaned (using a small brush and pressurized air) and then treated

with an anti-seize lubricant. The assembly procedure follows:

a. Fasten the pedestal, PD, to the bottom cap, BC. Steps 'b' and 'c' are only for hollow cylinder specimens.
b. Make all connections to the bore: two fittings for pressure, two for temperature and one for electrical wires. Bring the tubing and wiring out through the slots of the pedestal, PD. Position Cell No. 1 on the reaction frame cylinder.
c. Install the lower bore seal, SB, and then the bore membrane, MB. Make sure, before placing these parts, that the deairing tube, temperature coils and bore convergence device are in place and the wiring for temperature and bore convergence measurements connected. Fill the bore to approximately 15 mm below its top with silicone oil.
d. Fasten the specimen support, SS, to the bottom cap, BC. Make sure that the specimen support has the same diameter as the specimen and is adequate for the test to be performed, whether triaxial or hollow cylinder.
e. Fasten the bottom ring, BR, to the bottom cap, BC. Use the ring size adequate for the specimen diameter. Make sure that all O-rings are in place.
f. Place either the lower insulator cap, TS, or the lower platen, LP, followed by the specimen and the upper insulator cap. To avoid friction between the specimen and the bore membrane, MB, and between the specimen and the insulator caps, TS, a thin, uniform layer of dry lubricant (e.g., molybdenum disulphide, MoS_2) should be applied.
g. Slide the external membrane, MC, over the specimen. Again, dry lubricant between the membrane and the specimen should be applied.
h. Screw two bolts, BT, by hand on opposite sides into the bottom cap, BC.
i. Place the lower seal, SM, between the external membrane, MC, and the bottom ring, BR. To fully engage the seal, an accessory tool, consisting of a PVC cylinder with inner diameter larger than the outer diameter of the membrane and a flange at its bottom end of the same cross-sectional area as the seal, is used. This cylinder is forced against the seal using two bolts, BT, and a wood cross bar (e.g., 100 mm wide, 50 mm thick) as a reaction frame.
j. Fasten the air bleed tube to the bottom ring, BR, and place the four supporting columns.
k. Place the lower seal, SC, inside the bottom end of the cell chamber, CC.
l. Mount the cell chamber, CC, using the custom lift clamp. Two people are needed. Again, a custom PVC cylinder is used to engage the seal, SC. By visual inspection,

ensure that the lower lip seals are in place.

m. After installing the upper bore seal, SB, in the groove of the axial ram insert, place it over the insulator cap, TS, and bore membrane, MB. This step is only for hollow cylinder specimens.

n. Place the spherical ram seat over the insert. Make sure that they are properly aligned.

o. Place the top ring, TR, ensuring that all supporting columns and the deairing tube are aligned. Then place the upper seal, SM, by hand between the top ring, TR, and the external membr[illegible]

p. With a funnel, fill th[illegible] ith silicone oil up to the lower face of the to[illegible] TR. This operation saves time during the charg[illegible] ocedure. Then, place the upper seal, SC, betwee[illegible] op ring, TR, and the cell chamber, CC. Agai[illegible], [illegible] reaction frame may be of assistance.

q. Place the the axial ram, RM, by hand over its spherical seat. Use a small screw driver to free the perimeter of the membrane, MC. Two people are needed.

Now, follow step 'r' for Cell No. 1 only.

r. Install all sixteen bolts, BT, into the bottom cap, BC, engaging threads fully. In case of difficulty, fasten two nuts against each other in the top thread and use a wrench.

s. When using specimens with diameters other than 140 mm, the diameter reducer, DR, has to be fastened to the top cap, TC. Then with a crane, place the top cap, TC. This is guided by both the axial ram, RM, and the bolts, BT. Striking with a rubber hammer may help this operation.

The next five steps ('t' to 'x') are for Cell No. 2 only. For assembling Cell No. 1, go to step 'y'.

t. Place the piston chamber, PC, again using the lift clamp. Make sure that the chamber slot is aligned with the LVDT adapter of the axial ram, RM.

u. Place the lower seal, SP, in the recessed groove of the axial piston, PP. Then fasten the seal cap, CS, to the axial piston.

v. Place the wear rings (molygard) into the axial piston sidewall grooves. Slide the axial piston, PP, carefully into the piston chamber, PC, holding it by an eye bolt screwed in its top end. Finally, ensure that both axial piston and ram are properly aligned.

Follow step 'r' for Cell No. 2, then advance to the next step.

w. Place the upper seal, SP, in the groove of the piston cap, CP.
x. With a crane, place the piston cap, CP, using the bolts, BT, to guide it. Apply an uniform pressure to place the upper seal, SP, between the piston chamber, PC, and the cap, CP.
y. Place washers and fasten nuts to all sixteen bolts, BT. Tighten them uniformly using a torquemeter setting of 70 N.m for final adjustments.

For assembling the loading frame for Cell No. 1, follow the next step.

z. Screw the four bolts in the bottom plate. With a crane, position the top plate so that it is just in contact with the axial ram, RM. Adjust the four lower nuts and then, fasten the upper nuts.

A.4.2 Charging Procedure

The charging procedure follows:

a. Connect the high pressure line to the pressure inlet of the axis to be charged, either axial, internal or external pressure.
b. Connect a plastic tube to the pressure outlet (air bleed), through which it is possible to determine the fluid level inside the cell.
c. Open the appropriate handpump valve and inject fluid until fully charged.
d. Disconnect the plastic tube from the pressure outlet and fasten a cap to it.
e. Keep jacking the handpump until zero pressure is indicated in the pressure gauge and then close the handpump valve.
f. Repeat the above steps for the other axes to be charged. Then, connect all instrument lines.

A.4.3 Purging Procedure

The purging procedure follows:

a. Release all pressure in the cell and then disconnect the pressure and instrument lines.
b. Place a fluid reservoir lower than the cell.
c. Connect the fluid reservoir to the pressure inlet of the axis to be purged.
d. Remove the cap from the pressure outlet and connect a compressed air line to it.
e. Apply air pressure (e.g., 350 kPa) until there is no more fluid inside the cell or bore. This operation usually takes 5 min.
f. Disconnect the fluid reservoir and compressed air lines. Filter the fluid before storage to prevent contamination by particles of metal, lubricant and dust. Repeat the above steps for the other axes to be purged.

A.4.4 Disassembly Procedure

Step 'a' applies only to the disassembly of the axial loading frame for Cell No. 1:

a. Take the upper nuts off. With a crane, remove the top squared plate, by means of an eye bolt placed at its center. Then, unscrew the four bolts.
b. Remove the nuts and washers from the sixteen bolts, BT. The next four steps ('c' to 'f') apply only to Cell No. 2.
c. Using a crane, take the piston cap, CP, off. Striking with a rubber hammer might help. Remove the upper seal, SP, from it.
d. Remove all bolts, BT. Again, the use of a wrench and two nuts fastened against each other might help.
e. Screw an eye bolt to the top end of the axial piston, PP. Then using the crane, remove it from the chamber, PC. Again, the rubber hammer is helpful. Disassembly of the seal cap, CS, lower seal, SP, and wear rings (molygard) is optional.
f. Remove the piston chamber, PC, using the lift clamp. User may opt to remove the whole set of piston and chamber without taking them apart.

Follow step 'd' for Cell No. 1. Then advance to the next steps for both cells.

g. Screw an eye bolt to the top end of the axial ram, RM, and lift it using a crane and striking with a rubber hammer.
h. Also using the crane, remove the top cap, TC.
i. Remove the cell chamber, CC, using the lift clamp.
j. Remove the upper seals, SC and SM, and the top ring, TR,

from the cell chamber, CC.

k. Take the supporting columns, air bleed tube and lower seal, SC, off.
l. Remove all screws from the bottom ring, BR, and move it to loosen the lower seal, SM. Then, take the bottom ring and seal off.
m. Remove the specimen with the external membrane, MC. Take apart the specimen, membrane and axial ram components.
n. Remove the bore membrane, MB, and disconnect all instruments in the bore. This step applies only to hollow cylinder specimens.

If the next test is to be performed in a specimen with the same diameter as the previous one, this completes the disassembly procedure. Otherwise, the specimen support, SS, must also be removed. Before reassembly, all parts, membranes and seals must be cleaned very carefully.

A.5 Structural Performance of the Testing Cells

Ten strain gauges were installed on Cell No. 1 in order to check the design criteria and assumptions. The gauges were located as follow:

- two gauges each at mid-height of bolts BT-1 and BT-9 (diametrically opposed) to measure their elongation;
- one gauge in the middle of the lower face of the bottom cap, BC, to measure its deflection;
- one gauge at mid-height of the bore of the aluminium hollow cylindrical specimen to help interpret cell performance and to conduct calibration tests;
- two gauges (diametrically opposed) at mid-height of the cell chamber, CC, to measure its expansion during loading;
- two gauges on the upper face of the top cap, TC, at radii of 105 mm and 130 mm, to measure its deflection.

These strain gauges were connected to a switch and balance unit which was connected to a strain indicator box. All strain measurements were read at regular intervals during loading and unloading. This procedure was followed during all structural performance tests and calibration of the equipment.

The predicted values were obtained using the same formulae as for design, but not incorporating the load and resistance factors. Expressions of strain as functions of the axial stress and confining pressure were obtained by

substituting the elastic properties and geometric dimensions for each cell component. Figure A.21 shows the predicted and measured strains for a test where the axial stress and confining pressure were hydrostatically increased to 60 MPa and then decreased to zero. Comparison shows that the cell chamber behaved exactly as predicted by the closed-form elastic solution for the thick-walled cylinder. All other elements presented smaller measured values than the predicted ones. This may be easily explained as the end caps are thick elements and the adopted formulation only a crude approximation, being on the conservative side (Roark and Young, 1982). With the bolts, different values by the gauges might be attributable to a non-uniform distribution of load. However, no reasonable explanation exists for them measuring less than half of the predicted value. Other performance and calibration test results are consistent with the above.

Table A.1 Materials and properties of the testing cell and axial loading system components

Parts	Material	Properties		
		E (GPa)	ν	σ_y (MPa)
BC	AISI 4140 (HRC=33)	200	0.27	850
BR	mild steel			
BT	AISI 4340	200	0.27	1040
CC	AISI 4140 (HRC=33)	200	0.27	850
CL	mild steel			
CP	AISI 4140 (HRC=33)	200	0.27	850
CS	6061-T6	70	0.3	250
DR	AISI 4140 (HRC=33)	200	0.27	850
LP	316-SS			
PC	AISI 4140 (HRC=33)	200	0.27	850
PD	mild steel			
PP	6061-T6	70	0.3	250
RM	316-SS			
SS	316-SS			
TC	AISI 4140 (HRC=33)	200	0.27	850
TR	mild steel			
TS	sulfaset			
MB	neoprene	Durometer Rating of 90		
MC	neoprene	Durometer Rating of 90		
SB	molythane	Parker Polypak		
SC	molythane	Parker Polypak		
SM	molythane	Parker Polypak		
SP	molythane	Parker Polypak		

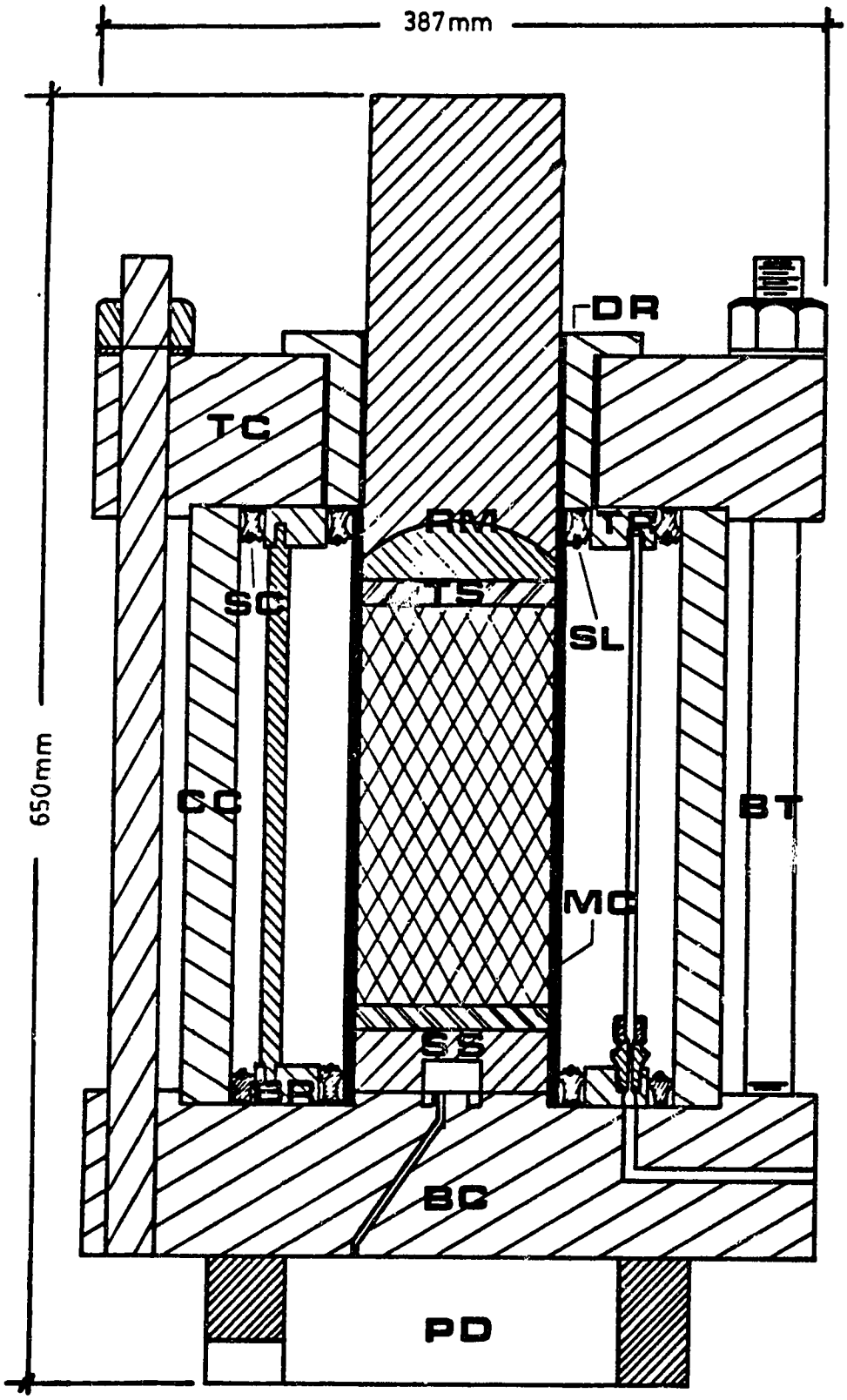

Figure A.1 Cell No. 1 - Triaxial test setup

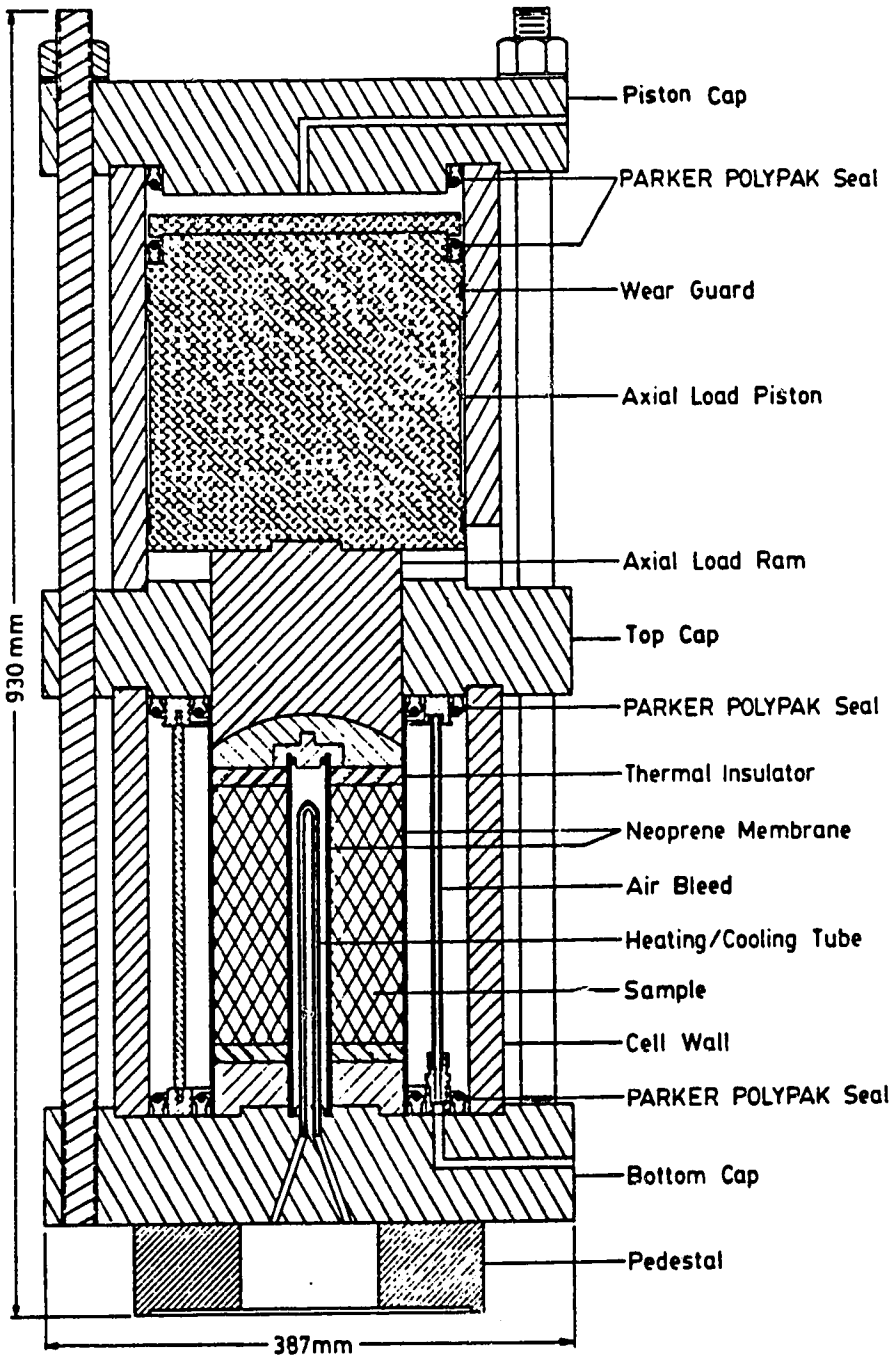

Figure A.2 Cell No. 2 - Hollow cylinder test setup

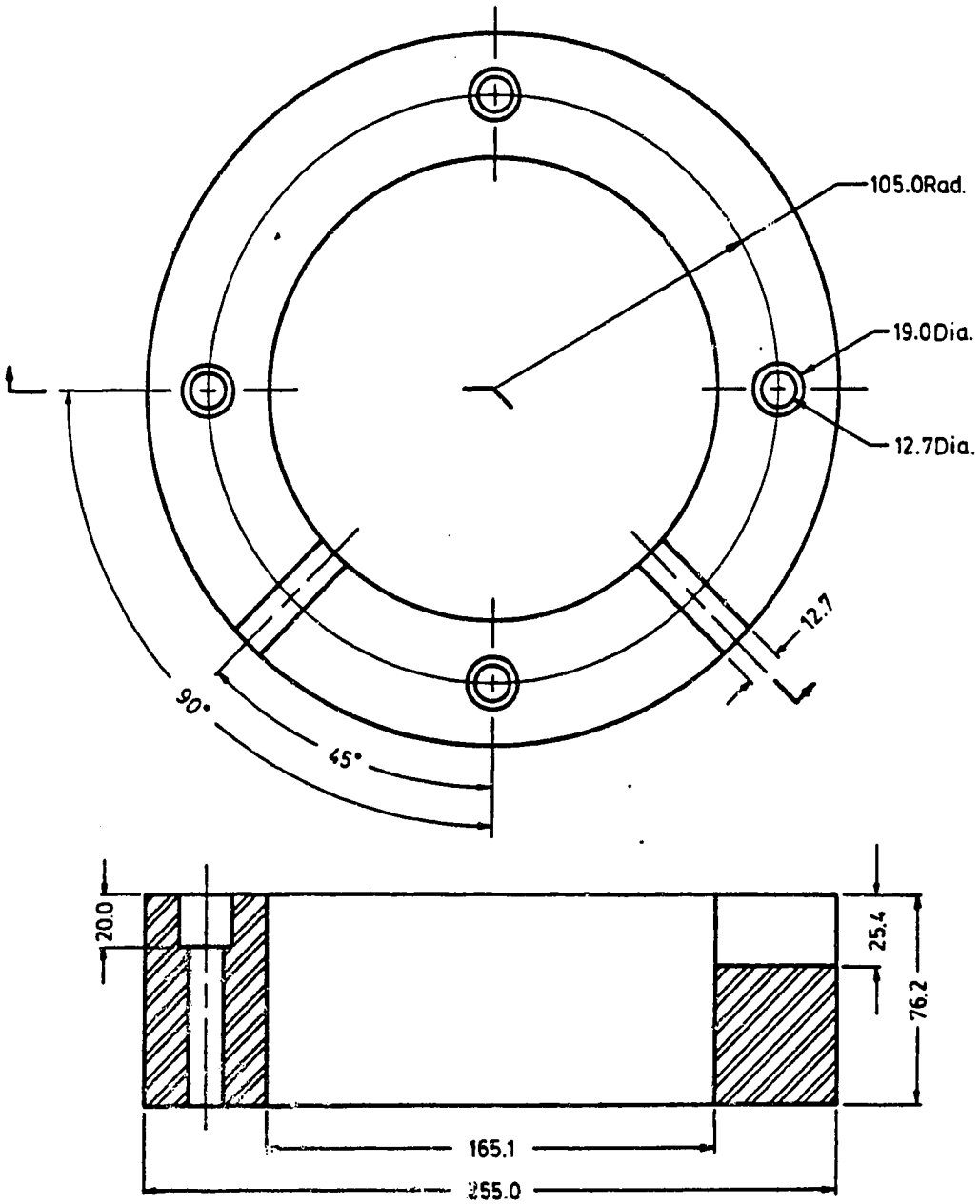

Figure A.3 Pedestal, PD

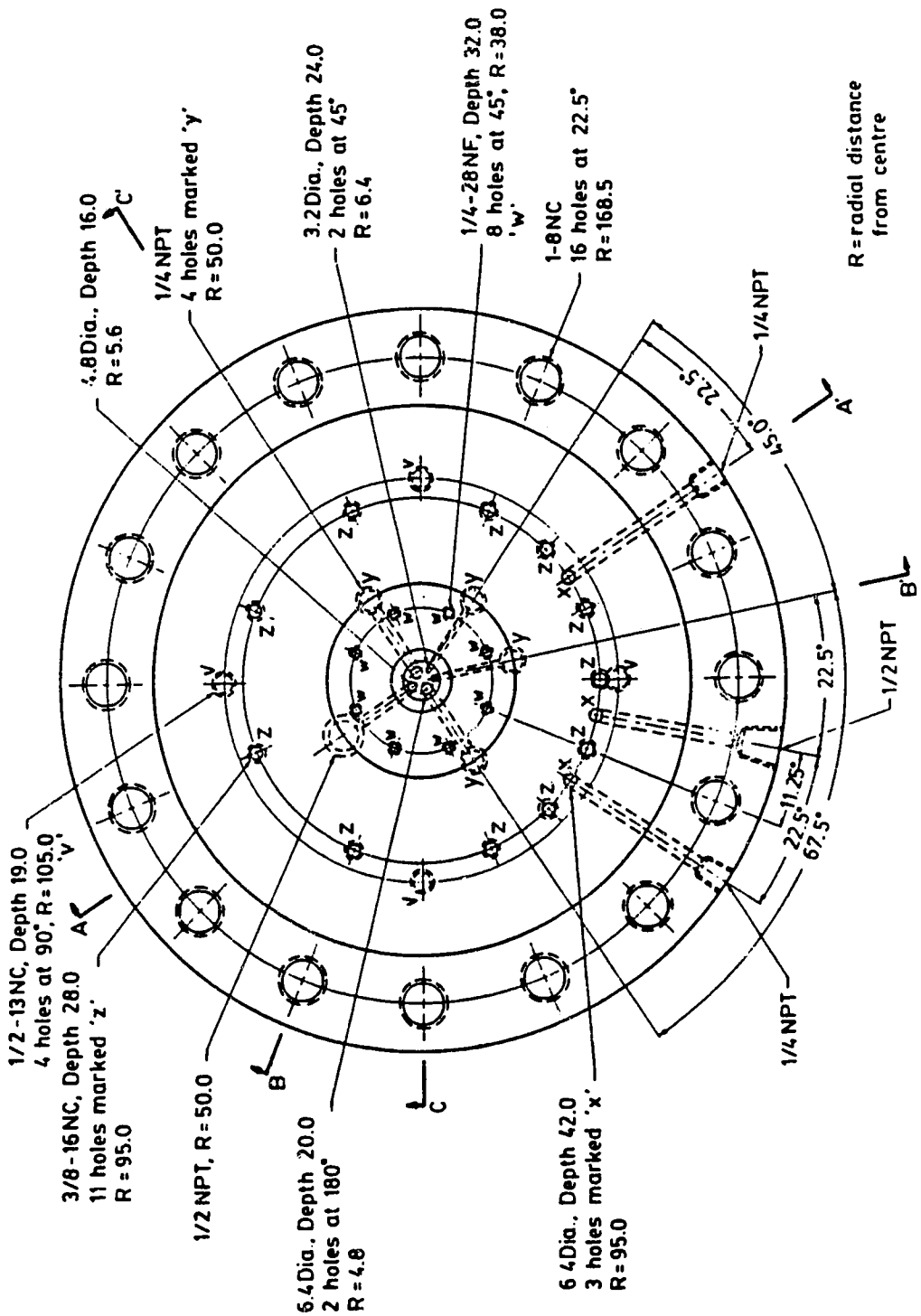

Figure A.4 Bottom cap, BC - Top view

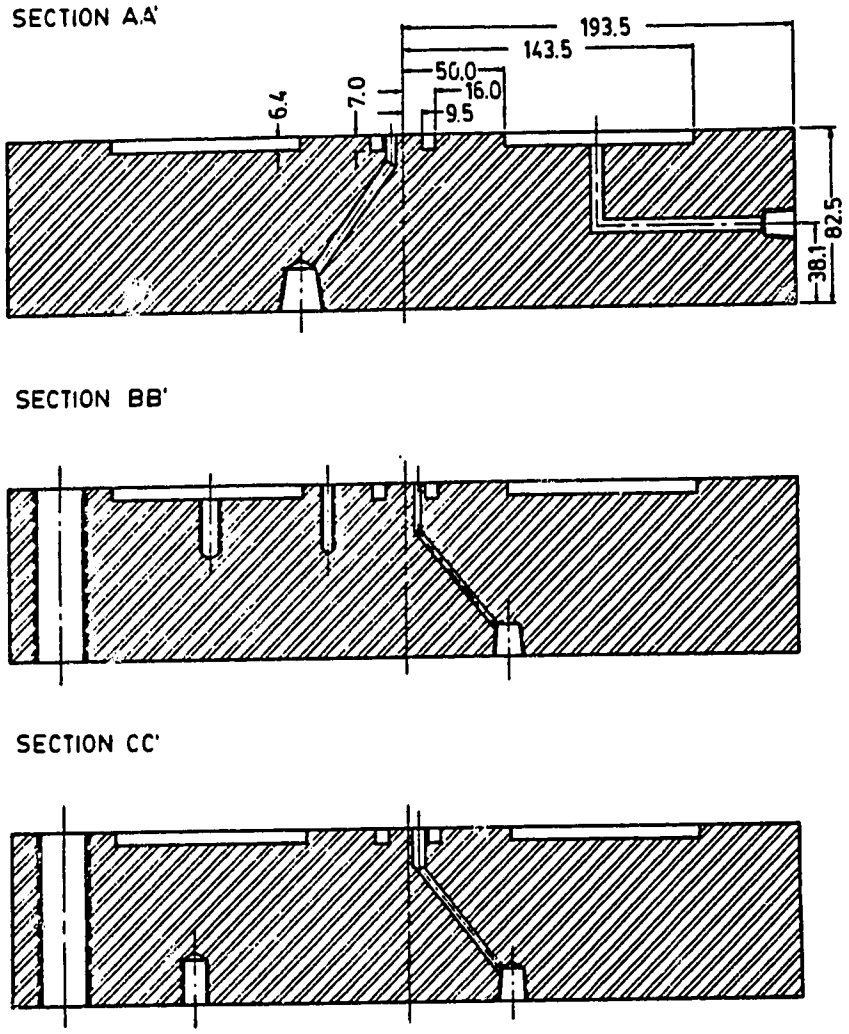

Figure A.5 Bottom cap, BC - Sections

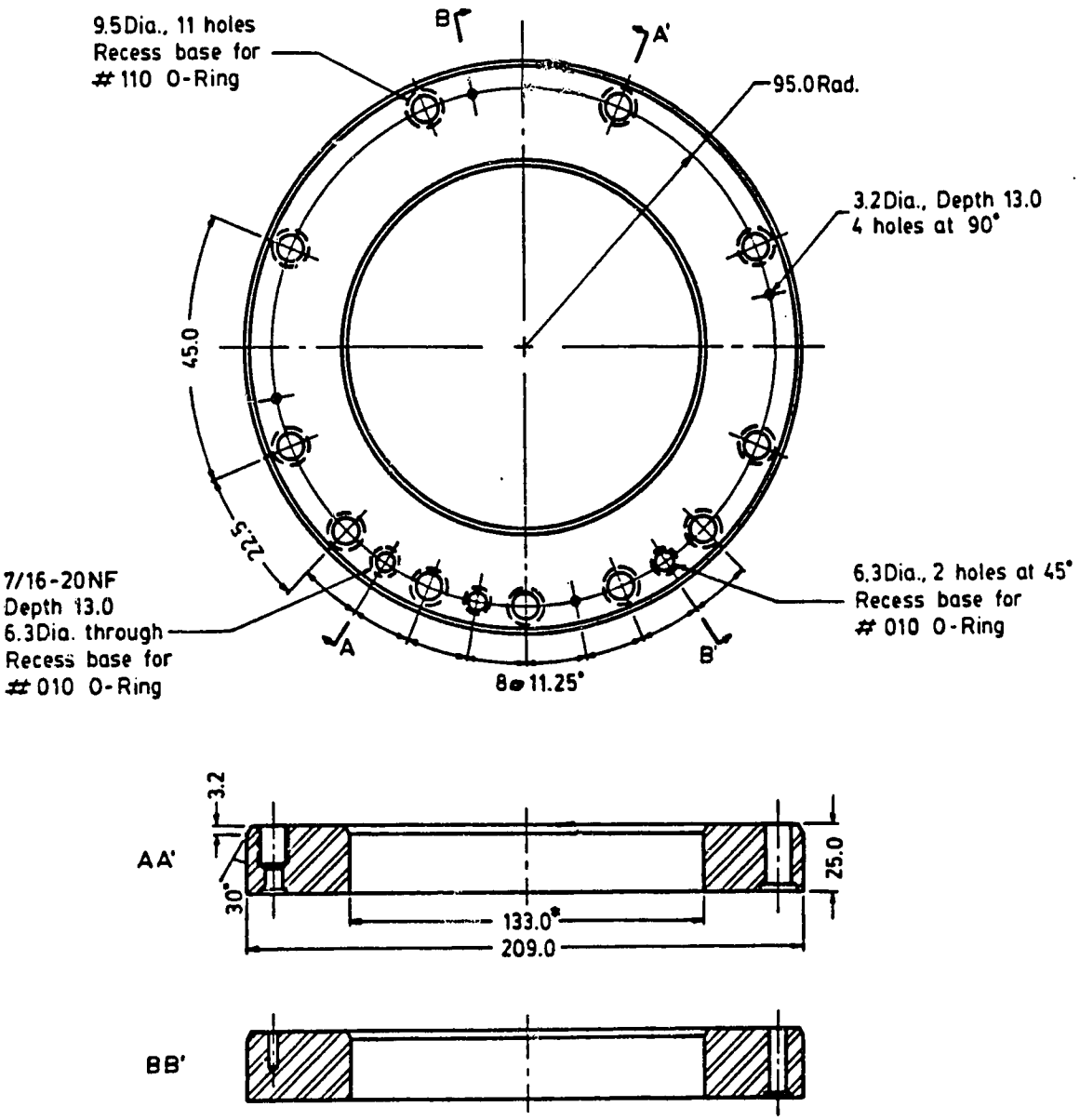

Figure A.6 Bottom ring, BR (* for 100 mm diameter specimen; 171.0 for 140 mm diameter specimen)

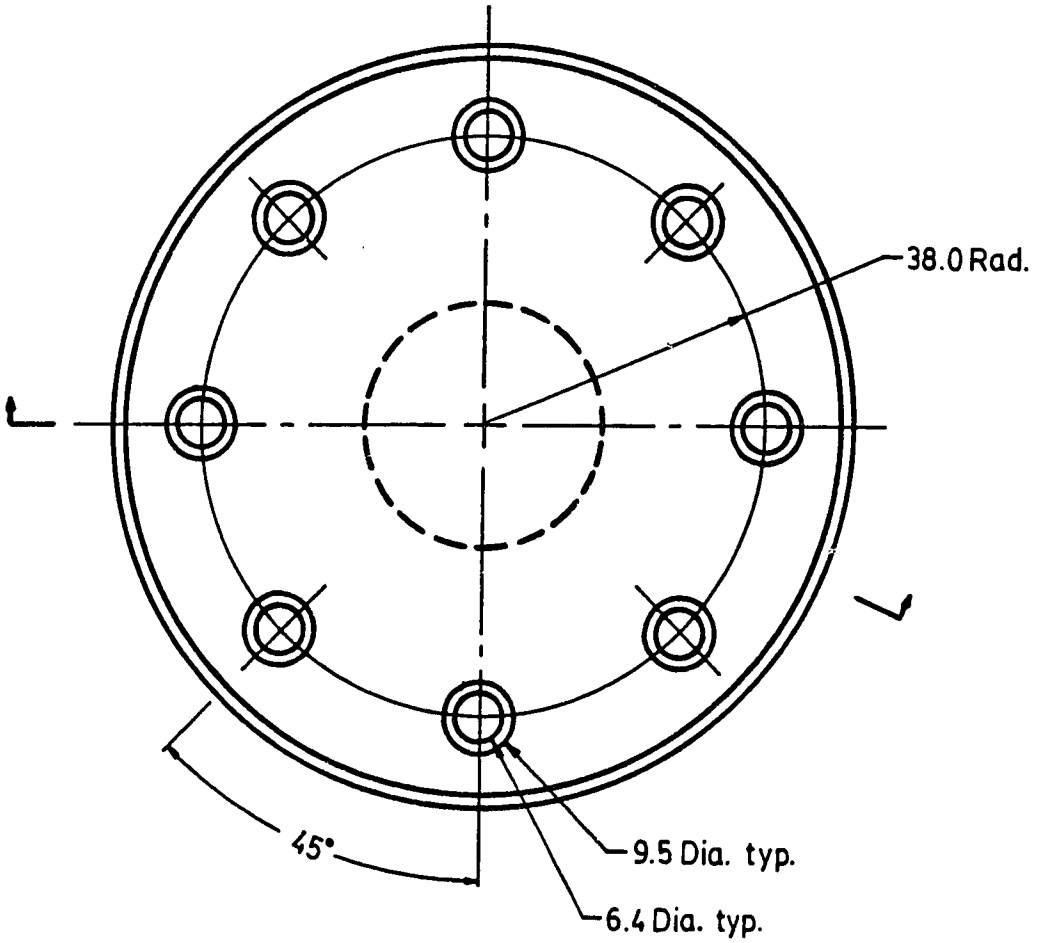

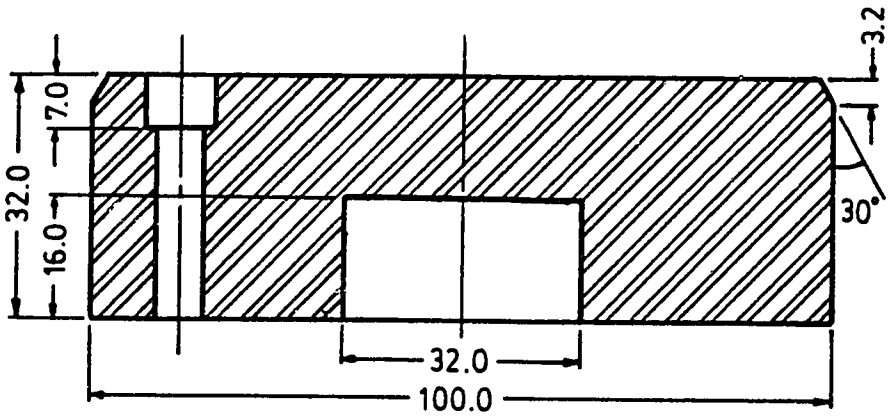

Figure A.7 Specimen support, SS - Cylindrical specimens

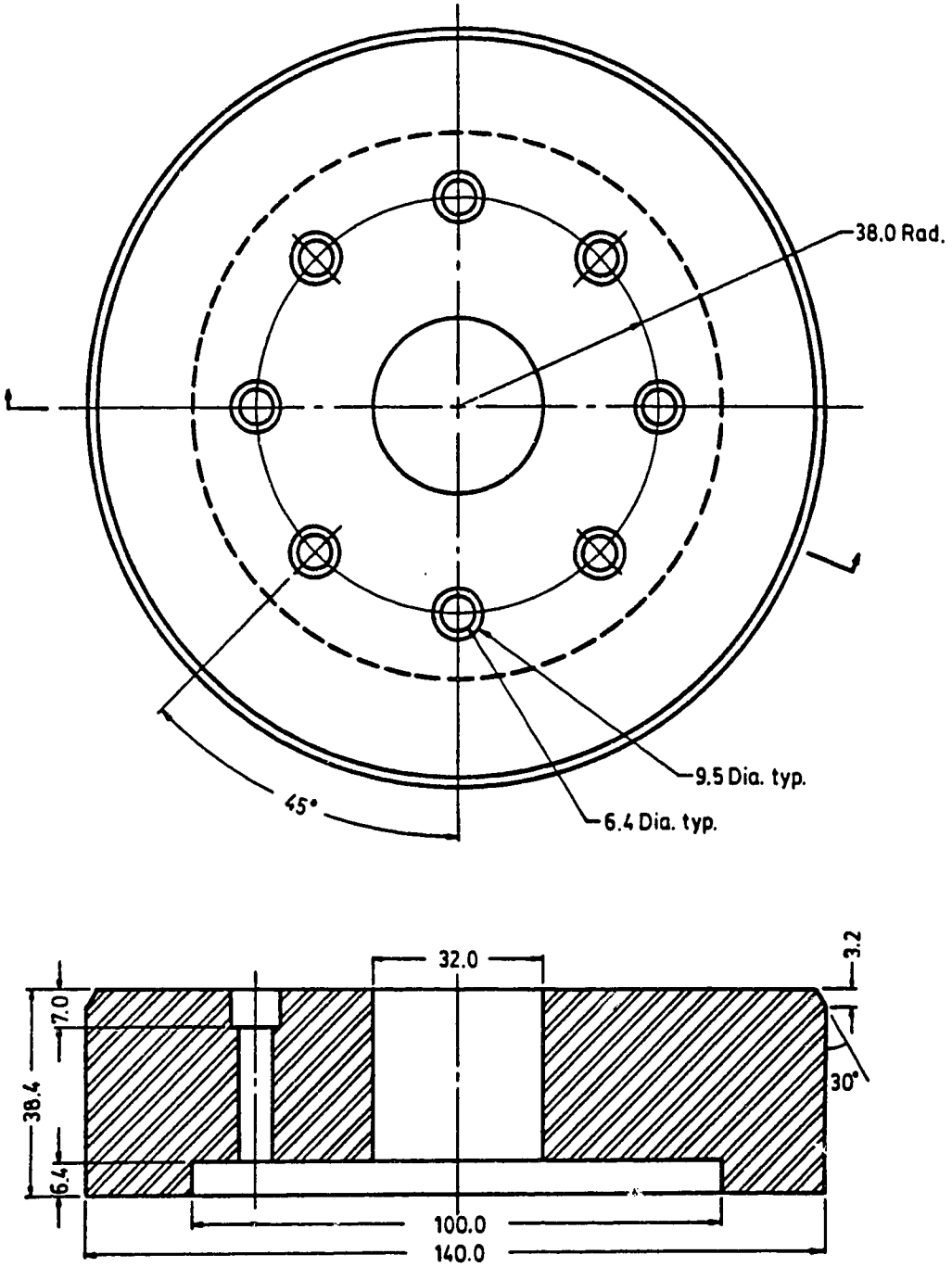

Figure A.8 Specimen support, SS - Hollow cylinder specimens

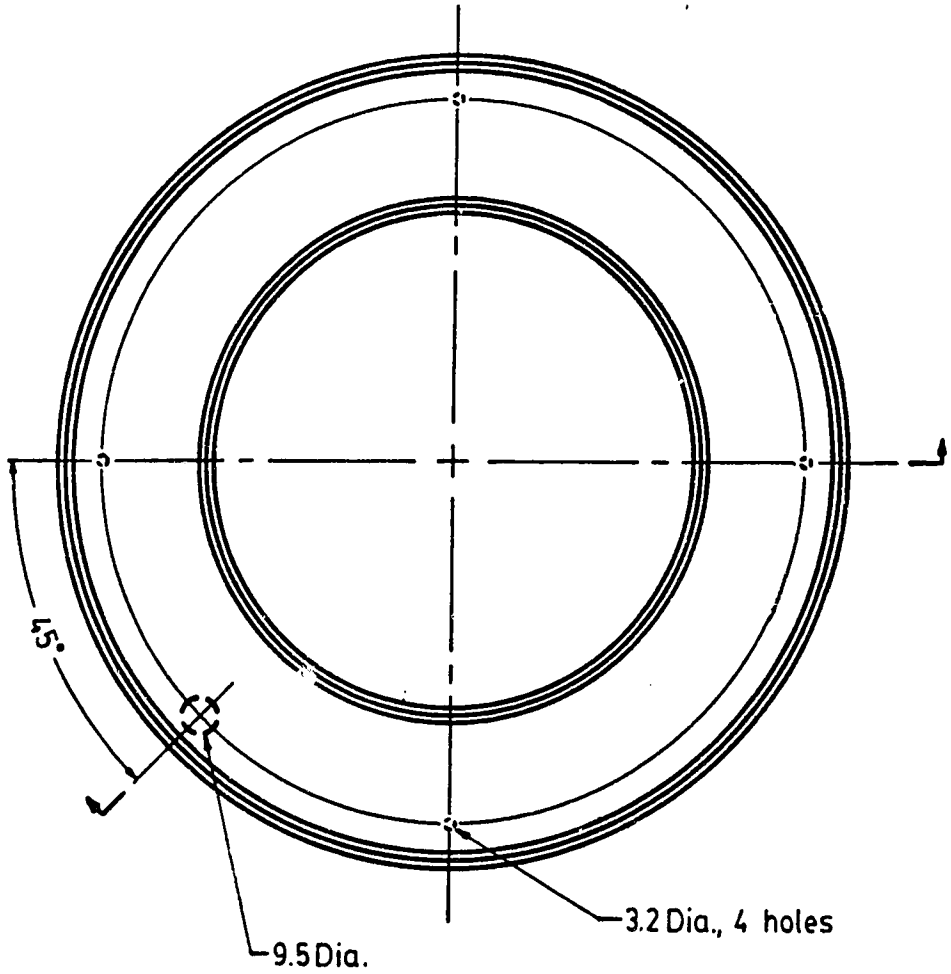

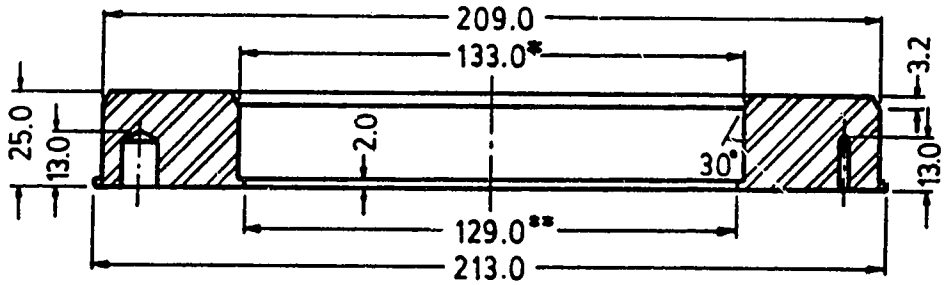

Figure A.9 Top ring, TR (* for 100 mm diameter specimen; 171.0 for 140 mm diameter specimen; **167.0 for 140 mm diameter specimen)

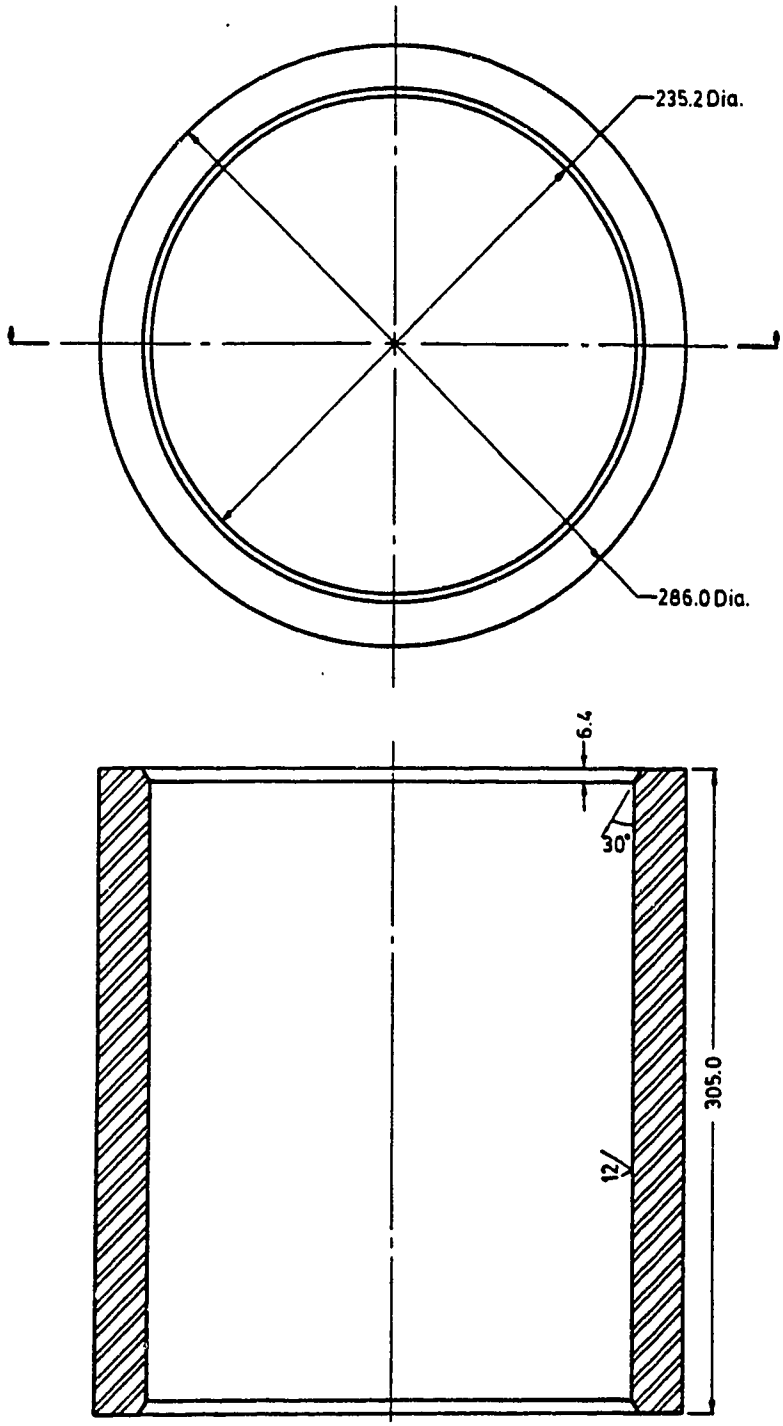

Figure A.10 Cell chamber, CC

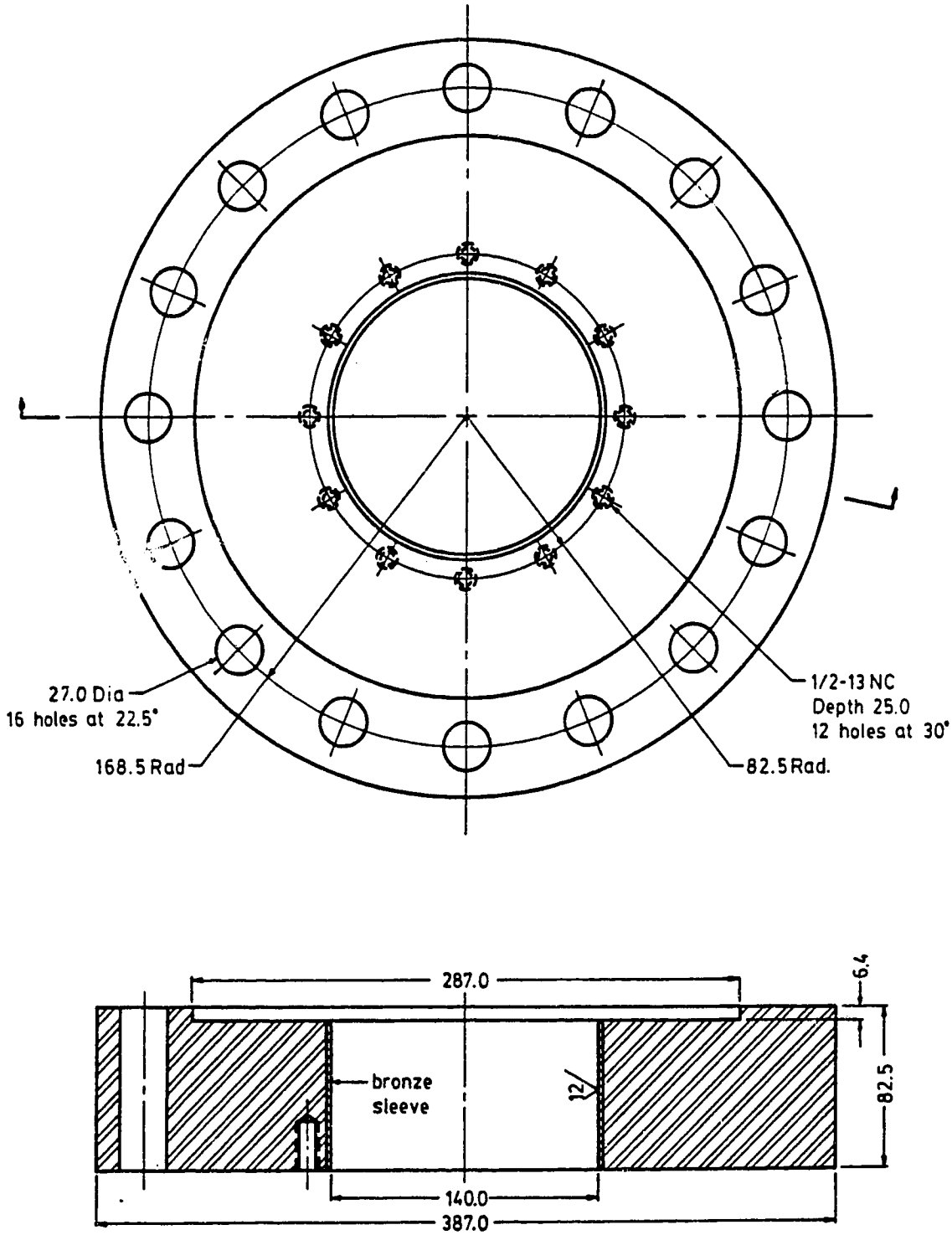

Figure A.11 Cell No. 1 - Top cap, TC

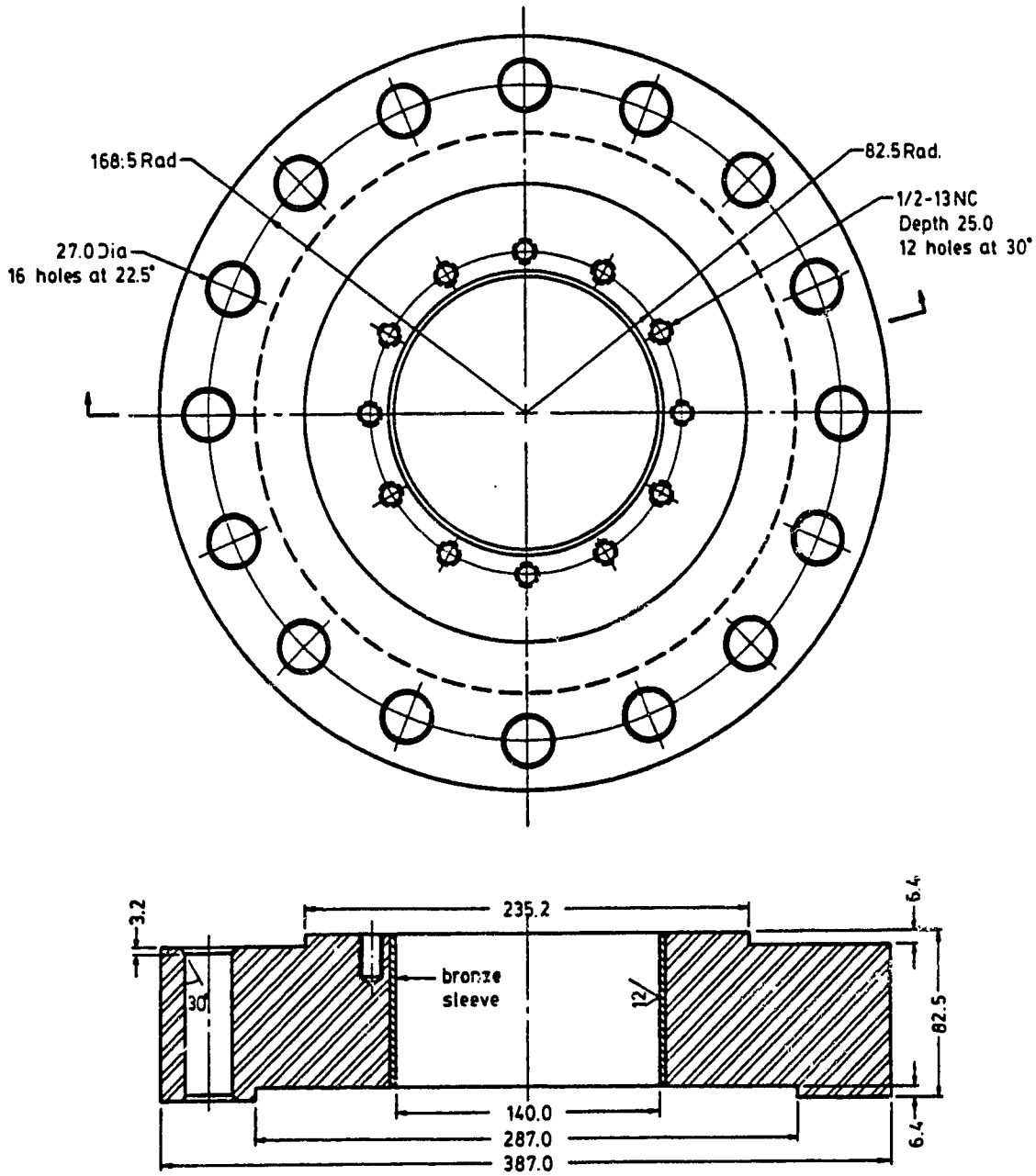

Figure A.12 Cell No. 2 - Top cap, TC

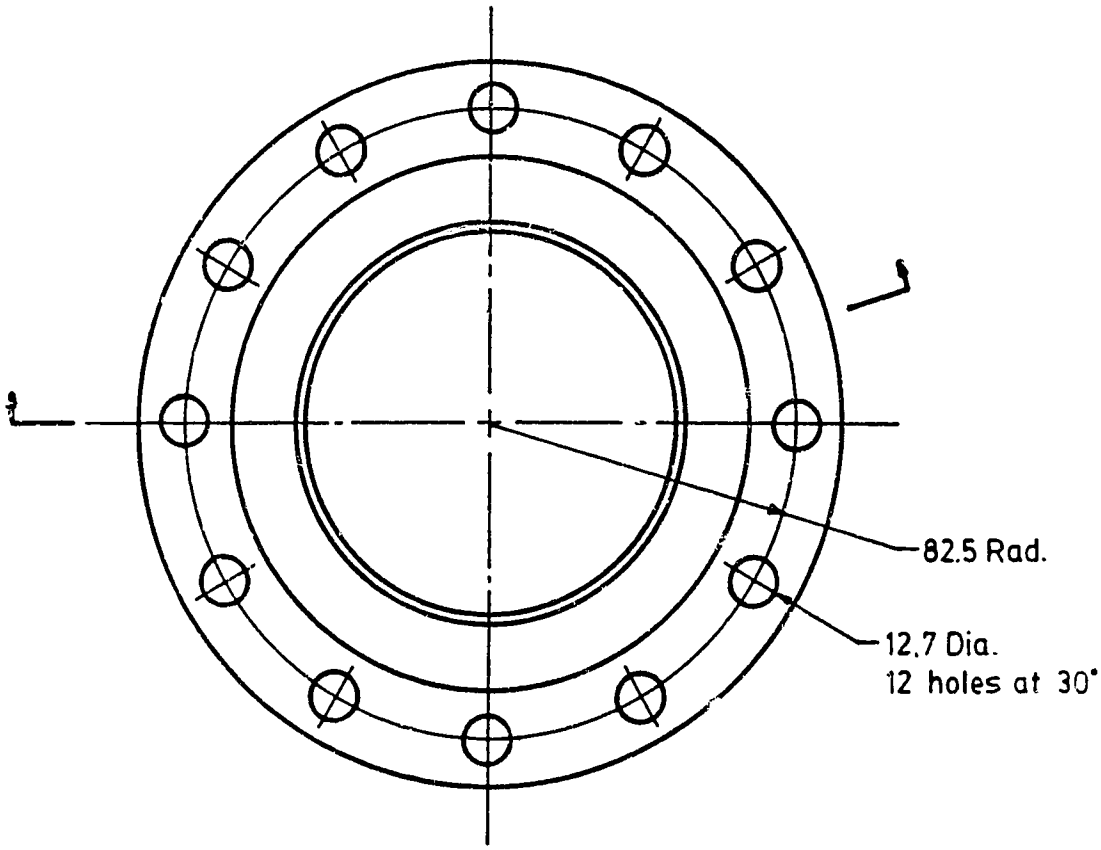

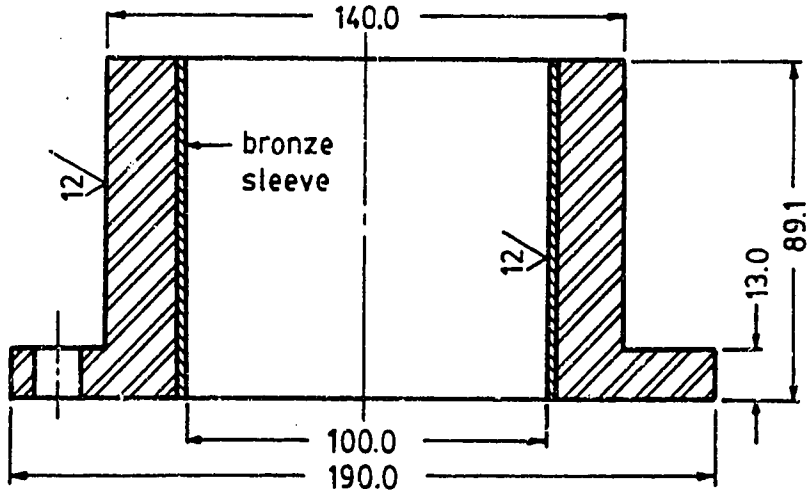

Figure A.13 Diameter reducer, DR - From 140 to 100 mm

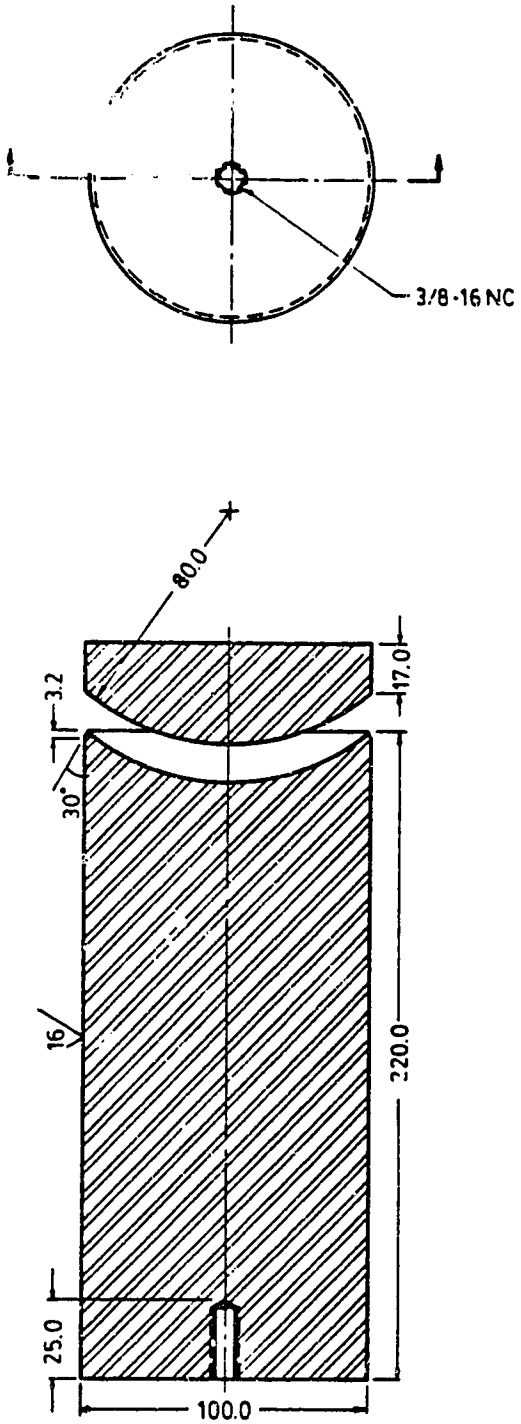

Figure A.14 Cell No. 1 - Axial ram, RM - Triaxial test setup

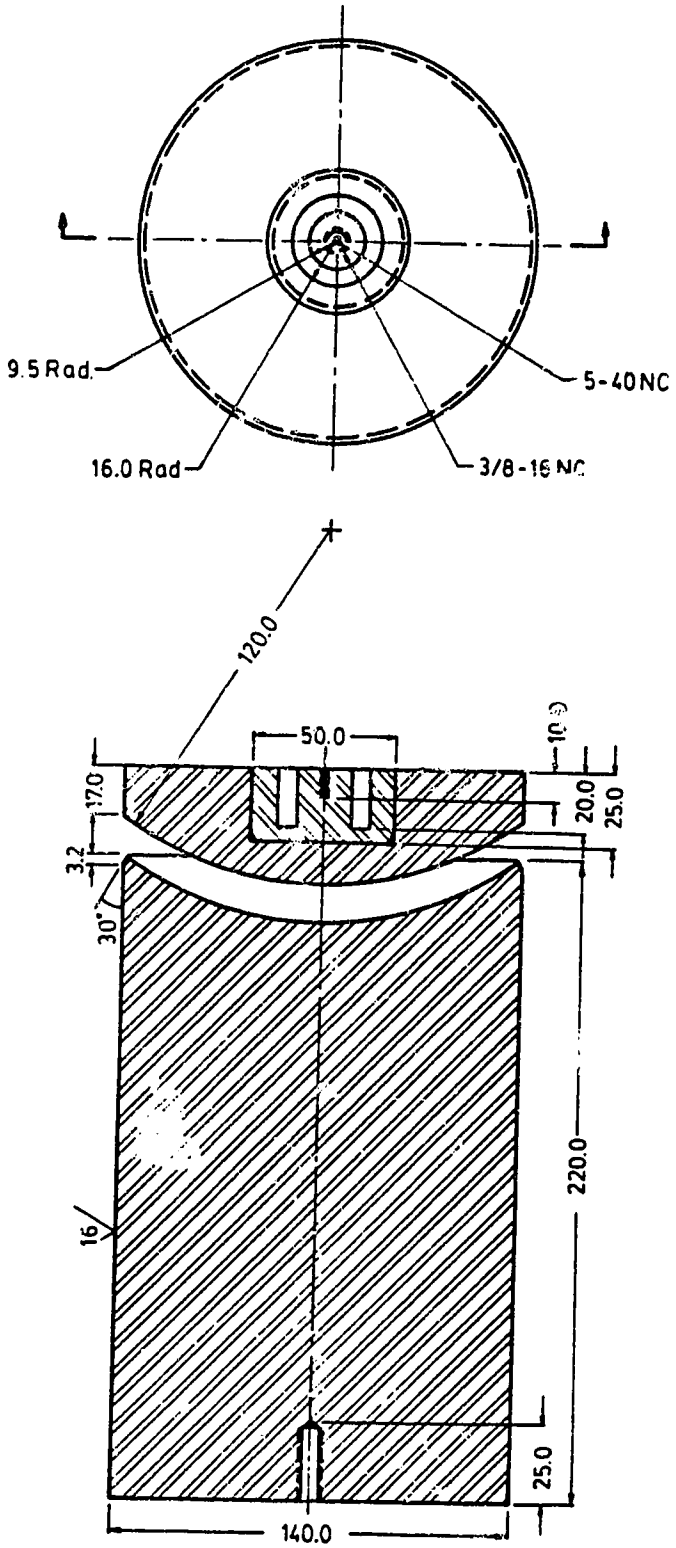

Figure A.15 Cell No. 1 - Axial ram, RM - Hollow cylinder test setup

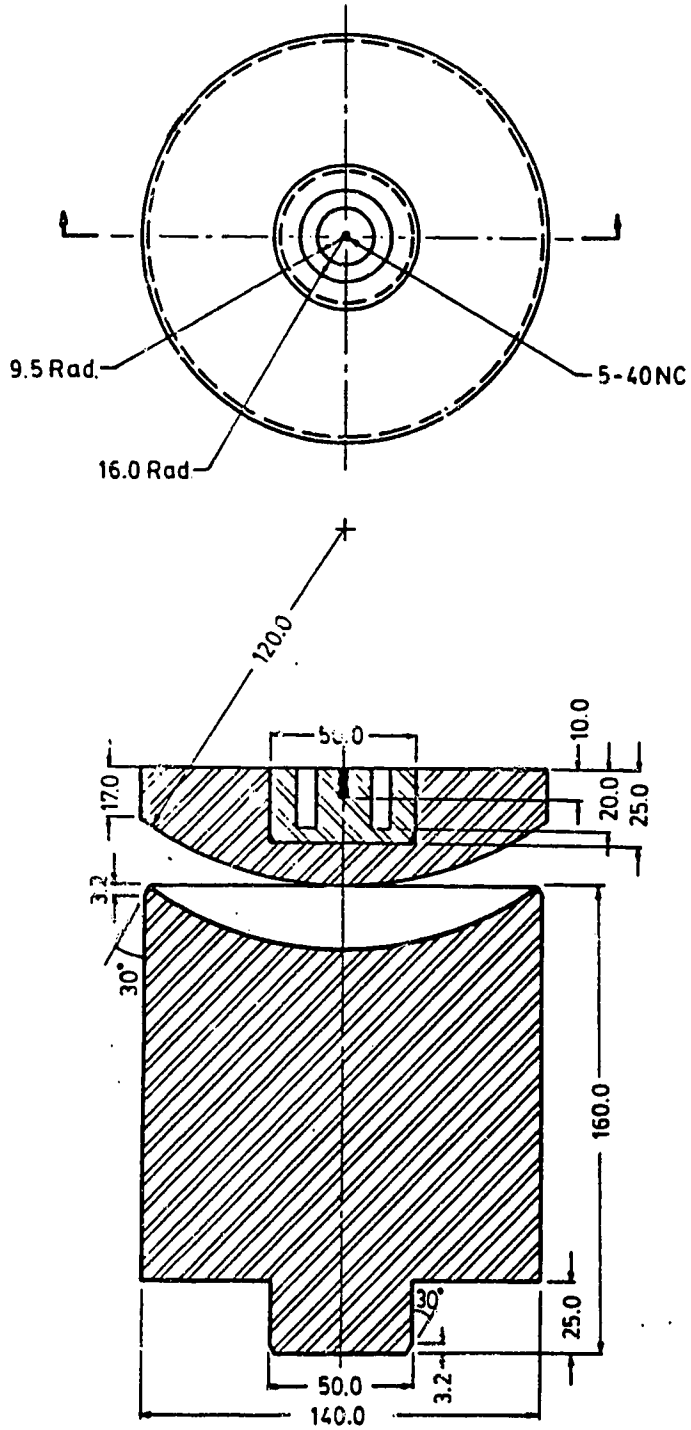

Figure A.16 Cell No. 2 - Axial ram, RM - Hollow cylinder test setup

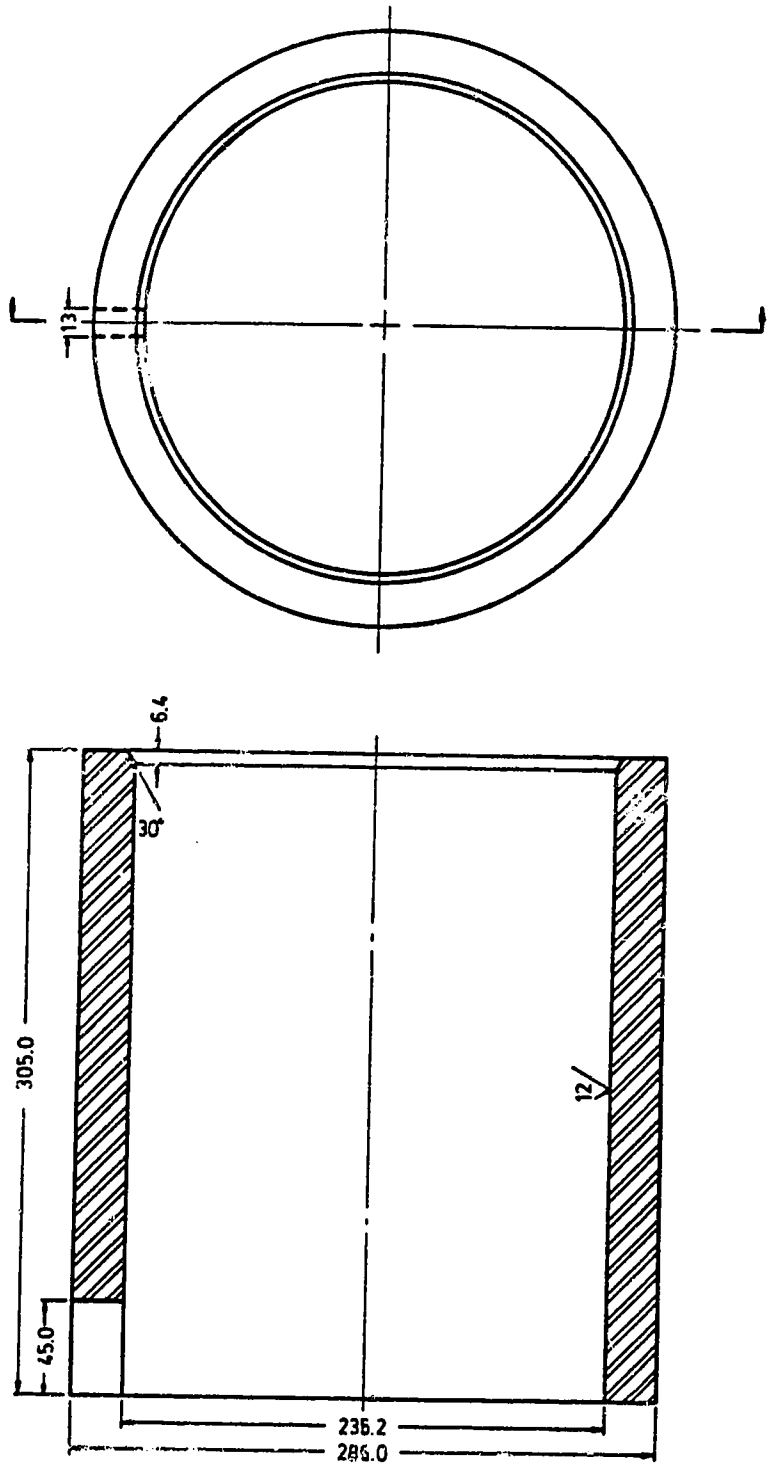

Figure A.17 Piston chamber, PC

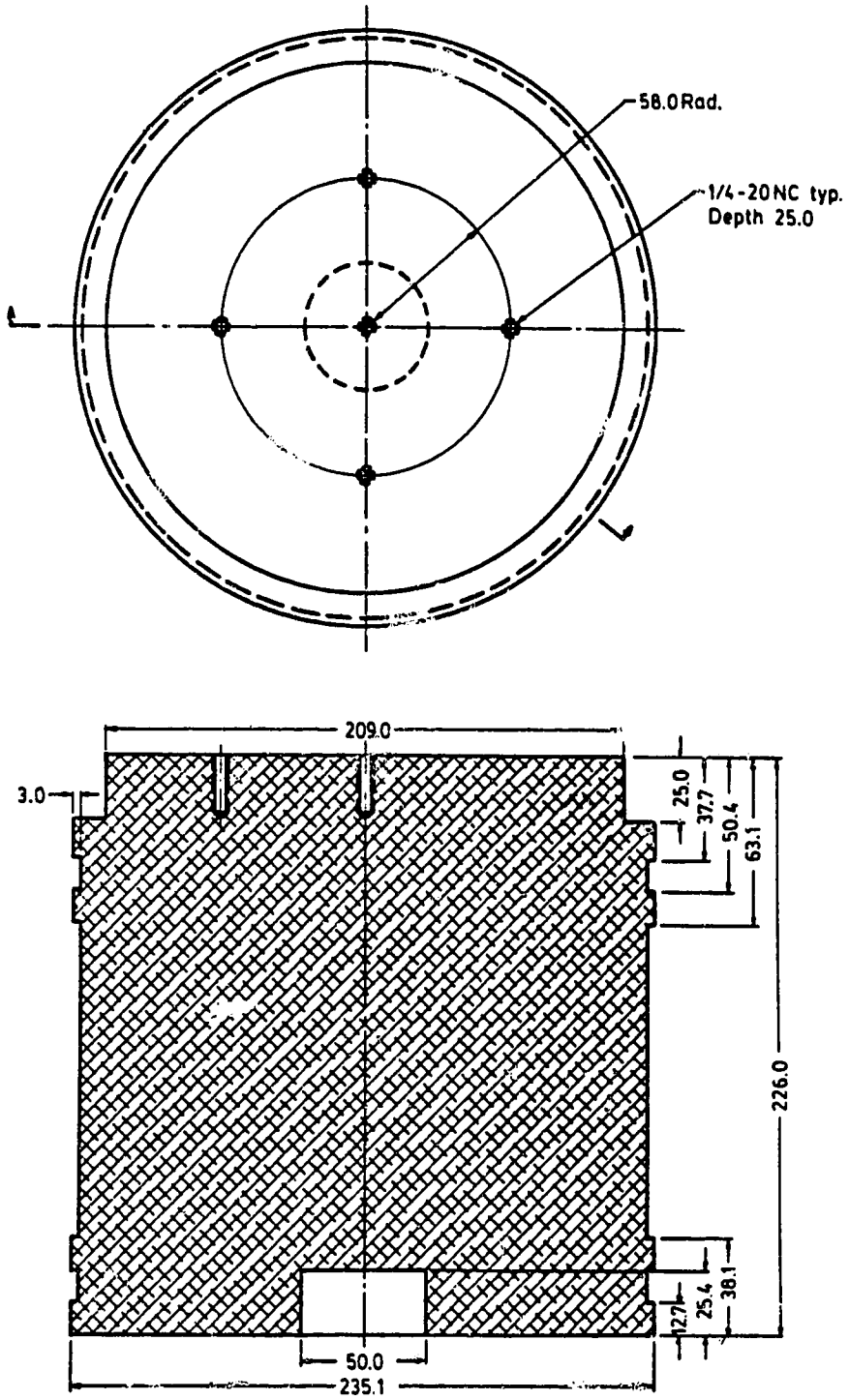

Figure A.18 Axial piston, PP

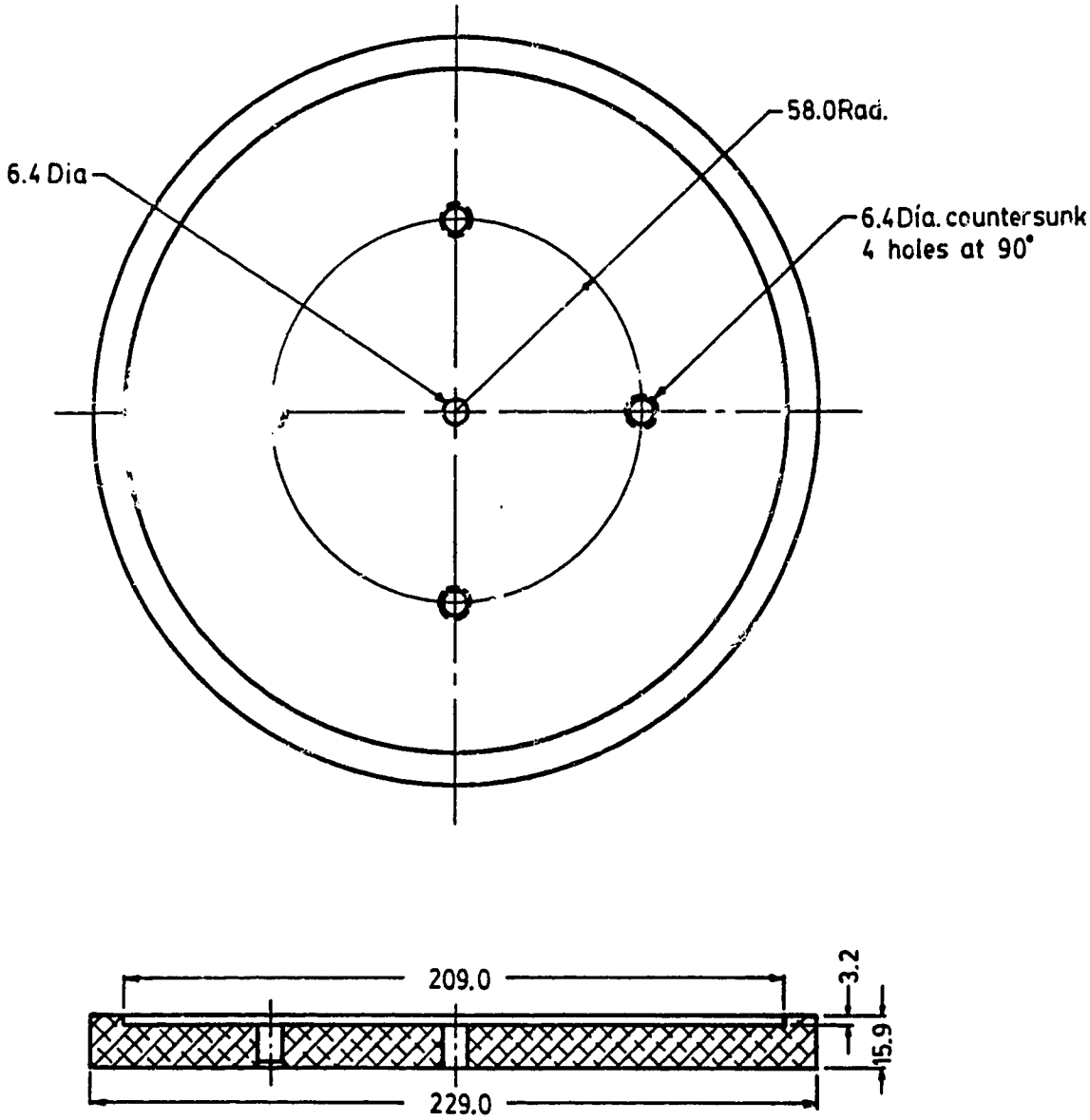

Figure A.19 Seal cap, CS

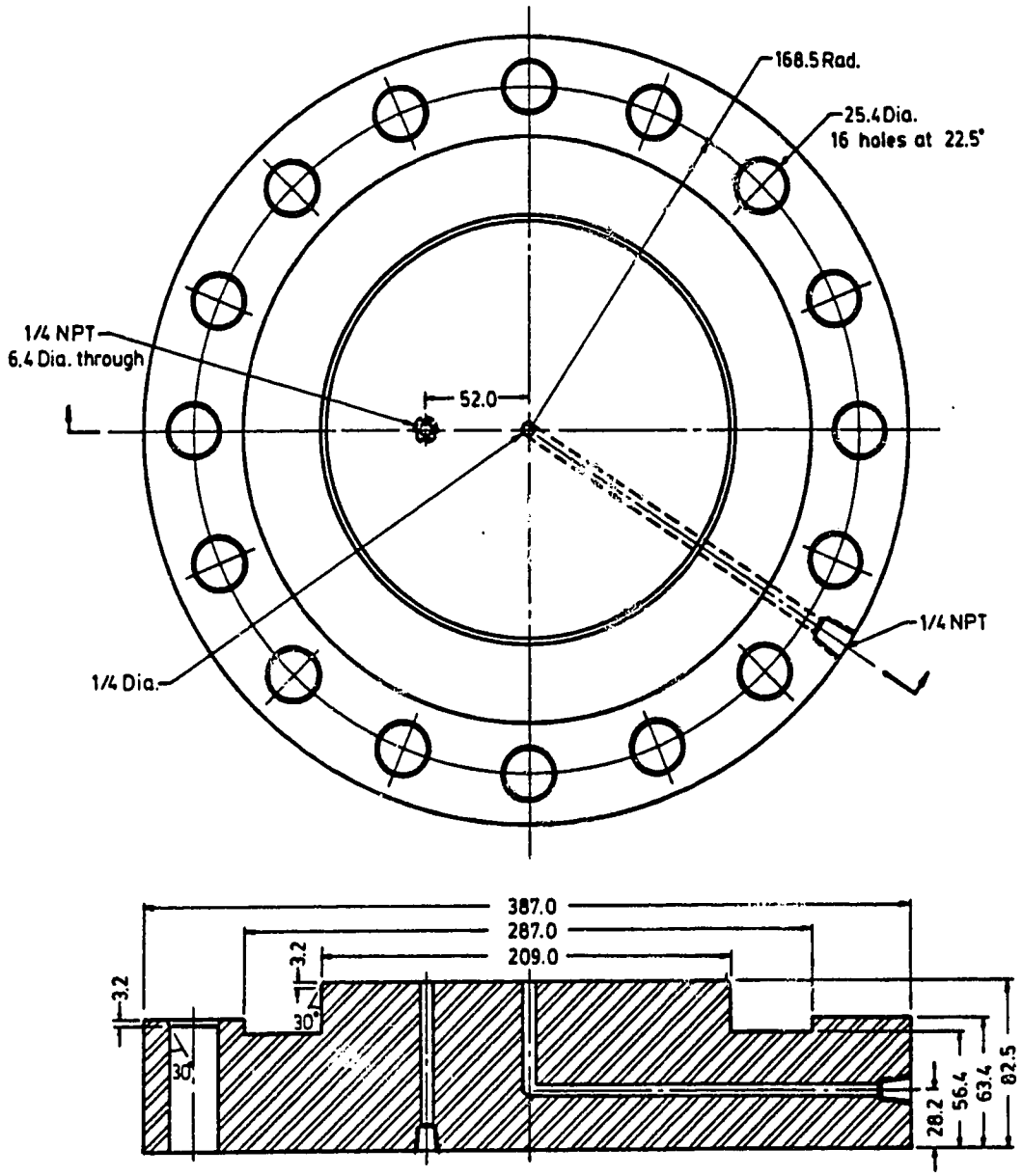

Figure A.20 Piston cap, CP

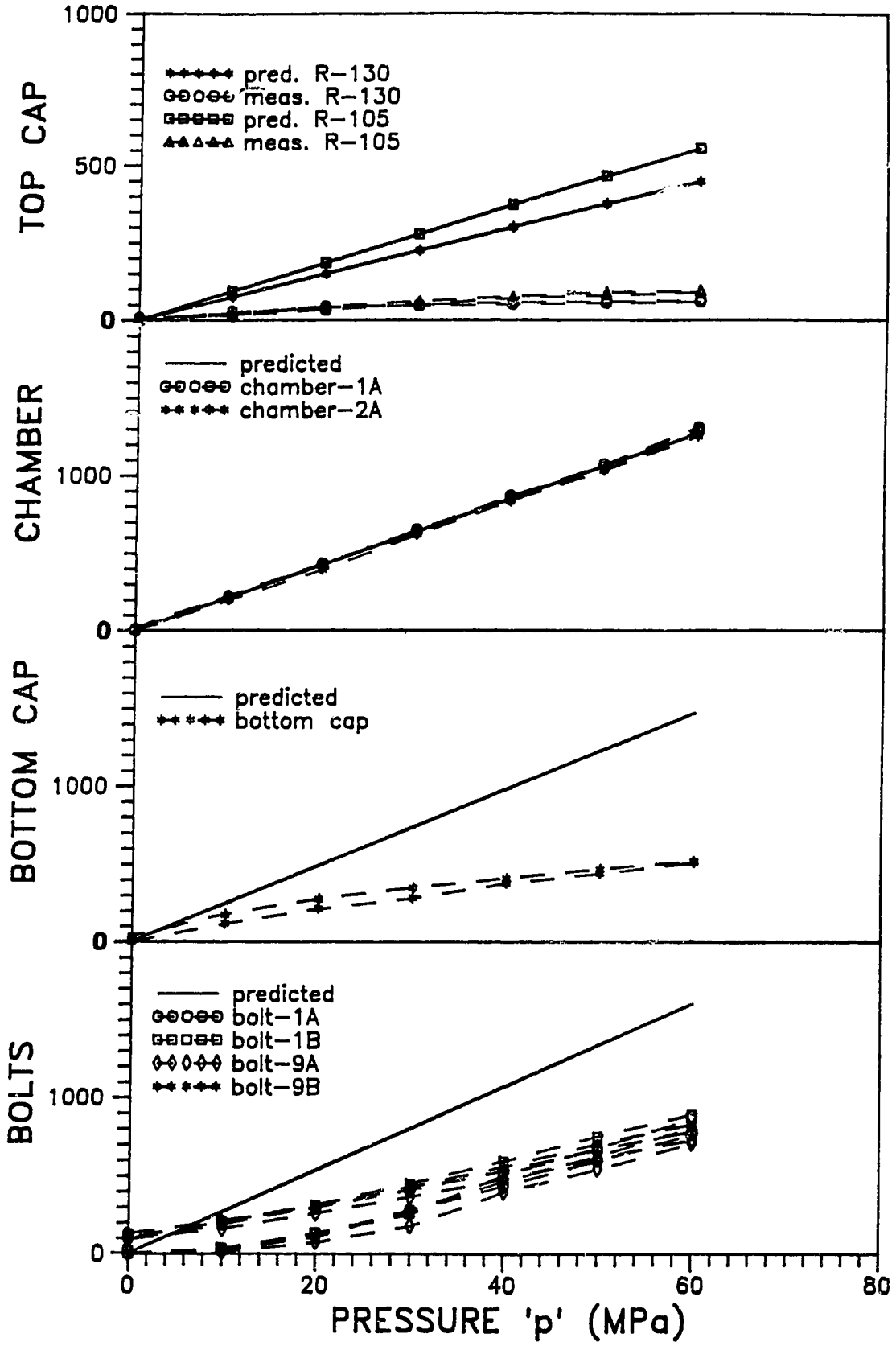

Figure A.21 Cell No. 1 - Structural performance tests - Strain gauge measurements (microstrain)

B. PRESSURE AND TEMPERATURE SYSTEMS

B.1 Introduction

The High Pressure and Temperature System, HPTS, developed at the University of Alberta was based on a similar triaxial testing system existing at the University of Waterloo (Baleshta and Dusseault, 1988). All modifications and complementary design implemented here were performed by Maloney (1986).

B.2 Pressure System

The HPTS controls two cells, each having three (axial, bore and cell) pressure axes. Each pressure axis is composed of a microprocessor-activated, low pressure side, a pressure intensifier and a high pressure side. Air pressure of 2 MPa is delivered to the low pressure side where it is controlled by a set of ball, metering and normally closed solenoid valves. The low pressure is then boosted by a pressure intensifier, delivered to the high pressure side and finally to the testing cells. The pressure control system and its operation are described in Appendix C. Figure B.1 shows the pressure system for both cells. The pressure system components are described below.

B.2.1 Low Pressure Side

The low pressure side consists of a source of air pressure and a set of valves to regulate this pressure. System control is effected on the low pressure side because of enhanced safety, reliability and economics.

The source of low pressure is bottled nitrogen, initially pressurized at 17.5 MPa. A pressure regulator with two gauges, one for the inlet bottle pressure and the other for the regulated outlet pressure, is attached to the bottle and set to deliver an outlet pressure of 2 MPa. This regulated pressure drives the low pressure side, which is shown in Fig. B.2. All tubing is copper and fittings are brass on this side. Ball valve V1 is a bypass valve. When open, air pressure goes directly to the intensifier chamber, bypassing the solenoid valves. Ball valve V2 permits manual venting to atmosphere in order to decrease the air pressure in the intensifier chamber. Ball valve V3 allows isolation of the low pressure side during maintenance.

When ball valves V1 and V2 are closed, air pressure is directed through the metering and solenoid valve system. Each solenoid valve is serially connected to a metering valve which controls the amount of air delivered by each pulse. Care must be exercised so that large overshots do not occur. The metering valves should be adjusted during the test according to system performance. When solenoid valve S1 is energized by the microprocessor, it opens for few milliseconds (the HPTS is set to 100 ms). Cyclical energizing allows the air pressure in the intensifier chamber to increase gradually from zero to the desired value (maximum of 2 MPa). If the pressure is higher than the reference value, then the computer energizes solenoid valve S2, which vents the intensifier chamber, thereby reducing the pressure. This process of increasing and decreasing pressure stops when the pressure is within user specified limits of the reference value (set independently for each axis and test). In this testing program, tolerances of 0.05% for the axial pressure axis and 0.1% for the bore and cell pressure axes have been adopted.

Manual intervention in the system is needed to replace an empty nitrogen bottle. The procedure for exchanging the nitrogen bottle is:

a. Interrupt computer control by pressing F3 and/or F4.
b. Isolate specimen from pressure system by closing all cell valves (high pressure side).
c. Take note of the pressure values shown in all pressure gauges (high pressure side).
d. Close the pressure regulator valves (nitrogen bottle) and wait for pressure release.
e. Exchange the nitrogen bottle.
f. Open the pressure regulator valves and resume gas pressure to 2 MPa.
g. Return pressure in the system to the previous values for each axis (item c) by opening ball valves V1.
h. Reconnect specimen to pressure system by opening all cell valves.
i. Resume computer control by pressing F9 and/or F10 and by following the menu of options displayed on the screen. Function 'C' for continuing the test at the same point as leaving is usually chosen.

B.2.2 Accumulator/Intensifier/Volume Change Device

The accumulator/intensifier/volume change device, AIVC (Fig. B.3), receives the controlled air pressure from the low pressure side. It acts as an accumulator by storing a quantity of compressed air which buffers pressure

fluctuations induced by changes in the pressurized volume, due to valve operation, leakage and temperature fluctuations.

The AIVC device also acts as a pressure intensifier due to the difference in the piston cross-sections. The low pressure (up to 2 MPa) is boosted either up to 24 MPa in the modified intensifier (ratio 1:12) or up to 70 MPa in the standard intensifier (ratio 1:35). A rolling diaphragm seal (Bellofram #4-500-(450)-500-FCJ) is used to minimize both static and dynamic friction on the low pressure piston (Fig. B.3).

Finally, this device also acts as a volume change indicator (Appendix D). By measuring the displacement of the low pressure piston, via the displacement rod (Fig. B.3), and multiplying it by the cross-sectional area of the high pressure piston, it is possible to determine the volume that enters and leaves the cell. The maximum stroke is limited by the Bellofram seal travel distance. For the chosen seal, it is 190 mm, giving high pressure supply volumes of 65 and 180 ml for the standard and modified intensifiers respectively.

When the piston is fully advanced during loading, it is necessary to manually return it to its initial position. This procedure is called recharging the piston. It is described below for a generic axis:

a. Interrupt computer control by pressing either F3 for System 1 or F4 for System 2.
b. Isolate specimen from pressure system by closing the cell valve (high pressure side).
c. Take note of the pressure value shown in the pressure gauge (high pressure side).
d. Reduce pressure in the low pressure side by opening ball valve V2 to vent.
e. Open the handpump valve (high pressure side) and jack the intensifier piston to the top of the cylinder, using the appropriate handpump.
f. Close both the handpump valve and ball valve V2.
g. Return pressure in the system to the pre-recharging value (item c) by opening ball valve V1.
h. Reconnect specimen to pressure system by opening the cell valve.
i. Resume computer control by pressing either F9 for System 1 or F10 for System 2 and by following the menu of options displayed on the screen. Function 'C' for continuing the test at the same point as leaving is usually used.

A similar procedure, called discharging, is needed during unloading and for the sake of completeness, it is also described. Steps 'a' to 'c' are the same as for recharging:

d. Open the handpump relief valve to allow fluid to drain into the pump reservoir.
e. Gradually open the handpump valve (high pressure side) to allow the intensifier piston to move downwards. If necessary to drive piston downwards, increase pressure in the low pressure side by opening ball valve V1.
f. Close the handpump valve.
g. Return pressure in the system to the pre-discharging value (item c) by opening either ball valves V1 or V2, depending on the pressure shown in the gauge.

Steps 'h' and 'i' are the same as for recharging. These procedures could be totally automated but the costs of high pressure solenoid valves and electric pump would be high.

Specifications, materials and design calculations of the AIVC device are presented by Maloney (1986). Figure B.5 depicts the performance curve for one of the six pressure intensifiers. It is worth noting that the internal friction of the pistons is not significant when compared to the magnitude of the working pressures. Furthermore, it does not affect performance as the feedback signal for pressure control is provided by a pressure transducer mounted on the high pressure side.

B. [illegible] Pressure Side

After intensification, pressure is delivered to the cells. Figure B.4 sketches the high pressure system for one axis. All high pressure tubing and fittings are stainless steel. The handpump is for recharging and discharging the AIVC device. The pressure gauges and transducers measure the pressure on the high pressure side just before delivery to the cells. The bleed cap is the highest point in the tubing system and provides deairing during the oil saturation procedure. The three high pressure valves (handpump, cell and gauge) are for isolating each part of the system in case of maintenance, recharging or discharging the AIVC device. The high pressure lines are connected to the cells by quick-connectors. They are convenient, easy to operate and avoid loss of fluids.

Finally, two kinds of fluid are used in the high pressure side. The axial axis uses ordinary hydraulic oil while the bore and cell axes use silicone oil due to its very low electrical conductivity (exposed thermocouple, RTD and strain gauge connections present).

B.3 Temperature System

It is known that temperature changes may cause significant hydraulic pressure fluctuations and affect the response of materials under testing. The HPTS facilities can control the temperature in two ways. First, all equipment is housed in a temperature controlled room. Room temperature is set at a certain value (e.g. 25°C), controlled to +/- 0.5°C and monitored by a thermograph (Bacharach Instrument). Second, the HPTS can independently control the oil temperature in the bore and cell. The cell fluid is not stirred and the temperature is transferred to the specimen by convection which may lead to some non-uniformity.

B.3.1 Cell Temperature

The cell temperature is controlled by a system of heaters, resistance temperature devices (RTDs) and a microprocessor. The heaters consist of two heating mats, 150 mm wide, 375 mm long, drawing 412 W each (WATLOW, #J-3125-60), wrapped around the cell chamber and either bonded with silicone rubber cement or just strapped. They are connected to the heater controller which is computer directed. The RTDs, placed within the cell, measure the temperature of the silicone oil, which is then used as a feedback signal to the computer. Depending on the temperature, the computer either energizes or de-energizes the heating elements. The tolerance set in the software (Appendix C) can be as low as 0.1°C. The room temperature air is used as the cooling medium. Only cell temperatures higher than it (up to 80°C) can be controlled by this system.

B.3.2 Bore Temperature

For hollow cylinder specimens, it is also possible to control the bore temperature. A temperature controlled fluid basin and circulation system are needed. The fluid is then circulated through the bore coils. The temperature of the silicone oil within the specimen bore is monitored by thermocouples connected to the data acquisition system (Appendix C). Presently, the HPTS is not able to control the

bore temperature by a closed loop process, but it could easily be implemented.

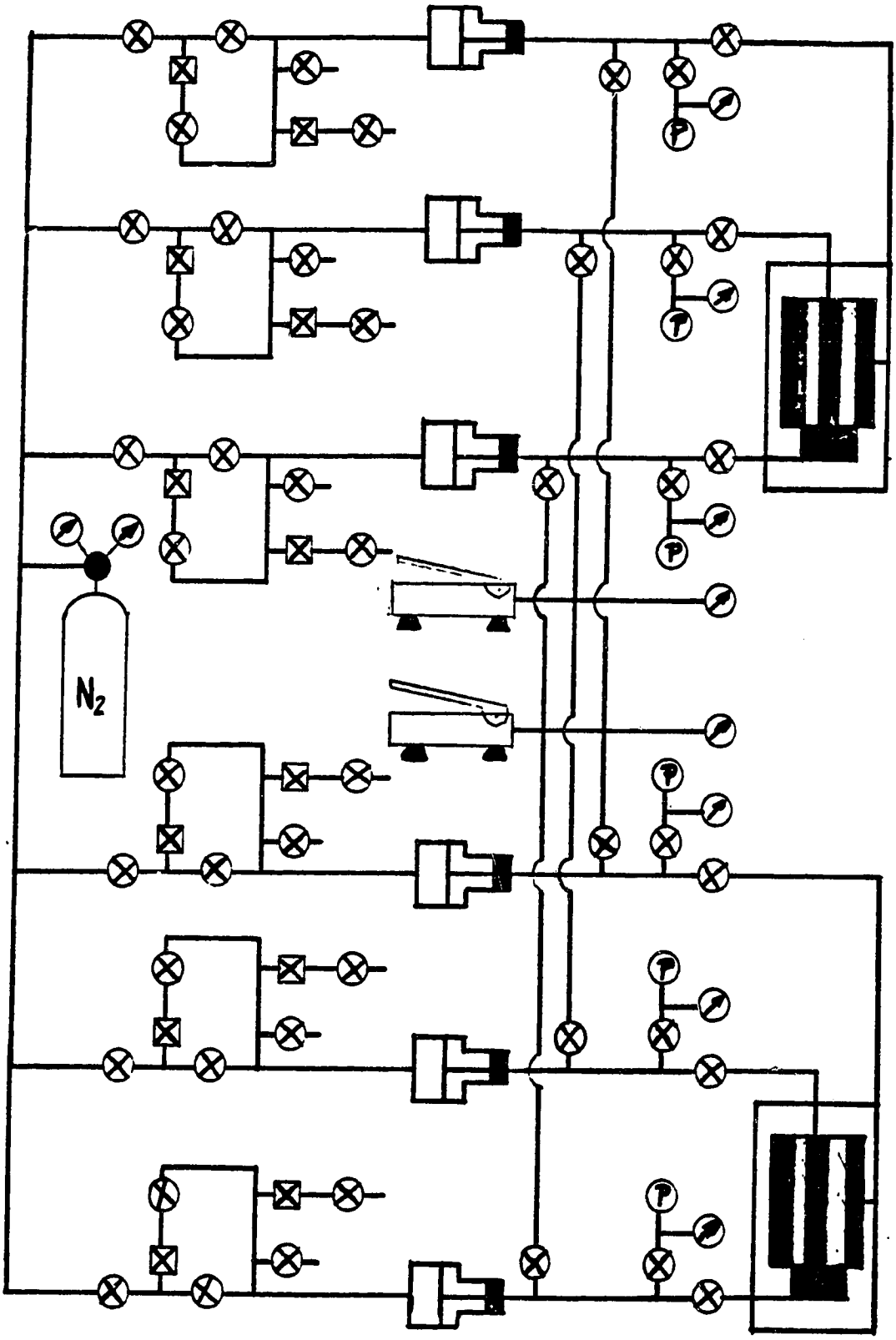

Figure B.1 Pressure system for two testing cells (symbols are defined on Figs. B.2 to B.4)

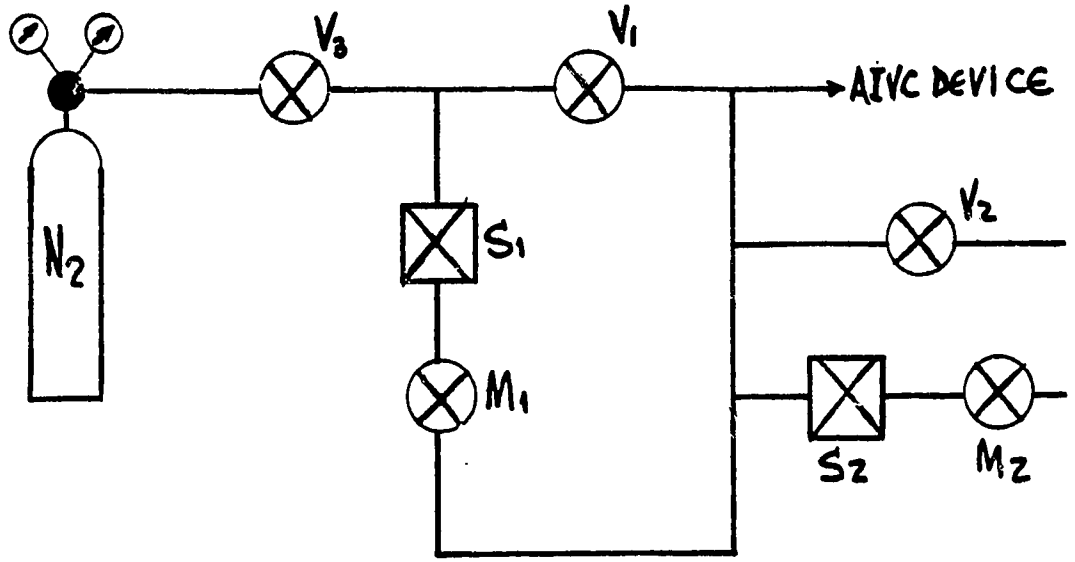

V OPEN / CLOSE VALVES (WHITEY B-4254)

M METERING VALVES (NUPRO B-4JR-PM)

NORMALLY CLOSED SOLENOID VALVES
(ASCO miniature, 2 way, 8262 C1, 120 VAC, 60 Hz

PRESSURE REGULATOR WITH GAUGES
(CIRCLE SEAL PR55 B 1311G)

LOW PRESSURE LINE (Brass, d= 1/4 in)

NITROGEN BOTTLE (compressed gas)

Figure B.2 Low pressure side

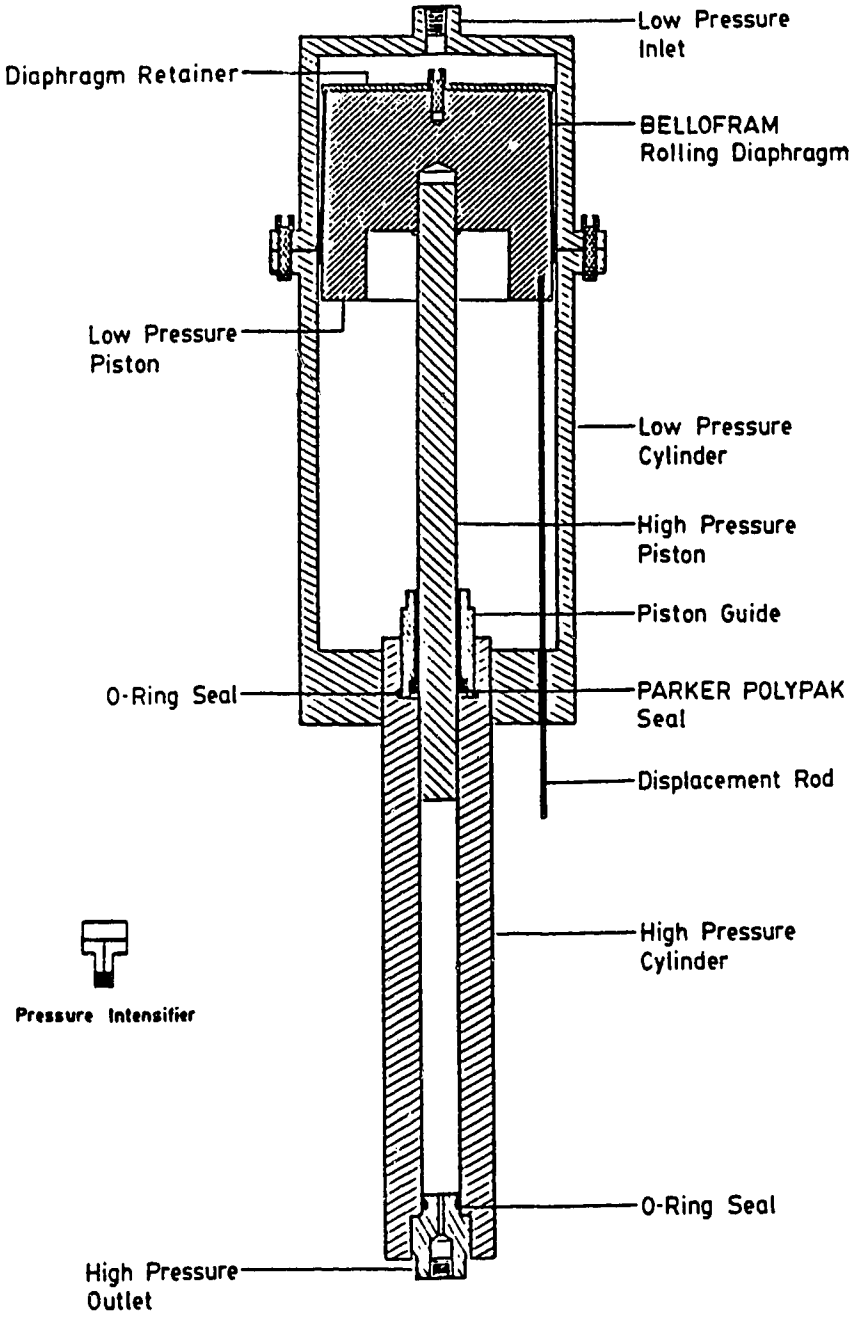

Figure B.3 AIVC device (modified after Maloney, 1986)

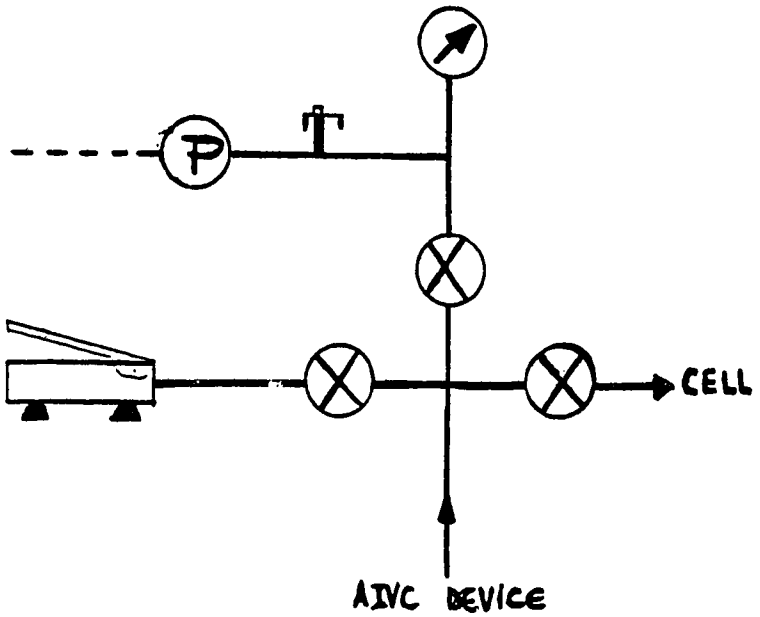

HIGH PRESSURE VALVES (SNO-TRIK SS-410-FP)

PRESSURE GAUGE (WIKA, 10000 psi)

PRESSURE TRANSDUCERS

CAP FOR BLEEDING AIR

HAND PUMP (OTC OWATONNA TOOL #4006A, 2 stages, 10000 psi)

HIGH PRESSURE LINE (stainless steel, d= 1/4 in)

ELECTRONIC WIRE

Figure B.4 High pressure side

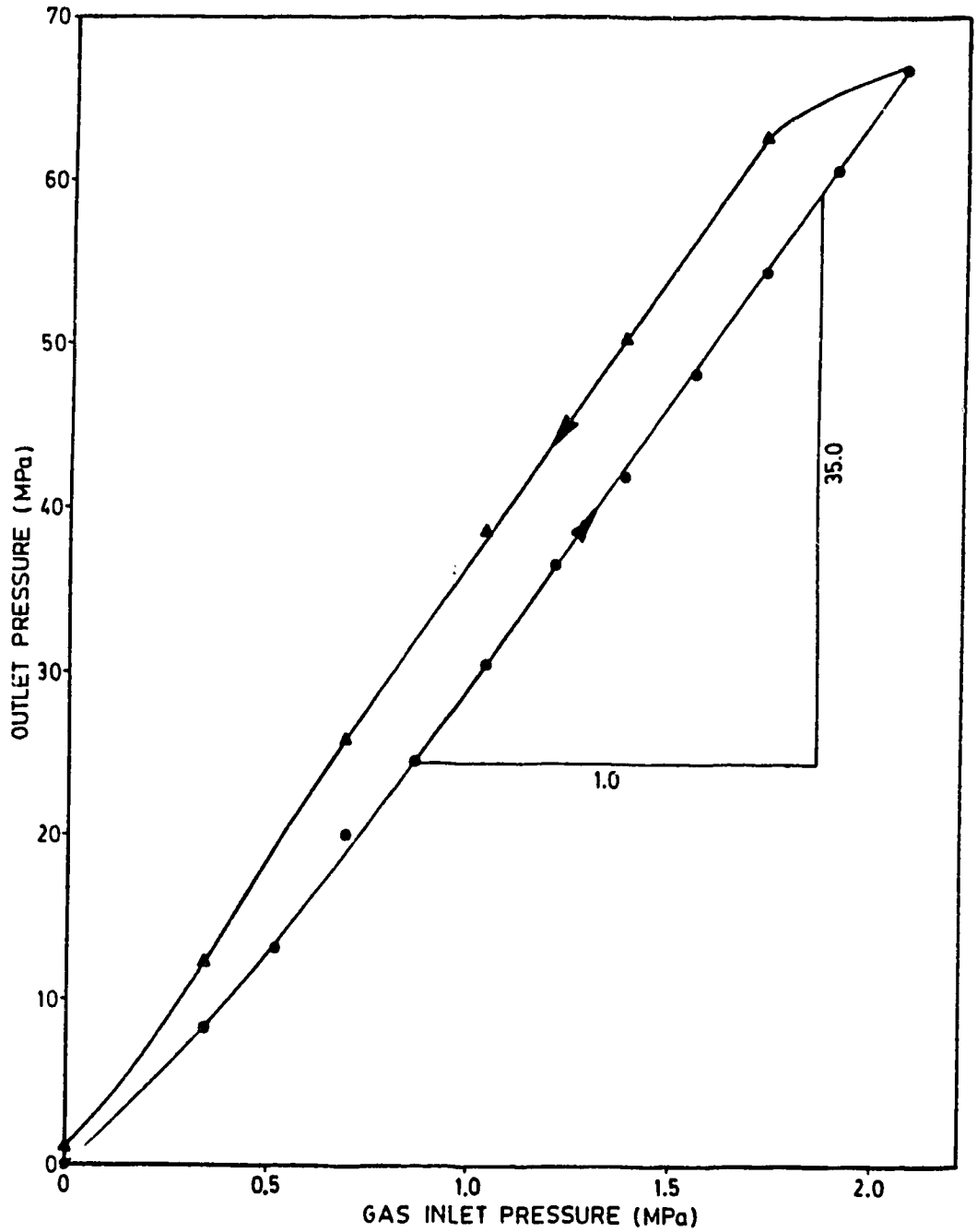

Figure B.5 Performance curve - AIVC No. 2 (modified after Maloney, 1986)

C. CONTROL AND DATA ACQUISITION SYSTEM

C.1 Introduction

The control and data acquisition system constitutes the core of the laboratory facilities developed for this research. It is able to simultaneously control two cells, with up to three independent loading axes each. A closed loop control process was necessary to regulate the system parameters (pressure, displacement, volume change and temperature) due to the importance of precise load and temperature application and to the long duration of the tests. Monitoring (signal acquisition) is by electronic instruments (pressure transducers, LVDTs, volume change, bore convergence and diameter deformation devices, thermocouples and RTDs), described in Appendix D. They convert a continuously varying physical quantity into a continuously varying directly proportional electrical signal (analog output). The analog output is sent to the analog/digital (A/D) converter board, DASH-8, and transformed into digital data. The system parameters are compared to the reference values prescribed by the software. Regardless of the kind of axis control, whether pressure, displacement or volume change, the computer transmits a digital signal which causes the appropriate normally-closed solenoid valve (two per loading axis) to be energized, thereby opening for few milliseconds (e.g., 100 ms). This process adjusts the axis pressure so that the system parameter is equal to the reference value, within the tolerance limits. A similar closed-loop control process exists for the cell temperature. The computer also acquires data at the end of load steps and time intervals specified by the software. Figure C.1 shows the interaction between pressure and control systems for one cell. More information on electronics applied to geotechnical problems can be found in a series of papers by Moore (1980a to f, 1981a and b). For the sake of simplicity, hardware and software are described separately.

C.2 Hardware

The hardware employed by the HPTS for testing control and data acquisition is composed of a computer system, a data acquisition and control interface board and extension boards (Fig. C.2). The computer system consists of an IBM-XT compatible personal computer with multifunction and graphic cards, clock, one hard (10 MBytes) and two floppy (360 kBytes each) disks, monochrome display monitor and printer.

The data acquisition and control interface board, DASH-8, is manufactured by Metrabyte. It is an eight channel, twelve bit, high speed A/D converter and timer/counter board. The full scale input of each A/D converter channel is +/- 5 V converted into +/- 2048 bits, yielding a resolution of 0.00244 V/bit. It also has three timer/counter registers, sixteen bits each, that provide periodic interrupts for the A/D converter permitting event counting, pulse and wave form generation and frequency and period measurements. One timer/counter is connected to the system clock and the others are for input/output (I/O) functions. The DASH-8 software package includes an I/O driver (machine language) for control of A/D, timer and digital I/O channel functions. It is accessed from BASIC by a single line CALL statement. A/D conversion time is typically 25 microseconds, but the speed of the BASIC compiler is the major limitation for the final execution time and consequently for the sampling rate. Up to 4000 samples/s can be obtained when using the DASH-8 routines and operating under BASIC. For details on installation, programming and specifications, see the DASH-8 Manual (1984).

The expansion multiplexer and instrumentation amplifier board, EXP-16 (Metrabyte), can be connected to one of the eight single analog input channels (DASH-8) to extend the capacity of the DASH-8 board. Each EXP-16 board multiplexes sixteen differential analog input channels and also provides signal amplification for low level voltage instruments (gains of 0.5, 1, 2, 10, 50, 100, 200 and 1000), filtering and conditioning. An EXP-16 board is connected to DASH-8 analog input channel No. 6 (gain of one) for LVDTs and another to channel No. 7 (gain of 100) for pressure transducers, strain gauge devices, thermocouples and resistance temperature devices, RTDs (Table C.1). When the EXP-16 board is used for monitoring temperature by thermocouples, a cold junction compensation (CJC) has to be connected to one of the DASH-8 analog input channels (e.g., No. 5). It produces a compensation signal with zero°C at 100 mV and a resolution of 0.05939°C/bit. For details on installation, operation and specifications, see the EXP-16 Manual (1985).

A 24 bit parallel, digital I/O interface, model PIO12 (Metrabyte), is connected to the computer for signal transmission. It consists of three ports (PA, PB and PC), of eight bits each. All ports are set to I/O modes. Ports PA and PC are for outputting signals to the twelve solenoid valves (pressure system) and to the four heater lines (heater controller). The solenoid valve lines are monitored by liquid electronic displays (LED), shown on the HPTS control panel. There are two lines for each heater, one

transmits a digital output signal to turn the heater on and the other, a signal to turn it off, depending on the comparison between the RTD output and the reference value prescribed by the software. Port PB is for signal input from the timer/counters 0 and 1 (DASH-8).

C.3 Software

The HPTS is controlled by three computer programs (software) which are written in QUICKBASIC and compiled to fast speed executable versions (EXE). Because the programs run in the EXE.version, open other files and call routines from the DASH-8 package, each disk has to have a set of files and routines to operate properly (Table C.2). The main program, called HPTS.EXE, manages the interaction of files and routines in disks and does the test control and data acquisition. Two accessory programs HPTSCAL.EXE and HPTSCON.EXE complement the software.

C.3.1 Program HPTSCAL (Fig. C.3)

Program HPTSCAL provides for instrument calibration and checking the initial readings of instruments prior to test commencement. It simply shows the number of bits and corresponding voltage that the set channel is experiencing. It accesses the 32 instruments connected to the two EXP-16 boards. The instrument calibration procedure is described in Appendix D.

C.3.1.1 Running Program HPTSCAL

To run Program HPTSCAL, follow these steps:

a. Turn on or boot the computer with DOS in the default disk drive (e.g., disk drive C).
b. Insert the diskette HPTS#1 into disk drive A. Change the default disk drive to A.
c. Load the program by typing HPTSCAL and pressing the Enter key.
d. The HPTSCAL logo appears on the monitor screen and also the following questions (steps 'e' to 'g'). Table C.1 shows the information for each instrument.
e. 'ENTER CHANNEL NUMBER?'. It ranges from zero to 31. Channel numbers less than zero or greater than 31 are assumed as zero and 31, respectively.
f. 'ENTER GAIN SETTING?'. The gain is important in calculating the voltage in the instrument. Gain settings less than one are assumed as one.

g. 'ENTER AVERAGE NUMBER?'. The average number 'N' means that the program reads the set channel 'N' times and gives the average as output. Average numbers of ten and 50 are normally used for checking initial readings and for calibrating instruments, respectively. Average numbers less than one are assumed as one.
h. The program starts monitoring the set channel. An F-key menu is displayed on the monitor screen, permitting changes of the channel number, gain setting and average number.
i. To stop the program, press the combination of CRTL-BREAK keys. The program returns to the system (DOS).

C.3.1.2 Listing of Program HPTSCAL

This listing corresponds to the last version run the the author:

```
10 '+++++++++++++++++++++++++++++++++++++++++++++++++++++++++++
15 '+                                                         +
20 '+ PROGRAM " HPTSCAL " - JUNE, 1986                        +
25 '+ ELECTRONICS DIVISION, CIVIL ENG. DEPT., U. OF A.        +
30 '+ BY ROY GITZEL                                           +
35 '+                                                         +
40 '+ HIGH PRESSURE AND TEMPERATURE SYSTEM                    +
45 '+ CALIBRATION AND INITIALIZATION OF CHANNELS              +
50 '+                                                         +
55 '+ THE FOLLOWING CONFIGURATION IS REQUIRED:                +
60 '+ XT COMPUTER ( 640K, 2 DISKS, CLOCK )                    +
65 '+ DASH-8 & 2 EXP-16 METRABYTE DATALOGGER                  +
70 '+                                                         +
75 '+ LAST MODIFICATIONS INSTALLED IN SEPTEMBER, 1988         +
80 '+ BY ANDRE ASSIS                                          +
85 '+                                                         +
90 '+++++++++++++++++++++++++++++++++++++++++++++++++++++++++++
100 '-RESET VARIABLES AND RELEASE DISK BUFFER--------------+
110 CLEAR
120 '-LOAD DASH-8 ADDRESS----------------------------------+
130 OPEN "DASH8.ADR" FOR INPUT AS #1
140 INPUT #1, BASADR%: CLOSE #1
150 '-DIMENSION VARIABLES----------------------------------+
160 DIM LT%(2)
170 '-INITIALIZE DASH-8------------------------------------+
180 MD%=0: CALL DASH8 (MD% ,BASADR%, FLAG%)
200 '-SETUP F-KEYS-----------------------------------------+
210 KEY (1)ON: KEY (2)ON: KEY (3)ON
215 KEY (4)ON: KEY (5)ON: KEY (6)ON
220 ON KEY (1) GOSUB 400: ON KEY (2) GOSUB 500
230 ON KEY (3) GOSUB 600: ON KEY (4) GOSUB 700
240 ON KEY (5) GOSUB 800: ON KEY (6) GOSUB 900
250 GOTO 1000
300 '-EVENT TRAPPING ROUTINES------------------------------+
```

```
400 CN%=CN%+1: RETURN
500 CN%=CN%-1: RETURN
600 AV%=AV%+1: RETURN
700 AV%=AV%-1: RETURN
800 LOCATE 8,1: INPUT "Enter New Channel Number ";CN%
810 LOCATE 8,1: PRINT "                                    "
820 KEY (5) ON: GOTO 1200
900 LOCATE 8,1: INPUT "Enter New  Gain  Setting ";GA
910 LOCATE 8,1: PRINT "                                    "
920 KEY (6) ON: GOTO 1200
1000 '-INPUT DATA-----------------------------------------+
1010 CLS: AV%=1: AVT=0
1020 PRINT "*********************************************
***************"
1030 PRINT "*********************************************
***************"
1040 PRINT " ": PRINT " "
1050 PRINT "     HH  HH  PPPP   TTTTTT   SSSS   CCCCCC   AAA
A   LL"
1060 PRINT "     HH  HH  PP  P  TTTTTT  SS      CCC     AA
AA  LL"
1070 PRINT "     HHHHHH  PPPP     TT     SSSS   CC      AAAA
AA  LL"
1080 PRINT "     HH  HH  PP       TT   S    SS  CCC     AA
AA  LLL"
1090 PRINT "     HH  HH  PP       TT    SSSSS   CCCCCC  AA
AA  LLLLLL"
1100 PRINT " ": LOCATE 11,43: PRINT "by R.GITZEL & A.ASSIS"
1110 PRINT "*********************************************
***************"
1120 PRINT "*********************************************
***************"
1130 PRINT " ": PRINT " "
1140 INPUT "Enter Channel Number ";CN%
1150 INPUT "Enter  Gain  Setting ";GA
1160 INPUT "Enter Average Number ";AV%: CLS: GOSUB 2000
1200 '-CHECKING FOR VARIABLE LIMITS-----------------------+
1210 IF AV%<1 THEN AV%=1
1220 IF GA<1 THEN GA=1
1230 IF CN%<0 THEN CN%=0
1240 IF CN%>31 THEN CN%=31
1250 IF CN%<16 THEN CH%=6: SB%=CN%: GOTO 1300
1260 IF CN%<32 THEN CH%=7: SB%=CN%-16: GOTO 1300
1300 '-MAIN ROUTINE---------------------------------------+
1310 VCON=5/(GA*2048)
1400 '-SET MULTIPLEXER SCAN LIMITS------------------------+
1410 MD%=1: LT%(0)=CH%: LT%(1)=CH%
1420 CALL DASH8 (MD%, LT%(0), FLAG%)
1500 '-WRITE DIGITAL OUTPUT OP1-4-------------------------+
1510 MD%=14: CALL DASH8 (MD%, SB%, FLAG%)
1600 FOR I%=1 TO AV%
1700 '-A/D CONVERSION-------------------------------------+
1710 MD%=4: CALL DASH8 (MD%, DIO%, FLAG%)
1800 '-SCREEN DISPLAY-------------------------------------+
```

```
1810 LOCATE 10,1: PRINT "Channel Number = ";USING "###";CN%
1820 LOCATE 11,1: PRINT "Gain   Setting = ";USING "###";GA
1830 LOCATE 12,1: PRINT "Average Number = ";USING "###";AV%
1840 LOCATE 13,1: PRINT "Dash-8 Channel = ";USING "###";LT%(
0)
1850 LOCATE 16,1: PRINT "Output = ";USING "#####";DIO%
1860 LOCATE 17,1: PRINT USING "+#.######";DIO%*VCON
1870 LOCATE 17,12: PRINT "Volts"
1880 AVT=AVT+DIO%: NEXT I%: AN=AVT/AV% :AVT=0
1890 LOCATE 20,1: PRINT "Average = ";USING "#####.#";AN
1900 LOCATE 20,19: PRINT "Bits": GOTO 1200
2000 '-MENU OF OPTIONS-------------------------------------+
2010 PRINT "F1...Advance  Channel Number by one"
2020 PRINT "F2...Decrease Channel Number by one"
2030 PRINT "F3...Advance  Average Number by one"
2040 PRINT "F4...Decrease Average Number by one"
2050 PRINT "F5...Ask  for  New  Channel  Number"
2060 PRINT "F6...Ask  for  New   Gain   Setting"
2070 RETURN
```

C.3.2 Program HPTSCON (Fig. C.4)

Program HPTSCON writes the conversion factors, obtained from instrument calibration (Program HPTSCAL.EXE), to the file CONFACT.DFN (disk A). This file contains the conversion factors for all HPTS instruments. Having a separate file with conversion factors is advantageous since, if for any reason an instrument is replaced, the test need not be stopped nor the main program edited, only the new conversion factor input to the file CONFACT.DFN. The main program then accesses this file and reads the new conversion factor.

C.3.2.1 Running Program HPTSCON

To run Program HPTSCON, follow these steps:

a. Turn on or boot the computer with DOS in the default disk drive (e.g., disk drive C).
b. Insert the diskette HPTS#1 into disk drive A. Change the default disk drive to A.
c. Load the program by typing HPTSCON and pressing the Enter key.
d. The program reads the old conversion factors stored in the file CONFACT.DFN. The HPTSCON logo appears on the monitor screen and also the following questions for each instrument.
e. 'ENTER CONVERSION FACTOR FOR SYSTEM (No.) TRANSDUCER (name) (0 TO SKIP)= (old value is displayed)'. Should the old conversion factor be correct, just press the Enter key. Otherwise, enter the new value including the

sign and press the Enter key. Zero is used to skip an instrument not used.

f. Information on the full scale output of the respective instrument follows and then the question 'IS THIS CORRECT?'. If positive, the program goes to the next instrument. If not, it returns to step 'e'.

g. When the conversion factors for all instruments are entered, the program asks 'PRINT CONVERSION FACTORS?'. It is good practice to have a hard copy of them for each test.

h. After printing, the program asks once more if the list of conversion factors is correct. If not, it goes to step 'e' and repeats the same procedure for all instruments. If yes, it stores the new conversion factors in the file CONFACT.DFN and returns to the system (DOS).

It is very important to understand how the signs of the system parameter conversion factors affect the pressure control done by the main program HPTS.EXE (HPTS Routine 8000). For instance, to run a plane strain test in the axial direction, if the specimen presents a positive displacement (shortening), the system must respond with a relief of the axial stress to produce the final zero displacement.

C.3.2.2 Listing of Program HPTSCON

This listing corresponds to the last version run by the author:

```
10 '++++++++++++++++++++++++++++++++++++++++++++++++++++++++++++
15 '+                                                          +
20 '+ PROGRAM " HPTSCON " - JUNE, 1986                         +
25 '+ ELECTRONICS DIVISION, CIVIL ENG. DEPT., U. OF A.         +
30 '+ BY ROY GITZEL                                            +
35 '+                                                          +
40 '+ HIGH PRESSURE AND TEMPERATURE SYSTEM                     +
45 '+ CONVERSION FACTORS OF TRANSDUCERS                        +
50 '+                                                          +
55 '+ THE FOLLOWING CONFIGURATION IS REQUIRED:                 +
60 '+ XT COMPUTER ( 640K, 2 DISKS, CLOCK )                     +
65 '+ DASH-8 & 2 EXP-16 METRABYTE DATALOGGER                   +
70 '+                                                          +
75 '+ LAST MODIFICATIONS INSTALLED IN SEPTEMBER, 1988          +
80 '+ BY ANDRE ASSIS                                           +
85 '+                                                          +
90 '++++++++++++++++++++++++++++++++++++++++++++++++++++++++++++
100 '-DIMENSION VARIABLES---------------------------------+
110 DIM CS(2,15),CB(7,15)
200 '-SETUP TRAPPING ERROR ROUTINE-----------------------+
```

```
210 ON ERROR GOTO 2000
300 '-READ OLD CONVERSION FACTORS-------------------------+
310 GOSUB 1600
400 '-INPUT DATA------------------------------------------+
410 RESTORE: CLS
420 PRINT "*****************************************************
**************"
430 PRINT "*****************************************************
**************"
440 PRINT " ": PRINT " "
450 PRINT "     HH  HH  PPPP   TTTTTT   SSSS   CCCCCC   OOOO
   NN   NN"
460 PRINT "     HH  HH  PP  P  TTTTTT  SS      CCC     OO  O
O  NNN  NN"
470 PRINT "     HHHHHH  PPPP     TT     SSSS   CC      OO  O
O  NN N NN"
480 PRINT "     HH  HH  PP       TT   S    SS  CCC     OO  O
O  NN  NNN"
490 PRINT "     HH  HH  PP       TT    SSSSS   CCCCCC   OOOO
   NN   NN"
500 PRINT " ": LOCATE 11,43: PRINT "by R.GITZEL & A.ASSIS"
510 PRINT "*****************************************************
**************"
520 PRINT "*****************************************************
**************"
530 PRINT " "
535 PRINT "FOR QUESTIONS (Y OR N)?, ALL ANSWERS OTHER THAN (
n OR N) ARE ASSUMED AS YES."
540 FOR SY%=1 TO 2: FOR X%=0 TO 15: READ TRANS$,D%,E%
550 LOCATE 17,1
555 PRINT "ENTER CONVERSION FACTOR FOR SYSTEM"SY%"TRANSDUCER
 "TRANS$" (0 TO SKIP)= ";: VER%=CSRLIN: HOR%=POS(0): PRINT C
S(SY%,X%)
560 GOSUB 1200
570 IF TS1%=1 THEN TS1%=0: GOTO 590
580 CS(SY%,X%)=VAL(FS$): FS$=""
590 CB(D%,E%)=CS(SY%,X%): IF CS(SY%,X%)=0 THEN 700
600 '-CHECK FOR TRANSDUCER UNITS--------------------------+
610 IF X%>-1 AND X%<3 THEN UNITS$="ml"
620 IF X%>2 AND X%<8 THEN UNITS$="mm"
630 IF X%>7 AND X%<11 THEN UNITS$="MPa"
640 IF X%>10 AND X%<13 THEN UNITS$="mm"
650 IF X%>12 AND X%<14 THEN UNITS$="MICROSTRAIN"
660 IF X%=14 OR X%=15 THEN UNITS$="Deg C"
670 LOCATE 19,1
675 PRINT "FULL SCALE OUTPUT OF TRANSDUCER "TRANS$" = "(CS(S
Y%,X%)*4096)" "UNITS$
680 LOCATE 21,1: INPUT "IS THIS CORRECT (Y OR N)";Y$
690 IF Y$="N" OR Y$="n" THEN GOSUB 800: GOTO 550
700 GOSUB 800: NEXT X%: NEXT SY%: CLS: GOTO 1000
800 '-CLEAR SCREEN----------------------------------------+
810 LOCATE 17,1
815 PRINT "
                                                  "
```

```
820 LOCATE 19,1
825 PRINT "
                    "
830 LOCATE 21,1
835 PRINT "                                                  "
840 RETURN
900 '-STRING CONSTANTS-------------------------------------+
910 DATA VCA1,6,0, VCI1,6,1, VCE1,6,2, DA1,6,3, LVDT0,6,8, L
VDT1,6,9, LVDT2,6,10, LVDT3,6,11, PA1,7,0, PI1,7,1, PE1,7,2,
IDA1,7,3, IDB1,7,4, ODA1,7,5, TI1, 7,6, TE1,7,7
920 DATA VCA2,6,4, VCI2,6,5, VCE2,6,6, DA2,6,7, LVDT4,6,12,
LVDT5,6,13, LVDT6,6,14, LVDT7,6,15, PA2,7,8, PI2,7,9, PE2,7,
10, IDA2,7,11, IDB2,7,12, ODA2,7,13 , TI2,7,14, TE2,7,15
1000 '-FINAL ROUTINE---------------------------------------+
1010 LOCATE 1,1
1015 PRINT "ENTERING OF CONVERSION FACTORS IS COMPLETE"
1020 GOSUB 1800
1030 LOCATE 5,1
1035 INPUT "IS IT CORRECT (Y OR N (REPEAT LIST))";Y$
1040 IF Y$="N" OR Y$="n" THEN 400
1050 GOSUB 1400
1060 LOCATE 7,1
1065 PRINT "CONVERSION FACTORS HAVE BEEN SAVED IN FILE A:CON
FACT.DFN"
1070 SYSTEM
1080 '----------------------------------------------------+
1200 '-TRAPPING ERROR ROUTINE FOR CONVERSION FACTORS-------+
1210 FST$=INKEY$: IF FST$="" THEN 1210
1220 IF ASC(FST$)=13 THEN 1280
1230 IF ASC(FST$)=46 THEN 1260
1240 IF ASC(FST$)=43 OR ASC(FST$)=45 THEN 1260
1250 IF ASC(FST$)>57 OR ASC(FST$)<48 THEN 1210
1260 IF TS%=0 THEN FS$=""
1270 FS$=FS$+FST$: TS%=TS%+1: LOCATE VER%,(HOR%+1)
1275 PRINT FS$: GOTO 1210
1280 IF LEN(FS$)=0 THEN TS%=0: TS1%=1: RETURN
1290 FST$="": TS%=0: RETURN
1400 '-SAVE DATA ROUTINE----------------------------------+
1410 OPEN "A:CONFACT.DFN" FOR OUTPUT AS #1
1420 FOR SY%=1 TO 2: FOR X%=0 TO 15
1430 PRINT #1,CS(SY%,X%): NEXT X%: NEXT SY%
1440 FOR D%=6 TO 7: FOR E%=0 TO 15
1450 PRINT #1,CB(D%,E%): NEXT E%: NEXT D%
1460 CLOSE #1: RETURN
1600 '-READ DATA ROUTINE----------------------------------+
1610 OPEN "A:CONFACT.DFN" FOR INPUT AS #1
1620 FOR SY%=1 TO 2: FOR X%=0 TO 15
1630 INPUT #1,CS(SY%,X%): NEXT X%: NEXT SY%
1640 FOR D%=6 TO 7: FOR E%=0 TO 15
1650 INPUT #1,CB(D%,E%): NEXT E%: NEXT D%
1660 CLOSE #1: RETURN
1800 '-PRINTING ROUTINE-----------------------------------+
1810 LOCATE 3,1
1815 INPUT "PRINT CONVERSION FACTORS (Y OR N)";Y$
```

```
1820 IF Y$="N" OR Y$="n" THEN RETURN
1830 RESTORE
1835 LPRINT "    HPTS   -   CONVERSION FACTOR FILE 'A:CONFAC
T.DFN'"
1840 LPRINT "": LPRINT ""
1850 LPRINT "TRANSDUCER#","CONVERSION FACTOR","FULL SCALE OU
TPUT"
1855 LPRINT ""
1860 FOR SY%=1 TO 2: FOR X%=0 TO 15: READ TRANS$,D%,E%
1870 IF X%>-1 AND X%<3 THEN UNITS$="ml"
1880 IF X%>2 AND X%<8 THEN UNITS$="mm"
1890 IF X%>7 AND X%<11 THEN UNITS$="MPa"
1900 IF X%>10 AND X%<13 THEN UNITS$="mm"
1910 IF X%>12 AND X%<14 THEN UNITS$="MICROSTRAIN"
1920 IF X%=14 OR X%=15 THEN UNITS$="Deg C"
1930 LPRINT TRANS$,CS(SY%,X%),,CS(SY%,X%)*4096,UNITS$
1940 NEXT X%: NEXT SY%: RETURN
2000 '-ERROR CHECKING ROUTINE-----------------------------+
2010 IF ERR=62 THEN 2200
2020 IF ERR=53 THEN 2300
2100 CLS: LOCATE 1,1: PRINT "ERROR" ERR "ON LINE" ERL
2110 INPUT "PRESS ENTER TO STOP"; Y$
2120 IF Y$="" THEN SYSTEM
2130 GOTO 2110
2200 CLS: LOCATE 1,1: PRINT "FILE EMPTY, NEW DATA REQUIRED"
2210 RESUME 400
2300 CLS: LOCATE 1,1: PRINT "FILE NOT FOUND"
2310 INPUT "GENERATE NEW FILE (Y OR N)";Y$
2320 IF Y$="N" OR Y$="n" THEN SYSTEM
2330 RESUME 400
```

C.3.3 Program HPTS

Program HPTS is summarized in Figs. C.5 to C.14. The main program (Fig. C.5) starts by resetting the variables, releasing the disk buffer and setting up the trapping error routine (Routine 21000). Then, it loads the DASH-8 address from the file DASH8.ADR, dimensions and sets up variables, sets up the F-keys routines (Routines 2000 to 2900) and initializes the datalogger (DASH-8 and accessories). Lastly, the program reads the conversion factors from the file CONFACT.DFN (disk A), goes through the enter test parameter setup routine (Routine 30000, Fig. C.13, Secs. C.3.3.2 and C.3.3.3) and starting routines (Sec. C.3.3.4). All system and reference parameters are displayed on the monitor when the system is ready to be started.

When initiated, the program is under screen control (Sec. C.3.3.5) and enters a loop process through the main routines (Fig. C.6). Routines 3000 and 3500 synchronize with the hardware timing pulse (timer/counter 0) and wait for it

to go high (timer/counter 1). Routine 10000 controls the menu of options displayed on the monitor screen during a test execution, when either F9 for System 1 or F10 for System 2 is pressed. Routine 4000 (Fig. C.7) checks the system in creep control. If under creep control, it adjusts the time controller and sets a flag for data acquisition at the end of each time interval. Routine 4500 (Fig. C.8) checks the system for loading control. If under loading control, it sets a flag for data acquisition at the end of each load step and calculates the reference limits for the next step. Routine 5000 stores data from all instruments in data files (Sec. C.3.3.6) every time that a flag for data acquisition exists. Routine 6000 (Fig. C.9) reads each of the DASH-8/EXP-16 channels ten times, averages them and keeps the averages for further comparison, displaying and occasionally storing. Routine 7000 (Fig. C.10) controls the cell temperature. It checks if the actual cell temperature is within the set limits and returns an output digital signal to turn the heaters either on or off. Routine 8000 (Figs. C.11 and C.12) is for loading control. It compares the actual system parameters (either pressure, displacement or volume change) to the reference values. If they are not within the tolerance limits, it activates the appropriate solenoid valve to open, either increasing or decreasing the axis pressure, in order to make the system parameter meet the desired value. Finally, Routine 9000 provides for the display of system and reference parameters, creep time and load stages on the monitor screen.

C.3.3.1 Running Program HPTS

Before starting Program HPTS, check the conversion factors and get a hard copy of them (Sec. C.3.2). Then, verify the initial readings for all key instruments (i.e., those monitoring the system parameters). Also verify that other instruments are not out of range. As a guide, pressure transducers should be close to -2048 bits, leaving the full range available for loading during the test. This is also true for LVDTs traveling in one direction only, but for LVDTs measuring expansion and contraction, the initial reading should be close to zero bit, leaving half the range on each side. In conclusion, the initial reading for each instrument has to be analysed individually, with consideration of the test load path and the expected response of the instrument.

The running procedure is described below:

a. Turn on or boot the computer with DOS in the default disk drive (e.g., disk drive C).
b. Change the default disk drive to C.

c. Change the default directory to HPTS by typing CD\HPTS and pressing the Enter key.
d. Insert the diskette HPTS#1, containing the file CONFACT.DFN, into disk drive A.
e. Load the program by typing HPTS and pressing the Enter key. Routine 30000 (Fig. C.13) manages the test parameter entry setup. It shows the HPTS logo on the monitor screen and also the following question.
f. 'ENTER INPUT DATA FROM KEYBOARD OR DISKETTE (K OR D)?'. If a test parameter setup file (*.PRM) already exists in the diskette HPTS#1 (disk A), type 'D' and press the Enter key. Then follow the steps described in Sec. C.3.3.2. If not, the data is input via keyboard. Type 'K' and press the Enter key. Then, follow the steps in Sec. C.3.3.3.

C.3.3.2 Entering Test Parameter Setup from Disk A (Fig. C.13)

If there already exists a test parameter file, follow these steps:

a. All test parameter setup files (*.PRM), stored in disk A, are displayed on the monitor screen. Type the appropriate file name and press the Enter key. Routine 24000 reads the test parameters, including instrument initial readings, stored last time.
b. Routine 29000 asks if initializing transducers. If no, it uses the old initial readings, read from the test parameter setup file. If yes, it asks if transducers are ready to be initialized. As soon as they are, press the Enter key.
c. Routine 22000 restores the test parameters, including the new instrument initial readings, in the same test parameter setup file name (disk A). Then, using the test parameters, Routine 35000 recalculates the current and total load reference parameters for all loading stages. Finally, the program goes through the starting routines (Sec. C.3.3.4).

C.3.3.3 Entering Data from the Keyboard (Fig. C.13)

Program HPTS controls pressure so as to follow the desired stress, displacement or volume change path for each of the three axes of control (axial, bore or cell). The desired total load reference parameter (pressure, displacement or volume change) for each axis has to be divided into stages (up to 25). Each stage is divided into two parts, the loading and creep parts. In the loading part (also divided in up to 25 steps), the system controls the pressure in each axis to keep the

system parameter within the tolerance limits. It goes axis by axis for each load step. The axial axis has the priority over the bore axis and this over the cell axis. System 1 has priority over System 2. When the last load step is complete for all three axes, the final load stage parameters can be maintained constant for a prescribed period of time (creep part). Creep is only controlled when the loading part has finished for all axes of both systems. In other words, the loading part has the priority over the creep control. The remaining stages follow.

Figure C.15 illustrates an example of an uniaxial test with three stages. It assists understanding of the data input methodology. This is important in ensuring correct entry of the test parameter setup (Fig. C.13). The procedure for entering data from the keyboard is:

a. Routine 29000 asks if transducers are ready to be initialized. As soon as they are, press the Enter key.
b. Routine 31000/32000 (Fig. C.14) enters the test parameter setup from keyboard. It starts defining the system to be entered. If entering data for both systems, start with System 1.
c. The program goes to Routine 28000 for selecting the control transducers (key instruments) for each axis. Four options of control are available, either pressure, displacement, volume change or disable axis control (axis not used in a particular test). In terms of displacement control, the axial axis is controlled by the axial displacement LVDT, the bore axis by the bore convergence device and the cell axis by the diameter deformation device. Finally, the program confirms the options of control for the three axes and returns to Routine 31000.
d. The statement 'ENTERING LOADING DATA FOR SYSTEM # (number)' is displayed on the monitor screen and also the following questions (steps 'e' to 'g'), for each load stage.
e. 'ENTER THE NUMBER OF DATA READINGS AT EACH OF THE FOLLOWING TIME INTERVALS IN STAGE (number) (1,2,5,15,60,120 MIN):?'. The summation of the numbers of data readings multiplied by the respective time intervals gives the total creep time for a stage. For instance, typing '60,60,30,10,2,1' and pressing the Enter key gives a total of 720 (60x1 + 60x2 + 30x5 + 10x15 + 2x60 + 1x120) minutes of creep control. It is advisable to use longer creep times when the material creep response is not known, since there is always the option of stopping creep control, but not the opposite.
f. 'ENTER NUMBER OF LOAD STEPS FOR SYSTEM (number), STAGE (number) (MAX 25)?'. The number of steps is the same for

all three axes. The more steps, the smaller the differential loads amongst the axes during loading. In each load step, the axial axis is loaded first, followed by the bore axis and then the cell axis.

g. 'ENTER TOTAL (reference load parameter) IN (physical units) OF SYSTEM (number), STAGE (number), FOR AXIS (name)?'. This question appears for all axes being used in the test. For stage one only, information on the full range of monitoring for the axis' key instrument is also shown. Enter the reference load value and press the Enter key. Negative signs preceding load values are assumed as unloading (decrease of the current stage load). The message 'LOAD OUT OF RANGE' is displayed when the key instrument range is overloaded and in this case, step 'g' is repeated for the axis under consideration.

h. The program asks if the data for each stage, loading and creep parts, are correct. If no, it returns to step 'd' and repeats the procedure. If yes, it goes to the next stage.

i. Data for each new stage are added, considering the load stage signs, to the previous one. There are two options to enter a new stage, either through the stage duplication routine (Routine 32000) when data for both loading and creep parts have to be exactly equal to the previous stage, or by repeating steps 'e' to 'g' for the new stage. The program asks a set of questions which allows the user to select the best option to enter data for each new stage.

j. When either the number of stages is greater than 25 or an answer 'N' (no) is given to the question 'ENTER ANOTHER STAGE?', the data entry is assumed as complete.

k. Routine 33000 is called for entry of the control tolerance (%) for each axis being used in the test. Type the percentage number and press the Enter key. The program then returns to Routine 31000.

l. Routine 27000 is called for entry of the starting cell temperature (zero to 80°C). Only enter cell temperatures above room temperature. Entering zero disables the cell temperature control. Type the temperature value and press the Enter key. If it is not zero, the program asks for the temperature tolerance (0.1 to 5°C). Type the tolerance value and press the Enter key. The program checks if the cell temperature and tolerance values are within the limits. If they are out of range, the procedure is repeated. The program then returns to Routine 31000.

m. When the data entry for System 1 is finished, the program asks for data entry for System 2. If yes, it repeats the same procedure (steps 'd' to 'l'). If no, or if the data entry for System 2 is already finished, the program goes through the starting routines.

C.3.3.4 Starting Routines

These routines do the final adjustments before starting the test control itself. Routine 26000 asks for printing the test parameter setup. It is good practice to have a hard copy of the test loading history for comparison with data during the test and for checking the accuracy of the input data. Routine 25000 asks for the data file name. Type the data file name and press the Enter key. The program adds the characters, 01.PRN and 02.PRN, to the data file name, creating two separate data files, one for System 1 and the other for System 2. The first character '0' (zero) is a counter incremented by one each time the system is restarted (i.e., when the function 'R' of the menu of options is accessed, Sec. C.3.3.5). Routine 34000 prints, on the monitor screen, a message saying that the test is ready to be started. Press the Enter key to start it. Finally, Routine 23000 sets up the monitor screen, displaying the loading and creep control headers, legend of control modes and the F-key menu.

C.3.3.5 Monitor Screen Control

As soon as the monitor screen control starts, the program goes through the main routines. Routine 9000 displays all major test information. The creep control header shows the system number (SY), time interval in minutes between readings (INTERVAL), number of data readings for each time interval (READING#), total set (TOTIME) and actual (ACTIME) creep times in minutes for the current time interval and the total actual creep time (CPTIME) for the current stage. The loading control header shows the system (SY), stage (SN) and step (ST) numbers, key instrument axis name (AXIS), tolerance (TOL%), set (STEMP) and actual (ATEMP) cell temperatures, increment of load per step (INCLOAD), set load for the current step (SETLOAD), actual load read from the key instrument (ACTLOAD), set load for the current stage (TOTLOAD) and the mode of control.

The modes of control are explained in a legend, displayed on the monitor screen. The monitor mode sign, MON, means the test is not under control and is awaiting input from the keyboard, following either the F-key menu or the menu of options. The axis disable control sign, OFF, is displayed for the axes not used in the test. The loading control mode, LOD, indicates that that axis is under loading control. As soon as the load step for this axis is complete, the step complete sign, S/C, is shown. When all axes have been loaded for a particular stage, the creep control starts and the creep control mode, CRP, plus the active creep, *, signs are displayed. The active creep sign is not displayed,

if one of the systems starts being loaded and the creep control stops momentarily for the other system, although creep time is still counting. When a stage, loading and creep parts, is complete, the creep complete sign, CPT, is shown. Finally, when all stages are complete, the test finished sign, FIN, is displayed.

Two menus allow test control from the monitor screen. The F-key menu has ten options (F1 to F10), five for each system. The odd F-keys are for System 1 and the even for System 2. They are for starting a test (F1 or F2), stopping a test at any point (F3 or F4) and either increasing (F5 or F6) or decreasing (F7 or F8) the set cell temperature by 1°C. F9/F10 menu is only displayed before a test is started or when a test is stopped by pressing either F3 or F4 (monitor mode, MON). The pressing of either F9 or F10 accesses the menu of options for the respective system.

All functions of the menu of options are activated by pressing the appropriate letter, either upper or lower case. Before starting a test, only the functions 'L' and 'E' are effective. A flag for data acquisition is set on when the functions 'C', 'S', 'N', 'R' and 'L' are accessed. Function 'C' continues the test from the same point as leaving. For instance, it resumes the test after either recharging or discharging the AIVC device (Appendix B). Function 'S' continues the test to the next load step and function 'N' to the next stage. They can be used for skipping either a particular load step or stage. Function 'N' provides for starting a new stage when the previous one is complete (creep complete mode, CPT) and function 'R' for restarting a test. It uses the same instrument initial readings and test parameter setup. Every time that a system is restarted, Program HPTS creates a new data file, with the same name as the original one, but increasing the counter by one. After the first restarting of System 1, the new data file is called DATA11.PRN. After the second restarting, the new data file is DATA21.PRN and so on. Function 'T' provides for transferring data from the current data file to disk B, during the test. This is helpful if a partial analysis of the data is needed without losing computer control of the test. Function 'L' loads the redefined test parameter setup file (*.PRM) from disk A and recalculates the new test load parameters. This is executed, if a change of instrument is required. Just input the new conversion factor, edit properly the test parameter setup file (*.PRM) in disk A and then access the function 'L'. Finally, function 'E' exits the menu of options without any interference with the system and returns the monitor screen control to the F-key menu.

C.3.3.6 HPTS Data Output

Data from all instruments are recorded at the end of load steps and stages, time intervals during creep control and when certain functions of the menu of options and F-keys are accessed. They are stored on the hard disk, directory C:\HPTS\DATA, into two data files, one for each system (*1.PRN and *2.PRN). The data output sequence for each line is date, time, system number, stage number, step number, creep increment, axial volume change, bore volume change, cell volume change, axial displacement, four spare LVDTs, axial pressure, bore pressure, cell pressure, bore convergence strain gauge A, bore convergence strain gauge B, diameter deformation device, cell temperature and bore temperature. Each number is followed by a space. The data files can be easily accessed or imported by any numerical, graphics and spread sheet software which facilitates data interpretation.

C.3.3.7 Listing of Program HPTS

This listing corresponds to the last version run by the author:

```
10 '+++++++++++++++++++++++++++++++++++++++++++++++++++++++++++
15 '+                                                         +
20 '+ PROGRAM " HPTS " - JUNE, 1986                           +
25 '+ ELECTRONICS DIVISION, CIVIL ENG. DEPT., U. OF A.        +
30 '+ BY ROY GITZEL                                           +
35 '+                                                         +
40 '+ HIGH PRESSURE AND TEMPERATURE SYSTEM                    +
45 '+ DATA ACQUISITION AND SYSTEM CONTROL                     +
50 '+                                                         +
55 '+ THE FOLLOWING CONFIGURATION IS REQUIRED:                +
60 '+ XT COMPUTER (640K, 2 FLOPPY AND 1 HARD DISKS, CLOCK)    +
65 '+ DASH-8 & 2 EXP-16 METRABYTE DATALOGGER                  +
70 '+                                                         +
75 '+ LAST MODIFICATIONS INSTALLED IN SEPTEMBER, 1988         +
80 '+ BY ANDRE ASSIS                                          +
85 '+                                                         +
90 '+++++++++++++++++++++++++++++++++++++++++++++++++++++++++++
100 '-------------------------------------------------------+
110 ' COMMENTS AND LAST MODIFICATIONS
120 '-------------------------------------------------------+
130 '-EVALUATION OF LOAD PARAMETERS USING REAL NUMBERS,
140 ' THAT MAKES APPROXIMATIONS MORE ACCURATE
150 '-IMPLEMENTATION OF THE NEXT STEP ROUTINE (SUB 20000)
160 '
170 '-SUB 20000 ALREADY TESTED AND IT IS OK
180 '-SUB 14000 NOT WORKING PROPERLY
190 '
```

```
200 '-----------------------------------------------------+
201 ' LIST OF CONSTANTS, VARIABLES, STRINGS AND FILE NAMES
202 '-----------------------------------------------------+
204 '
206 'A%..INTEGER, FOR...NEXT VARIABLE (SUB 6000)
208 'AN%..INTEGER, NUMBER OF READINGS TO BE AVERAGED
210 'AT%..INTEGER, AXIS NUMBER (0 TO 2)
212 'AV%..INTEGER, AVERAGE OF READINGS TAKEN FROM CHANNELS
214 'AW$..STRING, TYPE OF AXIS CONTROL (SUB 28000)
216 'AX%..INTEGER, AXIS NUMBER (0 TO 2)
218 'AX$..STRING, AXIS OR INSTRUMENT NAME CONTROLING AXIS
220 '
222 'BADR%..INTEGER, BASE ADDRESS FOR ROUTINE DASH8
224 '
226 'CB..REAL, CONVERSION FACTOR (PER EXP-16 BOARD)
228 'CH%..INTEGER, DATA PARAMETER IN ROUTINE DASH8 (CHANNEL
NUMBER)
230 'CONFACT.DFN..FILE CONTAINING CONVERSION FACTORS (DISK
A:)
232 'CS..REAL, CONVERSION FACTOR (PER SYSTEM)
234 '
236 'D%..INTEGER, DASH-8 CHANNEL NUMBER FOR EXP-16 (6 OR 7)
238 'DASH8..ROUTINE DASH8 (C:\HPTS)
240 'DASH8.ADR..FILE CONTAINING DASH8 ADDRESS (C:\HPTS)
242 'DD%..INTEGER, DASH-8 CHANNEL No. FOR EXP-16 (6 OR 7)
244 'DIO%..INTEGER, DATA PARAMETER IN ROUTINE DASH8
246 'DT..REAL, DATE
248 'DT$..STRING, DATE
250 '
252 'E%..INTEGER, EXP-16 CHANNEL NUMBER (0 TO 15)
254 'EB%..INTEGER, EXP-16 CHANNEL NUMBER (0 TO 15)
256 'EC%..INTEGER, EXP-16 CHANNEL NUMBER (0 TO 15)
258 'ERL..LINE NUMBER WHERE ERROR OCCURED
260 'ERR..ERROR NUMBER
262 '
264 'F%..INTEGER, COUNTER FOR DATA FILE NAME (SUB 17000 - RE
START)
266 'FB%..INTEGER, FLAG FOR SYSTEM INITIALIZATION (=0, NOT S
TARTED YET)
268 'FC%..INTEGER, TYPE OF AXIS CONTROL (SUB 28000)
270 'FD%..INTEGER, FLAG FOR DEFINING SOLENOID VALVE TO BE OP
EN
272 'FDD$..STRING, DATA FILE NAME
274 'FD1$..STRING, DATA FILE NAME FOR SYSTEM 1
276 'FD2$..STRING, DATA FILE NAME FOR SYSTEM 2
278 'FF%..INTEGER, FLAG FOR FINISHING TEST (=1, TEST FINISHE
D)
280 'FG%..INTEGER, FLAG FOR CONTROLING CREEP (=1, CREEP COMP
LETE)
282 'FH%..INTEGER, FLAG FOR STOPPING SYSTEM (=0, SYSTEM STOP
PED)
284 'FL%..INTEGER, FLAG INDICATING AXIS STEP COMPLETE (=1, A
XIS STEP COMPLETE)
286 'FLAG%..INTEGER, FLAG INDICATING ERROR CONDITION IN SUBR
```

```
OUTINE DASH8
288 'FM%..INTEGER, FLAG INDICATING MONITOR CONTROL (=1, MONI
TOR CONTROL)
290 'FN%..INTEGER, FLAG FOR DISPLAYING MENU OF OPTIONS (=1,
MENU IS ON)
292 'FP%..INTEGER, FLAG FOR DISPLAYING F9/F10 MENU (=1, MENU
 TO BE DISPLAYED)
294 'FPS$..STRING, FILE CONTAINING PARAMETER SETUP (DISK A:)
296 'FR%..INTEGER, FLAG FOR DATA RECORDING (=1, DATA TO BE S
TORED)
298 'FS%..INTEGER, FLAG FOR CONTROLING SYSTEM (=0, LOADING C
ONTROL IS ON)
300 'FTP$..STRING, DATA FILE TO BE TRANSFERED FROM C:\HPTS\D
ATA
302 'FTR$..STRING, DATA FILE NAME TRANSFERED TO DISK B:
304 'FY%..INTEGER, FLAG INDICATING AXIS USAGE (=0, NOT USED)
306 '
308 'G%..INTEGER, CONSTANT FOR CONTROLING LINE DISPLAY (SUB
9000)
310 '
312 'H%..INTEGER, SET MULTIPLEXER SCAN LIMITS IN SUBROUTINE
DASH8
314 '
316 'I%..INTEGER, CONSTANT CONTROLING LEGEND DISPLAY (SUB 23
000)
318 'IC%..INTEGER, TIME INTERVAL BETWEEN READINGS (MINUTES)
320 'IM%..INTEGER, NUMBER OF READINGS FOR EACH INCREMENT OF
THE CREEP STAGE
322 'IN%..INTEGER, INCREMENT NUMBER
324 'IT..REAL, SET TIME FOR EACH INCREMENT OF THE CREEP STAG
E (MINUTES)
326 'ITT..REAL, SET TOTAL TIME OF THE CREEP STAGE (MINUTES)
328 '
330 'J$..STRING, ANSWER FOR STARTING ROUTINE (SUB 34000)
332 '
334 'K%..INTEGER, PORT PB (PIO12) INPUT
336 'KEY$..STRING, OPTION FROM THE MENU
338 '
340 'LB..REAL, LOAD PER STEP
342 'LC%..INTEGER, CURRENT STEP LOAD (BITS)
344 'LD%..INTEGER, DIF. BETWEEN TOTAL STAGE AND CURRENT STEP
 LOADS (BITS)
346 'LL..REAL, TOTAL STAGE LOAD
348 'LM%..INTEGER, DIFFERENCE BETWEEN CURRENT STEP AND ACTUA
L LOADS (BITS)
350 'LN%..INTEGER, ABSOLUTE VALUE OF LM% (BITS)
352 'LR%..INTEGER, INITIAL READINGS OF ALL INSTRUMENTS/CHANN
ELS (BITS)
354 'LS%..INTEGER, NUMBER OF STEPS OF EACH STAGE
356 'LT..REAL, TOTAL STAGE LOAD
358 'LT%..INTEGER, TOTAL STAGE LOAD (BITS)
360 '
362 'M%..INTEGER, CONSTANT FOR CONTROLING LEGEND DISPLAY
364 'MC..REAL, TOTAL TIME OF THE CREEP STAGE (MINUTES)
```

```
366 'MD%..INTEGER, MODE OF OPERATION OF THE SUBROUTINE DASH8
368 '-----MODE 0, INITIALIZE DASH-8 AND INPUT BASE ADDRESS
370 '-----MODE 1, SET MULTIPLEXER SCAN LIMITS
372 '-----MODE 4, COMMAND SINGLE A/D CONVERSION AND INCREMEN
T MULTIPLEXER
374 '-----MODE 10, SET TIMER/COUNTER CONFIGURATION
376 '-----MODE 11, LOAD TIMER/COUNTER
378 '-----MODE 14, WRITE DIGITAL OUTPUT OP1-4
380 'MN%..INTEGER, CURRENT TIME WITHIN EACH TIME INTERVAL (M
INUTES)
382 'MT..REAL, CURRENT TIME WITHIN EACH INCREMENT OF THE CRE
EP STAGE (MINUTES)
384 '
386 'OP%..INTEGER, DATA PARAMETER IN ROUTINE DASH8 (SUB 6000
)
388 '
390 'P%..INTEGER, FOR...NEXT VARIABLE
392 '
394 'S$..STRING, STAR INDICATING ACTIVE CREEP
396 'SF%..INTEGER, SYSTEM NUMBER (1 OR 2)
398 'SM%..INTEGER, SYSTEM NUMBER (1 OR 2)
400 'SN%..INTEGER, STAGE NUMBER (1 TO 25)
402 'SS%..INTEGER, STEP NUMBER (1 TO 25)
404 'ST%..INTEGER, TOTAL NUMBER OF STAGES
406 'SY%..INTEGER, SYSTEM NUMBER (1 OR 2)
408 '
410 'TB%..INTEGER, AXIS LOAD TOLERANCE (BITS)
412 'TC%..INTEGER, COUNTER FOR ADJUSTING TIME
414 'TEA..REAL, ACTUAL EXTERNAL TEMPERATURE
416 'TEA%..INTEGER, ACTUAL EXTERNAL TEMPERATURE (BITS)
418 'TES..REAL, SET EXTERNAL TEMPERATURE
420 'TES%..INTEGER, SET EXTERNAL TEMPERATURE (BITS)
422 'TIA..REAL, ACTUAL INTERNAL TEMPERATURE
424 'TL..REAL, LOAD TOLERANCE
426 'TM..REAL, TIME
428 'TM$..STRING, TIME
430 'TT..REAL, EXTERNAL TEMPERATURE TOLERANCE
432 'TZ..REAL, AXIS LOAD TOLERANCE (%)
434 '
436 'VSA%..INTEGER, SOLENOID VALVE PORT (PA OR PC) ADDRESS
438 'VSL%..INTEGER, SOLENOID VALVE BIT (0 TO 7) ADDRESS
440 '
442 'WD%..INTEGER, EXP-16 BOARD NUMBER OF THE KEY-INSTRUMEN
T (6 OR 7)
444 'WE%..INTEGER, CHANNEL NUMBER OF THE KEY-INSTRUMENT (0
TO 15)
446 '
448 'X%..INTEGER, CHANNEL NUMBER (0 TO 15)
450 '
452 'Y$..STRING, ANSWER FOR QUESTIONS (Y OR N)
454 '
456 'Z%..INTEGER, FOR...NEXT VARIABLE (SUB 1100)
458 '
500 '-RESET VARIABLES AND RELEASE DISK BUFFER--------------+
```

```
510 CLEAR
600 '-SETUP TRAPPING ERROR ROUTINE-------------------------+
610 ON ERROR GOTO 21000
700 '-LOAD DASH8 ADDRESS-----------------------------------+
710 OPEN "DASH8.ADR"  FOR INPUT AS #1
720 INPUT #1, BADR%: CLOSE #1
800 '-DIMENSION VARIABLES----------------------------------+
810 DIM AV%(7,15),CB(7,15),CH%(7,15),CS(2,15),DIO%(1),FB%(2)
820 DIM FC%(2,2),FF%(2),FG%(2),FH%(2),FL%(2,25,2),FM%(2)
830 DIM FN%(2),FP%(2),FR%(2),FS%(2),FY%(2,25,2),H%(1),IC%(5)
840 DIM IM%(2,25,5),IN%(2),IT(2,25,5),LB(2,25,2),LC%(2,25,2)
850 DIM LD%(2,2),LR%(7,15),LS%(2,25),LT(2,25,2),LT%(2,25,2)
860 DIM MC(2),MN%(2),MT(2),SN%(2),SS%(2),ST%(2),TB%(2,2)
870 DIM TC%(2),TEA(2),TEA%(2),TES(2),TES%(2),TIA(2),TT(2)
880 DIM TZ(2,2),VSA%(2,2,1),VSL%(2,2,1),WD%(2,2),WE%(2,2)
900 '-SETUP VARIABLES--------------------------------------+
910 VSL%(1,0,0)=64: VSL%(1,0,1)=8: VSL%(1,1,0)=128
920 VSL%(1,1,1)=4: VSL%(2,0,0)=4: VSL%(2,0,1)=8
925 VSL%(2,1,0)=2: VSL%(2,1,1)=16: VSL%(1,2,0)=1
930 VSL%(1,2,1)=2: VSL%(2,2,0)=1: VSL%(2,2,1)=32
940 VSA%(1,0,0)=784: VSA%(1,0,1)=786: VSA%(1,1,0)=784
950 VSA%(1,1,1)=786: VSA%(2,0,0)=784: VSA%(2,0,1)=784
960 VSA%(2,1,0)=784: VSA%(2,1,1)=784: VSA%(1,2,0)=786
970 VSA%(1,2,1)=786: VSA%(2,2,0)=784: VSA%(2,2,1)=784
975 IC%(0)=1: IC%(1)=2: IC%(2)=5
980 IC%(3)=15: IC%(4)=60: IC%(5)=120
990 FS%(1)=1: FS%(2)=1
1000 '-SETUP F-KEYS----------------------------------------+
1010 ON KEY(1) GOSUB 2000: ON KEY(2) GOSUB 2100
1020 ON KEY(3) GOSUB 2200: ON KEY(4) GOSUB 2300
1030 ON KEY(5) GOSUB 2400: ON KEY(6) GOSUB 2500
1040 ON KEY(7) GOSUB 2600: ON KEY(8) GOSUB 2700
1050 ON KEY(9) GOSUB 2800: ON KEY(10) GOSUB 2900
1100 '-INITIALIZE DATALOGGER AND PIO12---------------------+
1110 DASH8=0: FLAG%=0: MD%=0: CALL DASH8 (MD%,BADR%,FLAG%)
1120 FOR Z%=0 TO 2: MD%=10: DIO%(0)=Z%
1130 IF Z%=1 THEN DIO%(1)=0: GOTO 1150  'PULSE HIGH ON TERMI
NAL COUNTER 1
1140 DIO%(1)=3  'SQUARE WAVE GENERATOR FOR COUNTERS 0 AND 2
1150 CALL DASH8 (MD%,DIO%(0),FLAG%): NEXT Z%
1160 MD%=11: DIO%(0)=0: DIO%(1)=200  'LOAD COUNTER 0, 200 FO
R TIMESET=2SEC
1170 CALL DASH8 (MD%,DIO%(0),FLAG%)
1180 DIO%(0)=2: DIO%(1)=23846  'LOAD COUNTER 2, FREQUENCY OF
 100 HZ
1190 CALL DASH8 (MD%,DIO%(0),FLAG%)
1200 OUT &H313,&H82  'CONTROL WORD=10000010, PA0-7 AND PC0-7
 OUT, PB0-7 IN
1210 OUT &H310,&H0: OUT &H312,&H0  'SET OUTPUTS LOW
1300 '-READ INSTRUMENT CONVERSION FACTORS------------------+
1310 OPEN "A:CONFACT.DFN" FOR INPUT AS #1
1320 FOR SY%=1 TO 2: FOR X%=0 TO 15
1330 INPUT #1,CS(SY%,X%): NEXT X%: NEXT SY%
1340 FOR D%=6 TO 7: FOR E%=0 TO 15
```

```
1350 INPUT #1,CB(D%,E%): NEXT E%: NEXT D%: CLOSE #1
1400 '-ENTER TEST PARAMETER SETUP--------------------------+
1410 CLS: GOSUB 30000
1500 '-STARTING ROUTINES-----------------------------------+
1510 GOSUB 26000  'PRINT TEST PARAMETER SETUP
1520 GOSUB 25000  'ENTER DATA FILE NAME
1530 GOSUB 34000  'START SYSTEM
1540 GOSUB 23000  'SETUP MONITOR SCREEN
1600 '-----------------------------------------------------+
1610 ' MAIN ROUTINES
1620 '-----------------------------------------------------+
1630 GOSUB 3000  'SYNCHRONIZE WITH HARDWARE TIMING PULSE
1640 GOSUB 3500  'WAIT FOR TIMING PULSE TO GO HIGH
1650 GOTO 10000  'CONTROL KEYS
1660 GOSUB 4000  'ADJUST TIME CONTROLLER FOR CREEP
1670 GOSUB 4500  'LOAD INCREMENT
1680 GOTO 5000   'STORE DATA TAKEN LAST TIME
1690 GOSUB 6000  'LOW SPEED DATA LOGGING
1700 GOSUB 7000  'EXTERNAL (CELL) TEMPERATURE CONTROL
1710 GOSUB 8000  'LOADING CONTROL
1720 GOSUB 9000  'SCREEN UPDATE
1730 GOTO 1630   'DO IT AGAIN
1800 '-----------------------------------------------------+
1810 ' SUB-ROUTINES
1820 '-----------------------------------------------------+
1900 '-----------------------------------------------------+
1910 ' EVENT TRAPPING ROUTINES
1920 '-----------------------------------------------------+
2000 '-ON KEY 1 - START SYSTEM #1--------------------------+
2010 SM%=1: GOSUB 19000: FR%(1)=1: FS%(1)=0: KEY(1) OFF
2020 FB%(1)=1: LOCATE 13,37: PRINT "                    "
2030 RETURN
2100 '-ON KEY 2 - START SYSTEM #2--------------------------+
2110 SM%=2: GOSUB 19000: FR%(2)=1: FS%(2)=0: KEY(2) OFF
2120 FB%(2)=1: LOCATE 13,62: PRINT "                    "
2130 RETURN
2200 '-ON KEY 3 - STOP SYSTEM #1---------------------------+
2210 FH%(1)=0: KEY(3) OFF: FR%(1)=1: RETURN
2300 '-ON KEY 4 - STOP SYSTEM #2---------------------------+
2310 FH%(2)=0: KEY(4) OFF: FR%(2)=1: RETURN
2400 '-ON KEY 5 - DECREASE EXTERNAL TEMPERATURE ON SYSTEM #1
2410 TES(1)=TES(1)-1: TES%(1)=CINT(TES(1)/CS(1,15)): RETURN
2500 '-ON KEY 6 - DECREASE EXTERNAL TEMPERATURE ON SYSTEM #2
2510 TES(2)=TES(2)-1: TES%(2)=CINT(TES(2)/CS(2,15)): RETURN
2600 '-ON KEY 7 - INCREASE EXTERNAL TEMPERATURE ON SYSTEM #1
2610 TES(1)=TES(1)+1: TES%(1)=CINT(TES(1)/CS(1,15)): RETURN
2700 '-ON KEY 8 - INCREASE EXTERNAL TEMPERATURE ON SYSTEM #2
2710 TES(2)=TES(2)+1: TES%(2)=CINT(TES(2)/CS(2,15)): RETURN
2800 '-ON KEY 9 - DISPLAY MENU OF OPTIONS FOR SYSTEM #1----+
2810 FP%(1)=1: KEY(1) OFF: RETURN
2900 '-ON KEY 10 - DISPLAY MENU OF OPTIONS FOR SYSTEM #2---+
2910 FP%(2)=1: KEY(2) OFF: RETURN
3000 '-----------------------------------------------------+
3010 ' SYNC. WITH HARDWARE TIMING PULSE, TIMER/COUNTER 0
```

```
3020 '-----------------------------------------------------+
3030 K%=INP(&H311): IF (K% AND 1)=0 THEN RETURN
3040 GOTO 3030
3500 '-----------------------------------------------------+
3510 ' WAIT FOR TIMING PULSE TO GO HIGH, TIMER/COUNTER 1
3520 '-----------------------------------------------------+
3530 K%=INP(&H311): IF (K% AND 1)=1 THEN RETURN
3540 GOTO 3530
4000 '-----------------------------------------------------+
4010 ' ADJUST TIME CONTROLLER FOR CREEP ROUTINE
4020 '-----------------------------------------------------+
4030 AT%=AT%+1: IF AT%>2 THEN AT%=0
4040 IF FH%(1)=1 AND FH%(2)=1 THEN SF%=((SF%-1) XOR 1)+1: GO
TO 4070
4050 IF FH%(1)=1 THEN SF%=1: GOTO 4070
4060 IF FH%(2)=1 THEN SF%=2
4070 FOR SY%=1 TO 2
4075 IF FH%(SY%)=1 AND FS%(SY%)=1 THEN 4085  'IS CREEPING?
4080 NEXT SY%: RETURN
4085 IF IM%(SY%,SN%(SY%),0)=0 AND IM%(SY%,SN%(SY%),1)=0 AND
IM%(SY%,SN%(SY%),2)=0 AND IM%(SY%,SN%(SY%),3)=0 AND IM%(SY%,
SN%(SY%),4)=0 AND IM%(SY%,SN%(SY%), 5)=0 THEN 4200
4090 TC%(SY%)=TC%(SY%)+1  'ADJUST TIMER
4100 IF TC%(SY%)=30 THEN TC%(SY%)=0: GOTO 4120  '1 MINUTE?
4110 GOTO 4080
4120 MN%(SY%)=MN%(SY%)+1: MT(SY%)=MT(SY%)+1
4125 MC(SY%)=MC(SY%)+1
4130 IF IM%(SY%,SN%(SY%),IN%(SY%))=0 THEN 4170
4140 IF MN%(SY%)=IC%(IN%(SY%)) THEN FR%(SY%)=1: MN%(SY%)=0
4150 IF MT(SY%)=IT(SY%,SN%(SY%),IN%(SY%)) THEN 4170
4160 GOTO 4080
4170 MT(SY%)=0: IN%(SY%)=IN%(SY%)+1  'GOTO NEXT INCREMENT
4180 IF (IN%(SY%)=6) THEN IN%(SY%)=5: GOTO 4200  'LAST INCRE
MENT?
4190 GOTO 4130
4200 FH%(SY%)=0: FG%(SY%)=1  'TURN SYSTEM OFF-CREEP COMPLETE
4205 IF SN%(SY%)=ST%(SY%) THEN FF%(SY%)=1
4210 IF FH%(1)=1 THEN SF%=1
4220 IF FH%(2)=1 THEN SF%=2
4230 MC(SY%)=0: GOTO 4080
4500 '-----------------------------------------------------+
4510 ' LOAD INCREMENT ROUTINE
4520 '-----------------------------------------------------+
4530 FOR SY%=1 TO 2: IF FS%(SY%)=0 THEN 4550
4540 NEXT SY%: RETURN
4550 FOR AX%=0 TO 2
4560 IF FY%(SY%,SN%(SY%),AX%)=1 AND FH%(SY%)=1 THEN FL%(SY%,
SN%(SY%),AX%)=1
4570 NEXT AX%
4580 IF FL%(SY%,SN%(SY%),0)=1 AND FL%(SY%,SN%(SY%),1)=1 AND
FL%(SY%,SN%(SY%),2)=1 THEN FL%(SY%,SN%(SY%),0)=0: FL%(SY%,SN
%(SY%),1)=0: FL%(SY%,SN%(SY%),2)=0: GOTO 4600
4590 RETURN
4600 IF FH%(SY%)=1 THEN 4620
```

```
4610 RETURN
4620 SS%(SY%)=SS%(SY%)+1
4630 IF SS%(SY%)>LS%(SY%,SN%(SY%)) THEN SS%(SY%)=LS%(SY%,SN%
(SY%))
4640 FOR AX%=0 TO 2
4645 LD%(SY%,AX%)=LT%(SY%,SN%(SY%),AX%)-LC%(SY%,SN%(SY%),AX%
)
4650 IF LD%(SY%,AX%)0 THEN LC%(SY%,SN%(SY%),AX%)=CINT((LT(
SY%,(SN%(SY%)-1),AX%)+LB(SY%,SN%(SY%),AX%)*SS%(SY%))/CB(WD%(
SY%,AX%),WE%(SY%,AX%)))+LR%(WD%(SY% ,AX%),WE%(SY%,AX%)): FR%
(SY%)=1
4660 NEXT AX%
4665 IF LD%(SY%,0)=0 AND LD%(SY%,1)=0 AND LD%(SY%,2)=0 THEN
FS%(SY%)=1: FR%(SY%)=1
4670 RETURN
5000 '-----------------------------------------------------+
5010 ' STORE DATA ROUTINE
5020 '-----------------------------------------------------+
5030 IF FR%(1)=1 THEN FR%(1)=0: SY%=1: GOTO 5100
5040 IF FR%(2)=1 THEN FR%(2)=0: SY%=2: GOTO 5200
5050 GOTO 1690
5100 OPEN FD1$ FOR APPEND AS #2
5110 DT$=LEFT$(DATE$,2)+MID$(DATE$,4,2)+RIGHT$(DATE$,2)
5115 DT=VAL(DT$)
5120 TM$=LEFT$(TIME$,2)+MID$(TIME$,4,2)+RIGHT$(TIME$,2)
5125 TM=VAL(TM$)
5130 PRINT #2, DT;TM;SY%;SN%(SY%);SS%(SY%);IN%(SY%);
5140 DD%=6: EB%=0: EC%=3: GOSUB 5300
5150 EB%=8: EC%=11: GOSUB 5300
5160 DD%=7: EB%=0: EC%=7: GOSUB 5300
5170 PRINT #2,"": CLOSE #2: GOTO 1630
5200 OPEN FD2$ FOR APPEND AS #2
5210 DT$=LEFT$(DATE$,2)+MID$(DATE$,4,2)+RIGHT$(DATE$,2)
5215 DT=VAL(DT$)
5220 TM$=LEFT$(TIME$,2)+MID$(TIME$,4,2)+RIGHT$(TIME$,2)
5225 TM=VAL(TM$)
5230 PRINT #2, DT;TM;SY%;SN%(SY%);SS%(SY%);IN%(SY%);
5240 DD%=6: EB%=4: EC%=7: GOSUB 5300
5250 EB%=12: EC%=15: GOSUB 5300
5260 DD%=7: EB%=8: EC%=15: GOSUB 5300
5270 PRINT #2,"": CLOSE #2: GOTO 1630
5300 '-----------------------------------------------------+
5310 D%=DD%: FOR E%=EB% TO EC%
5315 PRINT #2,((AV%(D%,E%)-LR%(D%,E%))*CB(D%,E%));
5320 NEXT E%: RETURN
6000 '-----------------------------------------------------+
6010 ' LOW SPEED DATA LOGGING ROUTINE
6020 '-----------------------------------------------------+
6030 AN%=10  'SET AVERAGE NUMBER
6040 FOR A%=1 TO AN%: MD%=1: H%(0)=0: H%(1)=5
6045 CALL DASH8 (MD%,H%(0),FLAG%)
6050 FOR D%=0 TO 5: E%=0: MD%=4
6055 CALL DASH8 (MD%,CH%(D%,E%),FLAG%)
6060 IF A%=1 THEN AV%(D%,E%)=CH%(D%,E%): GOTO 6080
```

```
6070 AV%(D%,E%)=AV%(D%,E%)+CH%(D%,E%)
6080 NEXT D%: FOR D%=6 TO 7
6090 MD%=1: H%(0)=D%: H%(1)=D%
6095 CALL DASH8 (MD%,H%(0),FLAG%)
6100 FOR E%=0 TO 15: OP%=E%: MD%=14
6105 CALL DASH8 (MD%,OP%,FLAG%)
6110 MD%=4: CALL DASH8 (MD%,CH%(D%,E%),FLAG%)
6120 IF A%=1 THEN AV%(D%,E%)=CH%(D%,E%): GOTO 6140
6130 AV%(D%,E%)=AV%(D%,E%)+CH%(D%,E%)
6140 NEXT E%: NEXT D%: NEXT A%
6150 FOR D%=0 TO 5: E%=0
6155 AV%(D%,E%)=AV%(D%,E%)/AN%: NEXT D%
6160 FOR D%=6 TO 7: FOR E%=0 TO 15
6165 AV%(D%,E%)=AV%(D%,E%)/AN%: NEXT E%: NEXT D%
6170 RETURN
7000 '-----------------------------------------------------+
7010 ' EXTERNAL (CELL) TEMPERATURE CONTROL ROUTINE
7020 '-----------------------------------------------------+
7030 TEA%(1)=AV%(7,7): TEA%(2)=AV%(7,15): FOR SY%=1 TO 2
7040 IF TES(SY%)=0 THEN 7070
7050 IF TEA%(SY%)>(TES%(SY%)+INT(TT(SY%)/CS(SY%,15))) THEN G
OTO 7100
7060 IF TEA%(SY%)<(TES%(SY%)-INT(TT(SY%)/CS(SY%,15))) THEN G
OTO 7200
7070 NEXT SY%: RETURN
7100 '-TURN HEATERS OFF-------------------------------------+
7110 IF SY%=1 THEN OUT &H312,(INP(&H312) AND &HDF): GOTO 707
0
7120 IF SY%=2 THEN OUT &H312,(INP(&H312) AND &HBF): GOTO 707
0
7200 '-TURN HEADERS ON--------------------------------------+
7210 IF SY%=1 THEN OUT &H312,(INP(&H312) OR &H20): GOTO 7070
7220 IF SY%=2 THEN OUT &H312,(INP(&H312) OR &H40): GOTO 7070
8000 '-----------------------------------------------------+
8010 ' LOADING CONTROL ROUTINE
8020 '-----------------------------------------------------+
8030 IF FH%(1)=1 OR FH%(2)=1 THEN 8050  'IS SYSTEM ON?
8040 RETURN  'NO SYSTEM ON
8050 FOR SY%=1 TO 2: IF FH%(SY%)=0 THEN 8080
8060 FOR AX%=0 TO 2
8065 IF FL%(SY%,SN%(SY%),AX%)=0 AND FS%(SY%)=0 AND FY%(SY%,S
N%(SY%),AX%)=0 AND FM%(SY%)=0 THEN GOSUB 8200: RETURN
8070 NEXT AX%: IF FS%(1)=1 AND FS%(2)=1 THEN 8090
8080 NEXT SY%: RETURN
8090 IF FY%(SF%,SN%(SF%),AT%)=0 THEN SY%=SF%: AX%=AT%: GOSUB
 8200: RETURN
8100 RETURN
8200 '-CHECK IF WITHIN TOLERANCE LIMITS---------------------+
8210 LN%=LC%(SY%,SN%(SY%),AX%)-AV%(WD%(SY
8510 IF LN%>0 THEN FD%=1: DIO%(1)=5: GOSUB 8600: RETURN  'PR
ESSURE IN
8520 FD%=0: DIO%(1)=10: GOSUB 8600: RETURN  'PRESSURE OUT
8600 '-ENERGIZE SOLENOID VALVES-----------------------------+
8610 KEY (3) OFF: KEY (4) OFF  'DISABLE STOP KEYS WHILE SOLE
```

```
NOID IS ON
8620 VSL%=VSL%(SY%,AX%,FD%)
8625 VSA%=VSA%(SY%,AX%,FD%)  'SET DOWN FLAG
8630 MD%=11: DIO%(0)=1: CALL DASH8 (MD%,DIO%(0),FLAG%)
8640 OUT &H312,(INP(&H312) XOR &H10)
8650 OUT VSA%,(INP(VSA%) XOR VSL%)  'TIMER AND SOLENOID ON
8660 IF (INP(&H311) AND 2)=2 THEN 8680
8670 GOTO 8660
8680 OUT &H312,(INP(&H312) XOR &H10)
8690 OUT VSA%,(INP(VSA%) XOR VSL%)  'TIMER AND SOLENOID OFF
8700 IF ST%(1)>0 THEN KEY (3) ON  'ENABLE KEYS
8710 IF ST%(2)>0 THEN KEY (4) ON  'ENABLE KEYS
8720 RETURN
9000 '-----------------------------------------------------+
9010 ' DISPLAY ROUTINE
9020 '-----------------------------------------------------+
9030 TEA(1)=AV%(7,7)*CS(1,15): TEA(2)=AV%(7,15)*CS(2,15)
9035 TIA(1)=AV%(7,6)*CS(1,14): TIA(2)=AV%(7,14)*CS(2,14)
9040 LOCATE 25,37: PRINT "DATE ";DATE$;
9045 LOCATE 25,67: PRINT "TIME ";TIME$;
9050 G%=6: FOR SY%=1 TO 2: IF ST%(SY%)=0 THEN 9350
9060 FOR AX%=0 TO 2: IF FC%(SY%,AX%)=3 THEN AX$=" OFF"
9070 IF AX%=0 AND FC%(SY%,AX%)=0 THEN AX$=" PA "
9080 IF AX%=0 AND FC%(SY%,AX%)=1 THEN AX$=" DA "
9090 IF AX%=0 AND FC%(SY%,AX%)=2 THEN AX$=" VCA"
9100 IF AX%=1 AND FC%(SY%,AX%)=0 THEN AX$=" PI "
9110 IF AX%=1 AND FC%(SY%,AX%)=1 THEN AX$=" IDA"
9120 IF AX%=1 AND FC%(SY%,AX%)=2 THEN AX$=" VCI"
9130 IF AX%=2 AND FC%(SY%,AX%)=0 THEN AX$=" PE "
9140 IF AX%=2 AND FC%(SY%,AX%)=1 THEN AX$=" ODA"
9150 IF AX%=2 AND FC%(SY%,AX%)=2 THEN AX$=" VCE"
9160 G%=G%+1
9170 LOCATE G%,1: PRINT SY%
9175 LOCATE G%,4: PRINT USING "##"; SN%(SY%)
9180 LOCATE G%,7: PRINT USING "##"; SS%(SY%)
9185 LOCATE G%,10: PRINT AX$
9190 IF FC%(SY%,AX%)=3 THEN LOCATE G%,15: PRINT "----": GOTO
 9200
9195 LOCATE G%,15: PRINT USING "#.##"; TZ(SY%,AX%)
9200 IF AX%=0 THEN LOCATE G%,21: PRINT "-----": LOCATE G%,28
: PRINT "------": GOTO 9220
9205 IF AX%=1 THEN LOCATE G%,21: PRINT "-----": LOCATE G%,28
: PRINT USING "+###.#"; TIA(SY%): GOTO 9220
9210 LOCATE G%,21: PRINT USING "+##.#"; TES(SY%)
9215 LOCATE G%,28: PRINT USING"+###.#"; TEA(SY%)
9220 LOCATE G%,36
9225 PRINT USING "+####.##"; LB(SY%,SN%(SY%),AX%)
9230 LOCATE G%,46
9235 PRINT USING "+####.##"; ((LC%(SY%,SN%(SY%),AX%)-LR%(WD%
(SY%,AX%),WE%(SY%,AX%)))*CB(WD%(SY%,AX%),WE%(SY%,AX%)))
9240 LOCATE G%,56
9245 PRINT USING "+####.##"; ((AV%(WD%(SY%,AX%),WE%(SY%,AX%)
)-LR%(WD%(SY%,AX%),WE%(SY%,AX%)))*CB(WD%(SY%,AX%),WE%(SY%,AX
%)))
```

```
9250 LOCATE G%,66
9255 PRINT USING "+####.##"; ((LT%(SY%,SN%(SY%),AX%)-LR%(WD%
(SY%,AX%),WE%(SY%,AX%)))*CB(WD%(SY%,AX%),WE%(SY%,AX%)))
9260 IF FF%(SY%)=1 THEN LOCATE G%,77: PRINT "FIN ": GOTO 933
0
9270 IF FY%(SY%,SN%(SY%),AX%)=1 THEN LOCATE G%,77: PRINT "OF
F ": GOTO 9330
9280 IF FH%(SY%)=0 AND FG%(SY%)=0 THEN LOCATE G%,77: FM%(SY%
)=1: PRINT "MON ": GOTO 9340
9290 IF FH%(SY%)=1 AND FS%(SY%)=0 AND FL%(SY%,SN%(SY%),AX%)=
0 THEN LOCATE G%,77: PRINT "LOD ": GOTO 9330
9300 IF FH%(SY%)=1 AND FS%(SY%)=0 AND FL%(SY%,SN%(SY%),AX%)=
1 THEN LOCATE G%,77: PRINT "S/C ": GOTO 9330
9310 IF FH%(SY%)=1 AND FS%(SY%)=1 THEN GOSUB 9500: LOCATE G%
,77: PRINT "CRP"+S$: GOTO 9330
9320 IF FH%(SY%)=0 AND FG%(SY%)=1 THEN LOCATE G%,77: PRINT "
CPT "
9330 FM%(SY%)=0
9340 NEXT AX%
9350 LOCATE (SY%+1),26: PRINT SY%
9360 IF ST%(SY%)=0 THEN LOCATE (SY%+1),34: PRINT "OFF": GOTO
 9420
9370 LOCATE (SY%+1),34
9375 PRINT USING "###"; IC%(IN%(SY%))
9380 LOCATE (SY%+1),43
9385 PRINT USING "####"; IM%(SY%,SN%(SY%),IN%(SY%))
9390 LOCATE (SY%+1),53
9395 PRINT USING "######"; IT(SY%,SN%(SY%),IN%(SY%))
9400 LOCATE (SY%+1),63: PRINT USING "######"; MT(SY%)
9410 LOCATE (SY%+1),73: PRINT USING "######"; MC(SY%)
9420 NEXT SY%: RETURN
9500 '-ACTIVE CREEP SIGN-----------------------------------+
9510 IF FS%((SY%-1) XOR 1)=0 AND SF%=2 AND SY%=2 THEN S$=" "
: RETURN
9520 IF FS%((SY%-1) XOR 1)=1 AND SF%=2 AND SY%=2 THEN S$="*"
: RETURN
9530 IF FS%((SY%-1) XOR 1)=0 AND SF%=2 AND SY%=1 THEN S$=" "
: RETURN
9540 IF FS%((SY%-1) XOR 1)=1 AND SF%=2 AND SY%=1 THEN S$=" "
: RETURN
9550 IF FS%((SY%-1) XOR 1)=0 AND SF%=1 AND SY%=1 THEN S$=" "
: RETURN
9560 IF FS%((SY%-1) XOR 1)=1 AND SF%=1 AND SY%=1 THEN S$="*"
: RETURN
9570 IF FS%((SY%-1) XOR 1)=0 AND SF%=1 AND SY%=2 THEN S$=" "
: RETURN
9580 IF FS%((SY%-1) XOR 1)=1 AND SF%=1 AND SY%=2 THEN S$=" "
: RETURN
10000 '-----------------------------------------------------+
10010 ' CONTROL KEY PICKUP
10020 '-----------------------------------------------------+
10030 FOR SY%=1 TO 2: IF FH%(SY%)=1 OR ST%(SY%)=0 THEN 10080
10040 LOCATE (13+SY%),1: PRINT "F"(8+SY%)
10050 LOCATE (13+SY%),6: PRINT "- SYSTEM#"SY%: KEY(8+SY%) ON
```

```
10060 IF FP%(SY%)=1 THEN GOSUB 11000
10070 IF FP%(SY%)=1 AND FN%(SY%)=1 THEN GOSUB 11500
10080 NEXT SY%: GOTO 1660
11000 '-MENU OF OPTIONS-----------------------------------+
11010 IF FN%(SY%)=1 THEN RETURN
11020 KEY$=INKEY$: IF KEY$"" THEN 11020
11030 LOCATE 17,1: PRINT "SYSTEM#"SY%
11040 LOCATE 18,2: PRINT "C - CONTINUE"
11050 LOCATE 19,2: PRINT "S - NEXT STEP"
11060 LOCATE 20,2: PRINT "N - NEXT STAGE"
11070 LOCATE 21,2: PRINT "R - RESTART"
11080 LOCATE 22,2: PRINT "T - TRANSFER DATA (C: TO B:)"
11090 LOCATE 23,2: PRINT "L - LOAD REDEFINED PARAMETERS"
11100 LOCATE 24,2: PRINT "E - EXIT TO MAIN";
11110 FN%(SY%)=1: RETURN
11500 '-SELECT A MENU FUNCTION----------------------------+
11510 KEY$=INKEY$: IF KEY$="" THEN RETURN
11520 IF FP%(1)=1 THEN SM%=1: FTP$=FD1$: GOTO 11540
11530 SM%=2: FTP$=FD2$
11540 IF FB%(SM%)=0 THEN 11600
11550 IF KEY$="C" OR KEY$="c" THEN 12000
11560 IF KEY$="S" OR KEY$="s" THEN 20000
11570 IF KEY$="N" OR KEY$="n" THEN 13000
11580 IF KEY$="R" OR KEY$="r" THEN 17000
11590 IF KEY$="T" OR KEY$="t" THEN 15000
11600 IF KEY$="L" OR KEY$="l" THEN 14000
11610 IF KEY$="E" OR KEY$="e" THEN 16000
11620 KEY$=INKEY$: IF KEY$="" THEN RETURN
11630 GOTO 11620
12000 '-CONTINUE TEST AT SAME POINT AS LEAVING-------------+
12010 GOSUB 18000: GOSUB 19000
12020 KEY(SM%+2) ON: FR%(SM%)=1: RETURN
13000 '-CONTINUE TEST TO NEXT STAGE------------------------+
13010 SN%(SM%)=SN%(SM%)+1: GOSUB 18000: GOSUB 19000
13020 FS%(SM%)=0: FG%(SM%)=0
13030 IF SN%(SM%)=ST%(SM%)+1 THEN SN%(SM%)=SN%(SM%)-1: FG%(S
M%)=1: FH%(SM%)=0: FS%(SM%)=1: FF%(SM%)=1 13040 FR%(SM%)=1:
IN%(SM%)=0: MT(SM%)=0: MC(SM%)=0
13050 SS%(SM%)=1: KEY(SM%+2) ON: RETURN
14000 '-LOAD REDEFINED TEST PARAMETERS---------------------+
14010 GOSUB 24050: GOSUB 35000
14020 IF FB%(SM%)=0 THEN KEY(SM%) ON
14030 FR%(SM%)=1: RETURN
15000 '-TRANSFER DATA FROM C: TO B:------------------------+
15010 LOCATE 16,1: FTR$="COPY "+FTP$+" B:": SHELL FTR$
15020 LOCATE 17,1: PRINT "                                  "
15030 RETURN
16000 '-EXIT MENU OF OPTIONS-------------------------------+
16010 FN%(SM%)=0: FP%(SM%)=0: GOSUB 18000
16020 IF FB%(SM%)=0 THEN KEY(SM%) ON
16030 RETURN
17000 '-RESTART SYSTEM-------------------------------------+
17010 F%=F%+1: FG%(SM%)=0: FF%(SM%)=0
17020 FR%(SM%)=1: SN%(SM%)=1: SS%(SM%)=1
```

```
17030 IF SM%=1 THEN FD1$="C:\HPTS\DATA\"+FDD$+RIGHT$(STR$(F%
),1)+"1.PRN": OPEN FD1$ FOR OUTPUT AS #1: CLOSE #1
17040 IF SM%=2 THEN FD2$="C:\HPTS\DATA\"+FDD$+RIGHT$(STR$(F%
),1)+"2.PRN": OPEN FD2$ FOR OUTPUT AS #2: CLOSE #2
17050 GOSUB 18000: GOSUB 19000
17060 FS%(SM%)=0: KEY(SM%+2) ON: RETURN
18000 '-ERASE MENU OF OPTIONS-----------------------------+
18010 FOR I%=16 TO 24: LOCATE I%,1
18020 PRINT"                                        ";
18030 NEXT I%: RETURN
19000 '-ERASE F9/F10 MENU---------------------------------+
19010 FN%(SM%)=0: FP%(SM%)=0: FH%(SM%)=1
19020 LOCATE (13+SM%),1: PRINT "                          "
19030 RETURN
20000 '-CONTINUE TEST TO NEXT STEP------------------------+
20010 GOSUB 18000: GOSUB 19000: SS%(SM%)=SS%(SM%)+1
20020 IF SS%(SM%)=SN%(SM%)+1 THEN SS%(SM%)=SS%(SM%)-1: GOTO
20060
20030 FOR AX%=0 TO 2: IF FC%(SM%,AX%)=3 THEN 20050
20040 LC%(SM%,SN%(SM%),AX%)=CINT((LT(SM%,(SN%(SM%)-1),AX%)+L
B(SM%,SN%(SM%),AX%)*SS%(SM%))/CB(WD%(SM%,AX%),WE%(SM%,AX%)))
+LR%(WD%(SM%,AX%),WE%(SM%,AX%))
20050 NEXT AX%
20060 KEY(SM%+2) ON: FR%(SM%)=1: RETURN
21000 '---------------------------------------------------+
21010 ' ERROR TRAPPING ROUTINE
21020 '---------------------------------------------------+
21030 IF ERR=53 AND ERL=22030 THEN 21600
21040 IF ERR=53 AND ERL=25030 THEN 21700
21050 IF ERR=53 AND ERL=24030 THEN 21500
21060 IF ERR=53 AND ERL=24050 THEN RESUME 24030
21070 IF ERR=52 AND ERL=24050 THEN RESUME 24030
21080 IF ERR=64 AND ERL=24050 THEN RESUME 24030
21090 IF ERR=71 AND ERL=1330 THEN 21800
21400 CLS: LOCATE 12,1: PRINT "ERROR " ERR "ON LINE " ERL
21410 INPUT "PRESS ENTER TO STOP ";Y$: IF Y$="" THEN SYSTEM
21420 GOTO 21410
21500 CLS: LOCATE 1,1
21505 PRINT "NO EXISTING PARAMETER SETUP FILES"
21510 INPUT "PRESS ENTER TO INPUT FROM KEYBOARD";Y$
21515 IF Y$="" THEN RESUME 30300
21520 GOTO 21510
21600 CLS: LOCATE 1,1
21605 PRINT "NO EXISTING PARAMETER SETUP FILES"
21610 INPUT "PRESS ENTER TO CONTINUE";Y$
21615 IF Y$="" THEN RESUME NEXT
21620 GOTO 21610
21700 CLS: LOCATE 1,1: PRINT "NO EXISTING DATA FILES"
21710 INPUT "PRESS ENTER TO CONTINUE";Y$
21715 IF Y$="" THEN RESUME NEXT
21720 GOTO 21710
21800 CLS: LOCATE 12,1: PRINT "ERROR! DISK A:> NOT READY"
21810 INPUT "WHEN READY, PRESS ENTER KEY TO CONTINUE ";Y$
21815 IF Y$="" THEN RESUME
```

```
21820 GOTO 21810
22000 '-----------------------------------------------------+
22010 ' SAVE TEST PARAMETER SETUP ROUTINE
22020 '-----------------------------------------------------+
22030 CLS: LOCATE 1,1: FILES "A:*.PRM"
22040 LOCATE 22,1
22045 PRINT "FILE NAME EXTENTION .PRM WILL BE AUTOMATICALLY
ADDED"
22050 LOCATE 23,1
22055 PRINT "ENTERING AN EXISTING FILE NAME WILL OVERWRITE T
HE OLD FILE"
 22060 LOCATE 20,1
22065 INPUT "SAVE PARAMETER SETUP UNDER FILE NAME (MAX. 7 CH
AR.)";FPS$
22070 IF LEN(FPS$)>7 THEN LOCATE 22,52: PRINT "
      ": GOTO 22060
22080 OPEN "A:"+FPS$+".PRM" FOR OUTPUT AS #1
22090 FOR SY%=1 TO 2: IF ST%(SY%)=0 THEN  22155
22100 PRINT #1,SY%;ST%(SY%)
22105 FOR SN%=1 TO ST%(SY%): FOR AX%=0 TO 2
22110 PRINT #1,LB(SY%,SN%,AX%);FY%(SY%,SN%,AX%): NEXT AX%
22120 PRINT #1,LS%(SY%,SN%): FOR P%=0 TO 5
22130 PRINT #1,IM%(SY%,SN%,P%);IT(SY%,SN%,P%): NEXT P%
22135 NEXT SN%: FOR AX%=0 TO 2
22140 PRINT #1,TZ(SY%,AX%);TB%(SY%,AX%);FC%(SY%,AX%);WD%(SY%
,AX%);WE%(SY%,AX%)
22150 NEXT AX%: PRINT #1,TES(SY%);TT(SY%)
22155 NEXT SY%
22160 FOR D%=6 TO 7: FOR E%=0 TO 15
22165 PRINT #1,LR%(D%,E%);CB(D%,E%): NEXT E%
22170 NEXT D%: CLOSE 1: RETURN
23000 '-----------------------------------------------------+
23010 ' SETUP SCREEN ROUTINE
23020 '-----------------------------------------------------+
23030 CLS: LOCATE 1,1
23035 PRINT "CREEP  CONTROL (t=min)   SY   INTERVAL  READING
#    TOTIME    ACTIME    CPTIME"
23040 LOCATE 5,1
23045 PRINT "SY SN ST AXIS TOL%  STEMP   ATEMP   INCLOAD   S
ETLOAD   ACTLOAD   TOTLOAD   MODE"
23050 LOCATE 13,37
23055 PRINT "F1=START SYSTEM# 1       F2=START SYSTEM# 2"
23060 LOCATE 14,37
23065 PRINT "F3=STOP  SYSTEM# 1       F4=STOP  SYSTEM# 2"
23070 LOCATE 15,37
23075 PRINT "F5=DECREASE TEMP 1       F6=DECREASE TEMP 2"
23080 LOCATE 16,37
23085 PRINT "F7=INCREASE TEMP 1       F8=INCREASE TEMP 2"
23090 LOCATE 18,37
23095 PRINT "                    MODE                    "
23100 LOCATE 20,37
23105 PRINT "MON - MONITOR MODE      S/C - STEP COMPLETE"
23110 LOCATE 21,37
23115 PRINT "LOD - CONTROL LOADING   FIN - TEST FINISHED"
```

```
23120 LOCATE 22,37
23125 PRINT "CRP - CONTROL CREEP     OFF - AXIS NOT USED"
23130 LOCATE 23,37
23135 PRINT "CPT - CREEP COMPLETE     *  -  ACTIVE CREEP"
23140 IF ST%(1)=0 THEN M%=37: GOSUB 23200: GOTO 23160
23150 KEY(1) ON: KEY(5) ON: KEY(7) ON: SN%(1)=1: SS%(1)=1
23160 IF ST%(2)=0 THEN M%=62: GOSUB 23200: GOTO 23180
23170 KEY(2) ON: KEY(6) ON: KEY(8) ON: SN%(2)=1: SS%(2)=1
23180 RETURN
23200 '-ERASE F-KEY MENU NOT USED-------------------------+
23210 FOR I%=13 TO 16
23215 LOCATE I%,M%: PRINT "                    "
23220 NEXT I%: RETURN
24000 '-----------------------------------------------------+
24010 ' LOAD TEST PARAMETER SETUP FROM DISK ROUTINE
24020 '-----------------------------------------------------+
24030 CLS: LOCATE 1,1: FILES "A:*.PRM"
24040 LOCATE 20,1
24045 INPUT "ENTER SETUP FILE NAME (DON'T ENTER .PRM)";FPS$
24050 OPEN "A:"+FPS$+".PRM" FOR INPUT AS #1
24060 FOR SY%=1 TO 2: IF ST%(SY%)=0 THEN 24125
24070 INPUT #1,SY%,ST%(SY%)
24075 FOR SN%=1 TO ST%(SY%): FOR AX%=0 TO 2
24080 INPUT #1,LB(SY%,SN%,AX%),FY%(SY%,SN%,AX%): NEXT AX%
24090 INPUT #1,LS%(SY%,SN%): FOR P%=0 TO 5
24100 INPUT #1,IM%(SY%,SN%,P%),IT(SY%,SN%,P%): NEXT P%
24105 NEXT SN%: FOR AX%=0 TO 2
24110 INPUT #1,TZ(SY%,AX%),TB%(SY%,AX%),FC%(SY%,AX%),WD%(SY%
,AX%),WE%(SY%,AX%)
24120 NEXT AX%: INPUT #1,TES(SY%),TT(SY%)
24125 NEXT SY%
24130 FOR D%=6 TO 7: FOR E%=0 TO 15
24135 INPUT #1,LR%(D%,E%),CB(D%,E%): NEXT E%
24140 NEXT D%: CLOSE 1: RETURN
25000 '-----------------------------------------------------+
25010 ' ENTER DATA FILE NAME ROUTINE
25020 '-----------------------------------------------------+
25030 CLS: LOCATE 1,1: FILES "C:\HPTS\DATA\*.PRN"
25040 LOCATE 22,1
25045 PRINT "SYSTEM NUMBER AND EXTENTION .PRN WILL BE AUTOMA
TICALLY ADDED TO DATA FILE NAME"
25050 LOCATE 23,1
25055 PRINT "ENTERING AN EXISTING FILE NAME WILL OVERWRITE T
HE OLD FILE"
25060 LOCATE 20,1
25065 INPUT "ENTER DATA FILE NAME (MAX. 6 CHAR.)";FDD$
25070 IF LEN(FDD$)>6 THEN LOCATE 20,36: PRINT "
        ": GOTO 25060
25080 FD1$="C:\HPTS\DATA\"+FDD$+RIGHT$(STR$(F%),1)+"1.PRN"
25085 OPEN FD1$ FOR OUTPUT AS #1: CLOSE 1
25090 FD2$="C:\HPTS\DATA\"+FDD$+RIGHT$(STR$(F%),1)+"2.PRN"
25095 OPEN FD2$ FOR OUTPUT AS #2: CLOSE 2
25100 RETURN
26000 '-----------------------------------------------------+
```

```
26010 ' PRINT TEST PARAMETER SETUP ROUTINE
26020 '-----------------------------------------------------+
26030 CLS: LOCATE 23,1
26035 PRINT "( MAKE SURE THAT PRINTER IS ON LINE )"
26040 LOCATE 22,1
26045 INPUT "PRINT PARAMETER SETUP TO PRINTER (Y OR N)";Y$
26050 IF Y$="N" OR Y$="n" THEN RETURN
26060 LPRINT "": LPRINT ""
26070 LPRINT "  HPTS - CONTROL TEST PARAMETER SETUP FILE A:"
+FPS$+".PRM";"   DATE = ";DATE$
26080 LPRINT ""
26090 FOR SY%=1 TO 2: IF ST%(SY%)=0 THEN 26340
26100 LPRINT "": LPRINT ""
26105 LPRINT "                                SYSTEM ";SY%
26110 LPRINT ""
26115 LPRINT "- - - - - - - - - - - - - - - - - - - - - - - - +
- - - - - - - - - - - - - - - - -"
26120 FOR SN%=1 TO ST%(SY%): LPRINT "": LPRINT ""
26130 LPRINT "STAGE NUMBER ";SN%: LPRINT"": LPRINT"
                  LOAD/STEP    TOTAL LOAD   STEPS/STAGE  TO
LERANCE% ": LPRINT ""
26140 FOR AX%=0 TO 2
26145 IF FC%(SY%,AX%)=3 THEN LPRINT "AXIS OFF": GOTO 26270
26150 IF AX%=0 AND FC%(SY%,AX%)=0 THEN AX$="PA  (MPa) "
26160 IF AX%=0 AND FC%(SY%,AX%)=1 THEN AX$="DA  (mm)  "
26170 IF AX%=0 AND FC%(SY%,AX%)=2 THEN AX$="VCA (ml)  "
26180 IF AX%=1 AND FC%(SY%,AX%)=0 THEN AX$="PI  (MPa) "
26190 IF AX%=1 AND FC%(SY%,AX%)=1 THEN AX$="IDA (mm)  "
26200 IF AX%=1 AND FC%(SY%,AX%)=2 THEN AX$="VCI (ml)  "
26210 IF AX%=2 AND FC%(SY%,AX%)=0 THEN AX$="PE  (MPa) "
26220 IF AX%=2 AND FC%(SY%,AX%)=1 THEN AX$="ODA (mcST)"
26230 IF AX%=2 AND FC%(SY%,AX%)=2 THEN AX$="VCE (ml)  "
26240 LPRINT "AXIS "AX$, LB(SY%,SN%,AX%),
26250 LPRINT ((LT%(SY%,SN%,AX%)-LR%(WD%(SY%,AX%),WE%(SY%,AX%
)))*CB(WD%(SY%,AX%),WE%(SY%,AX%))),
26260 LPRINT LS%(SY%,SN%) TAB(71) TZ(SY%,AX%)
26270 NEXT AX%: LPRINT ""
26280 LPRINT "NUMBER OF DATA READINGS AT 1,2,5,15,60,120 MIN
UTE INTERVALS :"
26290 ITT=IT(SY%,SN%,0)+IT(SY%,SN%,1)+IT(SY%,SN%,2)+IT(SY%,S
N%,3)+IT(SY%,SN%,4)+IT(SY%,SN%,5)
26300 LPRINT IM%(SY%,SN%,0);IM%(SY%,SN%,1);IM%(SY%,SN%,2);IM
%(SY%,SN%,3);IM%(SY%,SN%,4);IM%(SY%,SN%,5);"     TOTAL CREEP
 TIME (min) =";ITT
26305 NEXT SN%
26310 LPRINT "": LPRINT ""
26315 LPRINT "STARTING EXTERNAL (CELL) TEMPERATURE";TES(SY%)
"Deg C  TEMPERATURE TOLERANCE";TT(SY%)"Deg C"
26320 LPRINT ""
26325 LPRINT ""
26330 LPRINT CHR$(13) CHR$(13)
26340 NEXT SY%: RETURN
27000 '-----------------------------------------------------+
27010 ' ENTER STARTING EXTERNAL (CELL) TEMPERATURE ROUTINE
```

```
27020 '-----------------------------------------------------+
27030 LOCATE 2,1
27035 PRINT "ENTER STARTING ENTERNAL (CELL) TEMPERATURE OF S
YSTEM #"SY%"(0 TO 80 Deg C - 0 WILL DISABLE TEMPERATURE CONT
ROL)": INPUT;TES(SY%)
27040 IF TES(SY%)<0 OR TES(SY%)>80 THEN LOCATE 4,1: PRINT "
       ": GOTO 27030
27050 TES%(SY%)=CINT(TES(SY%)/CS(SY%,15))
27055 IF TES(SY%)=0 THEN 27080
27060 LOCATE 5,1
27065 PRINT "ENTER EXTERNAL (CELL) TEMPERATURE CONTROL TOLER
ANCE (0.1 TO 5 Deg C)": INPUT;TT(SY%)
27070 IF TT(SY%)<0.1 OR TT(SY%)>5 THEN LOCATE 6,1: PRINT "
       ": GOTO 27060
27080 RETURN
28000 '-----------------------------------------------------+
28010 ' SELECT CONTROL TRANSDUCER FOR EACH AXIS ROUTINE
28020 '-----------------------------------------------------+
28030 CLS: PRINT "SELECT CONTROL TRANSDUCER FOR EACH AXIS (E
NTERING 'OFF' WILL DISABLE THE AXIS)."
28040 IF SY%=2 THEN 28230
28050 LOCATE 4,1
28055 INPUT "ENTER (PA OR DA OR VCA) FOR AXIAL AXIS, SYSTEM
#1";AW$
28060 IF AW$="PA" OR AW$="pa" THEN FC%(1,0)=0: WD%(1,0)=7: W
E%(1,0)=0: GOTO 28110
28070 IF AW$="DA" OR AW$="da" THEN FC%(1,0)=1: WD%(1,0)=6: W
E%(1,0)=3: GOTO 28110
28080 IF AW$="VCA" OR AW$="vca" THEN FC%(1,0)=2: WD%(1,0)=6:
 WE%(1,0)=0: GOTO 28110
28090 IF AW$="OFF" OR AW$="off" THEN FC%(1,0)=3: GOTO 28110
28100 LOCATE 4,51: PRINT "                    ": GOTO 28050
28110 LOCATE 6,1
28115 INPUT "ENTER (PI OR IDA OF VCI) FOR INTERNAL (BORE) AX
IS, SYSTEM #1";AW$
28120 IF AW$="PI" OR AW$="pi" THEN FC%(1,1)=0: WD%(1,1)=7: W
E%(1,1)=1: GOTO 28170
28130 IF AW$="IDA" OR AW$="ida" THEN FC%(1,1)=1: WD%(1,1)=7:
 WE%(1,1)=3: GOTO 28170
28140 IF AW$="VCI" OR AW$="vci" THEN FC%(1,1)=2: WD%(1,1)=6:
 WE%(1,1)=1: GOTO 28170
28150 IF AW$="OFF" OR AW$="off" THEN FC%(1,1)=3: GOTO 28170
28160 LOCATE 6,61: PRINT "                    ": GOTO 28110
28170 LOCATE 8,1
28175 INPUT "ENTER (PE OR ODA OR VCE) FOR EXTERNAL (CELL) AX
IS, SYSTEM #1";AW$
28180 IF AW$="PE" OR AW$="pe" THEN FC%(1,2)=0: WD%(1,2)=7: W
E%(1,2)=2: GOTO 28410
28190 IF AW$="ODA" OR AW$="oda" THEN FC%(1,2)=1: WD%(1,2)=7:
 WE%(1,2)=5: GOTO 28410
28200 IF AW$="VCE" OR AW$="vce" THEN FC%(1,2)=2: WD%(1,2)=6:
 WE%(1,2)=2: GOTO 28410
28210 IF AW$="OFF" OR AW$="off" THEN FC%(1,2)=3: GOTO 28410
28220 LOCATE 8,61: PRINT "                    ": GOTO 28170
```

```
28230 LOCATE 4,1
28235 INPUT "ENTER (PA OR DA OR VCA) FOR AXIAL AXIS, SYSTEM
#2";AW$
28240 IF AW$="PA" OR AW$="pa" THEN FC%(2,0)=0: WD%(2,0)=7: W
E%(2,0)=8: GOTO 28290
28250 IF AW$="DA" OR AW$="da" THEN FC%(2,0)=1: WD%(2,0)=6: W
E%(2,0)=7: GOTO 28290
28260 IF AW$="VCA" OR AW$="vca" THEN FC%(2,0)=2: WD%(2,0)=6:
 WE%(2,0)=4: GOTO 28290
28270 IF AW$="OFF" OR AW$="off" THEN FC%(2,0)=3: GOTO 28290
28280 LOCATE 4,51: PRINT "                    ": GOTO 28230
28290 LOCATE 6,1
28295 INPUT "ENTER (PI OR IDA OR VCI) FOR INTERNAL (BORE) AX
IS, SYSTEM #2";AW$
28300 IF AW$="PI" OR AW$="pi" THEN FC%(2,1)=0: WD%(2,1)=7: W
E%(2,1)=9: GOTO 28350
28310 IF AW$="IDA" OR AW$="ida" THEN FC%(2,1)=1: WD%(2,1)=7:
 WE%(2,1)=11: GOTO 28350
28320 IF AW$="VCI" OR AW$="vci" THEN FC%(2,1)=2: WD%(2,1)=6:
 WE%(2,1)=5: GOTO 28350
28330 IF AW$="OFF" OR AW$="off" THEN FC%(2,1)=3: GOTO 28350
28340 LOCATE 6,61: PRINT "                    ": GOTO 28290
28350 LOCATE 8,1
28355 INPUT "ENTER (PE OR ODA OR VCE) FOR EXTERNAL (CELL) AX
IS, SYSTEM #2";AW$
28360 IF AW$="PE" OR AW$="pe" THEN FC%(2,2)=0: WD%(2,2)=7: W
E%(2,2)=10: GOTO 28410
28370 IF AW$="ODA" OR AW$="oda" THEN FC%(2,2)=1: WD%(2,2)=7:
 WE%(2,2)=13: GOTO 28410
28380 IF AW$="VCE" OR AW$="vce" THEN FC%(2,2)=2: WD%(2,2)=6:
 WE%(2,2)=6: GOTO 28410
28390 IF AW$="OFF" OR AW$="off" THEN FC%(2,2)=3: GOTO 28410
28400 LOCATE 8,61: PRINT "                    ": GOTO 28350
28410 LOCATE 20,1
28415 INPUT "ARE THE ABOVE INPUTS CORRECT (Y OR N)";Y$
28420 IF Y$="N" OR Y$="n" THEN 28030
28430 RETURN
29000 '-----------------------------------------------------+
29010 ' INITIALIZE TRANSDUCER READING ROUTINE
29020 '-----------------------------------------------------+
29030 CLS: INPUT "INITIALIZE TRANSDUCERS (Y OR N)";Y$
29040 IF Y$="N" OR Y$="n" THEN RETURN
29050 CLS: INPUT "ARE TRANSDUCERS READY TO BE INITIALIZED (Y
 OR N)";Y$
29060 IF Y$="N" OR Y$="n" THEN 29050
29070 GOSUB 6000  'LOW SPEED DATA LOGGING
29080 FOR D%=6 TO 7: FOR E%=0 TO 15
29090 LR%(D%,E%)=AV%(D%,E%): NEXT E%: NEXT D%: RETURN
30000 '-----------------------------------------------------+
30010 ' ENTER TEST PARAMETER SETUP ROUTINE
30020 '-----------------------------------------------------+
30030 PRINT "*********************************************
*****************"
30040 PRINT "*********************************************
```

```
*****************"
30050 PRINT " ": PRINT " "
30060 PRINT "     HHH    HHH   PPPPPPPPP     TTTTTTTTTTT
  SSSSSSS"
30070 PRINT "     HHH    HHH   PPPPPPPPPP    TTTTTTTTTTT
SSSS   SSS"
 30080 PRINT "     HHH    HHH   PPP     PPP   TTTTTTTTTTT
S
SSS"
30090 PRINT "     HHHHHHHHHH   PPP     PPP       TTT
SSSSSS"
30100 PRINT "     HHHHHHHHHH   PPPPPPPPPP        TTT
    SSSSSSS"
30110 PRINT "     HHHHHHHHHH   PPPPPPPPP         TTT
        SSSS"
30120 PRINT "     HHH    HHH   PPP               TTT
         SSSS"
30130 PRINT "     HHH    HHH   PPP               TTT       S
SSS     SSSS"
30140 PRINT "     HHH    HHH   PPP               TTT
SSSSSSSSSSS"
30150 PRINT " ": LOCATE 15,45: PRINT "by R.GITZEL & A.ASSIS"
30160 PRINT "*********************************************
*****************"
30170 PRINT "*********************************************
*****************"
30180 PRINT " "
30185 PRINT "FOR QUESTIONS (Y OR N)?, ALL ANSWERS OTHER THAN
 (n OR N) ARE ASSUMED AS YES."
30190 LOCATE 21,1
30195 INPUT "ENTER TEST PARAMETER SETUP FROM DISK OR KEYBOAR
D (D OR K)";Y$
30200 IF Y$="k" OR Y$="K" THEN 30300
30210 IF Y$="d" OR Y$="D" THEN 30400
30220 LOCATE 21,59: PRINT "                ": GOTO 30190
30300 '-TEST PARAMETER SETUP FROM KEYBOARD----------------+
30310 GOSUB 29050  'INITIALIZE TRANSDUCER READINGS
30320 GOSUB 31000  'ENTER TEST PARAMETER SETUP FROM KEYBOARD
30330 GOSUB 22000  'SAVE TEST PARAMETER SETUP
30340 GOTO  30500  'GO TO STARTING ROUTINES
30400 '-TEST PARAMETER SETUP FROM DISK--------------------+
30410 GOSUB 24000  'LOAD TEST PARAMETER SETUP FROM DISK
30420 GOSUB 29000  'INITIALIZE TRANSDUCER READINGS
30430 GOSUB 22080  'SAVE TEST PARAMETER SETUP
30440 GOSUB 35000  'RECALCULATE TEST LOAD PARAMETERS
30500 RETURN       'GO TO STARTING ROUTINES
31000 '-----------------------------------------------------+
31010 ' ENTER TEST PARAMETER SETUP FROM KEYBOARD ROUTINE
31020 '-----------------------------------------------------+
31030 CLS: LOCATE 1,1
31035 INPUT "ENTER LOADING DATA FOR SYSTEM #1 (Y OR N)";Y$
31040 IF Y$="n" OR Y$="N" THEN 31550
31050 SY%=1: SN%=1
31060 GOSUB 28000  'SELECT CONTROL TRANSDUCERS
```

```
31070 FOR AX%=0 TO 2: IF FC%(SY%,AX%)=3 THEN 31090
31080 LT%(SY%,0,AX%)=LR%(WD%(SY%,AX%),WE%(SY%,AX%))
31085 LT(SY%,0,AX%)=0
31090 NEXT AX%
31100 CLS: LOCATE 1,1
31105 PRINT "ENTERING LOADING DATA FOR SYSTEM #"SY%
31110 LOCATE 2,1: PRINT ""
31120 LOCATE 3,1
31125 PRINT "ENTER THE NUMBER OF DATA READINGS AT EACH OF TH
E FOLLOWING INTERVAL TIMES" CHR$(13) "IN STAGE"SN%"(1,2,5,15
,60,120 MINS):"
31130 LOCATE 5,1
31140 INPUT;IM%(SY%,SN%,0),IM%(SY%,SN%,1),IM%(SY%,SN%,2),IM%
(SY%,SN%,3),IM%(SY%,SN%,4),IM%(SY%,SN%,5)
31150 FOR P%=0 TO 5
31160 IT(SY%,SN%,P%)=IM%(SY%,SN%,P%)*IC%(P%): NEXT P%
31170 LOCATE 7,1
31175 PRINT "ENTER NUMBER OF LOADING STEPS FOR SYSTEM"SY%",S
TAGE"SN%"(MAX 25):": INPUT;LS%(SY%,SN%)
31180 PRINT ""
31185 IF LS%(SY%,SN%)<1 OR LS%(SY%,SN%)>25 THEN LOCATE 8,1:
PRINT "                ": GOTO 31170
31190 FOR AX%=0 TO 2
31195 IF FC%(SY%,AX%)=3 THEN FY%(SY%,SN%,AX%)=1: GOTO 31420
31200 IF FC%(SY%,AX%)=1 THEN 31260
31210 IF FC%(SY%,AX%)=2 THEN 31310
31220 IF AX%=0 THEN AX$=" PA ": LOCATE 12,1: PRINT "
     ": LOCATE 10,1
31230 IF AX%=1 THEN AX$=" PI ": LOCATE 14,1: PRINT "
     ": LOCATE 14,1
31240 IF AX%=2 THEN AX$=" PE ": LOCATE 20,1: PRINT "
     ": LOCATE 18,1
31250 PRINT "ENTER TOTAL LOAD IN (MPa) OF SYSTEM#"SY%",STAGE
#"SN%",AXIS#"AX$: GOTO 31350
31260 IF AX%=0 THEN AX$=" DA ": LOCATE 12,1: PRINT "
     ": LOCATE 10,1: GOTO 31300
31270 IF AX%=1 THEN AX$=" IDA ": LOCATE 14,1: PRINT "
     ": LOCATE 14,1: GOTO 31300
31280 IF AX%=2 THEN AX$=" ODA ": LOCATE 20,1: PRINT "
     ": LOCATE 18,1
31290 PRINT "ENTER TOTAL DEFORMATION IN (MICROSTRAIN) OF SYS
TEM#"SY%",STAGE#"SN%",AXIS#"AX$: GOTO 31350
31300 PRINT "ENTER TOTAL DISPLACEMENT IN (mm) OF SYSTEM#"SY%
",STAGE#"SN%",AXIS#"AX$: GOTO 31350
31310 IF AX%=0 THEN AX$=" VCA ": LOCATE 12,1: PRINT "
     ": LOCATE 10,1
31320 IF AX%=1 THEN AX$=" VCI ": LOCATE 14,1: PRINT "
     ": LOCATE 14,1
31330 IF AX%=2 THEN AX$=" VCE ": LOCATE 20,1: PRINT "
     ": LOCATE 18,1
31340 PRINT "ENTER TOTAL VOLUME CHANGE IN (ml) OF SYSTEM#"SY
%",STAGE#"SN%",AXIS#"AX$
31350 IF SN%>1 THEN PRINT "": GOTO 31370
31360 PRINT "(MAX="((2048-LR%(WD%(SY%,AX%),WE%(SY%,AX%)))*CB
```

```
(WD%(SY%,AX%),WE%(SY%,AX%)))"AND MIN="((-2048-LR%(WD%(SY%,AX
%),WE%(SY%,AX%)))*CB(WD%(SY%,AX%),W E%(SY%,AX%)))")"
31370 INPUT;LL: LOCATE 22,1
31375 PRINT "                                                  "
31380 LB(SY%,SN%,AX%)=LL/LS%(SY%,SN%)
31390 LC%(SY%,SN%,AX%)=CINT((LT(SY%,(SN%-1),AX%)+LB(SY%,SN%,
AX%))/CB(WD%(SY%,AX%),WE%(SY%,AX%)))+LR%(WD%(SY%,AX%),WE%(SY
%,AX%))
31400 LT(SY%,SN%,AX%)=LB(SY%,SN%,AX%)*LS%(SY%,SN%)+LT(SY%,(S
N%-1),AX%)
31405 LT%(SY%,SN%,AX%)=CINT(LT(SY%,SN%,AX%)/CB(WD%(SY%,AX%),
WE%(SY%,AX%)))+LR%(WD%(SY%,AX%),WE%(SY%,AX%))
31410 IF LT%(SY%,SN%,AX%)>2047 OR LT%(SY%,SN%,AX%)<-2048 THE
N LOCATE 22,1: PRINT " LOAD OUT OF RANGE - REENTER VALUE": G
OTO 31200
31420 NEXT AX%
31430 LOCATE 22,1
31435 INPUT "ARE THE ABOVE INPUTS CORRECT (Y OR N)";Y$
31440 IF Y$="N" OR Y$="n" THEN 31100
31450 LOCATE 22,38: PRINT "                    "
31460 LOCATE 22,1
31465 INPUT "ENTER ANOTHER STAGE (MAX 25) (Y OR N)";Y$
31470 IF Y$="N" OR Y$="n" THEN 31510
31480 SN%=SN%+1
31490 IF SN%>25 THEN 31510
31500 CLS: GOTO 32000  'STAGE DUPLICATION
31510 CLS: ST%(SY%)=SN%: IF SN%>25 THEN ST%(SY%)=25
31520 CLS: GOSUB 33000  'ENTER CONTROL TOLERANCE
31530 CLS: GOSUB 27000  'ENTER CELL TEMPERATURE
31540 IF SY%=2 THEN RETURN
31550 CLS: LOCATE 1,1
31555 INPUT "ENTER LOADING DATA FOR SYSTEM #2 (Y OR N)";Y$
31560 IF Y$="N" OR Y$="n" THEN RETURN
31570 SY%=2: SN%=1: GOTO 31060
32000 '-STAGE DUPLICATION ROUTINE-------------------------+
32010 LOCATE 1,1
32020 PRINT "SYSTEM #"SY%; "     CURRENT STAGE # ="SN%
32030 LOCATE 3,1
32040 INPUT "WOULD YOU LIKE TO DUPLICATE THE LAST STAGE (Y O
R N)";Y$
32050 IF Y$="N" OR Y$="n" THEN 31100
32060 CLS: GOTO 32080
32070 IF SN%>25 THEN 31510
32080 LOCATE 1,1
32085 PRINT "SYSTEM# "SY%; "     STAGE#= "SN%" DUPLICATED
32090 FOR P%=0 TO 5: IM%(SY%,SN%,P%)=IM%(SY%,(SN%-1),P%)
32100 IT(SY%,SN%,P%)=IM%(SY%,SN%,P%)*IC%(P%): NEXT P%
32110 LS%(SY%,SN%)=LS%(SY%,(SN%-1))
32120 FOR AX%=0 TO 2
32125 IF FC%(SY%,AX%)=3 THEN FY%(SY%,SN%,AX%)=1: GOTO 32180
32130 LB(SY%,SN%,AX%)=LB(SY%,(SN%-1),AX%)
32140 LC%(SY%,SN%,AX%)=CINT((LB(SY%,SN%,AX%)+LT(SY%,(SN%-1),
AX%))/CB(WD%(SY%,AX%),WE%(SY,AX%)))+LR%(WD%(SY%,AX%),WE%(SY%
,AX%))
```

```
32150 LT(SY%,SN%,AX%)=LB(SY%,SN%,AX%)*LS%(SY%,SN%)+LT(SY%,(S
N%-1),AX%)
32160 LT%(SY%,SN%,AX%)=CINT(LT(SY%,SN%,AX%)/CB(WD%(SY%,AX%),
WE%(SY%,AX%)))+LR%(WD%(SY%,AX%),WE%(SY%,AX%))
32170 IF LT%(SY%,SN%,AX%)>2047 OR LT%(SY%,SN%,AX%)<-2048 THE
N LOCATE 22,1: PRINT " LOAD OUT OF RANGE - REENTER STAGE": G
OTO 31100
32180 NEXT AX%
32190 LOCATE 3,1
32195 INPUT "DUPLICATE ANOTHER STAGE (Y OR N)";Y$
32200 IF Y$="N" OR Y$="n" THEN 32220
32210 SN%=SN%+1: CLS: GOTO 32070
32220 LOCATE 22,1
32225 INPUT "ENTER ANOTHER STAGE (Y OR N)";Y$
32230 IF Y$="N" OR Y$="n" THEN 31510
32240 SN%=SN%+1: IF SN%>25 THEN 31510
32250 GOTO 31100
33000 '-----------------------------------------------------+
33010 ' ENTER CONTROL TOLERANCE ROUTINE
33020 '-----------------------------------------------------+
33030 FOR AX%=0 TO 2: IF FC%(SY%,AX%)=3 THEN 33110
33040 IF AX%=0 THEN AX$=" AXIAL "
33050 IF AX%=1 THEN AX$=" INTERNAL (BORE) "
33060 IF AX%=2 THEN AX$=" EXTERNAL (CELL) "
33[illegible] LOCATE 22,1
33[illegible] PRINT "ENTER TOLERANCE IN (%) FOR SYSTEM #"SY%","AX$"A
XI
33[illegible] INPUT;TL
33[illegible] TZ(SY%,AX%)=TL: TB%(SY%,AX%)=INT((TL/100)*4096)
33[illegible] LOCATE 23,1: PRINT "                    "
33[illegible] IF TL<0 OR TL>100 THEN 33070
33[illegible] NEXT AX%: RETURN
34000 '-----------------------------------------------------+
34010 ' START SYSTEM ROUTINE
34020 '-----------------------------------------------------+
34030 CLS: LOCATE 10,1
34040 PRINT "THE SYSTEM IS  NOW  READY  TO  BE  STARTED."
34045 PRINT ""
34050 PRINT "TEMPERATURE CONTROL WILL START AND CONTROL"
34060 PRINT "VALUES  WILL  BE  DISPLAYED ON THE  SCREEN."
34065 PRINT ""
34070 PRINT "CONTROL OF THE SYSTEM  IS STARTED WITH THE"
34080 INPUT "FUNCTION KEYS. ->PRESS ENTER KEY TO START ";J$
34090 RETURN
35000 '-----------------------------------------------------+
35010 ' RECALCULATE TEST LOAD PARAMETER ROUTINE
35020 '-----------------------------------------------------+
35030 FOR SY%=1 TO 2: FOR AX%=0 TO 2
35040 IF FC%(SY%,AX%)=3 THEN FY%(SY%,0,AX%)=1: GOTO 35060
35050 LT%(SY%,0,AX%)=LR%(WD%(SY%,AX%),WE%(SY%,AX%))
35055 LT(SY%,0,AX%)=0
35060 NEXT AX%: NEXT SY%
35065 FOR SY%=1 TO 2: FOR SN%=1 TO ST%(SY%): FOR AX%=0 TO 2
35070 IF FC%(SY%,AX%)=3 THEN 35110
```

```
35080 LC%(SY%,SN%,AX%)=CINT((LB(SY%,SN%,AX%)+LT(SY%,(SN%-1),
AX%))/CB(WD%(SY%,AX%),WE%(SY%,AX%)))+LR%(WD%(SY%,AX%),WE%(SY
%,AX%))
35090 LT(SY%,SN%,AX%)=LB(SY%,SN%,AX%)*LS%(SY%,SN%)+LT(SY%,(S
N%-1),AX%)
35100 LT%(SY%,SN%,AX%)=CINT(LT(SY%,SN%,AX%)/CB(WD%(SY%,AX%),
WE%(SY%,AX%)))+LR%(WD%(SY%,AX%),WE%(SY%,AX%))
35110 NEXT AX%: NEXT SN%: NEXT SY%: RETURN
```

Table C.1 Electronic instrument parameters

Instrum. Name	System	Axis	DASH-8 Port	EXP-16 Gain	EXP-16 Channel	HPTSCAL Channel
VCA1	1	AXIAL	6	1	0	0
VCI1	1	BORE	6	1	1	1
VCE1	1	CELL	6	1	2	2
DA1	1	AXIAL	6	1	3	3
VCA2	2	AXIAL	6	1	4	4
VCI2	2	BORE	6	1	5	5
VCE2	2	CELL	6	1	6	6
DA2	2	AXIAL	6	1	7	7
LVDT0	1		6	1	8	8
LVDT1	1		6	1	9	9
LVDT2	1		6	1	10	10
LVDT3	1		6	1	11	11
LVDT4	2		6	1	12	12
LVDT5	2		6	1	13	13
LVDT6	2		6	1	14	14
LVDT7	2		6	1	15	15
PA1	1	AXIAL	7	100	0	16
PI1	1	BORE	7	100	1	17
PE1	1	CELL	7	100	2	18
IDA1	1	BORE	7	100	3	19
IDB1	1	BORE	7	100	4	20
ODA1	1	CELL	7	100	5	21
TI1	1	BORE	7	100	6	22
TE1	1	CELL	7	100	7	23
PA2	2	AXIAL	7	100	8	24
PI2	2	BORE	7	100	9	25
PE2	2	CELL	7	100	10	26
IDA2	2	BORE	7	100	11	27
IDB2	2	BORE	7	100	12	28
ODA2	2	CELL	7	100	13	29
TI2	2	BORE	7	100	14	30
TE2	2	CELL	7	100	15	31

NOTE ON THE INSTRUMENT NAMES

VC ... volume change device
P ... pressure transducer
D ... LVDT for axial displacement
ID ... bore convergence device
OD ... specimen diameter deformation device
T ... thermocouple or RTD

Table C.2 Files and routines contained in the disk drives

DISK A	DISK B	DISK C	
HPTS#1	HPTS#2	\HPTS	\HPTS\DATA
COMMAND.COM USERLIB.EXE BRUN30.EXE DASH8.ADR DASH8.BIN HPTSCAL.EXE HPTSCON.EXE CONFACT.DFN *.PRM	used for dumping datafiles from directory C:\HPTS\DATA during tests	HPTS.EXE DASH8.BIN DASH8.ADR	datafiles for Systems 1 and 2 *1.PRN *2.PRN

NOTE:

*.PRM ... test parameter setup files
*1.PRN ... datafiles for System 1
*2.PRN ... datafiles for System 2

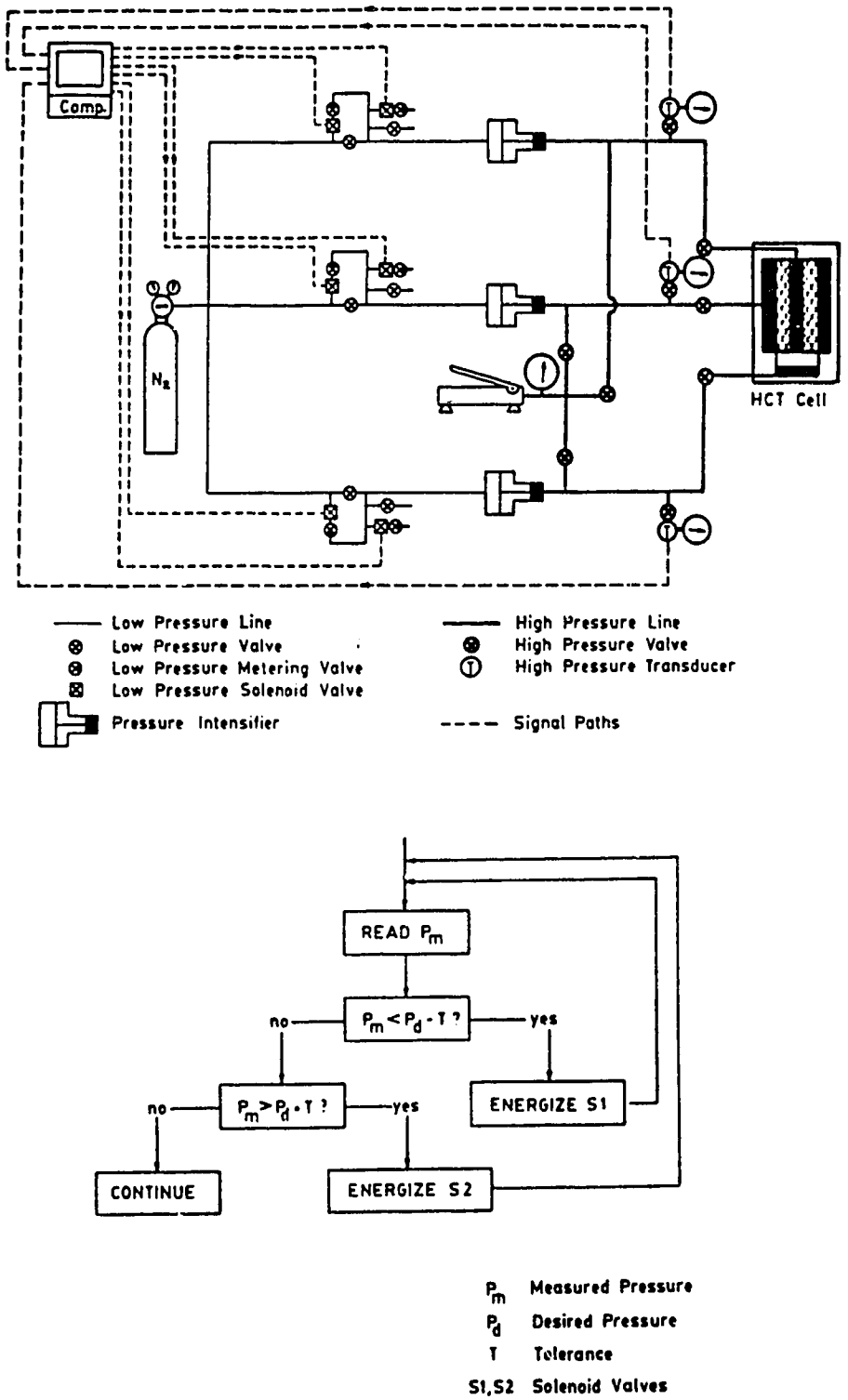

Figure C.1 Pressure and control system (modified after Maloney, 1986)

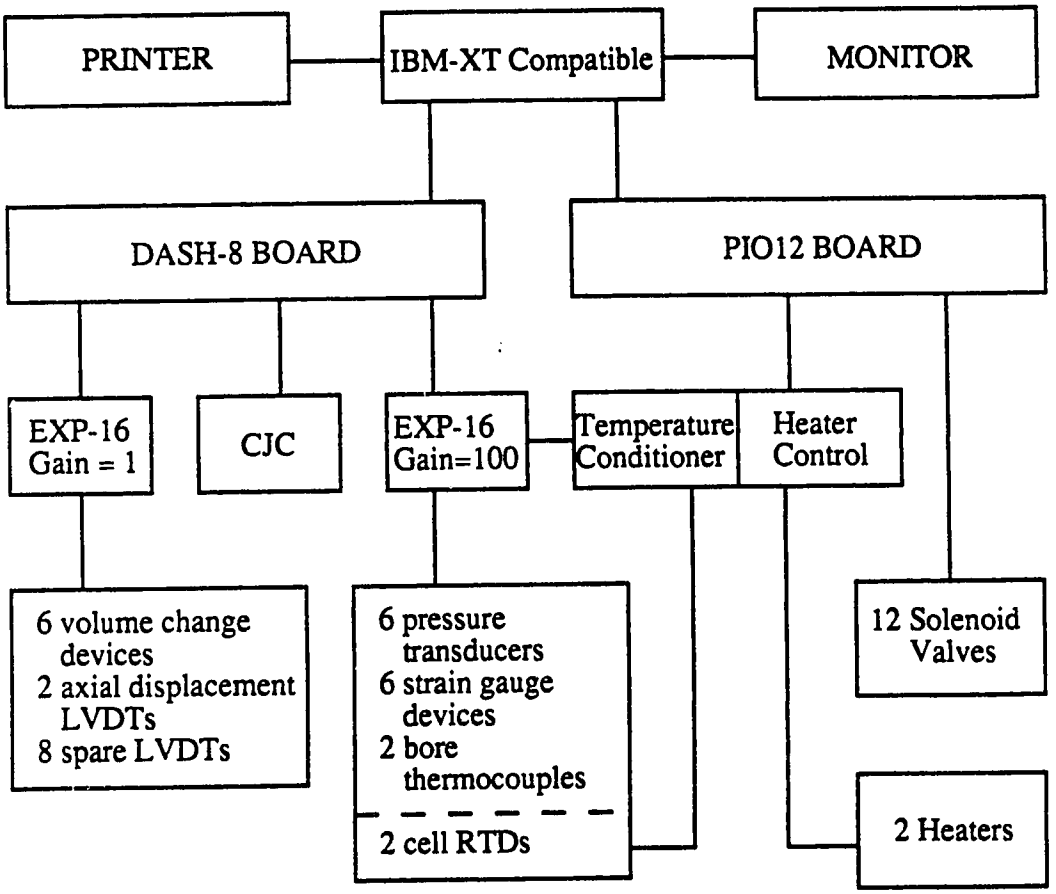

Figure C.2 Hardware layout

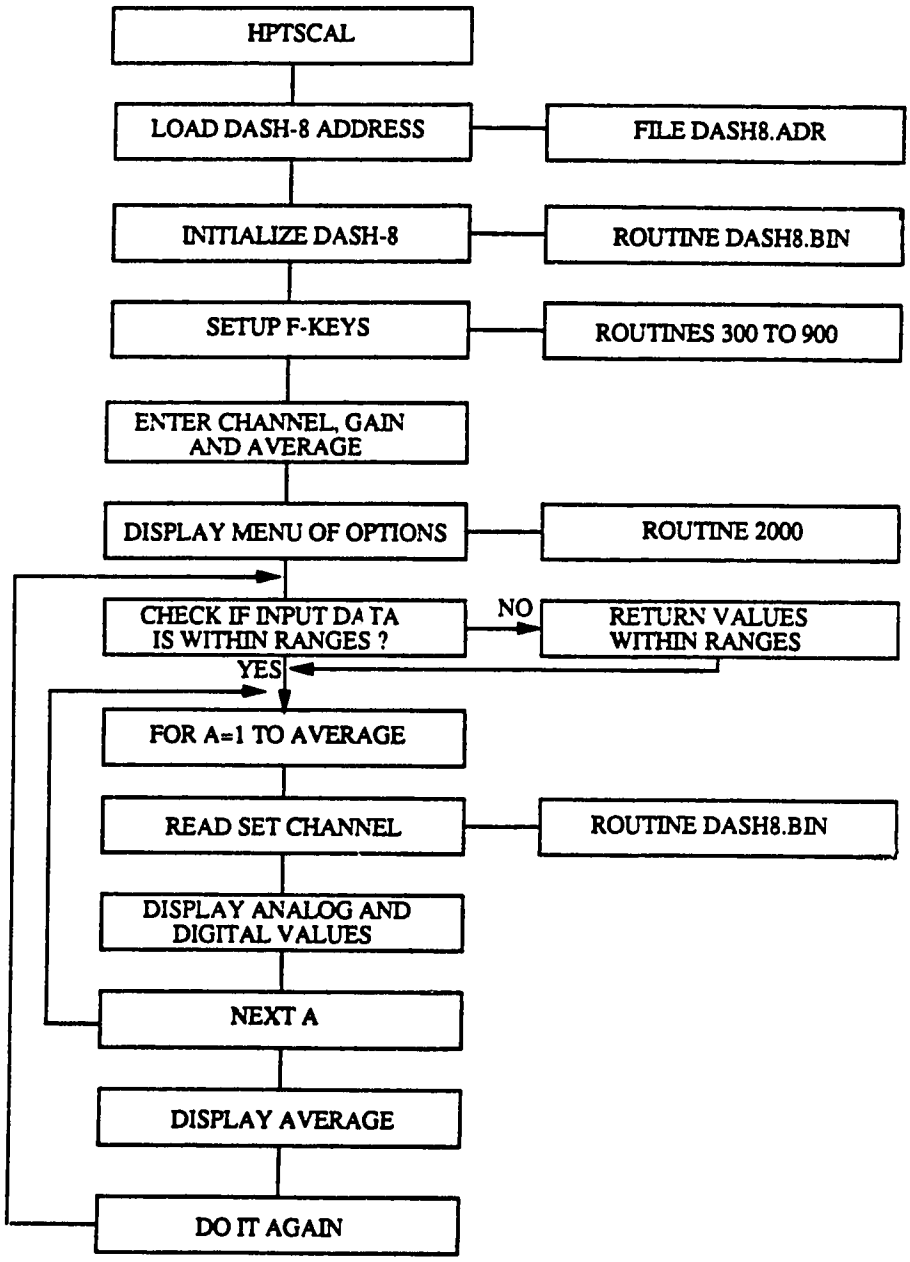

Figure C.3 Flow chart for Program HPTSCAL

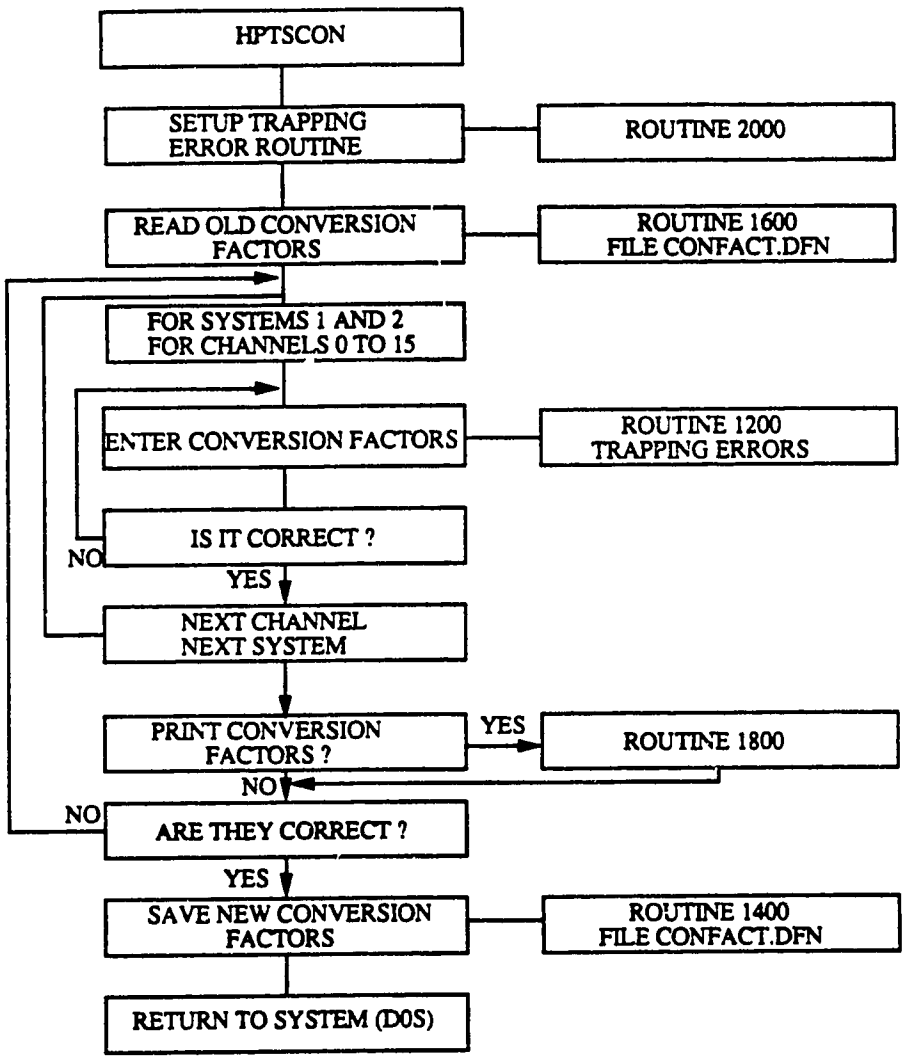

Figure C.4 Flow chart for Program HPTSCON

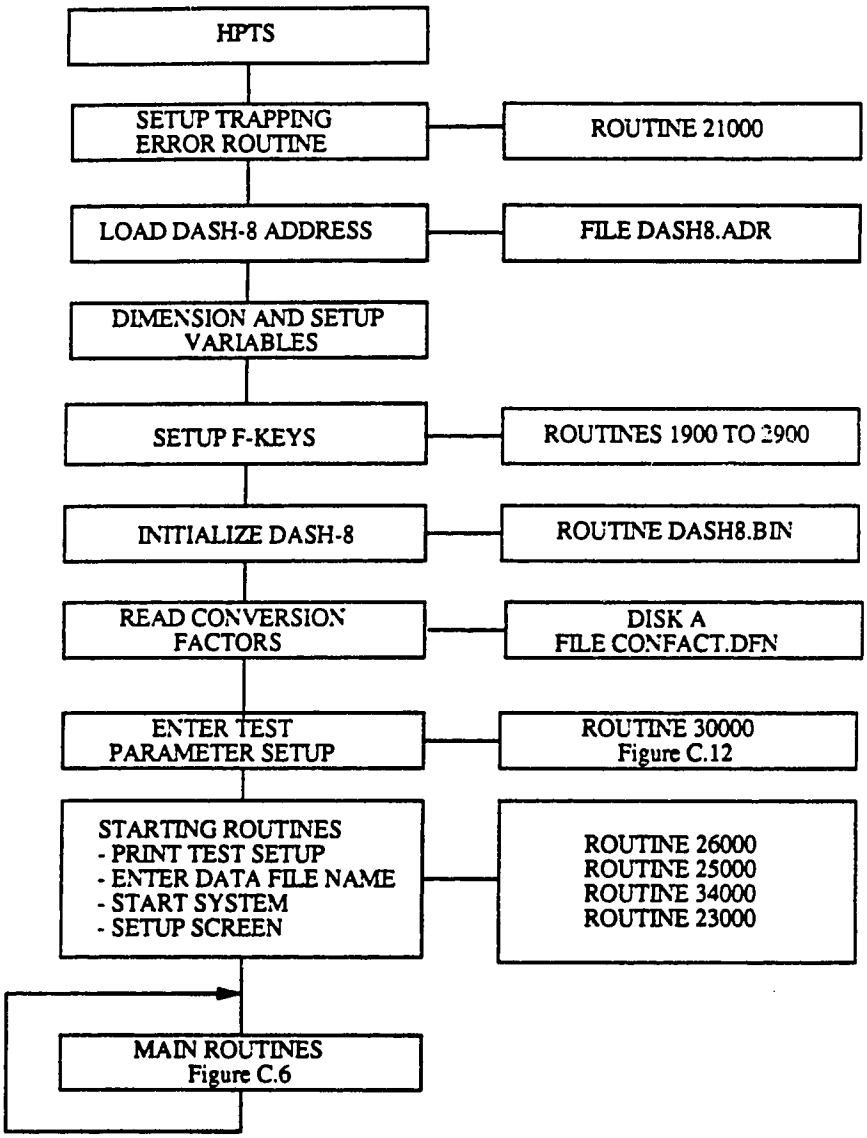

Figure C.5 Flow chart for Program HPTS

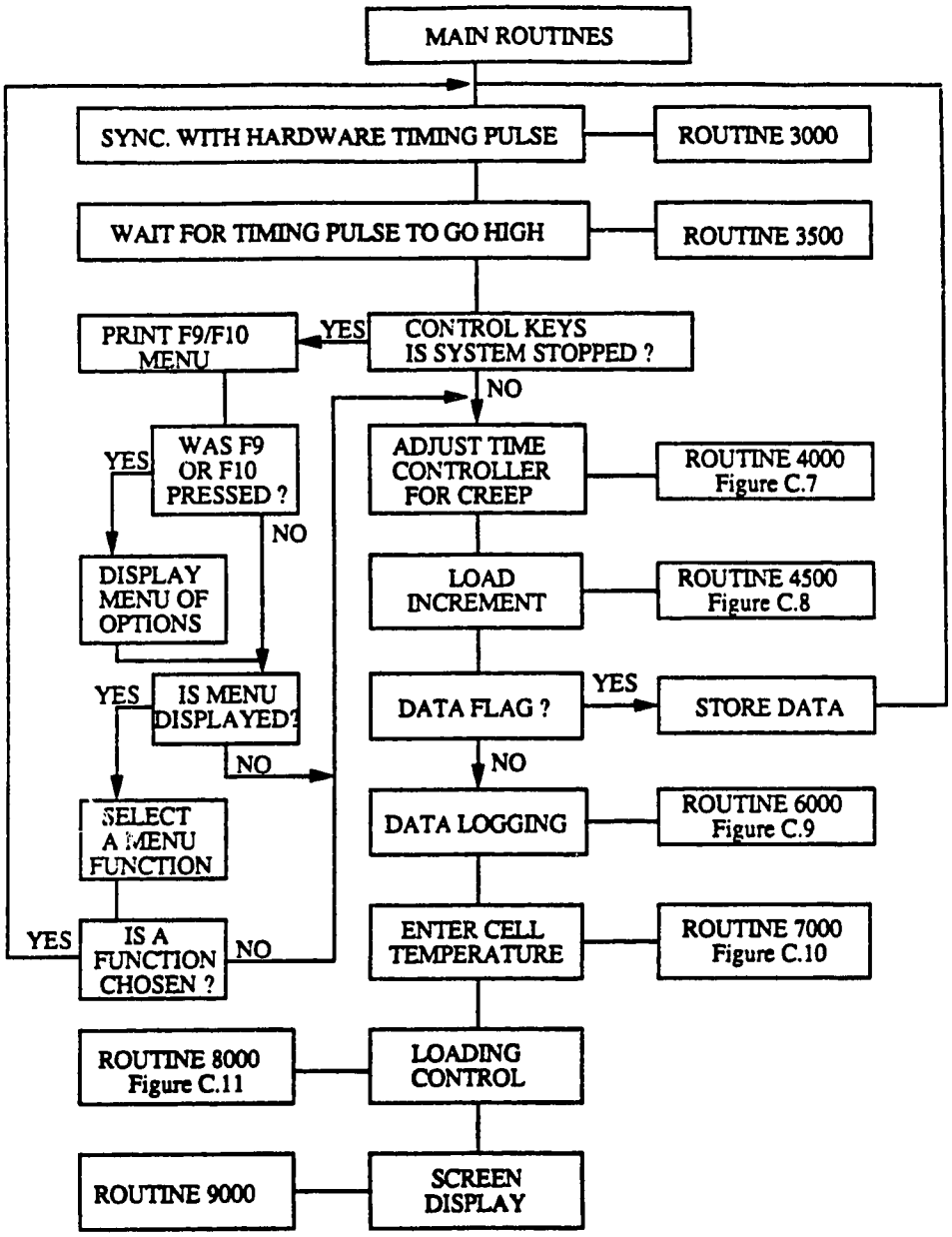

Figure C.6 Program HPTS - Flow chart for the main routines

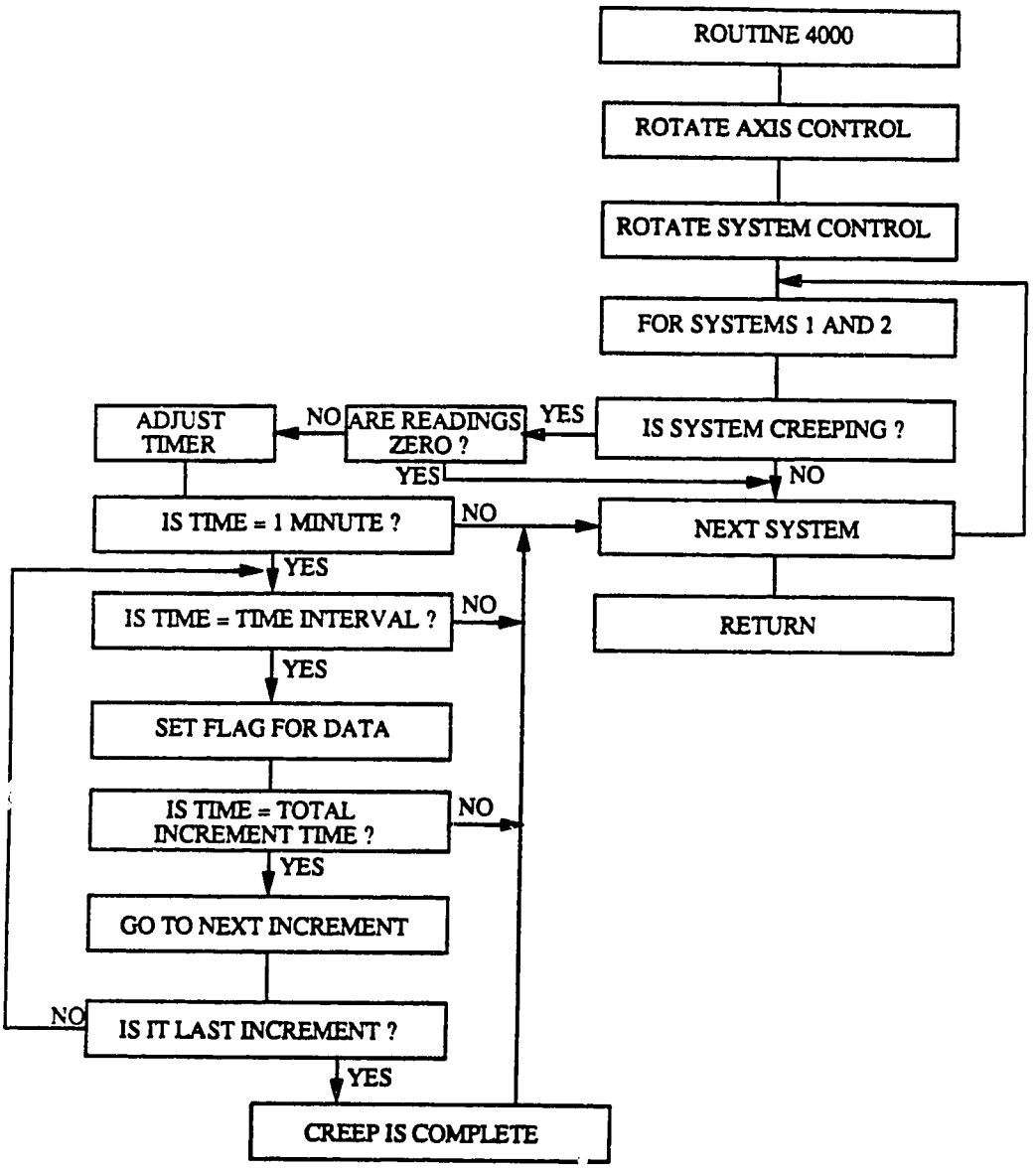

Figure C.7 Program HPTS - Flow chart for Routine 4000

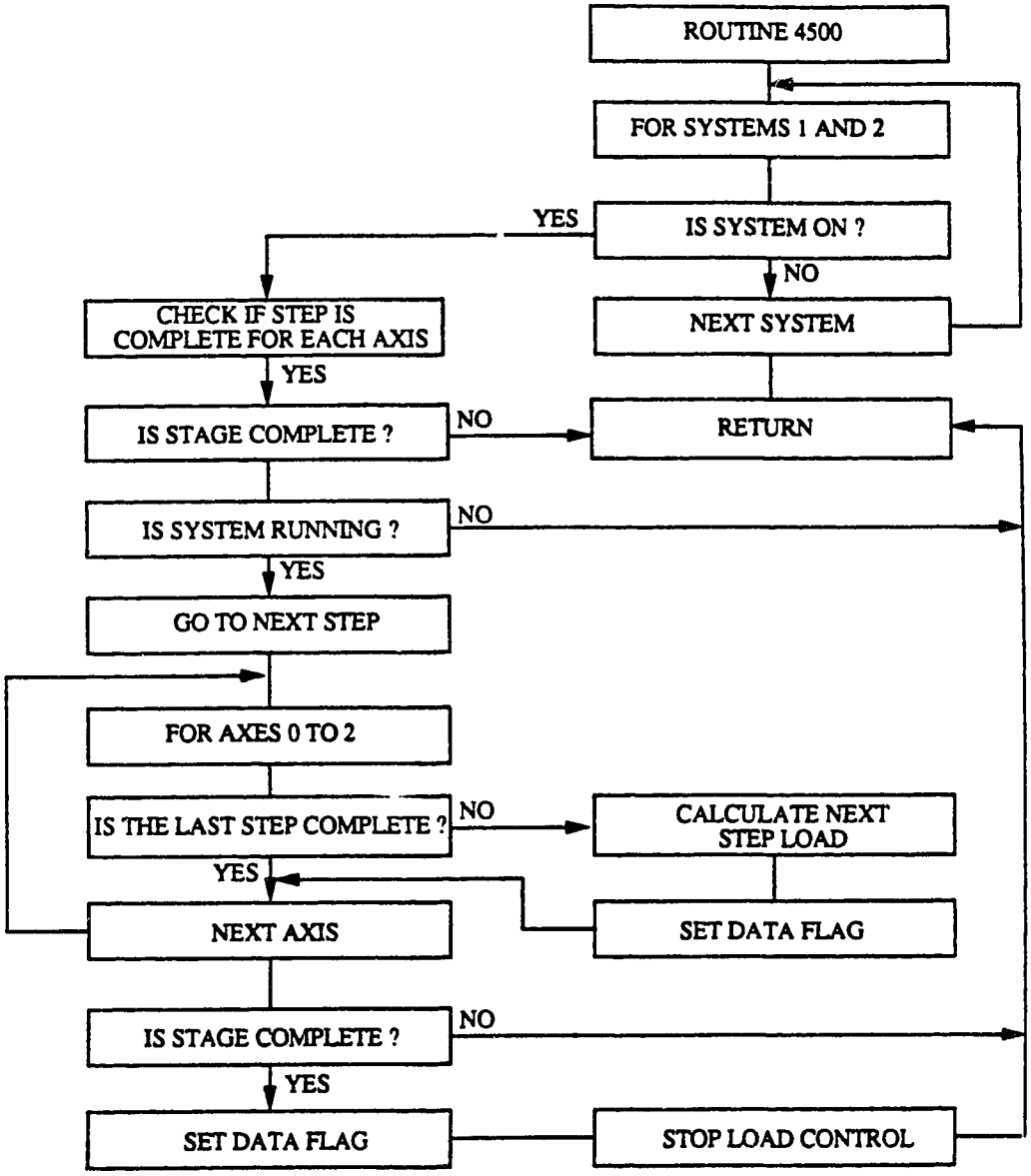

Figure C.8 Program HPTS - Flow chart for Routine 4500

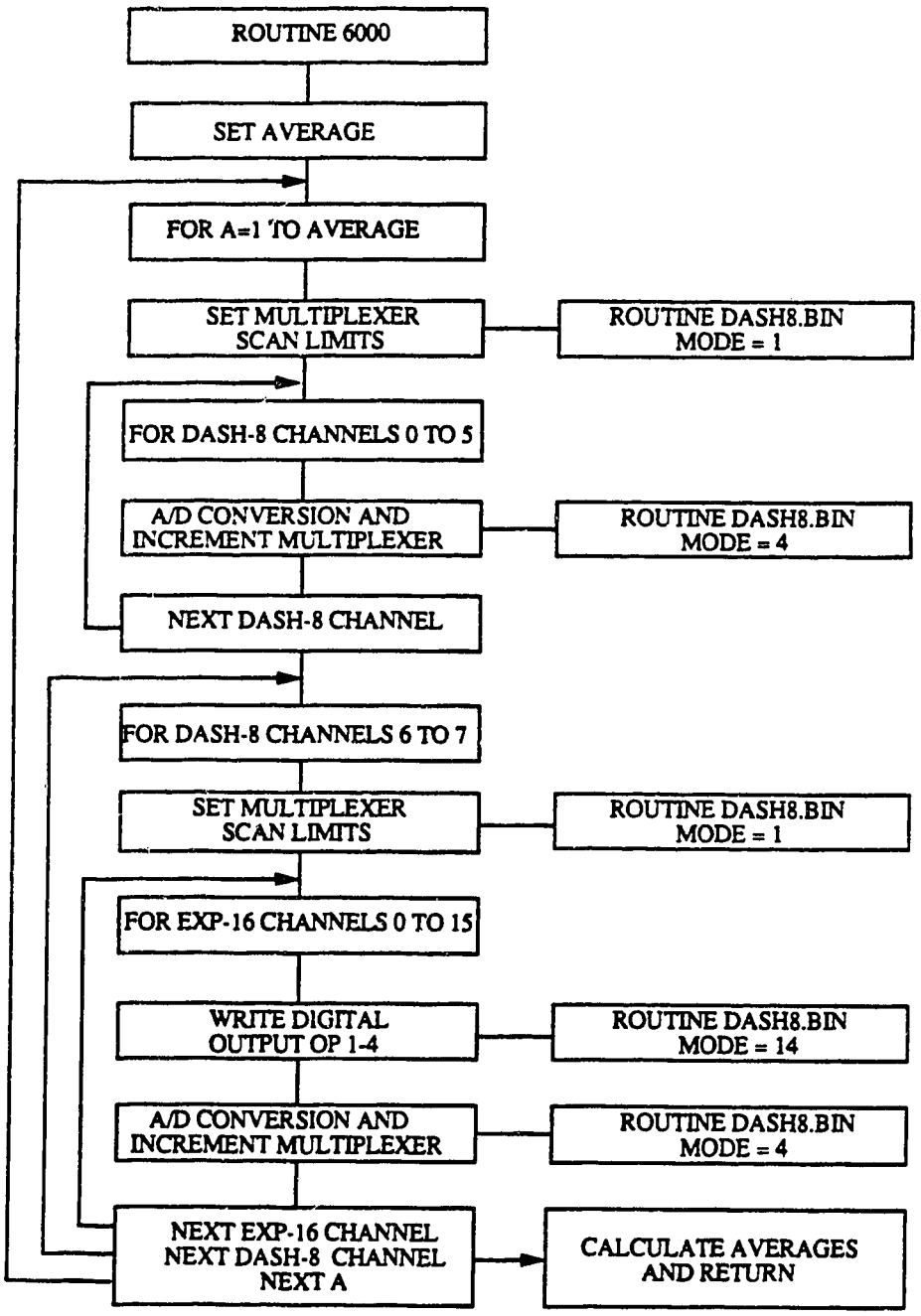

Figure C.9 Program HPTS - Flow chart for Routine 6000

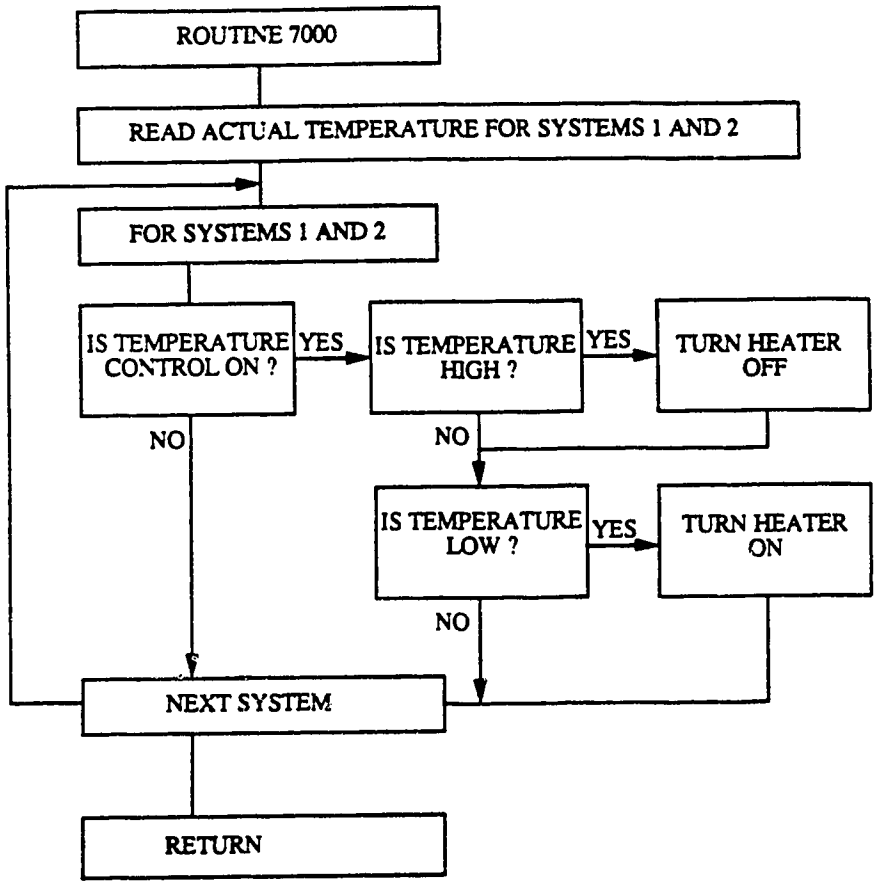

Figure C.10 Program HPTS - Flow chart for Routine 7000

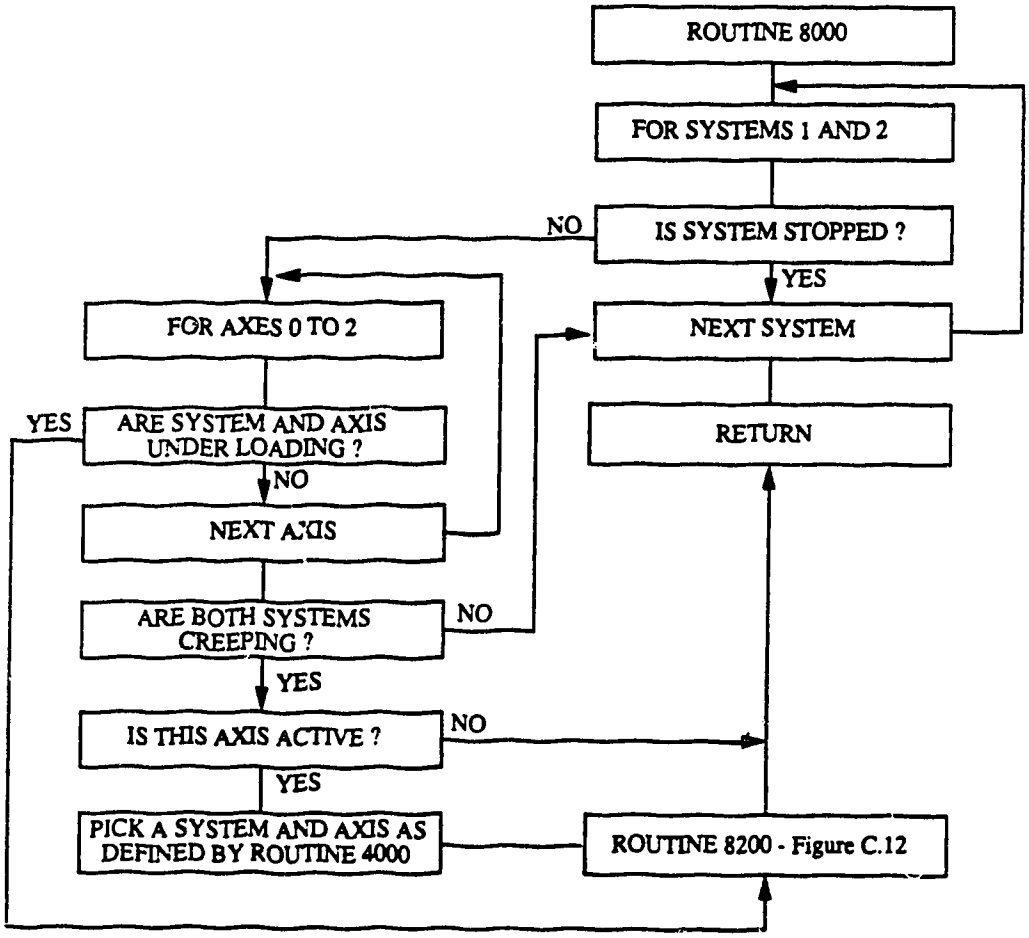

Figure C.11 Program HPTS - Flow chart for Routine 8000 - Part 1

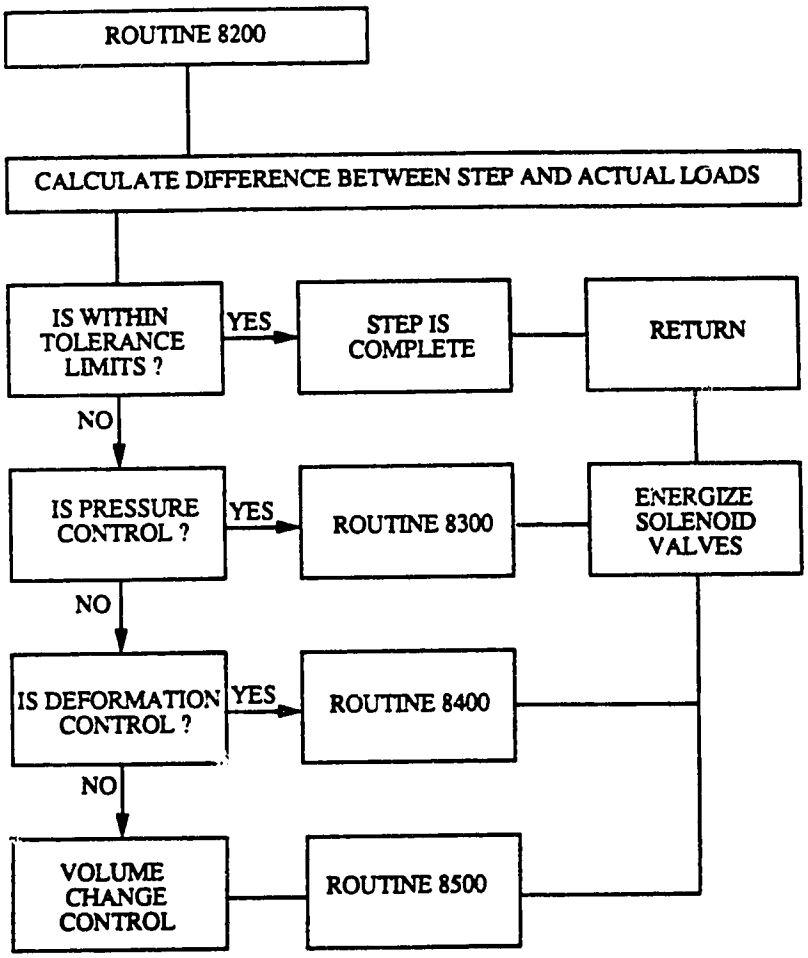

Figure C.12 Program HPTS - Flow chart for Routine 8000 - Part 2

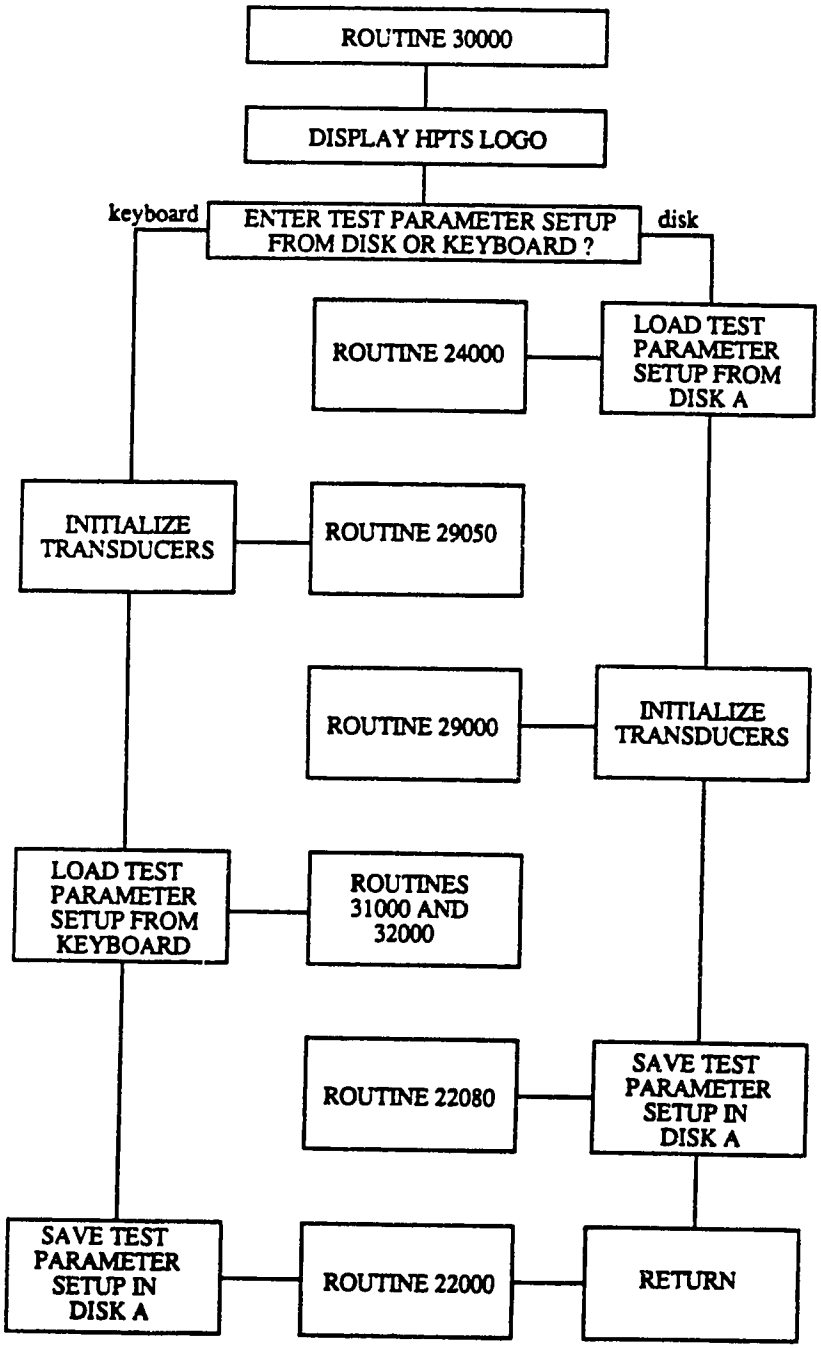

Figure C.13 Program HPTS - Flow chart for Routine 30000

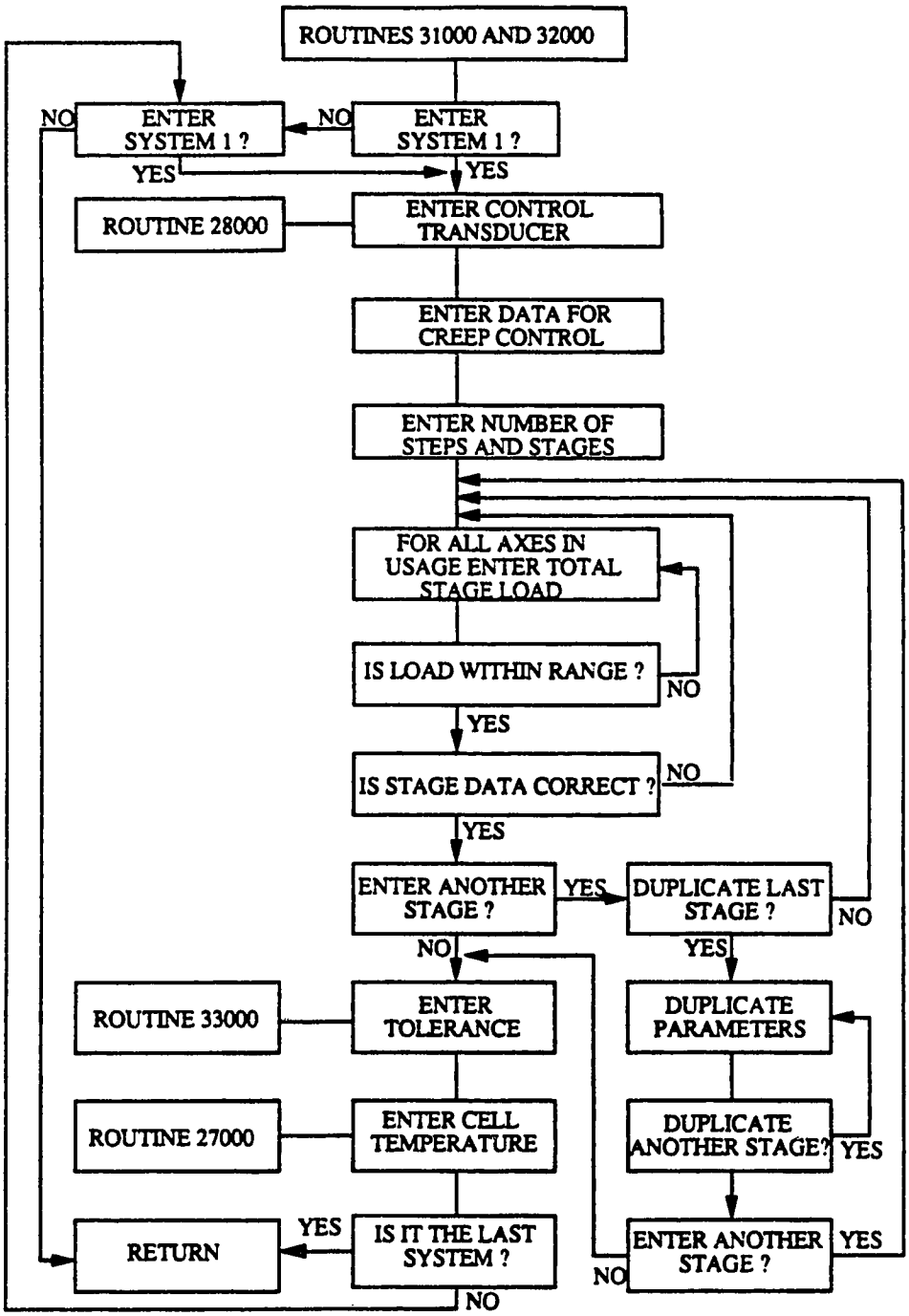

Figure C.14 Program HPTS - Flow chart for Routine 31000/32000

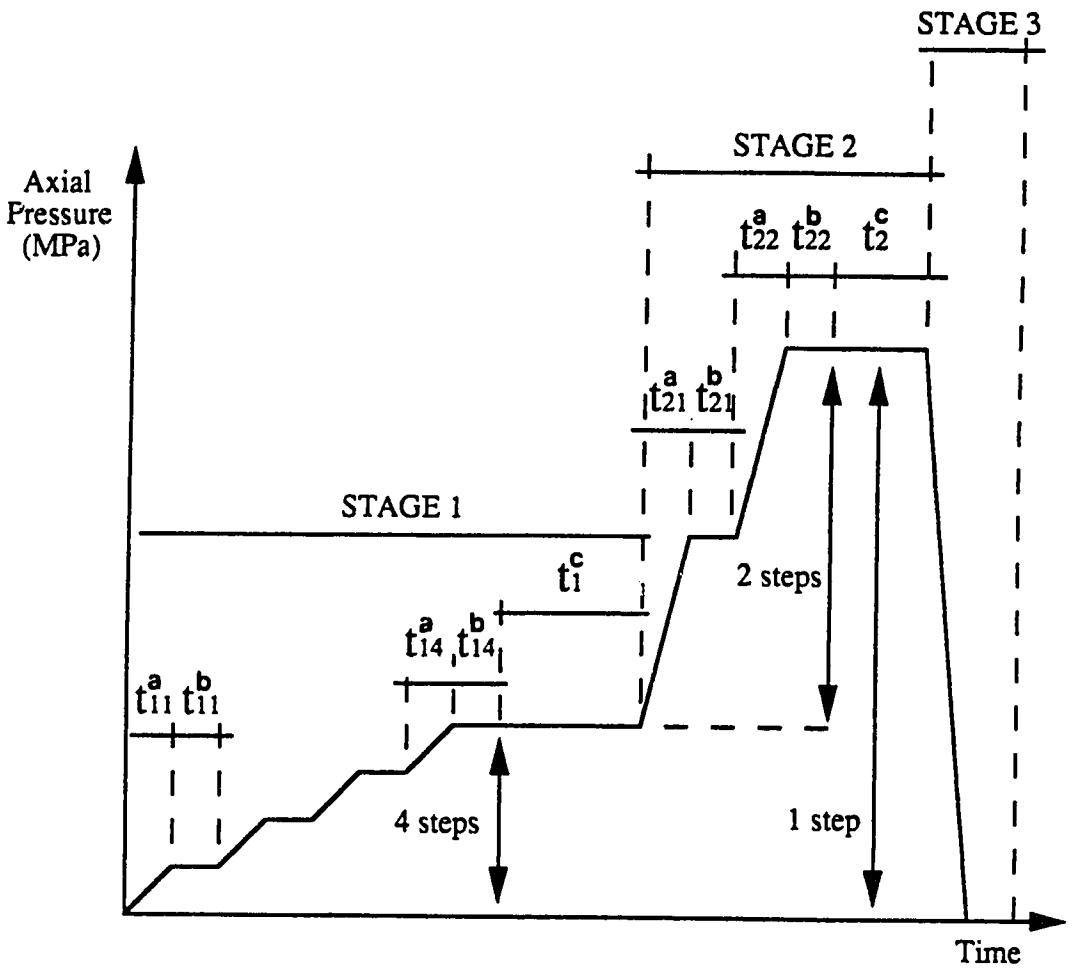

t_{ij} ... time for loading stage i, step j

t_{ij}^a ... time for loading one axis

t_{ij}^b ... time for loading the other axes

t_i^c ... creep time

Figure C.15 Example of data input methodology

D. INSTRUMENTATION AND SYSTEM CALIBRATION

D.1 Introduction

The High Pressure and Temperature System, HPTS, has the capability of controlling and monitoring up to 32 transducers, sixteen for each cell. The transducer configuration for each system is composed of three volume change devices (VCA, VCI, VCE), one axial displacement LVDT (DA), four spare LVDTs, three pressure transducers (PA, PI, PE), one bore convergence device with two strain gauge pairs (IDA, IDB), one specimen diameter deformation device (ODA), one thermocouple (TI) and one RTD (TE).

The methodology for system calibration consists of running tests along the same stress and temperature paths and ranges as the actual tests, using an aluminium specimen. For a system as complex as the HPTS, this procedure is necessary, since it is very difficult to determine the contribution of isolated components to the calibration curves. The whole system presents a unique response for each specific condition. So, a set of calibration curves have to be determined to provide correction data for all pressure and temperature ranges used for the laboratory testing program.

In order to get parameters for the system calibration curves, individual transducer calibrations are needed. This appendix presents the transducer and system calibration procedures.

D.2 Transducer Calibration

A transducer transforms a continuously varying physical quantity (pressure, displacement, volume change or temperature) into a directly proportional, continuously varying analog output (voltage). The HPTS data acquisition system (Appendix C) converts this analog output into digital output (bits). The transducers were calibrated using a transducer calibrator and the HPTS data acquisition system, controlled by Program HPTSCAL (Appendix C). The general procedure for transducer calibration consists of applying a known physical quantity to the calibrator and reading the transducer digital output shown on the monitor screen. Every coordinate point (physical quantity versus digital output) of the calibration curves is the average of 100 samples taken by the program. The relationship between the physical quantity and digital output is plotted. The transducer

conversion factor is simply the slope of the best-fit, directly-proportional relationship, determined by linear regression. Table D.1 shows conversion factors and correlation coefficients for the transducers used in the laboratory testing program carried out in this research.

D.2.1 Pressure Transducers

All six pressure transducers were manufactured by PSI-TRONIX/CELESCO. The two transducers for axial pressure, PA (model PLC5000), work in the zero to 35 MPa range, the others, PI and PE (model PLC10000), in the zero to 70 MPa range and the pressure calibrator (PRESSUMENTS Ltd., model M1900-3) in the zero to 28 MPa range. The transducers were tested to pressures up to 28 MPa, following the calibration procedure given by the calibrator manufacturer. To check whether the transducers had also a linear relationship for pressures higher than 28 MPa, they were tested to pressures up to their nominal limits, using a 70 MPa hydraulic jack (ENERPAC) and pressure gauge (MARSH). The results confirmed the linear relationships obtained from the pressure calibrator.

The pressure measured by axial transducers is acting on the axial loading system piston (Appendix A) and not on the specimen. Therefore, the conversion factors for axial pressure transducers (Table D.1) have to be corrected, based on the relationship between axial loading system piston and specimen cross-sections. Table D.2 shows correction factors for both cells and for solid and hollow cylindrical specimens with external diameters of 100 and 140 mm.

D.2.2 Linear Variable Displacement Transducers

In the HPTS, LVDTs are used for measuring axial displacement and volume change. This section only describes those employed for axial displacement (DA). They are manufactured by HEWLETT PACKARD (model 7DTDC-500) and have a range of 25 mm. These LVDTs actually measure the axial displacement between the bottom end cap and axial ram (Appendix A). The calibration procedure is very simple. A known displacement is applied to the LVDT calibrator (MITUTOYO, range of 50 mm) and the digital output monitored. All LVDTs showed some non-linearity at both 5% extremes of the nominal range, suggesting that, whenever possible, use be limited to only the middle 90% of the nominal range. These extreme points were not considered in the conversion factor calculation (Table D.1).

D.2.3 Volume Change Device

The volume change device, VC, was designed by Maloney (1986) to monitor the displacement of the AIVC low pressure piston (Appendix B). It consists of a linear motion reducer that reduces the large displacement of the intensifier rod which is connected to the AIVC low pressure piston, to a value measurable by the VC device LVDT (HEWLETT PACKARD, model 7DTDC-1000), with 50 mm of range. The calibration procedure comprises two stages. First, a long range (500 mm) LVDT (SCHAWITZ Eng., model 5000 HR-DC), having the intensifier rod as its core, is calibrated using a caliper (MAUSER, 350 mm of range), following a procedure similar to that described for the axial displacement LVDTs. A relationship between the intensifier rod displacement and the long range LVDT digital output is obtained. Second, the volume change device is mounted, having the intensifier rod in one side and the VC device LVDT core in the other side of the linear motion reducer. A generic displacement (in the order of 10 mm) is applied to the intensifier rod and the two digital outputs, long range LVDT and VC device LVDT, are monitored simultaneously by Program HPTSCAL. Using the first calibration, the exact intensifier rod displacement is calculated. Then, the relationship between it and the VC device LVDT digital output is obtained. The slope of this linear relationship is called the displacement factor. Finally, volume change conversion factors (Table D.1) are obtained by multiplying the displacement factor by the cross-sectional area of the AIVC high pressure cylinder, which is 3.3451 cm^2 for the standard and 9.5939 cm^2 for the modified intensifiers (Appendix B).

D.2.4 Bore Convergence Device

The bore convergence device (Fig. D.1) measures local deformations of the bore wall of hollow cylinder specimens. It has a thin-walled cylindrical shape but its wall is composed of eight narrow beams with prominent contact points at their mid section. Two strain gauge pairs, IDA and IDB, are installed on the internal face of these points, in two perpendicular diameters. The remaining four beams are used as spares. In terms of design, the beams were assumed to be fixed supported and expected to measure a maximum deflection of 2 mm. This device is fabricated from aluminium (6061-T6), which is easy to machine and has an adequate strength.

The calibration procedure consists of mounting the bore convergence device, BC, on the LVDT calibrator (MITUTOYO), applying a known displacement to two diametrically opposed contact points and reading the digital output. Finally, the

relationship between displacement (bore convergence) and digital output gives the conversion factor, shown on Table D.1. This relationship, although elastic, showed some non-linearity for diametric convergence greater than 3 mm. Therefore, only bore convergences less than this limit were considered for the conversion factor calculation.

D.2.5 Thermocouples and RTDs

The conversion fac[illegible] (voltage output per °C) for these two devices are [illegible] iven by the manufacturer. It is only necessary to c[illegible] em to °C/bit, according to either the temperatur[illegible] ioner or cold junction compensation specificati[illegible] endix C). Thermocouples are used for monitoring [illegible] perature (TI) and resistance temperature devices, RTD[illegible] 20, for [illegible]ell temperature (TE). These devices were not used in this laboratory testing program.

D.3 System Calibration

A series of calibration tests was performed using solid and hollow cylindrical aluminium specimens with the same dimensions as the actual specimens. Aluminium is a material with known properties, Young's modulus of 70 MPa and Poisson's ratio of 0.3 (Popov, 1978; Roark and Young, 1982), making it possible to calculate, from the theory of elasticity, the specimen deformation under certain load conditions (Tables D.3 and D.5). The differences between deformations, measured by the system transducers and calculated for the aluminium specimen, give the correction or calibration curve, due to fluid compressibility and system compliance. A set of calibration curves for all transducers was generated for different load conditions, yielding sufficient data for the interpolation of any correction needed for the laboratory testing program described in this thesis.

All calibration tests started by hydrostatically loading (HL) the specimens to a certain stress level. Then, four types of stress paths, conventional triaxial compression, CTC, J1-constant triaxial compression, JTC, hollow cylinder under axisymmetric loading, HCAL and hollow cylinder under plain strain, HCPS, were followed. For data interpretation, each test was divided in load stages according to the stress path. Data were separated and interpreted for each load stage. Data files for all load stages were screened to eliminate data which did not belong to that particular stress path. For instance, in the JTC

tests, data with the first stress invariant different from the specified one, within tolerance limits, were neglected. This kind of data may have originated from loss of system control due to the limited intensifier stroke travel or from system stoppages for either recharge or discharge of intensifiers.

As the calibration or correction curves for each transducer would be used to correct actual specimen data, it was decided to find a equation that would best fit the calibration test data. Among the alternatives offered by the best fitting technique, only those curves whose shapes were representative of the data trend were tried. Restrictions, such as forcing the curve through the origin (0,0), were also imposed in order to select those with some significance for the physical phenomena. Tables D.4 and D.6 show the best fit equations for calibration test data and also the correlation coefficients, which define the degree of fit of these curves. The calibration or correction curve equation for a certain transducer is the difference between the best fit equation for calibration test data and the respective deformation equation for the aluminium specimen. Using this calibration curve equation, actual specimen data could easily be automatically corrected by either a custom computer program or canned software such as spread sheet programs.

Triaxial calibration tests, CTC and JTC, were performed on an aluminium cylindrical specimen with diameter of 101.6 mm and height of 203.2 mm, using System 1. Hollow cylinder calibration tests, HCAL and HCPS, were conducted on an aluminium hollow cylinder specimen of 139.7 mm external diameter and 31.8 mm internal diameter with height of 203.2 mm, using System 2. Three curves, CAL, measured and aluminum, are shown in all figures. 'Measured' is the curve that best fits the experimental data. 'Aluminum' is the curve that represents the calculated deformation for the specimen. 'CAL' is the curve that represents the correction of the system. It is the difference between the two former curves.

D.3.1 Hydrostatic Loading (HL) Tests

Tests started by hydrostatically loading specimens to a desired stress level, defined by a mean pressure 'p' and by allowing time for system accommodation. Figure D.2 shows the calibration curves for axial displacement and volume change, using the aluminium cylindrical specimen and System 1. The axial displacement data show some dispersion but could be well fitted using a linear regression. The dispersion

(maximum of 0.1 mm) is not significant compared to the magnitude of actual displacements. Volume change data are very consistent and show a clear non-linearity due to entrapped air. At low pressures, there are air bubbles in the confining fluid and consequently fluid compressibility is higher. As soon as the pressure increases, air bubbles are incorporated in the fluid and compressibility reduces.

Figures D.3 and D.4 show the calibration curves for axial displacement, bore convergence and bore and cell volume changes using the aluminium hollow cylinder specimen and System 2. All curves are consistent and could be well fitted. The best-fit curve equations are presented in Tables D.4 and D.6 for triaxial and hollow cylinder tests, respectively. It is interesting to note that the calculated volume changes for the aluminium specimen are negligible when compared to those measured by the system.

D.3.2 Conventional Triaxial Compression (CTC) Tests

Four CTC calibration tests were carried out, two using sulfaset insulator caps (CTC-CAL Tests 1 and 2) and two using a lower platen with a spherical seat, instead of insulator caps (CTC-CAL Tests 3 and 4). Tests CTC1CAL and CTC2CAL have confining pressures of 15 and 35 MPa and tests CTC3CAL and CTC4CAL 25 and 35 MPa, respectively. Axial displacement data (Fig. D.5) were well fitted by a linear regression. Volume change data (Fig. D.5) show some scatter, demonstrating that the system was unable to consistently monitor such small volume changes (less than a millilitre). Again these values are not significant compared to those expected to be measured in actual specimens. The best-fit linear equation only explains 50% of the data and it is not statistically representative. A data equation (VC=0) was assumed, since during CTC tests there is no confining pressure change. Best-fit curve equations are presented in Table D.4.

D.3.3 J1-Constant Triaxial Compression (JTC) Tests

Two JTC calibration tests were performed using the lower platen with spherical seat instead of sulfaset insulator caps. Test JTC1CAL has the first stress invariant of 75 MPa and test JTC2CAL 105 MPa. Figure D.6 shows the calibration curves for axial displacement and volume change which are consistent and could be well fitted by a linear and a polynomial regression, respectively (Table D.4).

D.3.4 Hollow Cylinder (HC) Tests

Four calibration tests (two HCAL and two HCPS) were run in System 2 (Figs D.7 to D.10). In all tests, aluminium washers were used instead of sulfaset insulator caps. Tests HCAL1CAL and HCPS1CAL were consolidated at a mean pressure of 15 MPa and tests HCAL2CAL and HCPS2CAL at 35 MPa. The axial displacement (HCAL tests) and axial stress (HCPS tests) data are not consistent with what was expected. This might be caused by the test control tolerance limits. External volume change data are also not consistent, mainly due to the measurement of very small values. On the other hand, the bore convergence and bore volume change data are consistent and could be well fitted by linear regression.

D.4 Conclusion

Electronic transducers were calibrated to obtain conversion factors which transform physical quantity changes into the equivalent digital output changes. Conversion factors are input to Program HPTS which does the system control and data acquisition. Then, calibration tests were performed on aluminium specimens. The data for each transducer under a given stress path were reduced, plotted and analysed. Best-fit curves for the calibration test data were found. The difference of deformations given by the best fit curve and aluminium specimen equation generated the correction or calibration curve for a particular transducer under a given stress path. Using these equations, data from actual specimens subjected to the same loading conditions were corrected.

Table D.1 Transducer conversion factors

Transducer Name	Reference No.	Excitation Voltage	Conversion Factor	Correlation Coefficient
VCA1				
VCI1	SNo. 1186	6	0.042844	0.998126
VCE1	SNo. 1286	6	0.039984	0.999589
DA1	7DTDC-500	6	0.009872	0.999876
LVDT0				
LVDT1				
LVDT2				
LVDT3				
PA1	DC 86/09	10	0.008757	0.999997
PI1	SNo. 4867	10	0.018362	0.999995
PE1	SNo. 5308	10	0.018697	0.999973
IDA1				
IDB1				
ODA1				
TI1				
TE1				
VCA2				
VCI2	SNo. 1286	6	0.033035	0.999177
VCE2	SNo. 1286	6	0.036457	0.999876
DA2	7DTDC-500	6	0.009345	0.999936
LVDT4				
LVDT5				
LVDT6				
LVDT7				
PA2	DC 86/09	10	0.008724	0.999998
PI2	SNo. 5776	10	0.018674	0.999987
PE2	SNo. 5769	10	0.018655	0.999991
IDA2		6	0.004197	0.997526
IDB2		6	0.004489	0.997977
ODA2				
TI2				
TE2				

NOTE ON CONVERSION FACTOR UNITS:

volume change, VC ... ml/bit
axial displacement, DA ... mm/bit
pressure, P ... MPa/bit
bore convergence, ID ... mm/bit
specimen diameter deformation, OD ... strain/bit
temperature, T ... °C/bit

Table D.2 Correction factors for axial pressure transducers

	Triaxial Specimens		Hollow Cylinder Specimens	
	d = 100 mm	d = 140 mm	d = 100 mm	d = 140 mm
System 1	5.062500	2.677686	5.610390	2.823529
System 2	5.347656	2.828512	5.926407	2.982571

Table D.3 Deformation equations for aluminium cylindrical specimens

DEFORMATION EQUATIONS FOR TRIAXIAL SPECIMENS		
HL	DA	$[(1-2\nu)/E] \cdot L \cdot p$
	VC	$2 \cdot [(1-2\nu)/E] \cdot V \cdot p$
CTC	ΔDA	$[(PA-PE)/E] \cdot L$
	ΔVC	$-2 \cdot (\nu/E) \cdot V \cdot (PA-PE)$
JTC	ΔDA	$(2/3) \cdot [(1+\nu)/E] \cdot (PA-PE) \cdot L$
	ΔVC	$(-2/3) \cdot [(1+\nu)/E] \cdot (PA-PE) \cdot V$

p ... mean pressure = (PA+2PE)/3
E ... Young's modulus
ν ... Poisson's ratio
L ... specimen length
V ... specimen volume

Table D.4 Best-fit equations for aluminium cylindrical specimens

Best-Fit Equations for Calibration Test Data			Correlation Coefficient
HL	DA	$= 0.009593 \cdot p$	0.944145
	VC	$= -0.093695 \cdot (p)^2 + 15.2661 \cdot p$	0.99
CTC	$\triangle$DA	$= 0.005750 \cdot (PA-PE)$	0.997446
	$\triangle$VC	= 0 (assumed)	
JTC	$\triangle$DA	$= 0.003866 \cdot (PA-PE)$	0.996374
	$\triangle$VC	$= -0.005798 \cdot (PA-PE)^2 - 2.84961 \cdot (PA-PE)$	-0.99[illegible]8

p ... mean pressure = (PA+2PE)/3
PA ... axial pressure
PE ... confining pressure

Table D.5 Deformation equations for aluminium hollow cylinder specimens

HCHL	DA	$= C \cdot p \cdot L$
	VCI	$= \pi L a^2 (-C^3p^3 + 3C^2p^2 - 3Cp)$
	VCE	$= \pi L b^2 (+C^3p^3 - 3C^2p^2 + 3Cp)$
	BC	$= C \cdot p \cdot a$
HCAL	ΔDA	$= R \cdot \Delta pi$
	ΔVCI	$= \pi [-(S^2R) \Delta pi^3 + (S^2L - 2aSR) \Delta pi^2 - (a^2R - 2aLS) \Delta pi$
	ΔVCE	$= \pi [-(T^2R) \Delta pi^3 + (T^2L - 2bTR) \Delta pi^2 - (b^2R - 2bLT) \Delta pi$
	ΔBC	$= -S \cdot \Delta pi$
HCPS	ΔPA	$= -O \cdot \Delta pi$
	ΔVCI	$= \pi \cdot L [M^2 \Delta pi^2 + (2aM) \Delta pi]$
	ΔVCE	$= \pi \cdot L [N^2 \Delta pi^2 + (2bN) \Delta pi]$
	ΔBC	$= -M \cdot \Delta pi$

Constants, C, M, N, O, R, S and T, are defined in Section 3.2.3

$p = (PA+PE+PI)/3$
$\Delta pi = PI - (PA+PE)/2$ for HCAL tests
or $= PI - PE$ for HCPS tests

Table D.6 Best-fit equations for aluminium hollow cylinder specimens

HCHL	DA	$= 0.24738 \cdot p$	$r^2 = 0.990$
	VCE	$= 0.00199\ p^3 - 0.16069\ p^2 + 12.2135\ p$	$r^2 = 0.990$
	VCI	$= 0.00032\ p^3 - 0.01873\ p^2 + 0.638\ p$	$r^2 = 0.993$
	BC	$= 0.00354\ p$	$r^2 = 0.973$
HCAL	$\triangle$DA	$= -0.00026\ \triangle pi$	$r^2 = 0.246$
	$\triangle$VCE	$= 0.02717\ \triangle pi$	$r^2 = 0.216$
	$\triangle$VCI	$= 0.32727\ \triangle pi$	$r^2 = 0.630$
	$\triangle$BC	$= -0.00420\ \triangle pi$	$r^2 = 0.704$
HCPS	$\triangle$PA	$= 0.01538\ \triangle pi$	$r^2 = 0.213$
	$\triangle$VCE	$= 0.00144\ \triangle pi$	$r^2 = 0.700$
	$\triangle$VCI	$= 0.32730\ \triangle pi$	$r^2 = 0.715$
	$\triangle$BC	$= -0.00428\ \triangle pi$	$r^2 = 0.875$

$p = (PA+PE+PI)/3$

$\triangle pi = PI - (PA+PE)/2$ for HCAL tests

or $= PI - PE$ for HCPS tests

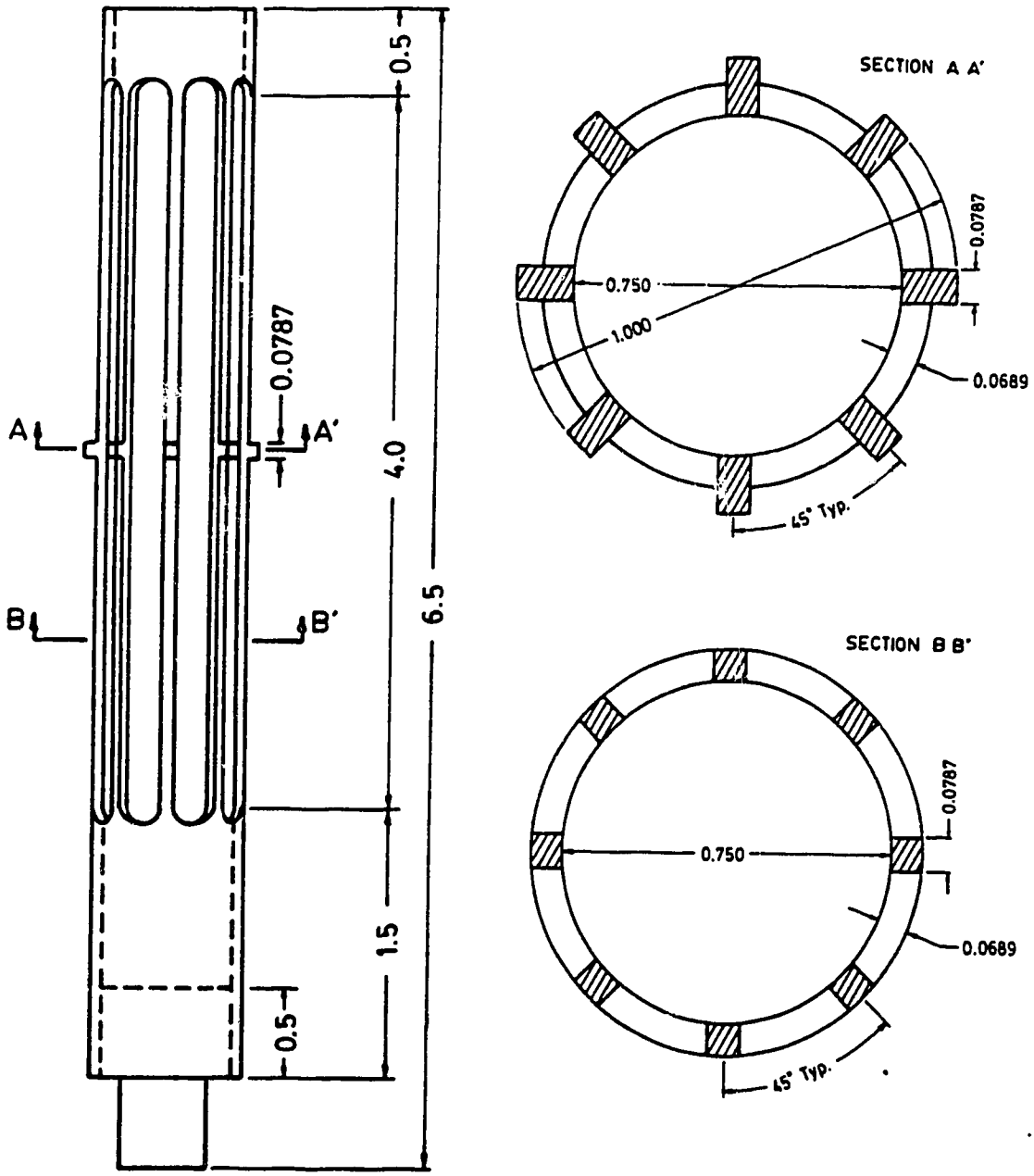

Figure D.1 Bore convergence device (units in inches)

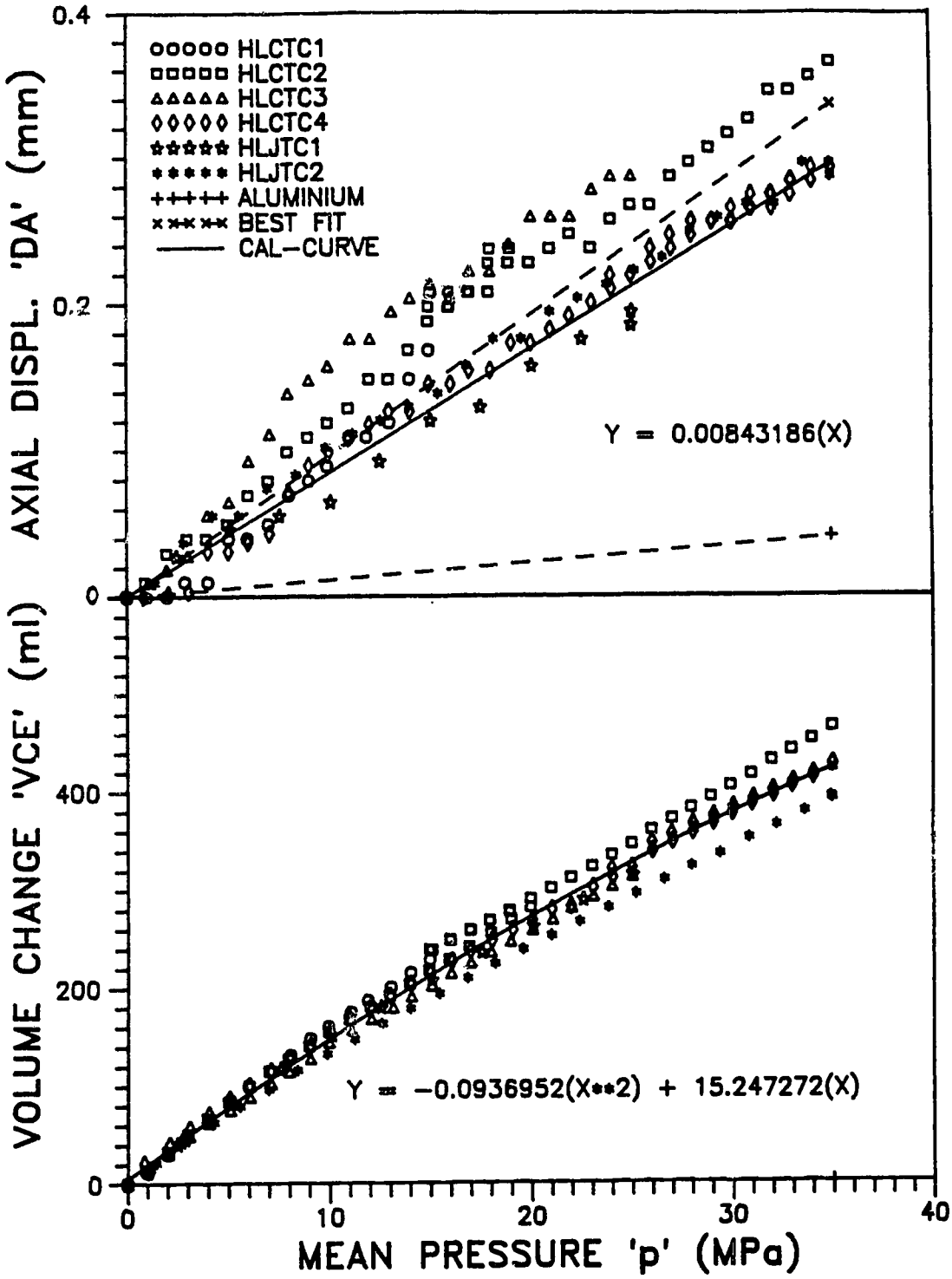

Figure D.2 System 1 - HL calibration tests for cylindrical specimens

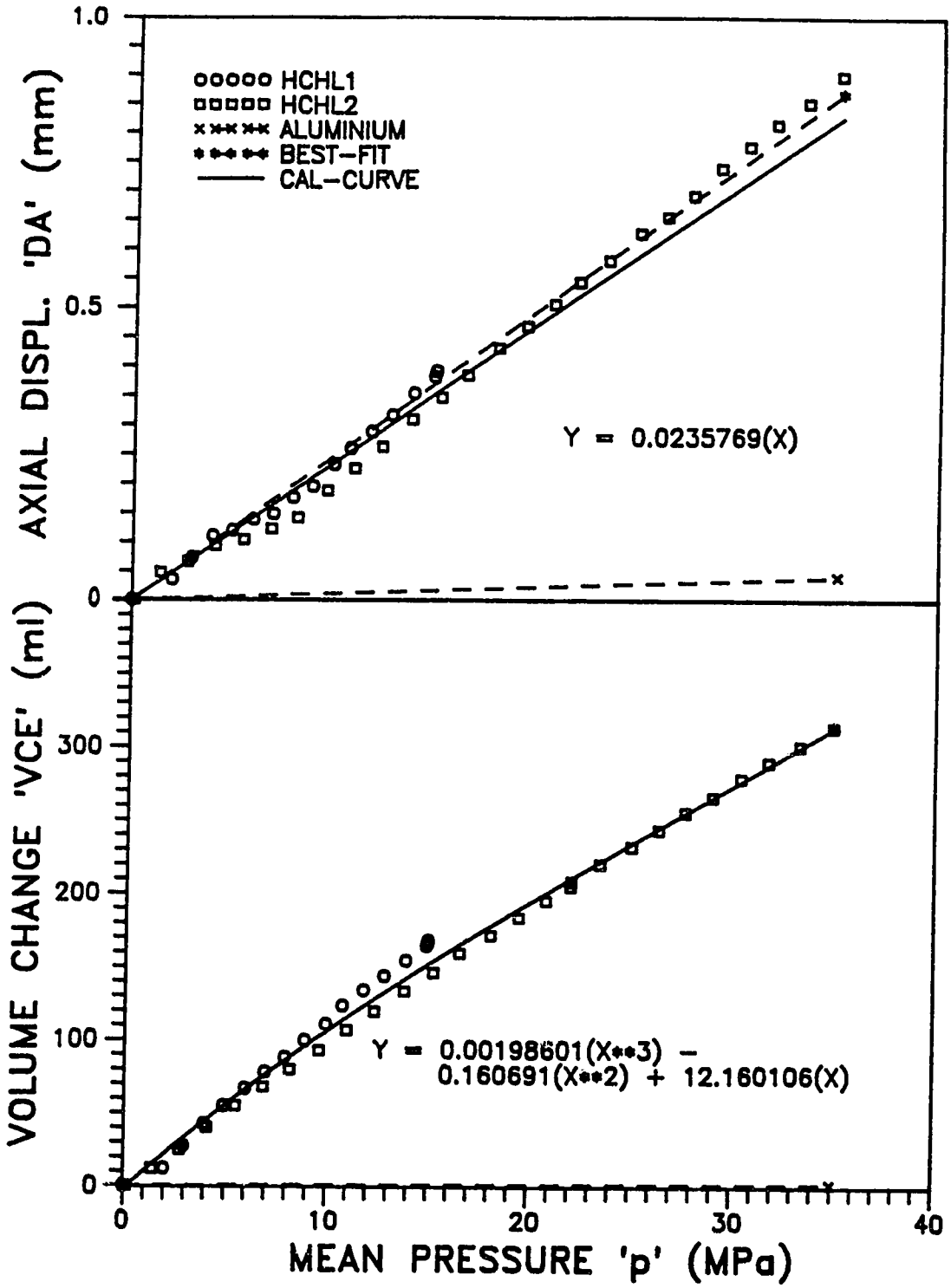

Figure D.3 System 2 - HL calibration tests for hollow cylinder specimens - A

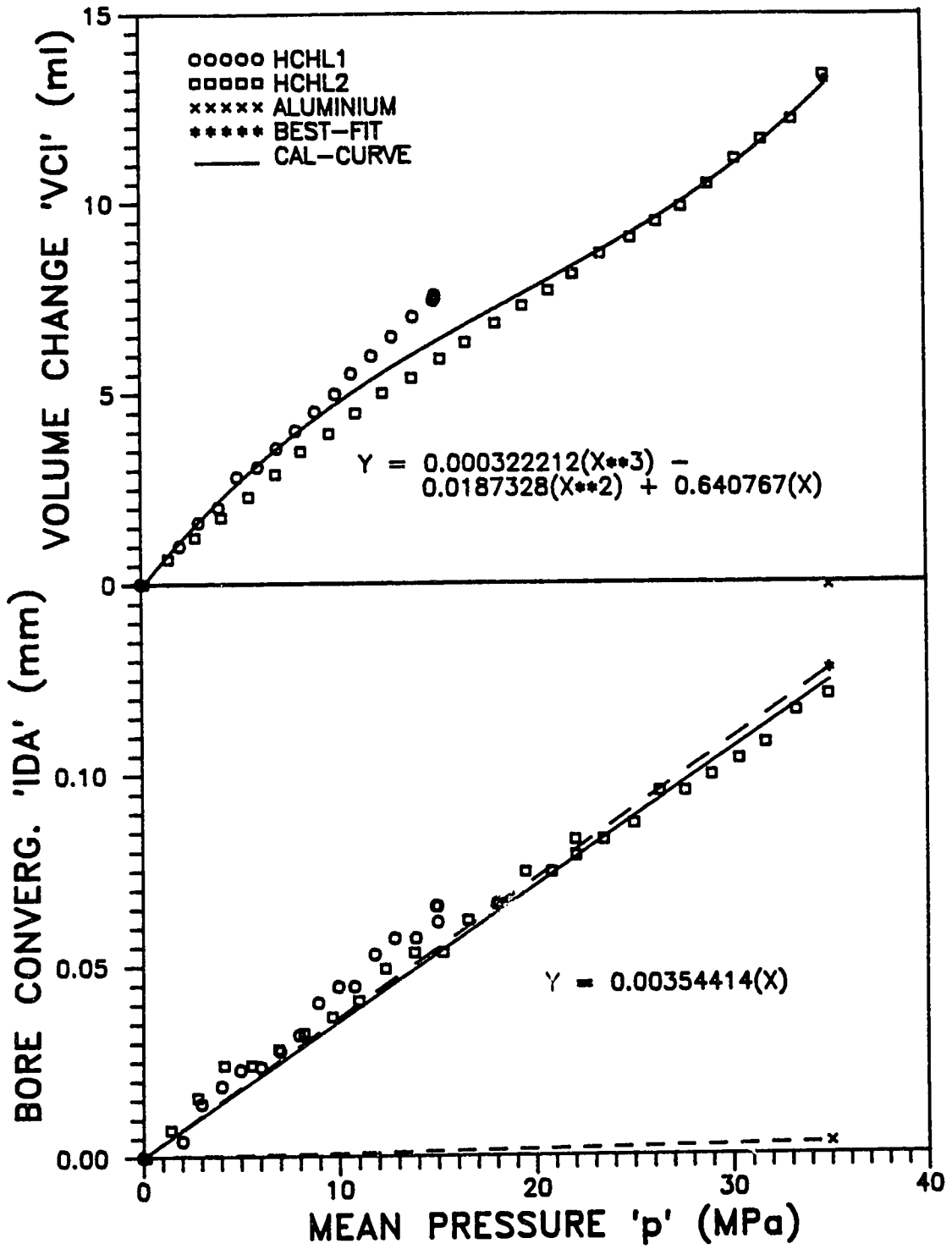

Figure D.4 System ℓ - HL calibration tests for hollow cylinder specimens - B

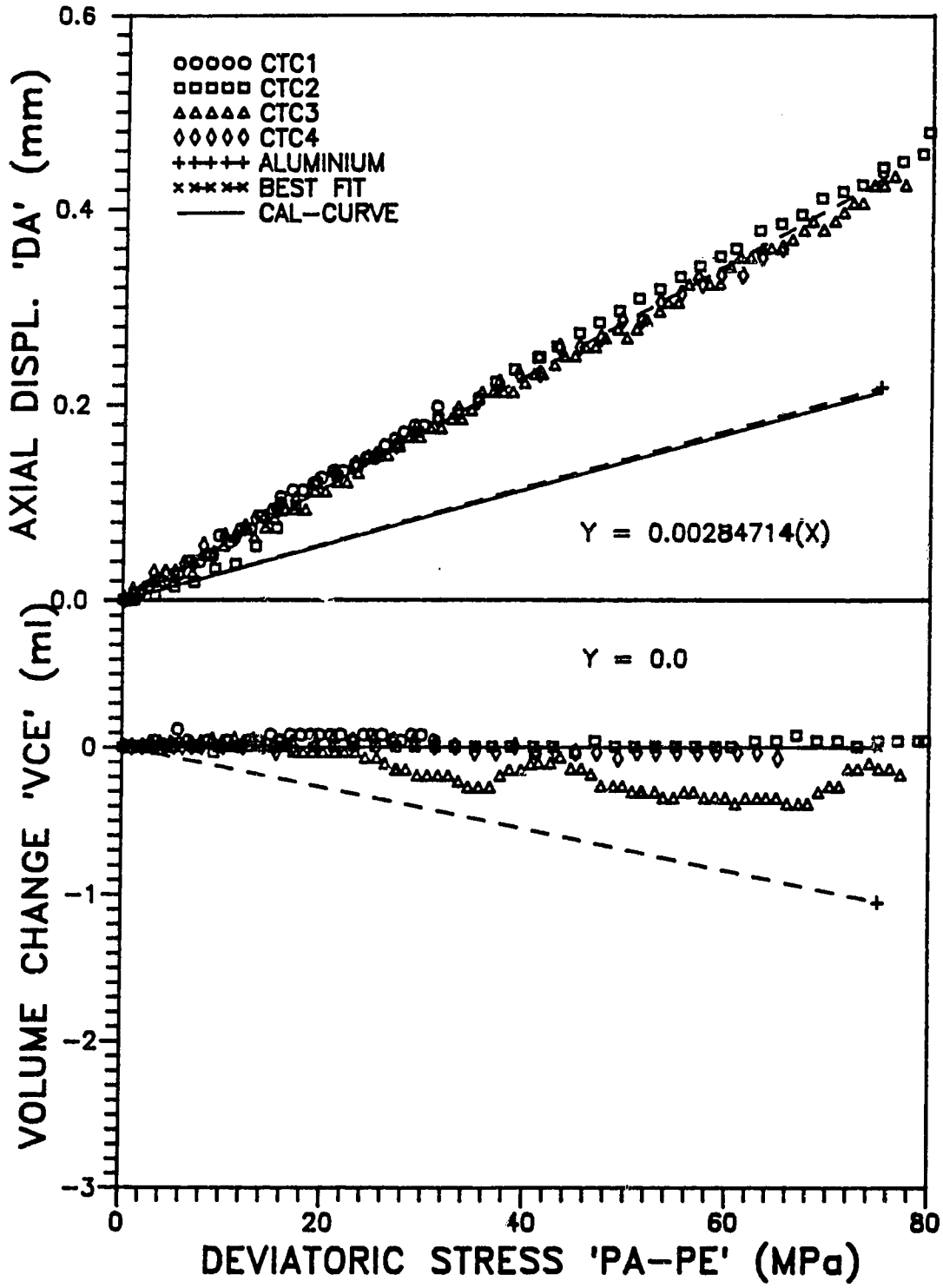

Figure D.5 System 1 - CTC calibration tests

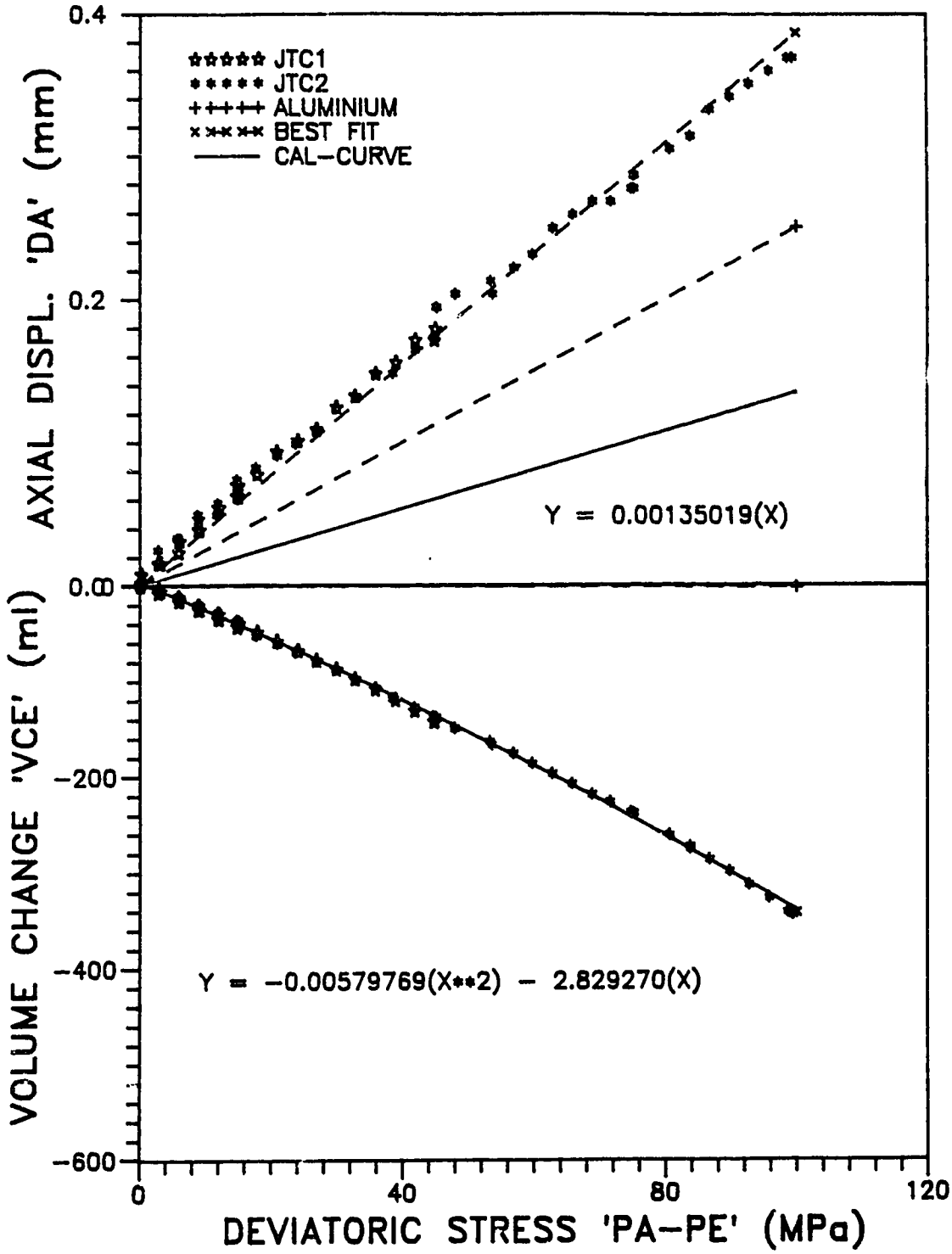

Figure D.6 System 1 - JTC calibration tests

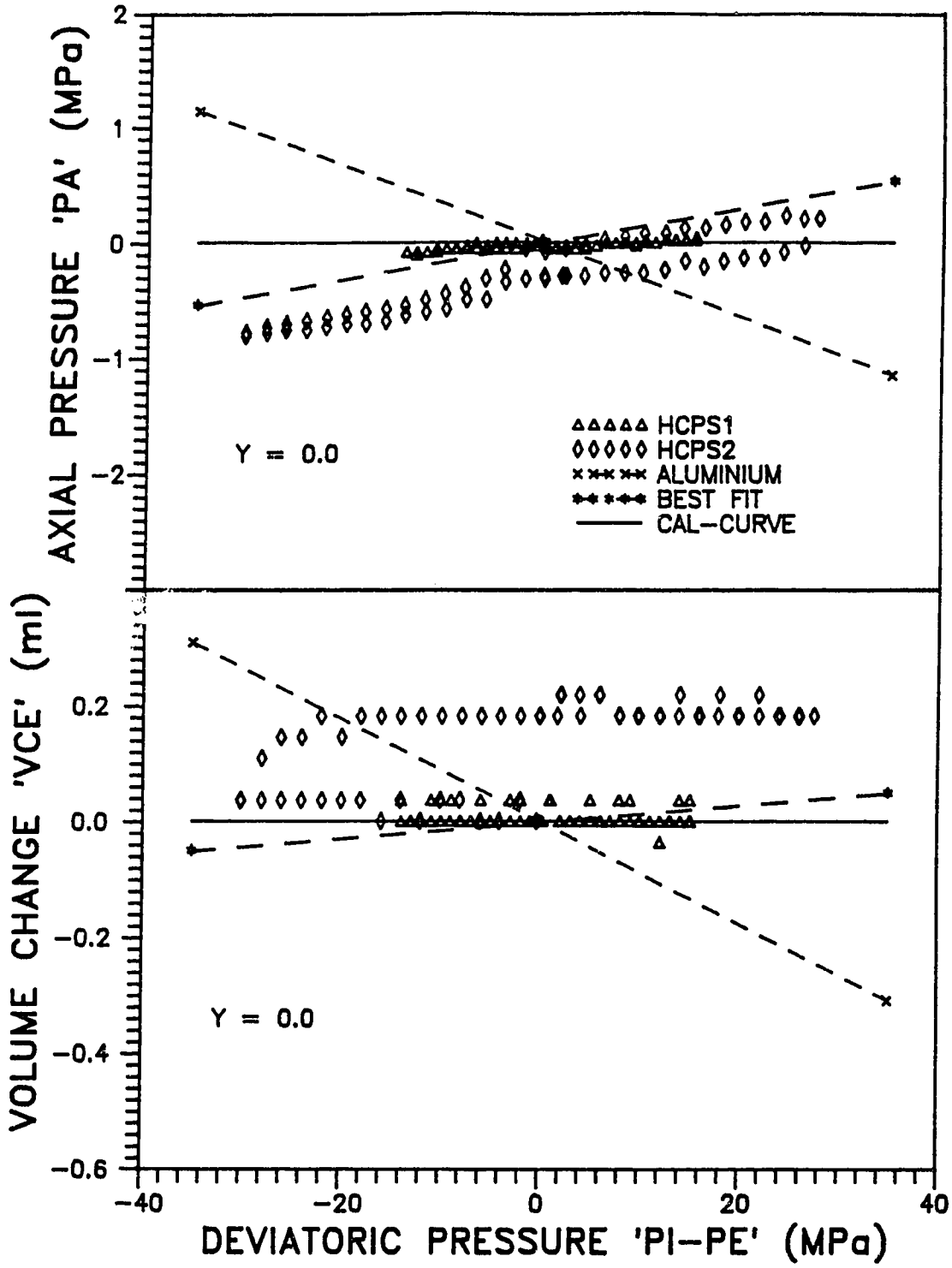

Figure D.7 System 2 - HC calibration tests under plane strain - A

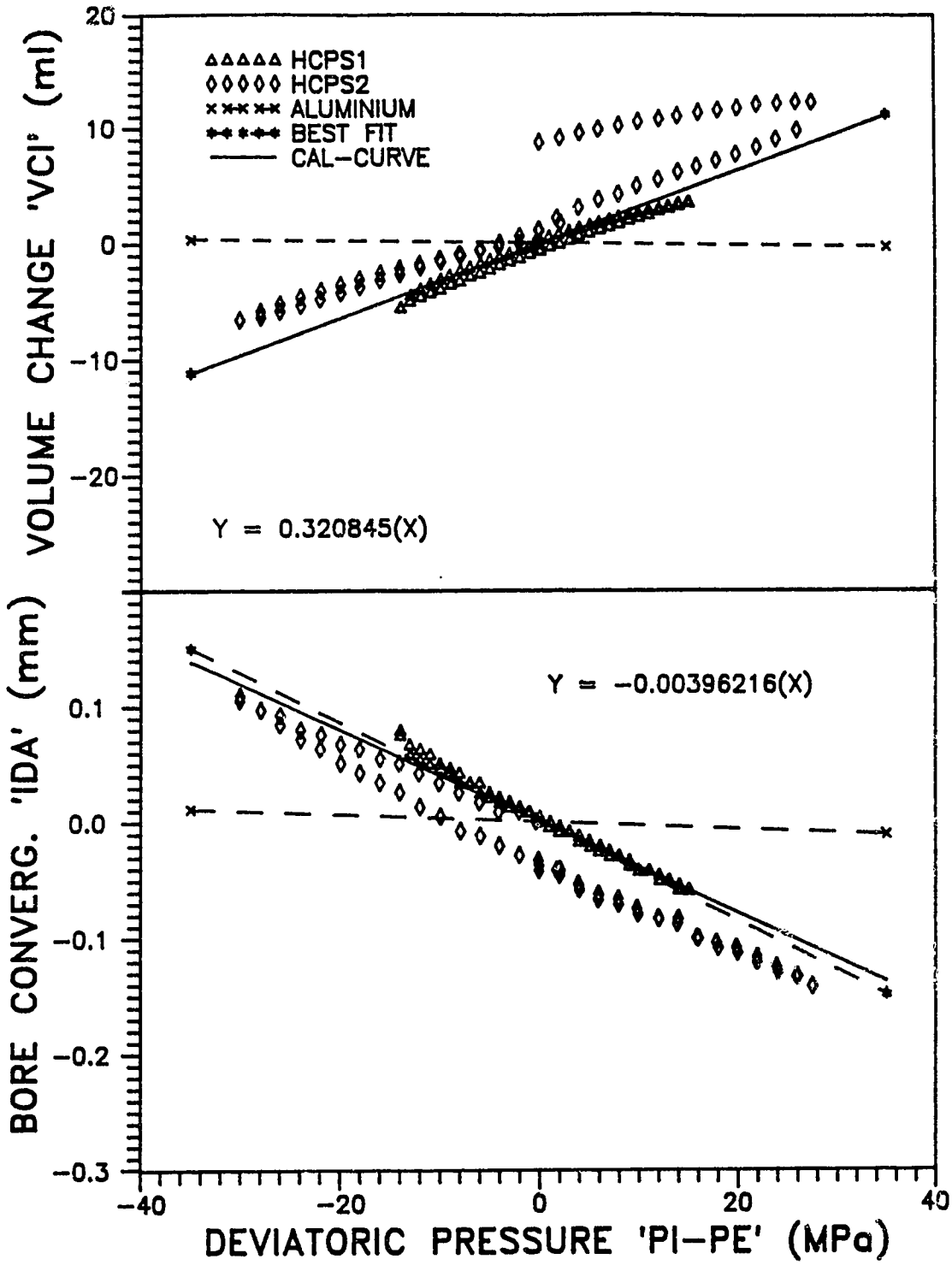

Figure D.8 System 2 - HC calibration tests under plane strain - B

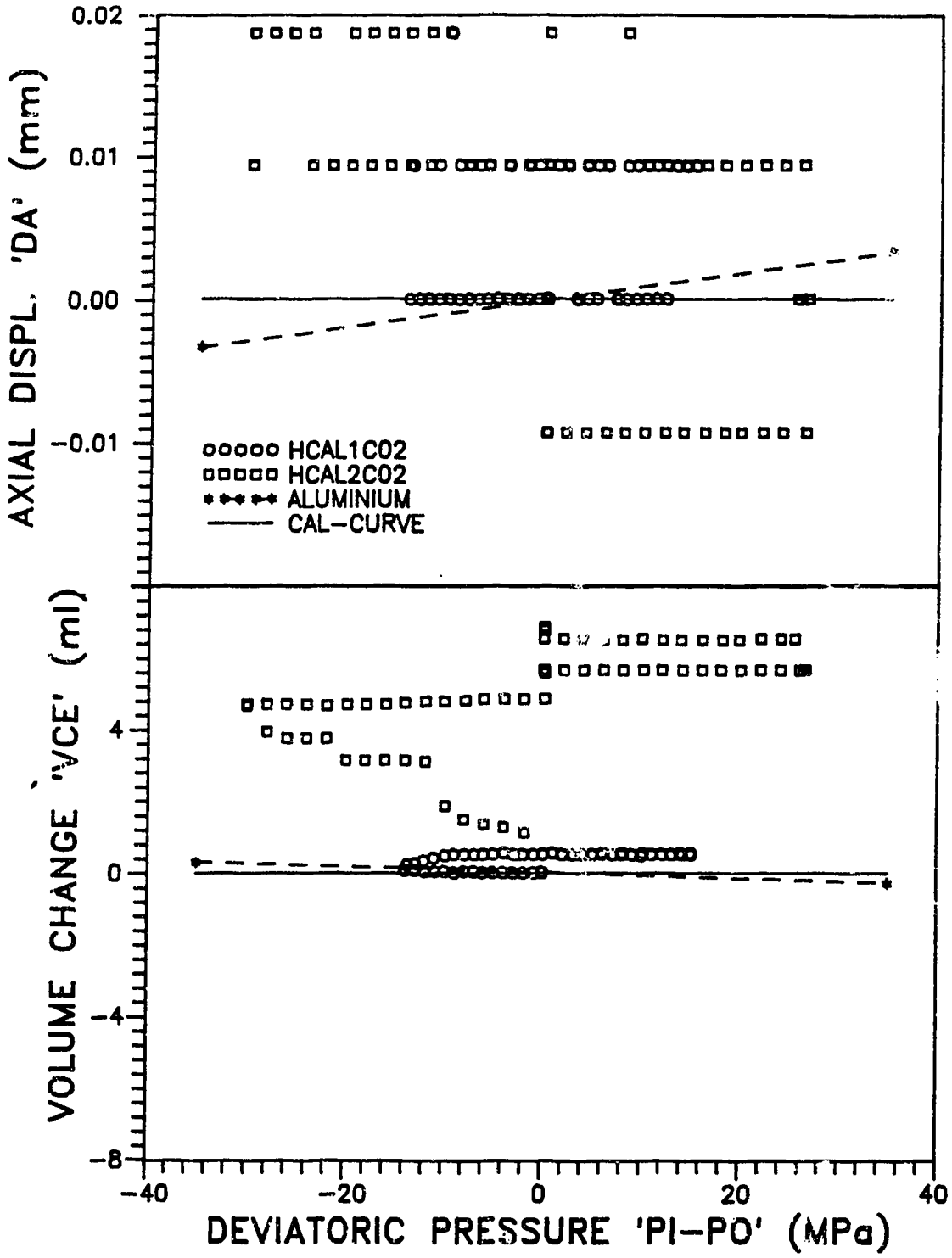

Figure D.9 System 2 - HC calibration tests under axisymmetric loading - A

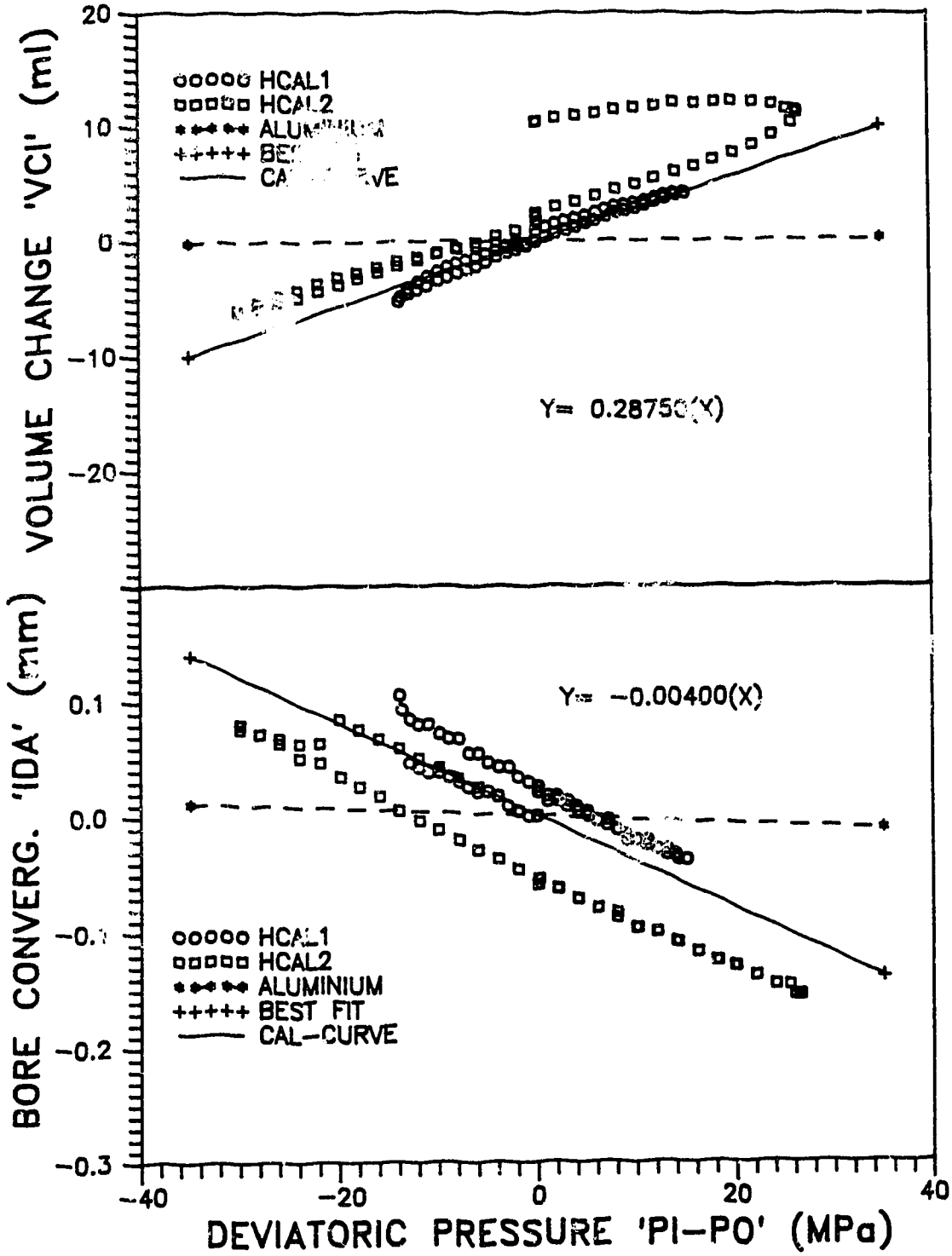

Figure D.10 System 2 - HC calibration tests under axisymmetric loading - B

E. TRIAXIAL TESTING PROGRAM DATA

Recorded data from the triaxial tests are presented. These data were corrected using the calibration equations shown on Table 4.1, according to the loading condition whether hydrostatic, conventional triaxial compression or J1-constant triaxial compression paths. Tables present the current dimensions of specimens, measured deformation, average stress rate, time and number of data for each test stage. The average stress rate is assumed to be the total change of load in all axes divided by the time taken by the system to perform it. The prescribed stress path graphs are only approximated in the time scale, therefore they are sketches showing all executed (not programmed) stages.

Table E.1 CTC Test 1

Stage	Initial Volume (ml)	Volume Change (ml)	Initial Length (mm)	Length Change (mm)	Load per Step (MPa)	Time (min)	Load Rate (MPa/min)	No. of Data Points
A-HLF	1283.0	90.9	171.20	1.75	0.5	45	1.8	69
B-HLC	1192.1	6.9	169.45	0.83	-x-	4007	-x-	276
C-HLF	1185.2	(?)	168.62	-0.18	0.5	27	1.8	54
D-CTCF	(?)	(?)	168.80	6.30	0.5	118	1.0	253
E-CTCC	(?)	(?)	162.50	4.90	-x-	2583	-x-	262
Σ=	(?)	(?)	157.60	13.60	-x-	6780	-x-	914

(?) VCE device stopped recording

Table E.2 CTC Test 2

Stage	Initial Volume (ml)	Volume Change (ml)	Initial Length (mm)	Length Change (mm)	Load per Step (MPa)	Time (min)	Load Rate (MPa/min)	No. of Data Points
A-HLF	1361.0	96.9	179.62	0.36	0.5	45	1.3	74
B-HLC	1264.1	18.4	179.26	0.13	-x-	4317	-x-	278
C-HLF	1245.7	-1.9	179.13	0.03	0.5	19	1.0	26
D-CTCF	1247.6	-112.4	179.10	17.08	0.5	74	0.6	113
Σ=	1360.0	1.0	162.02	17.60	-x-	4455	-x-	491

Table E.3 CTC Test 3

Stage	Initial Volume (ml)	Volume Change (ml)	Initial Length (mm)	Length Change (mm)	Load per Step (MPa)	Time (min)	Load Rate (MPa/min)	No. of Data Points
A-HLF	1411.0	15.8	180.25	0.03	0.5	47	0.9	70
B-HLC	1395.2	18.7	180.22	0.09	-x-	6476	-x-	275
C-HLF	1376.5	-1.8	180.13	0.00	0.5	32	0.6	26
D-CTCF	1378.3	-0.7	180.13	0.08	0.5	13	0.8	19
E-CTCC	1379.0	-0.6	180.05	0.25	-x-	5280	-x-	265
F-CTCF	1379.6	-2.5	179.80	0.14	0.5	6	1.6	21
G-CTCC	1382.1	-34.5	179.66	3.06	-x-	4360	-x-	30
H-CTCF	1416.6	-5.1	176.60	0.62	0.5	8	1.3	21
I-CTCC	1421.7	80.3	175.98	21.59	-x-	4747	-x-	35
Σ=	1341.4	69.6	154.39	25.86	-x-	20969	-x-	762

Table E.4 CTC Test 4

Stage	Initial Volume (ml)	Volume Change (ml)	Initial Length (mm)	Length Change (mm)	p (MP	Time (min)	Load Rate (MPa/min)	No. of Data Points
A-HLF	1467.0	72.0	192.81	0.54	0.8	43	1.4	54
B-HLC	1395.0	23.8	192.27	0.21	-x-	4277	-x-	223
C-HLF	1371.2	-7.2	192.06	0.05	0.8	31	1.6	39
D-CTCF	1378.4	1.1	192.01	0.71	1.0	9	2.7	28
E-CTCC	1377.3	-5.3	191.30	0.57	-x-	5738	-x-	36
F-CTCF	1382.6	-3.4	190.73	0.55	1.0	11	2.3	25
G-CTCC	1386.0	-6.2	190.18	0.52	-x-	5722	-x-	38
H-CTCF	1392.2	7.3	189.66	-0.53	1.0/-3.0	25	4.0	56
I-HLF	1384.9	-12.0	190.19	-0.25	0.6	26	1.2	32
J-CTCF	1396.9	-2.6	190.44	0.13	1.0	8	3.1	26
K-CTCC	1399.5	-7.7	190.31	0.03	-x-	5709	-x-	236
L-CTCF	1407.2	-0.1	190.28	0.16	1.0	10	2.5	26
M-CTCC	1407.3	-6.2	190.12	0.17	-x-	1398	-x-	9
N-CTCF	1413.5	-0.7	189.95	-0.38	1.0/-3.0	25	4.2	40
0-HLF	1414.2	-22.7	190.33	-0.67	-1.0/1.0	196	1.5	26
P-HLC	1436.9	5.0	191.00	1.70	-x-	1173	-x-	84
Q-CTCF	1431.9	-20.2	189.30	2.34	2.0	19	2.7	28
R-CTCC	1452.1	-23.5	186.96	1.02	-x-	2958	-x-	23
S-CTCF	1475.6	-14.6	185 94	1.46	2.0	14	3.5	27
T-CTCC	1490.2	-63.1	184.48	12.96	-x-	1375	-x-	14
Σ=	1553.3	-86.3	171.2	21.29	-x-	28767	-x-	1070

Table E.5 JTC Test 1

Stage	Initial Volume (ml)	Volume Change (ml)	Initial Length (mm)	Length Change (mm)	Load per Step (MPa)	Time (min)	Load Rate (MPa/min)	No. of Data Points
A-HLF	1452.0	68.4	187.67	0.60	1.0	29	1.0	20
B-HLC	1383.6	17.9	187.07	0.29	-x-	4355	-x-	127
C-HLF	1365.7	-1.2	186.78	0.00	1.0	42	1.1	14
D-JTCF	1366.9	-15.3	186.78	0.83	2.0/-1.0	16	1.0	7
E-JTCC	1382.2	-7.3	185.95	1.72(?)	-x-	8685	-x-	56
F-JTCF	1454.5	-39.5	184.23(?)	(?)	2.0/-1.0	15	1.0	7
Σ=	1494.0	-42.0	(?)	(?)	-x-	13142	-x-	231

(?) LVDT 'DA' stopped recording

Table E.6 JTC Test 2

Stage	Initial Volume (ml)	Volume Change (ml)	Initial Length (mm)	Length Change (mm)	Load per Step (MPa)	Time (min)	Load Rate (MPa/min)	No. of Data Points
A-HLF	1580.0	41.8	200.52	1.40	1.0	100	0.9	51
B-HLC	1538.2	16.9	199.12	0.29	-x-	4642	-x-	146
C-JTCF	1521.3	-14.1	198.83	1.00	2.0/-1.0	18	0.8	7
D-JTCC	1535.4	-91.0	197.83	10.86	-x-	8770	-x-	56
E-JTCF	1626.4	-27.0	186.97	2.93	2.0/-1.0	18	0.8	7
F-JTCC	1653.4	-23.0	184.04	5.63	-x-	939	-x-	15
Σ=	1676.4	-96.4	178.41	22.11	-x-	14487	-x-	282

Table E.1 JTC Test 3

Stage	Initial Volume (ml)	Volume Change (ml)	Initial Length (mm)	Length Change (mm)	Load per Step (MPa)	Time (min)	Load Rate (MPa/min)	No. of Data Points
A-HLF	1619.0	33.1	205.13	0.73	1.4	183	0.6	55
B-HLC	1585.9	6.2	204.40	0.33	-x-	4188	-x-	163
C-JTCF	1579.7	-68.6	204.07	8.38	2.0/-1.0	40	0.7	17
D-JTCC	1648.3	-91.5	195.69	14.73	-x-	1090	-x-	114
Σ=	1739.8	-120.8	180.96	24.17	-x-	5501	-x-	349

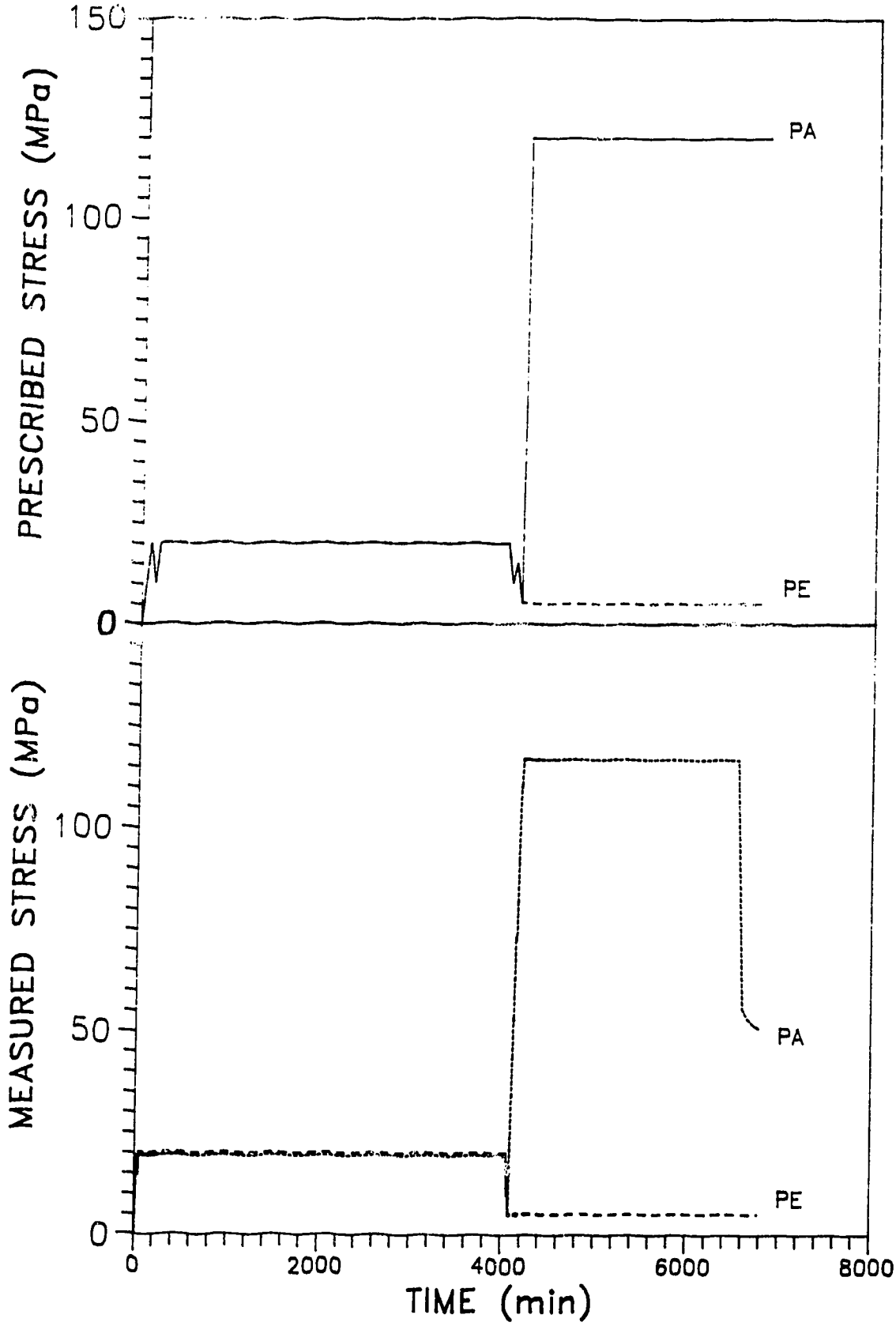

Figure E.1 CTC Test 1 (899 points) - Measured and prescribed stress paths

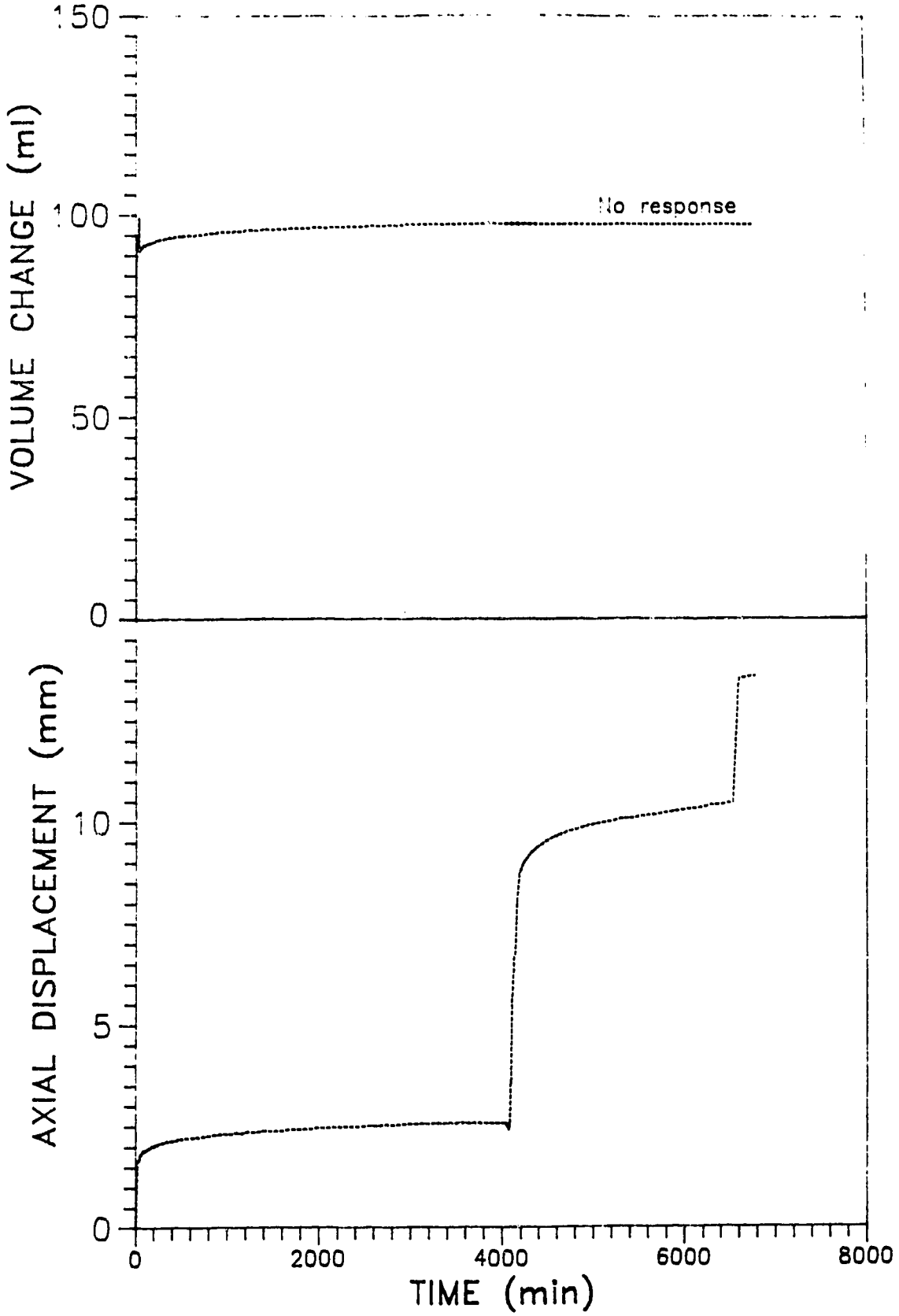

Figure E.2 CTC Test 1 (899 points) - Axial displacement and volume change responses

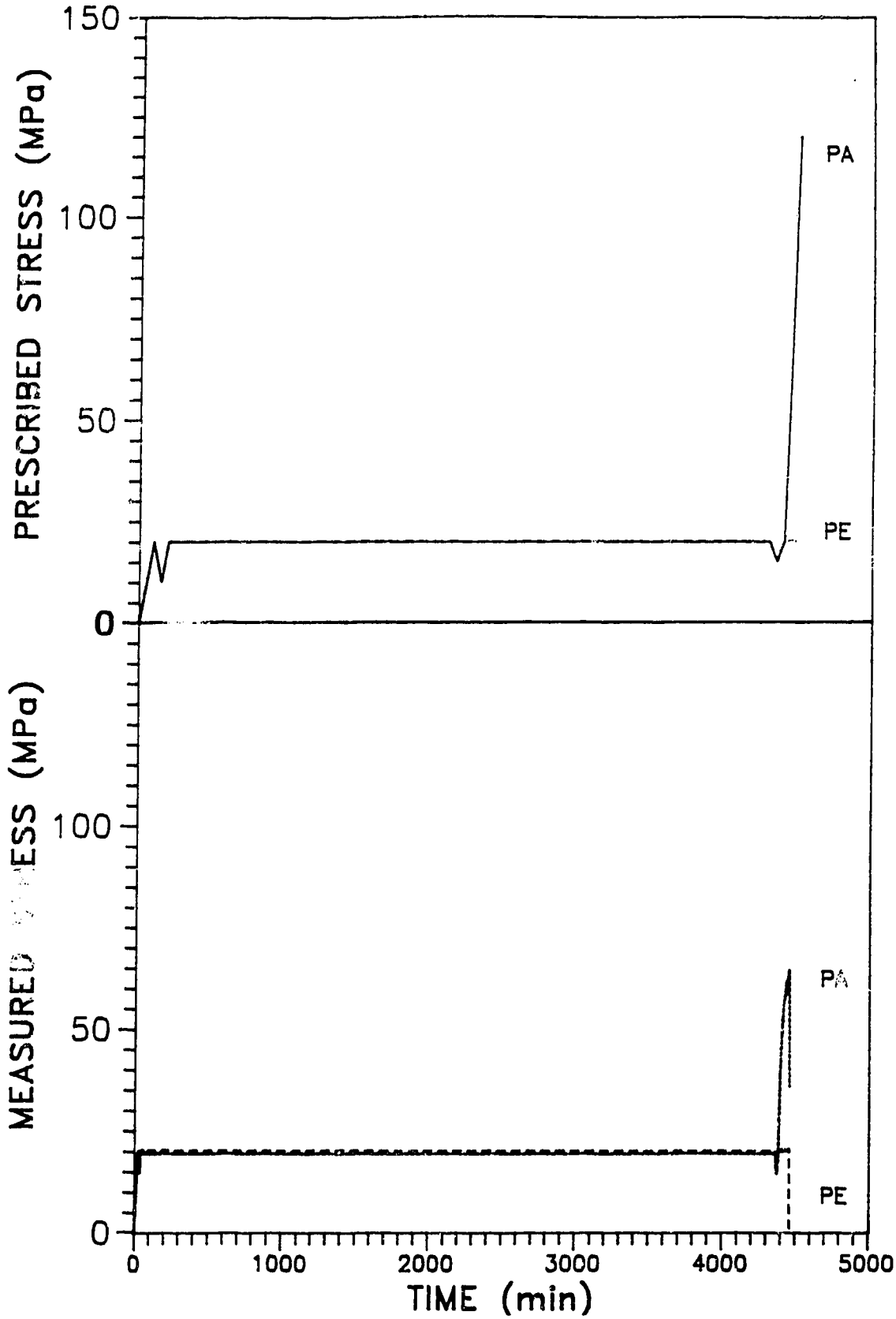

Figure E.3 CTC Test 2 (483 points) - Measured and prescribed stress paths

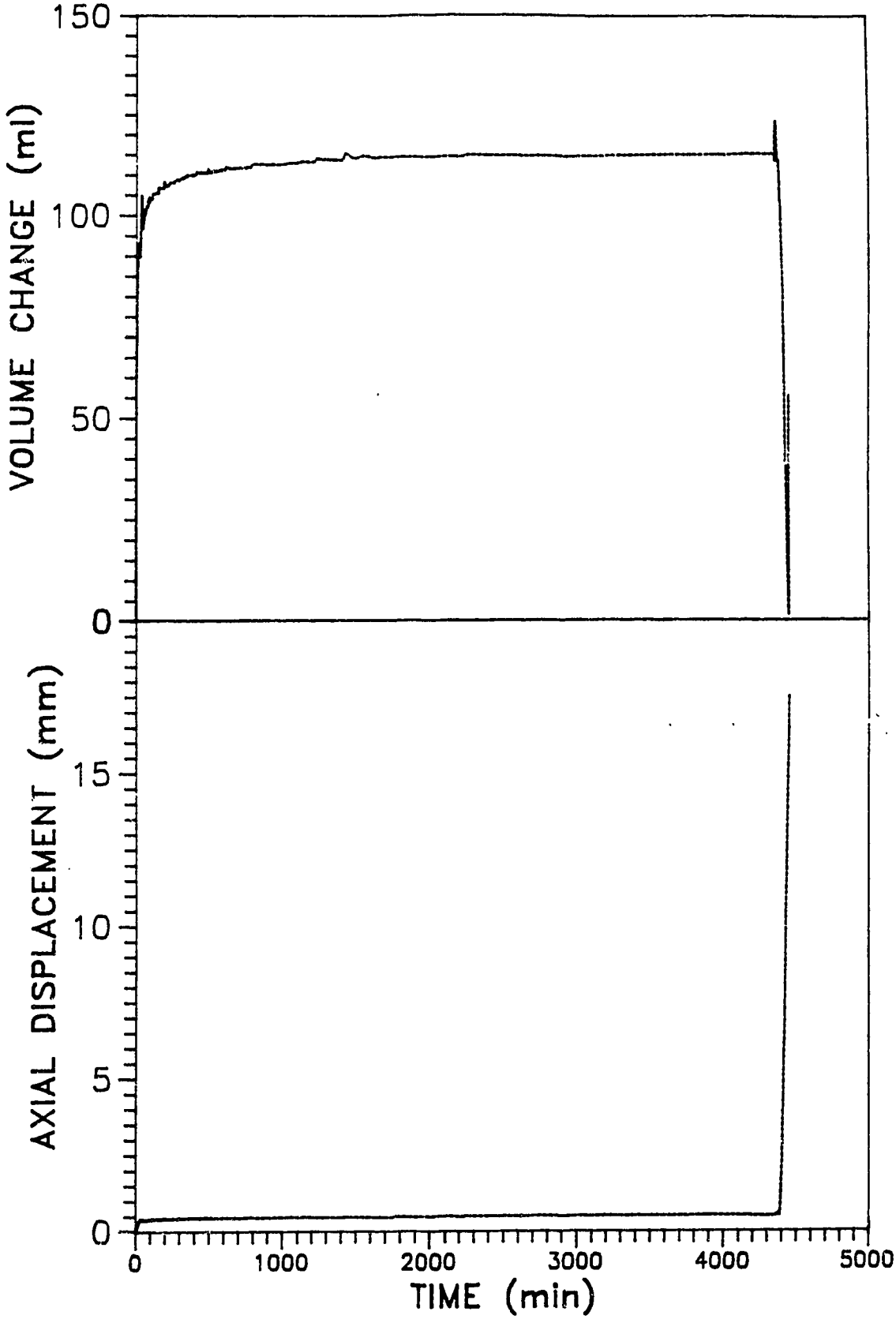

Figure E.4 CTC Test 2 (483 points) - Axial displacement and volume change responses

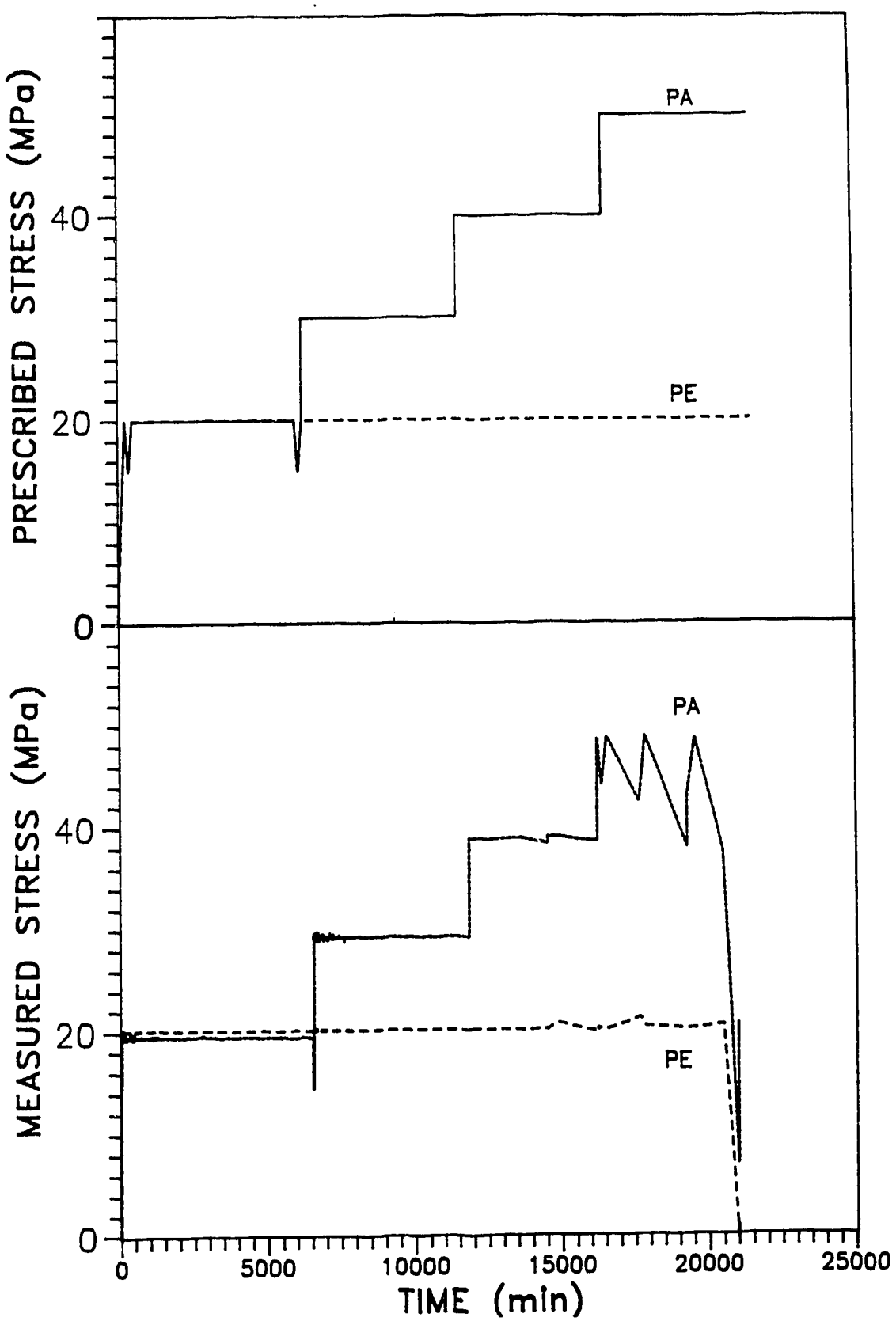

Figure E.5 CTC Test 3 (762 points) - Measured and prescribed stress paths

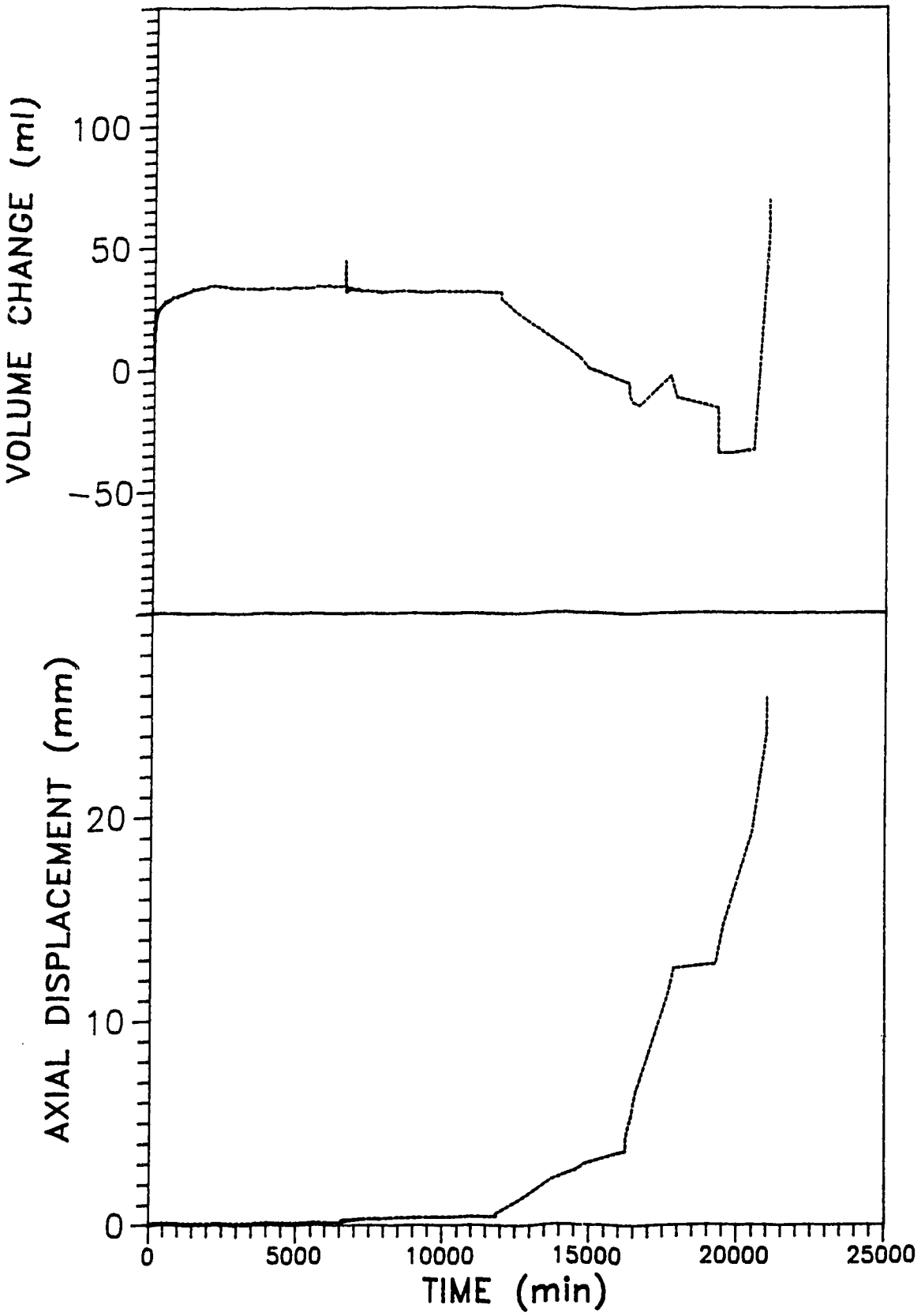

Figure E.6 CTC Test 3 (762 points) - Axial displacement and volume change responses

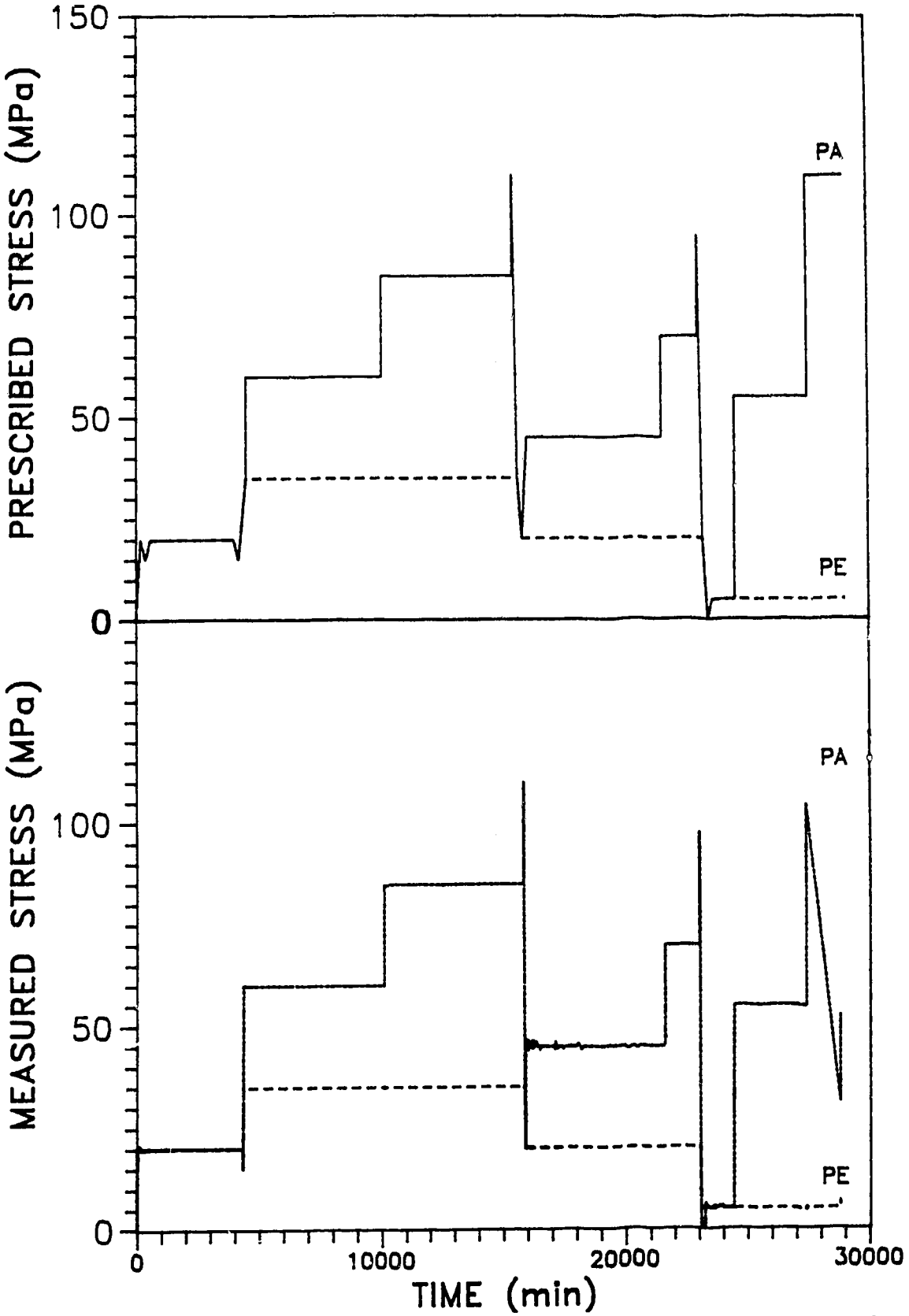

Figure E.7 CTC Test 4 (1058 points) - Measured and prescribed stress paths

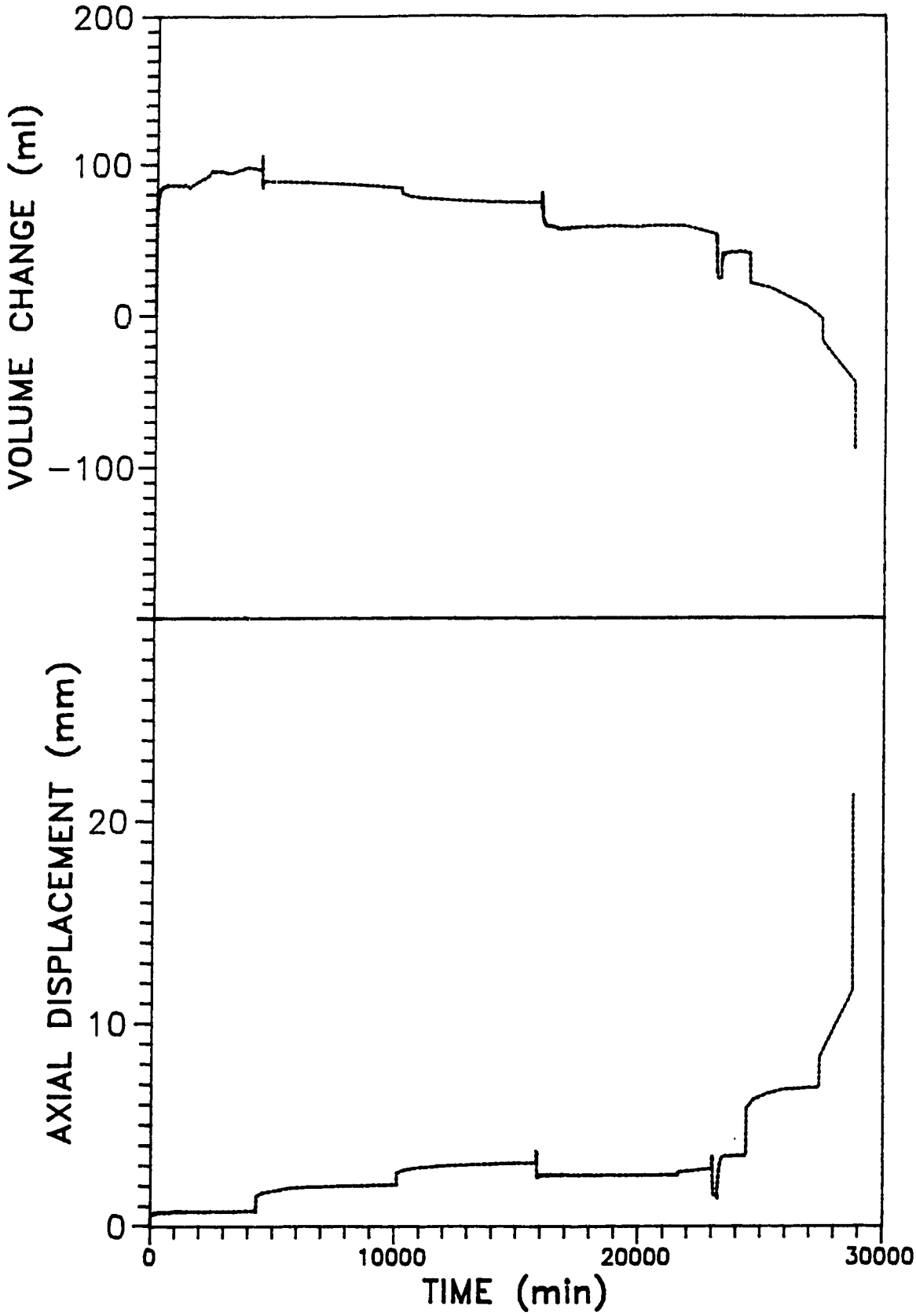

Figure E.8 CTC Test 4 (1058 points) - Axial displacement and volume change responses

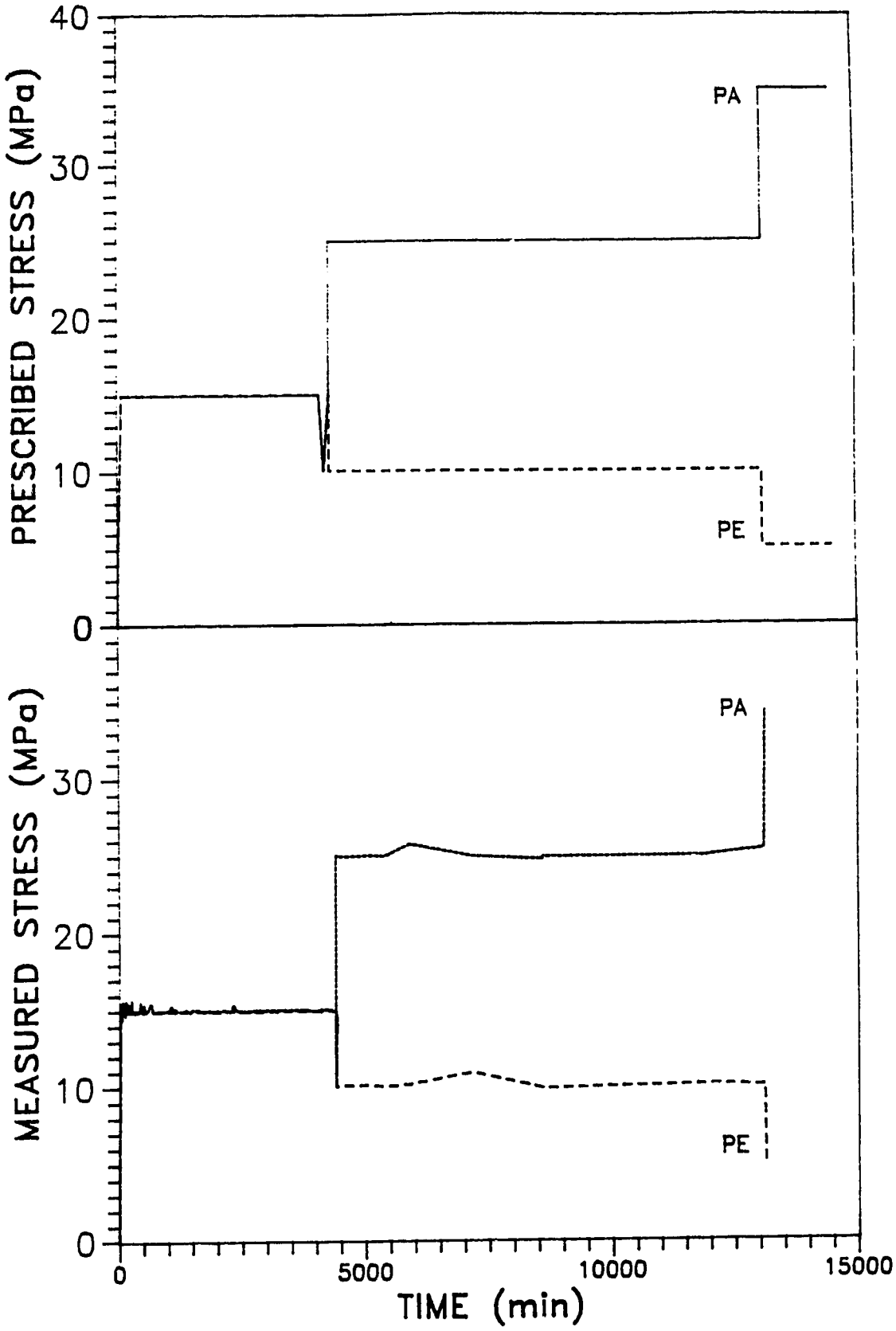

Figure E.9 JTC Test 1 (224 points) - Measured and prescribed stress paths

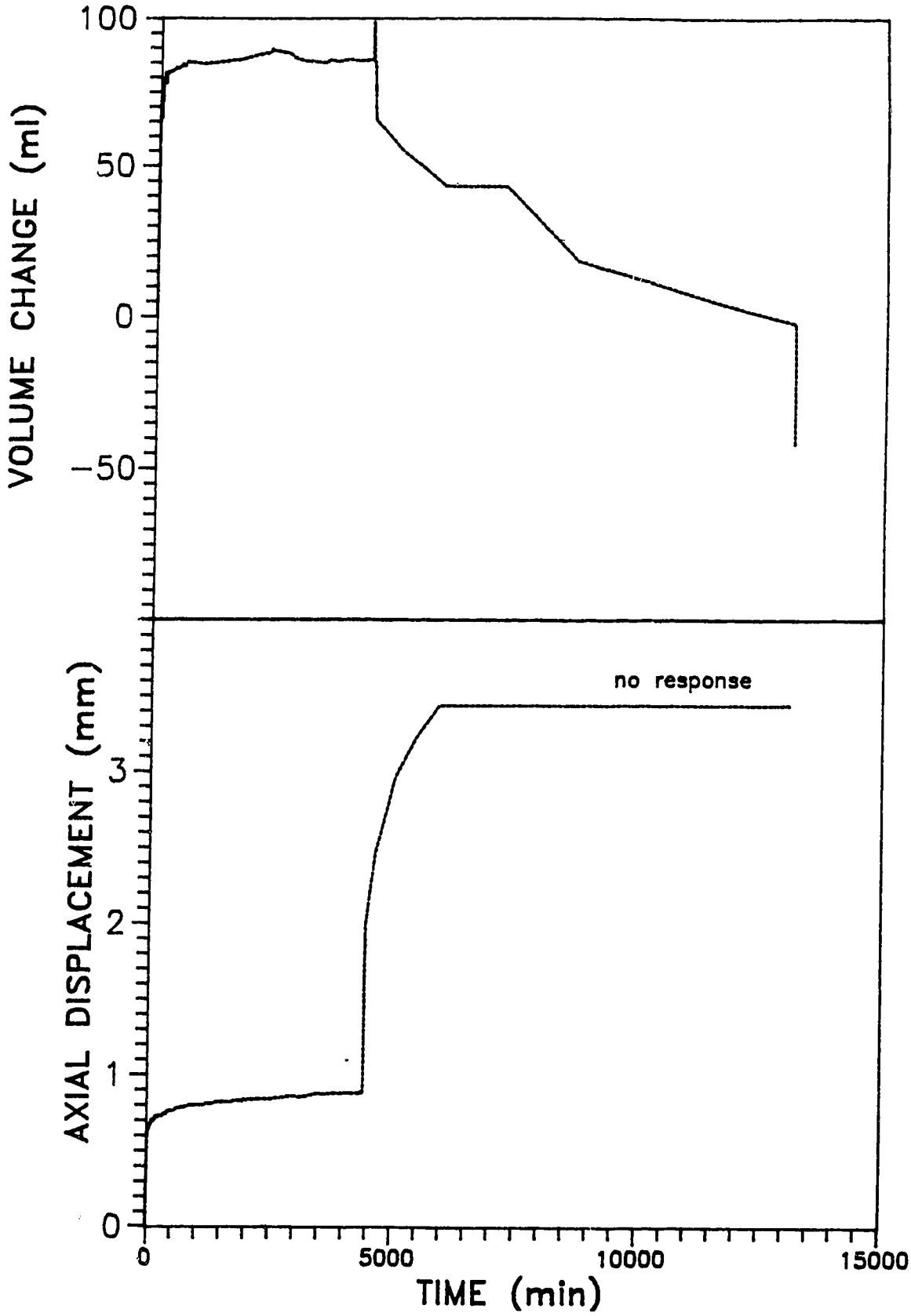

Figure E.10 JTC Test 1 (224 points) - Axial displacement and volume change responses

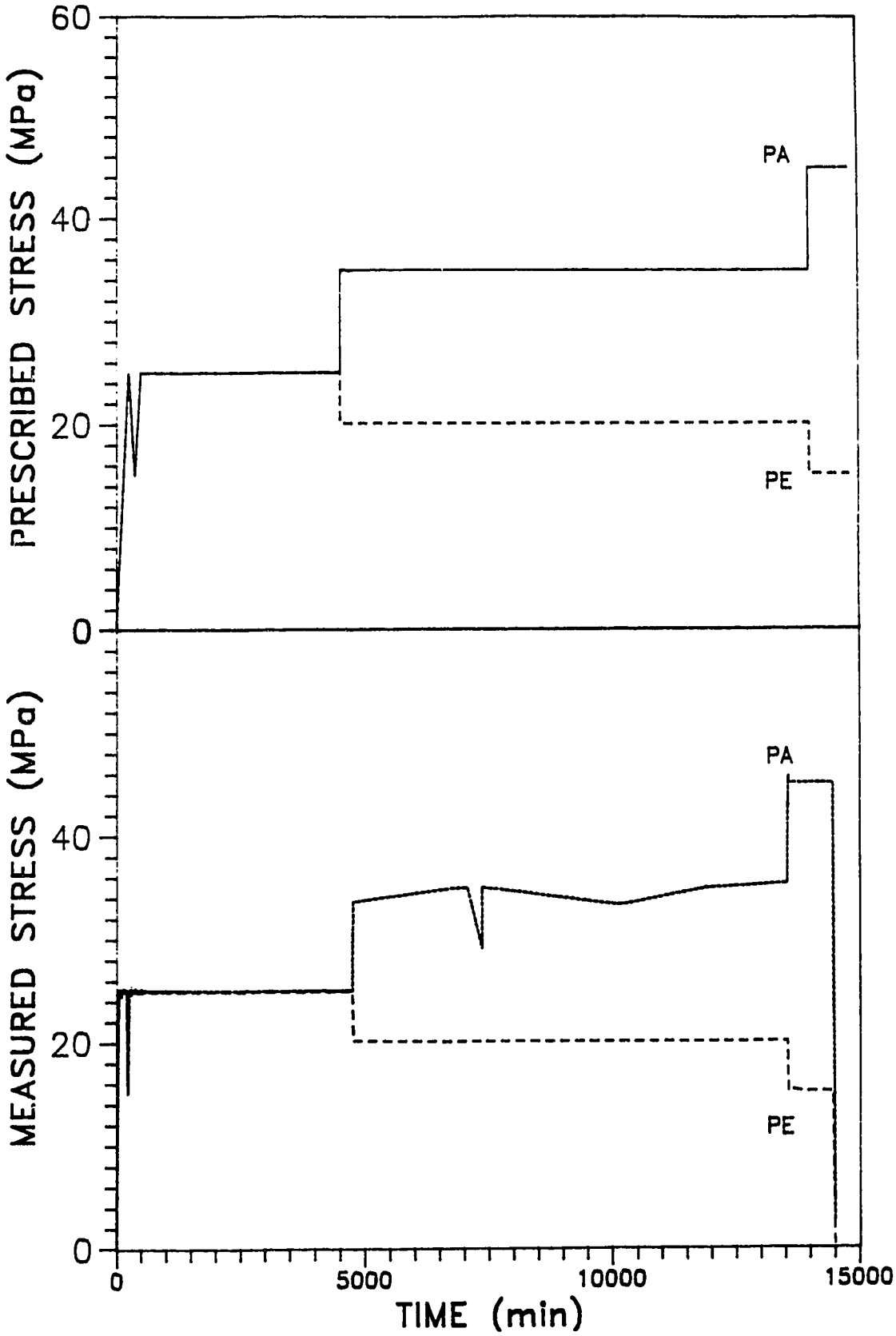

Figure E.11 JTC Test 2 (276 points) - Measured and prescribed stress paths

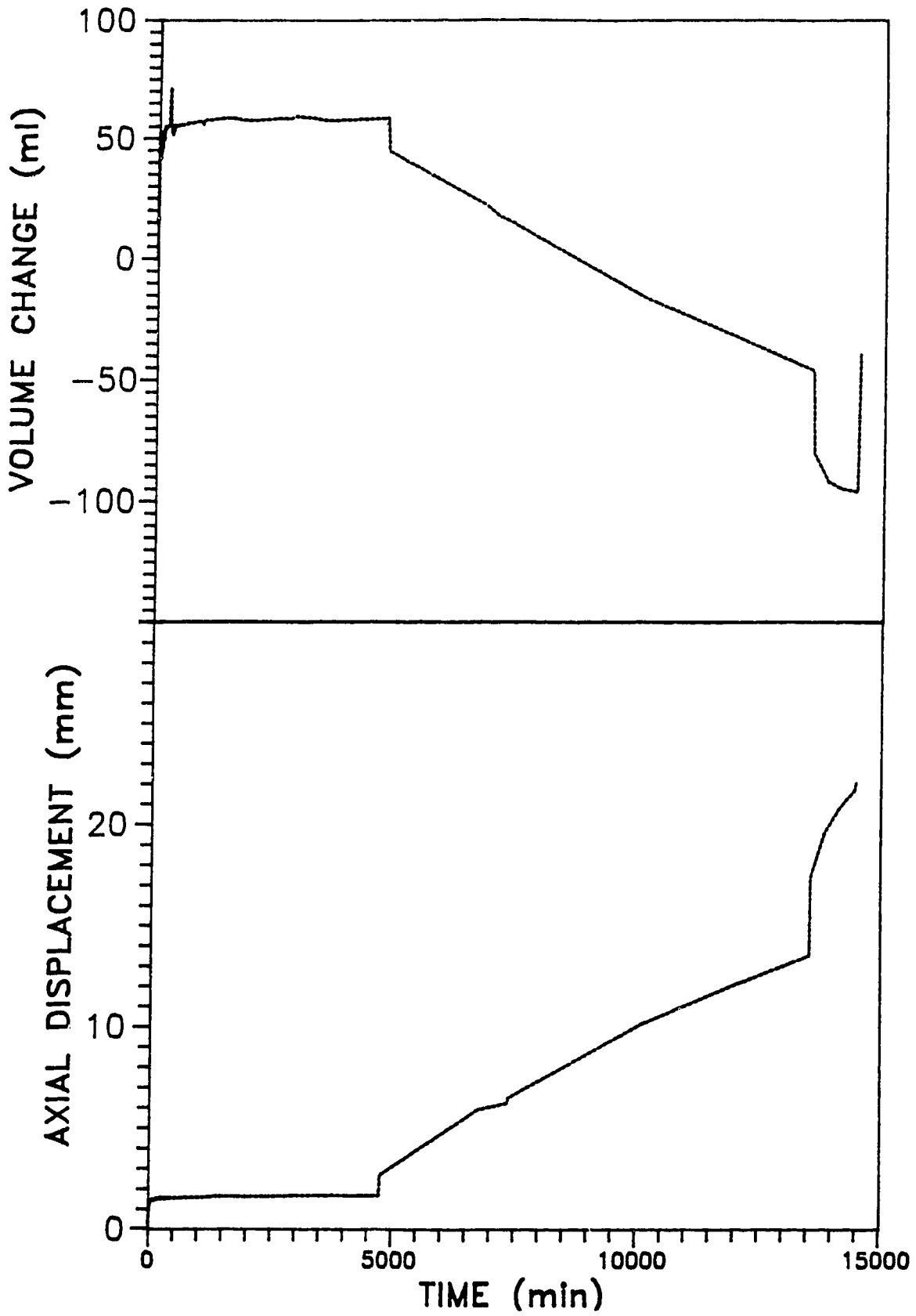

Figure E.12 JTC Test 2 (276 points) - Axial displacement and volume change responses

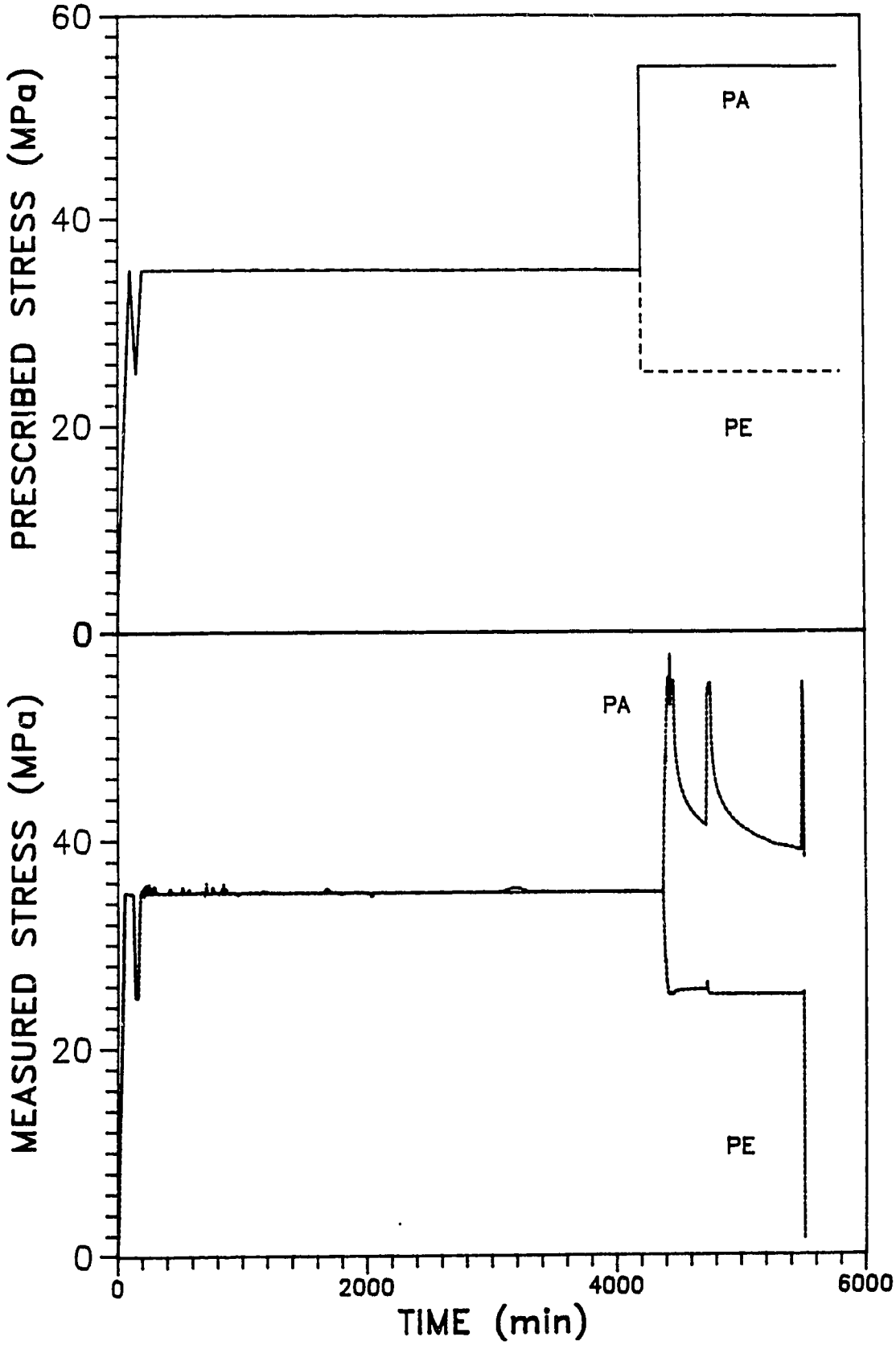

Figure E.13 JTC Test 3 (349 points) - Measured and prescribed stress paths

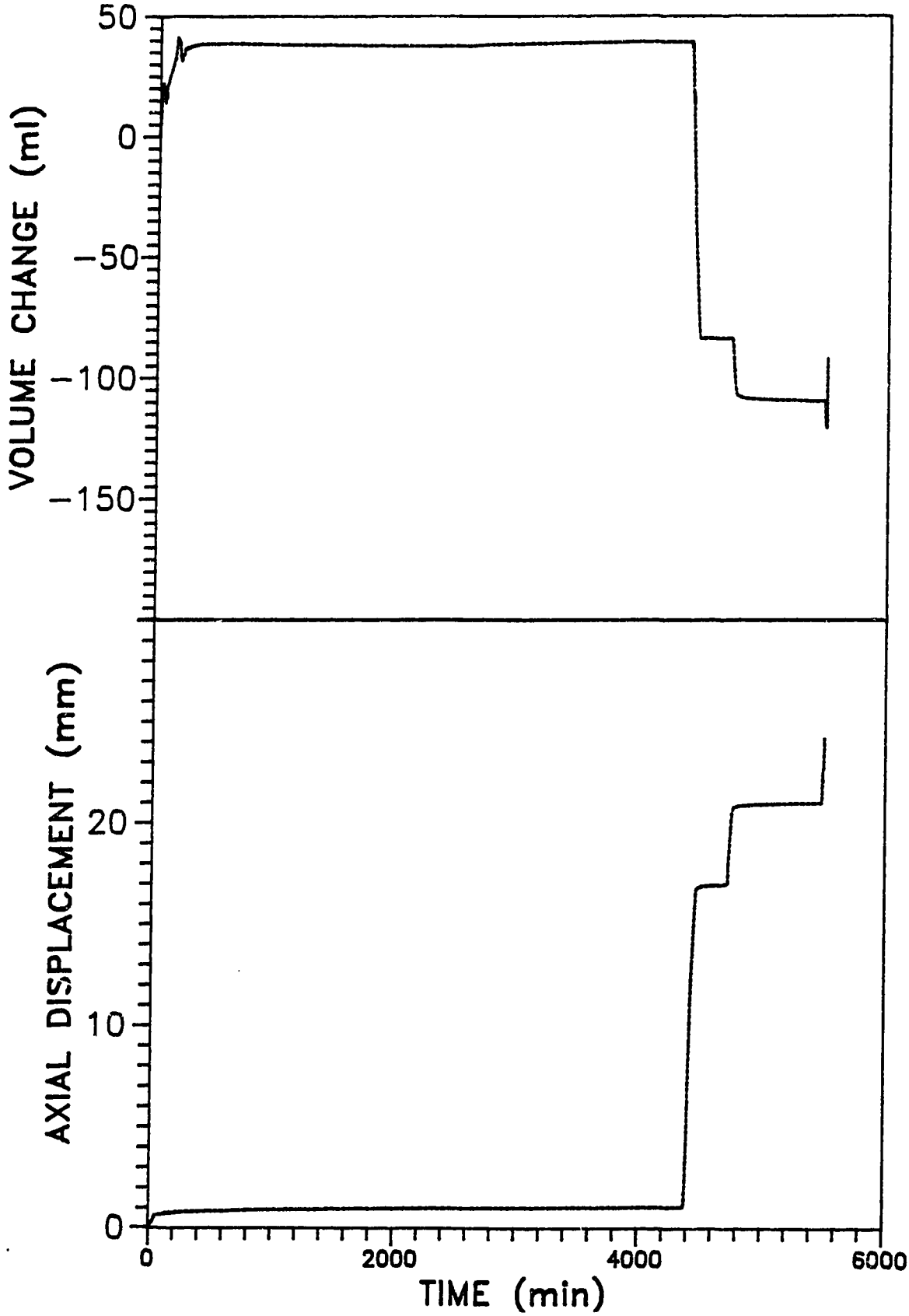

Figure E.14 JTC Test 3 (349 points) - Axial displacement and volume change responses

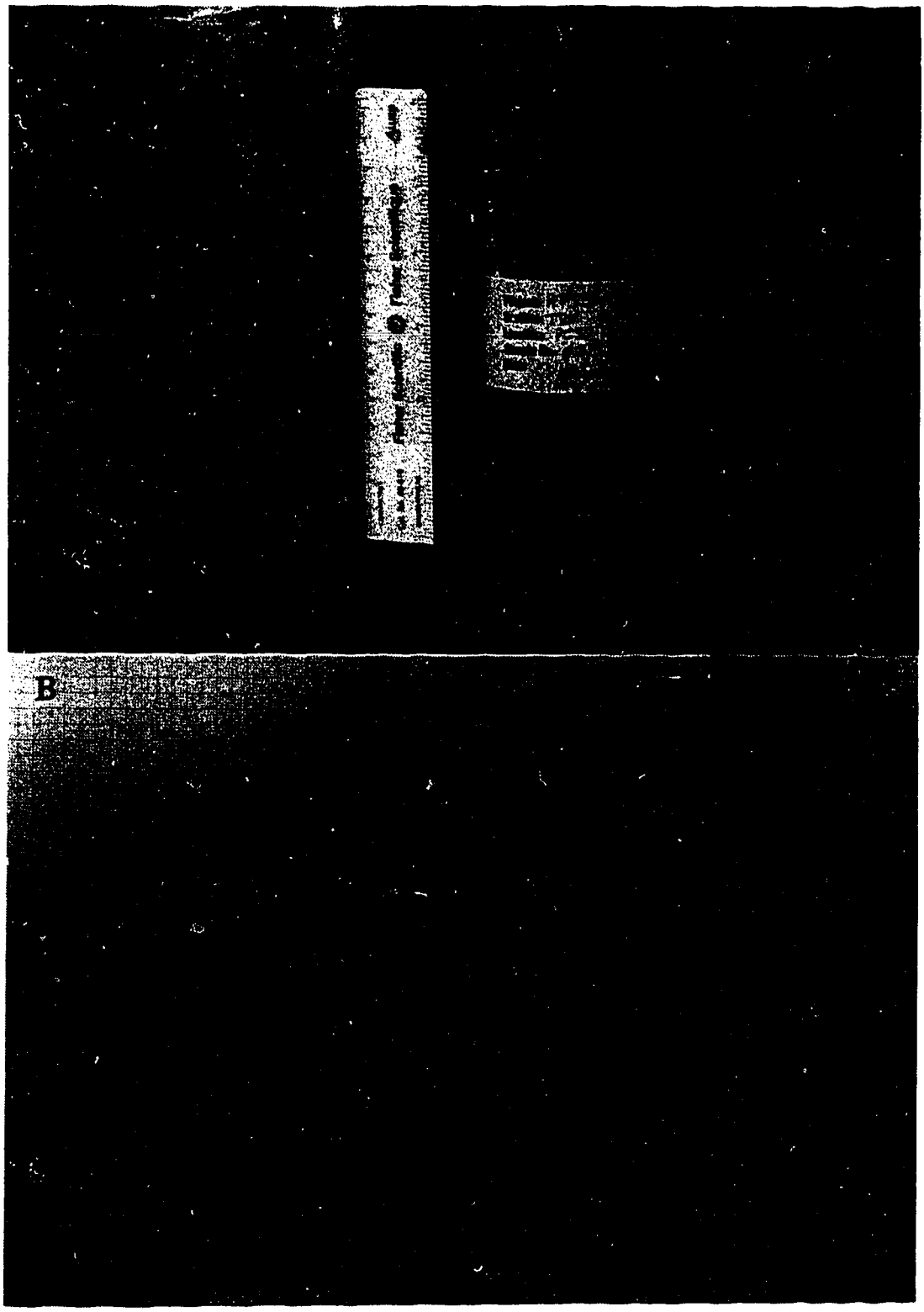

Plate E.1 CTC Test 1 - Specimen TR02; (A) Before testing; (B) After testing

A

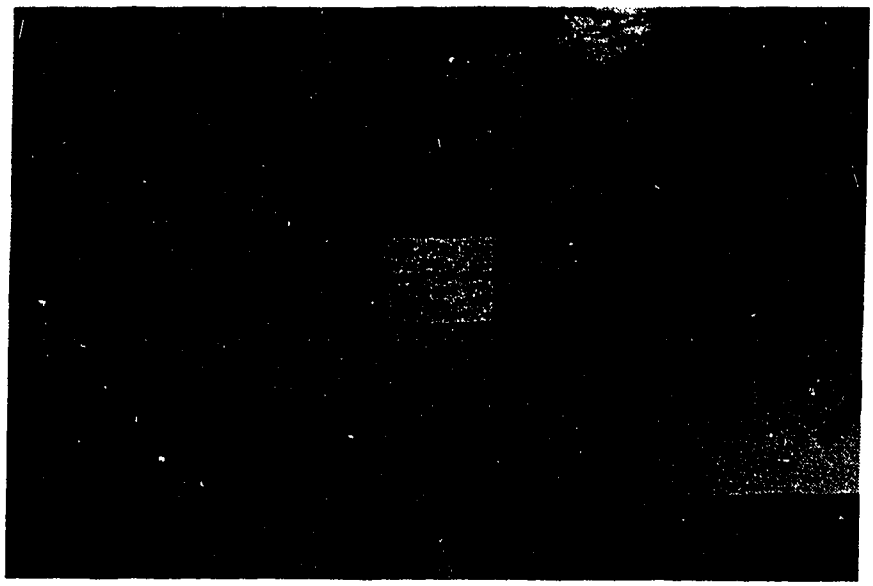

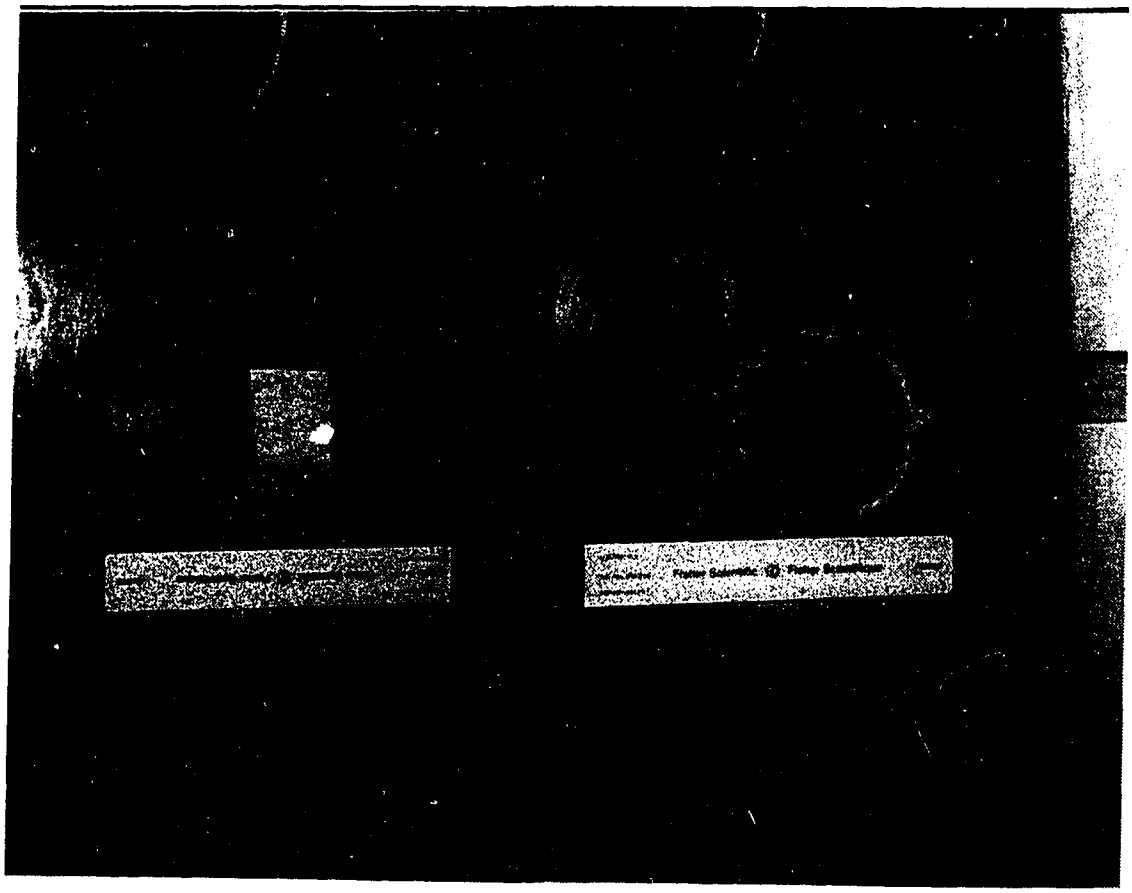

Plate E.2 CTC Test 2 - Specimen TR03; (A) Before testing; (B) After testing

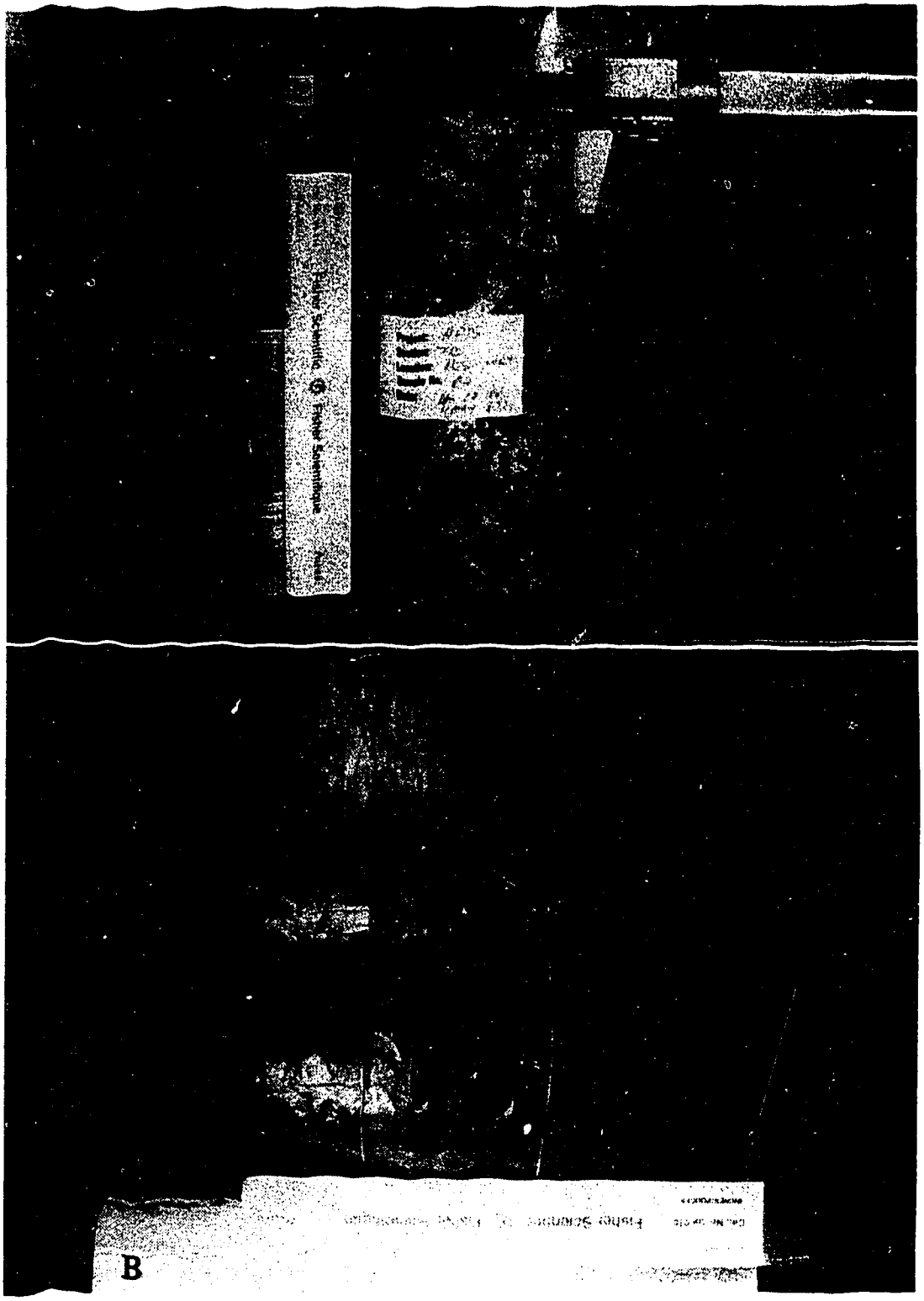

Plate E.3 CTC Test 3 - Specimen TR04; (A) Before testing; (B) After testing

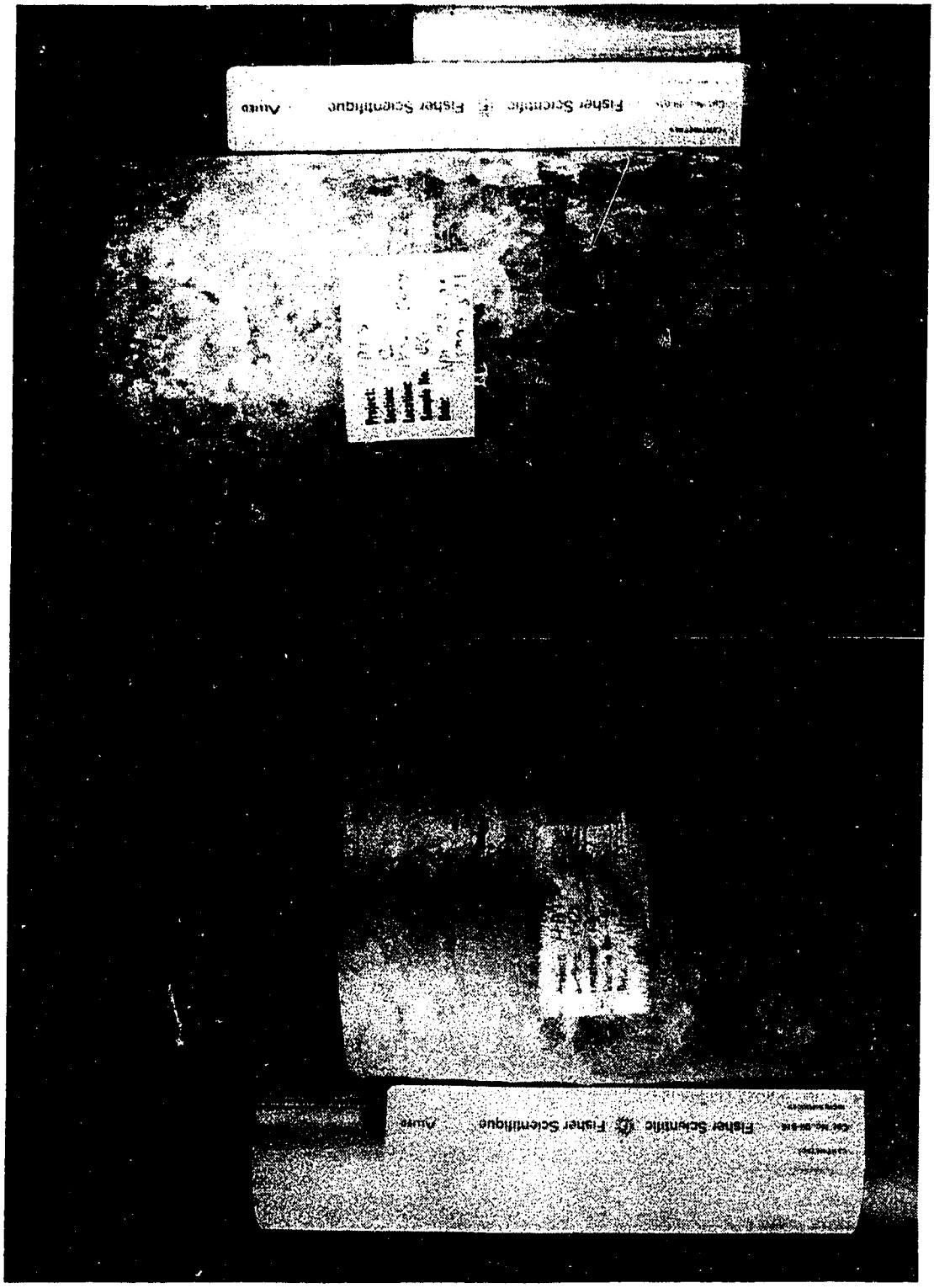

Plate E.4 CTC Test 4 - Specimen TR06; (A) Before testing; (B) After testing

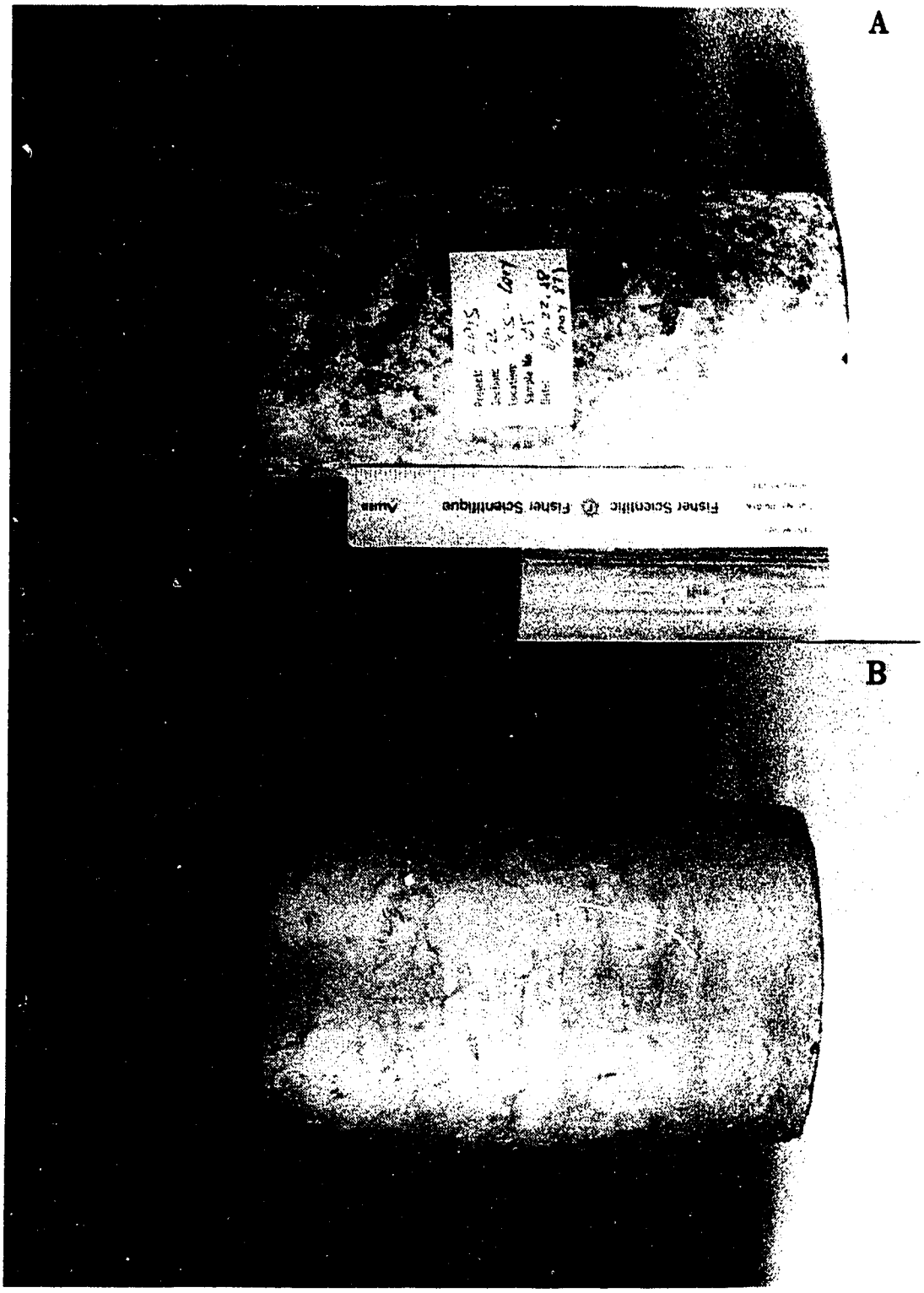

Plate E.5 JTC Test 1 - Specimen TR05; (A) Before testing; (B) After testing

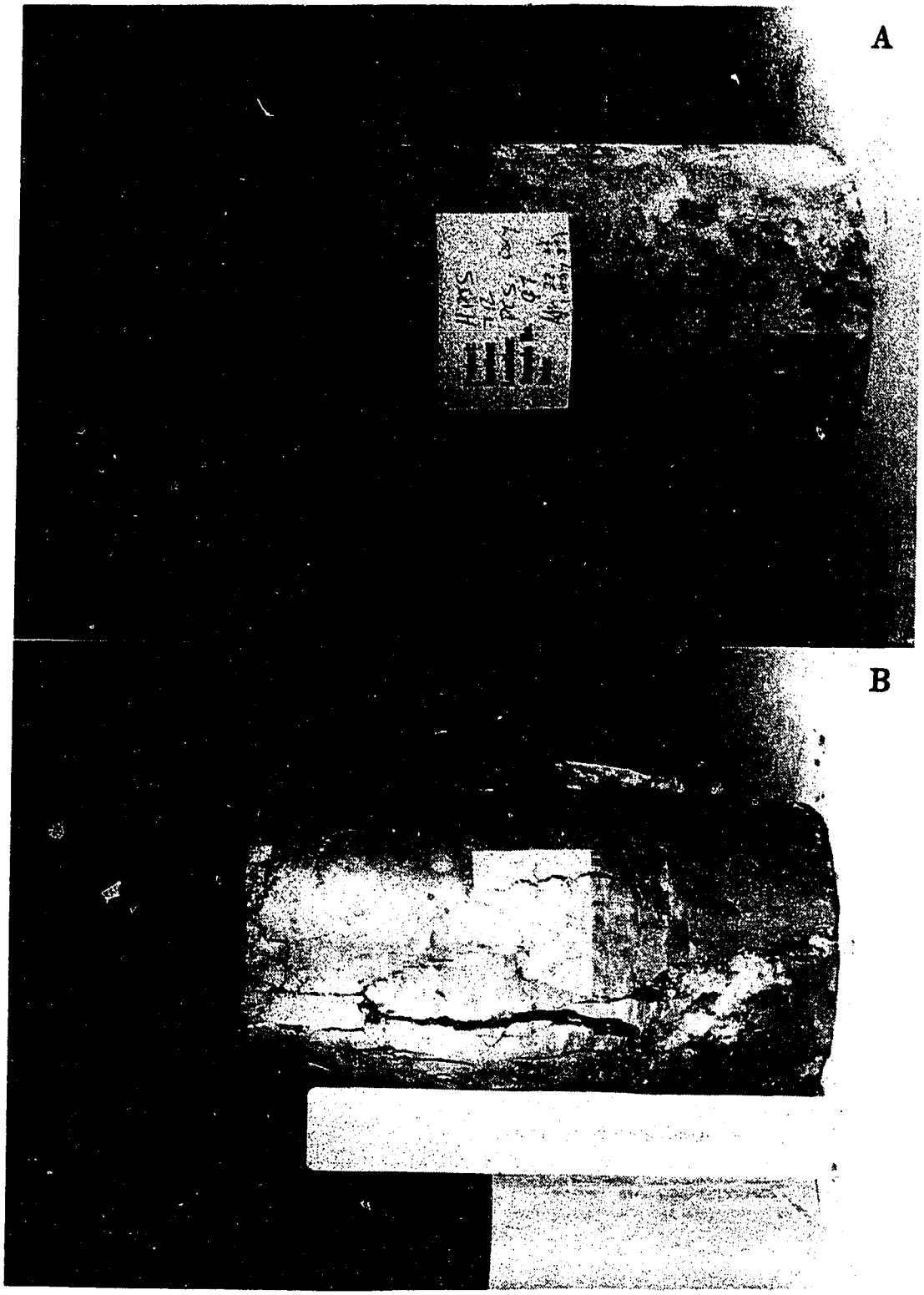

Plate E.6 JTC Test 2 - Specimen TR07; (A) Before testing; (B) After testing

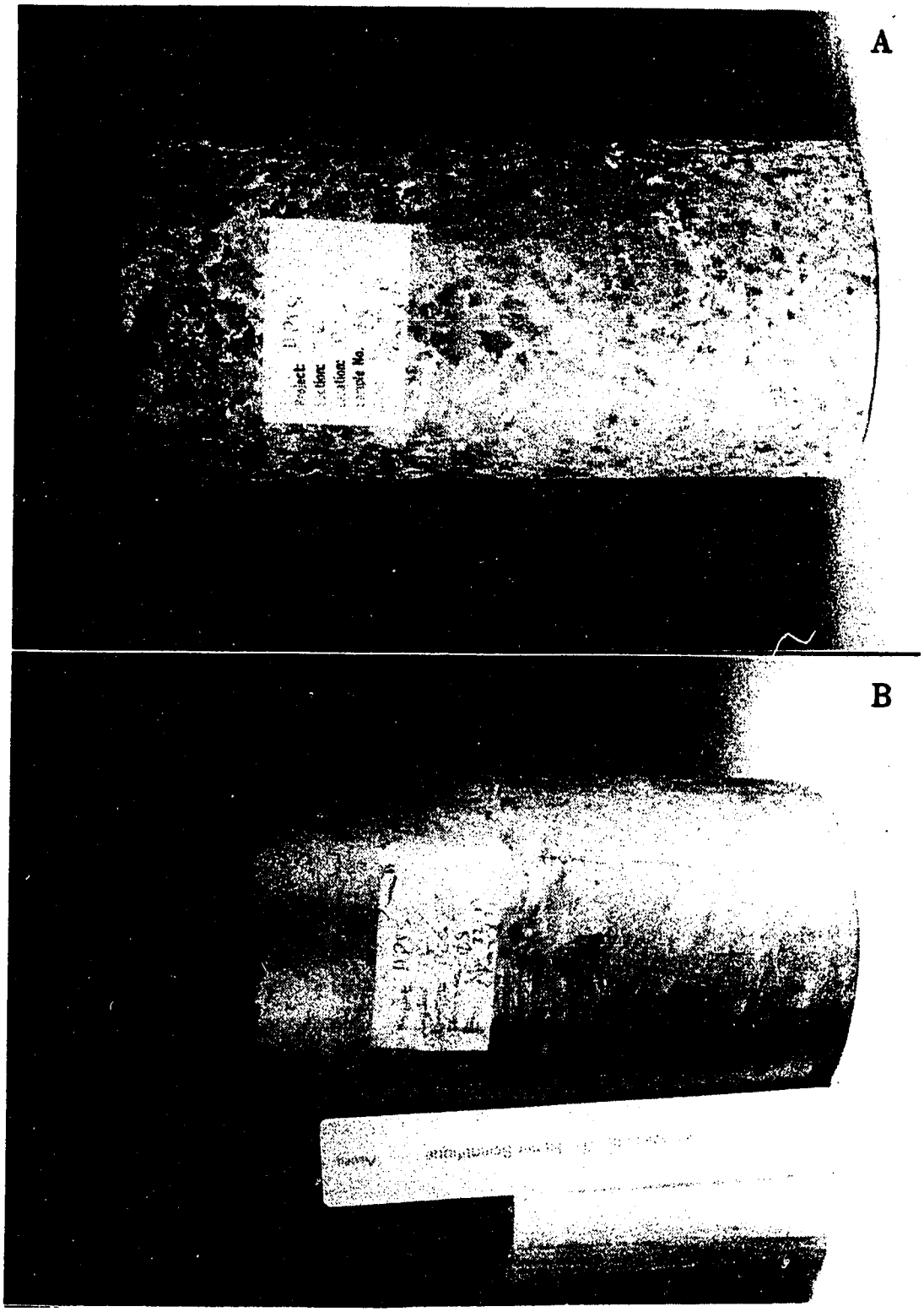

Plate E.7 JTC Test 3 - Specimen TR08; (A) Before testing; (B) After testing